International Journal of Polymer Science

Polysaccharides for Biomedical Applications

Lead Guest Editor: Mingqiang Li
Guest Editors: Jianxun Ding, Yu Tao, Bingyang Shi, and Jing-Hua Chen

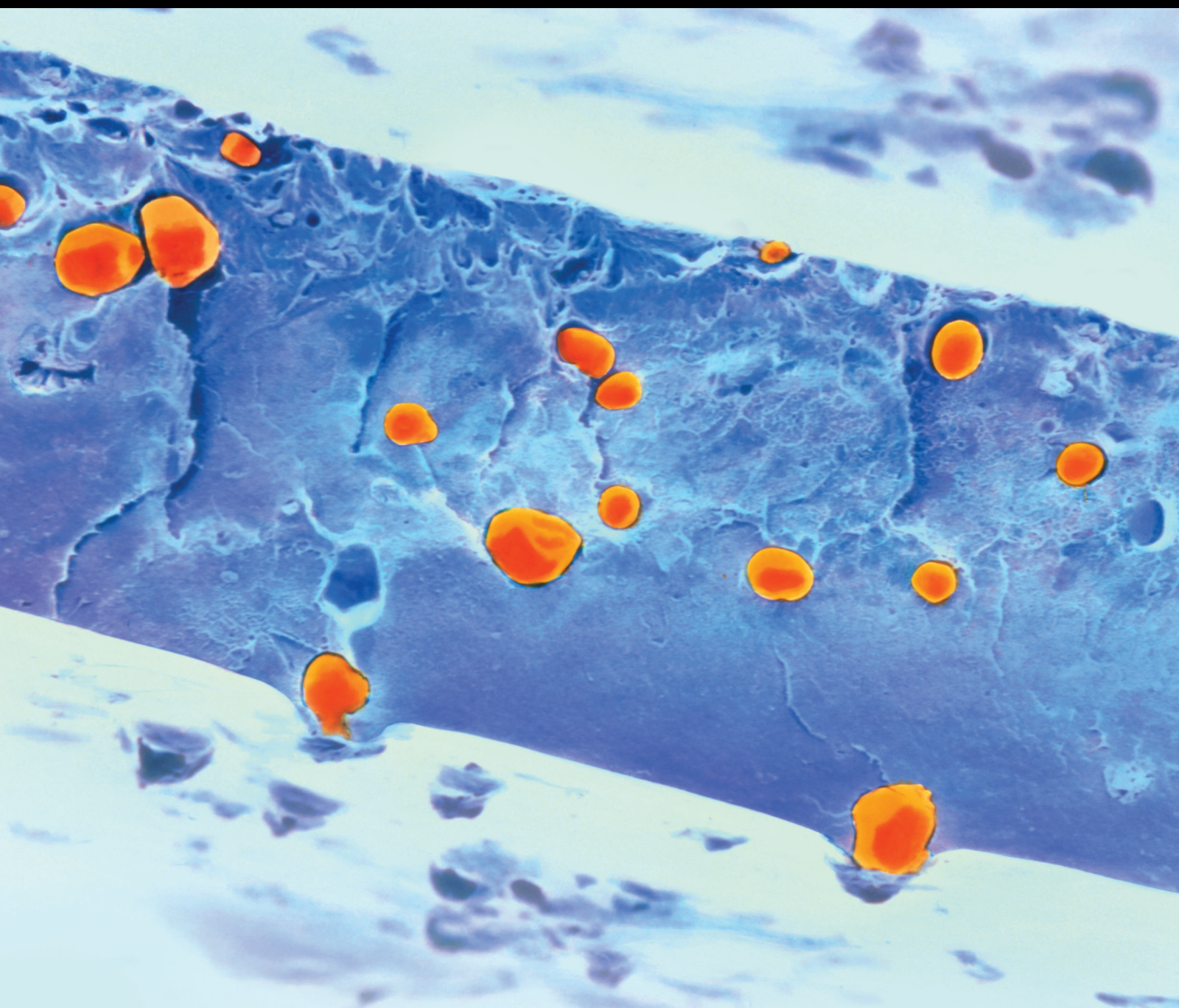

Polysaccharides for Biomedical Applications

International Journal of Polymer Science

Polysaccharides for Biomedical Applications

Lead Guest Editor: Mingqiang Li
Guest Editors: Jianxun Ding, Yu Tao, Bingyang Shi, and Jing-Hua Chen

Editorial Board

Contents

Hindawi
International Journal of Polymer Science
Volume 2019, Article ID 7841836, 2 pages
https://doi.org/10.1155/2019/7841836

Editorial

Polysaccharides for Biomedical Applications

Mingqiang Li,[1,2] **Jianxun Ding**,[3] **Yu Tao**,[2,4] **Bingyang Shi**,[5] **and Jing-Hua Chen**[6]

[1]*Department of Biomedical Engineering, Columbia University, New York, NY 10027, USA*
[2]*Laboratory of Biomaterials and Translational Medicine, The Third Affiliated Hospital, Sun Yat-sen University, Guangzhou 510630, China*
[3]*Key Laboratory of Polymer Ecomaterials, Changchun Institute of Applied Chemistry, Chinese Academy of Sciences, Changchun 130022, China*
[4]*Institute for Cancer Genetics, Columbia University Medical Center, New York, NY 10032, USA*
[5]*International Joint Center for Biomedical Innovation, School of Life Sciences, Henan University, Kaifeng, Henan 475004, China*
[6]*School of Pharmaceutical Sciences, Jiangnan University, Wuxi 214122, China*

Correspondence should be addressed to Mingqiang Li; limq567@mail.sysu.edu.cn, Jianxun Ding; jxding@ciac.ac.cn, and Yu Tao; taoy28@mail.sysu.edu.cn

Received 18 February 2019; Accepted 18 February 2019; Published 9 April 2019

Polysaccharides have been recognized and applied as promising candidates for diverse biomedical and biotechnological applications, such as diagnosis, bioactive therapy, controlled drug delivery, gene therapy, theranostics, cell encapsulation, tissue engineering, and medical devices, as a benefit of their biocompatibility, biodegradability, inherently low immunogenicity, and unique bioactive properties. The current special issue is motivated by the observed increasing interest and emerging innovative research output shown in the field of polysaccharide-based biomaterials. It aims to disseminate researches and advancements based on the polysaccharides, which can be used alone or applied as part of a hybrid system for biomedical researches and applications.

Seventeen original research articles and a review paper have been collected in this special issue. These articles are themed on the polysaccharide applied for antitumor, antimicrobial, antioxidant, anti-inflammation, tissue engineering, treatment of asthma, acute lung injury, rheumatoid arthritis, and so forth.

Seven papers focus on the biomedical applications of chitosan. S. Kim summarized the biological activities (antimicrobial, antioxidant, anticancer, and anti-inflammatory activities) of chitosan and its derivatives. E. Szymańska et al. developed the β-glycerophosphate-modified chitosan hydrogels for controlled drug release. D.-L. He et al. applied the hyaluronic acid-conjugated chitosan for the encapsulation of novel anticancer oligopeptide (*Perilla* seed oligopeptide (PSO)), showing a broad spectrum of anticancer activities. Guo et al. synthesized a cationic chitosan-based nanogel with an average diameter of 55.8 nm for the delivery of 10-hydroxycamptothecin. L. Zhang et al. prepared the alphastatin-loaded chitosan nanoparticles that could inhibit the SphK1-S1P signaling pathway and enhance the antiangiogenic effect of alphastatin. C.-L. Li et al. developed the chitosan-polyethylenimine as an effective gene (pCGRP) transfection system for the early healing of fractures. Nguyen et al. investigated the antibacterial activity of poly(vinyl alcohol)-chitosan-silver nanoparticle hybrid hydrogels.

Seven articles report the investigations on the biological activities of natural polysaccharides. L. Zhang et al. found that *Dendrobium officinale* polysaccharides (DOPS) could reduce the pentetrazol-induced brain inflammation and seizures by inhibiting the IL-1β, TNF-α, and MAPK signal pathways. J.-M. Wang et al. discovered that *Astragalus* polysaccharides could be utilized as potential antioxidative drugs for renal protection. Q. Sun et al. demonstrated the vaccine immune effect of *Robinia pseudoacacia* polysaccharides (RPPS). J. Sun et al. combined anti-IL-5 mAb and *Achyranthes bidentata* polysaccharide (ABPS) to improve airway function in a mouse asthma model. C. Peng et al. studied

the anticancer effects of nanoyam polysaccharides and the *Cyclocarya paliurus* polysaccharide in prostate cancer and thyroid cancer models, respectively. L. Cao et al. obtained the high quality of *Astragalus* polysaccharide by applying the cellulase method and proved its biological features against rheumatoid arthritis.

Four more studies deal with hydrogel or nanoparticle systems for bone regeneration, controlled drug release, and antimicrobial against skin pathogens.

Overall, this special issue bridges the polysaccharide and biomedical applications. We expect that related researchers will get inspired.

Conflicts of Interest

The guest editorial team declares no conflict of interest regarding the publication of this special issue.

Acknowledgments

We greatly appreciate the contributions of all the authors to the special issue and the constructive critiques, comments, and suggestions of all the reviewers and the editorial staff members.

Mingqiang Li
Jianxun Ding
Yu Tao
Bingyang Shi
Jing-Hua Chen

Hindawi
International Journal of Polymer Science
Volume 2019, Article ID 2751384, 9 pages
https://doi.org/10.1155/2019/2751384

Research Article

Alphastatin-Loaded Chitosan Nanoparticle Preparation and Its Antiangiogenic Effect on Lung Carcinoma

Li Zhang and Yaoren Hu

Second Hospital of Ningbo, Ningbo, China

Correspondence should be addressed to Yaoren Hu; hu510@126.com

Received 15 September 2018; Revised 15 December 2018; Accepted 24 December 2018; Published 7 April 2019

Guest Editor: Mingqiang Li

Alphastatin is a 24-amino acid peptide and can suppress tumor angiogenesis by inhibiting both the migration and tubule formation of vascular endothelial cells. However, the anticancer effect of Alphastatin is limited due to the short half-life and degradation in the body. In this study, Alphastatin-loaded chitosan nanoparticles (AsCs NPs) were prepared with an initial concentration of 2 mg/ml for chitosan and 1 mg/ml for Alphastatin. AsCs NPs presented the encapsulation efficiency of 32.4%, the mean particle size of 387.4 nm, the polydispersity index of 0.223, and the zeta potential of +28.1 mV. AsCs NPs have a sustained release for 6 days and were stable in serum for at least 24 hours. And the NPs could preserve the integrity of encapsulated Alphastatin and released Alphastatin for 24 hours. In a subcutaneous LA975 lung carcinoma xenograft T739 mouse model, AsCs NPs significantly inhibited the tumor growth, tumor volume, and microvessel density (MVD), and the antitumor effect was even stronger than that of Alphastatin. In addition, the VEGF-induced tube formation of HUVEC could be inhibited by AsCs NPs *in vitro* and the serum containing AsCs NPs, and the protein level of SphK1 in HUVEC was also decreased by AsCs NPs, suggesting an inhibitory effect of AsCs NPs on the SphK1-S1P signaling pathway. Furthermore, hemolysis assay showed a safety on blood compatibility of AsCs NPs. Our study indicated that AsCs NPs inhibited the SphK1-S1P signaling pathway and enhanced the antiangiogenic effect of Alphastatin both *in vitro* and *in vivo*.

1. Introduction

Lung cancer is a serious and life-threatening malignant tumor. Though great progress has been made in detection and treatment, the 5-year survival rate of lung cancer remains less than 15%. The invasion and metastasis of tumor are the underlying causes of treatment failure and mortality, and angiogenesis is the prerequisite and foundation for invasion and metastasis of tumor cells [1]. Thus, inhibition of tumor angiogenesis has emerged as an important strategy for antitumor therapy. Alphastatin is a designed and synthetic peptide containing 24 amino acids [2], whose structure is according to the fibrinogen E fragment (FgnE), a potent antiangiogenic factor [3]. It has been reported that Alphastatin acts on activated vascular endothelial cells in the tumor to inhibit tumor angiogenesis [4]. However, as a peptide, due to easy degradation by widely distributed proteolytic enzymes, Alphastatin has a short half-life; therefore, its antitumor angiogenesis could not be fully exerted [5].

Chitosan is a natural cationic polysaccharide and has been widely used as a biomaterial due to its chemical stability, safety, nontoxicity, biocompatibility, and biodegradability. Chitosan is often used as a carrier material to prepare drug-loaded nanoparticles [6]. Previous studies have shown that chitosan can entrap protein and peptide drugs and protect them from hydrolysis by proteolytic enzymes, so that the drug retention time in the body can be prolonged [7]. In addition, the preparation method of drug-loaded chitosan nanoparticles is relatively simple with moderate conditions. And the process has little effect on the bioactivity of proteins or peptides because organic solvent is not involved. Moreover, it has been reported that chitosan and its derivatives have inhibitory effects on cervical cancer, gastric cancer, and other tumor cells.

In view of the excellent carrier properties of chitosan, we speculated that Alphastatin-loaded chitosan nanoparticles (AsCs NPs) may enhance the antitumor effect of Alphastatin. In this study, AsCs NP was prepared and its efficacy against tumor angiogenesis was investigated both *in vivo* and *in vitro*.

2. Materials and Methods

2.1. Materials. Unless stated otherwise, all chemical reagents were purchased from Sigma-Aldrich. Chitosan has a 95% deacetylation degree and 100 kDa of average molecular weight. Alphastatin was purchased from GL Biochem (Shanghai) Ltd., and the amino acid sequence is ADSGEGDFLAEGGG VRGPRVVERH. 2 mice bearing LA975 lung tumor and 44 T739 mice were purchased from the Center for Laboratory Animals, Ningbo University. The T739 mice were 5 weeks old. The mice were all bred in a specific pathogen-free (SPF) room. Human umbilical vein endothelial cells (HUVECs) were obtained from Fuyang Biotech (Shanghai, China). Matrigel was purchased from Corning Inc. (Shanghai, China). The EGM2 medium was purchased from Lonza.

2.2. Preparation of AsCs NPs and Measurement of Encapsulation Efficiency (EE%). Different final concentrations of chitosan at 1.0 or 2.0 mg/ml were dissolved in acetic acid solution (0.1 M, pH = 5.0). 4 ml of chitosan/acetic acid solution was taken, and then a high concentration of Alphastatin was slowly added. The different mass ratios of chitosan to Alphastatin at 1 : 4, 1 : 2, 1 : 1.5, 1;1, 2 : 1, 4 : 1, and 8 : 1 were produced, corresponding to final concentrations of Alphastatin at 8 mg/ml, 4 mg/ml, 3 mg/ml, 2 mg/ml, 1 mg/ml, 0.5 mg/ml, and 0.25 mg/ml. After mixing well and incubating overnight at room temperature, 2.0 mg/ml sodium tripolyphosphate (TPP) was slowly added into the solution under magnetic stirring to a 4 : 1 mass ratio of chitosan to TPP, and the mixture was stirred continuously for 30 min. Then, the mixture was centrifuged at 4°C, 13,000 g for 30 min, and the sediment was collected. The sediment was resuspended in deionized water and lyophilized by freeze-drying. The powder was named AsCs NPs. Similarly, the blank chitosan nanoparticles (Cs NPs) were prepared following the above process without adding Alphastatin.

For EE% measurement, after adding TPP and stirring for 30 min, the mixture was centrifuged at 4°C, 13,000 rpm for 30 min, then the supernatant was collected and the protein concentration of free Alphastatin was measured using the colorimetric bicinchoninic acid (BCA) method according to the protocol provided with the BCA assay kit (Thermo Fisher). EE% was calculated according to the following formula, and the supernatant from the blank chitosan mixture without Alphastatin was set as the blank control.

$$\text{EE\%} = 100\% \times (\text{total amount of alphastatin used} - \text{amount of free alphastatin}) \div \text{total amount of alphastatin used}. \quad (1)$$

2.3. Nanoparticle Characterization. The nanoparticle size, polydispersity index (PDI), and surface charges were determined in water by using the DelsaNano C particle size and zeta potential analyzer (Beckman Coulter, CA, USA).

2.4. Morphology. Transmission electron microscopy (Philips CM12, Eindhoven, Netherlands) was used to examine the morphology of AsCs NPs developed in this study. Before microscopy observation, the NPs were stained with 2 wt% of phosphotungstic acid and placed on a copper grid coated with Formvar/carbon films.

2.5. In Vitro Drug Release. AsCs NPs was prepared with 2.0 mg/ml chitosan and 1 mg/ml Alphastatin in a mixture (a 2 : 1 mass ratio of chitosan to Alphastatin), and the mixture was centrifuged at 13,000 rpm for 30 min and lyophilized to obtain the powder. 2 mg AsCs NPs was precisely weighed and mixed in 10 ml PBS (pH = 7.4). The mixture was placed in a constant temperature shaker at 37°C and 200 rpm/min. At various intervals of 1 hour, 2 hours, 4 hours, 8 hours, 12 hours, 24 hours, 48 hours, 96 hours, and 144 hours, the mixture was centrifuged for 30 min (13,000 rpm), then 2 ml supernatants were collected and 2 ml fresh PBS was added to the mixture. Then, the concentrations of free Alphastatin were determined using the BCA method.

2.6. Stability Study of the AsCs NPs in Serum. 1 mg AsCs NPs (a 2 : 1 mass ratio of chitosan to Alphastatin in preparation) were precisely weighed and mixed in 5 ml DMEM medium containing 10% fetal bovine serum (FBS). Then, the mixture was placed in an incubator at 25°C or 37°C. At various intervals of 0 hours, 4 hours, 8 hours, 16 hours, and 24 hours, mixtures in different tubes were centrifuged and lyophilized and the nanoparticle size was measured.

2.7. Integrity Study of Alphastatin. 2 mg AsCs NPs were weighed, mixed in 2 ml PBS (pH = 7.4), placed at 37°C, and shaken at 200 rpm/min. After 24 hours, the mixture was centrifuged for 30 min at 13,000 rpm. The supernatant and the sediment were collected. Then, the synthetic Alphastatin, supernatant, and sediment were analyzed by Tricine-sodium dodecyl sulfate-polyacrylamide gel electrophoresis (Tricine-SDS-PAGE) using a 16.5% gel [8]. The molecular mass of samples was investigated compared with the ultra low range molecular weight marker of MW 1060–26,600 (M3546, Sigma). Peptides were stained with 0.2% Coomassie Brilliant Blue G-250 (Sigma).

2.8. Tumor Model and Treatments. The study was approved by the Ningbo University Institutional Animal Care and Use Committee (Ningbo, China). 2 mice have been

subcutaneously implanted with LA975 cells, and the tumors have grown for 2 weeks. The tumor-bearing mice were sacrificed, and the tumors were stripped and weighed. After washing twice with PBS, sterile saline was added at a mass-to-volume ratio of 1 g tumor to 4 ml saline. Then, the tumor was grounded using the syringe, and the mixture was filtered by a 200-mesh sieve to make a suspension of single cells. The cell density was diluted to 1×10^7 cells per ml. Then, each T739 mouse was subcutaneously implanted with 0.2×10^7 cells in 0.2 ml in the lower dorsal region. After 10 days of injection, 24 T739 mice were randomly divided into 4 groups with half female and half male: saline group (0.2 ml saline/day), Alphastatin group (0.25 mg/kg/day), AsCs NP group (AsCs NPs containing 0.25 mg Alphastatin for one kg weight, once a day), and Cs NP group (Cs NPs containing the same amount of chitosan as in the AsCs NP group, once a day). The reagents were all intravenously injected once daily for 14 consecutive days.

2.9. Quantification of Tumor Microvessel Density (MVD). Tumors were fixed by formalin and cut into 5 μm frozen sections. Immunohistochemistry was performed using the monoclonal antibody against Factor VIII (DAKO) specific for endothelial cells of microvessels [9] and visualized by the streptavidin–peroxidase conjugated method. MVD was assessed according to the literature previously reported [10]. Briefly, the most vascularized intratumoral area was scanned under low magnification. The number of factor VIII-positive vessels was counted in 10 randomly hot spot areas under 400x magnification. Then, the mean value was calculated from 3 images under low magnification.

2.10. Preparation of Serum Containing AsCs NPs. 20 T739 mice were randomly divided into 4 groups and administrated by intravenous injection once daily for 14 consecutive days with saline (0.2 ml saline/day), Alphastatin (0.25 mg/kg/day), AsCs NPs (AsCs NPs containing 0.25 mg Alphastatin for one kg weight), or Cs NPs (Cs NPs containing the same amount of chitosan as it in AsCs NPs group). On the last day, after 2 hours of injection, blood samples were collected by removing the eyeball from mice, immediately centrifuged at 3,000 rpm for 15 min. Then, the serums were stored at 4°C immediately.

2.11. HUVEC Tube Formation Assay. Matrigel assay was performed in a 96-well plate as described previously [11]. Briefly, 80 μl Matrigel was added into each well of the 96-well plate and incubated at 37°C for 45 min for hardening. HUVEC was trypsinized and washed by PBS. The cell density was diluted to 3×10^5 per ml using EGM2 medium. 100 μl cells were added into the Matrigel-precoated plate. Saline, 100 nM Alphastatin, AsCs NPs containing 100 nM Alphastatin, and Cs NPs containing the same amount of chitosan were added to individual wells. For the serum sample test, different serums were diluted to 20% final concentration. Then, the plate was incubated at 37°C for 24 hours. Images of the HUVEC tube-like structure were then captured under a digital microscope, and the mean tube length was calculated.

2.12. Western Blot Assay. HUVEC was trypsinized, washed by PBS, and diluted to 3×10^5 per ml using EGM2 medium. 100 μl cells were added into each well of the 96-well plate. After overnight incubation, the medium was replaced with EGM2 containing saline, 100 nM Alphastatin, AsCs NPs containing 100 nM Alphastatin, or Cs NPs containing the same amount of chitosan. Then, the plate was incubated at 37°C for 24 hours. The protein was extracted using ice-clod RIPA lysis buffer. 20 μg proteins were kept 5 min in boiling water, separated by gel electrophoresis, and then transferred to polyvinylidene fluoride (PVDF) membranes. After blocking, PVDF membranes were incubated with primary antibody, anti-SphK1 (1 : 500, Santa Cruz Biotechnology), and anti-β-actin (1 : 1000) at 4°C overnight. Furthermore, the membranes were washed and incubated with HRP-conjugated secondary antibodies (1 : 10,000) at room temperature for 2 hours. Then the bands were visualized using ECL chemiluminescence reagents (Pierce, USA) and quantified using Image-Pro Analysis software.

2.13. Hemolysis Assay. The heparinized blood was drawn from healthy mice and centrifuged at 1000 rpm for 5 min to collect the packed red blood cells (RBC). The RBC was washed three times with isotonic saline buffer with pH 7.4 before diluting to prepare 2% erythrocyte dispersion. Hemolysis assay was studied by adding 500 μl RBC to the equal volume of CS and AsCs NPs in isotonic saline buffer to get a final concentration of 0.1 mg/ml, 0.05 mg/ml, and 0.025 mg/ml of polymer. The distilled water (100% hemolysis) and isotonic saline buffer (0% hemolysis) were employed as the positive and negative control, respectively. After incubation for 2 hours at 37°C, the mixtures were centrifuged at 1,000 rpm for 5 min. The obtained supernatant determined the absorbance at 545 nm. The hemolysis ratio (HR%) was calculated according to $\text{HR\%} = 100\% \times (\text{OD}_{\text{Sample}} - \text{OD}_{\text{negative}}) \div (\text{OD}_{\text{positive}} - \text{OD}_{\text{negative}})$.

2.14. Statistical Analysis. Quantitative data were expressed as mean ± SD. All analyses were performed by using Prism software (GraphPad 5.0). The statistical differences were determined by Student's t-test or one-way ANOVA, with $P < 0.05$ considered statistically significant.

3. Results and Discussion

3.1. The Effect of the CS/Alphastatin Ratio on EE%. In order to prepare chitosan nanoparticle-loaded adequate amounts of Alphastatin, we used EE% as a detection index and focused on investigation of the effect of the mass ratio of chitosan and Alphastatin to EE%. As shown in Figure 1, we found a significant EE% increase along with the increase in the mass ratio of chitosan to Alphastatin. When the chitosan concentration was 1.0 mg/ml and the CS/Alphastatin ratio was 8 : 1, EE% of chitosan to Alphastatin could increase to 40.2%. When the chitosan concentration was 2.0 mg/ml and the CS/Alphastatin ratio was 8 : 1, EE% could increase to 51.2%. Furthermore, when the CS/Alphastatin ratio was greater than 1 : 1.5, EE% from the 2.0 mg/ml chitosan concentration was always higher than EE% from the 1.0 mg/ml chitosan concentration, although both EE% decreased dramatically when the ratio

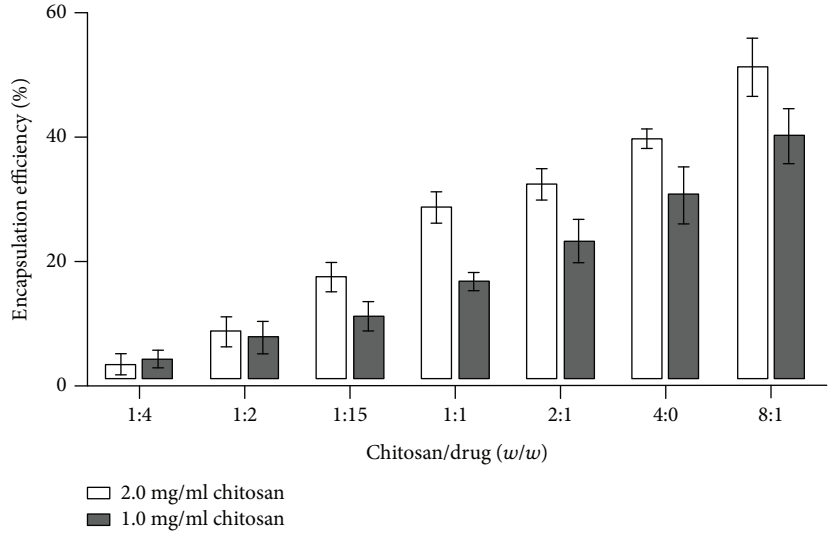

Figure 1: Effect of the mass ratio of chitosan to Alphastatin on Alphastatin encapsulation efficiency (%).

Table 1: Effect of the mass ratio of chitosan to Alphastatin on nanoparticle size and zeta potential. Chitosan concentration is 2 mg/ml.

	Mass ratio of chitosan to Alphastatin						
	1 : 4	1 : 2	1 : 1.5	1 : 1	2 : 1	4 : 1	8 : 1
Size (nm)	544.5 ± 16.5	526.8 ± 11.3	488.6 ± 12.9	412.9 ± 15.1	387.4 ± 12.5	334.2 ± 17.4	322.8 ± 21.6
Zeta potential (mV)	+13.6 ± 0.7	+17.6 ± 0.6	+23.1 ± 0.7	+26.8 ± 0.5	+28.1 ± 0.7	+27.4 ± 0.8	+27.6 ± 1.2

was less than 1 : 1. This result indicated that the increase in chitosan concentration could increase the encapsulation efficiency. Consistent with our results, Xu and Du [12] have reported that EE% was highly increased by an increase in the chitosan to BSA concentration, when BSA was used as a model protein. However, there are also contrary reports that show that the increase in chitosan to BSA concentration resulted in EE% decrease [13]. One possible reason is that the increase in chitosan concentration might lead to the increase in the viscosity of chitosan mixture and cause the failure of the combination of protein to chitosan [14]. Furthermore, some studies report that when the chitosan initial concentration is less than 4 mg/ml, EE% increases along with the increase in chitosan to protein concentration, whereas when the chitosan concentration is more than 4 mg/ml, EE% would decrease [15]. Based on previous reports and our own results, we choose 2 mg/ml as the chitosan concentration. In addition, since Alphastatin will be relatively less as the increased ratio of CS/Alphastatin, 1 mg/ml was chosen as Alphastatin concentration (CS/Aphastatin ratio = 2 : 1).

3.2. The Effect of the CS/Alphastatin Ratio on Characteristics. The average particle size and zeta potential of Cs NPs were 305.1 ± 13.8 nm and +26.5 ± 1.1 mV, respectively. When Alphastatin was loaded, the particle size of AsCs NPs increased when the chitosan concentration was 2 mg/ml. Table 1 shows the effect of different mass ratios of chitosan to Alphastatin on particle size at pH 5. The particle size increased with the decrease of the ratio. This indicated that Alphastatin played a part in the ionic cross-linking. In a strict

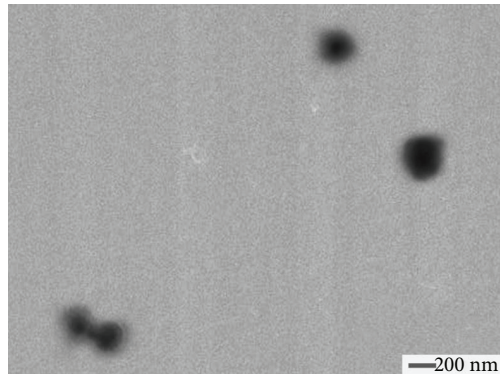

Figure 2: The transmission electron micrographs of AsCs NPs at the mass ratio of chitosan to Alphastatin on 2 : 1.

definition, the particle size of the nanomaterial should be between 1 and 100 nm [16], but the diameter of the nanoparticles made by polymer material may be larger than 100 nm, ranging from 10 to 500 nm, and cannot exceed 1000 nm [17]. In this study, AsCs NPs at the mass ratio of 2 : 1 were still nanoparticles since their average particle size was 387.4 ± 12.5 nm. There is little effect on zeta potential with the increase of the mass ratio from 1 : 1 to 8 : 1, and the AsCs NPs displayed a positive zeta potential in the range of +26 to +28 mV (Table 1). However, at the mass ratio from 1 : 1.5 to 1 : 4, the zeta potential decreased from +23.1 ± 0.7 mV to +13.6 ± 0.7 mV with the decrease of the ratio although they were still the positive zeta potential, which indicated that the negative charge of Alphastatin interacted with the

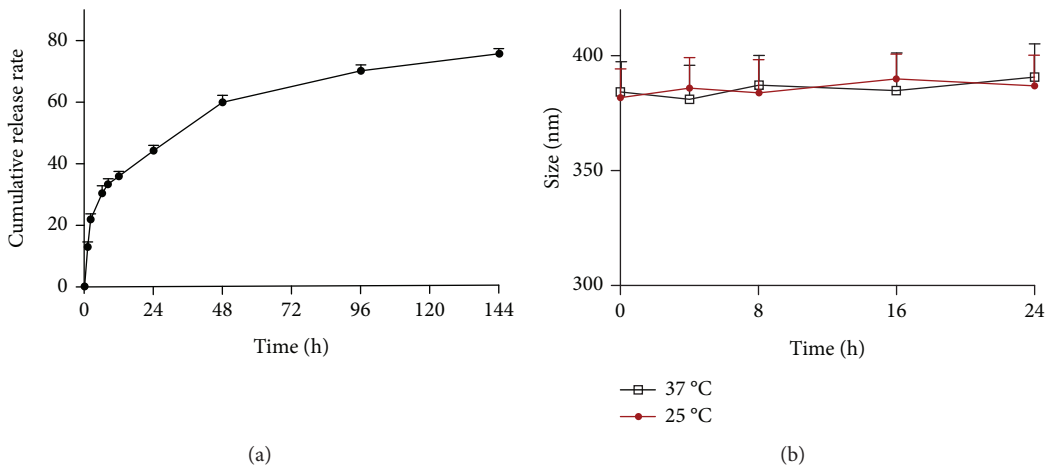

Figure 3: *In vitro* drug release characteristics of AsCs NPs. (a) Cumulative release of AsCs NPs in PBS (pH = 7.4). (b) 24-hour stability study of AsCs NPs in 10% FBS.

positive charge of chitosan via ionic cross-linking. In addition, at the specified mass ratio of 2 : 1, the zeta potential of AsCs NPs was +28.1 ± 0.7 mV (Table 1), and the polydispersity index was 0.223 ± 0.06. And Figure 2 presents the TEM morphology of the AsCs NPs and confirmed the spherical shape. These particles had a small size range of around 270–420 nm in diameter, which was consistent with the result from the particle size analyzer.

3.3. Release and Protection to Alphastatin by AsCs NPs In Vitro. As shown in Figure 3(a), the cumulative release (%) of Alphastatin was from 13.1% to 76.2%. At the first 6 hours, 30.5% Alphastatin was released, and at 12 hours, the cumulative release reached 35.9%, whereas 44.3% Alphastatin was released at 24 hours. This indicated a rapid initial burst release in AsCs NPs. The release decreased to a slower rate at some later stages since 24 hours, with a cumulative release of 60.1% at 48 hours and 70.5% at 96 hours. Then, AsCs NPs were released continuously for 6 days. Because FBS contains a variety of proteases, AsCs NPs were incubated in DMEM containing 10% FBS at 25 and 37°C, respectively. After 24 hours of incubation, it was observed that there was no obvious flocculus or any precipitates in any mixture. The average particle size of nanoparticles in each mixture decreased little at any intervals within 24 hours, which proved that AsCs NPs could be stably present in a liquid system with various proteases (Figure 3(b)). The integrity of encapsulated Alphastatin and released Alphastatin at 24 hours of release was analyzed by Tris-Tricine-SDS-PAGE (Figure 4). The electrophoresis revealed only a single band in the range of 1.0-3.0 kDa for every sample. The band positions were consistent of all samples indicating the integrity of encapsulated Alphastatin and released Alphastatin. The existence form of the drug in chitosan nanoparticles has been discussed in the previous study [18], including simple adsorption on the surface of nanoparticles, and wrapped in the interior of the nanoparticles. Since a small amount of Alphastatin was simply adsorbed on the surface of the nanoparticles, this led to the occurrence of the burst release in the first 12 hours in

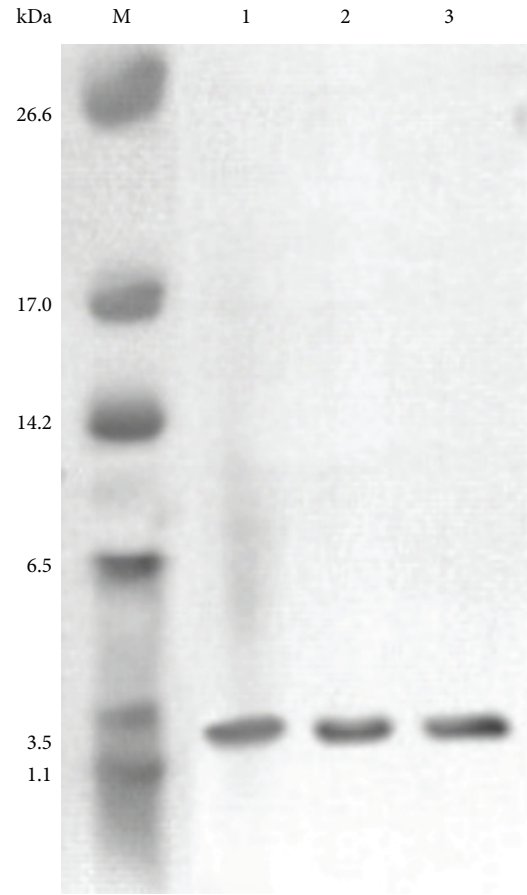

Figure 4: Analysis of Alphastatin integrity by Tricine-SDS-PAGE. M: molecular mass (1060–26,600 Da); 1: AsCs NPs precipitate after a 24-hour release in PBS (pH = 7.4); 2: the supernatant after a 24-hour release of AsCs NPs; 3: the synthetic Alphastatin.

Figure 3(a). Subsequently, Alphastatin inside AsCs NPs was stably released by diffusion through the pores of nanoparticles, and on day 6, 76.2% Alphastatin was released. In a further study, it was observed that after 24 hours of release, both the Alphastatin encapsulated in AsCs NPs and the

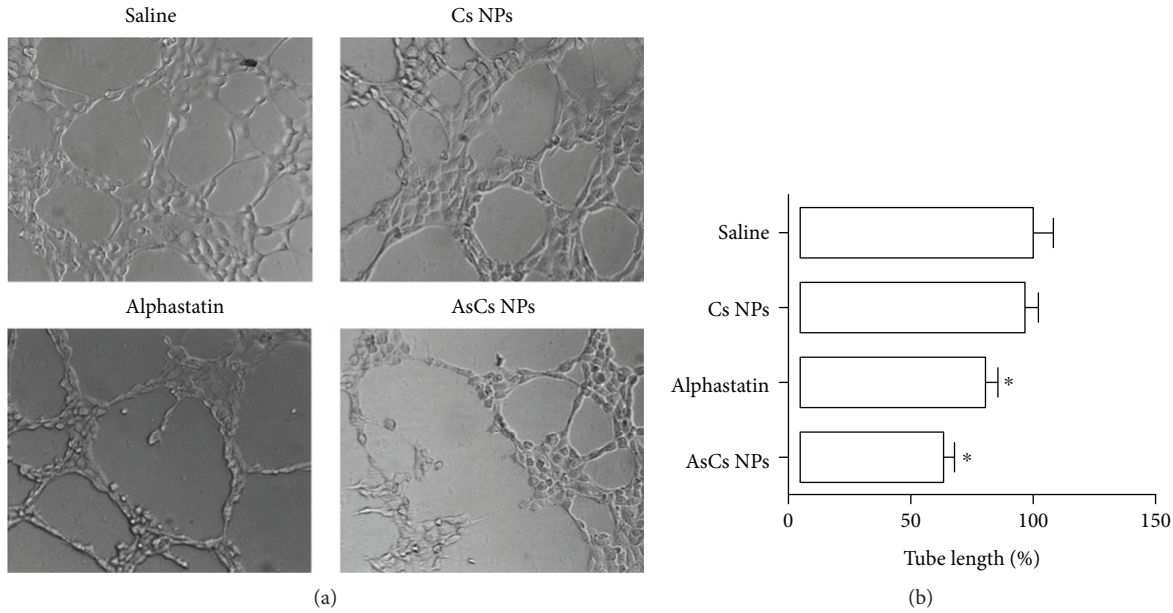

Figure 5: Impact of AsCs NPs on tube formation. (a) Representative images showing HUVEC tube formation under different nanoparticles at 100x magnification. (b) Tube length index. $^{*}P < 0.05$ versus saline control.

released Alphastatin preserved the same molecular mass, indicating the integrity of Alphastatin. For *in vivo* study, the complexity of the circulation system and humoral immune system can affect the stability of nanoparticles. In order to observe whether chitosan could play a basic role in the protection of Alphastatin, FBS was used as a substitute to simulate various proteases [19]. We found that AsCs NPs were stable in the system containing 10% FBS at least 24 hours, suggesting that AsCs NPs may be suitable for *in vivo* administration. Overall, the sustained release and Alphastatin integrity, as well as the stability in serum of AsCs NPs, made the *in vivo* administration possible.

3.4. Inhibition to the Tumor Growth and Angiogenesis In Vivo and In Vitro. It has been reported that Alphastatin inhibits tumor growth mainly by inhibiting the formation of neovasculars in tumors. In order to verify whether AsCs NPs still retained the ability to inhibit tumor growth and angiogenesis, HUVECs and LA975 tumor-bearing mice were used to observe the antiangiogenic effect of AsCs NPs *in vivo* and *in vitro*. As shown in Figure 5(a), in the HUVEC tube formation assay, tubular structures reduced significantly by Alphastatin and AsCs NPs, compared with the saline group. Quantitative analysis (Figure 5(b)) indicated that the tube length was significantly reduced by Alphastatin and AsCs NPs. For the *in vivo* effect of AsCs NPs, we observed that tumor developed in all mice and there was no death in each group. In the saline-treated group (control group), mice moved gradually slowly with tumor growth and presented lack of energy, loss of appetite, and hair loss, whereas mice treated with Alphastatin and AsCs NPs exhibited a better status and did not show the manifestations above. After 14 days of treatment, the tumor weight in all intervention groups was lower than that in the saline-treated group (Figure 6), and the inhibition to tumor growth by AsCs NPs was the strongest

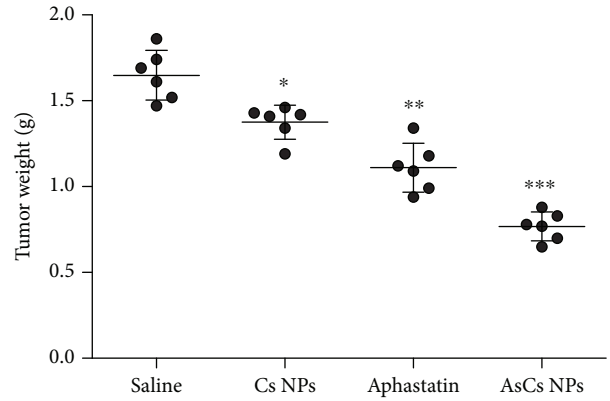

Figure 6: Effects of AsCs NPs on tumor weights from LA975 tumor-bearing mice. $^{*}P < 0.05$, $^{**}P < 0.01$, and $^{***}P < 0.001$ versus saline group.

($P < 0.001$). MVD inside the tumor was further detected. As shown in Figure 7(a), compared with the saline-treated group, the MVD of the AsCs NP ($P < 0.001$) or Alphastatin ($P < 0.05$) group was much lower, and the MVD of the AsCs NP group decreased most obviously. In addition, Figure 7(b) shows that HUVEC tube formation was inhibited by serums containing AsCs NPs ($P < 0.001$) or Alphastatin ($P < 0.05$) after a 2-hour injection, and the serum containing AsCs NPs presented stronger inhibition than did serum containing Alphastatin ($P < 0.001$). In contrast, the serum containing chitosan showed no significant difference in comparison with the blank serum control. It indicated that the increased inhibition by serum containing AsCs NPs could be attributed to the protection of chitosan to Alphastatin. This result is similar to the previous studies [2, 20, 21], indicating that Alphastatin from AsCs NPs could exert the inhibitive ability to angiogenesis both *in vivo* and *in vitro*. Chitosan could inhibit

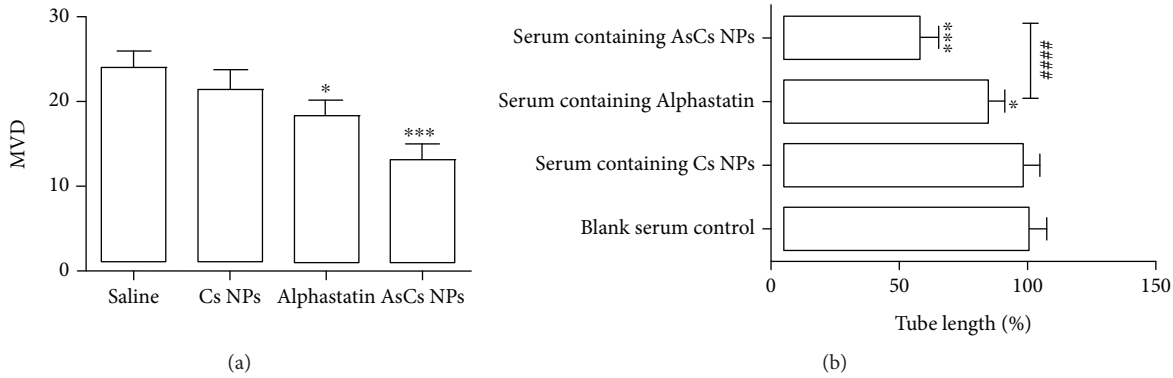

Figure 7: The inhibitory effect on angiogenesis by different nanoparticles. (a) Microvessel density expression in tumor from LA975 tumor-bearing mice treated with different nanoparticles. $^{*}P < 0.05$ and $^{***}P < 0.001$ versus saline group. (b) The inhibitory effect of mouse serums containing drugs against HUVEC tube formation. $^{*}P < 0.05$ and $^{***}P < 0.001$ versus blank serum control, $^{\#\#\#}P < 0.001$ versus serums containing Alphastatin.

tumor growth by directly killing and inducing apoptosis of tumor cells or by an indirect effect through improvement of the immune system of the animal model [22, 23]. Therefore, chitosan inhibited tumor weight ($P < 0.05$) in Figure 6, whereas the inhibition to angiogenesis in tumor and HUVECs by chitosan was not statistically different in Figures 5 and 7. It could be explained that the inhibition to tumor growth by chitosan might be by way of other mechanisms except angiogenesis inhibition. Alphastatin has the ability to inhibit tumor angiogenesis and tumor growth. As shown in Figures 5–7, both tumor weights and MVD levels in Alphastatin and AsCs NP groups were significantly lower than those in the saline group. Since Alphastatin has common disadvantages of peptide and protein drugs, such as degradation by proteolytic enzymes, a short half-life, and disability retaining effective concentration in the tumor for a relative long time, it is necessary to develop a protective system from these disadvantages. Compared with the Alphastatin group, both tumor weight and MVD level in the AsCs NP group were much lower, indicating that chitosan could protect Alphastatin from biodegradation and prolong its effect *in vivo*, which might be contributed by the restrained release and relative stability of AsCs NPs in the circulating system. In addition, chitosan nanoparticles allow the permeation and accumulation in certain tumors through the hyperpermeable vasculature existing in solid tumors, and cannot be easily cleared away due to the absence of the tumor's lymphatic drainage, so that Alphastatin might be remained at the tumor site with possible high concentration. This also contributed to the strongest inhibition to tumor weight and MVD by AsCs NPs.

3.5. SphK1 Inhibition by AsCs NPs. As shown in Figure 8, compared to the saline group, western blot analysis showed that chitosan did not affect the expression level of SphK1, whereas AsCs NPs and Alphastatin downregulated the expression levels of SphK1 in HUVECs. Notably, AsCs NPs presented more potent inhibition than Alphastatin, indicating that the protective and sustained release of chitosan on Alphastatin and the nanoparticles prolonged the function of Alphastatin. Alphastatin inhibits angiogenesis by inhibiting JNK and ERK kinase activation pathways [24] and the S1P-Akt pathway [20, 21, 25], whereas there was no detectable effect on vessels in normal tissues such as the liver, lungs, and kidney [2, 26]. SphK1 phosphorylates sphingosine (Sp) to produce S1P, a key enzyme responsible for the formation of sphingosine-1-phosphate (S1P) [27]. S1P binds to G protein-coupled receptors (GPCRs) on endothelial cell membranes, especially endothelial differentiation gene 1 (EDG-1) which is a member of the S1P receptor family and is essential for vascular maturation. S1P-binded EDG-1 stimulates the synthesis of DNA in vascular endothelial cells and induces vascular endothelial cell migration [28]. The migration of vascular endothelial cells stimulated by SIP was even stronger than that stimulated by basic fibroblast growth factor (bFGF) and vascular endothelial growth factor (VEGF). Moreover, S1P can significantly promote the formation of tubular structures made by endothelial cells and participate in many other important processes of angiogenesis [29]. Thus, the decrease in S1P production will reduce the migration of vascular endothelial cells and the formation of tubular structures. SphK1 is the most important enzyme for S1P synthesis and present positive stimulation to S1P production. AsCs NPs exhibited an inhibitory effect on SphK1, which in turn might inhibit the S1P level. It might be a possible mechanism of inhibitive angiogenesis by AsCs NPs.

3.6. Preliminary Safety Evaluation of AsCs NPs. The blood compatibility of AsCs NPs was evaluated by the hemolysis analysis (Figure 9). The hemolytic effects of both Cs NPs and AsCs NPs were lower than 5% within the range of 0.025–0.1 mg/ml. Because the <5% hemolysis percentage is considered as a safe level [30], the hemolysis results demonstrated that Cs NPs and AsCs NPs had good hemocompatibility and were suitable for intravenous administration.

4. Conclusion

In this study, a chitosan nanoparticle loaded with Alphastatin was prepared with optimization of the mass ratio of chitosan to Alphastatin. Then, the nanoparticle's characteristics were determined. Because of the characteristics

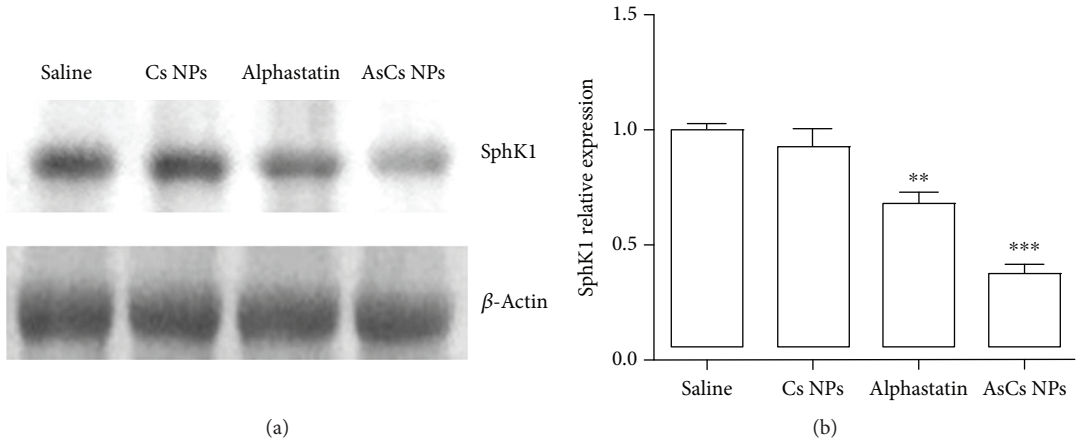

Figure 8: The downregulated SphK1 expression by AsCs NPs was detected by western blotting assay. (a) Representative images of SphK1. (b) The bar graphs show quantified levels of SphK1. $^{**}P < 0.01$ and $^{***}P < 0.001$ versus saline control.

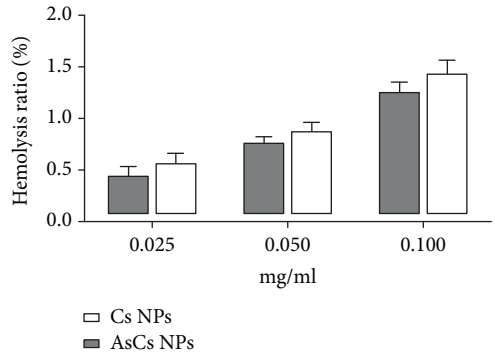

Figure 9: *In vitro* hemolysis assay of AsCs NPs. Hemolysis ratio of polymers at different concentrations.

including the restrained release, the stability in 10% FBS, and the remaining activity in serum-containing drugs, these nanoparticles present considerable antiangiogenic effects *in vivo* and *in vitro*. Additionally, the nanoparticles also present good hemocompatibility. Overall, chitosan could be used as a delivery carrier to strengthen the antitumor effect of Alphastatin.

Data Availability

All raw data used and analyzed during the current study can be available from the corresponding author on reasonable request.

Conflicts of Interest

The authors have no conflicts of interest regarding the publication of this paper.

References

[1] S. Sun and J. H. Schiller, "Angiogenesis inhibitors in the treatment of lung cancer," *Critical Reviews in Oncology/Hematology*, vol. 62, no. 2, pp. 93–104, 2007.

[2] C. A. Staton, N. J. Brown, G. R. Rodgers et al., "Alphastatin, a 24–amino acid fragment of human fibrinogen, is a potent new inhibitor of activated endothelial cells in vitro and in vivo," *Blood*, vol. 103, no. 2, pp. 601–606, 2004.

[3] C. A. Bootle-Wilbraham, S. Tazzyman, J. M. Marshall, and C. E. Lewis, "Fibrinogen E-fragment inhibits the mi-gration and tubule formation of human dermal microvascular endothelial cells in vitro," *Cancer Research*, vol. 60, no. 17, pp. 4719–4724, 2000.

[4] H. Che, J. Song, S. Guo, W. Wang, and G. Gao, "Inhibition of xenograft human glioma tumor growth by lentivirus-mediated gene transfer of alphastatin," *Oncology Reports*, vol. 29, no. 3, pp. 1101–1107, 2013.

[5] S. W. Guo, H. M. Che, and W. Z. Li, "Construction of recombinant lentivirus vector for tumor vasoinhibitory peptide alphastatin gene delivery," *Molecular Medicine Reports*, vol. 3, no. 6, pp. 923–928, 2010.

[6] K. C. Carter and M. Puig-Sellart, "Nanocarriers made from non-ionic surfactants or natural polymers for pulmonary drug delivery," *Current Pharmaceutical Design*, vol. 22, no. 22, pp. 3324–3331, 2016.

[7] M. Amidi, E. Mastrobattista, W. Jiskoot, and W. E. Hennink, "Chitosan-based delivery systems for protein therapeutics and antigens," *Advanced Drug Delivery Reviews*, vol. 62, no. 1, pp. 59–82, 2010.

[8] H. Schägger and G. von Jagow, "Tricine-sodium dodecyl sulfate-polyacrylamide gel electrophoresis for the separation of proteins in the range from 1 to 100 kDa," *Analytical Biochemistry*, vol. 166, no. 2, pp. 368–379, 1987.

[9] E. Jusufović, M. Rijavec, D. Keser et al., "let-7b and miR-126 are down-regulated in tumor tissue and correlate with microvessel density and survival outcomes in non–small–cell lung cancer," *PLoS One*, vol. 7, no. 9, article e45577, 2012.

[10] M. A. Mohammed, J. T. M. Syeda, K. M. Wasan, and E. K. Wasan, "An overview of chitosan nanoparticles and its application in non-parenteral drug delivery," *Pharmaceutics*, vol. 9, no. 4, 2017.

[11] N. Shen, R. Zhang, H. R. Zhang et al., "Inhibition of retinal angiogenesis by gold nanoparticles via inducing autophagy," *International Journal of Ophthalmology*, vol. 11, no. 8, pp. 1269–1276, 2018.

[12] Y. Xu and Y. Du, "Effect of molecular structure of chitosan on protein delivery properties of chitosan nanoparticles," *International Journal of Pharmaceutics*, vol. 250, no. 1, pp. 215–226, 2003.

[13] W. Yang, J. Fu, T. Wang, and N. He, "Chitosan/sodium tripolyphosphate nanoparticles: preparation, characterization and application as drug carrier," *Journal of Biomedical Nanotechnology*, vol. 5, no. 5, pp. 591–595, 2009.

[14] Q. Gan and T. Wang, "Chitosan nanoparticle as protein delivery carrier—systematic examination of fabrication conditions for efficient loading and release," *Colloids and Surfaces B: Biointerfaces*, vol. 59, no. 1, pp. 24–34, 2007.

[15] Z. Liu, Y. Jiao, F. Liu, and Z. Zhang, "Heparin/chitosan nanoparticle carriers prepared by polyelectrolyte complexation," *Journal of Biomedical Materials Research Part A*, vol. 83A, no. 3, pp. 806–812, 2007.

[16] The European Commission, "Commission recommendation of 18 October 2011 on the definition of nanomaterial (2011/696/EU)," *Official Journal of the European Union*, vol. L, no. 275, pp. 38–40, 2011.

[17] R. L. Heise, B. Adam Blakeney, and R. A. Pouliot, "Polymers in tissue engineering," in *Advanced Polymers in Medicine*, F. Puoci, Ed., Springer, Cham, Switzerland, 2015.

[18] S. A. Agnihotri, N. N. Mallikarjuna, and T. M. Aminabhavi, "Recent advances on chitosan-based micro- and nanoparticles in drug delivery," *Journal of Controlled Release*, vol. 100, no. 1, pp. 5–28, 2004.

[19] B. Shahbazi, M. Taghipour, H. Rahmani, K. Sadrjavadi, and A. Fattahi, "Preparation and characterization of silk fibroin/oligochitosan nanoparticles for siRNA delivery," *Colloids and Surfaces B: Biointerfaces*, vol. 136, pp. 867–877, 2015.

[20] T. Li and L. Chen, "Alphastatin inhibits tumor angiogenesis in nude mice bearing human gastric cancer xenografts," *Zhonghua Wei Chang Wai Ke Za Zhi*, vol. 12, no. 1, pp. 61–64, 2009.

[21] L. Chen, T. Li, R. Li, B. Wei, and Z. Peng, "Alphastatin downregulates vascular endothelial cells sphingosine kinase activity and suppresses tumor growth in nude mice bearing human gastric cancer xenografts," *World Journal of Gastroenterology*, vol. 12, no. 26, pp. 4130–4136, 2006.

[22] B. B. Aam, E. B. Heggset, A. L. Norberg, M. Sørlie, K. M. Vårum, and V. G. H. Eijsink, "Production of chitooligosaccharides and their potential applications in medicine," *Marine Drugs*, vol. 8, no. 5, pp. 1482–1517, 2010.

[23] H. T. Ta, C. R. Dass, and D. E. Dunstan, "Injectable chitosan hydrogels for localised cancer therapy," *Journal of Controlled Release*, vol. 126, no. 3, pp. 205–216, 2008.

[24] S. W. Guo, H. M. Che, and W. Z. Li, "Anti-tumor effect of lentivirus-mediated gene transfer of alphastatin on human glioma," *Cancer Science*, vol. 102, no. 5, pp. 1038–1044, 2011.

[25] L. Chen, T. Li, R. Li et al., "Inhibition of alphastatin on angiogenesis in human endothelial cells and the mechanism thereof: an experimental study," *Zhonghua Yi Xue Za Zhi*, vol. 86, no. 15, pp. 1061–1064, 2006.

[26] C. A. Staton, S. M. Stribbling, C. García-Echeverría et al., "Identification of key residues involved in mediating the in vivo anti-tumor/anti-endothelial activity of Alphastatin," *Journal of Thrombosis and Haemostasis*, vol. 5, no. 4, pp. 846–854, 2007.

[27] D. Hatoum, N. Haddadi, Y. Lin, N. T. Nassif, and E. M. McGowan, "Mammalian sphingosine kinase (SphK) isoenzymes and isoform expression: challenges for SphK as an oncotarget," *Oncotarget*, vol. 8, no. 22, pp. 36898–36929, 2017.

[28] Y. Takuwa, H. Okamoto, N. Takuwa, K. Gonda, N. Sugimoto, and S. Sakurada, "Subtype-specific, differential activities of the *EDG* family receptors for sphingosine-1-phosphate, a novel lysophospholipid mediator," *Molecular and Cellular Endocrinology*, vol. 177, no. 1-2, pp. 3–11, 2001.

[29] O. H. Lee, Y. M. Kim, Y. M. Lee et al., "Sphingosine 1-phosphate induces angiogenesis: its angiogenic action and signaling mechanism in human umbilical vein endothelial cells," *Biochemical and Biophysical Research Communications*, vol. 264, no. 3, pp. 743–750, 1999.

[30] Y. Xiao, Y. Liu, S. Yang et al., "Sorafenib and gadolinium co-loaded liposomes for drug delivery and MRI-guided HCC treatment," *Colloids and Surfaces B: Biointerfaces*, vol. 141, pp. 83–92, 2016.

Hindawi
International Journal of Polymer Science
Volume 2019, Article ID 1914976, 6 pages
https://doi.org/10.1155/2019/1914976

Research Article

Chitosan-Based Nanogel Enhances Chemotherapeutic Efficacy of 10-Hydroxycamptothecin against Human Breast Cancer Cells

Hui Guo, Faping Li, Heping Qiu, Qi Zheng, Chao Yang, Chao Tang, and Yuchuan Hou

Department of Urinary Surgery, The First Hospital of Jilin University, Changchun 130021, China

Correspondence should be addressed to Yuchuan Hou; hou63@163.com

Received 1 September 2018; Revised 15 October 2018; Accepted 6 February 2019; Published 4 April 2019

Guest Editor: Bingyang Shi

Chitosan (CS), the second most abundant polysaccharide in nature, has been widely developed as a nanoscopic drug delivery vehicle due to its intriguing characteristics. In this work, a positively charged CS-based nanogel was designed and synthesized to inhibit the proliferation of breast cancer cell lines. The model drug of 10-hydroxycamptothecin (HCPT) was entrapped into the core *via* a facile diffusion to form CS/HCPT. The characteristics of CS/HCPT were evaluated by assessing particle size, drug loading content, and drug loading efficiency. Furthermore, cell internalization, cytotoxicity, and apoptosis of CS/HCPT were also investigated *in vitro*. The present investigation indicated that the positively charged CS-based nanogel could be potentially used as a promising drug delivery system.

1. Introduction

Breast cancer is well known to be the most common malignant disease in women worldwide and is the second leading cause of death among US women [1]. The main subtypes of breast cancer are identified based on the expression of hormone receptors (HR), namely, estrogen receptor (ER), progesterone receptor (PR), and human epidermal growth factor receptor 2 (HER2) [2]. HR-positive breast cancer is one of the most common subtypes, which accounts for approximately 70–75% of all cases [3]. The prognosis of HR-positive breast cancer is better than that of HR-negative breast cancer [4]. Breast cancer is becoming a considerable public health problem because of its high morbidity and mortality. There are a variety of available treatment methods for breast cancer, including surgery, radiotherapy, chemotherapy, and hormone therapy [5]. It is proven that surgery is an efficient treatment for primary breast cancer. However, cancer cells may spread to distant sites in the body before the primary lesion is found and resected [6]. Chemotherapy, as a supplement to surgery, has become standard of treatment for locally advanced or poor-prognosis early-stage disease. Furthermore, neoadjuvant chemotherapy has been increasingly administered to reduce the size of primary tumor [7]. Although chemotherapy plays an important role in clinical application, it is still hindered by several unfavourable factors, such as rapid systemic elimination, low water solubility, and severe systemic toxicity [8].

To overcome these disadvantages, nanotechnology has been developed over the past few decades and offers promising perspectives for improving the therapeutic potency of chemotherapy [9]. Chitosan (CS), a biopolymer derived from chitin, is known as the second most abundant polysaccharide in nature [10]. CS has been widely developed as a nanoscopic drug delivery vehicle due to its intriguing characteristics, such as biocompatibility, biodegradability, antibacterial, nontoxicity, and low cost [11–13]. In addition to these advantages, the existence of primary amino (NH_2) and hydroxyl (OH) groups in the CS chain facilitates its surface engineering chemical reactions [14].

On the basis of these considerations, a positively charged CS-based nanogel was designed and synthesized as a drug delivery system to inhibit the proliferation of breast cancer cell lines. The model drug of 10-hydroxycamptothecin (HCPT) is a derivative of camptothecin (CPT) [15]. HCPT is an inhibitor of topoisomerase I, which can effectively inhibit DNA replication and RNA transcription in breast cancer cells [16, 17]. HCPT was entrapped into the CS *via* a

facile diffusion to form CS/HCPT. The characteristics of CS/HCPT were evaluated by assessing the particle size, drug loading content, and drug loading efficiency. Furthermore, cell internalization, cytotoxicity, and apoptosis of CS/HCPT were also investigated *in vitro*.

2. Experimental

2.1. Materials. 10-Hydroxycamptothecin (HCPT) was supplied by Beijing Huafeng United Technology Co. Ltd. (Beijing, China). Chitosan (CS) was obtained from Zhejiang Golden Shell Pharmaceutical Co. Ltd. (Zhejiang, China) and used as received. Clear polystyrene tissue culture-treated 96-well and 6-well plates were purchased from Corning Costar Co. (Cambridge, MA, USA). Culture medium fetal bovine serum (FBS) and Dulbecco's modified Eagle's medium (DMEM) were supplied by Gibco (Grand Island, NY, USA). Trypsin, penicillin, streptomycin, and methyl thiazolyl tetrazolium (MTT) were purchased from Sigma-Aldrich (Shanghai, China). Propidium iodide (PI) and Annexin V-FITC were purchased from Beijing Dingguo Changsheng Biotechnology Co. Ltd. (Beijing, China). Acetic acid was purchased from Sinopharm Chemical Reagent Co. Ltd. (Shanghai, China). Dimethylformamide (DMF) was sourced from Sigma-Aldrich (Shanghai, China) and dried over calcium hydride (CaH_2) at room temperature before vacuum distillation. The purified deionized water was prepared by the Milli-Q plus system (Millipore Co., Billerica, MA, USA).

2.2. Preparation of the HCPT-Loaded Nanogel. The CS/HCPT was prepared through a facile diffusion and dialysis method as described previously [18]. Briefly, CS (50.0 mg) was dissolved in 20.0 mL of acetic acid solution (pH 3.0), and HCPT (25.0 mg) was dissolved in 20.0 mL of DMF by vortex and sonication. Then, 20.0 mL of HCPT solution was dropped slowly into the CS solution while stirring. The mixed solution was then stirred at 30 rpm for 12 h at room temperature and then dialyzed against deionized water for 24 h. The dialysis medium was refreshed five times to completely remove the free HCPT and DMF. The whole procedure was performed in darkness. Finally, the solution was filtered and followed by lyophilization to obtain CS/HCPT.

2.3. Determination of Drug Loading Content and Drug Loading Efficiency. The drug loading content (DLC) and drug loading efficiency (DLE) were calculated as described in our previous work with slight modification [19]. In short, the freeze-dried CS/HCPT was accurately weighed and dissolved in acetic acid solution (pH 3.0). In CS/HCPT, the content of HCPT was then assayed by ultraviolet-visible (UV-vis) spectrophotometry at 365 nm. The standard curve method was used. The DLC and DLE of CS/HCPT were calculated according to equations (1) and (2), respectively.

$$\text{DLC}(\%) = \frac{\text{Amount of drug in nanogel}}{\text{Amount of loading nanogel}} \times 100\%. \quad (1)$$

$$\text{DLE}(\%) = \frac{\text{Amount of drug in nanogel}}{\text{Total amount of feeding drug}} \times 100\%. \quad (2)$$

2.4. Particle Size and Zeta Potential Measurements. The hydrodynamic radius (R_h) of CS/HCPT was measured by dynamic light scattering (DLS) measurements in a WyattQELS instrument with a vertically polarized He–Ne laser (DAWN EOS, Wyatt Technology Co., Santa Barbara, CA, USA). The scattering angle was fixed at 90°. The samples were prepared in aqueous solution at a concentration of 100.0 μg mL^{-1}. Before measurements, the solution was filtered through a 0.45 μm Millipore filter. The zeta potential of CS/HCPT was determined by a Zeta Potential/BI-90Plus Particle Size Analyzer (Brookhaven, USA). The sample was adjusted to a concentration of 100.0 μg mL^{-1} in aqueous solution as recommended. Both the particle size and zeta potential measurements were performed in triplicate, and the results were presented as means values ± standard deviation (SD).

2.5. Cell Uptake and Intracellular Drug Release. The cell uptake and intracellular HCPT release behavior of CS/HCPT by 4T1 cells were detected by confocal laser scanning microscopy (CLSM). Simply, 4T1 cells were suspended at a density of 0.8×10^5 cells mL^{-1} and taken 2.0 mL into a 6-well plate and incubated at 37°C in 5% (V/V) carbon dioxide (CO_2) atmosphere. After 24 h of incubation, the culture medium was replaced with free HCPT or CS/HCPT at a certain HCPT concentration of 1.25 μg mL^{-1}. The untreated cells incubated with phosphate-buffered saline (PBS) were used as a control. The cells were incubated for 2 h or 6 h and then rinsed with PBS for three times. The obtained cells were fixed with 4% paraformaldehyde for 15 min at room temperature. The cells were washed repeatedly with PBS. The cell uptake and intracellular drug release behavior of CS/HCPT were observed by CLSM.

2.6. In Vitro Cytotoxicity Assay. *In vitro* cytotoxicity of CS/HCPT, including free HCPT, was evaluated in 4T1 cells by a standard MTT assay. Briefly, 1.0×10^4 viable cells dispersed in 200.0 μL DMEM medium were seeded in 96-well plates and incubated overnight at 37°C. After that, the prepared free HCPT and CS/HCPT solution were added in cells and incubated for 48 h or 72 h. The concentrations of HCPT were ranged from 0 to 20.0 μg mL^{-1}. At predetermined time intervals, 20.0 μL of MTT solution was added to each well and the 96-well plates were incubated at 37°C for approximately 4 h. The obtained MTT products were measured with a Bio-Rad 680 microplate reader (Bio-Rad Laboratories, Hercules, CA, USA) at the absorbance of 490 nm. All experimental samples were performed for three times. The cell viability (%) was calculated as follows:

$$\text{Cell viability}(\%) = \frac{A_{\text{sample}}}{A_{\text{control}}} \times 100\%. \quad (3)$$

In equation (3), A_{sample} and A_{control} represented the absorbance of sample well and control well, respectively.

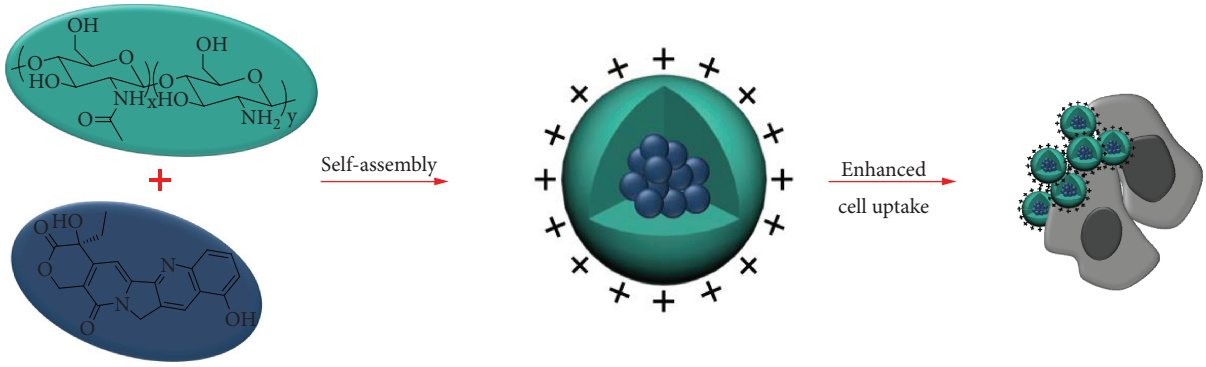

Scheme 1: Schematic illustration for the preparation of CS/HCPT and enhanced cell uptake by 4T1 cells.

2.7. Cell Apoptosis Analysis. The apoptosis percentage of 4T1 cells induced by CS/HCPT was detected by flow cytometry (FCM) analysis. 4T1 cells were incubated in 6-well plates at a density of 3×10^5 cells per well for 24 h. The incubation medium was then replaced with 2.0 mL of complete DMEM containing different HCPT formulations with a HCPT concentration of 0.1 μg mL^{-1}. The untreated cells were used as a control. The cells were incubated for additional 24 h at 37°C and then harvested by trypsinization, washed, and resuspended in 0.5 mL 1x Annexin V binding buffer. Before analyzing, the samples were stained with 5.0 μL of Annexin V-FITC and propidium iodide (PI) for 15 min in the dark. Finally, the cells were analyzed using FCM.

3. Results and Discussion

3.1. Preparations and Characterizations of CS/HCPT. The hydrophobic antitumor drug of HCPT was encapsulated into CS through facile diffusion (Scheme 1). Electrostatic interaction is the main reason for drug encapsulation [20]. The preparation method was simple and straightforward. The DLC and DLE of CS/HCPT were at high levels of 31.7 and 92.8 wt.%, respectively (Table 1). The resulting CS/HCPT exhibited an average diameter of 55.8 ± 1.4 nm, which was detected by DLS (Figure 1). The R_h of CS/HCPT was less than 200 nm, showing the maximum enhanced permeability and retention (EPR) effect, which was important for tumor targeting within the biomedical applications of nanomedicine [21, 22]. Furthermore, CS/HCPT has a positive surface charge with zeta potential of 10.6 ± 2.2 mV (Table 1). The zeta potential is important for evaluating the stability and dispersion of nanoparticles [23]. In addition, positively charged particles have a great efficiency in cell membrane infiltration and internalization [24]. Obviously, CS/HCPT is an excellent platform for drug delivery.

3.2. Cell Uptake and Intracellular Drug Release. The cell uptake and intracellular HCPT release behavior of CS/HCPT by 4T1 cells were monitored with CLSM. As depicted in Figure 2(a), after 2 h of treatment, the HCPT fluorescence signal was observed in the cells treated with free HCPT or CS/HCPT. The HCPT fluorescence was a little stronger in the cells incubated with free HCPT than in the cells with

Table 1: Particle size, DLC, DLE, and zeta potential of CS/HCPT.

Size (nm)	DLC (wt.%)	DLE (wt.%)	Zeta potential (mV)
55.8 ± 1.4	31.7	92.8	10.6 ± 2.2

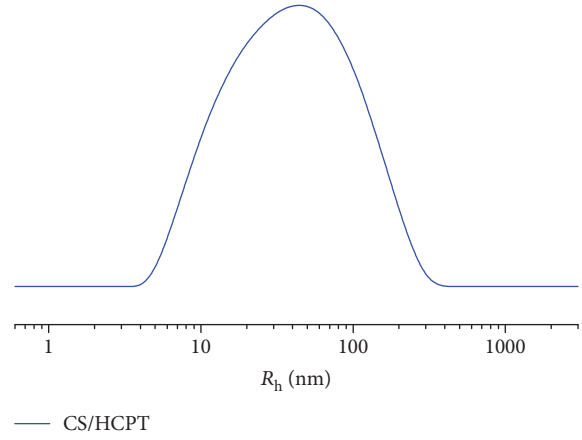

Figure 1: R_h of CS/HCPT.

CS/HCPT. However, after 6 h of incubation, the CS/HCPT-treated cells exhibited much higher HCPT fluorescence intensity than those of the free HCPT treatment group (Figure 2(b)). The results indicated that CS/HCPT could be preferentially internalized *via* endocytosis pathway, which had a temperate efficiency at the outset and then revealed the enhanced fluorescence signal after effective drug release [25]. On the contrary, free HCPT was transported into cells through passive diffusion [26, 27]. It was also reported that endocytosis of nanoparticles is often more efficient than passive diffusion of drug molecules [28]. Similar results have been reported in our previous work [29]. In that work, a positively charged polypeptide nanogel was synthesized mainly to enhance the mucoadhesiveness of HCPT for intravesical chemotherapy of bladder cancer. In this work, the positively charged nanogel was based on CS, which was the second most abundant polysaccharide in nature with good biocompatibility and biodegradability. The results of Figure 2 demonstrated that CS could increase the uptake and endocytosis of HCPT by 4T1 cells.

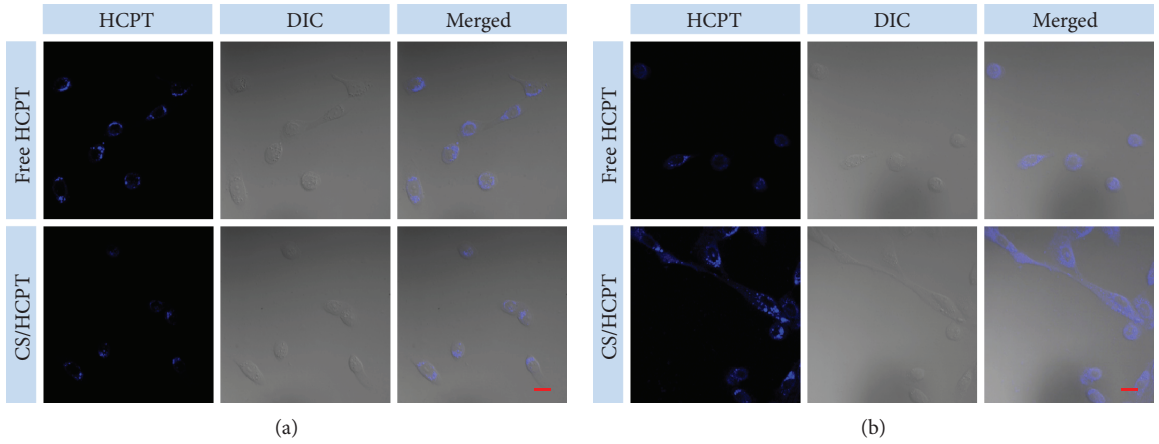

Figure 2: Representative CLSM microimages of 4T1 cells incubated with free HCPT and CS/HCPT for 2 (a) and 6 h (b). For each panel, the microimages from left to right showed HCPT fluorescence in cells (blue), differential interference contrast (DIC) image, and the overlay of two images. The scale bar represented 20 μm.

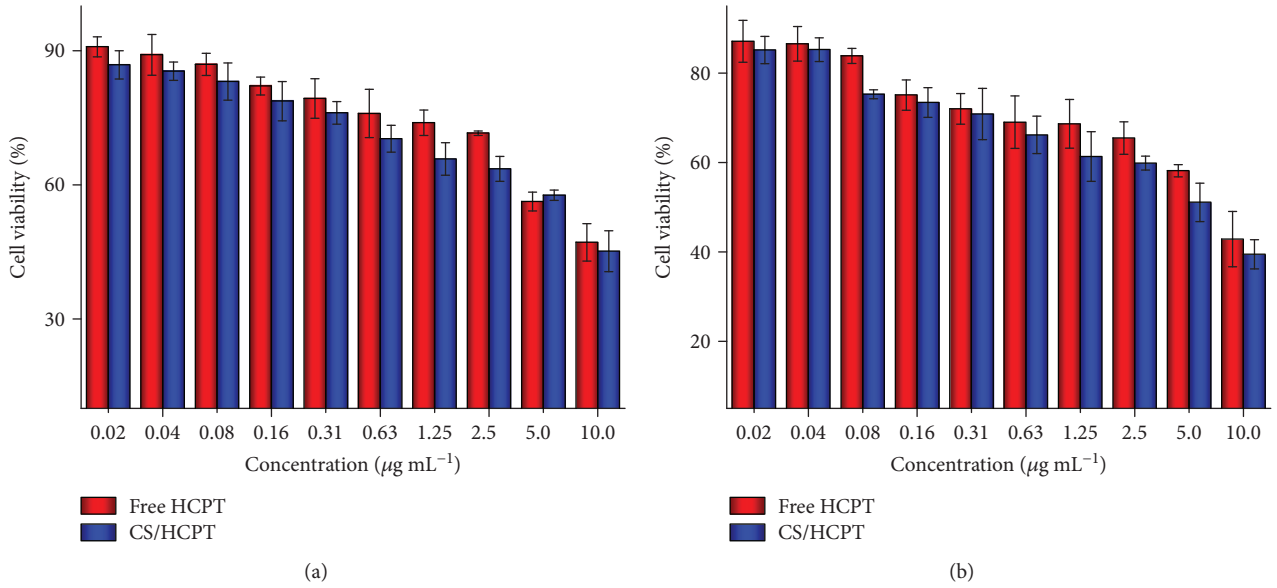

Figure 3: *In vitro* cytotoxicities of free HCPT and CS/HCPT after incubation with 4T1 cells for 48 h (a) and 72 h (b).

3.3. In Vitro Cytotoxicity Study of CS/HCPT. 4T1 is a representative cell line in breast cancer, and its growth and metastasis in BALB/c mice are very similar to that of human breast cancer. The kinetics of 4T1-induced tumors is similar in both postoperative and nonsurgical conditions, which can be used as a postoperative and nonsurgical model [30]. To investigate the enhanced therapeutic efficacy of CS/HCPT against the 4T1 cell line, a standard MTT assay was applied. As shown in Figure 3(a), after 48 h of exposure to either CS/HCPT or free HCPT, the metabolic activity of 4T1 cells decreased in a concentration-dependent manner. The CS/HCPT displayed an apparently higher cytotoxicity than free HCPT at any given equivalent concentration, indicating that the drug delivery platform can indeed enhance anticancer efficiency of HCPT. The enhanced cytotoxicity of CS/HCPT was probably due to the nonspecifically internalized into cells *via* endocytosis, phagocytosis, or pinocytosis after accumulating on the surface of the cells, while free HCPT was transported by passive diffusion [31, 32]. The similar results were obtained when the incubation time was expanded to 72 h (Figure 3(b)). In addition, the half maximal inhibitory concentration (IC_{50}) value of CS/HCPT was 8.7 μg mL^{-1} and 4.4 μg mL^{-1} at 48 h and 72 h, respectively. On the contrary, the IC_{50} value of free HCPT was 10.3 μg mL^{-1} and 7.5 μg mL^{-1} at 48 h and 72 h, respectively. The results indicated that the proliferation rate was time dependent.

3.4. Cell Apoptosis Analysis. The apoptotic activities of 4T1 cells induced by CS/HCPT were assessed by FCM analyses. The cells were incubated with free HCPT or CS/HCPT at a certain HCPT concentration of 0.1 μg mL^{-1} for 24 h and then double labeled for viability and apoptosis. As depicted in Figure 4, CS/HCPT remarkably decreased the percentage of normal cells and significantly increased the percentage of

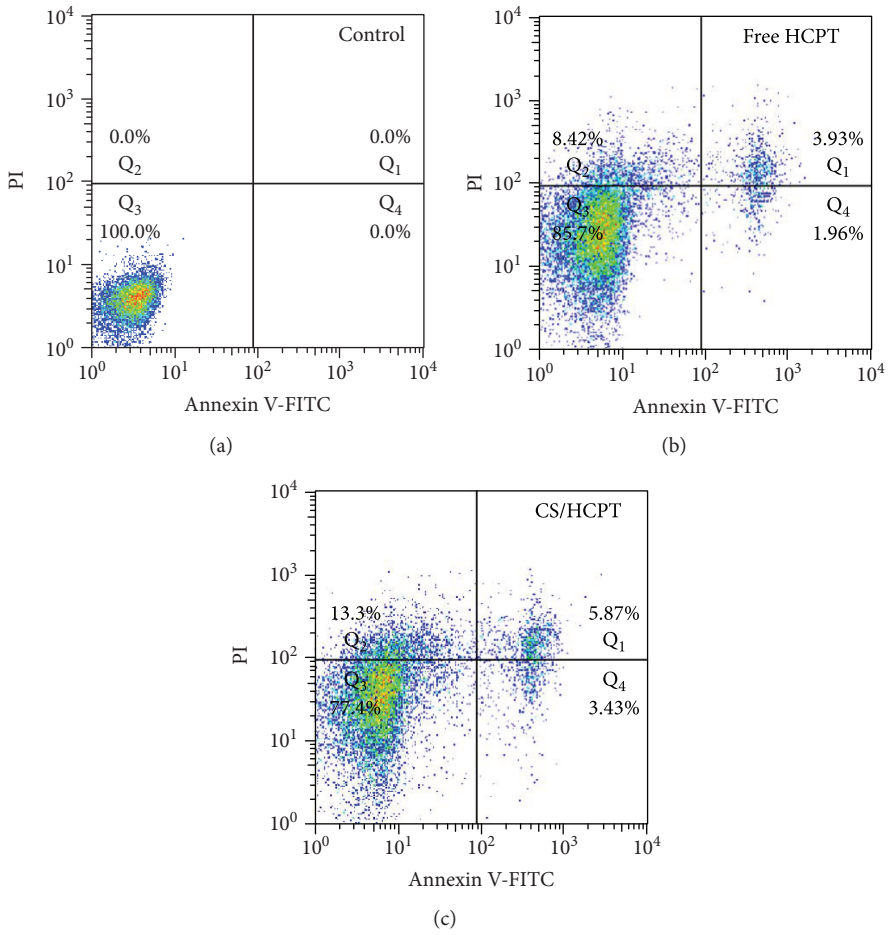

Figure 4: Apoptotic cell populations were determined by FCM analyses with Annexin V-FITC and PI staining after coincubating 4T1 cells with PBS, free HCPT, or CS/HCPT for 24 h. The lower left (Q3), lower right (Q4), upper right (Q1), and upper left (Q2) quadrants in each panel indicated the populations of normal, early and late apoptotic, and apoptotic necrotic cells, respectively.

necrotic/late apoptotic cells. The results were attributed to the positive charge of CS/HCPT, which increased the uptake of CS/HCPT by 4T1 cells and further induced enhanced cell apoptosis.

4. Conclusions

In summary, a cationic CS-based nanogel was successfully synthesized to inhibit the proliferation of breast cancer cells. The hydrophobic antitumor drug of HCPT was entrapped into the core *via* facile diffusion. The resulting CS/HCPT exhibited an average diameter of 55.8 ± 1.4 nm. The positive surface charge of CS/HCPT promoted intracellular drug internalization *via* endocytosis pathway. The cytotoxicity assay suggested excellent biocompatibility of CS/HCPT and also proved better cytotoxicity in comparison to free HCPT. The present investigation indicated that the positively charged CS-based nanogel could be potentially used as a promising drug delivery system.

Data Availability

The data used to support the findings of this study are included within the article.

Conflicts of Interest

The authors declare that they have no competing interests.

Acknowledgments

The study was financially supported by the Science and Technology Development Program of Jilin Province (no. 20180101167JC).

References

[1] C. E. DeSantis, J. Ma, A. G. Sauer, L. A. Newman, and A. Jemal, "Breast cancer statistics, 2017, racial disparity in mortality by state," *CA: A Cancer Journal for Clinicians*, vol. 67, no. 6, pp. 439–448, 2017.

[2] Y. Chen and Y. Zhang, "Application of the CRISPR/Cas9 system to drug resistance in breast cancer," *Advanced Science*, vol. 5, no. 6, 2018.

[3] S. Liu, X. Meng, H. Chen et al., "Targeting tyrosine-kinases and estrogen receptor abrogates resistance to endocrine therapy in breast cancer," *Oncotarget*, vol. 5, no. 19, pp. 9049–9064, 2014.

[4] A. Ferrari, A. Vincent-Salomon, X. Pivot et al., "A whole-genome sequence and transcriptome perspective on HER2-positive breast cancers," *Nature Communications*, vol. 7, no. 1, 2016.

[5] K. M. de Ligt, P. E. R. Spronk, A. C. M. van Bommel et al., "Patients' experiences with decisions on timing of chemotherapy for breast cancer," *Breast*, vol. 37, pp. 99–106, 2018.

[6] G. P. Gupta and J. Massague, "Cancer metastasis: building a framework," *Cell*, vol. 127, no. 4, pp. 679–695, 2006.

[7] A. Zapater-Moros, A. Gámez-Pozo, G. Prado-Vázquez et al., "Probabilistic graphical models relate immune status with response to neoadjuvant chemotherapy in breast cancer," *Oncotarget*, vol. 9, no. 45, pp. 27586–27594, 2018.

[8] C. Holohan, S. Van Schaeybroeck, D. B. Longley, and P. G. Johnston, "Cancer drug resistance: an evolving paradigm," *Nature Reviews Cancer*, vol. 13, no. 10, pp. 714–726, 2013.

[9] L. Yang, H. Tang, and H. Sun, "Progress in photo-responsive polypeptide derived nano-assemblies," *Micromachines*, vol. 9, no. 6, 2018.

[10] S. Wang, J. Sha, W. Wang, C. Qin, W. Li, and C. Qin, "Superhydrophobic surfaces generated by one-pot spray-coating of chitosan-based nanoparticles," *Carbohydrate Polymers*, vol. 195, pp. 39–44, 2018.

[11] S. Sharma, A. Kumar, Deepak, R. Kumar, N. K. Rana, and B. Koch, "Development of a novel chitosan based biocompatible and self-healing hydrogel for controlled release of hydrophilic drug," *International Journal of Biological Macromolecules*, vol. 116, pp. 37–44, 2018.

[12] C. Qi, L. Zhao, Y. Lin, and D. Wu, "Graphene oxide/chitosan sponge as a novel filtering material for the removal of dye from water," *Journal of Colloid and Interface Science*, vol. 517, pp. 18–27, 2018.

[13] M. Kurdtabar, R. N. Koutenaee, and G. R. Bardajee, "Synthesis and characterization of a novel pH-responsive nanocomposite hydrogel based on chitosan for targeted drug release," *Journal of Polymer Research*, vol. 25, no. 5, 2018.

[14] S. Yu, X. Zhang, G. Tan et al., "A novel pH-induced thermosensitive hydrogel composed of carboxymethyl chitosan and poloxamer cross-linked by glutaraldehyde for ophthalmic drug delivery," *Carbohydrate Polymers*, vol. 155, pp. 208–217, 2017.

[15] X. Ren, L. Zhang, Y. Zhang, L. Mao, and H. Jiang, "Mitochondria response to camptothecin and hydroxycamptothecine-induced apoptosis in *Spodoptera exigua* cells," *Pesticide Biochemistry and Physiology*, vol. 140, pp. 97–104, 2017.

[16] H. Guo, F. Li, W. Xu et al., "Mucoadhesive cationic polypeptide nanogel with enhanced penetration for efficient intravesical chemotherapy of bladder cancer," *Advanced Science*, vol. 5, no. 6, 2018.

[17] J. Li, W. Xu, D. Li et al., "Locally deployable nanofiber patch for sequential drug delivery in treatment of primary and advanced orthotopic hepatomas," *ACS Nano*, vol. 12, no. 7, pp. 6685–6699, 2018.

[18] J. Chen, J. Ding, W. Xu et al., "Receptor and microenvironment dual-recognizable nanogel for targeted chemotherapy of highly metastatic malignancy," *Nano Letters*, vol. 17, no. 7, pp. 4526–4533, 2017.

[19] J. Chen, J. Ding, Y. Wang et al., "Sequentially responsive shell-stacked nanoparticles for deep penetration into solid tumors," *Advanced Materials*, vol. 29, no. 32, 2017.

[20] Y. Zhang, L. Cai, D. Li et al., "Tumor microenvironment-responsive hyaluronate-calcium carbonate hybrid nanoparticle enables effective chemotherapy for primary and advanced osteosarcomas," *Nano Research*, vol. 11, no. 9, pp. 4806–4822, 2018.

[21] T. Doura, F. Tamanoi, and M. Nakamura, "Miniaturization of thiol-organosilica nanoparticles induced by an anionic surfactant," *Journal of Colloid and Interface Science*, vol. 526, pp. 51–62, 2018.

[22] W. Song, L. Shen, Y. Wang et al., "Synergistic and low adverse effect cancer immunotherapy by immunogenic chemotherapy and locally expressed PD-L1 trap," *Nature Communications*, vol. 9, no. 1, p. 2237, 2018.

[23] Y. Liu, K. Liu, X. Li et al., "A novel self-assembled nanoparticle platform based on pectin-eight-arm polyethylene glycol-drug conjugates for co-delivery of anticancer drugs," *Materials Science and Engineering: C*, vol. 86, pp. 28–41, 2018.

[24] Y. Liu, D. Zheng, Y. Ma et al., "Self-assembled nanoparticles platform based on pectin-dihydroartemisinin conjugates for codelivery of anticancer drugs," *ACS Biomaterials Science & Engineering*, vol. 4, no. 5, pp. 1641–1650, 2018.

[25] Y. Zhang, F. Wang, M. Li et al., "Self-stabilized hyaluronate nanogel for intracellular codelivery of doxorubicin and cisplatin to osteosarcoma," *Advanced Science*, vol. 5, no. 5, 2018.

[26] W. Xu, J. Ding, C. Xiao, L. Li, X. Zhuang, and X. Chen, "Versatile preparation of intracellular-acidity-sensitive oxime-linked polysaccharide-doxorubicin conjugate for malignancy therapeutic," *Biomaterials*, vol. 54, pp. 72–86, 2015.

[27] K. Zhao, D. Li, W. Xu et al., "Targeted hydroxyethyl starch prodrug for inhibiting the growth and metastasis of prostate cancer," *Biomaterials*, vol. 116, pp. 82–94, 2017.

[28] M. Zhou, X. Zhang, Y. Yang et al., "Carrier-free functionalized multidrug nanorods for synergistic cancer therapy," *Biomaterials*, vol. 34, no. 35, pp. 8960–8967, 2013.

[29] H. Guo, W. Xu, J. Chen et al., "Positively charged polypeptide nanogel enhances mucoadhesion and penetrability of 10-hydroxycamptothecin in orthotopic bladder carcinoma," *Journal of Controlled Release*, vol. 259, pp. 136–148, 2017.

[30] Y. Liu, Q. Qi, X. Li et al., "Self-assembled pectin-conjugated eight-arm polyethylene glycol-dihydroartemisinin nanoparticles for anticancer combination therapy," *ACS Sustainable Chemistry & Engineering*, vol. 5, no. 9, pp. 8097–8107, 2017.

[31] Y. Guo, Y. Zhao, T. Wang et al., "Hydroxycamptothecin nanorods prepared by fluorescently labeled oligoethylene glycols (OEG) codendrimer: antitumor efficacy in vitro and in vivo," *Bioconjugate Chemistry*, vol. 28, no. 2, pp. 390–399, 2017.

[32] F. Chen, K. Ma, B. Madajewski et al., "Ultrasmall targeted nanoparticles with engineered antibody fragments for imaging detection of HER2-overexpressing breast cancer," *Nature Communications*, vol. 9, no. 1, pp. 4141–4141, 2018.

Hindawi
International Journal of Polymer Science
Volume 2019, Article ID 7382717, 10 pages
https://doi.org/10.1155/2019/7382717

Research Article

In Vivo Study of the Antibacterial Chitosan/Polyvinyl Alcohol Loaded with Silver Nanoparticle Hydrogel for Wound Healing Applications

Tan Dat Nguyen,[1] **Thanh Truc Nguyen**,[1] **Khanh Loan Ly**,[1] **Anh Hien Tran**,[1] **Thi Thanh Ngoc Nguyen**,[1] **Minh Thuy Vo**,[1] **Hieu Minh Ho**,[1] **Ngoc Thao Nhi Dang**,[1] **Van Toi Vo**,[1] **Dai Hai Nguyen**,[2,3] **Thi Thu Hoai Nguyen**,[4] **and Thi Hiep Nguyen**[1]

[1]*Tissue Engineering and Regenerative Medicine Group, Department of Biomedical Engineering, International University, Vietnam National University-HCMC (VNU-HCMC), HCMC 700000, Vietnam*
[2]*Graduate School of Science and Technology Vietnam, Vietnam Academy of Science and Technology, HCMC 700000, Vietnam*
[3]*Institute of Applied Materials Science, Vietnam Academy of Science and Technology, HCMC 700000, Vietnam*
[4]*School of Biotechnology, International University, Vietnam National University-Ho Chi Minh City (VNU-HCM), HCMC 700000, Vietnam*

Correspondence should be addressed to Thi Hiep Nguyen; nthiep1981@gmail.com

Received 16 August 2018; Revised 28 November 2018; Accepted 12 December 2018; Published 21 March 2019

Guest Editor: Mingqiang Li

Silver nanoparticles have attracted great interests widely in medicine due to its great characteristics of antibacterial activity. In this research, the antibacterial activity and biocompatibility of a topical gel synthesized from polyvinyl alcohol, chitosan, and silver nanoparticles were studied. Hydrogels with different concentrations of silver nanoparticles (15 ppm, 30 ppm, and 60 ppm) were evaluated to compare their antibacterial activity, nanoparticles' sizes, and *in vivo* behaviors. The resulted silver nanoparticles in the hydrogel were characterized by TEM showing the nanoparticles' sizes less than 22 nm. The *in vitro* results prove that the antibacterial effects of all of the samples are satisfied. However, the *in vivo* results demonstrate the significant difference among different hydrogels in wound healing, where hydrogel with 30 ppm shows the best healing rate.

1. Introduction

In recent decades, nanoparticles (NPs) have been investigated for various biomedical applications and are considered to be the "material of the 21st century" because of their unique designs and property combinations compared with conventional materials [1, 2]. There is a wide range of applications of NPs such as in human health appliances, industrial fields, medical applications, biomedical fields, engineering, electronics, and environmental studies [1–7].

Basically, many benefits of using nanoparticles are proved over other drug delivery systems such as enhancing the solubility of highly hydrophobic drugs, providing sustained and controlled release of encapsulated drugs, and intensifying the stability of therapeutic agents by chemical or physical means and targeted treatments when modified with cell-specific ligands [2]. Among all of the nanomaterials, a variety of metallic nanoparticles have been considered as the foremost attention due to their antibacterial application to human health. Antibiotic resistance has always been one of the most significant health threats due to continuous adaptation of microbes to our antibiotic. This problem has risen the attention for metallic drugs that were used to treat infections before the era of antibiotics' total dominance. The most widely used delegate of metallic NPs is silver nanoparticles (AgNPs) because of their highly effective antibacterial activity both in solution and in components and their extremely large surface area, which provides better contact with

microorganisms [3–11]. When we apply AgNPs on the wound, they get attached to the cell membrane and also penetrate inside the bacteria. The bacterial membrane contains sulfur-containing proteins, and the AgNPs interact with these proteins in the cell as well as with the phosphorus-containing compounds like DNA. When AgNPs enter the bacterial cell, it forms a low molecular weight region in the center of the bacteria to which the bacteria conglomerate, thus protecting the DNA from the silver ions. The AgNPs preferably attack the respiratory chain and cell division, finally leading to cell death [12, 13]. AgNPs (ranging in size from ~1 to 100 nm) can be prepared with many methods: (i) chemical synthesis, (ii) physical dispersion, (iii) photochemical synthesis, and (iv) biological synthesis [8, 9].

Furthermore, to control the release rate of silver ion from AgNPs and increase the antibacterial effect, several studies have suggested combining AgNPs with other biocompatible polymers such as chitosan, polyvinyl alcohol, poly(vinyl alcohol), poly(vinyl pyrrolidone), and poly(lactic acid) to create wound healing application in the type of topical hydrogels, dressing, and mats [14–17]. For example, Zhou et al. created the matrix of gelatin/carboxymethyl chitosan loaded with silver nanoparticles. The results show that this matrix has good physical properties and long-time antibacterial activity [18]. The study of Gaafar et al. showed that AgNPs used singly or combined with chitosan NPs are promising drugs to eliminate the parasite [19]. However, the poor physical property of chitosan requires a combination of this natural polymer and other synthesized polymers [20, 21]. Recent studies showed that a promised alternative to enhance the benefits of chitosan properties is to blend chitosan with another water-soluble polymer such as poly(vinyl alcohol) (PVA) [3, 14, 15, 22]. Due to the high resistance to oil, grease, and solvents, high chemical stability, and excellent oxygen and aroma barrier properties, PVA presented itself as a factor in wound healing dressing to create a covered membrane-absorbing water, helping chitosan and AgNPs to easily access and kill bacteria.

However, the use of this chitosan/polyvinyl alcohol/AgNPs (PCA) gels carries some unpredictable risks regarding their interaction with biological systems [23, 24]. Several studies have suspected the negative effects of the strong oxidative activity of AgNPs releasing silver ions with biological systems by inducing cytotoxicity, genotoxicity, immunological responses, and even cell death [25–29]. Therefore, the profuse applications of AgNPs raise concerns about human exposure, because they can easily pass through the blood-brain barrier by transcytosis of capillary endothelial cells or into other critical areas or tissues [30]. Obviously, human became at risks induced by exposure to nanoparticles (NPs; diameter < 100 nm) either from ambient air or therapeutic uses as drug delivery [31]. According to Aueviriyavit et al., Ag products in colloidal form for medicinal or other purposes have activated Ag^+, which might have a direct effect on human health [32]. Moreover, it is hypothesized that Ag^+ possesses an enhanced toxicity potential than elemental Ag and AgNPs [28]. The interaction processes of nanomaterials with biological systems are unknown and consequently might be of great concern [24, 33]. The toxicity of other

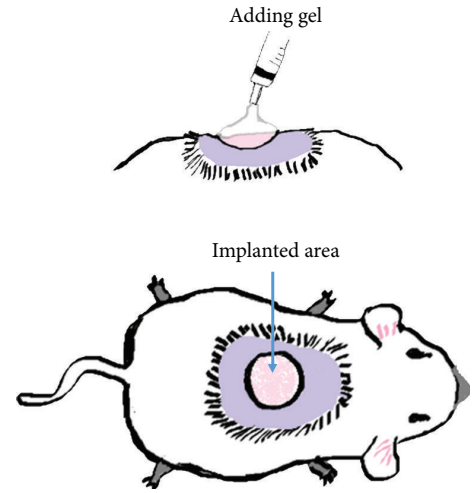

Figure 1: Cartoon depicting a surgical model for the in vivo study.

NPs in different organisms has been reported in various studies, whereas the toxicity of AgNPs has not been extensively explored. For example, titanium dioxide (TiO_2) NPs induce reactive oxygen species (ROS), which further initiate lipid peroxidation, protein dysfunction, and DNA degradation, finally triggering oxidative damage in the mouse brain [33]. Little is known about the diversified mechanisms of action of the cytotoxicity of AgNPs, as well as their short- or long-term exposure outcomes, on human physiology [34, 35]. Therefore, the toxicological studies on AgNPs have become a raising topic over the past few decades due to their unique properties on the nanoscale and being widespread in many commercial products that were launched into the market recently [36]. On the other hand, several studies of PCA system used cross-linkers such as glutaraldehyde, which causes risks to human health [37, 38].

In Vietnam, recently, medical products using the technology of silver nanoparticles have been developed. In 2016, Hiep et al. synthesized the PCA gels using microwave irradiation method [3]. Compared with other rays, for example, γ-ray and UV ray can induce the formation of AgNPs [39–41]; however, γ-ray causes structural changes in organic compounds [42] and the UV ray method is complicated and requires additional substances [40, 41]; the major impact of microwave is heating. Heating using microwave irradiation is simple, economical, and fast, which can be employed to form AgNPs. PVA in the PCA system under microwave exposure plays a role as a reducing agent, which leads to the reduction of Ag^+. The work also successfully cross-links PVA and chitosan without the need of any cross-linkers used in other studies [3, 38].

The aim of this study was to investigate the antibacterial activity and effects of hydrogel, containing polyvinyl alcohol, chitosan, and silver nanoparticles in our previous study, on wound healing to determine the optimal formulation of it [3]. In that research, Hiep et al. loaded AgNPs with two concentrations (5000 ppm and 10000 ppm) with the release rate of 40% and positive antibacterial effect. As mentioned above, the unproper concentration of AgNPs causes harmful effects

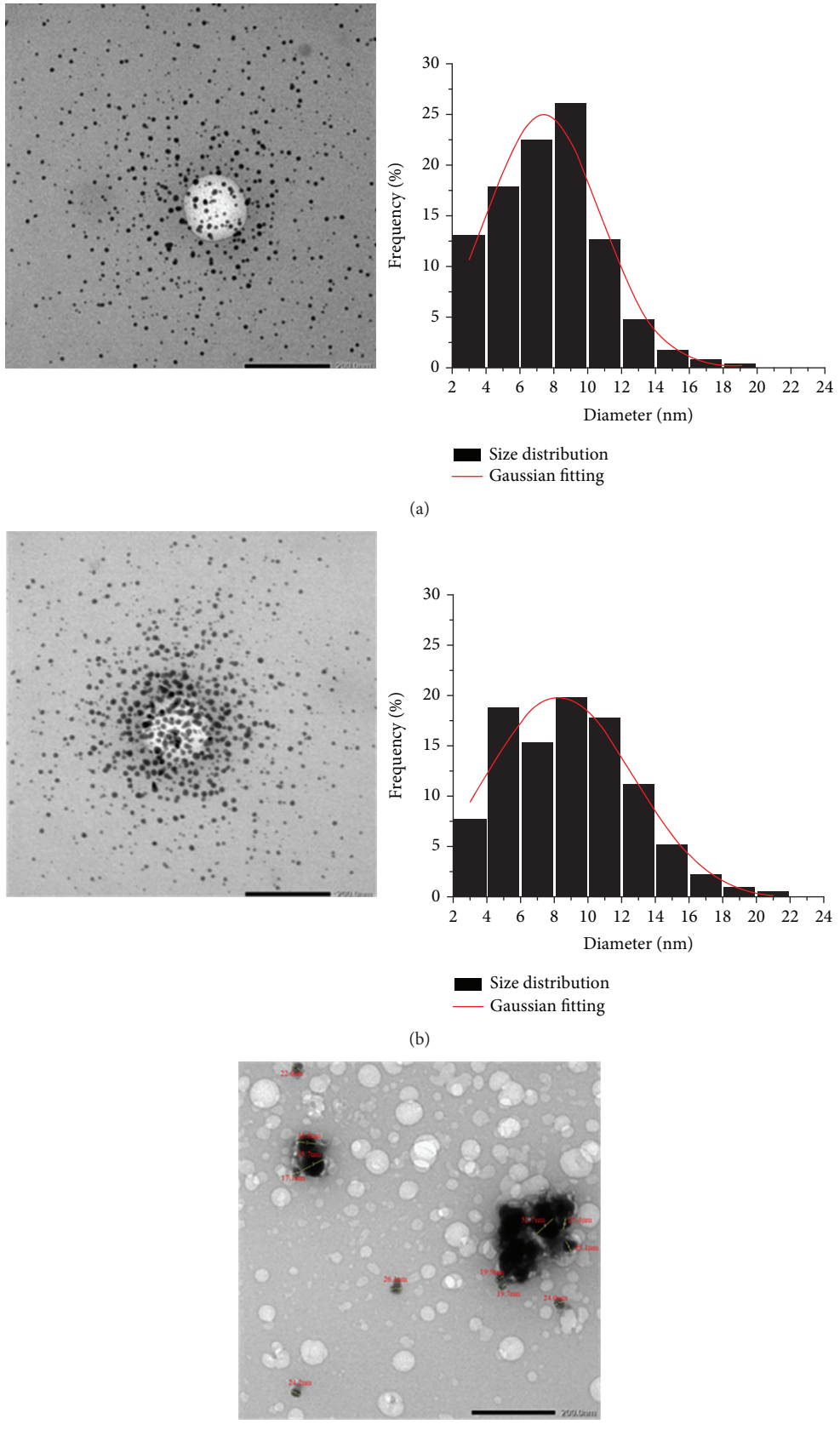

Figure 2: TEM images and particle size histograms of PCA15 (a), PCA30 (b), and PCA60 (c) fitted by log-normal distribution function; scale bar: 200 nm.

to our biological system. Consequently, this study introduces a topical hydrogel to treat infection and support wound healing and provides evidences of the appropriate concentration of AgNPs for the body and its importance to human health for further research on the field of metallic nanodrug.

2. Experimental Procedure

2.1. Materials. Chitosan powder (shrimp shells—low viscosity), Biebrich scarlet-acid fuchsin, phosphotungstic acid solution, phosphomolybdic acid solution, and aniline blue solution were purchased from Sigma-Aldrich, USA. Absolute alcohol, ethanol, xylene, hydrochloric acid, ferric chloride, silver nitrate ($AgNO3 \geq 99\%$), and acetic acid ($CH3COOH \geq 99.5\%$) were purchased from Xilong, China. Albino mice were supplied by the School of Biotechnology, International University, HCMC. The pathogens, such as *Staphylococcus aureus* ATCC 25913 and *Pseudomonas aeruginosa* ATCC 9028, were obtained from the American Type Culture Collection. ProGel® is a commercial gel containing 50 ppm AgNPs produced by C&D Company of Production and Application of New Materials, Hue City, Vietnam. All other chemicals used were of analytical grade.

2.2. Preparation of the CS/PVA Loaded with Silver Nanoparticle Gel. The silver nitrate solution that has silver ion concentrations of 15, 30, and 60 ppm was loaded into the PVA solution which has the concentration of 10 wt%. The mixture was put in a microwave oven with the setting wave time of 90 seconds and a power level of 800 W. This wave time was reported to be able to create silver nanoparticles with the size of 10–20 nm [3]. Each mixture solution including PVA and silver ions with four diverse concentrations was immersed in 2 wt% chitosan solution by the volume ratio of 1 : 1 [3]. Finally, four mixture gels were obtained as PCA15 (10 wt%-2 wt%-15 ppm), PCA30 (10 wt%-2 wt%-30 ppm), and PCA60 (10 wt%-2 wt%-60 ppm).

2.3. Transmission Electron Microscopy (TEM). Particle size and shape of AgNPs in PCA hydrogels were examined using transmission electron microscope (JEM-1400 Plus, JEOL, USA). The samples were prepared by applying a drop of PCA hydrogels onto a carbon-coated copper grid and drying. The diameters of AgNPs were measured by using image analysis software (ImageJ, NIH, USA).

2.4. Agar Diffusion Test. The antibacterial activity of AgNPs was evaluated by using the agar diffusion method against the gram-negative (*Pseudomonas aeruginosa*) and the gram-positive (*Staphylococcus aureus*) bacteria. The antibacterial activity of PCA gels was measured using the agar diffusion method. Briefly, 100 μl of the bacterial suspension was added and spread out Mueller-Hinton agar surface. Then, the samples were added to the suspension layer. The dishes were incubated upside down at 37°C, overnight. Zones of inhibition were evaluated by measuring the diameter of the bacterial growth inhibition zone around the membrane (in millimeter). The samples were performed with three replications for each bacterial strain. The positive control was a commercial gel, ProGel®, which contains ingredients including 50 ppm silver nanoparticles, Carbopol, and triethanolamine (TEA) (used as the control). The negative sample was the hydrogel which was prepared by polyvinyl alcohol and chitosan without silver.

Table 1: Measured average nanoparticle size.

Samples	Average size measurement (nm)	Standard deviation
PCA15	7.34	4.12
PCA30	8.31	5.22
PCA60	Undefined	Undefined

2.5. Animal Study. In order to evaluate the biocompatibility of five sample groups (PCA gels with four different concentrations and a commercial gel, ProGel®), prepared PCA gels were poured into a syringe and sterilized by autoclave before subcutaneously implanted at the dorsal region under general anesthesia and antiseptic conditions. The operation process was performed following the policy of Institutional Animal Care and Use Committee of International University, Vietnam National University-Ho Chi Minh City, Vietnam.

Mice were anesthetized with anesthesia Zoletil®, their hair was shaved at their back, and they were fixed on a table. The implanted site was cleaned by povidone solution and PBS buffer before making the laceration (8 mm × 8 mm) for samples' application. The experimental study used 15 male Swiss albino mice (3 mice for each group). Figure 1 illustrates the mouse model treated with samples.

Treatment with ProGel® and PCA gel was applied shortly after surgery. The control group was treated with ProGel®; PCA15, PCA30, and PCA60 animals were treated with gel containing the concentration of 15, 30, and 60 ppm silver ion, respectively. Once daily for 12 days, the test samples were applied topically and allowed to heal.

2.5.1. Wound Size Reduction. The wound area of each animal was measured on days 4, 8, and 12 postsurgery. The wound size measurements taken at the time of surgery and at the time of biopsy were used to calculate the percent wound contraction as follows:

$$\%\text{wound contraction} = \frac{A_o - A_t}{A_o} \times 100, \quad (1)$$

where A_o is the original wound area and A_t is the area of the wound at the time of biopsy.

2.5.2. Histological Examination. After 11 days, mice were sacrificed, and then the regenerated areas ($0.8 \times 0.8\ cm^2$) were extracted. The extracted samples were fixed by 10% formaldehyde, embedded in paraffin, and then sectioned (3-5 μm) using a microtome before staining with hematoxylin and eosin (H&E) stain. The stained samples were observed by a light microscope (Nikon Eclipse, Ti-U series, Japan).

2.6. Analysis of Data. All data are presented as the mean ± standard deviation (S.D.). Data were analyzed by one-way analysis of variance (ANOVA) using the IBM SPSS 20®

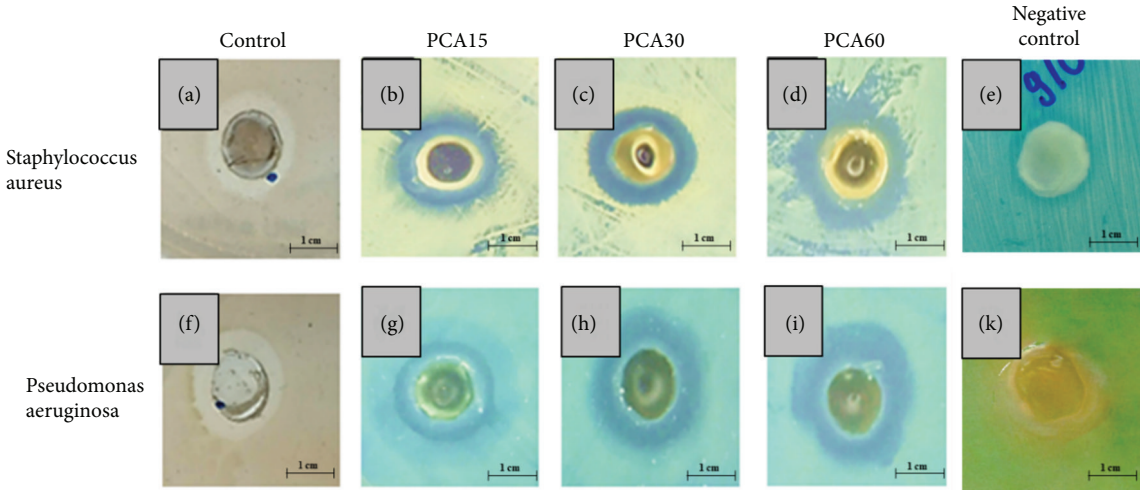

Figure 3: Inhibition area of the positive control group treated with ProGel® (a, f), negative control (e, k), and other groups treated with PCA15 (b, g), PCA30 (c, h), and PCA60 (d, i) in the antibacterial test with *Staphylococcus aureus* (a–e) and *Pseudomonas aeruginosa* (f–j).

statistical package. Statistical differences yielding $p \leq 0.05$ were considered significant.

3. Results

3.1. TEM Analysis. The TEM images of PCA hydrogels providing the shape and size of AgNPs are presented in Figure 2. In Figure 2(a), AgNPs in PCA15 hydrogel are smooth and spherical, and the diameter ranges from 2 to 20 nm, showing PVA under microwave is an excellent reducing agent for AgNPs. Furthermore, the average size determined from the histogram is 7.34 nm (Table 1). However, when increasing the concentration of $AgNO_3$ up to 30 ppm, Figure 2(b) shows that the rate of AgNPs over 10 nm enhances while the aggregation appears slightly, and the average diameter increases up to 8.31 nm (Table 1). On the other hand, the result of AgNPs in PCA60 hydrogel Figure 2(c) indicates instability of AgNPs when there are massive agglomerates of them, which caused incapability of exact measurement, and separate AgNPs are at least 17 nm.

3.2. Antibacterial Activity. The antibacterial properties of PCA gels with different concentrations of silver ions were evaluated using the agar diffusion method. Figures 3 and 4 show the inhibition zones of each sample for gram-negative strains (*P. aeruginosa*) and gram-positive strain (*S. aureus*). The overview of inhibition diameter proves that both strains were significantly inhibited for all samples, except the negative controls which were fabricated by polyvinyl alcohol and chitosan only. Among these, the gram-negative strain *P. aeruginosa* was more susceptible by a topical gel containing silver nanoparticles than the gram-positive strain *S. aureus*, especially with the positive control group which has the lowest inhibition area, except the PCA15 because they have a higher antimicrobial activity for gram-positive *S. aureus* than that for gram-negative *P. aeruginosa*. PCA30 and PCA60 show the predominant inhibition zones against *P. aeruginosa* compared to the ones with *S. aureus*. The group treated with ProGel® (50 ppm AgNPs) represents the

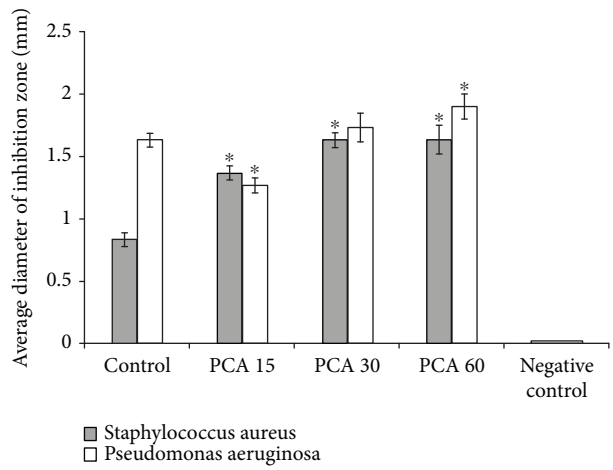

Figure 4: The average diameter of the inhibition zone (mm) of 5 samples against bacterial strains (*S. aureus* and *P. aeruginosa*) in agar media. The error bars presented as mean ± SD. Asterisks on the bar graph indicate significant ($p < 0.05$) difference with respect to the control group.

average diameter of the inhibition zone as well as the group treated with gel PCA30.

Particularly, the inhibition diameter of each sample yields significantly statistical meaning with $p < 0.05$ with the control group. When doubling the concentration of silver ions from 15 ppm to 30 ppm, we observed the increase in inhibition diameter. Clearly, the gram-positive *S. aureus* is inhibited with 1.6 ± 0.3 mm diameter treated with the gel PCA30, 0.2 mm diameter more than the gel PCA15 and the gel PCA60 keep that inhibition zone against *S. aureus*. Meanwhile, the increase could be observed more clearly with the gel PCA30 against *P. aeruginosa* (1.7 ± 0.3 mm diameter), more than 0.4 mm diameter compared with the gel PCA15. The gel PCA60 eventually increases the inhibition zone against *P. aeruginosa* (1.9 ± 0.3 mm diameter) compared to *S. aureus* (1.6 ± 0.3 mm diameter).

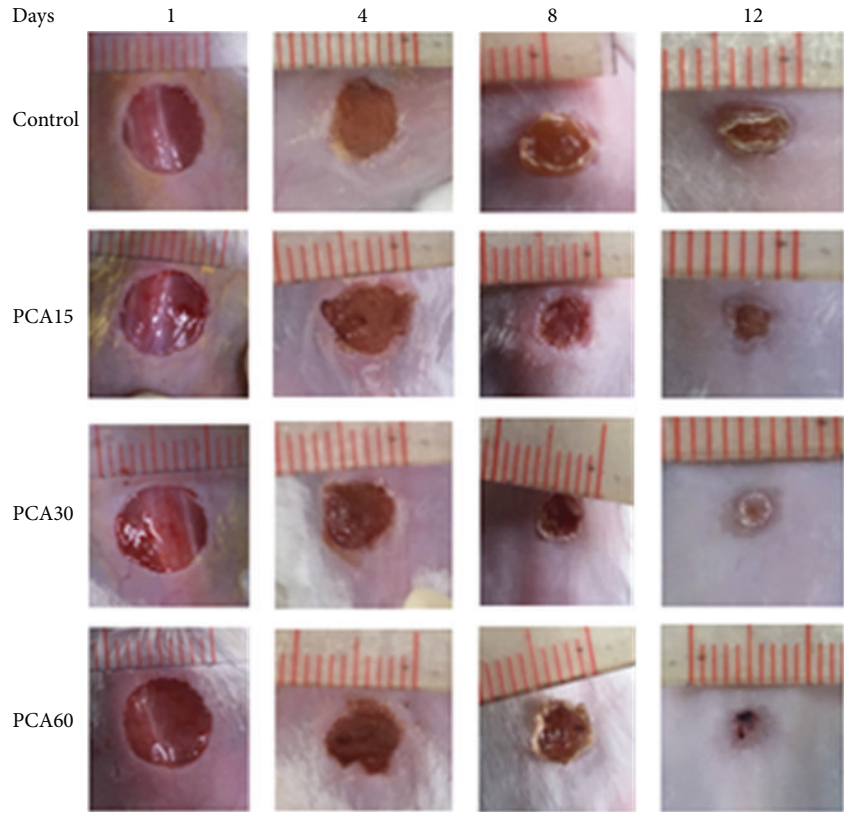

Figure 5: Representation images of the implanted area from day 1 to day 12.

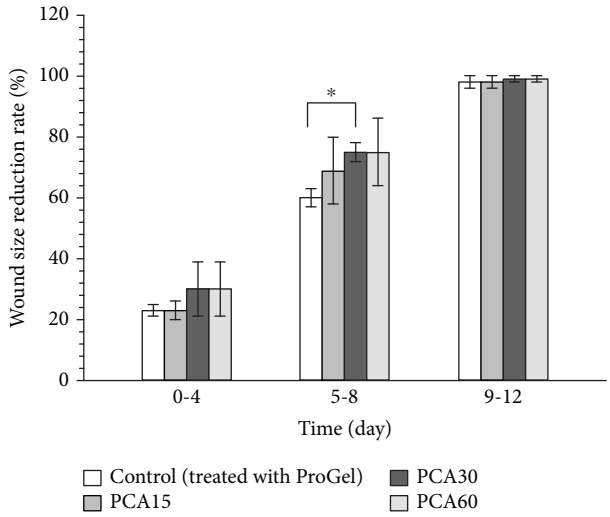

Figure 6: The rate of wound size reduction measured after 4 days, 8 days, and 12 days ($n = 3$). The asterisk on the bar graph indicates significant difference ($p < 0.05$).

3.3. Wound Size Reduction. Figure 5 illustrates the critical changes in wound size during the wound healing progression of each sample, which is measured for the calculation of wound size reduction rate as shown in Figure 6. The wounds of the control group closed slower than those of other groups (Figure 5). However, the measurement was relative, which makes the difference of samples compared to the control group not significant. On day 4, all the wounds had started healing from 23 ± 2 to 30 ± 9 (%). Then, there is a scab formation that covered the defected area, which led to the limitation in the observation of the diameter of wound size. On day 8, all groups reveal partial wound closing, from 60 ± 3 to 75 ± 11 (%). On day 12, the mice were euthanized, and the scabs on wounds were removed. It showed that all wounds closed up to 98 ± 4 to 99 ± 1 (%). The subjects treated with PCA gel showed better wound size reduction than the control group; however, among the gels, the PCA30 and PCA60 were considered to be more effective. Specifically, wounds of PCA30 and PCA60 groups reduced (30 ± 9 (0-4), 75 ± 3 for PCA30, 75 ± 11 for PCA60 (5-8), and 99 ± 1 (9-12) (%)), while those of PCA15 groups healed slower (23 ± 3 (0-4), 69 ± 11 (5-8), and 98 ± 2 (9-12) (%)).

3.4. Histological Analysis of the Skin Lesions. Histological results are presented in Figures 7–10. On the 12th day of postwound, complete epidermal covering forms over the wound surface in all groups, except PCA15. In Figure 7, PCA15 shows large necrosis and zones of necrotic inflammatory cells in the top of the wound site, which was considered to be caused by infection.

On the other hand, in the dermis, PCA15, PCA30, and PCA60 samples have granulation tissue and infiltrated inflammatory cells. Noticeably, wound of PCA30 was covered with necrotic tissue which is separated with the regenerative epidermis and prevents new tissue from the invasion of bacteria. This leads to stable growth of granule tissue, which

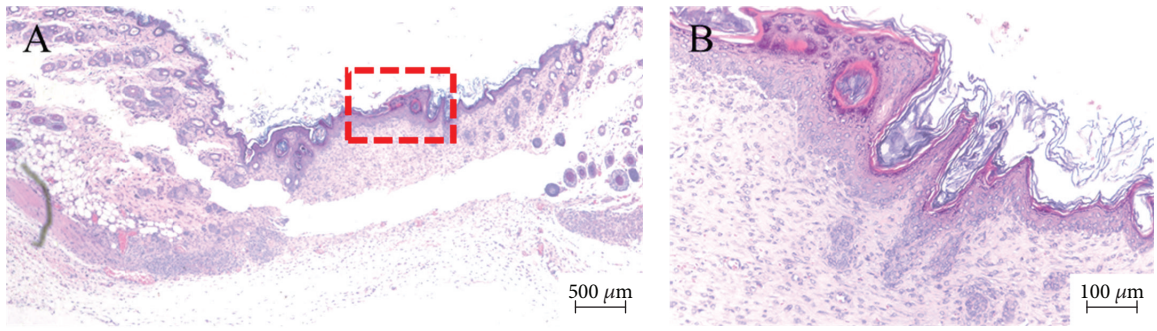

(a) (b)

Figure 7: H&E staining (a, b) images of the full defected area of the skin treated with ProGel® captured at 4x magnification and each enlarged part captured at 20x magnification.

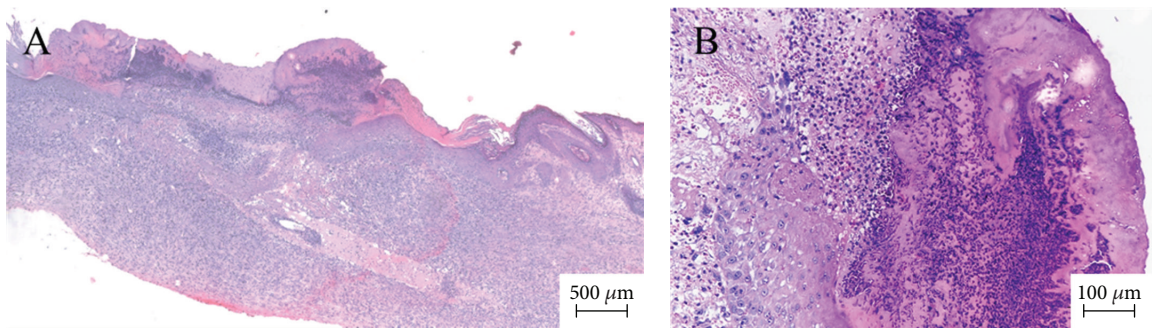

(a) (b)

Figure 8: H&E staining (a, b) images of the full defected area of the skin treated with PCA15 captured at 4x magnification and each enlarged part captured at 20x magnification.

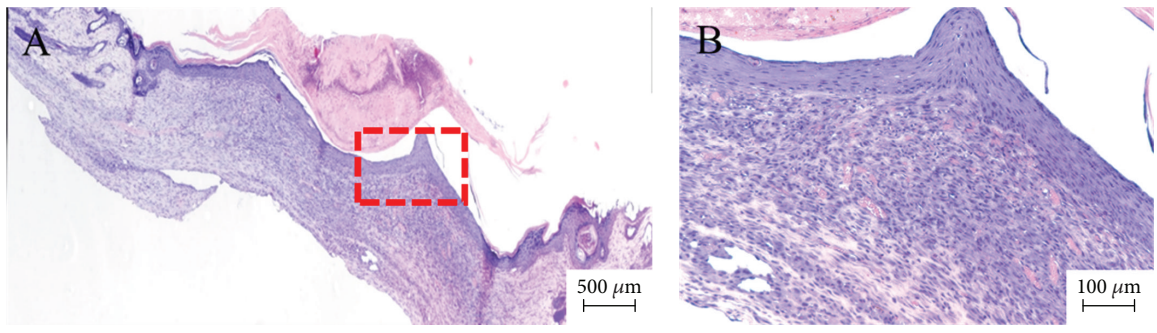

(a) (b)

Figure 9: H&E staining (a, b) images of the full defected area of the skin treated with PCA30 captured at 4x magnification and each enlarged part captured at 20x magnification.

enhances the healing rate. Furthermore, there are lesions appearing in the epidermis of the control and the dermis of PCA60 sample. This may result from the agglomerates of AgNPs. Those lesions resulted in necrosis to control samples and hemorrhage to PCA60 samples.

4. Discussion

In this study, three different concentrations of silver nanoparticles, 15 ppm, 30 ppm, and 60 ppm, were selected to create three types of samples: PCA15, PCA30, and PCA60. The ratio of PVA and CS, 10 wt% and 2 wt%, respectively, was unchanged following the previous study. These synthesized samples were compared with a commercial topical gel, ProGel®, containing 50 ppm AgNPs to evaluate the possibility for synthesized gel in the market.

Agar diffusion results indicate that increase of the concentration of silver ions leads to more positive antibacterial effect. These observations also reconfirm the results from the previous study that as the number of released Ag ions

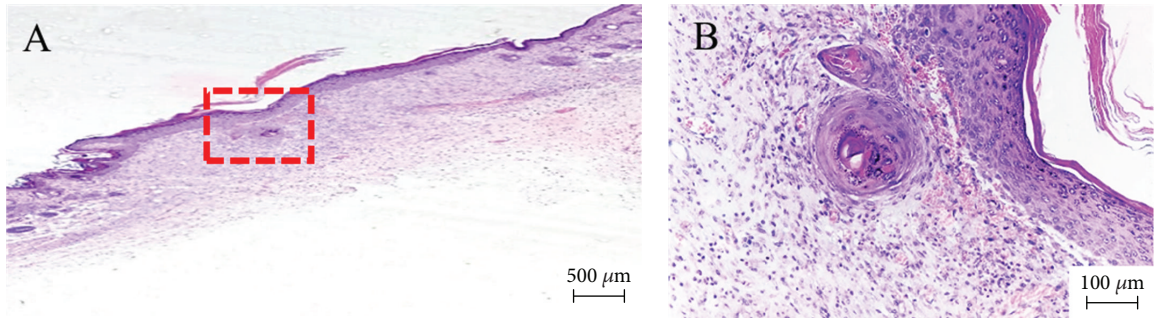

(a) (b)

Figure 10: H&E staining (a, b) images of the full defected area of the skin treated with PCA60 captured at 4x magnification and each enlarged part captured at 20x magnification.

increased, the inhibition zone enlarged [3]. Those synthesized hydrogels were aimed at entrapping the silver nanoparticle biopolymer matrix including both natural polymer (chitosan) and synthetic polymer (PVA). Those products take advantages of both polymer sources and enhanced the antibacterial property of silver nanoparticle.

However, the histological results illustrate a different view comparing with *in vitro* results. The PCA15 group shows severe necrosis and inflammation caused by infection, although the agar diffusion test proves antibacterial properties of PCA15 and TEM image displays the proper size of AgNPs. This means that the amount of AgNPs should be higher to assure effective antibacterial activity. Nevertheless, the excessive concentration of AgNPs could bring negative effects on wound healing, which can be seen in Figures 7(b) and 10(b). The PCA60 and control groups (50 ppm) induce lesions caused by the agglomerates of AgNPs which were shown in TEM images. Furthermore, there is a higher level of inflammation around lesions in mice treated with PCA60 and control gel. Studies suggest that AgNPs possess anti-inflammatory properties [43]. However, inferring from the findings of this study, it indicates that AgNPs do induce inflammation, and they generate reactive oxygen species (ROS) inside the cell, which enhances inflammation [5, 24, 44]. As a result, a higher concentration of AgNPs produces better antibacterial effects; however, the stability of them plays a more important role in minimization of side effects of AgNP application. Overall, when the regenerative tissue of the PCA30 group was compared with the regenerative tissue of the PCA60 and control groups, PCA30 samples show a better healing status with no harmful signs to the tissue.

5. Conclusion

In summary, we successfully determine the optimal formula of hydrogel composed of polyvinyl alcohol, chitosan, and AgNPs in terms of antibacterial properties and biocompatibility. The formation of AgNPs was confirmed via TEM imaging. PCA30 hydrogel possesses excellent antibacterial activity to *P. aeruginosa* and *S. aureus*. Besides, in vivo experiment proves the ability to promote wound healing of the PCA30 sample. Therefore, the hydrogel polyvinyl alcohol/chitosan loaded with AgNPs is a potential application as an antibacterial topical gel.

Data Availability

The data supporting the conclusions of this article are included within the article.

Conflicts of Interest

The authors declare that there is no conflict of interest regarding the publication of this paper.

Acknowledgments

This research is funded by the Vietnam National University Ho Chi Minh City (VNU-HCM) under grant number C2018-28-02.

References

[1] R. Goyal, L. K. Macri, H. M. Kaplan, and J. Kohn, "Nanoparticles and nanofibers for topical drug delivery," *Journal of Controlled Release*, vol. 240, pp. 77–92, 2016.

[2] P. H. C. Camargo, K. G. Satyanarayana, and F. Wypych, "Nanocomposites: synthesis, structure, properties and new application opportunities," *Materials Research*, vol. 12, no. 1, pp. 1–39, 2009.

[3] N. T. Hiep, H. C. Khon, V. V. T. Niem et al., "Microwave-assisted synthesis of chitosan/polyvinyl alcohol silver nanoparticles gel for wound dressing applications," *International Journal of Polymer Science*, vol. 2016, Article ID 1584046, 11 pages, 2016.

[4] P. L. Nadworny, J. F. Wang, E. E. Tredget, and R. E. Burrell, "Anti-inflammatory activity of nanocrystalline silver in a porcine contact dermatitis model," *Nanomedicine: Nanotechnology, Biology and Medicine*, vol. 4, no. 3, pp. 241–251, 2008.

[5] C. Rigo, L. Ferroni, I. Tocco et al., "Active silver nanoparticles for wound healing," *International Journal of Molecular Sciences*, vol. 14, no. 3, pp. 4817–4840, 2013.

[6] M. Hamzeh and G. I. Sunahara, "In vitro cytotoxicity and genotoxicity studies of titanium dioxide (TiO_2) nanoparticles in Chinese hamster lung fibroblast cells," *Toxicology in Vitro*, vol. 27, no. 2, pp. 864–873, 2013.

[7] S. Marin, G. Vlasceanu, R. Tiplea et al., "Applications and toxicity of silver nanoparticles: a recent review," *Current Topics in Medicinal Chemistry*, vol. 15, no. 16, pp. 1596–1604, 2015.

[8] R. Singh, U. U. Shedbalkar, S. A. Wadhwani, and B. A. Chopade, "Bacteriagenic silver nanoparticles: synthesis, mechanism, and applications," *Applied Microbiology and Biotechnology*, vol. 99, no. 11, pp. 4579–4593, 2015.

[9] T. Zhang, Y. J. Song, X. Y. Zhang, and J. Y. Wu, "Synthesis of silver nanostructures by multistep methods," *Sensors*, vol. 14, no. 4, pp. 5860–5889, 2014.

[10] S. Yu, Y. Yin, and J. Liu, "Silver nanoparticles in the environment," *Environmental Science: Processes & Impacts*, vol. 15, no. 1, pp. 78–92, 2013.

[11] S. B. N. Krishna, P. Govender, and J. K. Adam, "Biomedical applications and toxicity of nanosilver: a review," *Medical Technology SA*, vol. 29, no. 2, pp. 13–19, 2016.

[12] M. Rai, A. Yadav, and A. Gade, "Silver nanoparticles as a new generation of antimicrobials," *Biotechnology Advances*, vol. 27, no. 1, pp. 76–83, 2009.

[13] Q. L. Feng, J. Wu, G. Q. Chen, F. Z. Cui, T. N. Kim, and J. O. Kim, "A mechanistic study of the antibacterial effect of silver ions on *Escherichia coli* and *Staphylococcus aureus*," *Journal of Biomedical Materials Research*, vol. 52, no. 4, pp. 662–668, 2000.

[14] T. H. Nguyen, Y. H. Kim, H. Y. Song, and B. T. Lee, "Nano Ag loaded PVA nano-fibrous mats for skin applications," *Journal of Biomedical Materials Research Part B: Applied Biomaterials*, vol. 96B, no. 2, pp. 225–233, 2011.

[15] T.-H. Nguyen, K.-H. Lee, and B.-T. Lee, "Fabrication of Ag nanoparticles dispersed in PVA nanowire mats by microwave irradiation and electro-spinning," *Materials Science and Engineering: C*, vol. 30, no. 7, pp. 944–950, 2010.

[16] D. J. Ostlie, D. Juang, P. Aguayo et al., "Topical silver sulfadiazine vs collagenase ointment for the treatment of partial thickness burns in children: a prospective randomized trial," *Journal of Pediatric Surgery*, vol. 47, no. 6, pp. 1204–1207, 2012.

[17] A. M. Abdelgawad, S. M. Hudson, and O. J. Rojas, "Antimicrobial wound dressing nanofiber mats from multicomponent (chitosan/silver-NPs/polyvinyl alcohol) systems," *Carbohydrate Polymers*, vol. 100, pp. 166–178, 2014.

[18] Y. Zhou, Y. Zhao, L. Wang, L. Xu, M. Zhai, and S. Wei, "Radiation synthesis and characterization of nanosilver/gelatin/carboxymethyl chitosan hydrogel," *Radiation Physics and Chemistry*, vol. 81, no. 5, pp. 553–560, 2012.

[19] M. R. Gaafar, R. F. Mady, R. G. Diab, and T. I. Shalaby, "Chitosan and silver nanoparticles: promising anti-toxoplasma agents," *Experimental Parasitology*, vol. 143, pp. 30–38, 2014.

[20] M. Kong, X. G. Chen, K. Xing, and H. J. Park, "Antimicrobial properties of chitosan and mode of action: a state of the art review," *International Journal of Food Microbiology*, vol. 144, no. 1, pp. 51–63, 2010.

[21] P. I. Morgado, P. F. Lisboa, M. P. Ribeiro et al., "Poly(vinyl alcohol)/chitosan asymmetrical membranes: highly controlled morphology toward the ideal wound dressing," *Journal of Membrane Science*, vol. 469, pp. 262–271, 2014.

[22] S. Hajji, R. B. S. B. Salem, M. Hamdi et al., "Nanocomposite films based on chitosan–poly(vinyl alcohol) and silver nanoparticles with high antibacterial and antioxidant activities," *Process Safety and Environmental Protection*, vol. 111, pp. 112–121, 2017.

[23] C. Beer, R. Foldbjerg, Y. Hayashi, D. S. Sutherland, and H. Autrup, "Toxicity of silver nanoparticles—nanoparticle or silver ion?," *Toxicology Letters*, vol. 208, no. 3, pp. 286–292, 2012.

[24] C. Carlson, S. M. Hussain, A. M. Schrand et al., "Unique cellular interaction of silver nanoparticles: size-dependent generation of reactive oxygen species," *The Journal of Physical Chemistry B*, vol. 112, no. 43, pp. 13608–13619, 2008.

[25] S. Chernousova and M. Epple, "Silver as antibacterial agent: ion, nanoparticle, and metal," *Angewandte Chemie International Edition*, vol. 52, no. 6, pp. 1636–1653, 2013.

[26] X. Chen and H. J. Schluesener, "Nanosilver: a nanoproduct in medical application," *Toxicology Letters*, vol. 176, no. 1, pp. 1–12, 2008.

[27] A. Simon-Deckers, B. Gouget, M. Mayne-L'Hermite, N. Herlin-Boime, C. Reynaud, and M. Carrière, "In vitro investigation of oxide nanoparticle and carbon nanotube toxicity and intracellular accumulation in A549 human pneumocytes," *Toxicology*, vol. 253, no. 1–3, pp. 137–146, 2008.

[28] J. G. Cho, K. T. Kim, T. K. Ryu et al., "Stepwise embryonic toxicity of silver nanoparticles on *Oryzias latipes*," *BioMed Research International*, vol. 2013, Article ID 494671, 7 pages, 2013.

[29] M. Akter, M. T. Sikder, M. M. Rahman et al., "A systematic review on silver nanoparticles-induced cytotoxicity: physicochemical properties and perspectives," *Journal of Advanced Research*, vol. 9, pp. 1–16, 2018.

[30] J. Tang, L. Xiong, G. Zhou et al., "Silver nanoparticles crossing through and distribution in the blood-brain barrier in vitro," *Journal of Nanoscience and Nanotechnology*, vol. 10, no. 10, pp. 6313–6317, 2010.

[31] T.-T. Win-Shwe and H. Fujimaki, "Nanoparticles and neurotoxicity," *International Journal of Molecular Sciences*, vol. 12, no. 9, pp. 6267–6280, 2011.

[32] S. Aueviriyavit, D. Phummiratch, and R. Maniratanachote, "Mechanistic study on the biological effects of silver and gold nanoparticles in Caco-2 cells – induction of the Nrf2/HO-1 pathway by high concentrations of silver nanoparticles," *Toxicology Letters*, vol. 224, no. 1, pp. 73–83, 2014.

[33] Y. Ze, L. Zheng, X. Zhao et al., "Molecular mechanism of titanium dioxide nanoparticles-induced oxidative injury in the brain of mice," *Chemosphere*, vol. 92, no. 9, pp. 1183–1189, 2013.

[34] A. Nel, T. Xia, L. Mädler, and N. Li, "Toxic potential of materials at the nanolevel," *Science*, vol. 311, no. 5761, pp. 622–627, 2006.

[35] A. R. Mishra, J. Zheng, X. Tang, and P. L. Goering, "Silver nanoparticle-induced autophagic-lysosomal disruption and NLRP3-inflammasome activation in HepG2 cells is size-dependent," *Toxicological Sciences*, vol. 150, no. 2, pp. 473–487, 2016.

[36] M. M. Ahmed and M. M. A. Hussein, "Neurotoxic effects of silver nanoparticles and the protective role of rutin," *Biomedicine & Pharmacotherapy*, vol. 90, pp. 731–739, 2017.

[37] T. Takigawa and Y. Endo, "Effects of glutaraldehyde exposure on human health," *Journal of Occupational Health*, vol. 48, no. 2, pp. 75–87, 2006.

[38] S. Agnihotri, S. Mukherji, and S. Mukherji, "Antimicrobial chitosan–PVA hydrogel as a nanoreactor and immobilizing matrix for silver nanoparticles," *Applied Nanoscience*, vol. 2, no. 3, pp. 179–188, 2012.

[39] R. N. Oliveira, R. Rouze, B. Quilty et al., "Mechanical properties and in vitro characterization of polyvinyl alcohol-nano-silver hydrogel wound dressings," *Interface Focus*, vol. 4, no. 1, 2013.

[40] Z. Yang, D. Zhai, X. Wang, and J. Wei, "In situ synthesis of highly monodispersed nonaqueous small-sized silver nano-colloids and silver/polymer nanocomposites by ultraviolet photopolymerization," *Colloids and Surfaces A: Physicochemical and Engineering Aspects*, vol. 448, pp. 107–114, 2014.

[41] N.-T. Nguyen and J.-H. Liu, "A green method for in situ synthesis of poly(vinyl alcohol)/chitosan hydrogel thin films with entrapped silver nanoparticles," *Journal of the Taiwan Institute of Chemical Engineers*, vol. 45, no. 5, pp. 2827–2833, 2014.

[42] C. R. Harrell, V. Djonov, C. Fellabaum, and V. Volarevic, "Risks of using sterilization by gamma radiation: the other side of the coin," *International Journal of Medical Sciences*, vol. 15, no. 3, pp. 274–279, 2018.

[43] K. K. Y. Wong, S. O. F. Cheung, L. Huang et al., "Further evidence of the anti-inflammatory effects of silver nanoparticles," *ChemMedChem*, vol. 4, no. 7, pp. 1129–1135, 2009.

[44] R. Foldbjerg, P. Olesen, M. Hougaard, D. A. Dang, H. J. Hoffmann, and H. Autrup, "PVP-coated silver nanoparticles and silver ions induce reactive oxygen species, apoptosis and necrosis in THP-1 monocytes," *Toxicology Letters*, vol. 190, no. 2, pp. 156–162, 2009.

Hindawi
International Journal of Polymer Science
Volume 2019, Article ID 7651810, 11 pages
https://doi.org/10.1155/2019/7651810

Research Article

Fabrication of an Original Transparent PVA/Gelatin Hydrogel: *In Vitro* Antimicrobial Activity against Skin Pathogens

Naila Imtiaz,[1,8] Muhammad Bilal Khan Niazi,[2] Fehmida Fasim,[3] Barkat Ali Khan,[4] Syeda Asma Bano,[5] Ghulam Mujtaba Shah,[6] Malik Badshah,[7] Farid Menaa,[8] and Bushra Uzair[1]

[1]*Department of Bioinformatics and Biotechnology, International Islamic University, Islamabad, Pakistan*
[2]*Department of Chemical Engineering, National University of Sciences & Technology, Islamabad, Pakistan*
[3]*Discipline of Biomedical Science, Sydney Medical School, The University of Sydney, Sydney, NSW, Australia*
[4]*Department of Pharmaceutics, Gomal University, Dera Ismail Khan, Khyber Pakhtunkhwa, Pakistan*
[5]*Department of Microbiology, University of Haripur, Haripur, Pakistan*
[6]*Department of Microbiology, Hazara University, Mansehra, Pakistan*
[7]*Department of Microbiology, Quaid-i-Azam University, Islamabad 45320, Pakistan*
[8]*Department of Advanced Technologies, California Innovations Corporation, San Diego, CA, USA*

Correspondence should be addressed to Bushra Uzair; bushra.uzair@iiu.edu.pk

Received 11 October 2018; Revised 20 December 2018; Accepted 31 December 2018; Published 14 March 2019

Guest Editor: Mingqiang Li

The design of actively efficient and low-toxicity formulations against virulent bacterial strains causing skin infections remains a challenging task. The aim of the present study was to develop and evaluate *in vitro* a hydrogel impregnated with a known plant extract for topical applications against major skin bacteria. A poly(vinyl alcohol) (PVA)/gelatin hydrogel, namely HG, was prepared by esterification following the solution casting method. The gelling process was realized by cross-linking the synthetic polymer PVA and the biopolymer gelatin in the presence of hydrochloric acid (HCl). A crude extract of *Nigella sativa* seeds was then encapsulated in HG, and the resulting HGE was characterized morphologically (by Scanning Electron Microscopy (SEM)), structurally (by X-ray powder diffraction (XRD) and Fourier Transform Infrared (FTIR) spectroscopy), behaviorally (by swelling behavior), and biologically (by the agar well diffusion method). The results of HGE were compared to HG and HG impregnated with 10% acetic acid (HGAA). SEM sections of HGE revealed a dense and porous surface, suggesting a good hydrophilicity. X-ray diffractograms indicated that HGE and HG had a similar degree of crystallinity. FTIR spectra confirmed that esterification occurred between PVA and gelatin suggesting that the amine group is involved in the intercalation of the plant extract components in HG. Further, HGE was found to be as wettable and swellable as HG, suggesting a good biocompatibility. Eventually, HGE exerted a pronounced inhibitory effect against two major skin pathogens, the Gram-negative *Pseudomonas aeruginosa* and the Gram-positive *Staphylococcus aureus*, suggesting a good extract release. Taken together, the experimental data indicated that HGE might be a promising wound dressing.

1. Introduction

Despite advancements in the standards of healthcare and medical technology (i.e., sterilization and aseptic techniques), diseases caused by pathogens (e.g., bacteria, viruses, parasites, or fungi) remain major public health threats leading to struggling socioeconomic issues. Indeed, according to a World Health Organization (WHO) report, infectious diseases represent the second leading cause of mortality worldwide [1]. The increasing prevalence of infections, especially those associated with impaired wound healing and biomedical implant or device (e.g., catheter) failure [2], has spurred the development of new polymer formulations capable of exerting an antimicrobial activity [3].

S. aureus and *P. aeruginosa* represent the most common pathogens isolated from both acute and chronic injuries of different etiologies (e.g., wounds and burns), and so the current research is mainly focused in controlling their spread to avoid sepsis [4].Interestingly, wound and burn healing occurs more quickly with the help of dressing biopolymers such as hydrogels [4]. Hydrogels represent a class of highly hydrated 3D materials made of synthetic and natural polymers (e.g., polysaccharides such as alginate, starch, dextran, chitosan, or their derivatives, proteins such as gelatin and fibrin, polypeptides, and polynucleotides) [5, 6]. Their valuable properties, including hydrophilicity, biocompatibility, biodegradability, flexibility, and other mechanical properties similar to natural tissues, represent a tremendous interest in medicine. Thereby, their end use is quite noticeable in the tissue engineering (e.g., healing burns and wound dressing/wound fillers, contact lenses, absorbable sutures, hybrid-type organs such as encapsulated living cells, prostheses, and coated implants), pharmaceutical (e.g., drug delivery), and biomedical fields (e.g., asthma and osteoporosis treatments) [7].

Since the last decade, much attention was gained in the preparation and characterization of hydrogels, which are considered as a starting point when engineering antimicrobial materials [5]. Indeed, in addition to their possible inherent antimicrobial activities, particularly against multidrug resistant strains [8], they can be designed to convey acting antimicrobial agents that can be locally released over time, either through (noncovalent) encapsulation and/or (covalent) immobilization/coating [9]. Recently, Marchesan et al. described a relatively safe antimicrobial hydrogel that is formed *via* the self-assembly of the hydrophobic tripeptide ((D) Leu-Phe-Phe), which in the presence of ciprofloxacin took an active part in the integration of the drug into the peptide network allowing its eventual controlled release [10]. Nowadays, hydrogels made of PVA cross-linked with natural polymers (e.g., gelatin and polysaccharides) are well-studied for their biomedical applications and have long been particularly designed as wound dressing materials [11]. Interestingly, hydrogel features, including behavioral (e.g., swelling) and mechanical (e.g., strength) properties, may be modulated/optimized by the quantity of a given cross-linking agent or by the number of repeated freezing and thawing (F-T) cycles [12]. To date, there is still a paucity of reports on hydrogels impregnated with a plant extract exerting an antimicrobial activity. *N. sativa* L. (aka, black cumin) is largely considered as a marvelous herb that can cure numerous infirmities [13] and infections [14]. Nonetheless, the encapsulation of antimicrobial extracts from *N. sativa* has not been explored in hydrogels yet.

In this original *in vitro* study, we prepared and characterized HGE for its possible use as a scaffold for faster wound recovering/healing or for burn or skin infection management. The preparation was done according to a previously optimized method [15] using the casting method and a chemical cross-linker easily removable by washings. The morphology, structure, behavior, and potential antibacterial activity of HGE against the major skin pathogens, *S. aureus* and *P. aeruginosa*, were assessed.

2. Material and Methods

2.1. Chemicals, Strains, and Apparatus. The following commercially available chemicals were purchased from the indicated manufacturer and applied throughout this work without further purification. PVA (molecular weight: 125,000), HCl (35% pure), acetic acid, and Type B gelatin (~225 Bloom, for bacteriological purposes) were all purchased from Sigma-Aldrich Corp., St. Louis, MO, USA. Ethyl acetate was purchased from BDH Laboratory Supplies, England. Ethanol was purchased from Merck KGaA, Darmstadt, Germany.

Dry seeds of *N. sativa* were purchased locally and converted to powder form. Microbiological Oxoid™ culture media (i.e., Mueller-Hinton broth (MHB) and tryptone soy agar (TSA)) were supplied by Thermo Fisher Scientific Inc. *P. aeruginosa* (ATCC 27853) and *S. aureus* (ATCC 9144) were obtained from the American Type Culture Collection (ATCC), Manassas, VA 20108, USA. Oxoid™ Vancomycin (# CT0058B) and Gentamycin (# CT0024B) antimicrobial susceptibility discs were purchased from Thermo Fisher Scientific Inc.

The thermostatic incubator DHP-9052, the high-speed refrigerated centrifuge TGL20MC, and the multifrequency ultrasonic cleaning machine NB-600 DTY were all purchased from Zhengzhou Nanbei Instrument Equipment Co. Ltd., China. The X-ray diffractometer IPDS II was purchased from STOE & Cie GmbH, Darmstadt, Germany. The SEM Quanta 450 FEG was purchased from Thermo Fisher Scientific Inc. The FT/IR-4100 type A spectroscope was purchased from JASCO Inc., Easton, MD, USA.

2.2. Preparation of N. sativa Crude Extract. 2 grams of *N. sativa* seeds were crushed to granules using a stone rotor and poured into a beaker. Then, following a routine protocol [16], 8 mL of ethyl acetate (10%) was added to the beaker and the extract (1 : 4 w/v) was kept at room temperature for three days. The beaker remained uncovered to evaporate the maximum amount of solvent. The resulting concentrated extract was stored in a sterile container in a refrigerator until further use.

2.3. Preparation of Hydrogels. PVA/gelatin hydrogels were prepared with a weight composition of 75/25 under sterile conditions using the method described by Uzair et al. [14], with little modification. Briefly, 10 g of PVA was added into 100 mL of DD water (10% w/v), which was heated at 100°C for 1 hour under constant mechanical stirring (3500 rpm) to obtain total dissolution. The resulting homogeneous transparent aqueous solution was then mixed with 2.5 mg of gelatin and 0.05 mL of HCL (35%). The subsequent dispersion was stirred at 70°C for 30-45 minutes under constant mechanical stirring (100 ± 5 rpm) to carry out the esterification reaction between PVA and gelatin. Eventually, 100 mL of the thick dispersion solution was subdivided into three equal parts (33.3 mL each). Solution 1, in which nothing was added, served as the "internal control." Solution 2, in which 5 mL of acetic acid (10%) was added, served as the "external control." Solution 3, in which

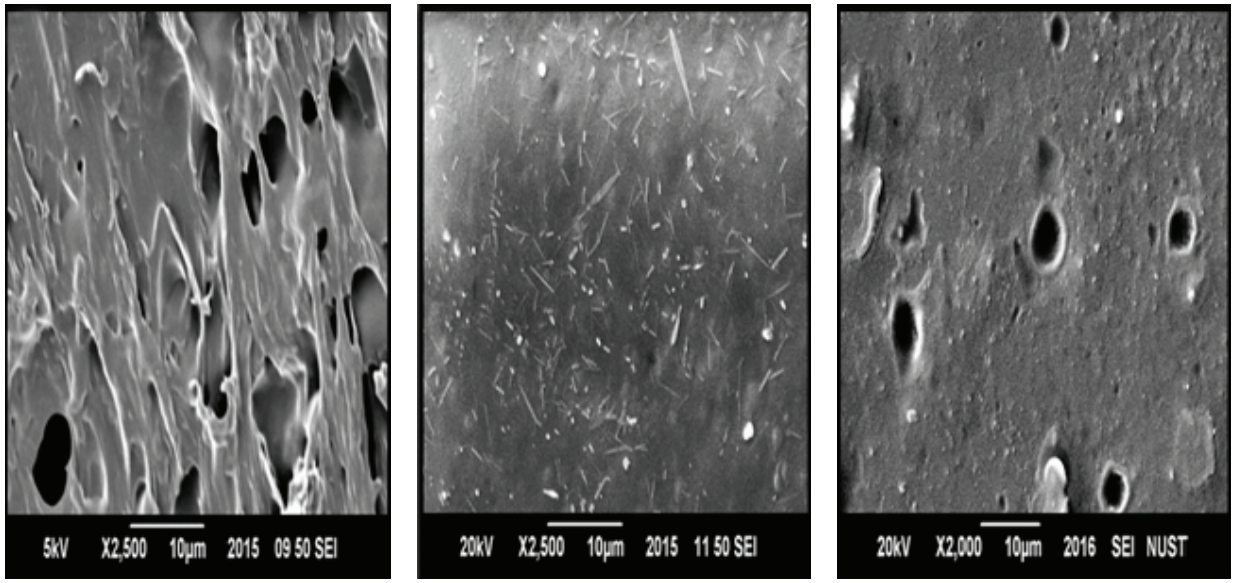

(a) (b) (c)

Figure 1: SEM micrographs representing the topographic view of the prepared hydrogels: (a) HG; (b) HGAA; (c) HGE.

5 mL (equivalent to 1 g) of the crude extract of *N. sativa* was added, served as "test."

These three solutions were separately mixed and exposed to ultrasonic waves for 2 hours in order to homogenize and remove bubbles/air, respectively. Then, each solution was converted into a membrane by the conventional solution casting method. Thereby, the three solutions were poured independently in standard 90 mm petri dishes and left overnight for drying at room temperature. Importantly, they were washed thoroughly with DD water to remove HCl and subsequently dried at 37°C for 3 hours in an oven. Then, 2 mL of glycerol was added to overcome the brittleness of the membrane. Eventually, the prepared hydrogels, i.e., HG (PVA/gelatin), HGAA (HG+acetic acid), and HGE (HG+extract), were peeled off with the help of forceps and stored in airtight pouches/ziplock packets until further use.

2.4. Characterizations of the Prepared Hydrogels

2.4.1. Scanning Electron Microscopy (SEM). To obtain high-resolution imaging of surface morphology, all the sterile hydrogels were subjected to SEM measurements using 1/1 cm samples coated with gold. This coating is required to obtain a clear image/micrograph of an insulating material, although it is so thin (200 Å) that it does not hinder the identification of specific minerals [17].

2.4.2. X-Ray Powder Diffraction (XRD). In order to determine the crystallinity of all the hydrogels, XRD (STOE & Cie GmbH, Darmstadt, Germany, θ-θ) was performed using Cu radiation generated at 40 kV and 40 mA. The range of the diffraction angle was 10 to 70° 2θ. The 0.02° step size of 2θ was maintained at a scan speed of 2 s/step. PVA 10% was used as a supplementary control.

2.4.3. Fourier Transform Infrared (FTIR) Spectroscopy. FTIR spectroscopy was employed to characterize the presence of specific functional chemical groups and their interactions/complexations in HG and HGE. The cross-linking of PVA with gelatin was also checked with this technique [10]. The prepared hydrogels were milled and mixed at a ratio of 1.0% to KBr powder dried for 24 hours at 120°C. FTIR spectra were obtained in the range of 4000-400 cm^{-1}, with a scanning speed of 2 mm/sec and a 4 cm^{-1} resolution.

2.4.4. Swelling Behavior. The dynamic swelling behavior of HG and HGE was investigated to determine the mechanism of water transport through these hydrogels. Thereby, the hydrogels were cut and the initial weight was determined (W_i). The samples were then kept in DD water (swelling medium) at room temperature. Subsequently, the samples were taken out from the DD water (pH~5.6) at regular intervals of time (i.e., every 2 hours for 8 hours), and each sample weight was determined at room temperature (W_f). Special care was taken to ensure that there was no water present during weighting. The process was continued until the saturation of final weight is observed. Swelling percentage was calculated using the following formula [18]:

$$\text{Swelling\%} = \left[\frac{W_f - W_i}{W_i}\right] \times 100, \quad (1)$$

where W_f is the weight of the product after hydration, and W_i is the weight of the dried product.

2.4.5. Antimicrobial Activity. Skin pathogens, i.e., *Pseudomonas aeruginosa* and *Staphylococcus aureus*, were cultured aerobically in Mueller-Hinton broth (MHB) and subcultured on tryptone soy agar (TSA), as reported by another group [19]. The antimicrobial potential of the prepared gel was tested

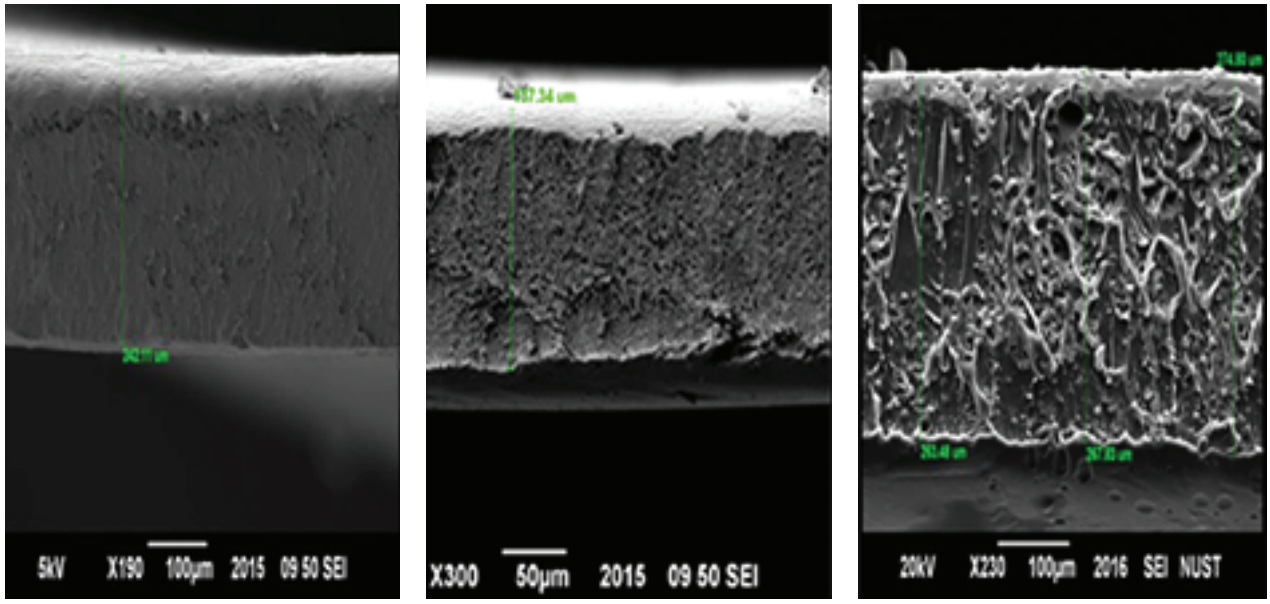

(a) (b) (c)

Figure 2: SEM micrographs representing the transverse view of the prepared hydrogels: (a) HG; (b) HGAA; (c) HGE.

by the agar well diffusion method described elsewhere [20], with little modification. Inoculums of *S. aureus* (ATCC 9144, the so-called "Oxford *Staphylococcus*") [21] or *P. aeruginosa* (ATCC 27853) were prepared from a 24-hour culture on *Luria-Bertani* (LB) broth, and the turbidity of the suspension made in a sterile saline solution (0.85%) was adjusted with a spectrophotometer at 530 nm to obtain a final concentration that matches a 0.5 McFarland standard ($0.5\text{-}2.5 \times 10^3$). 20 mL of Mueller-Hinton *agar* (*MHA*) was melted, cooled to 55°C, and poured into a 90 mm petri dish. The plates were allowed to cool down on a leveled surface. Once the medium had solidified, each bacterial strain was swabbed uniformly across a MHA plate. Then, 6 mm wells were cut out of the agar, and hydrogels (i.e., HG, HGAA, and HGE) cut in 6 mm diameter pieces were placed into each of these wells. Control antibiotic discs, i.e., Gentamycin (10 μg) for *S. aureus* or Vancomycin (30 μg) for *P. aeruginosa*, were placed on the respective plates. Eventually, the inoculated plates were incubated at 37°C for 24 hours, after which the respective sizes of the zones of inhibition were measured (in mm). CLSI disc diffusion breakpoints were used for the interpretation of the zones of inhibition against the control antibiotic discs [22].

2.5. Statistics. The statistical analysis of most results (i.e., SEM, swelling behavior, and antimicrobial assays) was performed using the software package SPSS Statistics 17.0 following one-way analysis of variance (ANOVA), at a significance level of 95%. ANOVA statistical analysis was used to determine whether the difference between the groups studied was significant. To ensure accuracy, all data were obtained from three sets of independent experiments. Data were presented as means ± standard error of the mean (SEM) with statistical annotations when required. Differences with $p < 0.05$ were considered statistically significant.

3. Results and Discussion

3.1. Microarchitecture of the Synthesized Hydrogels. Topographic view (i.e., surface) and transverse view (i.e., thickness) of HG, HGAA, and HGE were obtained by SEM (Figures 1 and 2). The topographic microscopic view of HG (Figure 1(a)) revealed a complex surface, i.e., a crispy 3D inner structure containing irregular voids arranged within disorganized/nondirectional lamellas, suggesting valuable hydrophilic characteristics. However, the topographic view of HGAA (Figure 1) indicated a unique crystallized surface, exempt of voids, which may be due to the partial dissolution of acetic acid in the final solution. Interestingly, the topographic analysis of HGE (Figure 1) depicted a less complex microarchitecture than HG, i.e., a granular, rough, and porous surface containing a few aerosols with clearer delimited voids, which is representative of a good hydrophilicity. Besides, we noticed that the expected impregnation of the extract did not appear to have a significant effect on membrane structure distortion. The preparation, properties, and applications of such type of hydrogel have been previously described [15]. SEM analyses of HGE reveal a dense and porous-like inner structure with a less complex microarchitecture than HG, although the size and distribution of macropores were not completely investigated by porosimetry. These data are usually indicative of a good hydrophilicity, a natural characteristic of hydrogels [23]. The SEM images of HG also evolve a dense membrane and evidence a typical 3D structure, the data of which are consistent with a previous study [24].

The transverse microscopic view of HG (Figure 2) revealed a significantly ($p < 0.05$) higher average thickness ($241.49 \pm 0.55\,\mu$m) than HGAA (Figure 3(b)) ($138.37 \pm 0.51\,\mu$m). Interestingly, the average thickness of HGE ($270.32 \pm 1.54\,\mu$m) was significantly ($p < 0.05$) the highest (Figure 2), and it could be explained by a higher

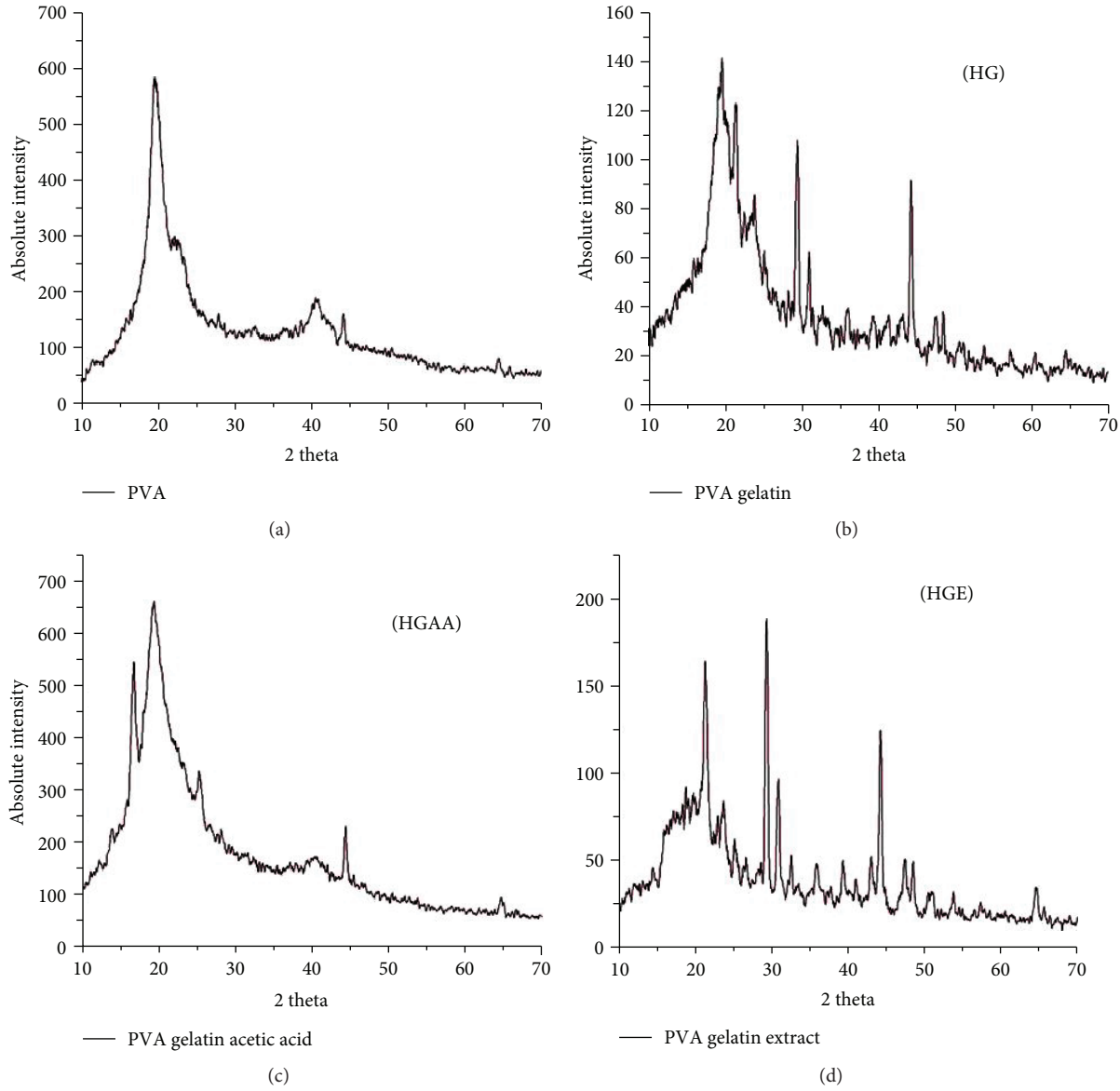

Figure 3: X-ray diffractograms of the prepared hydrogels: (a) PVA; (b) HG; (c) HGAA; (d) HGE.

viscosity, an important parameter for the hydrogel composition. Nie et al. [11] reported that composite or hybrid hydrogels (e.g., PVA/gelatin hydrogel) are the best choice of material compared to other dressing forms because they fit the requirements for the ideal wound dressing, including better mechanical stability at the swollen state (its intrinsic properties include biocompatibility, hydrophilicity/high degree of swelling in aqueous solution, elasticity, resemblance to rubber, and absence of detectable toxicity) [3]. Besides, gelatin is a natural polymer that is able to activate macrophages, displays a high hemostatic effect, and increases the swelling % capacity of a PVA hydrogel, making it very useful for a wide variety of wound dressings [25]. The possible reason why the topographic view of HG and HE showed a significant difference may be because the system turned acidic in the gel with acetic acid, and there is a possibility that the nature of the gelation mechanism was changed.

Table 1: Absolute intensities of the main peaks at 2θ from XRD patterns of the prepared hydrogels.

Hydrogels types	20° 2θ	28° 2θ	40° 2θ	44° 2θ
PVA	582	ND*	186	160
HG	142	108	36	188
HGAA	665	340	175	234
HGE	164	92	50	124

Nie et al. [11] reported that the in acidic system, the nature of the gelation mechanism is deprotonation and entanglement. The difference in the gelation mechanism leads to a great difference in the gelation process, hence the topography of different gels was changed. The HE cross-linked mesh-like structure, with interconnected micropores evident in Figure 2(c), provides efficient channels for rapid water

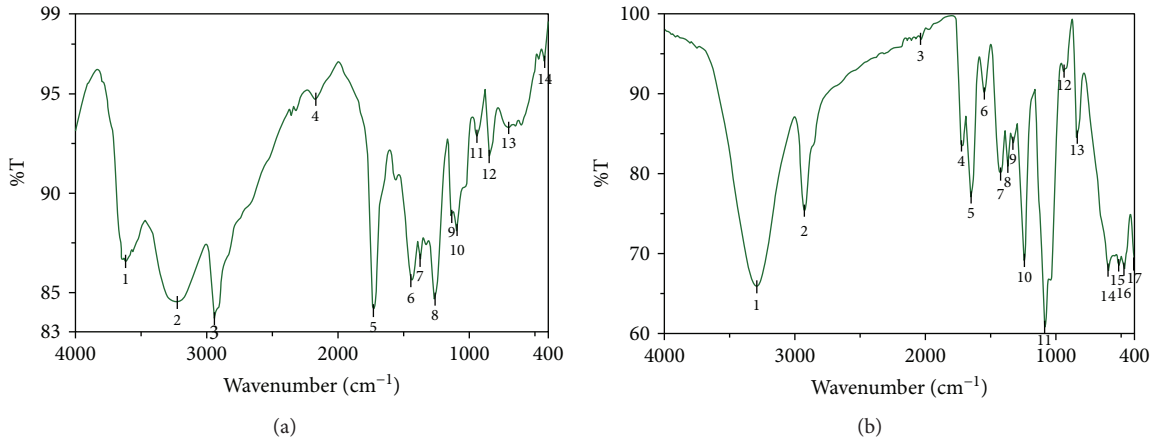

Figure 4: FTIR spectra of the prepared hydrogels: (a) HG; (b) HGE.

Table 2: Main FTIR spectral assignments in the prepared hydrogels.

Hydrogel	Wave number (cm^{-1})	Peak intensity	Nature of bond(s)	Spectral assignment #
HG	3615	Low	O—H	1
	3222	Low	H—H	2
	1730	Low	C=O	5
	1443	Medium	C—H	7
HE	3291	Low	—NH_3^+	1
	1652	Strong	C=O and NH_2	6
	1087	Low	C—O	11
	943	Strong	CH_2	12

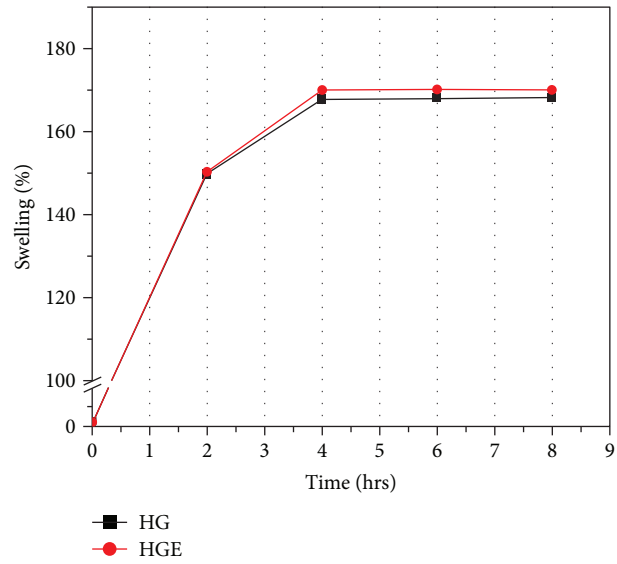

Figure 5: Swelling behavior of the prepared hydrogels over a period of 8 hours.

transport, which explains the potential of our hydrogel samples reaching equilibrium swelling in only 8 hours. In the acidic system, the gelation process is promoted by the diffusion of OH^- from the coagulation bath instead of the formation of cross-links in the whole system as observed in Figure 1(b).

3.2. Structural Characterization of the Prepared Hydrogels. The XRD patterns of PVA, HG, HGAA, and HGE are presented in Figure 3. The absolute intensities of the main peaks corresponding to each hydrogel are presented in Table 1. The XRD pattern of PVA, used as a supplementary control, displayed a sharp peak of relatively high intensity (~582) at around 20° 2θ and peaks of much smaller intensity at around 40° 2θ (~186) and at around 44° 2θ (~160) (Figure 3). Importantly, the XRD patterns of HG (Figure 4(b)), HGAA (Figure 3(c)), and HGE (Figure 3) also elicited prominent peaks of relative intensity at around 20° 2θ (~142, ~665, and ~164, respectively), at around 40° 2θ (~36, ~175, and ~50, respectively), and at around 44° 2θ (~188, ~234, and ~124, respectively). These data confirmed the presence of PVA in their composition. Furthermore, we noticed sharp peaks at around 28° 2θ (~108, ~340, and ~92, respectively), strongly suggesting that the respective peak was due to the presence of gelatin in these three hydrogels. Nevertheless, considering that in similar previously published experimental conditions [15] the crystallinity of HG < crystallinity PVA < crystallinity of gelatin, the peak observed at around 28° 2θ due to gelatin, once cross-linked to PVA, is related to lower crystallinity. Eventually, HGAA has an XRD pattern close to the one observed for PVA, displaying a peak of low relative (and not absolute) intensity at around 28° 2θ, suggesting that acetic acid is likely to be involved in maintaining a better crystalline state of HG.

Besides, in order to ensure the cross-linking of PVA with gelatin [14] and to identify specific functional chemical groups involved in the intercalation of the plant extract components in the hydrogel, major FTIR spectral assignments obtained for HGE were compared to that of HG (Table 2).

The FTIR spectrum of HG (Figure 5(a)) showed peaks of low intensity at 3615 cm^{-1} and 3222 cm^{-1} and a peak of medium intensity at 1443 cm^{-1}, which are commonly due to the stretching vibration of free O-H (hydroxyl) bonds [15] and H-H bonds and the bending vibrations of C-H bonds, respectively. Intramolecular and intermolecular hydrogen

Table 3: Water holding ability of a synthesized prepared hydrogel.

Type	0	2 hours	4 hours	6 hours	8 hours
HG	2 ± 0.07^{a}	149.67 ± 0.24^{b}	167.87 ± 0.22^{c}	168.00 ± 0.2^{c}	168.07 ± 0.11^{c}
HGE	2 ± 0.07^{a}	150.27 ± 0.18^{b}	169.97 ± 0.24^{c}	170.1 ± 0.27^{c}	170.05 ± 0.25^{c}

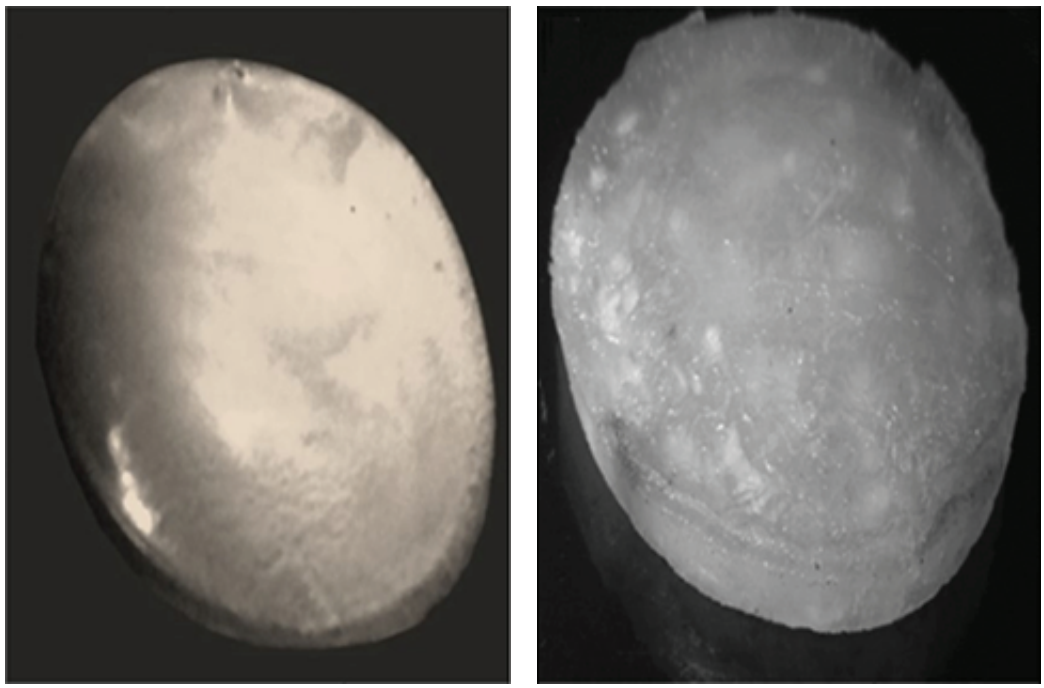

(a) (b)

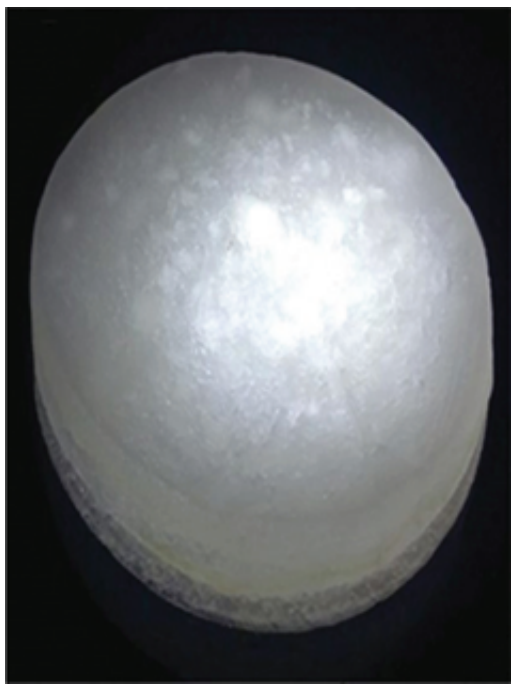

(c)

Figure 6: Water holding ability of the prepared hydrogels: (a) state of HGE prior to swelling; (b) state of HGE after 2 hours of swelling; (c) state of HGE after 8 hours of swelling.

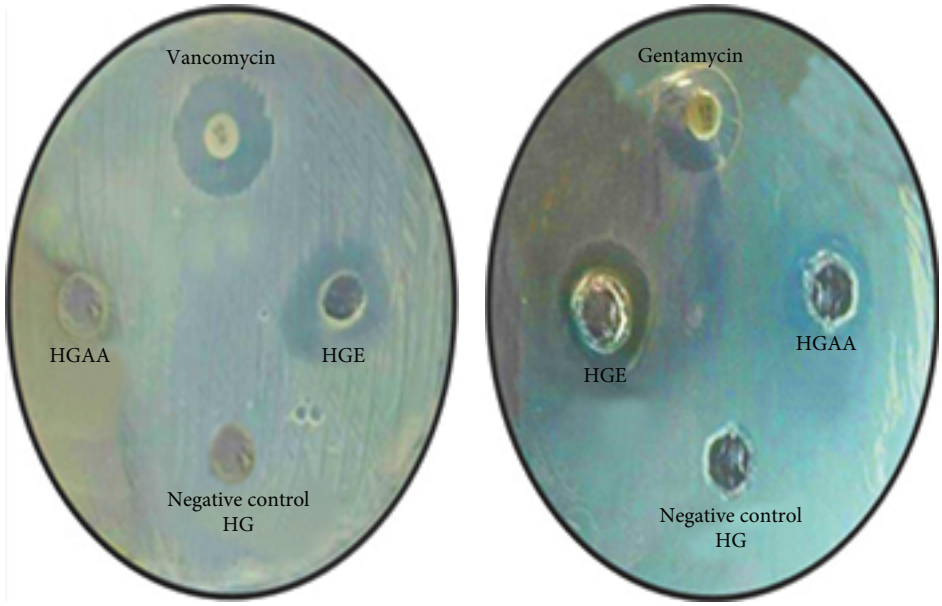

(a) (b)

Figure 7: Inhibition zones reflecting the activity of the prepared hydrogels against skin pathogens: (a) against *S. aureus*; (b) against *P. aeruginosa.*

Table 4: Inhibition zones (mm) caused by the prepared hydrogels against major skin pathogens.

	HGAA	HE	VAN	GEN	HG
S. aureus	ND*	20.07 ± 0.24^{b}	21.95 ± 0.45^{d}	—	ND*
P. aeruginosa	10.27 ± 0.38^{a}	18.00 ± 0.20^{c}	—	20.17 ± 0.31^{b}	ND*

ND* stands for "not detectable"; variables with the same letter means $p > 0.05$; variables having different letters means $p < 0.05$.

bonding are expected to occur among PVA chains due to high hydrophilic forces [26]. The peak of low intensity at 1730 cm^{-1} corresponded to a C=O ester bond, indicating the formation of an expected esterified product (i.e., esterification of all the free carboxylic groups of gelatin) [15]. Both C-H and C=C are typical of the alkane structure.

Besides, the FTIR spectrum of HGE (Figure 4) shows a peak of low intensity at 3291 cm^{-1} which indicates an asymmetrical stretching of $-NH_3^+$ in amino acids and a peak of strong intensity at 1652 cm^{-1} which is due to two bands stretching C=O and NH_2 in primary amides. The peak of low intensity at 1087 cm^{-1} is due to C-O stretching, and the peak of strong intensity at 943 cm^{-1} is due to CH_2 which is out-of-plane wagging in $CH{=}CH_2$ of vinyl compounds. Taken together, FTIR analysis confirmed the cross-linking between PVA and gelatin and determined a specific functional group (i.e., amine $-NH_3^+$) involved in the intercalation of the plant extract components in the hydrogel. FT-IR spectra analyses show that the esterification, induced by chemical cross-linking, occurred between the hydroxyl group of PVA and the carboxyl group of gelatin. Our data are concordant with other observations [16]. The infrared spectra of HGE also indicate that the plant extract did engage in $-NH_3^+$ bonds with the polymeric matrix, which may reduce its potential antimicrobial activity as hypothesized elsewhere [27]. Interestingly, the presence of free amine groups plays an important role in water uptake because of their hydrophilic nature [15].

3.3. Swelling Behavior of the Prepared Hydrogels. The swelling rates of HGE were compared to that of HG, and its water holding capacity (Figure 5 and Table 3) has been evaluated during 8 hours. The resulting curves obtained for HGE and HG were superposed, indicating no significant ($p > 0.05$) differences between the swelling rates (Figure 6). Thereby, in a first step, a quick increase in swelling percentage (about 150%) is observed during the first two hours of immersion/soaking which further increased gradually to about 170% for 2 hours before a saturation/equilibrium step occurred for 4 hours.

Overall, our data showed that the swelling behavior values were greater than 100% during many hours for both hydrogels, which may indicate that HGE has good biocompatibility *in vivo* and a valuable water holding capacity during the course period. Indeed, these data are of great interest in a clinical setting since swelling % decides the time of substitution of a wound dressing, which is usually short [18, 26]. Importantly, these superabsorbent hydrogels are usually biocompatible in nature and are nonirritating to soft tissues when in contact with them [28]. The potential capacity of HGE to uptake and retain wound liquids/exudates appears relatively good and sufficient for its application in a clinical setting. Indeed, in

the case of wound dressing, the shelf life of a hydrogel is not the problem, as the hydrogel is used once for a short period [29]. Eventually, we noticed that the original shape of the HG was maintained after impregnation of the plant extract in HG, which may be explained by the permanent junction-induced mechanical strength after chemical cross-linking [30].

3.4. Antimicrobial Activity of the Prepared Hydrogels. The antimicrobial activities of HGE were checked by the agar well diffusion method against two major skin pathogens, namely *S. aureus* (Figure 7(a)) and *P. aeruginosa* (Figure 7(b)). External positive controls included the glycopeptide antibiotic Vancomycin/VAN (30 μg) against *S. aureus* and the aminoglycoside antibiotic Gentamycin/GEN (10 μg) against *P. aeruginosa*. HG was used as a potential negative control, and HGAA as a potential positive control. A zone of inhibition smaller than 5 mm meant a resistance of the strain to the product (i.e., hydrogel or known antibiotic). Interestingly, HGE showed higher sensitivity zones against *S. aureus* (20 mm) and *P. aeruginosa* (18 mm) compared to that of HGAA which was only sensitive against *P. aeruginosa* (10 mm) (Table 4). The zones of inhibition for Vancomycin (22 mm) and Gentamycin (20 mm) were slightly larger compared to that of HGE when tested on *S. aureus* and *P. aeruginosa*, respectively (Table 4). Besides, both strains were resistant to HG (Figures 7(a) and 7(b) and Table 4), strongly demonstrating no inherent antimicrobial activity of the unloaded/unfilled HG. Vancomycin is a glycopeptide which is considered as the drug of choice for first-line treatment against *S. aureus*, including Methicillin Resistant *S. aureus* (MRSA) infections [31]. Gentamycin is an aminoglycoside widely recommended in the treatment of *P. aeruginosa* infections [31], since it is one of the only antibiotic agents to which strains are regularly sensitive [32, 33]. Besides, no zone of inhibition was observed using HG against the two strains. These observations indicate a sustained release of the plant extract and not an inherent antibacterial property of HG (at least when used against the selected strains).

4. Conclusions

This work was realized to explore a natural antimicrobial agent that can be used to design an original wound dressing material. In the current study, HGE was made by esterification using the conventional solution casting method. Based on its physical, behavioral, and biological characterizations, we found that HGE is able to maintain the hydrophilicity and crystallinity of HG. To the best of our knowledge, our study represents the first report about the *N. sativa* extract encapsulated into HG, which most importantly presented a good characteristic in relation to (i) the release of the active antimicrobial principle verified through a swelling test performed at dermatological pH and (ii) *in vitro* antimicrobial activity. Therefore, HGE showed a promising potential for application as a wound dressing biomaterial and may be a promising alternative formulation against at least certain Gram-positive and Gram-negative strains. To ensure its topical applicability, our ongoing project consists of further evaluating HGE regarding (i) the influence of weight ratios on properties, including gel content; (ii) its mechanical resistance/tensile strength; (iii) its thermal properties; (iv) its biodegradation rate; (v) its water vapor transmission rate; (vi) the release mechanism of extract from HG (e.g., Fickian diffusion); (vii) its bioactivity against a bunch of resistant skin strains including the determination of its bacteriostatic or microbicide effects; and (viii) its efficacy (e.g., cycles of use) and safety (e.g., cytocompatibility and biocompatibility by acute toxicity tests ex-vivo and *in vivo*).

Abbreviations

F-T:	Freezing-thawing
FTIR:	Fourier transform infrared (spectroscopy)
HG:	PVA/gelatin hydrogel
HGAA:	HG filled with acetic acid
HGE:	HG loaded with extract
MDR:	Multidrug resistant
MHB:	Mueller-Hinton broth
NA:	Not applicable
ND:	Not determined
ND*:	Not detectable
P. aeruginosa:	*Pseudomonas aeruginosa*
PEG:	Poly(ethylene glycol)
PVA:	Poly(vinyl alcohol)
S. aureus:	*Staphylococcus aureus*
SEM:	Scanning electron microscopy
TSA:	Tryptone soy agar
UV:	Ultraviolet
XRD:	X-ray powder diffraction.

Data Availability

All required data is available and can be provided on request.

Conflicts of Interest

The authors declare that they have no conflicts of interest.

Acknowledgments

The authors would like to acknowledge the Higher Education Commission of Pakistan for project no. PM IPFP/HRD/-HEC/2010/1815 and the International Islamic University, Islamabad, Pakistan for supporting this research project. The authors also thank Dr. Abder Menaa, MD, for his pertinent suggestions and ideas in translational medicine.

Supplementary Materials

Figure S1: flow chart of the methodology used for the preparation of hydrogels. Figure S2: preparation of hydrogels (A). The hydrogel is peeled off with the help of forceps from a 90 mm petri dish (B). The hydrogel is saved in a ziplock packet. *(Supplementary Materials)*

References

[1] C. Mathers, D. M. Fat, and J. Boerma, *The Global Burden of Disease: 2004 Update*, World Health Organization, 2008, http://www.who.int/healthinfo/global_burden_disease/2004_report_update/en/.

[2] R. Djeribi, W. Bouchloukh, T. Jouenne, and B. Menaa, "Characterization of bacterial biofilms formed on urinary catheters," *American Journal of Infection Control*, vol. 40, no. 9, pp. 854–859, 2012.

[3] E. A. Kamoun, X. Chen, M. S. Mohy Eldin, and E.-R. S. Kenawy, "Crosslinked poly(vinyl alcohol) hydrogels for wound dressing applications: a review of remarkably blended polymers," *Arabian Journal of Chemistry*, vol. 8, no. 1, pp. 1–14, 2015.

[4] S. Bhowmick, S. Mohanty, and V. Koul, "Fabrication of transparent quaternized PVA/silver nanocomposite hydrogel and its evaluation as an antimicrobial patch for wound care systems," *Journal of Materials Science. Materials in Medicine*, vol. 27, no. 11, p. 160, 2016.

[5] A. Salomé Veiga and J. P. Schneider, "Antimicrobial hydrogels for the treatment of infection," *Biopolymers*, vol. 100, no. 6, pp. 637–644, 2013.

[6] C. Y. Loo, P. M. Young, W. H. Lee, R. Cavaliere, C. B. Whitchurch, and R. Rohanizadeh, "Non-cytotoxic silver nanoparticle-polyvinyl alcohol hydrogels with anti-biofilm activity: designed as coatings for endotracheal tube materials," *Biofouling*, vol. 30, no. 7, pp. 773–788, 2014.

[7] C. M. González-Henríquez, M. A. Sarabia-Vallejos, and J. Rodriguez-Hernandez, "Advances in the fabrication of antimicrobial hydrogels for biomedical applications," *Materials*, vol. 10, no. 3, p. 232, 2017.

[8] V. W. L. Ng, J. M. W. Chan, H. Sardon et al., "Antimicrobial hydrogels: a new weapon in the arsenal against multidrug-resistant infections," *Advanced Drug Delivery Reviews*, vol. 78, pp. 46–62, 2014.

[9] S. C. Lee, I. K. Kwon, and K. Park, "Hydrogels for delivery of bioactive agents: a historical perspective," *Advanced Drug Delivery Reviews*, vol. 65, no. 1, pp. 17–20, 2013.

[10] S. Marchesan, Y. Qu, L. J. Waddington et al., "Self-assembly of ciprofloxacin and a tripeptide into an antimicrobial nanostructured hydrogel," *Biomaterials*, vol. 34, no. 14, pp. 3678–3687, 2013.

[11] J. Nie, Z. Wang, and Q. Hu, "Difference between chitosan hydrogels via alkaline and acidic solvent systems," *Scientific Reports*, vol. 6, no. 1, article 36053, 2016.

[12] Q. Chai, Y. Jiao, and X. Yu, "Hydrogels for biomedical applications: their characteristics and the mechanisms behind them," *Gels*, vol. 3, no. 1, p. 6, 2017.

[13] A. Ahmad, A. Husain, M. Mujeeb et al., "A review on therapeutic potential of *Nigella sativa*: a miracle herb," *Asian Pacific Journal of Tropical Biomedicine*, vol. 3, no. 5, pp. 337–352, 2013.

[14] B. Uzair, A. Hameed, S. Nazir et al., "Synergism between *Nigella sativa* seeds extract and synthetic antibiotics against Mec a gene positive human strains of *Staphylococcus aureus*," *International Journal of Pharmacology*, vol. 13, no. 8, pp. 958–968, 2017.

[15] K. Pal, A. K. Banthia, and D. K. Majumdar, "Preparation and characterization of polyvinyl alcohol-gelatin hydrogel membranes for biomedical applications," *AAPS PharmSciTech*, vol. 8, no. 1, pp. E142–E146, 2007.

[16] G.-Y. Zuo, X.-J. Zhang, C.-X. Yang, J. Han, G.-C. Wang, and Z.-Q. Bian, "Evaluation of traditional Chinese medicinal plants for anti-MRSA activity with reference to the treatment record of infectious diseases," *Molecules*, vol. 17, no. 3, pp. 2955–2967, 2012.

[17] J. E. Welton, *SEM Petrology Atlas, Chevron Oil Field Research Company, Methods in Exploration Series No. 4*, The American Association of Petroleum Geologists, Oklahoma, OK, USA, 2003.

[18] M. Kokabi, M. Sirousazar, and Z. M. Hassan, "PVA-clay nanocomposite hydrogels for wound dressing," *European Polymer Journal*, vol. 43, no. 3, pp. 773–781, 2007.

[19] M. A. Aziz, J. D. Cabral, H. J. L. Brooks, S. C. Moratti, and L. R. Hanton, "Antimicrobial properties of a chitosan dextran-based hydrogel for surgical use," *Antimicrobial Agents and Chemotherapy*, vol. 56, no. 1, pp. 280–287, 2012.

[20] C. Valgas, S. M. d. Souza, E. F. A. Smânia, and A. Smânia Jr., "Screening methods to determine antibacterial activity of natural products," *Brazilian Journal of Microbiology*, vol. 38, no. 2, pp. 369–380, 2007.

[21] A. M. Kearns, M. Ganner, and A. Holmes, "The "Oxford *Staphylococcus*": a note of caution," *Journal of Antimicrobial Chemotherapy*, vol. 58, no. 2, pp. 480-481, 2006.

[22] CLSI, "Performance standards for antimicrobial disk susceptibility tests, approved standard," in *CLSI Document M02-A11*, pp. 1–58, Clinical and Laboratory Standards Institute, Wayne, PA, USA, 7th edition, 2012.

[23] E. M. Ahmed, "Hydrogel: preparation, characterization, and applications: a review," *Journal of Advanced Research*, vol. 6, no. 2, pp. 105–121, 2015.

[24] S. Moscato, F. Ronca, D. Campani, and S. Danti, "Poly(vinyl alcohol)/gelatin hydrogels cultured with HepG2 cells as a 3D model of hepatocellular carcinoma: a morphological study," *Journal of Functional Biomaterials*, vol. 6, no. 1, pp. 16–32, 2015.

[25] E. A. Kamoun, E.-R. S. Kenawy, and X. Chen, "A review on polymeric hydrogel membranes for wound dressing applications: PVA-based hydrogel dressings," *Journal of Advanced Research*, vol. 8, no. 3, pp. 217–233, 2017.

[26] E. F. dos Reis, F. S. Campos, A. P. Lage et al., "Synthesis and characterization of poly(vinyl alcohol) hydrogels and hybrids for rMPB70 protein adsorption," *Materials Research*, vol. 9, no. 2, pp. 185–191, 2006.

[27] K. S. P. Jodar, V. M. Balcao, M. V. Chaud et al., "Development and characterization of a hydrogel containing silver sulfadiazine for antimicrobial topical applications," *Journal of Pharmaceutical Sciences*, vol. 104, no. 7, pp. 2241–2254, 2015.

[28] P. Gupta, K. Vermani, and S. Garg, "Hydrogels: from controlled release to pH-responsive drug delivery," *Drug Discovery Today*, vol. 7, no. 10, pp. 569–579, 2002.

[29] A. Hassan, M. B. K. Niazi, A. Hussain, S. Farrukh, and T. Ahmad, "Development of anti-bacterial PVA/starch based hydrogel membrane for wound dressing," *Journal of Polymers and the Environment*, vol. 26, no. 1, pp. 235–243, 2018.

[30] M. C. Hacker and A. G. Mikos, *Synthetic Polymers, Principles of Regenerative Medicine*, Elsiever, 2nd edition, 2011.

[31] C. N. Chaudhari, K. Tandel, N. Grover et al., "In vitro vancomycin susceptibility amongst methicillin resistant *Staphylococcus aureus*," *Medical Journal Armed Forces India*, vol. 70, no. 3, pp. 215–219, 2014.

[32] Y. Morita, J. Tomida, and Y. Kawamura, "Responses of *Pseudomonas aeruginosa* to antimicrobials," *Frontiers in Microbiology*, vol. 4, 2014.

[33] T. S. Sivanmaliappan and M. Sevanan, "Antimicrobial susceptibility patterns of *Pseudomonas aeruginosa* from diabetes patients with foot ulcers," *International Journal of Microbiology*, vol. 2011, Article ID 605195, 4 pages, 2011.

Hindawi
International Journal of Polymer Science
Volume 2019, Article ID 9432194, 10 pages
https://doi.org/10.1155/2019/9432194

Research Article

Preparation and *In Vivo* Expression of CS-PEI/pCGRP Complex for Promoting Fracture Healing

Chun-Liang Li,[1] Feng Qin,[2] Rong-rong Li,[3] Jia Zhuan,[4] Hai-Yong Zhu,[1] Yu Wang,[1] and Kai Wang[1]

[1]*Department of Orthopedics, Qinghai Provincial People's Hospital, Xining, Qinghai, China*
[2]*Department of Endocrinology, University Affiliated Hospital, Xining, Qinghai, China*
[3]*Qinghai Nationalities University, Xining, Qinghai, China*
[4]*Department of Clean Operation, Qinghai Provincial People's Hospital, Xining, Qinghai, China*

Correspondence should be addressed to Kai Wang; wkkw002@sina.com

Received 18 October 2018; Revised 11 November 2018; Accepted 22 November 2018; Published 19 February 2019

Guest Editor: Jianxun Ding

Background/Objective. CGRP is a calcitonin gene-related peptide that is capable of promoting bone development and bone regeneration. Chitosan is a nontoxic and degradable biomaterial. However, the gene transfection efficiency of chitosan is low, whereas PEI (polyethyleneimine) has higher capability of transfection efficiency. In this paper, PEI was covalently linked to chitosan, and the rat CGRP plasmid was encapsulated in a CS-PEI complex to construct CS-PEI/pCGRP nanoparticles. The characterization and biological effects of CS-PEI/pCGRP nanoparticles were investigated *in vivo*. *Methods*. CS-PEI/pCGRP nanoparticles were prepared by a complex coacervation method. The PEI distribution degree on chitosan was measured with a dialysis method and ^{1}H-NMR analysis. The particle size and zeta potential of CS-PEI/pCGRP nanoparticles were detected by dynamic light scattering. The binding of CS-PEI to pCGRP was detected by gel retardation assay. The transfection effect was evaluated by RT-qPCR. A rat femoral fracture model was established and treated with PBS, pCGRP, CS-PEI, and CS-PEI/pCGRP to detect the expression of CGRP and downstream genes in early healing of fractures by RT-qPCR, western blot, and immunohistochemistry (IHC). *Results*. The particle size and zeta potential of CS-PEI/pCGRP nanoparticles were stable when the mass ratio of CS-PEI and pCGRP was higher than 5 : 1, the ratio which could also effectively protect pCGRP from DNase I degradation. CS-PEI/pCGRP could obviously increase CGRP expression in rat bone marrow stromal cells. *In vivo* fracture healing experiments demonstrated that CGRP could be delivered to the body via the CS-PEI and expressed in situ after a 3-week treatment. Moreover, CS-PEI/pCGRP significantly enhanced the mRNA and protein levels of downstream RUNX2 and ALP. *Conclusion*. CS-PEI/pCGRP nanoparticles were an effective nonviral gene transfection system that could upregulate CGRP expression *in vivo* and accelerate the expression of key biomarkers for early healing of fractures.

1. Introduction

With the increase of people's activity and space, the possibility of bone fracture rises. And the increasing number of osteoporosis patients caused by aging results in continuous increase of fracture incidence. About 50% of women and 20% of men in their lifetime will experience fragility fractures [1–4] and consequent high cost of medical care (costs associated with fragility fractures). In 2006, China spent 1.6 billion USD on hip fracture care, which is projected to rise to 12.5 billion USD by 2020 and 265 billion USD by 2050 [5]. With the development of biomaterials, it has been the focus of bone repair research for tissue engineering biomaterials as transplant substitutes in recent years. Bone tissue engineering has made "local repair" of the fracture area and systematically enhanced bone repair ability to regenerate normal bone tissue, which has achieved considerable results.

Fracture healing is a complex physiological process accompanied by the formation of local hematoma and local inflammation. The healing process involves the proliferation, differentiation, and matrix mineralization of osteoblasts. The treatment strategies to control inflammation, promote blood

circulation, and stimulate bone regeneration can improve fracture healing. Gene therapy induces human normal genes or therapeutic genes into targeted cells in some certain ways to correct gene defects and has achieved clinical effect by induction of single or multiple genes to accelerate the fracture healing. CGRP is a calcitonin gene-related peptide, which is a neuropeptide that distributes in the active region of bone growth [6]. CGRP plays an important role in nourishing nerves and blood vessels; it also plays an anti-inflammatory role, directly promoting osteoblast proliferation, differentiation, and mineralization, thereby promoting bone development and bone regeneration [7]. For example, CGRP can induce differentiation of adipose-derived stem cells into osteoblasts and maintain high cell proliferative capacity, as well as induce exuberant secretion of extracellular matrix, and upregulate BMP2 expression which can promote osteogenic activity of osteoblasts [8]. However, there are still few studies on the role of CGRP in fracture healing, and it is beneficial to investigate how CGRP promotes bone regeneration.

Chitosan is a natural polycationic and weak alkaline polysaccharide with excellent biocompatibility and degradability [9]. It is safe and nontoxic, which is regarded as one of the most promising drug-loading materials [10]. Mumper et al. [11] first reported the use of chitosan in gene delivery *in vitro*. Many studies have shown that the physicochemical properties (size, zeta potential, and nucleic acid complexation efficiency) of chitosan/gene complex directly affect gene delivery efficiency [12, 13]. It is generally recognized that a diameter of complex, smaller than 200 nm with a positive potential [14], holds the highest transfection efficiency, so the ratio of chitosan to nucleic acid and the preparation method are the key factors affecting these physical and chemical properties [15]. Polyethyleneimine (PEI), like chitosan, is a cationic nonviral gene carrier that binds to proteoglycans on the cell surface and enters cells by endocytosis. PEI facilitates the escape of carriers from lysosomes by "proton sponge effect," thereby increasing transfection efficiency [16]. In this study, PEI with a small molecule mass was covalently grafted onto the chitosan backbone to prepare chitosan-PEI (CS-PEI) composite carrier, and CGRP plasmid (pCGRP) was packaged by CS-PEI to synthesize CS-PEI/pCGRP nanoparticles. The physical properties of CS-PEI/pCGRP nanoparticles were detected. *In vivo* gene transfection experiments were performed to study the role of CS-PEI/pCGRP complex in promoting fracture healing.

2. Method

2.1. Materials. The pCDNA3.1$^+$ plasmid containing the rat CGRP sequence (pCGRP) was constructed and transformed into *E. coli* to amplify and extract the plasmid.

2.2. Preparation of CS-PEI/pCGRP Nanoparticles. In Figure 1, according to previous reports by Tripathi et al. [17], 100 mg of chitosan (85% deacetylated, Sigma) was dissolved in a 1% hydrochloric acid (HCl) solution and stirred at 60°C overnight. Afterwards, 0.25 mL of epichlorohydrin was added, stirred for 3 hours, and concentrated to a white

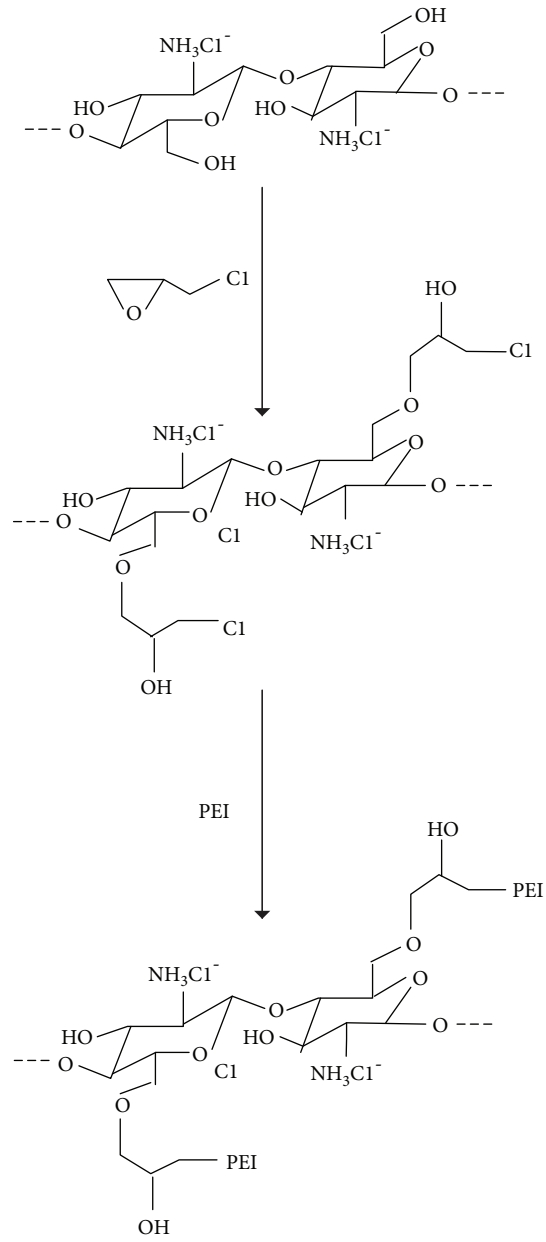

Figure 1: Reaction scheme of constructing CS-PEI.

powder on a rotary evaporator to achieve chitosan chlorohydrin hydrochloride (CC). CC and PEI (Sigma) with a mass ratio of 1 : 4 were dissolved in 100 mL of water, heated to 60°C, supplemented with NaOH solution (2 mol/L, 2 mL), and stirred at 60°C for 20 h. The resulting solution was purified with a dialysis method and lyophilized to obtain CS-PEI. The distribution degree of PEI on CS-PEI was calculated by the following equation:

$$\text{Distribution degree}\,(\%) = 100\%\times \frac{W_1 - W_0}{W_0}, \qquad (1)$$

where W_0 is the initial weight of chitosan and W_1 is the weight of CS-PEI.

CS-PEI was dissolved in water to prepare a solution of 0.5 μg/μL and stirred overnight. An appropriate amount of CGRP plasmid DNA was added to the CS-PEI solution and stirred for 2 min to prepare a CS-PEI/pCGRP nanoparticle solution.

2.3. ^{1}H-NMR Characterization of CS-PEI Nanoparticles. CS and CS-PEI were dissolved in a CD_3COOD/D_2O solvent, and the ^{1}H-NMR spectrum was determined using a Mercury-plus 400 NMR spectrometer (Varian, CA, USA).

2.4. Dynamic Light Scattering Detection of Particle Size and Zeta Potential. The CS-PEI/pCGRP complex containing different mass ratios (CS-PEI :) was sufficiently diluted, added to the sample cell, and placed in a nanoparticle-size analyzer (Delsa Nano C Particle Analyzer, Beckman Coulter Inc.) to measure the particle size and zeta potential of the sample.

2.5. Agarose Gel Retardation Electrophoresis Experiment. 5 U DNase I (Qiagen) was added into the CS-PEI/pCGRP complex solution containing CS-PEI and pCGRP in different mass ratios under 37°C water bath. One hour later, 25 mM EDTA was added to stop the reaction. 1% agarose gel electrophoresis was performed to analyze the binding ability of the CS-PEI carrier to plasmid, and pCGRP was used as control.

2.6. Culture of Rat Bone Marrow Stromal Cells and In Vitro Transfections by CS-PEI/pCGRP. As previously discussed [18], rat bone marrow stromal cells (BMSCs) were isolated from the femur and tibia and cultured in IMDM supplemented with 20% FBS. The adherent BMSCs were used for further assay after 3 days of culture.

Next, cells were trypsinized, washed, centrifuged, and seeded in a 6-well plate at the density of 100,000/well. After overnight culture, the medium was replaced with a serum-free medium containing CS-PEI/pCGRP with different mass ratios of CS-PEI to pCGRP from 1 : 2 to 8 : 1. The amount of pCGRP was 2 μg in every well. After 6 hours of culture, cells were then continuously cultured for 48 h with a complete medium. Then, CGRP mRNA levels of BMSCs were evaluated by gene quantification.

2.7. Preparation of Rat Femoral Fracture Model and Interventional Treatment of CS-PEI/pCGRP. 20-month-old Sprague-Dawley male rats were provided by the Experimental Animal Center of Lanzhou University (Lanzhou, China). All rats were prepared for the right femoral fracture model. In brief, the middle part of the right hind leg was surgically exposed after anesthesia and the middle part of the femur was sawn to induce a short transverse fracture. A 1 mm diameter Kirschner wire was then threaded into the medullary cavity of the femur. The fracture was fixed and the wound was closed after surgery. The rats were intraperitoneally injected with 100,000 U of penicillin sodium daily for 3 days. Three days after the operation, 48 rats were selected under imaging without obvious displacement at the broken site and loosening at the internal fixation.

The rats were randomly divided into 4 groups: PBS control group, pCGRP treatment group, CS-PEI treatment group, and CS-PEI/pCGRP treatment group. The rats were

Table 1: PCR primer sequences.

Gene	Primer sequences
CGRP	F:5′-AGCCCCAGATCTAAGCGGTGTG-3′
	R: 5′-TCCTTGGCCATATCCCTTTTCTTG-3′
ALP	F: 5′-CTCAACACCAATGTAGCCAAGAATG-3′
	R: 5′-GGCAGCGGTTACTGTGGAGA-3′
RUNX2	F: 5′-GCACAAACATGGCCAGATTCA-3′
	R: 5′-AAGCCATGGTGCCCGTTAG-3′
β-Actin	F: 5′-CATCCGTAAAGACCTCTATGCCAAC-3′
	R: 5′-ATGGAGCCACCGATCCACA-3′

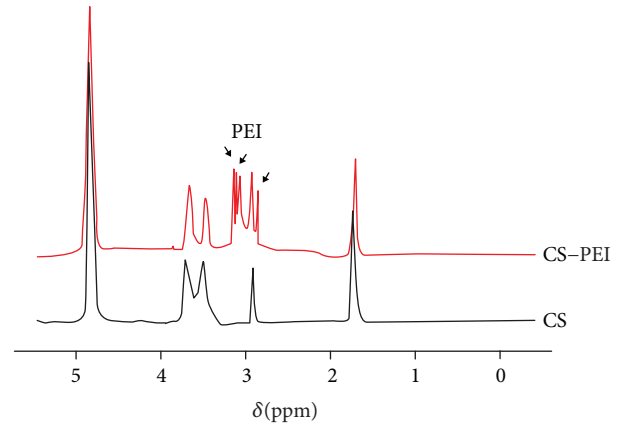

Figure 2: ^{1}H-NMR spectra of CS and CS-PEI.

fixed after anesthesia, and 250 μL of various solutions was slowly injected subcutaneously at the fracture site. The injection time was not shorter than 1 min. The amount of pCGRP was 20 μg, and the mass ratio of CS-PEI:pCGRP was 8 : 1. For the mice in the CS-PEI treatment group, the amount of CS-PEI was equal to the amount of CS-PEI/pCGRP in the mice of the CS-PEI/pCGRP treatment group.

2.8. Immunohistochemistry (IHC) Staining to Detect the Expression of CGRP in Bone Tissue. Animals were sacrificed 3 weeks after treatment. The femur samples from four rats in each group were taken and fixed in 4% paraformaldehyde for 12 h. Decalcification (Fuyang Biotek, Shanghai, China) was performed to make 5 μm thick paraffin sections. The sections were routinely dewaxed, hydrated, washed with PBS, and incubated with 3% hydrogen peroxide for 20 min at room temperature to block endogenous peroxidase activity. After blocking with rabbit serum, the slides were incubated with CGRP primary antibody (Bioss, Beijing, China) at 4°C overnight and then incubated with secondary antibody (Bioster, Wuhan, China), visualized with DAB (Bioster), and counterstained with hematoxylin for 2 min, then dehydrated and mounted.

2.9. Real-Time Quantitative Polymerase Chain Reaction (RT-qPCR). The callus was taken from each group with 4 rats. TRIzol reagent was added to the callus and placed in

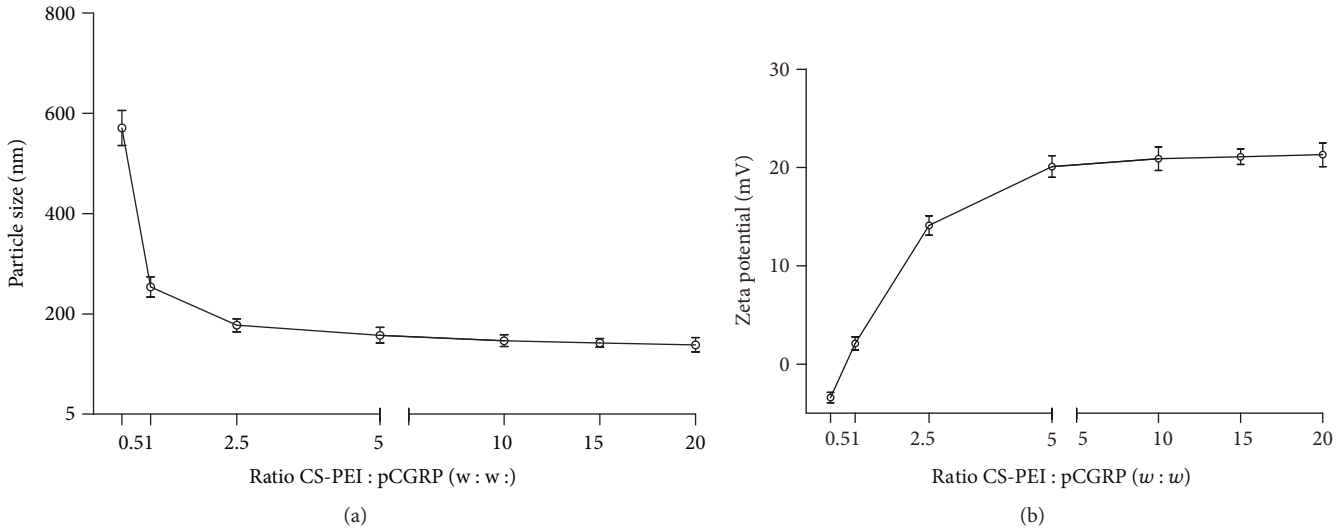

Figure 3: Physical properties of CS-PEI/pCGRP with different mass ratios of CS-PEI to pCGRP. (a) Particle size and (b) zeta potential of different CS-PEI/pCGRP nanoparticles.

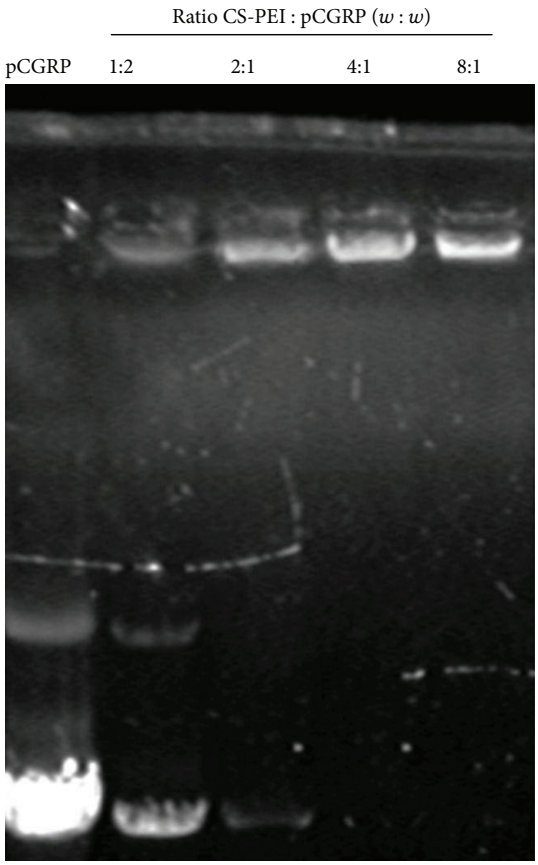

Figure 4: DNA binding capacity of CS-PEI in agarose gel retardation assay.

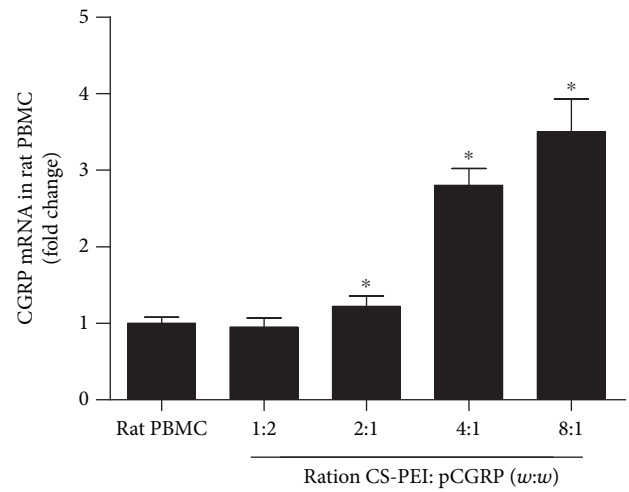

Figure 5: CGRP mRNA expression in rat bone marrow stromal cells (BMSCs) transfected with CS-PEI/pCGRP at different CS-PEI : pCGRP ratios ($w : w$). Data are mean ± standard deviation ($n = 3$). $^*P < 0.05$ vs. BMSCs.

liquid nitrogen. Afterwards, RNA was extracted, and 10 μg of total RNA was quantified by a spectrophotometer (BioPhotometer 6131, Eppendorf) and reverse-transcribed into cDNA. Then, a real-time PCR instrument (Light Cycler, Roche) was used to detect the relative expression of ALP, RUNX2, and CGRP, and β-actin was used as a reference gene for PCR reaction. The reaction conditions of the PCR were set to 95°C for 30 sec, then 40 cycles with 60°C for 30 sec and 72°C for 1 min, and finally incubated at 72°C for 1 min and 4°C for extension. Primer synthesis was provided by Guangzhou Funeng Gene Co. Ltd. (Guangzhou, China). The specific primer sequences were shown in Table 1. The results were analyzed using the $2^{-\Delta\Delta Ct}$ data method. The same procedure was used to detect the CGRP mRNA levels in CS-PEI/pCGRP-transfected BMSCs.

2.10. Western Blot. The total bone protein was extracted from 0.5 g frozen callus, and the total protein was adjusted to the same concentration by the Coomassie Brilliant Blue

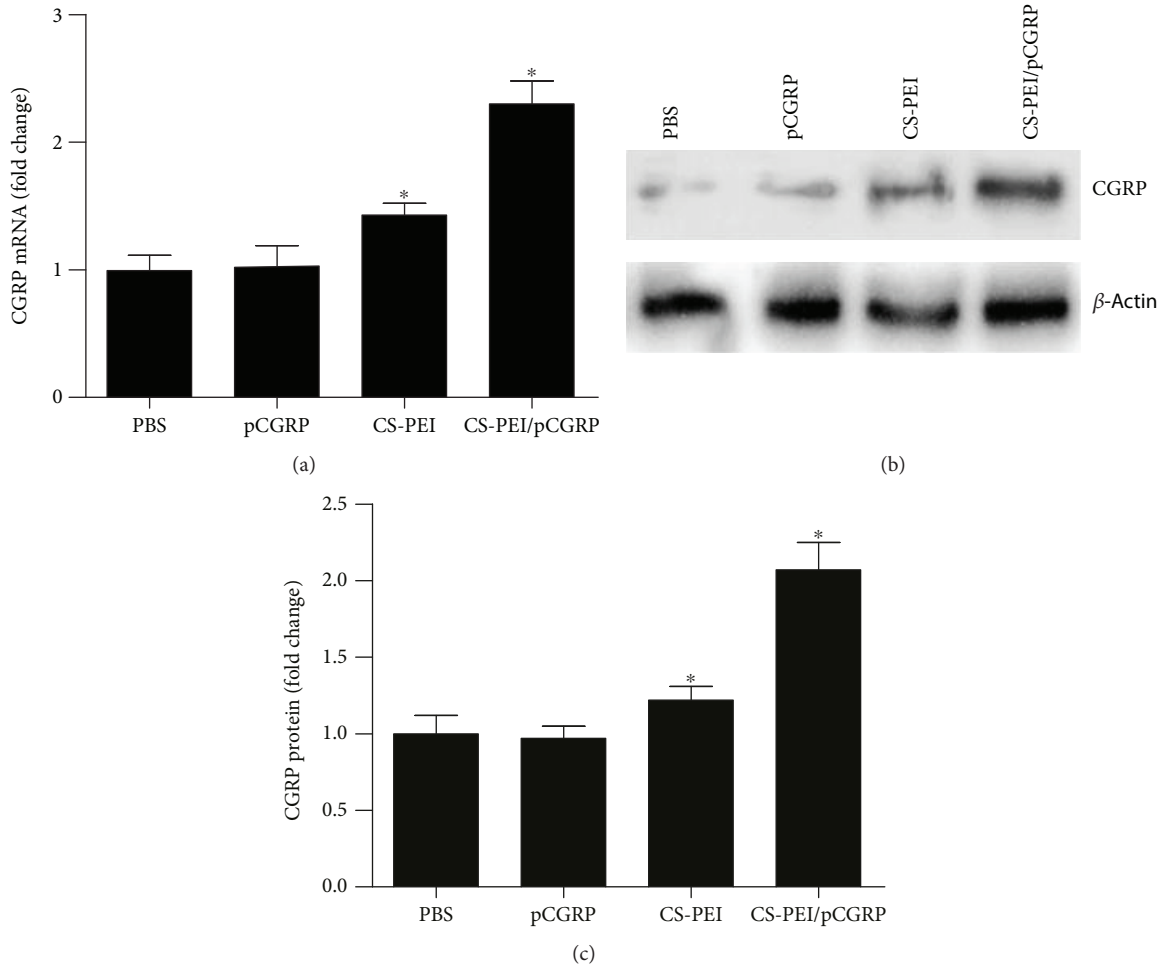

Figure 6: CGRP expression in callus of rat femoral fracture model after 3 weeks treatment with CS-PEI/pCGRP. (a) mRNA level of CGRP by RT-qPCR. (b) Representative image of CGRP bands for protein level by western blot. (c) The quantified result of CGRP bands. Data are mean ± standard deviation ($n = 4$). $^*P < 0.05$ vs. the PBS group.

method. The sample was loaded with 50 μg, electrophoresed on SDS-PAGE, and transferred to PCDF membrane. The electroporated nitrocellulose membrane was blocked with a 50 g/L skim milk blocking solution, after which ALP, RUNX2, CGRP, and β-actin antibodies were added and incubated at 4°C overnight and then incubated with horseradish peroxidase-labeled secondary antibody IgG (Bioster). Chemiluminescence method was applied for color development and gel quantitative software Quantity One 4.52 was used for analysis. RUNX2, CGRP, and β-actin antibodies were purchased from Bioss Inc., and ALP antibody was purchased from Boster Inc.

2.11. Hematoxylin and Eosin (H&E) Staining. After the rats were sacrificed, the livers were rapidly excised and fixed in 4% paraformaldehyde. Then, the fixed samples were dehydrated, embedded in paraffin, and sectioned to 5 μm slices. The sections were stained by hematoxylin and eosin for the detection of pathological changes.

2.12. Statistical Analysis. Statistical analysis was performed on SPSS19.0 statistical software. All data were presented as mean ± SD, statistically analyzed by a t-test and one-way ANOVA. $P < 0.05$ indicated that the difference was significant.

3. Results and Discussion

3.1. The Distribution Degree of PEI on CS-PEI. The initial weight of chitosan was 0.1 g, and the product weight of CS-PEI was 0.135 g, showing the distribution degree of PEI which was 35%. This indicated that the procedure could successfully graft PEI to chitosan.

3.2. ^{1}H-NMR Analysis and Composition of CS-PEI Nanoparticles. ^{1}H-NMR spectroscopy was used to investigate the composition of chitosan to PEI. As shown in the CS-PEI spectrum in Figure 2, the signals between 3.3 and 2.8 ppm showed the presence of hydrogen peaks, which was absent in the CS spectrum and was presumed to be the hydrogen peak of PEI. The ^{1}H-NMR confirms that PEI has been successfully covalently grafted onto chitosan. According to the analysis of peak areas, it could be concluded that one PEI is connected to an average of 29 D-glucosamine units of

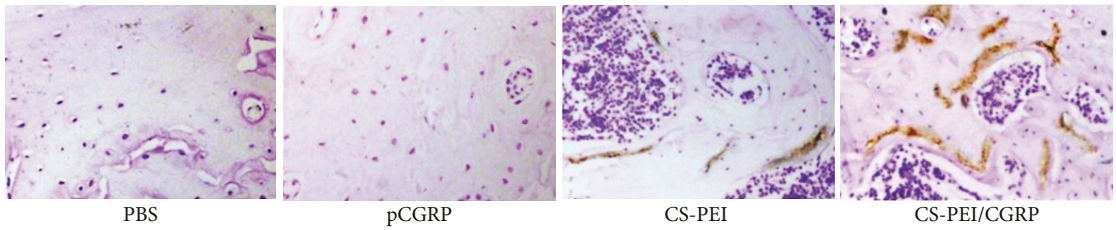

Figure 7: CGRP immunohistochemical result in callus of rat femoral fracture model after a 3-week treatment with CS-PEI/pCGRP.

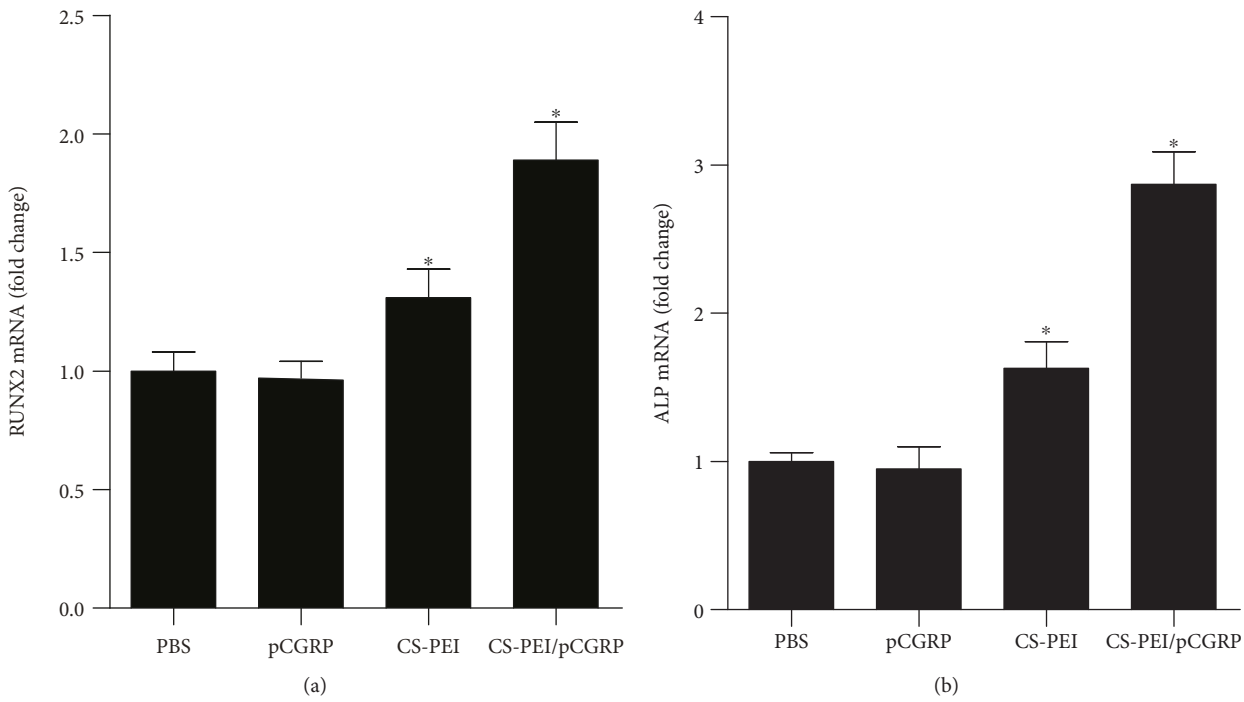

Figure 8: RUNX2 and ALP mRNA levels in the callus of rat femoral fracture model after a 3-week treatment with CS-PEI/pCGRP. Data are mean ± standard deviation ($n = 4$). $^*P < 0.05$ vs. the PBS group.

chitosan, which was consistent with the 35% distribution degree calculated by the above dialysis method.

3.3. Size and Potential of CS-PEI/pCGRP Nanoparticles. Figure 3 showed the particle size and zeta potential of CS-PEI/pCGRP nanoparticles. The results displayed that when the mass ratio was 1 : 2~1 : 1, the particle sizes of the nanoparticles were 571.1 ± 34.9 nm and 254.1 ± 20.3 nm (Figure 3(a)), respectively. When the mass ratio was 1 : 2 to 2.5 : 1, the zeta potential was increased from −3.4 ± 0.52 mV to 14.1 ± 0.98 mV (Figure 3(b)). With the increase of mass ratio, the particle sizes of composite nanoparticles decreased gradually and the zeta potential gradually increased. When the mass ratio is 5 : 1, the particle sizes and zeta potentials of CS-PEI/pCGRP nanoparticles tended to be stable and were 157.4 ± 15.6 nm (Figure 3(a)) and 20.1 ± 1.1 mV (Figure 3(b)), respectively. This indicated that the ability compressing DNA was improved as the proportion of CS-PEI polymer in the nanoparticles increased, and the zeta potential of the particles could be effectively increased. The advantage of chitosan is the good degradability and biocompatibility, and the main drawback is the low efficiency for gene transfection [17]. Studies have shown that the main reason for the low efficiency of chitosan-mediated gene transfection is the lack of buffered amine groups, which leads to the difficulty in escaping from endosomes and lysosomes. Another reason is the strong binding capability of chitosan to DNA, which results in low DNA disassembly and low target gene expression after entry into cells. PEI has a strong ion buffering capacity, which allows DNA to effectively escape the digestion of acidic lysosomes, thus achieving higher transfection efficiency [19, 20]. However, in gene transfection, PEI usually exhibits molecular weight-related cytotoxicity in a dose-dependent manner, mainly due to its significantly positive charge, which leads to strong electrostatic interaction with the cell membrane, resulting in intracellular functional disorder [21]. In addition, PEI is a nondegradable polymer that accumulates in the body and may present an unknown risk for long-term use. Therefore, we selected a relatively low-molecular-weight (1.8 kDa) PEI grafted onto chitosan and tried to produce a gene carrier with low toxicity and high transfection efficiency [20]. It is

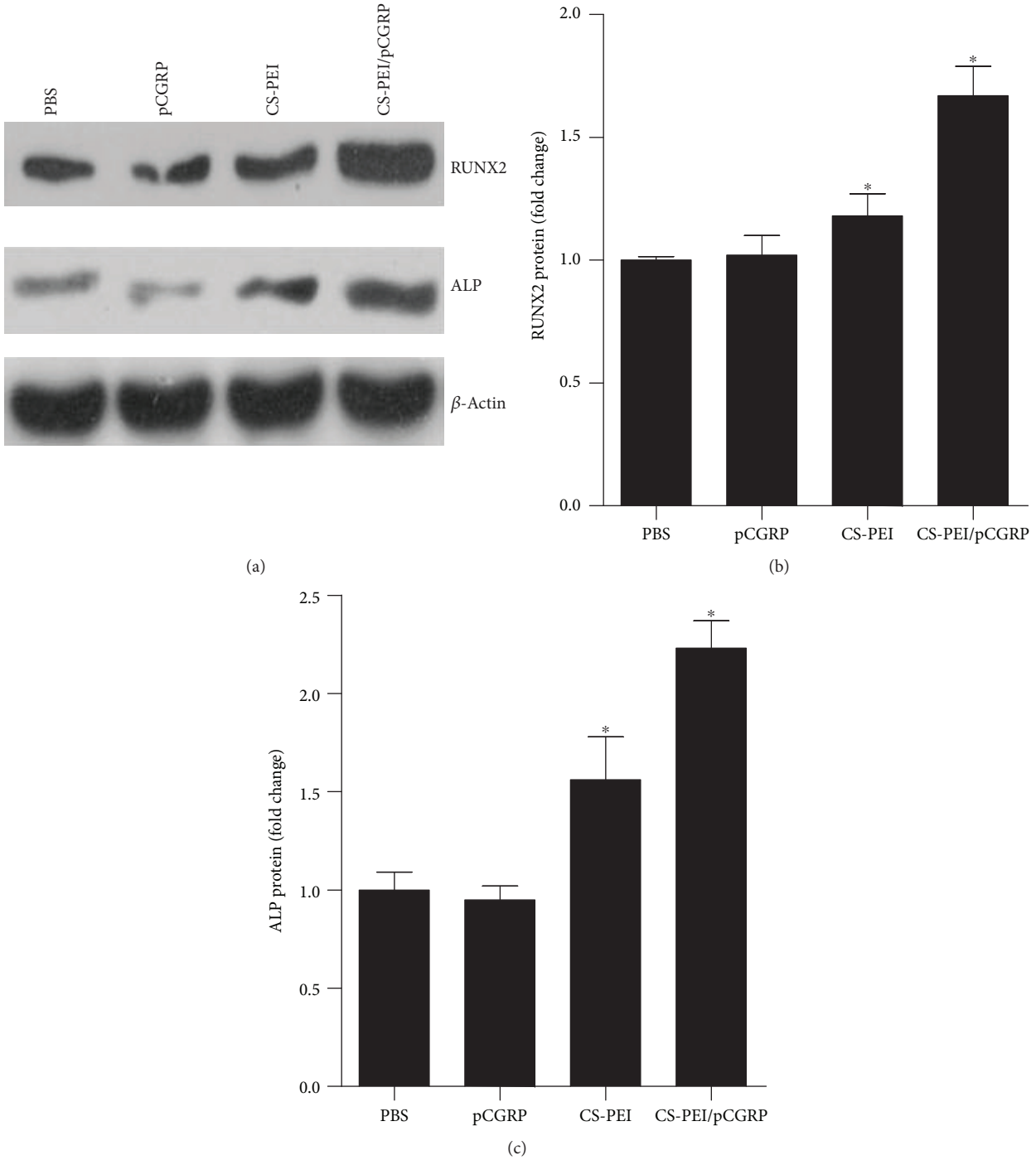

Figure 9: RUNX2 and ALP protein levels in callus of rat femoral fracture model after a 3-week treatment with CS-PEI/pCGRP. Data are mean ± standard deviation ($n = 4$). $^*P < 0.05$ vs. the PBS group.

generally believed that a diameter < 200 nm [14, 15] with positive potential is most beneficial for transfection. We found that the mass ratio of CS-PEI : pCGRP affected the particle size and zeta potential. When the mass ratio was higher than 5 : 1, the CS-PEI/pCGRP nanoparticles had a particle size of less than 200 nm.

3.4. Stability of CS-PEI/pCGRP Nanoparticles. To further determine the loading and protection capability of CS-PEI on pCGRP, we performed an agarose gel retardation assay. It could be observed from Figure 4 that when the mass ratio of CS-PEI copolymer to pCGRP was less than 2 : 1, some DNA bands appeared. When the mass ratio reached 4 : 1, no obvious DNA bands ran out, indicating that the CS-PEI copolymer could fully bind to the pCGRP plasmid when $w : w$ is higher than 4 : 1. The DNA plasmid is easily degraded by nucleases in the body. In the experiment, DNase I was used to represent the nuclease in the cells. The results

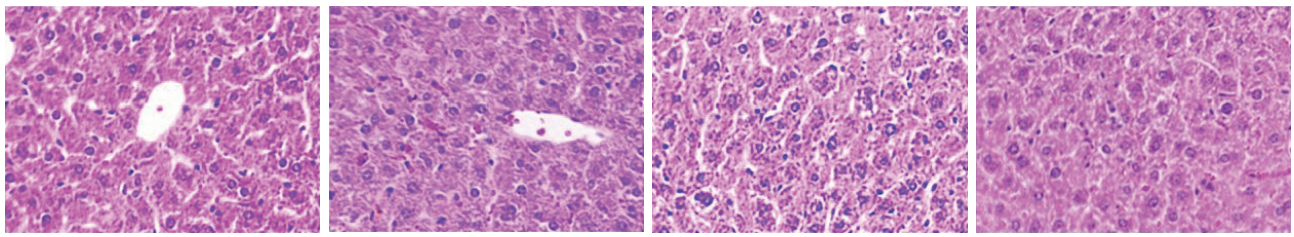

Figure 10: The histological section of rat liver after 3 weeks with different treatments of pCGRP, CS-PEI, or CS-PEI/pCGRP.

demonstrated that the antinuclease effect of CS-PEI on the pCGRP plasmid could effectively encapsulate and protect the gene from nuclease degradation. This advantage of CS-PEI would significantly contribute to the improvement of transfection efficiency.

3.5. CS-PEI/pCGRP Nanoparticles Enhance the In Vitro Expression of CGRP mRNA in Rat BMSCs. Figure 5 showed the CGRP mRNA levels in BMSCs transfected with CS-PEI/pCGRP. The CGRP mRNA levels increased with increasing of CS-PEI : pCGRP ratio ($w : w$). The level initially increased at the ratio of 2 : 1 and obviously increased from 4 : 1 to 8 : 1. It could be explained by the increased protective ability of CS-PEI.

3.6. CS-PEI/pCGRP Upregulates the Expression of CGRP and Its Downstream Genes in Early Stage of Fracture. In the early healing of fracture (3 weeks), there were no signs of nonhealing in the fracture site of rats in the 4 groups. The PBS control group and the pCGRP treatment group had less callus, the fracture line was clear, and the trabecular bone formation was less; the CS-PEI treatment group and the CS-PEI/pCGRP treatment group had more callus, the fracture line was blurred, and the trabecular bone generation was more. The CS-PEI/pCGRP treatment group had more quantities of callus and trabecular bone when compared with the CS-PEI treatment group. The mRNA and protein levels of CGRP in the callus site of rats were detected. It was found that the mRNA and protein expression levels of CGRP were the highest in CS-PEI/pCGRP treatment group, and the mRNA and protein levels of CGRP in the CS-PEI-treated group were increased in a certain level (Figure 6). Further IHC staining detection (Figure 7) showed that the expression of CGRP was the highest in the CS-PEI/pCGRP treatment group, and CGRP was mainly deposited on functionally active osteoblasts around the trabecular bone. These results indicated that CS-PEI had certain repair ability. After CS-PEI polymer delivery, pCGRP could be transfected into the cells of the fracture site to induce more obvious repair effect. Further, by RT-qPCR and western blot studies, it was found that the mRNA of osteogenesis molecules RUNX2 and ALP (Figure 8) and their protein expression levels (Figure 9) were also significantly increased after *in vivo* transfection of pCGRP. Wang et al. [22] have reported that chitosan has a certain effect on bone repair due to its osteoinductivity and progressive substitution of implants by host bones, which might explain the upregulated CGRP, RUNX2, and ALP expression in the CS-PEI treatment group. However, pCGRP delivered by a CS-PEI copolymer could further enhance the repair effect.

Furthermore, because of the known toxicity of polymeric cations, the biosafety of CS-PEI and CS-PEI/pCGRP was preliminary detected by investigating the appearance of internal organs and evaluating the histological changes in the liver. As shown in Figure 10, all livers in rats of the CS-PEI or CS-PEI/pCGRP treatment group did not present histological changes. And the appearance of the heart, liver, stomach, and kidney in all treatment groups was similar to that in the control group. This indicated that the dosage of CS-PEI or CS-PEI/pCGRP in this study did not show significant toxicity to rats.

The study found that CGRP levels were significantly elevated in the local fracture site and in the patient's plasma at the time of fracture [23, 24], suggesting that this small peptide was likely to be involved in the process of fracture repair. *In vivo* experiments confirmed that CGRP knockout mice showed more severe bone loss than wild-type mice [25]. *In vitro* experiments had also demonstrated that CGRP could induce osteoblast proliferation and differentiation [26]. ALP (alkaline phosphatase) is an important index for evaluating bone formation and bone turnover. During bone formation, osteoblast activity is enhanced. ALP in osteoblasts produces phosphoric acid by enzymatic action and is deposited in the bone with calcium phosphate. RUNX2 is also a specific osteogenic marker expressed by osteoblasts. It is an important transcription factor that activates and initiates the differentiation of BMSCs into osteoblasts and regulates the maturation of osteoblasts. A number of studies have confirmed that CGRP can increase the transcriptional level and protein level of RUNX2 *in vivo* through Hippo signaling pathway [27] and BMP2 signaling pathway [28], thereby accelerating the differentiation of BMSCs into osteoblasts *in vivo*, resulting in the difference in mineralization osteogenesis at the late stage of the fracture. The results of in this study demonstrated that CS-PEI polymer could not only transfect CGRP plasmid into *in vivo* fracture areas but also preserve the biological role of transfected CGRP plasmid.

4. Conclusion

In summary, this study developed a CS-PEI polymer that could encapsulate the rat CGRP plasmid, which could significantly induce bone differentiation into the osteogenesis and

increase calcium deposition. By upregulating the production of CGRP, CS-PEI/pCGRP nanoparticles might regulate the fracture healing process in the early stage and provide a new therapeutic approach for promoting early rehabilitation of patients with fractures in clinics, preventing delayed healing and nonunion of fractures.

Data Availability

The data used to support the findings of this study are available from the corresponding author upon request.

Ethical Approval

All animal experiments were approved by the Ethical Committee of Qinghai Provincial People's Hospital.

Conflicts of Interest

The authors declare that there are no conflicts of interest regarding the publication of this paper.

References

[1] O. Ström, F. Borgström, J. A. Kanis et al., "Osteoporosis: burden, health care provision and opportunities in the EU: a report prepared in collaboration with the International Osteoporosis Foundation (IOF) and the European Federation of Pharmaceutical Industry Associations (EFPIA)," *Archives of Osteoporosis*, vol. 6, no. 1-2, pp. 59–155, 2011.

[2] T. P. van Staa, E. M. Dennison, H. G. Leufkens, and C. Cooper, "Epidemiology of fractures in England and Wales," *Bone*, vol. 29, no. 6, pp. 517–522, 2001.

[3] US Department of Health and Human Services, *Bone Health and Osteoporosis: a Report of the Surgeon General. U.S*, Department of Health and Human Services, Office of The Surgeon General, Rockville, MD, USA, 2004.

[4] J. A. Kanis, E. V. McCloskey, H. Johansson et al., "European guidance for the diagnosis and manage-ment of osteoporosis in postmenopausal women," *Osteoporosis International*, vol. 24, pp. 23–57, 2013.

[5] International Osteoporosis Foundation, *The Asian Audit: Epidemiology, Costs and Burden of Osteoporosis in Asia 2009*, IOF, Nyon, 2009.

[6] T. Sekiguchi, N. Suzuki, N. Fujiwara et al., "Calcitonin in a protochordate, Ciona intestinalis–the prototype of the vertebrate calcitonin/calcitonin gene-related peptide superfamily," *The FEBS Journal*, vol. 276, no. 16, pp. 4437–4447, 2009.

[7] C. V. Vause and P. L. Durham, "CGRP stimulation of iNOS and NO release from trigeminal ganglion glial cells involves mitogen-activated protein kinase pathways," *Journal of Neurochemistry*, vol. 110, no. 3, pp. 811–821, 2009.

[8] Z. Fang, Q. Yang, W. Xiong et al., "Effect of CGRP-adenoviral vector transduction on the osteoblastic differentiation of rat adipose-derived stem cells," *PLoS One*, vol. 8, no. 8, article e72738, 2013.

[9] S. Q. Li, S. J. Dong, W. G. Xu et al., "Antibacterial hydrogels," *Advanced Science*, vol. 5, no. 5, article 1700527, 2018.

[10] Z. H. Tang, C. L. He, H. Y. Tian et al., "Polymeric nanostructured materials for biomedical applications," *Progress in Polymer Science*, vol. 60, pp. 86–128, 2016.

[11] R. J. Mumper, J. Wang, J. M. Claspell, and A. P. Rolland, "Novel polymeric condensing carriers for gene delivery," *Proceedings of the Controlled Release Society*, vol. 22, pp. 178-179, 1995.

[12] M. Köping-Höggård, I. Tubulekas, H. Guan et al., "Chitosan as a nonviral gene delivery system. Structure-property relationships and characteristics compared with polyethylenimine in vitro and after lung administration in vivo," *Gene Therapy*, vol. 8, no. 14, pp. 1108–1121, 2001.

[13] S. P. Strand, S. Lelu, N. K. Reitan, C. de Lange Davies, P. Artursson, and K. M. Vårum, "Molecular design of chitosan gene delivery systems with an optimized balance between polyplex stability and polyplex unpacking," *Biomaterials*, vol. 31, no. 5, pp. 975–987, 2010.

[14] K. Corsi, F. Chellat, L. Yahia, and J. C. Fernandes, "Mesenchymal stem cells, MG63 and HEK293 transfection using chitosan-DNA nanoparticles," *Biomaterials*, vol. 24, no. 7, pp. 1255–1264, 2003.

[15] S. Mao, W. Sun, and T. Kissel, "Chitosan-based formulations for delivery of DNA and siRNA," *Advanced Drug Delivery Reviews*, vol. 62, no. 1, pp. 12–27, 2010.

[16] Y. K. Wang, X. Yu, D. M. Cohen et al., "Bone morphogenetic protein-2-induced signaling and osteogenesis is regulated by cell shape, RhoA/ROCK, and cytoskeletal tension," *Stem Cells and Development*, vol. 21, no. 7, pp. 1176–1186, 2012.

[17] S. K. Tripathi, R. Goyal, P. Kumar, and K. C. Gupta, "Linear polyethylenimine-graft-chitosan copolymers as efficient DNA/siRNA delivery vectors in vitro and in vivo," *Nanomedicine*, vol. 8, no. 3, pp. 337–345, 2012.

[18] A. Gazdhar, N. Susuri, K. Hostettler et al., "HGF expressing stem cells in usual interstitial pneumonia originate from the bone marrow and are antifibrotic," *PLoS One*, vol. 8, no. 6, article e65453, 2013.

[19] Y. C. Li, H. Y. Tian, J. X. Ding et al., "Guanidinated thiourea-decorated polyethylenimines for enhanced membrane penetration and efficient siRNA delivery," *Advanced Healthcare Materials*, vol. 4, no. 9, pp. 1369–1375, 2015.

[20] J.-Q. Gao, Q.-Q. Zhao, T.-F. Lv et al., "Gene-carried chitosan-linked-PEI induced high gene transfection efficiency with low toxicity and significant tumor-suppressive activity," *International Journal of Pharmaceutics*, vol. 387, no. 1-2, pp. 286–294, 2010.

[21] V. Uskoković and D. P. Uskoković, "Nanosized hydroxyapatite and other calcium phosphates: chemistry of formation and application as drug and gene delivery agents," *Journal of Biomedical Materials Research. Part B, Applied Biomaterials*, vol. 96, no. 1, pp. 152–191, 2011.

[22] X. Wang, J. Ma, Y. Wang, and B. He, "Bone repair in radii and tibias of rabbits with phosphorylated chitosan reinforced calcium phosphate cements," *Biomaterials*, vol. 23, no. 21, pp. 4167–4176, 2002.

[23] J. Li, A. Kreicbergs, J. Bergström, A. Stark, and M. Ahmed, "Site-specific CGRP innervation coincides with bone formation during fracture healing and modeling: a study in rat angulated tibia," *Journal of Orthopaedic Research*, vol. 25, no. 9, pp. 1204–1212, 2007.

[24] G. N. Onuoha, "Circulating sensory peptide levels within 24 h of human bone fracture," *Peptides*, vol. 22, no. 7, pp. 1107–1110, 2001.

[25] A. K. Huebner, T. Schinke, M. Priemel et al., "Calcitonin deficiency in mice progressively results in high bone turnover,"

Journal of Bone and Mineral Research, vol. 21, no. 12, pp. 1924–1934, 2006.

[26] G. Tian, G. Zhang, and Y. H. Tan, "Calcitonin gene-related peptide stimulates BMP-2 expression and the differentiation of human osteoblast-like cells in vitro," *Acta Pharmacologica Sinica*, vol. 34, no. 11, pp. 1467–1474, 2013.

[27] W. Fei, Z. Huiyu, D. Yuxin, L. Shiting, Z. Gang, and T. Yinghui, "Calcitonin gene-related peptide-induced osteogenic differentiation of mouse bone marrow stromal cells through Hippo pathway in vitro," *Hua Xi Kou Qiang Yi Xue Za Zhi*, vol. 34, no. 3, pp. 286–290, 2016.

[28] C. Tuzmen and P. G. Campbell, "Crosstalk between neuropeptides SP and CGRP in regulation of BMP2-induced bone differentiation," *Connective Tissue Research*, vol. 59, Supplement 1, pp. 81–90, 2018.

Hindawi
International Journal of Polymer Science
Volume 2019, Article ID 8514247, 9 pages
https://doi.org/10.1155/2019/8514247

Research Article

Cellulase-Assisted Extraction, Characterization, and Bioactivity against Rheumatoid Arthritis of *Astragalus* Polysaccharides

Ling Cao,[1,2] Mi Yu,[1,2] Chonghui Wang,[1,2] Yunhui Bao,[1,2] Minghui Zhang,[1,2] Ping He,[1,2] Yan Zhang,[1,2] Tingting Yang,[1,2] Lulu Li,[1,2] Gang Li,[1,2] and Yun Gong[3]

[1]*Department of General Medicine, Renmin Hospital, Hubei University of Medicine, Shiyan, Hubei 442000, China*
[2]*Department of Rheumatic & Immunologic Diseases, Renmin Hospital, Hubei University of Medicine, Shiyan, Hubei 442000, China*
[3]*Department of Urinary Surgery, Renmin Hospital, Hubei University of Medicine, Shiyan, Hubei 442000, China*

Correspondence should be addressed to Gang Li; 439653434@qq.com and Yun Gong; 294361742@qq.com

Ling Cao and Mi Yu contributed equally to this work.

Received 10 September 2018; Revised 30 October 2018; Accepted 8 November 2018; Published 7 February 2019

Guest Editor: Jianxun Ding

This study investigated the effect of cellulase on the isolation of crude *Astragalus* polysaccharide (APS), analyzed the monosaccharide component of deproteinized APS, detected the molecular weights of purified APS, and examined the biological activities and the preliminary mechanism against rheumatoid arthritis (RA). Compared with water extraction method, cellulase-assisted extraction increased the yield of crude APS to 154% and polysaccharide contents to 121%. Crude APS was then purified by ethanol precipitation, Sevag deproteinization, and high-performance liquid chromatography (HPLC) analysis; monosaccharide contents of APS were different after cellulase-assisted method, especially galacturonic acid content which significantly increased. DEAE-52 cellulose column chromatography isolated three polysaccharide fractions, including a neutral polysaccharide (APS-water) and two acidic polysaccharides (APS-NaCl1 and APS-NaCl2). Using high-performance gel permeation chromatography (HPGPC), the molecular weights of APS-water, APS-NaCl1, and APS-NaCl2 were identified as 67.7 kDa, 234.1 kDa, and 189.4 kDa, respectively. Then their therapeutic effects and possible mechanism against RA were explored using type II collagen-induced arthritis (CIA) rat model. APS could significantly reduce paw swelling, serum concentration of IL-1β and TNF-α, and the expression levels of NF-κB-p65 and IκBα in synovial membranes in CIA rats. Our study indicated that cellulase significantly increases the yield and polysaccharide contents of crude APS, improves the product quality, and preserves the biological features against RA in CIA rats.

1. Introduction

Rheumatoid arthritis (RA) is a chronic, inflammatory, and systemic disease. The pathological features of RA are joint synovitis and pannus formation [1]. Currently, there is no known cure; the treatment aim is to prevent RA progression by keeping away from joint inflammation, destruction, and function loss [2]. Inflammation is the basis of RA development; therefore, it is an important target for RA therapy [3]. It has been proven that clinical agents targeting inflammatory mediators or various cytokines, such as antibody drugs (adalimumab and anakinra) which interfere with the progression of inflammation [4] and glucocorticoid drugs which inhibit cellular and humoral immunity [5], could prevent RA. Chemical drug treatment, alone or in combination, although can take significant effect in short term, is easy to illness relapses and side effects on patients. Biological agents, although work highly effective with low side effects, are very expensive [6]. Thus, there are still a lot of limitations in the clinical application of drugs against RA inflammation. It is necessary to continuously research and develop anti-inflammation, high-efficiency, low-toxicity, and moderate-priced drugs against RA.

Treatment of RA using Chinese herbal remedies has a long history [7]. In recent years, effective herbal medicine

extraction, such as tripterygium polyglycoside (TG), has shown good anti-inflammatory effects in the treatment of both RA animal models and patients [7]. It has been reported [8] that *Astragalus* polysaccharides (APS) inhibited cell growth and proinflammatory responses in IL-1β-stimulated fibroblast-like synoviocytes (FLSs). And APS is safe without any distinct toxicity and side effects [9], thus can be used for a long time. However, APS is mainly extracted using water extraction method, which has several disadvantages, such as low active ingredients (polysaccharide content), especially the yield (only about 2.5%) of crude APS [10], and high cost. All of these limit the development and utilization of APS. Enzyme engineering technology is a bioengineering technology used in recent years for the extraction of active constituents from natural plants [11]. Appropriate enzyme can decompose the plant tissues more gently and release the active ingredients faster, therefore increasing the extraction efficiency. The cell wall of *Astragalus membranaceus* is majorly composed of cellulose and is also the main barrier in releasing macromolecules, such as intracellular polysaccharides. The use of cellulase can hydrolyze cell walls and facilitate the dissolution of intracellular components [12].

In this study, cellulase was used to assist extraction of crude APS from *Astragalus membranaceus*, aimed at improving APS extraction efficiency, shortening the extraction time, preserving the biological activity of APS, and maximizing the utilization of APS. Then the crude APS was further purified and identified, and the effect and preliminarily mechanism of purified APS on treating RA in rat models were investigated.

2. Materials and Methods

2.1. Materials. Raw roots of *Astragalus membranaceus* (Fisch.) Bge. were obtained from Tongrentang Group Corporation (Beijing, China).

2.2. Extraction of Crude APS. The roots were dried and pulverized then were soaked in 80% ethanol overnight. After filtering with gauze, the residue was soaked with pure water at a mass ratio of 1 : 8 and was boiled for 2 h. When the temperature was lowered to 50°C, pH was adjusted to 5.5 with 0.5% sulfuric acid, and then cellulase (SDG-2425, Sunson, Beijing, China) was added to the final enzyme activity at 60 U per gram of raw materials. The residue was stirred for 90 min at 50°C and then was boiled for 1 h to inactive cellulase. After filtering with gauze again, the residue was soaked with pure water at a mass ratio of 1 : 5, then the cellulase hydrolysis process was repeated. The filtrates from two extraction processes were combined and concentrated by rotary evaporation, followed by removing impurity through stirring and soaking in 95% ethanol for 24 h. The precipitate was centrifuged, dried, and weighed, to be named crude APS. The crude APS extraction yield was calculated by the following:

$$\text{Crude APS extraction yield} = \left(\frac{\text{Weight of crude APS}}{\text{Weight of raw materials used}}\right) \times 100\%. \quad (1)$$

2.3. Determination of Polysaccharide Contents. The polysaccharide contents of crude APS were determined by phenol-sulfuric acid method. Crude APS was dissolved in deionized water, then 2.0 ml of each dissolved sample was mixed with 1.0 ml of 5% phenol, followed by shaking well. And then 5.0 ml of sulfuric acid was added and shaken vigorously at room temperature for 5 min. After boiling for 15 min and then cooling for 30 min, absorption at 490 nm was recorded on the basis of deionized water as blank control. Polysaccharide concentration was calculated according to the glucose standard curve. Then polysaccharide content was calculated by formula (2), and APS extraction yield was calculated by formula (3):

$$\text{APS content} = \left(\frac{\text{Weight of polysaccharide tested}}{\text{Weight of crude APS used}}\right) \times 100\%, \quad (2)$$

$$\text{APS extraction yield} = \text{APS content} \times \text{Crude APS extraction yield}. \quad (3)$$

2.4. Monosaccharide Composition Analyses. The protein in crude APS was removed with solvent of chloroform: n-butanol (3 : 1), and the supernatant was collected by centrifugation then was dried and weighed [13]. 10 mg APS was first hydrolyzed with 1 ml sulfuric acid solution (2 mol/l) at 110°C for 6 h. After precipitation and neutralization by barium sulfate, the sample was centrifuged and the supernatant was retained. Then HPLC was applied for monosaccharide composition analyses of vacuum dried APS. 1-Phenyl-3-methyl-5-pyrazolone (PMP) derivatives of various monosaccharide standards (Sigma, MO, USA) and monosaccharide from APSs were prepared by the reported method [14]. Then a Shimadzu LC-20A HPLC system (Kyoto, Japan) was used to analyze the monosaccharide composition of the APS according to the literature methods [15].

2.5. Isolation and Purification of APS. After purification by Sevag method and vacuum drying, APS was dissolved in deionized water to 0.2 g/ml and filtered using syringe filter (0.45 μm pore). 10 ml APS filtrate was loaded on a DEAE-52 cellulose column (2.4 × 70 cm, 4057-200, Whatman, Buckinghamshire, UK) that had been equilibrated with deionized water. The column was subsequently eluted with 400 ml deionized water, followed by 800 ml 0.5 M NaC1 aqueous solution with a flow rate of 1 ml per min. The eluate was collected into each tube (10 ml per tube), respectively. Polysaccharide content in each tube was measured through phenol-sulfuric acid method at 490 nm. The eluates of each major fraction were pooled, dialyzed, concentrated, and lyophilized. The three combined eluted fractions were denoted as APS-water, APS-NaCl1, and APS-NaCl2.

2.6. Molecular Weight Determination. High-performance gel permeation chromatography (HPGPC) was used to evaluate molecular weights and homogeneity of the three polysaccharide fractions from DEAE-52 cellulose column [16]. APS-water, APS-NaCl1, or APS-NaCl2 was dissolved in deionized water to 2 mg/ml and filtered through syringe filter (0.45 μm

pore). 20 μl filtrate was applied to a TSKgel G-3000PWXL liquid chromatography column which was eluted with deionized water with a flow rate of 0.6 ml/min. A series of different molecular weight of dextran standards (1.0-20.0 kDa, Sigma, MO, USA) were applied for calibration. The standard curve was obtained through plotting the logarithm of the known molecular weight of each standard against the corresponding retention time. Afterwards, the molecular weight was determined from the previously constructed standard curve according to the retention time of each sample.

2.7. RA Rat Model Establishment and Administration. Type II collagen-induced arthritis (CIA) rats were established using female adult Sprague-Dawley rats (200 g~220 g). All experiments were undertaken with the approval of Hubei Provincial Laboratory Animal Public Service Center (Wuhan, China). RA in rats was induced as previously described [17] with slight modification. Bovine type II collagen (MD Biosciences, MN, USA) was sterilely dissolved to 4 mg/ml final concentration using 0.1 M acetic acid then was further emulsified using the same volume of 1 mg/ml Freund's complete adjuvant (Sigma, MO, USA). After shaking overnight, the emulsion (CFA) was obtained with 1 mg collagen in 0.5 ml emulsion. After rats were allowed to acclimate for 1 week, rats were anesthetized with isoflurane and injected intradermally at both the base of the tail and the right hind paw with 0.1 ml CFA in each point. At day 7 after primary immunization, each rat was administered a booster injection of 0.1 ml CFA emulsion into the tail intradermally. At day 14, a total of 18 rats with ankle swelling were selected for further experiments. 6 female rats in the vehicle group were injected with phosphate buffer saline (PBS, pH 7.4) following the same steps as described above for CIA rats. Except the vehicle group, CIA rats were divided into the following groups with 6 rats: CIA group, APS group, and TG group. Rats were infused intragastrically with 4 g/kg·d^{-1} APS (1 g/ml dissolved in PBS) or 6 mg/kg·d^{-1} TG (0.01 g/ml dissolved in PBS) once daily. Rats in the vehicle and CIA groups were infused with the same volume of PBS.

2.8. Measurement of Paw Volume. All rats were monitored for hind paw swelling once a week at day 0, after CFA or PBS injection, and before and after treatments. Paw volume was measured to indicate the hind paw swelling using a plethysmometer (520-IITC, Thermo, MA, USA). The mean values of volume were calculated and plotted at each time point.

2.9. ELISA. 2 h after administration on day 28, all rats were sacrificed. Blood was collected from the femoral artery and was centrifuged for 15 min at 4000 rpm at 4°C. The serum (supernatant) was collected and kept at -80°C. Cytokine concentrations (TNF-α and IL-1β) were quantified through ELISA kits (Enzo, Raamsdonksveer, Netherlands) according to the manufacturer's procedure. Optical density (OD) values were recorded at 450 nm in a microplate reader. Concentrations were calculated according to the standard curve.

2.10. Western Blotting. After all rats were anesthetized and sacrificed on the last day of experiment, the synovial membranes were collected together in each group and immediately stored at -80°C. For western blotting, each tissue was lysed to extract total protein by using RIPA buffer (Sigma, MO, USA). Then the protein concentration for each sample was determined by BCA kit (Thermo, MA, USA) and loaded SDS by boiling for 5 min with loading buffer (Boston Biochem, MA, USA). The SDS-loaded protein was separated by SDS-PAGE according to procedures in Bio-Rad system (CA, USA), followed by transferring to PVDF membrane (Merck Millipore, MA, USA). The membranes were blocked with 5% goat serum (in TBST), then incubated in refrigerator overnight with the following primary antibodies, anti-NF-κB-p65 monoclonal (Cell Signaling Technology, 1 : 800, MA, USA) and anti-IκBα monoclonal (Cell Signaling Technology, 1 : 1000, MA, USA). Signals were further detected using appropriate IRDye 800CW-conjugated secondary antibodies at room temperature for 1 h. The complex was visualized with imaging systems (Li-Cor Biosciences, USA). GAPDH on the same membrane was used as a loading control. All western blotting analyses were performed in triplicate.

2.11. Data Analysis. All statistical analyses of this study were run with IBM SPSS 19.0. We performed one-way analysis of variance (ANOVA) to determine significant differences, followed by LSD-Q test for comparison between groups. Results were presented as means ± standard deviation. P values less than 5% reflected statistical significance.

3. Results and Discussions

Traditional Chinese medicine (TCM) has a long history of usage in treating RA [18]. Recently, a variety of TCM drugs and methods with good curative effect and few side effects have emerged. These can reduce the side effects in therapy with NSAIDs (nonsteroidal anti-inflammatory drugs) and glucocorticoids, showing the characteristics and advantages of TCM in treating RA [18]. Fangji Huangqi decoction is a common prescription for RA treatment, and its therapeutic effect has been clinically proven [19]. *Astragalus membranaceus* is the main component of Fangji Huangqi decoction. Pharmacological studies have shown that APS, as the main ingredient of *Astragalus membranaceus*, has various therapeutic functions, such as immune regulation [20, 21], anti-inflammation [7, 22], antioxidation [23], antivirus [24, 25], antibacterial [26], lowering blood sugar [27], and protecting the liver [28] and kidney [29]. Furthermore, it has been reported that APS could prevent RA progression [8, 30]. However, as a macromolecule, the extraction yield and purity of APS are greatly limited [10]. Thus, a variety of technologies are used to assist the water extraction process to elevate the yield and purity of APS. Cellulase can accelerate the release of APS from plant cells; more importantly, it also preserves the structural integrality and bioactivity of APS without destruction because cellulase swells the cell wall with high specificity [12]. This present study was to investigate the assisted effect of cellulase on crude APS extraction. Furthermore, the crude APS was purified and the physicochemical properties of purified APS were determined, and

Table 1: Yield and content of *Astragalus* polysaccharides extracted by different methods.

Group	Crude APS extraction yield (%)	APS content (%)	APS extraction yield (%)
Water extraction	2.45 ± 0.32	25.71 ± 1.82	0.63 ± 0.11
Cellulase-assisted extraction	3.78 ± 0.43*	31.24 ± 2.71*	1.18 ± 0.25*
P value	*0.013*	*0.043*	*0.026*

Values are expressed as mean ± standard deviation ($n = 3$). Significant effect compared to result by water extraction method: $^{*}P < 0.05$.

Table 2: Monosaccharide composition of *Astragalus* polysaccharides extracted by different methods.

Group	Glucose (%)	Galactose (%)	Arabinose (%)	Mannose (%)	Galacturonic acid (%)
Water extraction	65.11 ± 0.02	26.12 ± 0.81	6.56 ± 0.11	1.24 ± 0.07	0.97 ± 0.12
Cellulase-assisted extraction	47.32±0.03***	35.49±0.08***	12.23±0.18***	2.08±0.25**	2.88±0.08***
P value	*0.001*	*0.001*	*0.001*	*0.005*	*0.001*

Values are expressed as mean ± standard deviation ($n = 3$). Significant effect compared to result by water extraction method: $^{**}P < 0.01$; $^{***}P < 0.001$.

then the anti-inflammatory effect and possible mechanism of purified APS against RA in CIA rats were explored.

3.1. Cellulase Increased the Extraction Efficiency of Crude APS from Astragalus membranaceus. As shown in Table 1, crude APS yield increased from 2.45%±0.32% by water extraction method to 3.78%±0.43% with cellulase-assisted extraction method, increasing 54%. Polysaccharide content in crude APS increased from 25.71%±1.82% by water extraction method to 31.24%±2.71% with cellulase treatment. Thus, extraction yield of APS was increased to 187% by water extraction method, from 0.63%±0.11% to 1.18%±0.25%. Our results indicated that the yield and polysaccharide content of crude APS were greatly improved by cellulase-assisted extraction method, compared to conventional method. Chen et al. [11] studied the effect of various enzymes on the yield of APS; similar to our results, they found that cellulase could improve APS extraction yield nearly to 1.5-fold. The function of cellulase is to decompose cellulose [12], which is the main structural component of the cell wall. It helps to increase the release of polysaccharides from the cytoplasm, thereby ultimately increasing yield and polysaccharide content. In our cellulase-assisted extraction procedure, repeated water extraction and cellulase treatment after boiling are two key steps. On the one hand, softening of raw material by boiling contributes to the full functionality of the cellulase. On the other hand, a large amount of saccharides obtained by initial enzymatic hydrolysis might exert inhibitory feedback on cellulase function. It has been reported that sucrose and glucose in the extract have a negative effect on cellulase activity [31]. Therefore, the secondary enzymatic treatment to the filter residue after filtration is necessary, and it helps to improve the efficiency of cellulase in the second extraction and fully extract the remaining polysaccharides.

Our study showed that the isolation procedure with cellulase-assisted treatment is simple and feasible and can greatly increase APS yield, indicating that cellulase treatment is an effective process in utilizing *Astragalus membranaceus*. However, there is still a need for identifying the biological activity and effectiveness of APS obtained in this process.

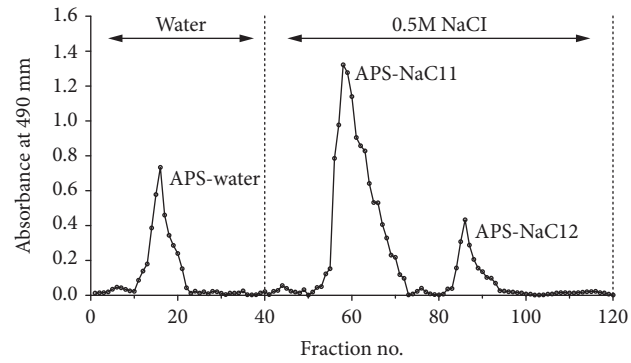

Figure 1: Elution curve of polysaccharide fractions from crude APS by DEAE-52 cellulose column chromatography.

3.2. Purification of APS, Monosaccharide Composition, and Molecular Weight Analyses. Crude APS was isolated by hot water extraction, cellulase hydrolysis, and ethanol precipitation. After purification by Sevag method, vacuum drying, decomposition, and HPLC analysis, APS was identified with the composition of glucose, galactose, arabinose, mannose, and galacturonic acid (Table 2), and it showed the homogeneity of monosaccharide types of APSs extracted by different methods. However, the extraction method significantly influenced the monosaccharide contents (%). The contents of galacturonic acid, mannose, and arabinose of APS from cellulase-assisted extraction were 2.88%, 2.08%, and 12.23%, respectively, which were significantly higher than those of APS from water extraction (0.97%, 1.24%, and 6.56%). The result was similar to a study by Shang et al. [32] and suggested a better antioxidant activity and potential bioactivity of APS extracted from cellulase-assisted method [33].

Then after DEAE-52 cellulose ion-exchange column chromatography, three purified polysaccharide fractions were obtained (Figure 1). Anionic DEAE-52 cellulose chromatography column was selected because polysaccharide was negatively charged. Tube 11-22, tube 51-72, and tube 82-94 were combined, respectively, and then dialyzed and

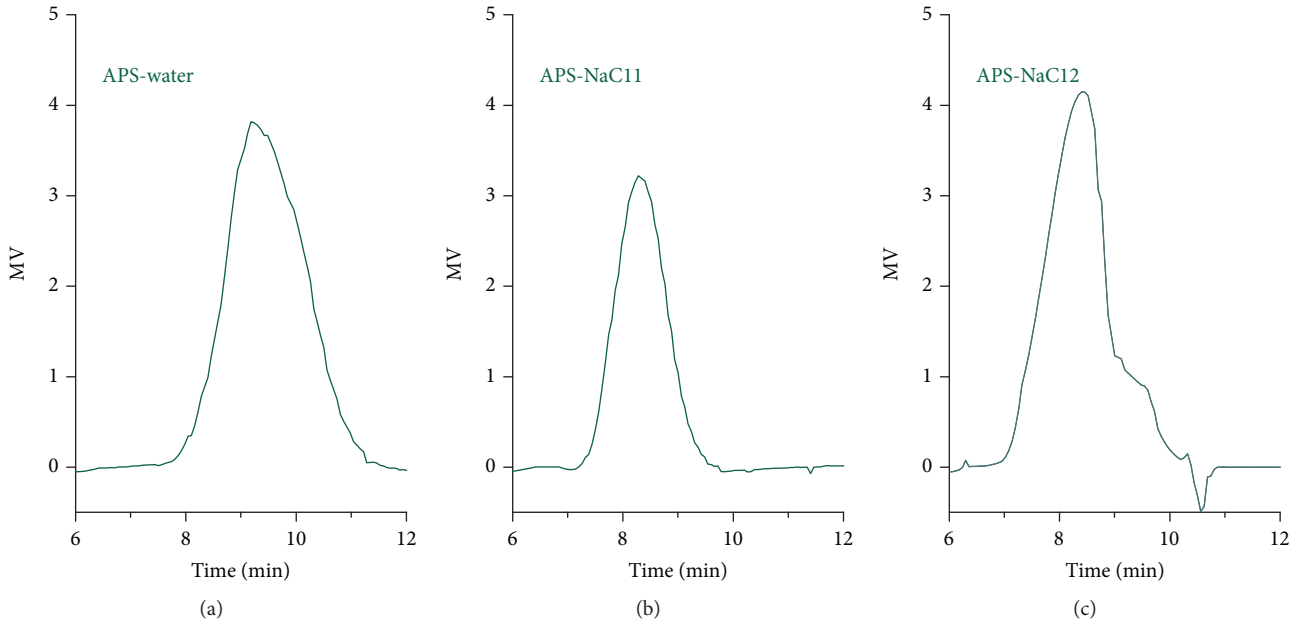

Figure 2: High-performance gel permeation chromatography (HPGPC) chromatogram of APS fractions (APS-water, APS-NaCl1, and APS-NaCl2) gained with a TSKgel G-3000PWXL liquid chromatography column. (a) APS-water in HPGPC. (b) APS-NaCl1 in HPGPC. (c) APS-NaCl2 in HPGPC.

lyophilized to obtain the fractions, APS-water, APS-NaCl1, or APS-NaCl2. APS-water is a neutral polysaccharide fraction which does not bind to the column and could be eluted by deionized water. APS-NaCl1 and APS-NaCl2 are acidic polysaccharides which bind to the column and could be eluted by 0.5 M NaCl solution.

Molecular weights of purified polysaccharide fractions were determined by HPGPC. As shown in Figure 2, three polysaccharide fractions exhibited a single peak, which indicated that the fractions were homogeneous. Based on the calibration curve of dextran standards, the average molecular weights of APS-water, APS-NaCl1, and APS-NaCl2 were 67.7 kDa (Figure 2(a)), 234.1 kDa (Figure 2(b)), and 189.4 kDa (Figure 2(c)), respectively. Different from our results, Yan et al. [34] reported that the molecular weight distribution of APS is extensive. One possible reason is that APS obtained by Yan et al. [34] may not be purified. Notably, consistent with Yan et al.'s result [34] that the molecular weights of most APS (57.6%) were more than 150 kDa, in our study, molecular weights of APS-NaCl1 and APS-NaCl2 were more than 150 kDa and constituted the main ingredients of purified APS.

3.3. Relief of RA Symptoms In Vivo by APS. In order to verify the biological activity of APS obtained by cellulase hydrolysis, the anti-RA effect of purified APS in CIA rats was investigated. There are two classical rodent models of RA, adjuvant arthritis (AA) rats and CIA rats. In previous reports, the anti-RA effect of APS was detected in AA rats [30]. However, compared with AA rat, CIA rat has more obvious and serious synovial hyperplasia, cartilage destruction, and other secondary lesions. Moreover, in CIA rats, RA duration is much longer, and signs are similar to human RA. Thus, the CIA rat model is more ideal for the study of RA [35]. Rat foot volume was measured by displacement method and significantly increased in CIA rats from day 7 to day 14 after the primary injection (Figure 3). Foot volumes in CIA rats were notably larger

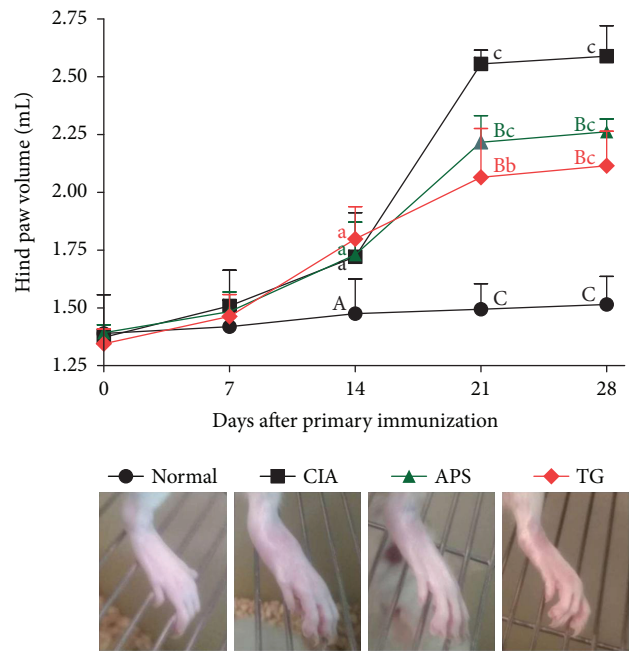

Figure 3: Paw volume evaluation before and after RA induction and drug administration. Data represent the mean ± SD of 6 rats per group. Significant effect compared to the normal group: (a) $P < 0.05$, (b) $P < 0.01$, (c) $P < 0.001$; significant effect compared to the CIA group: (A) $P < 0.05$, (B) $P < 0.01$, (C) $P < 0.001$.

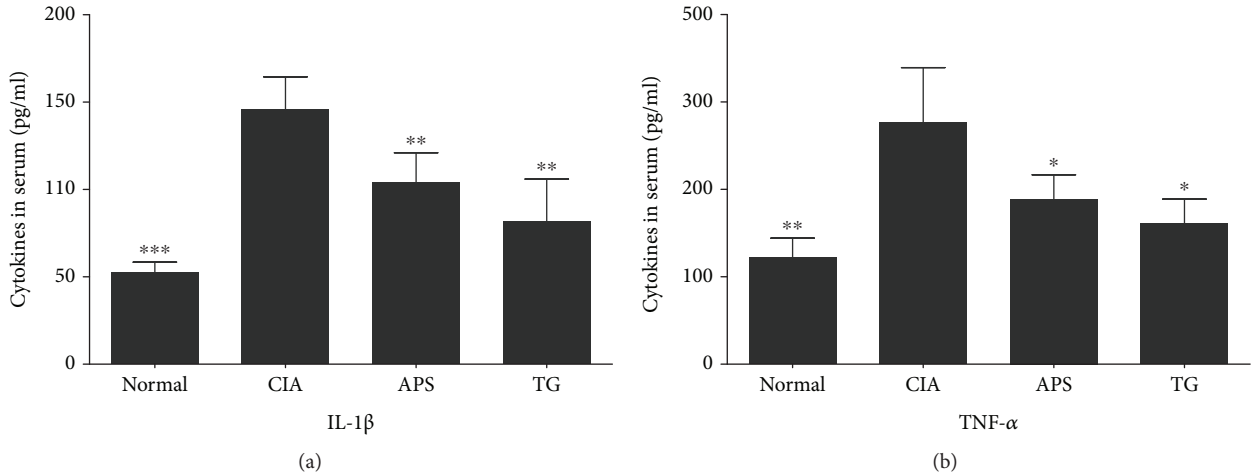

Figure 4: Serum levels of proinflammatory cytokines after 2 weeks of drug administration in type II collagen-induced arthritis (CIA) rats and vehicle rats. (a) Serum IL-1β levels. (b) TNF-α levels. Data represent the mean ± SD of 6 rats per group. Significant effect compared to the CIA group: $^{*}P < 0.05$, $^{**}P < 0.01$, $^{***}P < 0.001$.

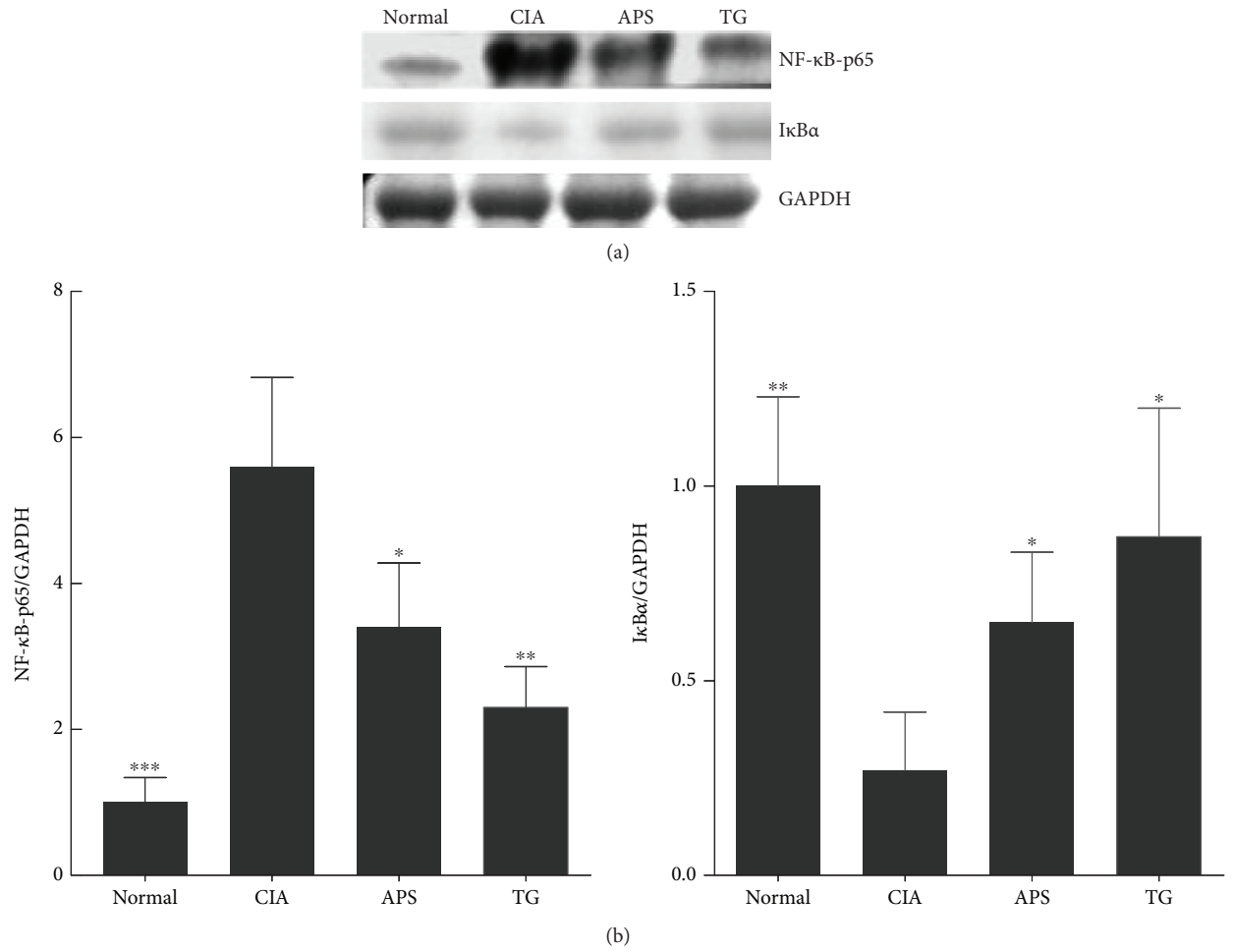

Figure 5: Western blotting analysis of the effects of APS administration on protein expression of NF-κB-p65 and IκBα, as well as GAPDH in synovial membrane homogenates from rats in each group. (a) Representative western blots are shown. (b) Ratios of optical density are calculated on NF-κB-p65 to GAPDH and IκBα to GAPDH. Data represent the mean ± SD of 6 rats per group. Significant effect compared to the CIA group: $^{*}P < 0.05$, $^{**}P < 0.01$, $^{***}P < 0.001$.

than those in vehicle rats on day 14 ($P < 0.05$), indicating the successful CIA rat models. After 2 weeks of administration, the hind paw volumes of rats in the CIA group continued to increase, while the volumes in the APS group or the TG group decreased notably ($P < 0.05$), compared to those in the CIA group. Although volume was slightly smaller in the TG group from day 21 to day 28, there was no statistical difference in the hind paw volumes in the TG group versus the APS group.

3.4. The Anti-inflammatory Activity on CIA Rats In Vivo by APS. Inflammation is the basic and core step in RA progression. Cytokines are involved in the regulation of various inflammatory responses and play a key role in each stage of the RA pathological process [36]. As shown in Figure 3, APS had an acceptable effect in reducing RA symptoms in CIA rats. And it was speculated that APS might decrease inflammation by reducing serum cytokines levels. Proinflammatory cytokines, TNF-α and IL-1β, are pleiotropic molecules which play central roles in swelling, pannus formation and perpetuation, and so on [37]. After 2 weeks of administration, rat serum IL-1β (Figure 4(a)) and TNF-α (Figure 4(b)) were significantly lower in the APS group than in the CIA group ($P < 0.05$), indicating that APS contributed to the inhibition of serum cytokines and alleviated inflammation. Interestingly, this result was consistent with previous studies [8]. Meng et al. [8] reported that APS could *in vitro* decrease TNF-α secreted in RA fibroblast-like synoviocytes. Jiang et al. [30] also verified that APS could *in vivo* diminish serum TNF-α and IL-1β in AA rats.

3.5. Inhibitory Effect to NF-κB Activation in CIA Rats by APS. NF-κB signaling pathway is considered as the main "switch" in secreting proinflammatory cytokines and can activate and regulate a variety of cytokines, including TNF-α and IL-1β [38]. In Figure 5, compared with the CIA group, APS and TG significantly decreased NF-κB-p65 expression ($P < 0.05$) and significantly increased IκBα expression ($P < 0.05$). In physical status, NF-κB binds to its inhibitory protein, IκB, to form a complex, which is stabilized in the cytoplasm and cannot function as a transcription factor. In pathological status, NF-κB releases from the complex because IκB is phosphorylated by IKK kinase and phosphorylated IκB is subsequently ubiquitinated and degraded by proteasome [39]. The dissociative NF-κB then travels into the cell nucleus, binds promoter sequences, and activates transcription of various genes to lead to transcriptional expression of downstream inflammatory molecules [40]. Numerous studies have shown that NF-κB exerts harmful and crucial effect in the positive feedback mechanism in RA inflammation. NF-κB not only upregulates the transcriptional levels and serum concentrations of IL-1β, TNF-α, and IL-6 but also can be activated by increased IL-1β and TNF-α through intracellular cascade responses. The positive feedback contributes to maintain and accelerate the inflammatory response of RA and leads to structural damage of the bone and cartilage ultimately [41, 42]. In this study, APS administration in CIA rats reversed the expression levels of NF-κB-p65 and IκBα, thereby blocking a harmful feedback and cycle (increased proinflammatory cytokines → activated NF-κB signaling → induced release and increasing of proinflammatory cytokines).

4. Conclusion

In summary, our results indicate that cellulase can significantly increase the APS yield and polysaccharide content, improve the product quality, and preserve the biological features in reducing RA symptoms, cytokine secretion, and NF-κB activation.

Data Availability

The data used to support the findings of this study are available from the corresponding author upon request.

Conflicts of Interest

No conflict of interest was declared by the authors.

References

[1] M. Yang, J. Ding, Y. Zhang et al., "Activated macrophage-targeted dextran-methotrexate/folate conjugate prevents deterioration of collagen-induced arthritis in mice," *Journal of Materials Chemistry B*, vol. 4, no. 12, pp. 2102–2113, 2016.

[2] Y. Kim, H. C. Oh, J. W. Park et al., "Diagnosis and treatment of inflammatory joint disease," *Hip & Pelvis*, vol. 29, no. 4, pp. 211–222, 2017.

[3] M. Yang, J. Ding, X. Feng et al., "Scavenger receptor-mediated targeted treatment of collagen-induced arthritis by dextran sulfate-methotrexate prodrug," *Theranostics*, vol. 7, no. 1, pp. 97–105, 2017.

[4] D. Wang, Y. Li, Y. Liu, and G. Shi, "The use of biologic therapies in the treatment of rheumatoid arthritis," *Current Pharmaceutical Biotechnology*, vol. 15, no. 6, pp. 542–548, 2014.

[5] S. Paolino, M. Cutolo, and C. Pizzorni, "Glucocorticoid management in rheumatoid arthritis: morning or night low dose?," *Reumatologia/Rheumatology*, vol. 4, no. 4, pp. 189–197, 2017.

[6] C. F. Allaart, F. C. Breedveld, and B. A. Dijkmans, "Treatment of recent-onset rheumatoid arthritis: lessons from the Best study," *Journal of Rheumatology Supplement*, vol. 80, pp. 25–33, 2007.

[7] X. Chu, X. J. Liu, J. M. Qiu, X. L. Zeng, H. R. Bao, and J. Shu, "Effects of Astragalus and Codonopsis pilosula polysaccharides on alveolar macrophage phagocytosis and inflammation in chronic obstructive pulmonary disease mice exposed to PM2.5," *Environmental Toxicology and Pharmacology*, vol. 48, pp. 76–84, 2016.

[8] Q. Meng, X. Du, H. Wang, H. Gu, J. Zhan, and Z. Zhou, "Astragalus polysaccharides inhibits cell growth and pro-inflammatory response in IL-1β-stimulated fibroblast-like synoviocytes by enhancement of autophagy via PI3K/AKT/m-TOR inhibition," *Apoptosis*, vol. 22, no. 9, pp. 1138–1146, 2017.

[9] S. Y. Yu, H. T. Ouyang, J. Y. Yang et al., "Subchronic toxicity studies of Radix Astragali extract in rats and dogs," *Journal of Ethnopharmacology*, vol. 110, no. 2, pp. 352–355, 2007.

[10] Y. Chen, F. Yao, K. Ming, D. Wang, Y. Hu, and J. Liu, "Polysaccharides from traditional Chinese medicines: extraction, purification, modification, and biological activity," *Molecules*, vol. 21, no. 12, article 1705, 2016.

[11] H. Chen, X. Zhou, and J. Zhang, "Optimization of enzyme assisted extraction of polysaccharides from Astragalus membranaceus," *Carbohydrate Polymers*, vol. 111, pp. 567–575, 2014.

[12] P. Phitsuwan, N. Laohakunjit, O. Kerdchoechuen, K. L. Kyu, and K. Ratanakhanokchai, "Present and potential applications of cellulases in agriculture, biotechnology, and bioenergy," *Folia Microbiologia (Praha)*, vol. 58, no. 2, pp. 163–176, 2013.

[13] L. Y. Xie, Y. Zhang, W. H. Peng, and B. C. Gan, "Study on methods of deproteinization from Phellinus baumii polysaccharide," *Zhong Yao Cai*, vol. 34, no. 2, pp. 293–295, 2011.

[14] S. L. Chen, H. M. Shang, J. Y. Yang, R. Li, and H. X. Wu, "Effects of different extraction techniques on physicochemical properties and activities of polysaccharides from comfrey (Symphytum officinale L.) root," *Industrial Crops and Products*, vol. 121, pp. 18–25, 2018.

[15] M. Y. Duan, H. M. Shang, S. L. Chen, R. Li, and H. X. Wu, "Physicochemical properties and activities of comfrey polysaccharides extracted by different techniques," *International Journal of Biological Macromolecules*, vol. 115, pp. 876–882, 2018.

[16] X. M. Li, X. L. Li, and A. G. Zhou, "Evaluation of antioxidant activity of the polysaccharides extracted from Lycium barbarum fruits in vitro," *European Polymer Journal*, vol. 43, no. 2, pp. 488–497, 2007.

[17] J. Y. Wang, Y. Yuan, X. J. Chen et al., "Extract from *Eucommia ulmoides* Oliv. ameliorates arthritis via regulation of inflammation, synoviocyte proliferation and osteoclastogenesis *in vitro* and *in vivo*," *Journal of Ethnopharmacology*, vol. 194, pp. 609–616, 2016.

[18] S. Lü, Q. Wang, G. Li, S. Sun, Y. Guo, and H. Kuang, "The treatment of rheumatoid arthritis using Chinese medicinal plants: from pharmacology to potential molecular mechanisms," *Journal of Ethnopharmacology*, vol. 176, pp. 177–206, 2015.

[19] R. Wang, T. M. Ma, F. Liu, and H. Q. Gao, "Research progress on pharmacological action and clinical application of Stephania Tetrandrae Radix," *Zhongguo Zhong Yao Za Zhi*, vol. 42, no. 4, pp. 634–639, 2017.

[20] Y. J. Gao, F. Zhu, J. M. Qian, and J. Y. Dai, "Therapeutic and immunoregulatory effect of GATA-binding protein-3/T-box expressed in T-cells ratio of astragalus polysaccharides on 2, 4, 6-trinitrobenzene sulfonic acid-induced colitis in rats," *Chinese Journal of Integrative Medicine*, vol. 22, no. 12, pp. 918–924, 2016.

[21] S. Sun, K. Zheng, H. Zhao et al., "Regulatory effect of astragalus polysaccharides on intestinal intraepithelial $\gamma\delta$T cells of tumor bearing mice," *Molecules*, vol. 19, no. 9, pp. 15224–15236, 2014.

[22] Y. C. Huang, H. J. Tsay, M. K. Lu et al., "*Astragalus membranaceus*-polysaccharides ameliorates obesity, hepatic steatosis, neuroinflammation and cognition impairment without affecting amyloid deposition in metabolically stressed APPswe/PS1dE9 mice," *International Journal of Molecular Sciences*, vol. 18, no. 12, article 2746, 2017.

[23] W. Chen, J. Ju, Y. Yang et al., "Astragalus polysaccharides protect cardiac stem and progenitor cells by the inhibition of oxidative stress-mediated apoptosis in diabetic hearts," *Drug Design, Development and Therapy*, vol. 12, pp. 943–954, 2018.

[24] P. Zhang, X. Liu, H. Liu et al., "Astragalus polysaccharides inhibit avian infectious bronchitis virus infection by regulating viral replication," *Microbial Pathogenesis*, vol. 114, pp. 124–128, 2018.

[25] J. Jiang, C. Wu, H. Gao, J. Song, and H. Li, "Effects of astragalus polysaccharides on immunologic function of erythrocyte in chickens infected with infectious bursa disease virus," *Vaccine*, vol. 28, no. 34, pp. 5614–5616, 2010.

[26] X. Yin, L. Chen, Y. Liu et al., "Enhancement of the innate immune response of bladder epithelial cells by Astragalus polysaccharides through upregulation of TLR4 expression," *Biochemical and Biophysical Research Communications*, vol. 397, no. 2, pp. 232–238, 2010.

[27] Y. C. Juan, Y. H. Kuo, C. C. Chang et al., "Administration of a decoction of sucrose- and polysaccharide-rich radix astragali (*huang qi*) ameliorated insulin resistance and fatty liver but affected Beta-cell function in type 2 diabetic rats," *Evidence--based Complementary and Alternative Medicine*, vol. 2011, Article ID 349807, 11 pages, 2011.

[28] M. Hamid, D. Liu, Y. Abdulrahim et al., "Amelioration of CCl4-induced liver injury in rats by selenizing Astragalus polysaccharides: role of proinflammatory cytokines, oxidative stress and hepatic stellate cells," *Research in Veterinary Science*, vol. 114, pp. 202–211, 2017.

[29] C. Yuan, X. Pan, Y. Gong et al., "Effects of Astragalus polysaccharides (APS) on the expression of immune response genes in head kidney, gill and spleen of the common carp, Cyprinus carpio L," *International Immunopharmacology*, vol. 8, no. 1, pp. 51–58, 2008.

[30] J. B. Jiang, J. D. Qiu, L. H. Yang, J. P. He, G. W. Smith, and H. Q. Li, "Therapeutic effects of astragalus polysaccharides on inflammation and synovial apoptosis in rats with adjuvant-induced arthritis," *International Journal of Rheumatic Diseases*, vol. 13, no. 4, pp. 396–405, 2010.

[31] X. M. Yang and J. C. Yang, "Effect of sugars on the stability of cellulase," *Journal of Tsinghua University (Science and Technology)*, vol. 40, no. 2, pp. 51–54, 2000.

[32] H. M. Shang, S. L. Chen, R. Li, H. Z. Zhou, H. X. Wu, and H. Song, "Influences of extraction methods on physicochemical characteristics and activities of Astragalus cicer L. polysaccharides," *Process Biochemistry*, vol. 73, pp. 220–227, 2018.

[33] Z. J. Zhang, F. H. Wang, M. C. Wang, L. P. Ma, H. Ye, and X. X. Zeng, "A comparative study of the neutral and acidic polysaccharides from Allium macrostemon Bunge," *Carbohydrate Polymers*, vol. 117, pp. 980–987, 2015.

[34] Q. J. An, L. J. Han, Z. Q. Jiang, and C. J. Huang, "Molecular mass distribution of astragalus polysaccharides," *Food Science*, vol. 25, no. 8, pp. 27–30, 2004.

[35] H. Lin, Y. H. He, Y. Li, Y. L. Lu, and B. F. Shen, "Rheumatoid arthritis model in rat induced by type II collagen and Freund's complete adjuvant," *Acta Laboratorium Animalis Scientia Sinica*, vol. 7, no. 1, pp. 1–6, 1999.

[36] M. Noack and P. Miossec, "Selected cytokine pathways in rheumatoid arthritis," *Seminars in Immunopathology*, vol. 39, no. 4, pp. 365–383, 2017.

[37] S. B. Abramson and A. Amin, "Blocking the effects of IL-1 in rheumatoid arthritis protects bone and cartilage," *Rheumatology*, vol. 41, no. 9, pp. 972–980, 2002.

[38] J. A. Roman-Blas and S. A. Jimenez, "NF-κB as a potential therapeutic target in osteoarthritis and rheumatoid arthritis," *Osteoarthritis and Cartilage*, vol. 14, no. 9, pp. 839–848, 2006.

[39] N. M. Blackwell, P. Sembi, J. S. Newson, T. Lawrence, D. W. Gilroy, and P. S. Kabouridis, "Reduced infiltration and increased apoptosis of leukocytes at sites of inflammation by systemic administration of a membrane-permeable IκBα repressor," *Arthritis & Rheumatism*, vol. 50, no. 8, pp. 2675–2684, 2004.

[40] M. S. Hayden and S. Ghosh, "Shared principles in NF-κB signaling," *Cell*, vol. 132, no. 3, pp. 344–362, 2008.

[41] S. S. Makarov, "NF-κB in rheumatoid arthritis: a pivotal regulator of inflammation, hyperplasia, and tissue destruction," *Arthritis Research*, vol. 3, no. 4, pp. 200–206, 2001.

[42] T. Okamoto, "NF-κ B and rheumatic diseases," *Endocrine, Metabolic & Immune Disorders - Drug Targets*, vol. 6, no. 4, pp. 359–372, 2006.

Hindawi
International Journal of Polymer Science
Volume 2019, Article ID 9542759, 7 pages
https://doi.org/10.1155/2019/9542759

Research Article

Immunomodulatory Effects of *Robinia pseudoacacia* Polysaccharides on Live Vaccine against Infectious Bronchitis in Immunosuppressive Chickens

Qiuyan Sun, Fang Li, Caixia Wang, and Meiyan Shen

Department of Veterinary Medicine, Shandong Vocational Animal Science and Veterinary College, Weifang 261061, China

Correspondence should be addressed to Fang Li; sdmylifang@163.com

Received 15 October 2018; Accepted 13 November 2018; Published 7 February 2019

Guest Editor: Jianxun Ding

In order to investigate the immunomodulatory effect of *Robinia pseudoacacia* Polysaccharides (RPPS) on vaccine against Infectious Bronchitis (IB) in immunosuppressive chickens, the artificial leukemia chicken model was established and then the IB live vaccine (H120 strain) was immunized. The immunomodulatory efficacy of RPPS was determined by the antibody titer, the lymphocyte transformation rate in peripheral blood, the $CD4^+$ and $CD8^+$ T lymphocyte levels in peripheral blood, and the cytokine levels in the serum. The results showed that RPPS could not only enhance the immune effect of IB live vaccine but also improve the immunity of immunosuppressive chickens. Thus, the function of RPPS immunopotentiator could be further developed.

1. Introduction

In China's large-scale chicken farms, reticuloendotheliosis virus (REV), Marek's disease virus (MDV), avian leukosis virus (ALV), chicken infectious bursal disease virus (IBDV), and other viruses could cause different levels of immunosuppression in chickens; therefore, diseases induced by the viruses are called immunosuppressive diseases. Immunosuppressive diseases have caused significant reduction in poultry production performance, immune system function, and the ability of poultry to respond to vaccine immunization, leading to huge damage and losses to the poultry industry [1, 2]. Studies have found that immunosuppressive diseases were very common in the poultry industry in China and had different levels of inhibitory effect on the antibody production after vaccine immunization in chicks. Avian leukosis (AL) is an avian infectious disease caused by avian leukosis virus (ALV). Infection of ALV could induce growth retardation, decreased production performance, increased mortality and feed consumption, increased development of multitissue tumors, and also immunosuppression in chicken flocks indirectly causing immune failure of other vaccines, which resulted in a huge economic loss to the poultry industry.

Infectious Bronchitis (IB) caused by infectious bronchitis virus (IBV) is characterized by cough, sneezing, tracheal vocalization, difficulty in breathing, asphyxia, kidney enlargement, paleness, urate deposition, "spotted kidney," and egg production and quality decline [3]. At present, it has seriously affected the development of China's poultry industry [4, 5]. Studies have shown that *Robinia pseudoacacia* Linn had various biological effects including antitumor, antioxidation, antibacterial, antiviral, and immune regulation function [6, 7] and had rare toxicity on the body. *Robinia pseudoacacia* Linn is a flower of the perennial deciduous tree eucalyptus of the genus Rhododendron. *Robinia pseudoacacia* Linn has a remarkable curative effect on blood vomiting, hematuria, hemorrhoid hemorrhage, wind-heat redness, hypertension, hyperlipidemia, cervical lymphatic tuberculosis, vascular sclerosis, diabetes, retinitis, psoriasis, etc. It can deworm and treat pharyngitis and has extremely high medicinal value [8, 9], so *Robinia pseudoacacia* Linn has high medical value and belongs to healthy products in people's life as a traditional Chinese medicine. *Robinia pseudoacacia* polysaccharides (RPPS) are a kind of plant polysaccharides. So far, there have been few reports on the immunomodulatory effects of *Robinia pseudoacacia*

polysaccharides (RPPS) on livestock and poultry, especially on RPPS for immunosuppressive chickens. The immune regulation of IB vaccine has not been reported at all. Therefore, we established a model of artificial leukemia chicken and then immunized them with live IB vaccine (H120 strain). The efficacy was determined by detecting the antibody titer, immune organ index, lymphocyte conversion rate in the peripheral blood, $CD4^+$ and $CD8^+$ T cell levels in the peripheral blood, and cytokine levels in the serum. The study will lay the foundation for further development of application value and market prospect of *Robinia pseudoacacia* polysaccharides and of green ecological animal husbandry in China.

2. Materials and Methods

2.1. Reagents. Concanavalin A (ConA), lymphocyte separation solution, IL-2 ELISA kit, and IFN-γ ELISA kit were purchased from Sigma, USA. RPMI-1640 (Gibco) and fetal bovine serum (Gibco) were purchased from Invitrogen, USA.

2.2. Instrument. PE-6800VET automatic animal blood analyzer was from Japan Sysmex company. Enzyme standard analyzer RT-6100 was from Rayto, Shenzhen, China.

2.3. Strains and Vaccines. The IBV H120 (infectious bronchitis H120) strain with $TCID_{50}$ of $10^{-7.32}$/0.1 mL was kindly provided by Professor Yuyan Wang from the Department of Pathogenic Biology of Fudan University, School of Medicine. ALV-J (Avian Leukosis virus-J) NX0102 strain $TCID_{50}$ of $10^{-5.96}$/0.1 mL was kindly provided by Professor Ruiliang Zhu of Shandong Agricultural University. IB H120 live vaccine was purchased from Qingdao Yibang Bioengineering Co. Ltd. (production batch number: 150132016).

2.4. Extraction and Determination of Robinia pseudoacacia Polysaccharides (RPPS) [10]. Fresh *Robinia pseudoacacia* flowers, collected from Shandong Animal Husbandry and Veterinary Vocational College in May, were cleaned and dried at 60°C, then pulverized by ultrafine pulverizer and extracted by boiled alcohol precipitation method. The flowers were deproteinized by sevage method and purified by C18 solid phase extraction column. The content of polysaccharides was measured by PMP (1-phenyl-3-methyl-5-pyrazolone) precolumn derivatization ultrahigh performance liquid chromatography tandem mass spectrometry.

2.5. Experimental Animals

2.5.1. Establishing the Model of Artificial Leukemia Chicken. 140 one-day-old SPF white-feathered chicks were intraperitoneally injected with ALV-J $10^{5.96}$ $TCID_{50}$/0.1 mL at a dose of 0.1 mL per chick; the artificial leukemia chicken model was established.

2.5.2. Grouping of Experimental Animals. The 1-day-old SPF white-feathered chicks were purchased from the SPAFAS chicken farm in Jinan, Shandong. The chickens used during the study were kept in strict accordance with the SPF chicken breeding management requirements in the SPF animal house of the Shandong Animal Husbandry and Veterinary Vocational College. 210 one-day-old SPF white-feathered chicks were randomly divided into 3 groups with 70 animals each; the three groups were group I, group IV, and group V. 140 artificial leukemia chicken model was divided into 2 groups, which were group II and group III. Three groups, groups I to II, were inoculated subcutaneously with 10 mg/mL of *Robinia pseudoacacia* polysaccharides daily at 2 days of age. The inoculation dose was 0.1 mL per chick for 3 days. In groups III and IV, the chicks were injected subcutaneously with saline, 0.1 mL/day for 3 days, and groups I to IV were inoculated intranasally with live IB vaccine at 7 days. Group V served as the blank control group. Ten chickens were randomly selected from each group at 7 d, 14 d, 21 d, 28 d, 35 d, 42 d, and 49 d after immunization for follow-up evaluation after being for 8 h before the test.

2.6. Determination of IB Antibody Titer in the Serum. 1.0 mL aseptically-collected heart blood from chickens was centrifuged with a speed of 3000 rpm/min for 25 min in a centrifuge tube, with the supernatant removed. The IB antibody titer was determined by a fixed virus dilution serum neutralization test.

2.7. Determination of Immune Organ Index. Each group of chickens was weighed and then the bursa, spleen, and thymus were removed. The organs, their surface water gently wiped with sterile filter paper, were weighed separately, and the bursa, spleen, and thymus indexes were calculated according to the formula: immune organ index (mg/g) = (immune organ mass/body weight).

2.8. Determination of Peripheral Blood Lymphocyte Transformation Rate. 2 mL heart blood, collected with EDTA-Na vacuum sterile blood collection tube, was shaken up and diluted with 2 mL RPMI-1640.4 mL human lymphocyte separation solution (density 1.085) which was added in the tube followed by centrifugation at 20°C with a speed of 2000 rpm/min for 20 min. Afterward, the supernatant was removed and the solution was centrifuged for 2 more times. After cell precipitation, RPMI-1640 containing 10% fetal bovine serum was added in for suspension cultivation, and a drop of the cell suspension was counted. The cell suspension was diluted to 2×10^6 cells/mL. Then the lymphocyte suspension was inoculated into a 96-well cell culture plate with a density of 0.1 mL/well. Each sample was replicated by 4 wells, in which 3 wells were added with Congo protein (ConA) at a final concentration of 50 μg/mL, and the last well was used as a negative control. All the samples were put into an incubator at 37°C with the volume of 5% CO_2 until the appearance of single-layer cells. Afterward, 5 μL of 5 mg/L MTT solution was added in each well for another 4 hours of incubation. Then the supernatant was gently discarded and 200 μL of DMSO solution was added into each well followed by a 10-minute shaking. The absorbance value was measured at 490 nm with a microplate reader for the calculation of the lymphocyte conversion rate.

2.9. Determination of $CD4^+$ and $CD8^+$ T Lymphocyte Levels in the Peripheral Blood. 2 mL heart blood was collected with EDTA-Na vacuum aseptic blood collection tube, and the

content of $CD4^+$ and $CD8^+$ T lymphocyte in the peripheral blood was measured and calculated by PE-6800VET automatic animal blood analyzer.

2.10. Determination of Cytokine Levels in the Serum. 2 mL aseptically-collected heart blood from chickens was centrifuged at 3000 rpm/min for 25 min in a centrifuge tube, with the supernatant removed and stored at −20°C. The content of cytokine IL-2 and IFN-γ in the serum was measured referring to the manufacturer instruction of IL-2 ELISA kit and IFN-γ ELISA kit.

2.11. Data Analysis. Data analysis was worked out based on SPSS Statistics 19.0 statistical analysis software. Multiple comparisons were performed using the LSD method, and the test data were expressed as mean ± standard deviation (Mean ± SD) and the significant difference was analyzed.

3. Results

3.1. Extraction and Content Determination of Polysaccharides from Robinia pseudoacacia (RPPS). Polysaccharide was extracted from the fresh locust flower, dried, and pulverized via water boiling and precipitation with ethanol, with the extract of 25.7%. The content of polysaccharide was 71.3% by PMP precolumn derivatization high-performance liquid chromatography tandem mass spectrometry.

3.2. Changes of IB Antibody Titer in the Serum. The IB antibody titer in each group of serum is shown in Figure 1. The titer of IB antibody in the serum of group I was significantly higher than that of the other groups ($P < 0.01$), and the retention time of the high-level antibody titer was longer. The difference of IB antibody titer in the serum between group II and group IV was not obvious ($P > 0.05$); however, the two groups were much higher than group III in antibody titer in the serum. The IB antibody titer in the serum of group V was 0. The IB antibody titer in the serum of groups I to IV peaked at 21 days after immunization and then began to decrease. The IB antibody titer in the serum of group III was extremely lower than that of group I ($P < 0.01$), group II, and group IV ($P < 0.05$).

3.3. Changes of the Immune Organ Index

3.3.1. The Change of the Bursal Index. The bursal index of group I was much higher than that of the other groups ($P < 0.01$). The difference of the bursal index between group II and group IV was not obvious ($P > 0.05$), but their indexes were significantly higher compared with that of group III. The bursal index of group III was obviously lower than that of group I ($P < 0.01$), group II, and group IV ($P < 0.05$), shown in Figure 2.

3.3.2. The Change of the Thymus Index. The thymus index of group I was significantly higher than that of the other groups ($P < 0.01$). The thymus index of group IV was much higher than that of groups II, III, and V ($P < 0.05$). The thymus index of group II was much higher than that of group III ($P < 0.05$). The thymus index of group III was obviously lower than that of group I ($P < 0.01$), group II, group IV, and group V ($P < 0.05$), shown in Figure 3.

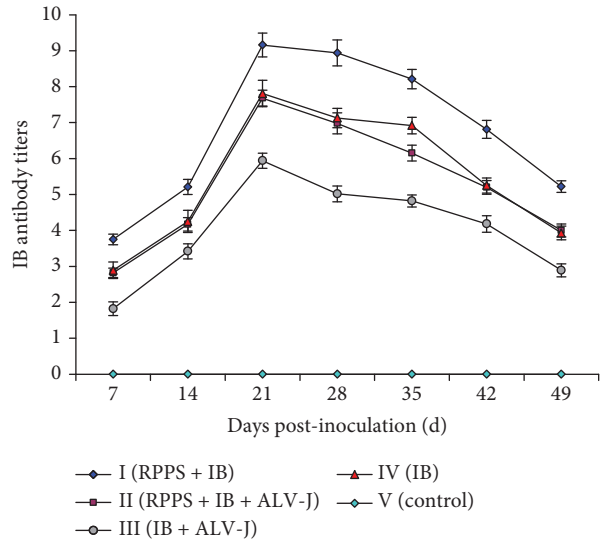

Figure 1: Changes of antibody titer in the serum.

3.3.3. The Change of the Spleen Index. The spleen index of group I was significantly higher than that of the other groups ($P < 0.01$). The spleen index of group IV was much higher than that of groups II, III, and V ($P < 0.05$). There was no remarkable difference in the spleen index between group II and group V ($P > 0.05$). The spleen index of group III was obviously lower than that of group I ($P < 0.01$), group II, group IV, and group V ($P < 0.05$), shown in Figure 4.

3.4. Changes of Peripheral Blood Lymphocyte Transformation Rate. The changes of transformation rate of peripheral blood lymphocytes of each group are shown in Figure 5. The results showed that the transformation rate of peripheral blood lymphocytes in group I was significantly higher than that of the other groups ($P < 0.05$). The transformation rate of peripheral blood lymphocytes in group II was obviously lower than that of group IV ($P < 0.05$). The transformation rate of peripheral blood lymphocytes of group III was much lower than that of the other groups ($P < 0.05$) and was decreased rapidly after 28 days.

3.5. Changes of $CD4^+$ T Lymphocytes in the Peripheral Blood. The changes of $CD4^+$ T lymphocytes in the peripheral blood are shown in Table 1. The content of $CD4^+$ T lymphocytes in the peripheral blood of group III was significantly lower than that of the other groups ($P < 0.01$). The content of $CD4^+$ T lymphocytes in the peripheral blood of group I was obviously higher than that of the other groups ($P < 0.05$). The content of $CD4^+$ T lymphocytes in the peripheral blood of group II and group IV showed no observable difference ($P > 0.05$). The content of $CD4^+$ lymphocytes in the peripheral blood of group II and IV was much higher than that of group V ($P < 0.05$). The content of $CD4^+$ lymphocytes in the peripheral blood of group I to group IV reached a peak after 21 days and then slowly decreased.

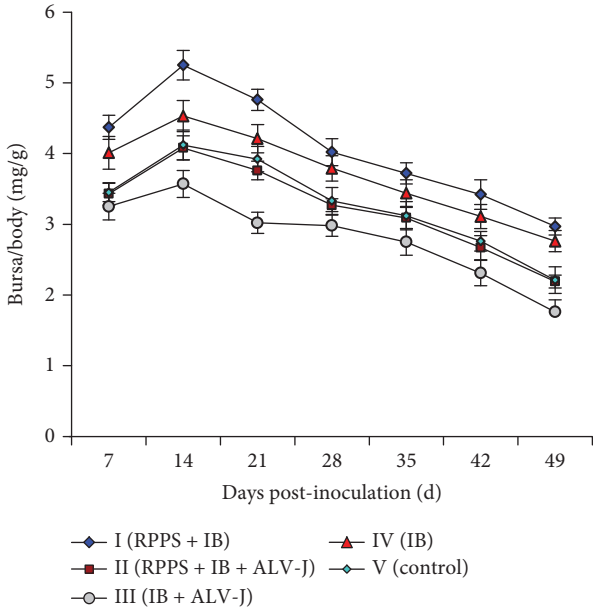

Figure 2: Changes of the bursa index.

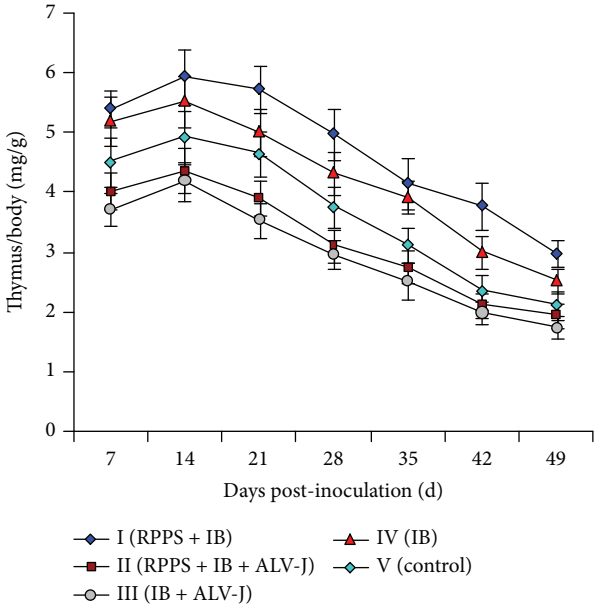

Figure 3: Changes of the thymus index.

3.6. Changes of $CD8^+$ T Lymphocytes in the Peripheral Blood. The changes of $CD8^+$ T lymphocytes in the peripheral blood are shown in Table 2. The content of $CD8^+$ lymphocytes in the peripheral blood of group I was significantly higher than that of the other groups ($P < 0.01$). The content of $CD8^+$ lymphocytes in the peripheral blood of group III was obviously lower than that of the other groups ($P < 0.01$). The content of $CD8^+$ lymphocytes in the peripheral blood of group II and group IV showed no observable difference ($P > 0.05$). The content of $CD4^+$ lymphocytes in the peripheral blood of group I to group IV reached a peak after 21 days and then decreased slowly.

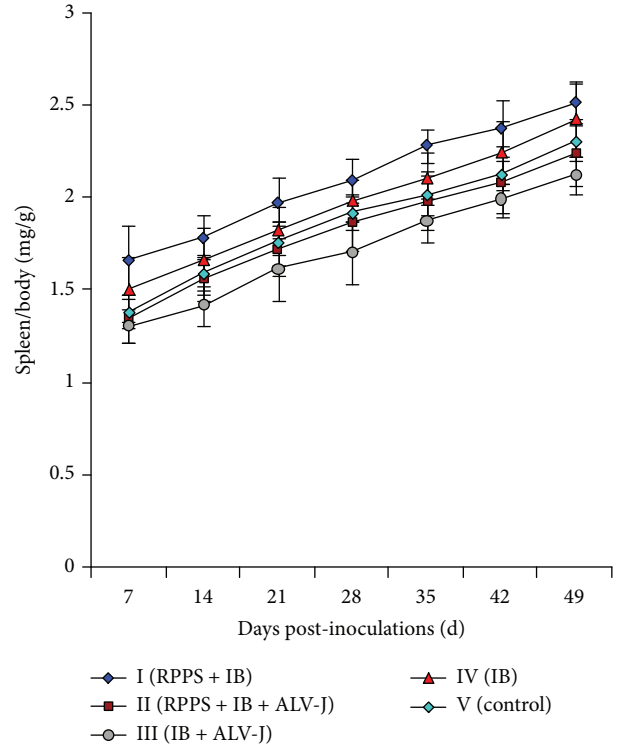

Figure 4: Changes of the spleen index.

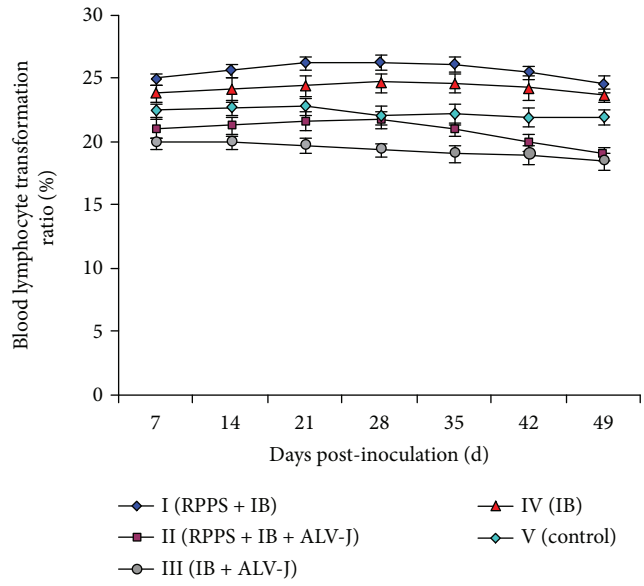

Figure 5: Effect of RPPS on blood lymphocyte transformation rate in chickens (%).

3.7. Changes of Cytokine IL-2 Level in the Serum. The results in Figure 6 showed that the level of cytokine IL-2 in the serum of group I was significantly higher than that of the other groups ($P < 0.01$). The level of cytokine IL-2 in the serum of group II was much higher than that of group III ($P < 0.05$). The level of cytokine IL-2 in the serum of group

Table 1: Effects of RPPS on $CD4^+$ T lymphocyte in the peripheral blood.

Groups	Days postinoculation and lymphocyte transformation rates						
	7	14	21	28	35	42	49
I (RPPS+IB)	34.53 ± 4.21^{a}	46.98 ± 5.11^{a}	49.28 ± 4.57^{a}	48.23 ± 4.22^{a}	45.69 ± 3.65^{a}	44.12 ± 3.52^{a}	40.78 ± 3.47^{a}
II (RPPS+IB+ALV-J)	31.98 ± 3.47^{b}	42.65 ± 3.78^{b}	45.02 ± 4.23^{b}	44.42 ± 3.57^{b}	41.88 ± 3.59^{b}	41.03 ± 3.43^{b}	37.67 ± 3.55^{b}
III (IB+ALV-J)	22.96 ± 3.76^{A}	24.02 ± 3.43^{A}	25.98 ± 4.42^{A}	25.55 ± 3.45^{A}	25.01 ± 3.54^{A}	24.9 ± 3.68^{A}	24.76 ± 3.71^{A}
IV (IB)	32.09 ± 3.41^{b}	42.77 ± 4.85^{b}	45.68 ± 3.98^{b}	44.79 ± 3.62^{b}	42.52 ± 3.73^{b}	41.78 ± 3.67^{b}	38.23 ± 4.02^{b}
V (control)	29.95 ± 2.97^{c}	35.27 ± 3.78^{c}	39.76 ± 4.52^{c}	39.02 ± 4.07^{c}	37.99 ± 3.82^{c}	35.03 ± 3.57^{c}	34.79 ± 3.24^{c}

Note: groups with different superscript lowercase letters are statistically different at $P < 0.05$; groups with superscript capital letters are statistically extremely different ($P < 0.01$).

Table 2: Effects of RPPS on $CD8^+$ T lymphocyte in the peripheral blood.

Groups	Days postinoculation and lymphocyte transformation rates						
	7	14	21	28	35	42	49
I (RPPS+IB)	18.32 ± 4.71^{A}	24.55 ± 5.43^{A}	27.87 ± 5.46^{A}	26.97 ± 5.22^{A}	25.12 ± 3.65^{A}	24.37 ± 3.52^{A}	23.05 ± 3.47^{A}
II (RPPS+IB+ALV-J)	15.32 ± 3.12^{a}	19.21 ± 3.41^{a}	22.94 ± 3.65^{a}	22.65 ± 2.89^{a}	21.19 ± 2.78^{a}	20.05 ± 3.21^{a}	19.53 ± 2.96^{a}
III (IB+ALV-J)	12.47 ± 2.76^{B}	13.53 ± 3.25^{B}	15.05 ± 3.76^{B}	14.76 ± 2.98^{B}	13.51 ± 2.74^{B}	11.65 ± 2.77^{B}	10.56 ± 2.12^{B}
IV (IB)	15.71 ± 2.92^{a}	19.65 ± 4.52^{a}	23.32 ± 4.78^{a}	22.77 ± 4.23^{a}	21.23 ± 3.42^{a}	20.45 ± 3.67^{a}	19.72 ± 3.02^{a}
V (control)	13.98 ± 2.21^{b}	18.21 ± 4.02^{b}	21.45 ± 4.33^{b}	20.98 ± 3.67^{b}	19.88 ± 3.82^{b}	18.21 ± 3.57^{b}	17.92 ± 2.96^{b}

Note: groups with different superscript lowercase letters are statistically different at $P < 0.05$; groups with superscript capital letters are statistically extremely different ($P < 0.01$).

II was obviously lower than that of group IV ($P < 0.05$). The levels of cytokine IL-2 within the first 7 days of group III and group V showed no observable difference ($P > 0.05$). However, the difference became significant from the 7^{th} day to the 28^{th} day and returned the value within the first 7 days after 28 days ($P > 0.05$).

3.8. Changes of Cytokine IFN-γ Level in the Serum. The results in Figure 7 showed that the level of cytokine IFN-γ in the serum of group I was significantly higher than that of the other groups ($P < 0.01$). There was no obvious difference in the IFN-γ level between group III and group V ($P > 0.05$). The level of cytokine IFN-γ of groups II and IV showed no observable difference within the first 14 days ($P > 0.05$), while the difference became significant after 14 days ($P < 0.05$). The cytokine IFN-γ content in the serum of group II was much higher than that of group III ($P < 0.05$).

4. Discussion

According to grouping of experimental animals, I marks the group of vaccine and RPPS (group I), II the group of chicken leukemia, vaccine, and RPPS (group II), III the group of chicken leukemia and vaccine (group III), IV the group of vaccine strain (group IV), and V the control group (group V).

Changes in the serum antibody titer of the body can accurately and intuitively reflect the state of humoral immunity [11]. The titer of IB antibody in the serum of group I was obviously higher than that of the other groups ($P < 0.01$), indicating that RPPS can significantly improve the serum antibody titer of IB live vaccine. IB antibody titer in the serum of both groups II and IV was not notably different ($P > 0.05$) but was much higher than that of group III, indicating that RPPS can significantly increase the serum antibody level in immunosuppressive chickens.

The brusa fabricius, thymus, and spleen are the main immune organs of birds. These organs are the main sites for immune cell formation, differentiation, and antibody formation. The developmental status of immune organs directly influences to resist pathogenic microorganisms. So the immune organ index can be used to reflect the immune status of birds; the increase of immune organ index is an enhancement of immune function. The detection of avian bursal, thymus, and spleen index changes can directly determine the immune status of animals [12]. The study observed the bursal index, thymus index, and spleen index of chickens. The results showed that the bursal index, thymus index, and spleen index of chickens in group I were all remarkably higher than those of the rest of the groups ($P < 0.01$). The bursal index, thymus index, and spleen index of chickens in group III were remarkably lower than those of both group I ($P < 0.01$) and group II ($P < 0.05$). This study found that RPPS could significantly increase the bursal index, thymus index, and spleen index of chickens and also the bursal index, thymus index, and spleen index of immunosuppressive chickens, suggesting that RPPS could enhance immune function in poultry.

Lymphocyte transformation rate is the most direct indicator of cellular immunity [13]. The conversion rate of lymphocytes in the peripheral blood of RPPS and IB vaccine group was significantly higher than the other groups; the infected ALV-J and IB vaccine groups decreased the

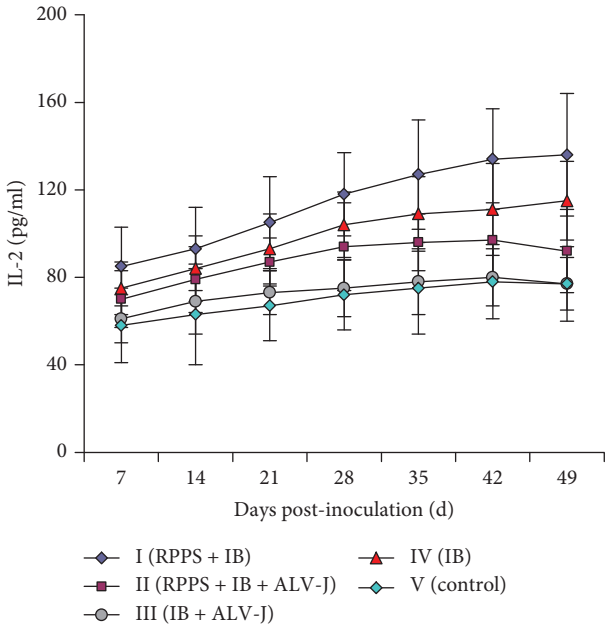

Figure 6: Changes of cytokine IL-2 level in the serum.

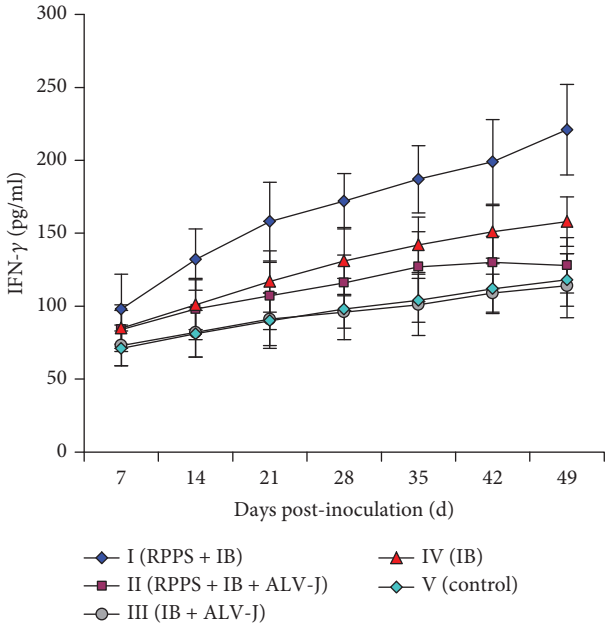

Figure 7: Changes of cytokine IFN-γ level in the serum.

conversion rate of lymphocytes in the peripheral blood compared with the other groups. These results imply that RPPS could increase the conversion rate of lymphocytes in the peripheral blood. And the immunosuppressive disease could reduce the lymphocyte transformation rate of chicken.

The mature $CD4^+$ and $CD8^+$ T cells in the peripheral blood are mutually exclusive subsets. $CD4^+$ T cells belong to T helper (Th) cells, which are divided functionally into Th1 and Th2 cells based on the distinct patterns of cytokine production. $CD8^+$ T cells are immune effector cells that belong to cytotoxic T lymphocytes and are responsible for the removal of target cells through the direct killing effect; the increased counts of $CD4^+$ and $CD8^+$ lymphocytes reflect the enhanced T cell-mediated immunity. So the content of $CD4^+$ and $CD8^+$ T in the peripheral blood is the basis for evaluation of immune status [14]. The content of $CD4^+$ lymphocytes in the peripheral blood of RPPS and IB vaccine group was significantly higher than that of the other groups ($P < 0.05$); the content of $CD4^+$ lymphocytes in the peripheral blood of infected ALV-J and IB vaccine group was extremely lower than the other groups ($P < 0.01$). The results indicate that RPPS could remarkably increase the content of $CD4^+$ lymphocytes in the peripheral blood of chickens and RPPS can increase the content of $CD4^+$ lymphocytes in the peripheral blood of chickens with immunosuppressive disease. The content of $CD8^+$ lymphocytes in the peripheral blood of group RPPS and IB vaccine group was remarkably higher than that of the other groups ($P < 0.01$); the content of $CD8^+$ lymphocytes in the peripheral blood of infected ALV-J and IB vaccine group was significantly lower than the other groups ($P < 0.01$); the difference of $CD8^+$ lymphocytes in the peripheral blood between groups II and IV is not significant ($P > 0.05$). The results indicate that RPPS could significantly increase the content of $CD8^+$ lymphocytes in the peripheral blood of chickens and the content of $CD8^+$ lymphocytes in the peripheral blood of immunosuppressive chickens.

IL-2 mainly produced by activated T lymphocytes has important immunoregulatory effects in the immune system and can enhance multiple functions of immune cells, stimulating helper T cells and natural killer cells to produce cytokines and facilitate their proliferation. Therefore, IL-2 level can indirectly reflect the level of immune response [15]. The content of cytokine IL-2 in the serum of group I was significantly higher than that of the other groups ($P < 0.01$), indicating that RPPS could remarkably increase the content of cytokine IL-2 in chicken serum. The content of cytokine IL-2 in the serum of group II was obviously higher than that of group III ($P < 0.05$), suggesting that RPPS could increase the cytokine IL-2 content in the serum of immunosuppressive chickens. The content of cytokine IL-2 in the serum of group II was much lower than that of group IV ($P < 0.05$), indicating that the immunosuppression disease could inhibit the production of cytokine IL-2 in chicken serum.

IFN-γ can stimulate natural killer cells and enhance their killing function. It can also promote macrophage and cytotoxic T lymphocyte maturation and stimulate B lymphocytes to secrete antibodies, thereby enhancing the body's immune function [16]. The cytokine IFN-γ level in the serum of group I was significantly higher than that of the other groups ($P < 0.01$), indicating that RPPS can remarkably increase cytokine IFN-γ production in chicken serum. The difference of cytokine IFN-γ in the serum between group III and group V was not obvious ($P > 0.05$), indicating that immunosuppressive disease can reduce the function of vaccine to stimulate IFN-γ production. The content of cytokine IFN-γ in the serum of group II was much higher than that of group III ($P < 0.05$), indicating that RPPS can dramatically increase the content of cytokine IFN-γ in the serum of immunosuppressive chickens.

5. Conclusion

RPPS can significantly enhance the vaccine immune effect and improve the immune function of immunosuppressive chickens. Thus, the efficacy of RPPS in immunity enhancement can be further studied.

Data Availability

The data used to support the findings of this study are available from the corresponding author upon request.

Conflicts of Interest

The authors declare that there are no conflicts of interest regarding the publication of this paper.

Acknowledgments

The article is supported by the poultry innovation team building projects of Shandong Province Modern Agricultural Industry Technology System (SDAIT-11-05) and the Science and Technology Institution of Higher Education Plan of Shandong Province (J17KB105).

References

[1] Z. Cui, S. Sun, Z. Zhang, and S. Meng, "Simultaneous endemic infections with subgroup J avian leukosis virus and reticuloendotheliosis virus in commercial and local breeds of chickens," *Avian Pathology*, vol. 38, no. 6, pp. 443–448, 2009.

[2] S.-h. Sun, Z.-z. Cui, and L.-x. Qu, "Maternal antibody protected chicks from growth retardation and immunosuppression induced by early reticuloendotheliosis virus infection," *Agricultural Sciences in China*, vol. 6, no. 6, pp. 762–768, 2007.

[3] M. Li, M. L. Mo, B. C. Huang et al., "Continuous evolution of avian infectious bronchitis virus resulting in different variants co-circulating in Southern China," *Archives of Virology*, vol. 158, no. 8, pp. 1783–1786, 2013.

[4] M. Li, X. Y. Wang, P. Wei, Q. Y. Chen, Z. J. Wei, and M. L. Mo, "Serotype and genotype diversity of infectious bronchitis viruses isolated during 1985-2008 in Guangxi, China," *Archives of Virology*, vol. 157, no. 3, pp. 467–474, 2012.

[5] J. Ji, J. Xie, F. Chen et al., "Phylogenetic distribution and predominant genotype of the avian infectious bronchitis virus in China during 2008-2009," *Virology Journal*, vol. 8, no. 1, p. 184, 2011.

[6] S.-D. Zhang, Y.-X. Yin, and Q. Wei, "Immunopotentiation on murine spleen lymphocytes induced by polysaccharide fraction of *Panax ginseng* via upregulating calcineurin activity," *APMIS*, vol. 118, no. 4, pp. 288–296, 2010.

[7] Y. Zhang, S. Yang, X. Zhao et al., "Immune enhancement of Taishan Robinia pseudoacacia polysaccharide on recombinant *Proteus mirabilis* OmpA in chickens," *International Immunopharmacology*, vol. 22, no. 1, pp. 236–241, 2014.

[8] Q. Wenwen, X. Bao, and S. Chuandao, "Nutrition and health protection function of Robinia pseudoacacia polysaccharides and prospects for food development," *Agriculture Products Processing*, vol. 9, pp. 59–61, 2016.

[9] K. Wei, Z. Sun, Z. Yan et al., "Effects of Taishan Pinus massoniana pollen polysaccharide on immune response of rabbit haemorrhagic disease tissue inactivated vaccine and on production performance of Rex rabbits," *Vaccine*, vol. 29, no. 14, pp. 2530–2536, 2011.

[10] L.-h. Wang, Y.-f. Duan, Y.-l. Ma, H.-j. Ding, and E.-c. Li, "Studies on extraction and antioxidant function of polysaccharides from Sophora japonica," *Journal of Northwest A & F University(Natural Science Edition)*, vol. 36, no. 8, pp. 213–218, 2008.

[11] G. Chattopadhyay, Q. Chen, J. Colino, A. Lees, and C. M. Snapper, "Intact bacteria inhibit the induction of humoral immune responses to bacterial-derived and heterologous soluble T cell-dependent antigens," *The Journal of Immunology*, vol. 182, no. 4, pp. 2011–2019, 2009.

[12] K. C. Mountzouris, P. Tsirtsikos, E. Kalamara, S. Nitsch, G. Schatzmayr, and K. Fegeros, "Evaluation of the efficacy of a probiotic containing *Lactobacillus*, *Bifidobacterium*, *Enterococcus*, and *Pediococcus* strains in promoting broiler performance and modulating cecal microflora composition and metabolic activities," *Poultry Science*, vol. 86, no. 2, pp. 309–317, 2007.

[13] C.-R. Li, S. Santoso, and D. D. Lo, "Quantitative analysis of T cell homeostatic proliferation," *Cellular Immunology*, vol. 250, no. 1-2, pp. 40–54, 2007.

[14] B. Li, K. Wei, S. Yang et al., "Immunomodulatory effects of Taishan *Pinus massoniana* pollen polysaccharide and propolis on immunosuppressed chickens," *Microbial Pathogenesis*, vol. 78, pp. 7–13, 2015.

[15] F. Guo, C. Xue, C. Wu et al., "Immunoregulatory effects of Taishan *Pinus massoniana* pollen polysaccharide on chicks co-infected with *avian leukosis* virus and *Bordetella avium* early in ovo," *Research in Veterinary Science*, vol. 96, no. 2, pp. 260–266, 2014.

[16] T. H. M. Ottenhoff and T. Mutis, "Role of cytotoxic cells in the protective immunity against and immunopathology of intracellular infections," *European Journal of Clinical Investigation*, vol. 25, no. 6, pp. 371–377, 1995.

Hindawi
International Journal of Polymer Science
Volume 2019, Article ID 1058410, 8 pages
https://doi.org/10.1155/2019/1058410

Research Article

The Investigation of LRP5-Loaded Composite with Sustained Release Behavior and Its Application in Bone Repair

Yanhai Xi,[1] Tingwang Jiang,[2] Jiangming Yu,[1] Mintao Xue,[1] Ning Xu,[1] Jiankun Wen,[1] Weiheng Wang,[1] Hailong He,[1] and Xiaojian Ye[1]

[1]*Department of Spine Surgery, Changzheng Hospital, Second Military Medical University, Shanghai 200003, China*
[2]*Department of Immunology and Microbiology, Institution of Laboratory Medicine of Changshu, Changshu, 215500 Jiangsu, China*

Correspondence should be addressed to Xiaojian Ye; xjyespine@smmu.edu.cn

Received 14 September 2018; Revised 8 December 2018; Accepted 31 December 2018; Published 5 February 2019

Guest Editor: Mingqiang Li

Low-density lipoprotein receptor-related protein 5 (LRP5) plays a vital role in bone formation and regeneration. In this study, we developed an injectable and sustained-release composite loading LRP5 which could gelatinize in situ. The sustained release of the composite and its efficacy in bone regeneration were evaluated. Sodium alginate, collagen, hydroxyapatite, and LRP5 formed the composite LRP5-Alg/Col/HA. It was found that the initial setting time and final setting time of LRP5-Alg/Col/HA containing 4% alginate were suitable for surgical operation. When the composite was loaded with 40 μg/mL LRP5, LRP5-Alg/Col/HA did not exhibit a burst-release behavior and could sustainably release LRP5 up to 21 days. Up to 18 days, LRP5 released from LRP5-Alg/Col/HA still present the binding activity with DKK1 (Wnt signaling pathway antagonist) and could increase the downstream β-catenin mRNA in bone marrow mesenchymal stem cells. Moreover, LRP5-Alg/Col/HA was found to significantly increase bone mineral density in the defect area after 6 weeks' implantation of LRP5-Alg/Col/HA into the rats' calvarial defect area. H&E staining detection demonstrated that LRP5-Alg/Col/HA could mediate the formation of a new bone tissue. Therefore, we concluded that Alg/Col/HA was a suitable sustained-release carrier for LRP5 and LRP5-Alg/Col/HA had a significant effect on repairing bone defects and could be a good bone regeneration material.

1. Introduction

With the development of society and the consequent industrial accidents, traffic accidents, and natural disasters, the number of patients with orthopedic trauma has also increased. Moreover, bone tumors [1] and orthopedic diseases such as skeletal tuberculosis and avascular necrosis have caused numerous patients with bone defects. Therefore, bone defects are not only a severe disease that potentially shorten the life span of individual patients but also an important public health issue that concerns the society. With the aging of the population, the improvement of people's health awareness and consumption capacity, and the improvement of the national medical security system, the demand for bone repair materials has increased dramatically [2]. In recent years, a variety of synthetic bone repair biomaterials have been widely used in clinics, and the injectable bone repair material is the most important one [3]. Firstly, the injectable bone repair material can be implanted into the body by injection with insignificant trauma, therefore eliminating many complications associated with traditional bone transplantation surgery. Secondly, it has good plasticity, which can fill bone defects of any shape or size, and can be gelatinized by physical or chemical action-mediated sol-gel phase transformation, forming a scaffold material with porous microstructure and exerting bone conduction [4, 5]. Finally, the implanted materials can degrade slowly, resulting in a hydrated network structure that can better simulate the physical and chemical microenvironment of the extracellular matrix and promote cell proliferation, differentiation and secretion of new extracellular matrix with efficient mass transfer performance [4, 6], good regeneration activity to damaged tissue [7, 8], and growth activity for a new bone in the host. Therefore, injectable materials have various

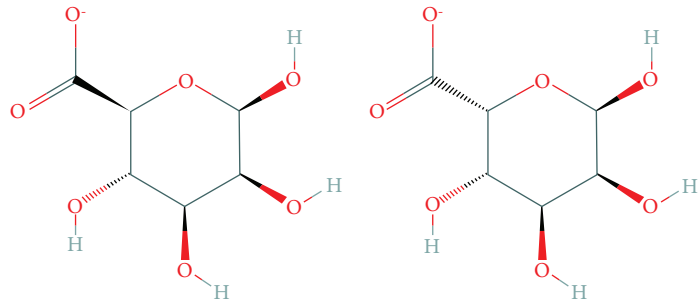

Figure 1: Two monosaccharide units of sodium alginate: (a) β-D-mannuronate (M) and (b) α-L-guluronate (G).

advantages and have attracted increasing attention as carriers capable of carrying compounds, macromolecular drugs, proteins, and cells.

Sodium alginate (NaAlg or Alg) is a cell wall component of brown algae with a chemical composition of 1,4-glycosidically linked β-D-mannuronate (M) and α-L-guluronate (G) combined linear chain anionic polymer, which has a molecular weight of about 50,000 to 250,000 Daltons [9]. The molecular formula is ($C_6H_7O_6Na$). Figure 1 shows the monomers constituting the alginate polymer. Alginate is easily bonded to most divalent cations, such as Ca^{2+}, Ba^{2+}, and Cu^{2+}, to form an ion cross-linked alginate hydrogel [10], which is metabolized into monomers of mannose and glucuronic acid by enzymatic hydrolysis in vivo that are nontoxic to humans [11]. In addition, alginate has the advantages of no immunogenicity and a certain biological sustained release [12]. However, alginate hydrogel shows a significant burst-release effect after swelling [13–15]. According to Tan's report [16], a gel-like composite containing alginate, collagen, and hydroxyapatite (HA) is prepared with sustained-release and injectable properties. On the one hand, collagen and hydroxyapatite act as a "stable stent" to effectively reduce the swelling of the alginate and improve the sustained-release effect of alginate hydrogel. On the other hand, the injectability property of alginate hydrogel can offset the disadvantages of collagen and hydroxyapatite and solid property and poor plasticity, although collagen and hydroxyapatite have the advantages of biodegradability, good biocompatibility, and biological activity [17, 18]. Additionally, local injection is a simple and effective minimally invasive surgery with low complications. Therefore, alginate hydrogel can be combined with collagen and hydroxyapatite to prepare a gel composite suitable for bone tissue repair.

Low-density lipoprotein receptor-related protein 5 (LRP5) is a member of the low-density lipoprotein receptor-related protein (LRP) family and is widely expressed in a variety of tissues, including the fibroblasts, macrophages, central nervous system, digestive tract epithelial cells, liver, and kidney [19]. In the bone tissue, LRP5 is mainly expressed in the osteoblasts on the endosteal and trabecular bone surfaces, but not in the osteoclasts that are not conducive to bone repair. The role of LRP5 is mainly to promote the accumulation of bone mass, and its loss-of-function mutation can lead to a decrease in bone mass [20], while a functionally acquired mutation can increase bone mass [21–23]. A peptide derived from an LRP5 gene also enhances stem cell aggregation and chondrogenic differentiation [24]. This effect is mainly through the Wnt signaling pathway. The Wnt and LRP5/6 complex regulate the classical β-catenin signaling pathway, which plays a vital role in the bone differentiation of the bone marrow mesenchymal stem cells, osteoblast proliferation, or apoptosis, and maintain normal bone. LRP5/6 activation is inhibited by secreted proteins belonging to the Dickkopf (DKK) family [25, 26]. Fleury et al. [27] showed DKK1 and LRP5 interaction in vitro. It suggests that the interference with LRP5/DKK1 interaction can be a viable approach for maintenance of normal Wnt signaling pathway and therapeutic intervention to increase bone mass. Clinically, bone defects with varying degrees of bone loss are extremely common and frequent, and the bone tissue has a limited self-repair ability. Therefore, various studies have tried to apply a variety of exogenous beneficial proteins to local bone defect areas to promote osteogenesis. However, the efficacy of LRP5 still lacks research reports on bone defect repair.

In this study, a composite containing alginate, hydroxyapatite, and collagen was used as a carrier. After loading with LRP5, the sustained-release capability, biocompatibility, and repair of bone defects in vivo were studied.

2. Method

2.1. LRP5-Alg/Col/HA Preparation. The preparation of calcium sulfate slurry consists of weighing calcium sulfate (Sigma) and deionized water, electromagnetic stirring until no obvious particles are seen, leaving for more than 24 hours, removing the static electricity, and standing for further use.

At less than 10°C, the bovine type I collagen (Sigma) was dissolved in HCl of pH = 2 and prepared an acidic collagen solution with a concentration of 5 mg/mL. Thereafter, $Na_3PO_4{\cdot}12H_2O$ solution and a certain proportion of sodium alginate (Sigma) solution were sequentially added with stirring. After that, NaOH solution was added to adjust the pH to 7.4, and different concentrations of LRP5 (Novus Biologicals) or BSA were added as needed. Afterward, hydroxyapatite slurry was added in equal volume and mixed evenly.

Finally, the above mixture was uniformly mixed with the calcium sulfate slurry and allowed to stand for 15 min. The inside of the mixture was cross-linked in situ to obtain a solid

bone repair material, which was named LRP5-Alg/Col/HA. The LRP5-Alg without collagen and hydroxyapatite was prepared in the same manner as above. BSA-Alg/Col/HA was prepared in the same manner as above with a different concentration of BSA. The final concentrations of each substance were calcium sulfate (5 mM), collagen (2.5 mg/mL), Na_3PO_4 (1.3 mM), alginate (2%, 3%, 4%, and 5%), and hydroxyapatite (10 mg/mL).

2.2. The Injectability Study. At 37°C, the gelation time of the liquid after mixing with the calcium sulphate slurry was recorded including the initial setting time and final setting time, using a tube rotation method.

2.3. Sustained-Release Behavior Investigation. BSA was used as a model protein to be loaded into Alg/Col/HA, and the release of protein was studied. BSA-Alg/Col/HA with final concentrations of 10, 20, 40, 80, 150, and 300 μg/mL BSA were prepared. 5 mL of saline was added as a drug-release medium in a test tube. 1 mL BSA-Alg/Col/HA gel was injected and placed in a 37°C water bath shaker (60 r/min) for 2 weeks. At 0.25, 1, 3, 6, 9, 12, and 15 days, 0.5 mL of the release medium was taken out, and an equal amount of the fresh saline solution was added. The BCA colorimetric method was used to detect the BSA concentration, and the OD value of the solution was measured at a wavelength of 570 nm. The BSA concentration in the solution was converted according to the standard curve of the concentration of the BSA solution.

The method for the sustained-release manner of LRP5-Alg/Col/HA or LRP5-Alg (no collagen and hydroxyapatite) was the same as above. The release time was recorded until 3 weeks, and the concentration of LRP5 in the release solution was detected at 0.25, 1, 3, 6, 9, 12, 15, 18, and 21 days. The method was performed by the enzyme-linked immunosorbent assay kit (PeproTech, USA) according to the manufacturer's instructions. The concentration of LRP5 in the released solution was determined by comparing with the standard curve; calculate the percentage of total BSA or LRP5 released at each time point and plot the cumulative release profile.

2.4. DKK1 Binding Activity Detection of LRP5 Released from LRP5-Alg/Col/HA. At day 1, day 6, day 12, and day 18, saline was replaced with DMEM. After 24 hours, DMEM was collected and filtered as the conditioned medium. The binding activity of LRP5 to DKK1 was detected using a competitive assay. After the overnight incubation of 10 yg/mL DKK1 solution in a 96-well plate, the plate was washed 3 times and then blocked using 5% BSA for 4 hours. Then, different conditioned mediums and 50 ng/mL LRP5-FITC were added and incubated for 2 hours at room temperature. After washing, FITC fluorescence was read immediately using an Envision plate reader.

2.5. Biological Activity of LRP5 Released from LRP5-Alg/Col/HA. The biological activity of LRP5 in the conditioned mediums collected at different times was indirectly evaluated by the expression level of the downstream gene β-catenin of the rat bone marrow-derived stem cells (MSCs). Rat MSCs (Fuyang Biotech, Shanghai, China) were seeded into 6-well plates at a concentration of 1×10^5 cells/well, incubated in a DMEM medium containing 10% fetal bovine serum and penicillin–streptomycin at 37°C in a 5% CO_2 incubator. After 24 hours of culture, the medium was removed, and the conditioned mediums of the Alg/Col/HA sample without LRP5 at different times were added as the negative control, and the conditioned mediums of the LRP5-Alg/Col/HA at different times were used as the experimental. Then, Wnt3a and DKK1 were added into every well of the final concentration of 100 ng/mL. After 2 days culture, the medium was removed and the cells were collected for detection. Then, RT-qPCR assay was preformed to detect the gene level of β-catenin.

2.6. Real-Time Quantitative PCR (RT-qPCR). Total RNA from rat MSCs were extracted using TRIzol (Invitrogen). First-strand cDNA was made using SuperScript III (Invitrogen). qPCR was run on the ViiA Real-Time PCR (Applied Biosystems) using the SYBR Green method. The β-catenin relative expression level was calculated by comparing the cycle times to those of β-actin. PCR primers were listed as follows: forward5′-ACCTCCCAAGTCCTTTATG-3′ and reverse5′-TACAACGGGCTGTTTCTAC-3′, for β-catenin and forward5′-CCCAGAGCAAGAGAGGCATC-3′ and reverse5′-CTCAGGAGGAGCAATGATCT-3′, for β-actin.

2.7. Bone Defect Model Preparation and Drug Administration. Twenty male Sprague-Dawley rats were randomly divided into 4 groups, with 5 rats in each group. Except for 5 healthy controls, in the other 3 groups, the rat parietal and frontal bones were exposed after the median incision of the skull. The parietal bone was made at 5 mm of full-thickness bone defect, and the dura mater should be kept intact. Three different experimental materials were randomly implanted; then, the periosteum, soft tissue, and skin were sutured layer-by-layer. Rats in the vehicle group were not treated; rats in the Alg/Col/HA group were implanted with Alg/Col/HA without LRP5; and rats in the LRP5-Alg/Col/HA group were implanted with LRP5-Alg/Col/HA. Rat activities, diet, mental state, and incision status were observed daily for 6 weeks.

2.8. Bone Mineral Density (BMD) Testing. The rats were euthanized at 6 weeks, and cranial bone samples were taken for microCT scan to analyze BMD of the rat calvarial defect area. The scanning conditions were 55 kVp, 109 μA, 10.5 μm resolution, and 200 ms exposure time.

2.9. Hematoxylin-Eosin (H&E) Staining. The formalin-fixed rat cranial bones were thoroughly washed with PBS and decalcified in a solution of 10% EDTA (pH 8.0) at 4°C for 20 days. The samples were treated with ethanol gradient dehydration, xylene transparent, paraffin-embedding, continuous longitudinal tissue section (5 μm thickness), and then H&E staining was performed. The bone tissue structure of each group was observed under a microscope.

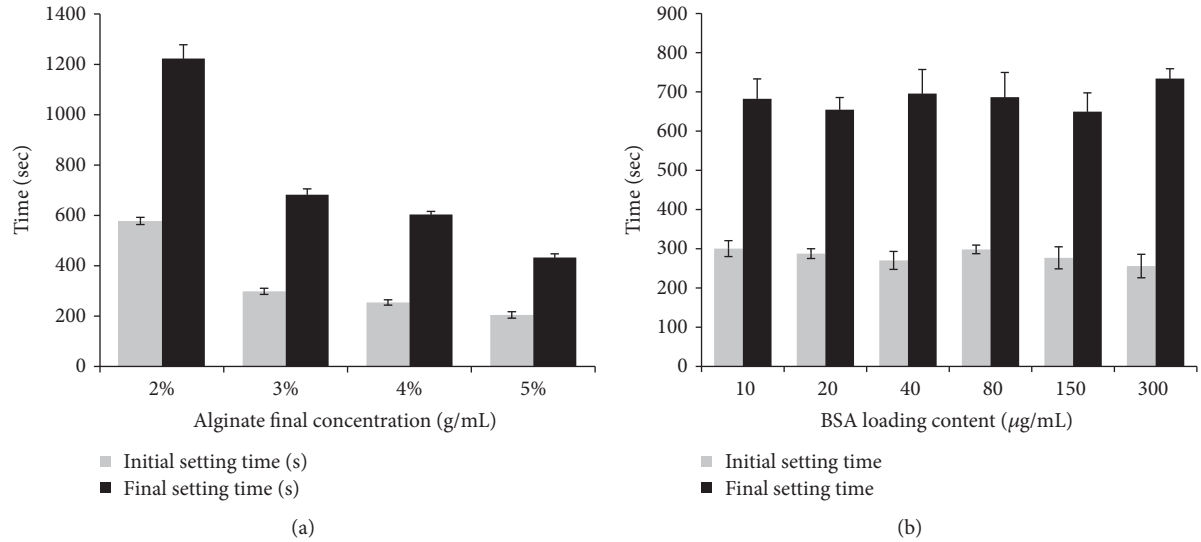

Figure 2: Effect to gelation time of Alg/Col/HA with different concentrations of alginate. (a) Effect of different concentrations of alginate on Alg/Col/HA gelation. (b) Effect of different concentrations of BSA on Alg/Col/HA gelation containing 4% alginate.

2.10. Statistical Analysis. SPSS19 statistical analysis software was used. Data was analyzed by the 2-tailed t-test or one-way analysis of variance (ANOVA), followed by the Tukey post hoc comparisons. Data was presented as mean ± SD, and P values less than 0.05 were considered statistically significant.

3. Results and Discussion

3.1. Effect of Alginate Concentration on Gelation Performance. After the cations are added to the aqueous sodium alginate solution, Na^+ on the α-L-guluronate (G) unit undergoes an ion-exchange reaction with the divalent ion, and the α-L-guluronate residues accumulate to form a cross-linked network, thus transforming into a hydrogel. In this process, Ca^{2+} is captured to form calcium alginate gel, which can inhibit the water flow. In this study, we examined the effect of different alginate concentrations on the gelation time of the composite according to the optimal criteria of solidification time including (1) "3 min initial setting time < 8 min" and (2) "final setting time ≤ 15 min" [28]. As shown in Figure 2(a), the Alg/Col/HA gelation rate was positively related to the alginate concentration. The higher alginate concentration induced the faster gelatinization. When the alginate concentration was 2%, 3%, 4%, and 5%, the initial setting times of the composite were 578.3 ± 14.3 sec, 298.5 ± 12.3 sec, 254.3 ± 10.5 sec, and 204.7 ± 12.7 sec, respectively, and the final setting times were 1,223.1 ± 54.9 sec, 682.4 ± 23.1 sec, 603.7 ± 12.3 sec, and 432.8 ± 14.6 sec, respectively. It indicated that 3%~5% of alginate concentration could provide relatively controllable initial and final setting times, which were suitable intervals for the surgical operation [28]. As the alginate concentration increased, the injectable ability of Alg/Col/HA decreased. The main reason is that the viscosity increases along with the increase of alginate [29]. However, when alginate concentration is too low, the formation of the network structure and the release efficiency are also affected. Therefore, the composite material

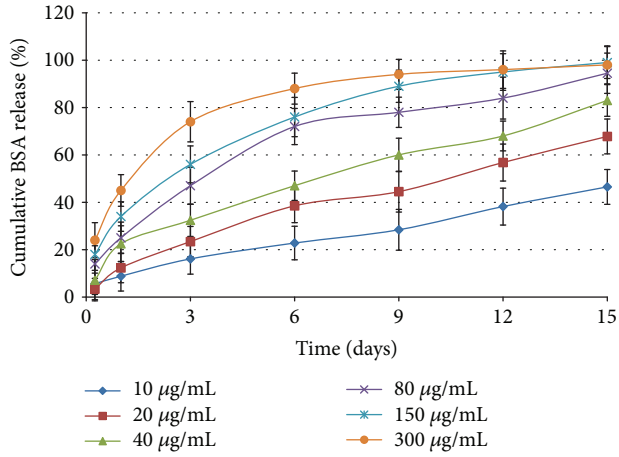

Figure 3: Effect of different concentrations of loaded BSA to the in vitro release profile of BSA-Alg/Col/HA.

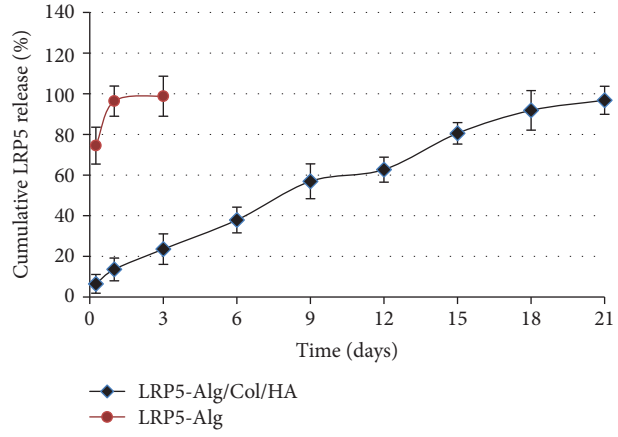

Figure 4: In vitro release of LRP5-Alg/Col/HA loaded with 40ug/mL LRP5.

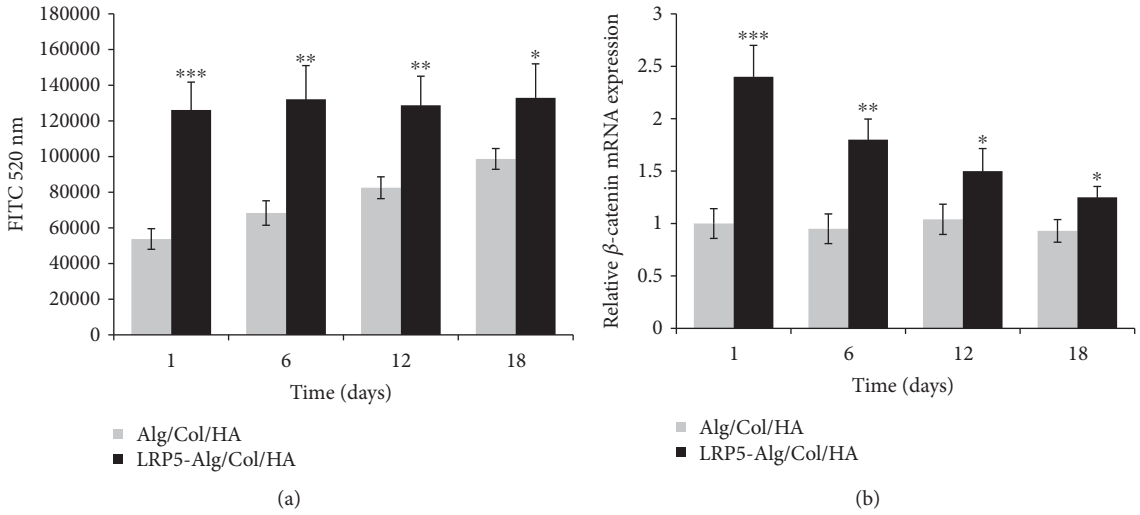

Figure 5: Effect of released LRP5 from LRP5-Alg/Col/HA to DKK1 binding and bioactivity in Wnt signaling pathway. (a) At different release times, the DKK1 binding activity of LRP5 released from LRP5-Alg/Col/HA. (b) At different release times, the effect of LRP5 released from LRP5-Alg/Col/HA on mRNA expression of β-catenin in rat BMCs. $^{*}P < 0.05$, $^{**}P < 0.01$ and $^{***}P < 0.001$ indicates the comparison with the Alg/Col/HA.

with 4% alginate concentration was selected as the material for subsequent research. Because the isoelectric point (pI) of LRP5 (5.11) is similar to BSA pI (4.70) and BSA is easy to obtain, we use BSA as the model protein to verify whether the loaded protein can affect the gelation time of the composite with 4% alginate concentration. As shown in Figure 2(b), when BSA concentration was in the range of 10~300 μg/mL, it was found that there were no obvious change trends in the initial and final setting times. It indicated that loaded protein had no influence on the gelation time.

3.2. Sustained-Release Performance Study of LRP5-Alg/Col/HA. As a protein, LRP5 is prone to be degraded. In order to overcome this, a few sustained-release carrier loaded LRP5 have been reported [24]. In this study, we investigated the in vitro sustained LRP5 release behavior of LRP5-Alg/Col/HA. Based on feasibility and cost considerations, BSA was first used as a model protein to study the feasibility of Alg/Col/HA as a protein sustained-release carrier. As shown in Figure 3, as the amount of loaded BSA increased, the release rate of BSA increased. It took 15 days to observe BSA release from BSA-Alg/Col/HA loaded with different amounts of BSA. When BSA concentrations were set at 20 μg/mL and 10 μg/mL, the cumulative release of BSA could exceed 60% and 40% within 2 weeks, respectively. When BSA concentration was 40 μg/mL, the cumulative release of BSA could reach more than 80% within 2 weeks. However, samples with BSA concentration of 80 μg/mL and 150 μg/mL, the cumulative release reached 80% within 1~1.5 weeks. Therefore, in the range of BSA concentration of 10~40 μg/mL, BSA-Alg/Col/HA had considerable controlled-release properties, and this concentration range might be a feasible condition to prepare LRP5-Alg/Col/HA.

Considering the largest loading and considerable sustained release, 40 μg/mL LRP5 was loaded into LRP5-Alg/Col/HA. In Figure 4, LRP5-Alg/Col/HA showed a good

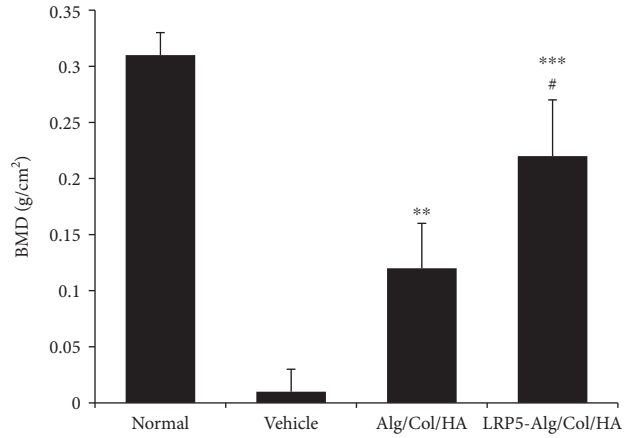

Figure 6: Effect of LRP5-Alg/Col/HA on bone mineral density (BMD) in defect sites of a rat model of calvarial critical defect after 6 weeks' treatment. $^{**}P < 0.01$ and $^{***}P < 0.001$ indicates the comparison with the vehicle group and $^{\#}P < 0.05$ indicates comparison with the Alg/Col/HA group.

sustained-release property at a relatively stable release rate for 21 days. No burst release of LRP5 was found on day 1 when compared to the same amount of loaded LRP5 in LRP5-Alg. However, the burst-release effect of LRP5-Alg without collagen and hydroxyapatite was obvious, and the cumulative release of LRP5 was nearly 80% in the first 6 hours and 96% in 24 hours. Previous reports have studied that alginate hydrogels have controlled-release properties, but their burst-release effects are apparent, due to the excessive swelling of the hydrogel [13]. In this study, the alginate hydrogel was modified by the addition of collagen and hydroxyapatite. Collagen and the alginate form an interpenetrating polymer network (IPN) [30, 31]. The two polymers are intertwined and entangled through the network, which retain not only the secondary structure

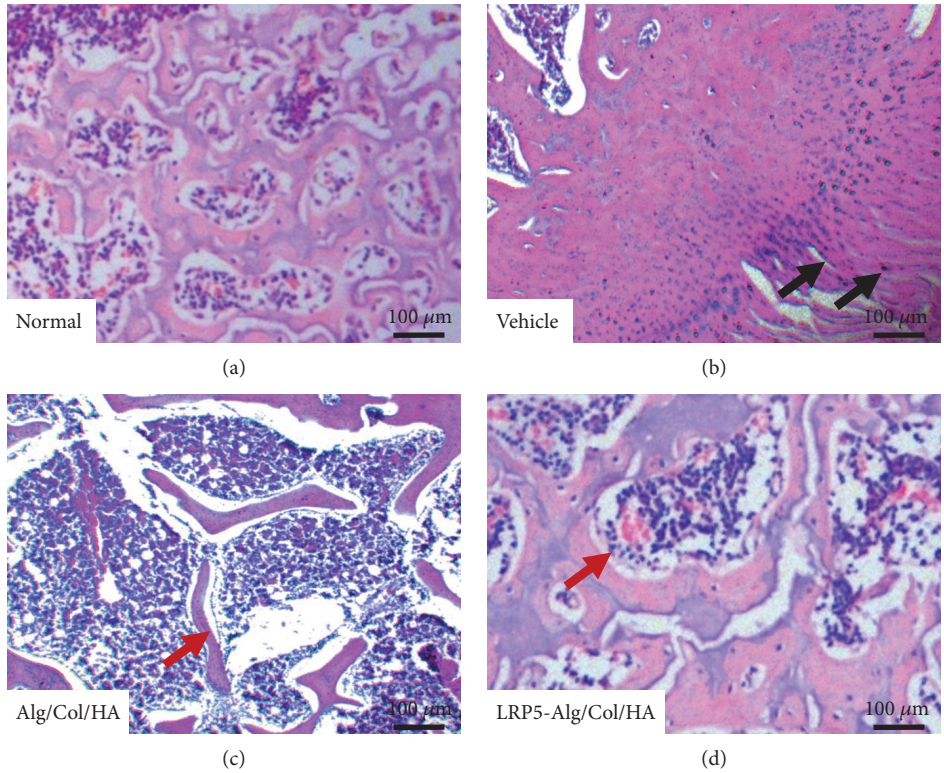

Figure 7: H&E staining of defect sites of a rat model of calvarial critical defect after 6 weeks' treatment. Black arrow indicates fibrous tissue, and red arrow indicates trabecular bones.

of collagen but also the network structure of calcium alginate, ensuring the normal biofunction of both polymers. Furthermore, collagen and hydroxyapatite also act as a "stable stent" for calcium alginate gels due to their significant ability of water absorption. Collagen absorbs water and greatly reduces the excessive swelling of the alginate gel, thereby increasing the sustained release of the composite. On the other hand, collagen and hydroxyapatite also adsorb protein drugs and improve the sustained-release performance.

3.3. Bioactivity of LRP5-Alg/Col/HA. The biological activity of LRP5 is mainly achieved by the Wnt signaling pathway. During the osteogenesis process, the Wnt/LRP5/β-catenin pathway plays an important role. The normal function of the Wnt/LRP5/β-catenin pathway mediates intracellular signals through LRP5 and stabilizes intracellular β-catenin, which enters the nucleus to bind to transcription factors, thereby regulating the expression of genes involved in osteoblast proliferation and functionality and promoting skeletal development. Loss of function of LRP5 leads to osteoblast dysfunction, which affects the accumulation of bone mass [32–34]. DKK1, a Wnt antagonist, has been reported to specifically inhibit the signaling pathway by binding to LRP, whereas the exogenous LRP5 prevents the interaction of endogenous LRP5 with DKK1. In order to study whether released LRP5 from LRP5-Alg/Col/HA still remained biologically active, we tested both the binding and biological activities of released LRP5 by competitive binding assay and cellular assay, respectively. Through the binding assay, FITC fluorescence increased on days 1, 6, 12, and 18, indicating that the LRP5 binding activity to DKK1 decreased over time in the conditioned mediums (Figure 5(a)). In cellular assay, the conditioned mediums containing released LRP5 were cultured with MSCs, and the downstream mRNA expression level was detected to indirectly identify LRP5 bioactivity. On days 1, 6, 12, and 18, compared with the Alg/Col/HA control group (Figure 5(b)), the LRP5-conditioned mediums in the LRP5-Alg/Col/HA group significantly increased the mRNA level of β-catenin in MSCs, indicating that LRP5-Alg/Col/HA could maintain the biological activity of LRP5 up to 18 days. Further, it was found that LRP5 release showed a uniform release rate during 1, 6, 12, and 18 days according to Figure 4. However, in Figure 5, the downstream β-catenin mRNA expression level decreased along with the release time, which was not consistent with the in vitro release. It was demonstrated that the released LRP5 has certain attenuation on biological activity over time. Taken together, it still had acceptable retention of binding activity and bioactivity, which was confirmed by the in vitro and cellular experiments in Figure 5. Overall, Alg/Col/HA was a good sustained-release carrier of LRP5, which not only had good controlled-release properties but also maintained the biological activity of LRP5.

3.4. Effect on the BMD of LRP5-Alg/Col/HA in Bone Repair. Compared with other bone defect models, the rat skull critical-size defect model is a reliable model for evaluating the repairing ability of bone biomaterials. This model does not have the ability to repair itself and requires certain material filling support to achieve healing [35–39]. Moreover,

experimental operation is relatively easy and repeatable. Therefore, we used this model to evaluate the ability to induce the osteogenesis of the LRP5-Alg/Col/HA composite. During the surgery, the composite could form into gel state in the defect area after injection. It implied the applicable possibility of LRP5-Alg/Col/HA in minimally invasive surgery to treat other types of bone defects according to the injectability of the LRP5-Alg/Col/HA composite. At 6 weeks, as shown by BMD measurement in the defect area in Figure 6, the density of the defect area in the LRP5-Alg/Col/HA group was significantly improved ($P < 0.05$) compared with the vehicle group, which was still a large gap in density compared to normal cranial bone density. Additionally, the improvement effect of LRP5-Alg/Col/HA was extremely obvious, and the bone density was significantly increased ($P < 0.05$) when compared with the Alg/Col/HA group. The histological evaluation results (Figure 7) revealed that the Alg/Col/HA group had an obvious new trabecular bone formation at the defect site, and no cartilage-like tissue was observed. Also, no cartilage-like tissue was observed in the LRP5-Alg/Col/HA group, but the trabecular bone distribution direction was more consistent, and the trabecular bone width was more uniform. In the vehicle group, the defect site was filled with fibrous tissue (black arrow in Figure 7), which affected cellular infiltration and growth. The results of the histological evaluation (Figure 7) and BMD (Figure 6) confirmed that LRP5-Alg/Col/HA had a potent ability to induce osteogenesis and had a great healing effect on the repair of bone defects. On the one hand, LRP5-Alg/Col/HA materials could facilitate the formation of a new bone in the defect site. Moreover, LRP5-Alg/Col/HA had good biocompatibility and osteogenic capability. In addition, the sustained release of LRP5 accelerated osteogenesis in vivo, which was consistent with previous reports. In the femoral fracture report [40], the healing effect of the whole-knockout LRP5 mice was significantly weaker than that of the wild-type mice, the healing area was smaller, and BMD was lower in the region.

4. Conclusion

LRP5-Alg/Col/HA has good injectability and is capable of the sustained release of LRP5 for up to 3 weeks and maintains the biological activity of LRP5 for more than 2 weeks. Furthermore, LRP5-Alg/Col/HA can promote the formation of a new bone in the rat calvarial defects and promote bone mineral density increase.

Data Availability

All the data is available with the handwritten notebook documented in our lab and could be provided from the corresponding author upon request.

Conflicts of Interest

The authors declare that there are no conflicts of interest regarding the publication of this paper.

Authors' Contributions

Yanhai Xi and Tingwang Jiang are equal contributors to this work.

Acknowledgments

This work was supported by the National Natural Science Foundation of China (Grant nos. 81472071 and 81301537), the Shanghai Science and Technology Committee Scientific research plan project (Grant no. 12nm0501202), and the Shanghai Changzheng Hospital Foundation (Grant no. 2017CZQN05).

References

[1] Z. Burningham, M. Hashibe, L. Spector, and J. D. Schiffman, "The epidemiology of sarcoma," *Clinical Sarcoma Research*, vol. 2, no. 1, p. 14, 2012.

[2] W. He, Y. Fan, and X. Li, "Recent research progress of bioactivity mechanism and application of bone repair materials," *Zhongguo Xiu Fu Chong Jian Wai Ke Za Zhi*, vol. 32, no. 9, pp. 1107–1115, 2018.

[3] Z. Chen, L. Kang, Q. Y. Meng et al., "Degradability of injectable calcium sulfate/mineralized collagen-based bone repair material and its effect on bone tissue regeneration," *Materials Science & Engineering. C, Materials for Biological Applications*, vol. 45, pp. 94–102, 2014.

[4] J. L. Drury and D. J. Mooney, "Hydrogels for tissue engineering: scaffold design variables and applications," *Biomaterials*, vol. 24, no. 24, pp. 4337–4351, 2003.

[5] Q. Hou, P. A. de Bank, and K. M. Shakesheff, "Injectable scaffolds for tissue regeneration," *Journal of Materials Chemistry*, vol. 14, no. 13, pp. 1915–1923, 2004.

[6] H. Tan and K. G. Marra, "Injectable, biodegradable hydrogels for tissue engineering applications," *Materials*, vol. 3, no. 3, pp. 1746–1767, 2010.

[7] G. D. Nicodemus and S. J. Bryant, "Cell encapsulation in biodegradable hydrogels for tissue engineering applications," *Tissue Engineering Part B: Reviews*, vol. 14, no. 2, pp. 149–165, 2008.

[8] B. V. Slaughter, S. S. Khurshid, O. Z. Fisher, A. Khademhosseini, and N. A. Peppas, "Hydrogels in regenerative medicine," *Advanced Materials*, vol. 21, no. 32-33, pp. 3307–3329, 2009.

[9] A. J. Wargacki, E. Leonard, M. N. Win et al., "An engineered microbial platform for direct biofuel production from brown macroalgae," *Science*, vol. 335, no. 6066, pp. 308–313, 2012.

[10] P. Agulhon, M. Robitzer, L. David, and F. Quignard, "Structural regime identification in ionotropic alginate gels: influence of the cation nature and alginate structure," *Biomacromolecules*, vol. 13, no. 1, pp. 215–220, 2011.

[11] S. Sudarsan, D. S. Franklin, M. Sakthivel, and S. Guhanathan, "Non toxic, antibacterial, biodegradable hydrogels with pH-stimuli sensitivity: investigation of swelling parameters," *Carbohydrate Polymers*, vol. 148, pp. 206–215, 2016.

[12] K. T. Campbell, D. J. Hadley, D. L. Kukis, and E. A. Silva, "Alginate hydrogels allow for bioactive and sustained release of VEGF-C and VEGF-D for lymphangiogenic therapeutic applications," *PLoS One*, vol. 12, no. 7, article e0181484, 2017.

[13] N. O. Dhoot and M. A. Wheatley, "Microencapsulated liposomes in controlled drug delivery: strategies to modulate drug release and eliminate the burst effect," *Journal of Pharmaceutical Sciences*, vol. 92, no. 3, pp. 679–689, 2003.

[14] W. Jie, D. Shijie, C. Jing, J. Jinlong, and W. Junjun, "Preparation and sustained release properties of acidified-attapulgite/alginate composite material," *CIESC Journal*, vol. 65, no. 11, pp. 4627–4632, 2014.

[15] Z. Li, P. Chen, X. Xu, X. Ye, and J. Wang, "Preparation of chitosan-sodium alginate microcapsules containing ZnS nanoparticles and its effect on the drug release," *Materials Science and Engineering: C*, vol. 29, no. 7, pp. 2250–2253, 2009.

[16] R. Tan, Z. She, M. Wang, X. Yu, H. Jin, and Q. Feng, "Repair of rat calvarial bone defects by controlled release of rhBMP-2 from an injectable bone regeneration composite," *Journal of Tissue Engineering and Regenerative Medicine*, vol. 6, no. 8, pp. 614–621, 2012.

[17] S. S. Liao, F. Z. Cui, W. Zhang, and Q. L. Feng, "Hierarchically biomimetic bone scaffold materials: nano-HA/collagen/PLA composite," *Journal of Biomedical Materials Research*, vol. 69B, no. 2, pp. 158–165, 2004.

[18] S. S. Liao, F. Z. Cui, and Y. Zhu, "Osteoblasts adherence and migration through three-dimensional porous mineralized collagen based composite: nHAC/PLA," *Journal of Bioactive and Compatible Polymers*, vol. 19, no. 2, pp. 117–130, 2016.

[19] B. O. Williams, "LRP5: from bedside to bench to bone," *Bone*, vol. 102, pp. 26–30, 2017.

[20] Y. Gong, R. B. Slee, N. Fukai et al., "LDL receptor-related protein 5 (LRP5) affects bone accrual and eye development," *Cell*, vol. 107, no. 4, pp. 513–523, 2001.

[21] M. L. Johnson, G. Gong, W. Kimberling, S. M. Recker, D. B. Kimmel, and R. R. Recker, "Linkage of a gene causing high bone mass to human chromosome 11 (11q12-13)," *American Journal of Human Genetics*, vol. 60, no. 6, pp. 1326–1332, 1997.

[22] R. D. Little, C. Folz, S. P. Manning et al., "A mutation in the LDL receptor-related protein 5 gene results in the autosomal dominant high-bone-mass trait," *The American Journal of Human Genetics*, vol. 70, no. 1, pp. 11–19, 2002.

[23] L. M. Boyden, J. Mao, J. Belsky et al., "High bone density due to a mutation in LDL-receptor-related protein 5," *The New England Journal of Medicine*, vol. 346, no. 20, pp. 1513–1521, 2002.

[24] J. W. Lee, H. An, and K. Y. Lee, "Introduction of N-cadherin-binding motif to alginate hydrogels for controlled stem cell differentiation," *Colloids and Surfaces. B, Biointerfaces*, vol. 155, pp. 229–237, 2017.

[25] C. Niehrs, "Function and biological roles of the Dickkopf family of Wnt modulators," *Oncogene*, vol. 25, no. 57, pp. 7469–7481, 2006.

[26] H. Clevers, "Wnt/β-catenin signaling in development and disease," *Cell*, vol. 127, no. 3, pp. 469–480, 2006.

[27] D. Fleury, B. Vayssiere, R. Touitou et al., "Expression, purification and functional characterization of Wnt signaling co-receptors LRP5 and LRP6," *Protein Expression and Purification*, vol. 70, no. 1, pp. 39–47, 2010.

[28] K. Y. Mao, F. H. Zhou, F. Z. Cui et al., "The preparation and evaluation of the combined artificial bone," *Applied Mechanics and Materials*, vol. 140, pp. 1–6, 2011.

[29] R. Tan, X. Niu, S. Gan, and Q. Feng, "Preparation and characterization of an injectable composite," *Journal of Materials Science. Materials in Medicine*, vol. 20, no. 6, pp. 1245–1253, 2009.

[30] C. Branco da Cunha, D. D. Klumpers, W. A. Li et al., "Influence of the stiffness of three-dimensional alginate/collagen-I interpenetrating networks on fibroblast biology," *Biomaterials*, vol. 35, no. 32, pp. 8927–8936, 2014.

[31] O. Chaudhuri, S. T. Koshy, C. Branco da Cunha et al., "Extracellular matrix stiffness and composition jointly regulate the induction of malignant phenotypes in mammary epithelium," *Nature Materials*, vol. 13, no. 10, pp. 970–978, 2014.

[32] D. Baksh, G. M. Boland, and R. S. Tuan, "Cross-talk between Wnt signaling pathways in human mesenchymal stem cells leads to functional antagonism during osteogenic differentiation," *Journal of Cellular Biochemistry*, vol. 101, no. 5, pp. 1109–1124, 2007.

[33] L. A. Davis and N. I. zur Nieden, "Mesodermal fate decisions of a stem cell: the Wnt switch," *Cellular and Molecular Life Sciences*, vol. 65, no. 17, pp. 2658–2674, 2008.

[34] P. S. Issack, D. L. Helfet, and J. M. Lane, "Role of Wnt signaling in bone remodeling and repair," *HSS Journal*, vol. 4, no. 1, pp. 66–70, 2008.

[35] S. H. Ahn, C. S. Kim, H. J. Suk et al., "Effect of recombinant human bone morphogenetic protein-4 with carriers in rat calvarial defects," *Journal of Periodontology*, vol. 74, no. 6, pp. 787–797, 2003.

[36] E. K. Pang, S. U. Im, C. S. Kim et al., "Effect of recombinant human bone morphogenetic protein-4 dose on bone formation in a rat calvarial defect model," *Journal of Periodontology*, vol. 75, no. 10, pp. 1364–1370, 2004.

[37] S. Hong, C. Kim, D. Han et al., "The effect of a fibrin-fibronectin/β-tricalcium phosphate/recombinant human bone morphogenetic protein-2 system on bone formation in rat calvarial defects," *Biomaterials*, vol. 27, no. 20, pp. 3810–3816, 2006.

[38] Y. C. Por, C. R. Barceló, K. E. Salyer et al., "Bone generation in the reconstruction of a critical size calvarial defect in an experimental model," *The Journal of Craniofacial Surgery*, vol. 19, no. 2, pp. 383–392, 2008.

[39] H. I. Canter, I. Vargel, P. Korkusuz et al., "Effect of use of slow release of bone morphogenetic protein-2 and transforming growth factor-beta-2 in a chitosan gel matrix on cranial bone graft survival in experimental cranial critical size defect model," *Annals of Plastic Surgery*, vol. 64, no. 3, pp. 342–350, 2010.

[40] D. E. Komatsu, M. N. Mary, R. J. Schroeder, A. G. Robling, C. H. Turner, and S. J. Warden, "Modulation of Wnt signaling influences fracture repair," *Journal of Orthopaedic Research*, vol. 28, no. 7, pp. 928–936, 2010.

Hindawi
International Journal of Polymer Science
Volume 2019, Article ID 9058161, 6 pages
https://doi.org/10.1155/2019/9058161

Research Article

Effects of Dendrobium Officinale Polysaccharides on Brain Inflammation of Epileptic Rats

Lin Zhang, Hua Peng, Jin Xu, Yixin Xu, You Yin, Bin He, and Jianhua Zhuang

Department of Neurology, Changzheng Hospital, Second Military Medical University, Shanghai 200003, China

Correspondence should be addressed to Jianhua Zhuang; jianhuazh11@126.com

Lin Zhang and Hua Peng contributed equally to this work.

Received 11 October 2018; Accepted 7 November 2018; Published 5 February 2019

Guest Editor: Mingqiang Li

Objective. To investigate the effects of Dendrobium officinale polysaccharides (DOPS) on the expression of inflammatory factors IL-1β and TNF-α and the MKP-1/MAPK signal pathway. *Methods*. PTZ-induced epileptic rat models were established. The rats were randomly divided into four groups: the control group, the DOPS group, the model group, and the DOPS intervention group. RT-PCR was used to measure the mRNA expression of IL-1β and TNF-α in the hippocampi of all groups; western blot was used to measure the protein expression of IL-1β and TNF-α and phosphorylation of ERK1/2, JNK, p38, and MKP-1 in the hippocampi of all groups at weeks 1, 2, 3, and 4 after modeling. *Results*. At weeks 1, 2, 3, and 4 after modeling, there were no significant differences between the control group and the DOPS group in the mRNA and protein expression of IL-1β and TNF-α and phosphorylation of ERK1/2, JNK, p38, and MKP-1 (all $P > 0.05$); the mRNA and protein expression of IL-1β and TNF-α and phosphorylation of ERK1/2, JNK, and p38 were significantly increased, while the phosphorylation of MKP-1 was decreased in the model group compared with the control group. The mRNA and protein expression of IL-1β and TNF-α and phosphorylation of ERK1/2, JNK, and p38 were significantly decreased, while the phosphorylation of MKP-1 was increased in the DOPS intervention group compared with the model group. *Conclusion*. DOPS can reduce PTZ-induced brain inflammation and seizures of epileptic rats by inhibiting IL-1β, TNF-α, and MAPK signal pathways.

1. Introduction

Epilepsy is one of the most common chronic brain diseases characterized by frequent recurrent seizures [1], as well as emotional and cognitive dysfunction [2]. The main cause of epilepsy is transient-distorted hypersynchronous electrical discharges of the brain network caused by imbalance between excitation and suppression [3]. Epilepsy imposes a huge burden on society and the economy, seriously affecting quality of life. It is reported that the expression of mRNA and the protein level of various proinflammatory cytokines in epileptics and rat models were increased, such as tumor necrosis factor-alpha (TNF-α) and interleukin-1 beta (IL-1β) [4, 5]. Studies have reported that seizure thresholds for the overexpression of TNF-α were lower in transgenic rats [6]. IL-1β single nucleotide polymorphism was associated with temporal lobe epilepsy [7], and downregulation of the IL-1β signal not only delayed the onset of seizures, preventing the generalization of epilepsy, but also elevated the threshold for post-discharge induction [8]. These studies indicated that inflammatory factors played a key role in the development of epilepsy. Therefore, regulating epilepsy-related inflammatory factors is important for the treatment of epilepsy.

Dendrobium officinale is a kind of traditional Chinese medicine of high medicinal value, and it has anti-inflammatory, antioxidative, and immunity-enhancement effects. The main active ingredient of Dendrobium officinale is Dendrobium officinale polysaccharides, which are water-soluble and used for the treatment of epilepsy due to their strong anti-inflammatory and antioxidative effects [9]. There are few reports about the effects of DOPS on inflammatory responses induced by epilepsy and its mechanism. This study will investigate the effects of DOPS on brain inflammation in SD epileptic rats and its mechanism.

2. Materials and Methods

2.1. Experimental Animals. 96 SD male rats, about 200-220 g, were purchased from Shanghai SLAC Experimental Animal Co. Ltd. The feeding condition was at 20-25°C under 12-hour light/day, with humidity of 60%-70%, and all the rats were allowed to drink and eat freely.

2.2. Reagent. Pentetrazol (PTZ) was purchased from Sigma-Aldrich Trade Co. Ltd. Air-dried Dendrobium officinale purchased from Baise Biological Products Chain Co. Ltd. in Lingyun County, Baise, was used to prepare 0.15 g/l diluent based on Yu et al.'s method of extraction, purification, and concentration determination of DOPS [10]. IL-1β, TNF-α, and β-actin primers were synthesized by GenScript Biotechnology Co. Ltd. The primer sequences are seen in Table 1. Kits for total RNA extract were purchased from Shanghai Doctor Biotechnology Co. Ltd. Fluorescence quantitative PCR kits were purchased from TaKaRa Company. Rat IL-1β and TNF-α ELISA kits were purchased from Invitrogen Company. Rat p-ERK1/2, p-JNK, and p-p38 ELISA kits were purchased from RayBiotech Company. Rat p38, ERK1/2, and MKP-1 ELISA kits were purchased from LifeSpan BioSciences. Rat JNK ELISA kits were purchased from R&D Systems.

2.3. Instruments. The following instruments were used: NanoDrop 2000 microvolume spectrophotometers, Thermo Fisher Scientific RT-PCR system, SDS-PAGE electrophoresis system, transblot turbo transfer packs, and 3H-2000TD automatic true density analyzer.

2.4. Animal Model Establishment. The experimental groups consisted of the control group ($n = 24$), the DOPS group ($n = 24$), the PTZ model group ($n = 24$), and the DOPS intervention group ($n = 24$). PTZ (35 mg/kg) was given to rats in the PTZ model group and the DOPS intervention group by intraperitoneal injection; equivalent normal saline (35 mg/kg) was given to rats in the control group and the DOPS group by intraperitoneal injection. The degree of seizure was assessed by changes in behaviour of the rats within 30-50 min after injection: no seizure: no convulsion; mild seizures: facial clonus, convulsionary nodding, or foreleg myoclonus; and severe seizures: hindlimb spasticity or aggravated foreleg clonus or falls due to lack of balance occurring on the basis of mild seizures. It took 4 weeks for modeling. Rats with severe seizures for a week were PTZ kindling models, and those failing to kindle were considered as failure.

2.5. Medications. Rats in the DOPS group and the DOPS intervention group were perfused with DOPS (1.5 g/kg) 1 hour before each intraperitoneal injection; rats in the control group and the DOPS group were perfused with equivalent normal saline and administrated for 4 weeks. Rats' behaviour during modeling was observed. Rats of each group were weighed before modeling, after the model establishment, and at weeks 1, 2, 3, and 4 after drug administration. SD rat hippocampi, 6 for each group, were isolated at low temperatures at weeks 1, 2, 3, and 4 after drug administration, and fresh hippocampi were stored in liquid nitrogen containers.

Table 1: IL-1β, TNF-α, and β-actin primers.

Primers	Primer sequences 5′-3′
IL-1β	5′-AGAGTGTGGATCCCAAACAA-3′ 5′-AGT CAA CTA TGT CCC GAC CA-3′
TNF-α	5 ′-CTCCAGCTGGAAGACTCCTCCCAG-3′ 5 ′-CCCGACTACGTGCTCCTCACC-3′
β-Actin	5′-TCAGGTCATCACTATCGGCAAT-3′ 5′-AAAGAAAGGGTGTAAAACGCA-3′

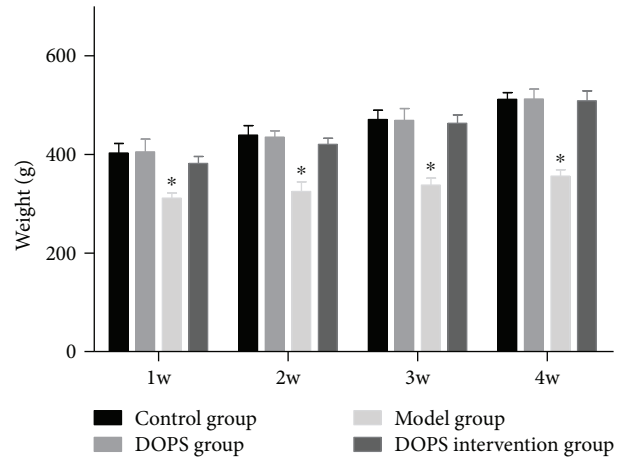

Figure 1: The weights of each group. $^*P < 0.05$ compared with the control group.

2.6. RT-PCR. Relative quantification was used to determine mRNA levels of IL-1β and TNF-α. An appropriate amount of hippocampi was obtained. The hippocampi were grinded and homogenized for subsequent RNA extraction. The extraction was guided by TRIzol kit instructions. O.D. value was measured to quantify RNA concentration, and then reverse transcription experiments were conducted with its product cDNA stored at -20°C. RT-PCR experiments were performed by using cDNA as a template according to the instructions of fluorescence quantitative PCR kits, and quantitative analysis was performed by using 2-ΔΔct.

2.7. ELISA. Hippocampi were obtained, with PBS buffer at a ratio of 10.0 ml buffer/1.0 g tissue slices added. The brain tissue was homogenized on ice and kept on ice for 1 h. Then the brain tissue was centrifuged in a 15 ml centrifuge tube at 2000 rpm for 20 min. The supernatant was transferred to a new centrifuge tube for ELISA analysis.

2.8. Analysis Methods. Measurement data for each group were expressed as mean ± standard deviation. Comparisons were based on t-tests. $P < 0.05$ indicated statistical significance.

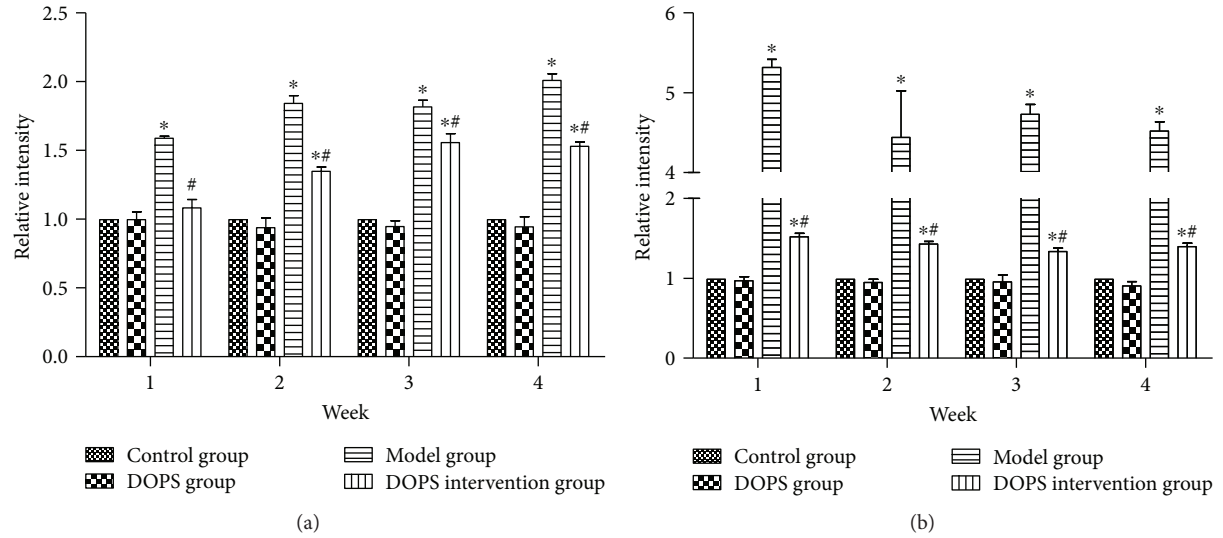

Figure 2: mRNA expression detection of IL-1β and TNF-α. (a) The mRNA transcription detection results of IL-1β. (b) The mRNA transcription detection results of TNF-α. $^{*}P < 0.05$ compared with the control group and $^{\#}P < 0.05$ compared with the model group.

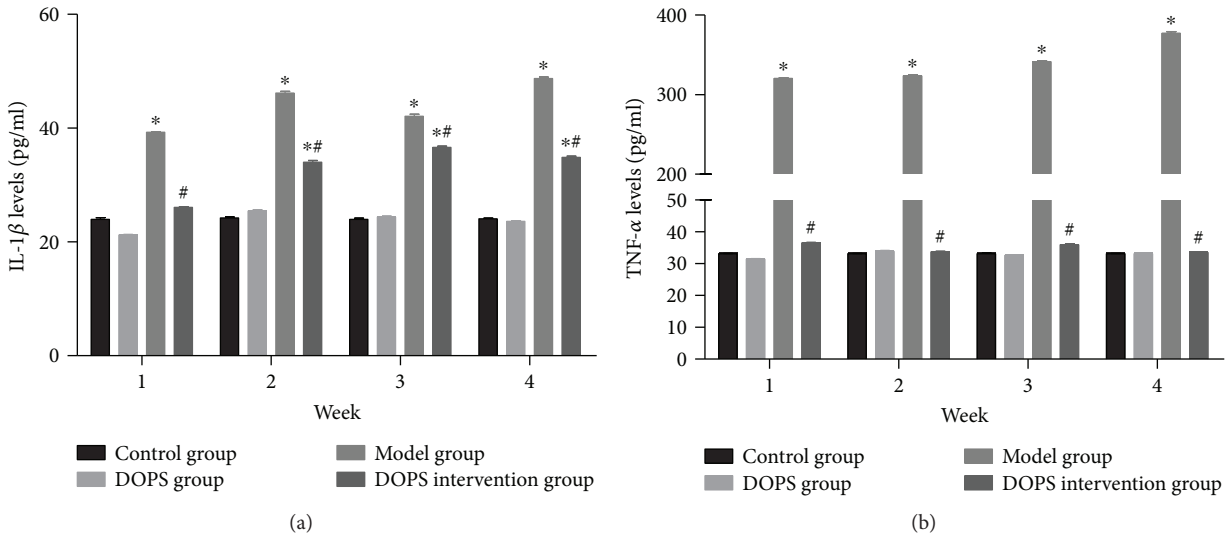

Figure 3: The levels of IL-1β and TNF-α by ELISA: (a) the levels of IL-1β; (b) the levels of TNF-α. $^{*}P < 0.05$ compared with the control group and $^{\#}P < 0.05$ compared with the model group.

3. Results

3.1. Behavioural Observation. Rats in the control group and the DOPS group had normal appetite, shiny hair, and no seizures. Rats in the PTZ model group had aggravating seizures, decreased appetite, and lost luster in hair within days after injection. Most rats developed severe seizures and overreacted to external sounds often with their bodies curled up one week after PTZ injection. Rats in the DOPS intervention group developed severe seizures two weeks after PTZ injection; however, they regained normal appetite and shiny hair with less overreactions to external sounds under continuous DOPS intervention.

3.2. Weight. The weights of each group are shown in Figure 1. The weights of each group were gradually increased. There were no significant differences in weights between the control group and the DOPS group at each time point. The weights of the model group at each time point were significantly different from those of the control group. The weights of the DOPS intervention group grew faster than those of the model group and had no significant differences with those of the control group.

3.3. mRNA Expression Detection of IL-1β and TNF-α. There were no significant differences between the DOPS group and the control group in the levels of transcription of IL-1β and TNF-α (all $P > 0.05$). The levels of transcription of IL-1β and TNF-α in the model group were significantly higher than those in the control group (all $P < 0.05$). The levels of transcription of IL-1β in the DOPS intervention group were significantly higher than those in the control group at weeks 2, 3, and 4 (all $P < 0.05$), and the levels of TNF-α in the DOPS intervention group were significantly

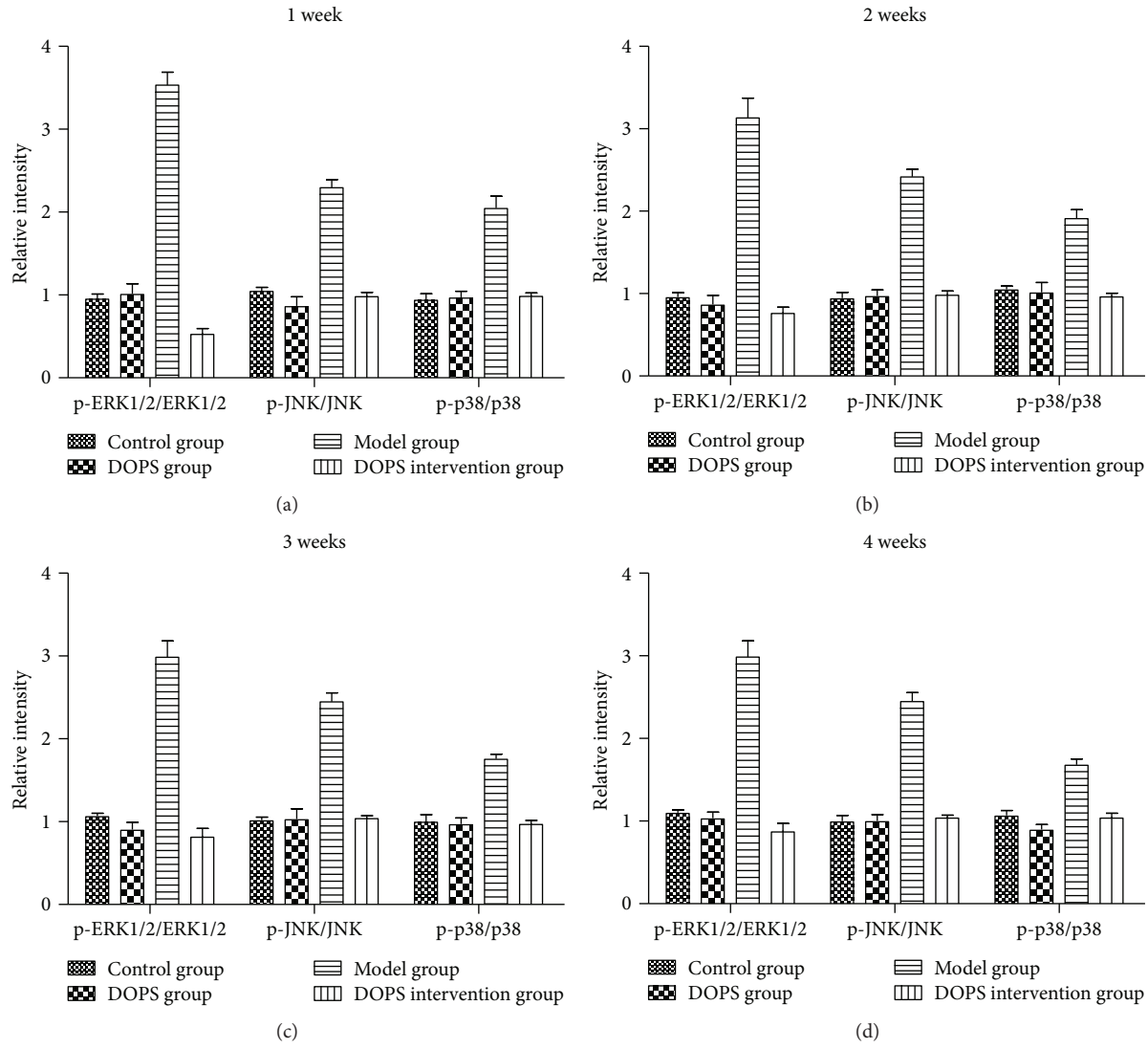

Figure 4: The quantitative analysis of the signaling of p-ERK1/2/ERK1/2, p-JNK/JNK, p-P38/P38. $^{*}P < 0.05$ compared with the control group and $^{\#}P < 0.05$ compared with the model group.

higher than those in the control group at each time point (all $P < 0.05$). At each time point, the levels of transcription of IL-1β and TNF-α in the DOPS intervention group were significantly lower than those in the model group (all $P < 0.05$). See Figure 2. The data further suggests that DOPS intervention can alleviate PTZ-induced neuroinflammation.

3.4. Protein Expression Detection of IL-1β and TNF-α. There were no significant differences between the DOPS group and the control group in levels of translation of IL-1β and TNF-α at each time point (all $P > 0.05$). The levels of translation of IL-1β and TNF-α in the model group were significantly increased at each time point (all $P < 0.05$). The levels of translation of IL-1β in the DOPS intervention group were significantly higher than those in the control group at weeks 2, 3, and 4 (all $P < 0.05$), and the levels of TNF-α in the DOPS intervention group were significantly higher than those in the control group at each time point (all $P < 0.05$). At each time point, the levels of translation of IL-1β and TNF-α in the DOPS intervention group were significantly lower than those in the model group (all $P < 0.05$). See Figure 3. The data further suggests that DOPS intervention can alleviate PTZ-induced neuroinflammation.

3.5. MKP-1/MAPK Signal Pathway in PTZ Model Rats Was Inhibited by DOPS. Detection found no differences between the four groups in total protein content of ERK1/2, JNK, and p38. Phosphorylation of ERK1/2, JNK, and p38 in the model group was significantly higher than that in the control group (all $P < 0.05$) and was significantly higher than that in the DOPS intervention group (all $P < 0.05$) (Figure 4). This suggests that the activation of the MAPK signal pathway in PTZ-induced brain dendrobium candidum was reduced by DOPS.

MKP-1 can dephosphorylate MAPK and inhibit the activity of ERK, JNK, and p38 in stress responses, thereby participating in the regulation of inflammatory responses; thus, MKP-1 was detected. The result showed that

phosphorylation of MKP-1 in the DOPS intervention group was higher than that in the model group (Figure 5). It suggests that MKP-1 activation is involved in the inhibition of MAPK intervened by DOPS.

4. Discussion

Epilepsy is a common neurological disease, yet its pathogenesis has not been fully understood; however, studies have shown that seizures may be associated with immune dysfunction in patients, and it was proposed to treat immune dysfunction in epileptics [11]. Studies indicated that seizures could be induced by oxidative stress injury. And a large number of oxygen free radicals could cause inflammatory reactions, synthesize and release many inflammatory factors in the brain, and activate the NF-κB pathway and the MAPK signal pathway [12]. Studies have shown that DOPS could reduce oxidative products to improve the antioxidant capacity and correct the oxidative/antioxidative imbalance [13]. DOPS can inhibit the NF-κB pathway and release of proinflammatory factors and enhance the activity of antioxidant enzymes in the blood [14]. In this study, DOPS had no effect on the growth and survival of normal SD rats, and there were no significant differences in weight gain between the DOPS group and the control group.

The NF-κB pathway controls the synthesis and release of such downstream inflammatory cytokines as IL-1β, TNF-α, and IL-10 during the development of epilepsy. IL-1β and TNF-α are proinflammatory cytokines released by brain inflammation-activated microglia, and PTZ and traumatic injuries can stimulate the production of IL-1β and TNF-α in the brain [15, 16]. The study found that DOPS can inhibit the expression of IL-1β and TNF-α transcription and translation of PTZ-induced rat hippocampi. Studies have shown that inhibition of IL-1β and TNF-α expression could reduce the effects of T lymphocytes and monocytes. Excessive proinflammatory cytokines produced by activated microglia were toxic to neurons [17, 18]. The inhibition of IL-1β and TNF-α expression in the study suggests that DOPS can reduce PTZ-induced seizures by regulating microglia-mediated inflammatory responses.

Pathological mechanisms such as inflammation, ischemia, and apoptosis are related to the regulation of the MAPK signal pathway [19]. MAPK consists of three major subsets, ERK1/2, JNK, and p38, and plays a key role in transmitting various extracellular signals to nuclei and regulating cell growth and differentiation. The expression of proinflammatory cytokines is under the control of various transcription factors and regulation of the MAPK signal pathway [20]. The result of the study indicates that DOPS can inhibit the MAPK signal pathway by reducing phosphorylation of ERK1/2, JNK, and p38 in vivo. This suggests that DOPS can enhance ERK1/2, JNK, and p38 dephosphorylation. MKP-1 is another member of the MAPK family that enables dephosphorylation and inactivation of various members of the family [21]. MKP-1 deficiency is known to enhance phosphorylation of p38 and JNK [22]. The study found that the level of MKP-1 phosphorylation was increased in rats given DOPS intervention. The data indicates that DOPS blocked the MAPK signal pathway by enhancing MKP-1 phosphorylation.

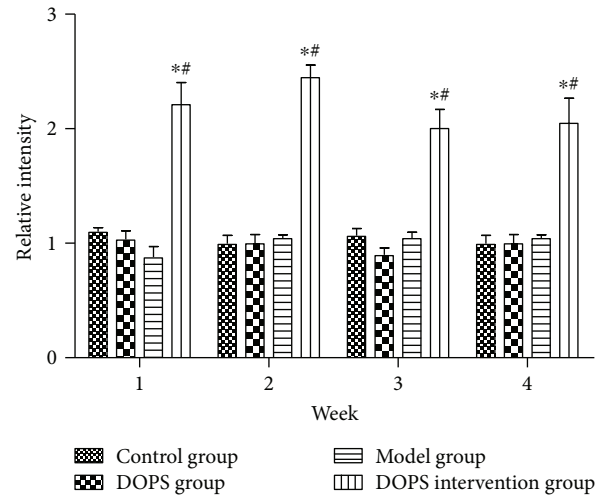

Figure 5: The quantitative analysis of p-MKP-1/MKP-1 signaling. $^{*}P < 0.05$ compared with the control group and $^{\#}P < 0.05$ compared with the model group.

In summary, DOPS can reduce the effects of PTZ-induced brain inflammation in epileptic rats as well as seizures by inhibiting the IL-1β, TNF-α, and MAPK signal pathway.

Data Availability

All the data is available in the handwritten notebook documented in our lab.

Conflicts of Interest

The authors declare that there are no conflicts of interest regarding the publication of this paper.

References

[1] B. S. Chang and D. H. Lowenstein, "Epilepsy," *The New England Journal of Medicine*, vol. 349, no. 13, pp. 1257–1266, 2003.

[2] S. Realmuto, L. Zummo, C. Cerami et al., "Social cognition dysfunctions in patients with epilepsy: evidence from patients with temporal lobe and idiopathic generalized epilepsies," *Epilepsy & Behavior*, vol. 47, pp. 98–103, 2015.

[3] J. Ozuna, "Seizure disorders and epilepsy," *Lippincott's Primary Care Practice*, vol. 4, no. 6, pp. 608–618, 2000.

[4] M. G. de Simoni, C. Perego, T. Ravizza et al., "Inflammatory cytokines and related genes are induced in the rat hippocampus by limbic status epilepticus," *The European Journal of Neuroscience*, vol. 12, no. 7, pp. 2623–2633, 2000.

[5] B. Feng and Z. Chen, "Generation of febrile seizures and subsequent epileptogenesis," *Neuroscience Bulletin*, vol. 32, no. 5, pp. 481–492, 2016.

[6] L. Probert, K. Akassoglou, G. Kassiotis, M. Pasparakis, L. Alexopoulou, and G. Kollias, "TNF-α transgenic and

knockout models of CNS inflammation and degeneration," *Journal of Neuroimmunology*, vol. 72, no. 2, pp. 137–141, 1997.

[7] M. A. Kauffman, D. G. Moron, D. Consalvo, R. Bello, and S. Kochen, "Association study between interleukin 1β gene and epileptic disorders: a HuGe review and meta-analysis," *Genetics in Medicine*, vol. 10, no. 2, pp. 83–88, 2008.

[8] T. Ravizza, F. Noé, D. Zardoni, V. Vaghi, M. Sifringer, and A. Vezzani, "Interleukin converting enzyme inhibition impairs kindling epileptogenesis in rats by blocking astrocytic IL-1β production," *Neurobiology of Disease*, vol. 31, no. 3, pp. 327–333, 2008.

[9] H. Jie, Z. Ying, Y. Jing et al., "Immunomodulatory effect of *Dendrobium officinale* polysaccharide on macrophage RAW264.7 induced by LPS," *Chinese Pharmaceutical Journal*, vol. 52, no. 7, pp. 548–552, 2017.

[10] Y. Li-li, W. Jiao-mei, and H. Suo-yi, "Study on antioxidation of polysaccharides from Lingyun, Guangxi wild Dendrobium officinale," *Lishizhen Medicine and Materia Medica Research*, vol. 25, no. 12, pp. 2842–2845, 2014.

[11] M. Fei, *The Effect of Recombinant Rat IL-10 on In Vitro Cytokine Production of Peripheral Blood Mononuclear*, Shanxi Medical University, 2006.

[12] I. Stanojkovic, J. Kotur-Stevuljevic, S. Spasic et al., "Relationship between bone resorption, oxidative stress and inflammation in severe COPD exacerbation," *Clinical Biochemistry*, vol. 46, no. 16-17, pp. 1678–1682, 2013.

[13] T. Han-qing, W. Yi, L. Lan, and C. Hua, "Experimental study on the effect of dendrobium officinale on the antioxidant ability of mice," *Chinese Journal of Health Laboratory Technology*, vol. 24, no. 21, pp. 3082–3084, 2014.

[14] L. Yinmin, *Study of Anti-aging Effect of Dendrobium Officinale Polysaccharides on Female Aging Mice Models and the Underlying Mechanisms*, Guangzhou University of Chinese Medicine, 2011.

[15] K. N. Nam, Y. M. Park, H. J. Jung et al., "Anti-inflammatory effects of crocin and crocetin in rat brain microglial cells," *European Journal of Pharmacology*, vol. 648, no. 1-3, pp. 110–116, 2010.

[16] C. R. Plata-Salamán, S. E. Ilyin, N. P. Turrin et al., "Kindling modulates the IL-1β system, TNF-α, TGF-β1, and neuropeptide mRNAs in specific brain regions," *Brain Research. Molecular Brain Research*, vol. 75, no. 2, pp. 248–258, 2000.

[17] J. Wang, H. Zhang, H. Ma et al., "Inhibitory effect of dietary n-3 polyunsaturated fatty acids to intestinal IL-15 expression is associated with reduction of TCR$\alpha\beta$+CD8α+CD8β– intestinal intraepithelial lymphocytes," *The Journal of Nutritional Biochemistry*, vol. 19, no. 7, pp. 475–481, 2008.

[18] B. C. Sydora, S. M. MacFarlane, J. W. Walker et al., "Epithelial barrier disruption allows nondisease-causing bacteria to initiate and sustain IBD in the IL-10 gene-deficient mouse," *Inflammatory Bowel Diseases*, vol. 13, no. 8, pp. 947–954, 2007.

[19] J. Campbell, C. J. Ciesielski, A. E. Hunt et al., "A novel mechanism for TNF-α regulation by p38 MAPK: involvement of NF-κB with implications for therapy in rheumatoid arthritis," *Journal of Immunology*, vol. 173, no. 11, pp. 6928–6937, 2004.

[20] H. Chanteux, A. C. Guisset, C. Pilette, and Y. Sibille, "LPS induces IL-10 production by human alveolar macrophages via MAPKinases- and Sp1-dependent mechanisms," *Respiratory Research*, vol. 8, no. 1, p. 71, 2007.

[21] B. C. Jang, K. J. Lim, M. H. Suh, J. G. Park, and S. I. Suh, "Dexamethasone suppresses interleukin-1beta-induced humanβ-defensin 2 mRNA expression: involvement of p38 MAPK, JNK, MKP-1, and NF-κB transcriptional factor in A549 cells," *FEMS Immunology and Medical Microbiology*, vol. 51, no. 1, pp. 171–184, 2007.

[22] J. Ye, M. Ding, X. Zhang, Y. Rojanasakul, and X. Shi, "On the role of hydroxyl radical and the effect of tetrandrine on nuclear factor–kappaB activation by phorbol 12-myristate 13-acetate," *Annals of Clinical and Laboratory Science*, vol. 30, no. 1, pp. 65–71, 2000.

Hindawi
International Journal of Polymer Science
Volume 2019, Article ID 9543526, 5 pages
https://doi.org/10.1155/2019/9543526

Research Article

Therapy of Prostate Cancer by Nanoyam Polysaccharide

Cheng Peng,[1] **Bo Han**,[1] **Baishan Wang**,[1] **Gaoyang Zhao**,[1] **Fang Yuan**,[2] **Yeyu Zhao**,[3] **Liang Liang**,[2] **Dingge Liu**,[4] **Zhaohui Zhai**,[5] **and Yanping Shen**[6]

[1]*Department of Clinical Laboratory, The Affiliated Hospital of Liaoning University of Traditional Chinese Medicine, Shenyang, Liaoning 110032, China*
[2]*Department of Nephrology, The Affiliated Hospital of Liaoning University of Traditional Chinese Medicine, Shenyang, Liaoning 110032, China*
[3]*Department of Rheumatology and Immunology, The Affiliated Hospital of Liaoning University of Traditional Chinese Medicine, Shenyang, Liaoning 110032, China*
[4]*Medical College of Soochow University, Suzhou, Jiangsu 215123, China*
[5]*Department of Plastic Surgery, Plastic Surgery Hospital of Weifang Medical University, Weifang, Shandong 261042, China*
[6]*Department of Nephrology, The First Affiliated Hospital of Soochow University, Suzhou, Jiangsu 215006, China*

Correspondence should be addressed to Zhaohui Zhai; zhaizhh@wfmc.edu.cn and Yanping Shen; shenyanping@suda.edu.cn

Received 20 October 2018; Revised 22 November 2018; Accepted 5 December 2018; Published 31 January 2019

Guest Editor: Jianxun Ding

We evaluated the effect and mechanism of yam polysaccharide on the proliferation of the prostatic cancer cell line and tumor-bearing mice. The effect of nanoyam polysaccharide on prostatic cancer cell line PC-3 was measured using the scratch adhesion test and flow cytometry. The growth effect induced by nanoyam polysaccharide was detected with the CCK-8 test. The levels of caspase-3 protein were determined with Western blot. In our data, nanoyam polysaccharide presented inhibitory effect on the proliferation of PC-3. The scratch adhesion test showed that the rate of wound healing in the intervention group was significantly lower than that in the control group ($p < 0.05$). Flow cytometry assay showed that, after treatment with nanoyam polysaccharide, the apoptosis rate in the intervention group was significantly lower than that in the control group (45.8%±2.6%, 25.8%±3.1%; $p < 0.05$). Western blot assay showed upregulated levels of caspase-3 in the intervention group, compared to the control group ($p < 0.05$). Our results suggested that nanoyam polysaccharide strongly suppressed the growth of prostatic cancer by inducing the overexpression of caspase-3 and may be a potent anticancer strategy.

1. Introduction

Prostate cancer, defined as one of the most common malignant tumors in male, ranks the second in global morbidity and the sixth in mortality [1]. Previously, prostate cancer was usually treated with surgery and local radiotherapy. However, due to the invisibility of early prostate cancer, most patients are diagnosed in the middle and late stage and miss the best opportunity for treatment. Testicular resection combined with endocrine therapy was mainly used in patients with advanced cancer. Patients may develop androgen-independent prostate cancer during endocrine therapy [2, 3].

With the continuous in-depth study of Chinese traditional pharmacology, which is often used in the comprehensive treatment of cancer and has achieved good results, Chinese medicine has become an important part of tumor treatment in China. Studies have shown that traditional Chinese medicine played multiple roles in preventing tumorigenesis and antitumor therapy, such as increasing efficacy and reducing toxicity, suppressing tumor recurrence and metastasis [4, 5]. Some studies have found that nanoyam polysaccharides could be used as antitumor active substances [6–8], but little research has been performed on prostate cancer.

Previous studies indicated that the hot water extraction could be used to separate pure Chinese yam polysaccharide

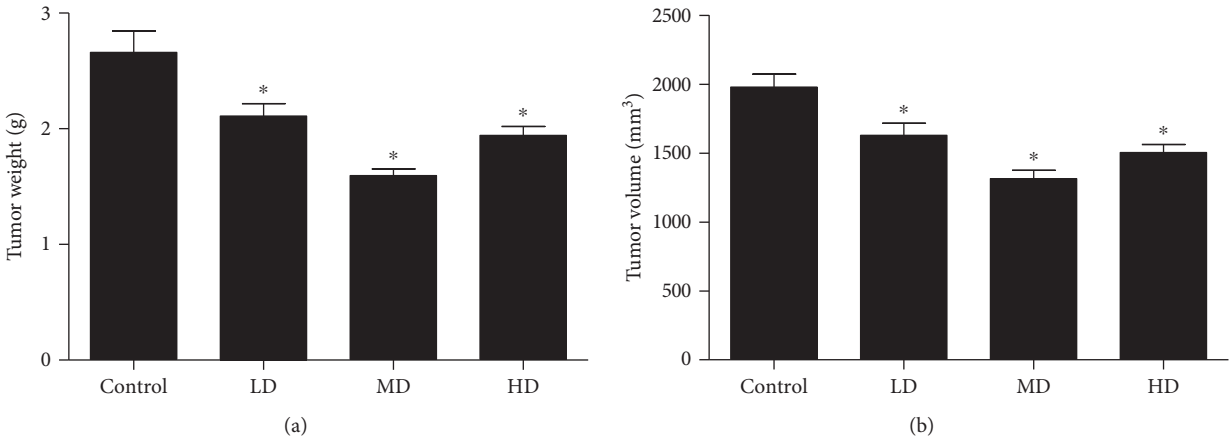

Figure 1: (a, b) The tumor weight and tumor volume of mice in different groups. Data were presented as mean ± SD. $^*p < 0.05$, compared with the control group.

[9]. There exists bioactive ingredients such as β-1,3-glucose, α-1-galactose, and α-1,6-galactose in the purified yam polysaccharide, which could be encapsulated into nanostructure. Nanoparticles are prepared by natural polymers with the size of approximately 100 nm [10]. In this study, the antitumor activity of nanoencapsulated yam polysaccharide was investigated in prostate cancer *in vitro* and *in vivo*.

2. Methods and Materials

2.1. Cell Line and Animals. Human prostatic cancer cell line was purchased from Shanghai Cell Institute, Chinese Academy of Sciences. Cells were cultured in medium RPMI1640 (Gibco) containing 10% bovine fetal serum (Thermo Fisher Scientific). Forty healthy male 5-6-week-old BALB/c mice (body weight, 18-22 g) were purchased from the Centre of Experimental Animals at Fudan University. All mice were kept on a 12 h light/dark cycle and given free access to food and water. The mice were divided into four groups randomly: control group ($n = 10$), low-dose group ($n = 10$), medium group ($n = 10$), and high-dose group ($n = 10$). The animal experiment and all associated procedures were approved by the Animal Ethical and Welfare Committee at Fudan University.

2.2. Reagents. Nanoyam polysaccharides were purchased from Shanxi Ciyuan Biotech Company. Caspase-3 primary antibody (ab13847, 1 : 1000, Abcam) and GAPDH (#4970, 1 : 1000, Abcam) were purchased. HRP-conjugated rabbit anti-mouse IgG were from Jackson ImmunoResearch Laboratories Inc. (West Grove, Pennsylvania, USA). FITC-Annexin V/PI kit was purchased from Sigma (APOAF-20TST, USA). Flow cytometry assay was performed in FACS-san440 (BD, USA). CCK-8 kit was purchased from Beyotime.

2.3. Tumor Xenograft Mouse Model. All animal experiment protocols were approved by the Institutional Review Board at the Immune Disease Institute. Breast cancer xenograft model was established in nude mice by the injection of PC-3 cells. Next, the mice received intravenous injection of PBS (as negative control), low-dose nanoyam polysaccharide, medium-dose nanoyam polysaccharide, and high-dose nanoyam polysaccharide every day for 4 weeks. The tumor growth and body weight of the mice were monitored until day 30 when the mice were sacrificed and the tumor tissues were excised for analysis.

2.4. Scratch Adhesion Test. PC-3 cell suspension was prepared at a density of 2×10^5 cells/mL. 2 mL cell suspension was inoculated in a 6-well plate and cultured for 12 h. After the cells were adhered to the wall, a straight line was drawn along the diameter of the hole with the nozzle of a 200 μL micropipette and the floating cells were washed away by PBS. The cells were divided into two groups. Normal medium was added to the control group, and nanoyam polysaccharide (80 mg/L) was added to the intervention group for 48 h after culture. The scratch was recorded at 0 h, 12 h, 24 h, and 48 h after microscopy. The relative ratio of the cell scratch spacing between the control group and the intervention group was calculated using the IPP software. The experiment was repeated three times, and the average value was calculated. The scratch healing rate = (0 h width-xh width)/0 h width.

2.5. CCK-8 Assay. A cell counting kit-8 (CCK-8) analysis kit (Thermo Fisher Scientific) was used to determine the PC-3 viability. The CCK-8 kit was put into each well 0, 12, 24, and 48 h, respectively, based on the manufacturer's protocol, and we recorded the absorbance at 450 nm.

2.6. Flow Cytometry Assay. Cells were obtained from the cell line, and mice were stained with FITC-labeled Annexin V and PI. After incubation at room temperature for 15 min, samples were washed once with PBS buffer. At least 10,000 cells were assayed by two-color FCM using flow cytometry. Data were analyzed by the CellQuest software (Becton Dickinson, Mountain View, CA).

2.7. Western Blot. Cells were then harvested and homogenized in ice-cold sodium dodecylsulfate (SDS) lysis buffer. After collection of total cell lysates, equal amount of

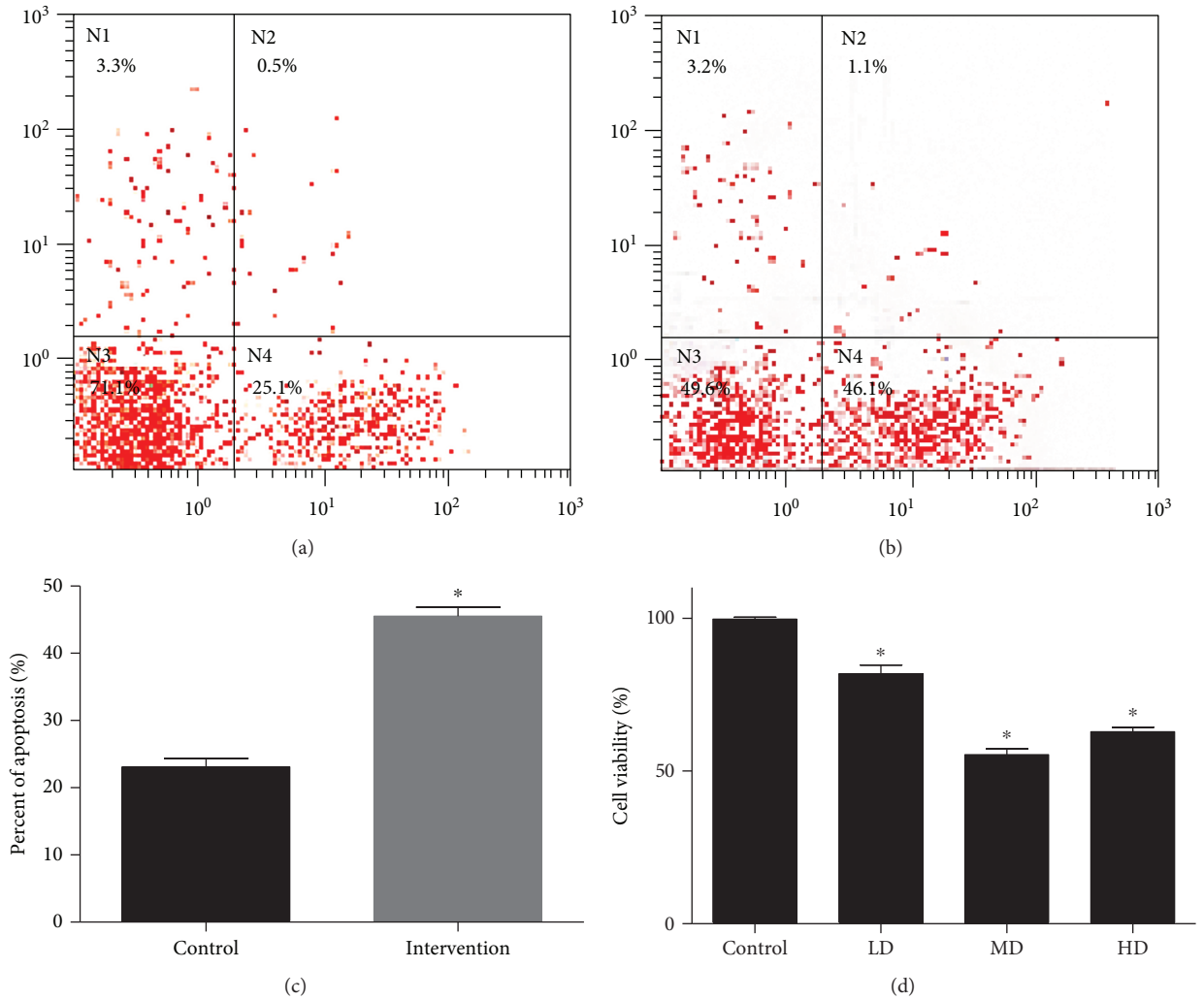

FIGURE 2: Flow cytometry assay and CCK-8 assay for prostatic cancer cells. (a, b) The representative data of flow cytometry assay for apoptosis of cell line PC-3. (c) The average percent of apoptosis of PC-3 cells was calculated. (d) CCK-8 results for tumor cells in mice. All experiments were triplicated. Data were presented as mean ± SD. $^*p < 0.05$, compared with the control group.

protein was separated by 10% SDS-PAGE and blotted onto a PVDF membrane. The PVDF membranes were blocked with Tris-buffered saline (TBS) containing 5% skimmed milk powder for 1 h and then incubated at 4°C overnight with caspase-3 mAb. After that, the membranes were washed with 16Tris-buffered saline/Tween-20 (TBS/T) buffer for three times (5 min each time) and incubated with HRP-conjugated polycolonal secondary antibody for 1 h at room temperature. The membranes were developed with the enhanced plus chemiluminescence assay (Pierce, USA) according to the manufacturer's instructions. Images were analyzed by the Image Pro Plus 6.0 software. The caspase-3 expressions were normalized to the GAPDH loading control.

2.8. Statistical Analysis. The data were presented as mean ± SD. All statistical analysis was performed using SPSS11.0. Unpaired Student's t-test was used for the comparisons between two different groups. p values less than 0.05 were considered significant.

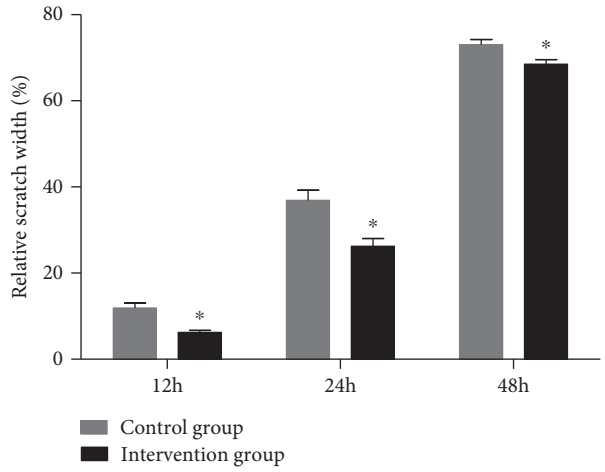

FIGURE 3: Scratch adhesion test at 12 h, 24 h, and 48 h was conducted. All experiments were triplicated. Data were presented as mean ± SD. $^*p < 0.05$, compared with the control group.

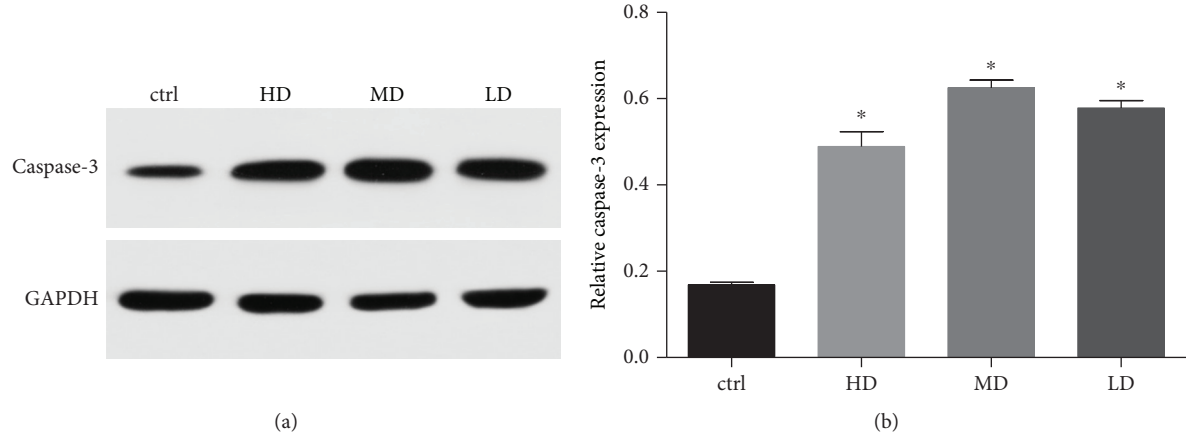

Figure 4: Western blot assay for caspase-3 protein levels of prostate cancer. (a, b) The effect of different doses of nanoyam polysaccharide on expressions of caspase-3 in mice tumor tissues. All experiments were triplicated. Data were presented as mean ± SD. $^*p < 0.05$, compared with the control group.

3. Results

3.1. Effect of Nanoyam Polysaccharide on Tumor Growth. The effect of nanoyam polysaccharide intervention on tumor growth in tumor-bearing mice was observed by detecting the volume and weight of the tumor body. Compared with the control group, different doses of nanoyam polysaccharide intervention could significantly inhibit the tumor weight of PC-3 tumor-bearing mice ($p < 0.05$), as shown in Figure 1(a). In the HD group and MD group, the tumor weight inhibition rate in the LD group was 20.60%±0.3%, 38.07%±0.4%, and 27.08%±0.1%, respectively. Compared with the negative control group, the nanoyam polysaccharide could significantly inhibit the volume of prostate cancer in tumor-bearing mice ($p < 0.05$), as shown in Figure 1(b).

3.2. Effect of Nanoyam Polysaccharide on Cell Viability. To determine the effect of nanoyam polysaccharide on apoptosis of prostatic cancer cells, Annexin V/PI staining was performed. As shown in Figures 2(a) and 2(b), apoptosis of prostatic cancer cells in the intervention group was significantly higher than that in the control group (45.8%±2.6%, 25.8%± 3.1%; $p < 0.05$). CCK-8 assay indicated that in the HD group and MD group, tumor cell activity in the LD group decreased to 81.80%±1.1%, 55.15%±1.6%, and 62.85%±0.9% of the control group, respectively, and the difference was significant ($p < 0.05$), as shown in Figure 2(d).

3.3. Effect of Nanoyam Polysaccharide on Cell Migration. Scratch adhesion test showed that the rate of wound healing in the intervention group at 12 h, 24 h, and 48 h were significantly lower than that in the control group (Figure 3, $p < 0.05$), indicating that nanoyam polysaccharide had a inhibitory effect on prostatic cancer cells.

3.4. Effect of Nanoyam Polysaccharide on Protein Levels. The expression of caspase-3 protein of prostate cancer in mice was detected by Western blotting. Compared with the control group, the expression of caspase-3 in prostate cancer tissues was downregulated in the HD group, MD group, and LD group, with statistical difference (Figure 4, $p < 0.05$).

4. Discussion

This study investigated the anticancer effect of polysaccharides of nanoyam. PC-3 cell line is one of the representative cell lines of human prostate cancer. *In vitro* study showed that the nanoyam polysaccharide presented inhibitory on the human prostate cancer cell line PC-3. Furthermore, the scratch test showed that nanoyam polysaccharide can significantly inhibit the migration of pc-3 cells. By using flow cytometry analysis, we found that the intervention of nanoyam polysaccharide could induce apoptosis of pc-3 cells. Subsequently, *in vivo* study of PC-3 tumor-bearing mice, we explored the inhibitory effect of nanoyam polysaccharide on human prostate cancer cells and its potential mechanism. Four weeks after the intervention of nanoyam polysaccharide, the weight and volume of the tumor were significantly reduced. The results of CCK-8 assay showed that the nanoyam polysaccharides had an inhibitory effect on the proliferation of prostate tumors, which was consistent with the results of *in vitro* flow cytometry analysis.

Tumor development and prognosis are closely related to apoptosis. Abnormal apoptosis is considered as one of the causes of tumor formation, and inducing apoptosis of tumor cells has become a new trend of tumor treatment over the years [11, 12]. Classic apoptotic pathways include exogenous death receptor pathways and endogenous mitochondrial cytochrome release pathways. Existing studies have shown that these two pathways are interrelated, rather than independent, and both of these pathways will eventually activate the apoptotic end-effector caspase 3 [13, 14]. In this study, the protein level of caspase-3 in tumor cells of PC-3 tumor-bearing mice was detected by Western blot. We found that the intervention of nanoyam polysaccharide could inhibit tumor development and metastasis by inducing the upregulated expression of caspase-3 protein. The cell apoptosis signal pathway of cancer cells is very complex, and the nanoyam polysaccharide contains many active components.

Therefore, the signal mechanism of nanoyam polysaccharide inducing cell apoptosis needs further exploration.

To sum up, nanoyam polysaccharides are potential therapeutic agents for prostate tumors by inducing high levels of caspase-3 protein expression and inhibiting the proliferation of prostate tumors.

Data Availability

The data used to support the findings of this study are available from the corresponding author upon request.

Conflicts of Interest

The authors declare that there are no conflicts of interest regarding the publication of this paper.

Authors' Contributions

Cheng Peng, Bo Han, Zhaohui Zhai, and Yanping Shen contributed equally to this work.

Acknowledgments

This work was supported by the Science and Technology Plan Project of Liaoning Province (Grant no. 20170540607).

References

[1] A. Jemal, F. Bray, M. M. Center, J. Ferlay, E. Ward, and D. Forman, "Global cancer statistics," *CA: A Cancer Journal for Clinicians*, vol. 61, no. 2, pp. 69–90, 2011.

[2] H. H. Cheng, D. W. Lin, and E. Y. Yu, "Advanced clinical states in prostate cancer," *The Urologic Clinics of North America*, vol. 39, no. 4, pp. 561–571, 2012.

[3] H. A. Adeola, J. M. Blackburn, T. R. Rebbeck, and L. F. Zerbini, "Emerging proteomics biomarkers and prostate cancer burden in Africa," *Oncotarget*, vol. 8, no. 23, pp. 37991–38007, 2017.

[4] C.-q. Ling, X.-q. Yue, and C. Ling, "Three advantages of using traditional Chinese medicine to prevent and treat tumor," *Journal of Integrative Medicine*, vol. 12, no. 4, pp. 331–335, 2014.

[5] X. Feng, D. Li, J. Han, X. Zhuang, and J. Ding, "Schiff base bond-linked polysaccharide–doxorubicin conjugate for upregulated cancer therapy," *Materials Science and Engineering: C*, vol. 76, pp. 1121–1128, 2017.

[6] L. Liu, M. Li, M. Yu et al., "Natural polysaccharides exhibit anti-tumor activity by targeting gut microbiota," *International Journal of Biological Macromolecules*, vol. 121, pp. 743–751, 2019.

[7] J. S. Chang, H. P. Kuo, K. L. B. Chang, and Z. L. Kong, "Apoptosis of hepatocellular carcinoma cells induced by nanoencapsulated polysaccharides extracted from *Antrodia Camphorata*," *PLoS One*, vol. 10, no. 9, article e0136782, 2015.

[8] J. Su, L. Jiang, J. Wu, Z. Liu, and Y. Wu, "Anti-tumor and anti-virus activity of polysaccharides extracted from *Sipunculus nudus* (SNP) on Hepg2.2.15," *International Journal of Biological Macromolecules*, vol. 87, pp. 597–602, 2016.

[9] W. Yang, Y. Wang, X. Li, and P. Yu, "Purification and structural characterization of Chinese yam polysaccharide and its activities," *Carbohydrate Polymers*, vol. 117, pp. 1021–1027, 2015.

[10] Y. Huang, Y. Zhao, F. Liu, and S. Liu, "Nano traditional Chinese medicine: current progresses and future challenges," *Current Drug Targets*, vol. 16, no. 13, pp. 1548–1562, 2015.

[11] K. Zhao, D. Li, W. Xu et al., "Targeted hydroxyethyl starch prodrug for inhibiting the growth and metastasis of prostate cancer," *Biomaterials*, vol. 116, pp. 82–94, 2017.

[12] M. Qiu, L. Chen, G. Tan et al., "JS-K promotes apoptosis by inducing ROS production in human prostate cancer cells," *Oncology Letters*, vol. 13, no. 3, pp. 1137–1142, 2017.

[13] Y. S. Kim, S. K. Kim, and S. J. Park, "Apoptotic effect of demethoxyfumitremorgin C from marine fungus Aspergillus fumigatus on PC3 human prostate cancer cells," *Chemico--Biological Interactions*, vol. 269, no. 269, pp. 18–24, 2017.

[14] J. C. Lee, E. A. Shin, B. Kim et al., "Auraptene induces apoptosis via myeloid cell leukemia 1-mediated activation of caspases in PC3 and DU145 prostate cancer cells," *Phytotherapy Research*, vol. 31, no. 6, pp. 891–898, 2017.

Hindawi
International Journal of Polymer Science
Volume 2019, Article ID 4597641, 10 pages
https://doi.org/10.1155/2019/4597641

Research Article

Acetylsalicylic Acid (ASA) on Hydroxyethylcellulose/Polyacrylamide Gel (HEC/PAAm) as a Proposal for a Dermatological Compress: Mathematical Modeling of ASA Release Kinetics

Claudia Alicia Castillo-Miranda,[1] Carlos Fernando Castro-Guerrero,[2] Hugo Alberto Velasco-Ocejo,[1] Jorge Alberto Gonzalez-Sanchez,[1] Gabriel Osmar Flores-Cerda,[1] Claudia Esmeralda Ramos-Galvan,[1] Jose Luis Rivera-Armenta,[1] and Ana Beatriz Morales-Cepeda[1]

[1]*Juventino Rosas y Jesús Urueta s/n, Col. Los Mangos, TecNM/Instituto Tecnológico de Ciudad Madero, C.P. 89318 Cd. Madero, Tamps, Mexico*
[2]*Departamento de Sistemas Mecánicos, Reforma 113, Col. Palmira.CONACyT–Instituto Nacional de Electricidad y Energías Limpias, Cuernavaca, Mor, C. P. 62490, Mexico*

Correspondence should be addressed to Ana Beatriz Morales-Cepeda; abmoralesc@itcm.edu.mx

Received 12 September 2018; Accepted 1 November 2018; Published 20 January 2019

Guest Editor: Mingqiang Li

Currently, acne in adolescents and adults is caused by an infection in follicles caused by hormonal changes, stress, water pollution, air, and earth; the last one comes into contact with the skin through the hands of patients. This project presents the incorporation of acetylsalicylic acid (ASA) to the hydroxyethylcellulose/polyacrylamide gel (HEC/PAAm) in the synthesis of gel or by its swelling. The results show us that the incorporation of ASA is possible by both methods; first, the incorporation by synthesis of degradation of the gel is more visible. The infrared spectroscopic analysis shows the functional groups of gel and ASA, 2921 and 2863 cm^{-1}, whose assignments correspond to CH_3 and CH_2 groups, which are part of both the polymer and the ASA molecule, which confirms the interaction between the two groups. The microscopy photographs (SEM) show on the surface the drug in irregular whitish orthorhombic forms due to swelling; arborescent structures are observed in the case of the incorporation of the ASA drug by synthesis. Swelling kinetics has a Fickian form. The Higuchi model conforms to the release of ASA because the level of confidence is 90%. This gel was allowed to release 0.35 mg/hour, thus allowing the patient to have a continuous form of the release, in the affected area in a short period of time.

1. Introduction

Acne is an inflammation of the follicles, due to the obstruction of sebaceous glands and hormonal changes (in adolescence or in adulthood); a statistic published in the year 2017 shows that 9.4% of the world population suffers from acne [1]. Depending on the degree of progress of acne, it goes from a teenage acne, rosacea, hormonal, with nodules, with cysts, severe. These types of acne cause psychological problems resulting in social segregation in adolescents and adults, this is because their possibilities of professional, work and personal growth (search for a partner, friendships) are affected, causing depression and low self-esteem [2].

Treatments to control or diminish acne go from washing the face and/or affected zones (back, chin, and neck), hand-washing, avoiding sun exposure, and applying ointments and astringent lotions, with benzoyl peroxide, acetylsalicylic acid, and antibiotics such as erythromycin and in severe cases isotretinoin; if it is hormonal-type acne, it should be treated with appropriate hormonal medications.

On the other hand, the release of drugs used in the last decades in body temperature control, contraceptive patches, the version of medications for the control of muscle pain, cancer, bones, as a palliative. These patches are based on gels where the drug is deposited for controlled release or for stimuli such as changes in body temperature or change of pH if ingested.

In general, hydrogels that present a critical temperature of higher miscibility (UCST (upper critical solution temperature)) expand as temperature increases, while those with an LCST contract. The LCST of a polymer can be varied by copolymerizing it with monomers with different degrees of hydrophilicity [3]. Hydrogels sensitive to temperature changes are characterized by having a critical temperature of lower miscibility (LCST (lower critical solution temperature)) of the polymer or copolymer in aqueous solution.

In essence, certain polymers with an appropriate cross-linking composition and density can swell greatly in water at room temperature and collapse to the LCST. Acetylsalicylic acid or ASA is a nonsteroidal anti-inflammatory drug (NSAID) of the family of salicylates, frequently used as an anti-inflammatory, analgesic for the relief of mild and moderate pain, and antipyretic for the reduction of fever and as an antiplatelet drug indicated for people at high risk of blood coagulation, mainly individuals who have already had an acute myocardial infarction. The adverse effects of aspirin are mainly gastrointestinal, that is, gastric ulcers and stomach bleeding, mainly when administered orally.

The incorporation of nonsteroidal drugs in gels for prolonged release is one of the options for patients with gastrointestinal problems. The incorporation of drugs such as ibuprofen on hydroxyethylcellulose gels has been studied as an option [4] where the capacity of HEC as a biodegradable and biocompatible gel was investigated, incorporating the drug by swelling, achieving the incorporation of 5 wt% of the drug.

Kalagasidis Krušić et al. [5] prepared copolymer hydrogels of N-isopropylacrylamide acid (PNIPAM) and itaconic acid (IA), crisscrossed with MBAAm by radical copolymerization, and investigated the composition ratios to find materials with good swelling and drug release properties. Paracetamol was used as a model drug, incorporating it by swelling in xerogels in aqueous solution of drug (10 mg/mL) at room temperature for 2 days. It was found that the swelling behavior of the investigated hydrogels depends on pH and temperature with limited swelling and the lowest degree of swelling is at lower pH values and temperatures above the LCST value of PNIPAM (around 34°C). The presence of "IA" incorporated into the network weakened the shear strength of the hydrogels. The pore size was calculated for the different PNIPAM/IA compositions, which range from 0.019 to 0.041 μm, which is why they are considered as microporous. On the other hand, paracetamol was released after 6 hours at pH 2.2 and after 2 hours at pH 6.8. In all the experiments, the drug was released in the first five hours. The values of the diffusion exponent indicated a release kinetics of Fickian paracetamol. According to the results obtained, the swelling behavior, mechanical properties, drug loading capacity, and drug release rate can be controlled by the hydrogel cross-linking composition and density, which is important for the application of hydrogels investigated as drug release systems.

In MojtabaTaghizadeh and Javan [6], a nanoparticulate, biocompatible, and biodegradable drug release system was prepared to increase the efficiency and bioavailability of oral drugs. They prepared, by the emulsion method, nanoparticles of chitosan containing salicylic acid. The morphology of the nanoparticles was characterized by SEM, and the particle size distribution was examined by laser light scattering. The release of the drug and the content was examined by UV spectroscopy using phosphate buffer at pH 7.4 and at 37°C. The effects of the different initial loads of the drug on the content and its release were investigated. The nanoparticles were spherical and their average size was 300 nm, and the content of the drug was in the range 20-35%. All nanoparticles have an initial release and a release behavior that better fits the Higuchi model. The release of salicylic acid from the chitosan nanoparticles was Fickian.

The synthesis of HEC/PAAm has been previously studied by Alonso et al. [7], by means of free radicals using potassium persulfate (KPS), demonstrating the dependence of pH and temperature on the swelling of gels. The gels showed a maximum swelling of 1200 wt%, at a temperature of 30°C, decreasing when the temperature and amount of HEC in the gel matrix increased.

Acetylsalicylic acid in gels is potentially accepted in the pharmaceutical industry in the treatment of dermatological problems, such as acne in adolescents and/or adults, and the exposure of acetylsalicylic acid in soaps, ointments, lotions, exfoliants, and emulsions, where they incorporated from 1 to 40 wt% of ASA, in cellulose gel with the help of isopropyl alcohol [8].

Castillo-Miranda et al. [9] investigated the mathematical model of Higuchi in the release of ibuprofen on the HPC/PAAm gel, in two solutions in the buffer and in saline, finding that this release is possible to predict at an average temperature between 36 and 39°C. In addition, it was found that ibuprofen crystallizes on the surface, due to the method of incorporation of the drug by swelling.

In the present investigation, we present the simulation of three mathematical models for the kinetics of drug release and nonsteroids such as acetylsalicylic acid (ASA), on the hydroxyethylcellulose/polyacrylamide gel (HEC/PAAm). Research was done to find the best way to investigate the incorporation of ASA into the proposed gel, and this was analyzed by infrared spectroscopy, X-ray, DSC, and DMA, to ensure that ASA does not degrade and is found in the gel.

2. Methodology

2-Hydroxyethyl cellulose (HEC) was obtained from Sigma-Aldrich, the viscosity (in water at 2% weight) of which is 4500 to 6500 cP. Its degree of substitution is 1.5, and the degree of molar substitution is 2.5. Other chemicals used in this study were as follows: acrylamide (AAm), 2-propenamide (C_3H_5NO, Sigma-Aldrich brand with 97% purity), ammonium persulfate (APS), $(NH_4)_2S_2O_8$ (the initiator of the polymerization of acrylates via free radicals, Sigma-Aldrich brand

with 98% purity), methylenebisacrylamide (MBAm), N,N′,-methylenebis(2-propenamide), $C_7H_{10}O_2N_2$ (cross-linker for polyacrylamide, Sigma-Aldrich brand with a purity of 99%), N,N,N′,N′,-tetramethylethylenediamine (TEMED), 1,2-di(dimethylamino)ethane, $C_6H_{16}N_2$ (co-catalyst for the formation of free radicals of APS, Sigma-Aldrich brand with 99% purity), and sodium hydroxide (NaOH; used at 1.0 M in deionized water to regulate the reaction at pH 12; Sigma-Aldrich brand with a minimum purity of 97%).

The buffer solution was a phosphate solution, pH 7.384 ± 0.003 at 37°C, and was obtained by HYCEL brand. The acetylsalicylic acid ($C_9H_8O_4$) was obtained by Sigma brand, 99% purity.

2.1. Synthesis of Gel Ratio 25/75 wt% [10]. The reaction was carried out in a four-neck flask with a temperature control medium at 40°C ± 1°C and an inert atmosphere with nitrogen. The solution consisted of 95% deionized water and 5% reagents in the desired amount to work. For the 50/50 ratio, 27.5 mL of deionized water was added, swept with nitrogen, and 1.875 g of AAm was added, which is in constant agitation while the temperature was increased to 40°C. In a vial with 10 mL of deionized water, 0.0375 g of APS was dissolved together with 0.0019 g of MBAm, and in another vial with the same amount of water, 0.0375 g of TEMED was dissolved. When the temperature was 40°C, HEC was added to the reactor, the first vial was immediately injected, and then the second vial with TEMED and then 0.19 mL of DVS was injected, all in an inert atmosphere. At the end, about 1 mL of 1.0 M NaOH was added and the pH of the solution was checked, which was 12. The reaction lasted 30 minutes; once the reaction was finished, it was allowed to dry at 40°C in an oven in a vacuum for a week. Once the film was dry, the gel was rinsed with deionized water and dried.

Standard solutions of the drug containing 5 mg/mL were prepared in the solvent (phosphate buffer, ethanol-water 50 vol%).

The synthesis of the gels was reported by Castro-Guerrero, where the amount of HEC, PAAm, and cross-linker was observed, observing that at a high level of divinyl sulfone (DVS, cross-linking), the network is more cross-linked and rigid, having agglomerates of particles of the smallest gels. Castro varied the amount of the cross-linker based on 0.18 g of DVS/g of polymer [11]; however, this is different from the effect of the pH in the network, and the alkaline pH catalyzes the cross-linking between the DVS and the cellulose derivative, which increases the percentage of swelling by preventing the gel from being diluted. This is based on the synthesis proposed by Castro (thesis), and as a cross-linker base of 0.18 g of DVS/g of the polymer.

2.2. Incorporation of Drugs by Swelling. The incorporation of the drug to the gels was according to what was reported by Kenawy et al. [12]; once the drug solutions were prepared, pieces of xerogels were cut and weighed, and their thickness was measured. The gels were immersed in a solution with the drug for 48 hours at room temperature; at the end of this time, the gels were removed, and the excess solution was removed and weighed. Subsequently, they were frozen at −10°C for 48 hours, then allowed to stand at room temperature until constant weight [13].

With the maximum amount of solution absorbed by the gel, the amount of drug theoretically absorbed is calculated. According to Makino et al. [14], the amount of drug inside the gel is equal to the solution incorporated in the drug.

2.3. Incorporation of the Drug by Synthesis. The drug acetylsalicylic acid (ASA) was added to 5% by weight relative to the reagents [15]; in the synthesis of the gels of HEC/PAAm previously described, ASA is added before the cross-linker.

2.4. Infrared Spectroscopy. For the qualitative identification of the functional groups of HEC/PAAM films, a Perkin-Elmer Fourier transform spectrometer model Spectrum One was used with the ATR accessory, with a frequency range of 4000-600 cm^{-1}.

2.5. Particle Size. A Tepper model TP1 spectrophotometer was used, with incident light at a wavelength of 670 nm for heating and 540 nm for cooling, the temperature range was 30 to 80°C, and for high concentrations of 5 at 95°C, the measurement speed was 10°C/min.

2.5.1. Analysis of Particle Size. This analysis was made using the PL-PSDA particle size distribution analyzer equipment from Polymer Laboratories with a series of quasi-monodisperse polystyrene latexes manufactured by Duke Scientific as calibration standards. A type I cartridge, with an operational range of 5 to 300 nm, was selected, and the effluent flow was 2 mL/min. Solutions containing 20 mg of sample in 20 mL of solvent were filtered through a Whatman filter of 2 μm before analysis, and the injection volume was 20 μL.

2.6. Differential Scanning Calorimetry (DSC). For this analysis, a PerkinElmer Pyris 1 differential scanning calorimeter was used, with a sample amount of 5 to 10 mg deposited in aluminum capsules, and a heating ramp of 10°C/min was used in a range of 25°C up to 200°C using a flow of nitrogen.

2.7. Mechanical Dynamic Analysis. The DMA analysis was made in a DMA equipment brand TA Instruments model 2980, in the multifrequency mode using a 35 mm long film tension-type clamp. The heating ramp was 5°C/min using a frequency of 1 Hz in a temperature range of 0 to 250°C.

2.8. SEM. The equipment used was a scanning electron microscope JEOL model JSM 6390LV; it was not necessary to modify with Au the surface of the samples since it was worked under low vacuum. This technique will be useful to observe the surface of the films and the incorporation of the drugs in them.

2.9. Atomic Force Microscopy (AFM). A Veeco di CP-II brand atomic force microscope with software Vr 5.01 was used. The analysis was done without cryo-fracture in non-contact tapping mode. The type of cantilever was rotated from monolithic silicone with a gold coating of 70 nm at a resonance frequency of 145-230 kHz.

2.10. Kinetics. The ultraviolet light spectrometer (Perkin Elmer model Lambda 10) was used for the calibration curves for the drug in ethanol-water and in buffer solution. With the data of the absorbances as a function of time, the release profiles (drug concentration released as a function of time) will be obtained, and the percentages of drug released from the gels will be calculated. In addition, the nature of the diffusion of the ASA drug in the HEC/PAAm gels will be determined to indicate which model is suitable. Among the most used mathematical models to analyze and describe the mechanism by which the liberation process occurs are those proposed by Higuchi in 1963 and Korsmeyer and Peppas in 1983 [16, 17].

Higuchi proposed a mathematical model used to describe the empirical drug release process, which complies with Fick's Law and is represented as follows:

$$\frac{M_t}{M_\infty} = K \cdot t^{1/2}, \quad (1)$$

where M_t/M_∞ is the fraction of drug released at time t and k is the release rate constant. On the other hand, Korsmeyer and Peppas proposed a mathematical model that is generally linear for values of $M_t/M_\infty < 0.6$. This model attempts to explain mechanisms of drug release where erosion and/or dissolution of the matrix occurs and is no more than a generalized form of the Higuchi equation that is expressed as:

$$\frac{M_t}{M_\infty} = K \cdot t^n, \quad (2)$$

where k is the release constant of the release system that incorporates structural and graphic factors of the drug release and release system.

The value of the exponent n provides information about the kinetics of drug release, so if n is equal to 0.5, the release of the drug takes place through a diffusion phenomenon of the Fickian type (mathematical model of Higuchi); if it does not take the values between 0.5 and 1, it indicates that the release of the drug is due to a non-Fickian or abnormal diffusion mechanism, and when it is equal to 1, the mechanism of drug release depends on the release process of the polymer chains [18]. To study the release of ASA from these polymer matrices, we proceeded with Equation (2). Matlab software 2016 was used to simulate the kinetic release.

3. Results

3.1. Infrared Spectroscopy. Figure 1 shows the spectrums for the HEC/PAAm gel and the gels with ASA incorporated by swelling and on the synthesis. The spectrum of HEC/-PAAm gel shows the corresponding peak stretches NH and OH to 3346 and 3186 cm^{-1}, respectively; the symmetrical and asymmetric stretches of CH_2 of the cellulose are located at 2921 and 2863 cm^{-1}, that of the stretching of the carbonyl group from PAAm is at 1672 cm^{-1}, that of the CN stretch of the polyacrylamide is seen at 1283 cm^{-1}, and finally that of the C-O-C stretch of HEC is located at 1088 cm^{-1}.

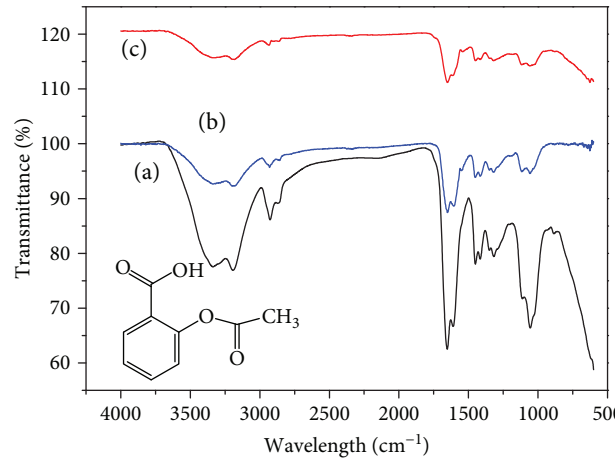

Figure 1: Infrared spectrum of (a) HEC/PAAm xerogel, (b) HEC/PAAm xerogel with ASA incorporated by swelling, and (c) HEC/PAAm xerogel with ASA incorporated on synthesis.

Bands belonging to the ASA drug are also observed: one of them coincides with that of the gel of OH at 3346 cm^{-1}, that of the asymmetric stretch C=O of the ester at 1754 cm^{-1}, a peak attributable to the C=O stretching of acid carboxyl at 1672 cm^{-1}, symmetric stretching for the acetoxy group at 1454, and symmetric stretching for the carboxyl group at 1411 cm^{-1}. The bands are located at 2921 and 2863 cm^{-1}, whose assignments correspond to the CH_3 and CH_2 groups that are part of both the polymer and the ASA molecule, thereby confirming the interaction between them. These results are similar to those reported by Nita [19] and Yang and Wang [20].

The IR spectrum of the HEC/PAAm sample with ASA incorporated on synthesis. In the same way as in the previous case, the functional groups of the gel is identified, as well as the main assignments of the drug; the vibration of OH at 3257 cm^{-1}, the asymmetric stretch C=O of the ester at 1676 cm^{-1}, and the stretch C=O of the carboxylic acid are not appreciated, perhaps because they moved to the right and are overlapped with the band of the carbonyl group of the gel. The peak of the symmetric stretch for the acetoxy group is located at 1454 cm^{-1}, and the symmetric stretch for the carboxyl group is at 1418 cm^{-1}.

3.2. Mechanical Dynamic Analysis (DMA). Figure 2 corresponds to the tan delta curved thermogram and the curved thermogram of the HEC/PAAm film storage module. In the curve tan delta against temperature, the secondary relaxations of the material between 50 and 75°C are observed, which are attributed to chain movements, rearrangements, or relaxations of an amorphous region; like the previous samples, there is a very pronounced peak that corresponds to T_g at 185° C.

Figure 3 shows the thermogram of the HEC/PAAm gel with ASA incorporated in synthesis; a transition that is attributed to T_g is identified around 115.3°C and then a peak at 117°C due to the active principle. It has been shown that the thermograms of the hydrogels with ASA do not coincide with those of the active principle nor with that of hydrogel

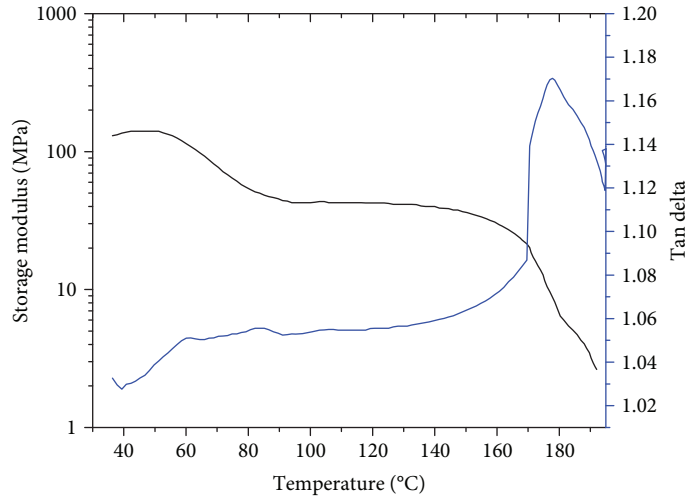

Figure 2: DMA from the xerogel HEC/PAAm.

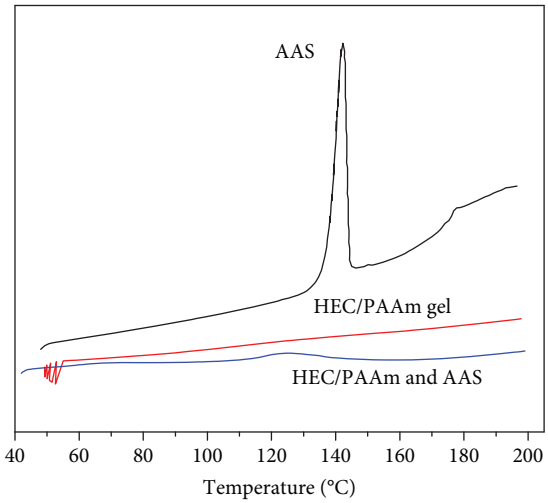

Figure 3: DSC-thermogram from the xerogel HEC/PAAm, ASA and HEC/PAAm and ASA.

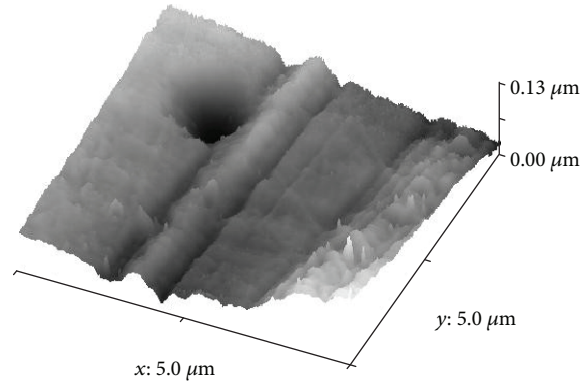

Figure 4: Atomic force micrograph of the HEC/PAAm xerogel.

alone. Therefore, we can say that a drug-polymer interaction occurs, which is an indication that the drug is inside the polymer matrix. This is consistent with that reported by Rodríguez-Llimos et al. [21].

3.3. Analysis of the Surface of the Gels. Figure 4 shows the atomic force micrograph of the HEC/PAAm xerogel; like the SEM photographs in AFM micrographs, the surface is a little warped and has some micelles on the surface that measure 0.05 to 0.1 μm. The micrograph shows a hole in the surface; the wrinkling of the surface is due to the shrinkage of the samples during drying, which is similar to what has been observed in other works, where the differences in the drying process lead to different types of pores and "wrinkles" on the surface of HEC gels. Pore sizes between 13 microns were found, similar to those obtained by Petrov et al., which reported between 20 and 200 microns in pore size, and the corrugated walls are approximately 0.25 microns [22, 23].

The surface morphology of HEC/PAAm xerogels is at 100x (Figure 5(a)). The xerogels show a uniform, smooth, homogeneous surface. In most of the film, crater-like reliefs are also observed after doing the washings and letting the film dry again; this type of behavior was observed when drying the gels of HEC either by a conventional method or by cryogenic HEC, which tends to form undulations as observed by Petrov et al. [22, 23]. The incorporation of ASA in HEC/PAAm xerogels by swelling is shown in Figure 5(b), where the morphology surface clearly shows the formation of irregular orthorhombic white crystals, from 4 to 10 μm long of the drug distributed on the surface of the film, which in turn has a homogeneous morphology with certain parts more pronounced as waves. The shade of the crystals is more transparent and opaque.

The HEC/PAAm xerogel with ASA incorporated in synthesis (5c); in the images, a homogeneous, smooth surface like the one that corresponds to the gel without the drug is seen in the background. In relief, the agglomeration of white particles is observed and in others the accumulation of particles in the form of arborescent branches; the shape of these structures had not been appreciated in the films with drug incorporated by swelling, so they are attributed to the way in which the

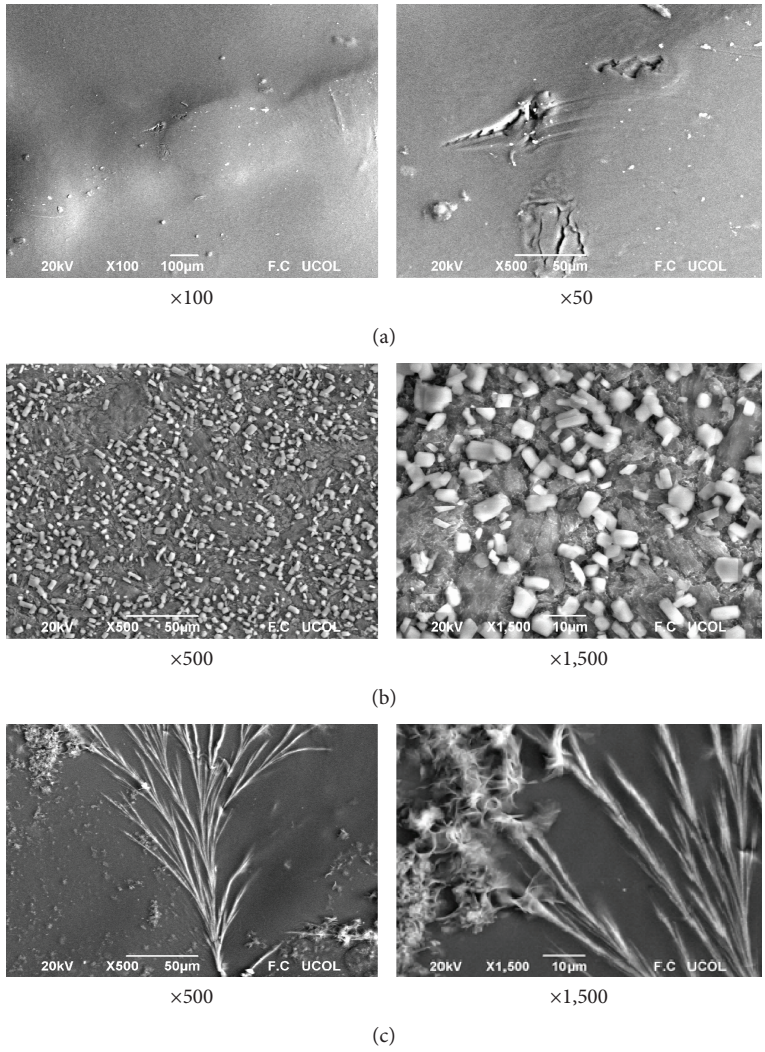

Figure 5: Micrographs with magnifications, the samples are (a) xerogel of HEC/PAAm without drug, (b) xerogel of HEC/PAAm with drug ASA incorporated by swelling, and (c) xerogel of HEC/PAAm with drug ASA incorporated in the synthesis.

incorporation of the drug was made, to all the conditions since it was in contact with reagents during the synthesis.

3.3.1. X-Rays. In Figure 6, the "X"-rays of xerogels with incorporated ASA are shown, either by swelling or by synthesis. Pure acetylsalicylic acid has definite peaks in the X-ray patterns, where the crystal size is 54 nm calculated with the Debye-Scherrer equation [24]. In the case of xerogels, the xerogels of HEC/PAAm, a broad peak ranging from 15 to 40° is completely amorphous. It is known that the growth of the crystals depends on the solvent, temperature, and pressure [25], and there is some confusion in the sizes of the crystals or the indexation. In the case of the gels, where ASA was incorporated by swelling, there is an increase in the height of the peak, compared to the xerogel with the ASA incorporated by synthesis.

3.3.2. Drug Release. Below the UCST and above the LCST, the polymer was insoluble in water and the solution was physically cloudy and whitish. Above the UCST and below the LCST, the polymer was soluble in water and the solution was clear, forming then a small "window of solubility"

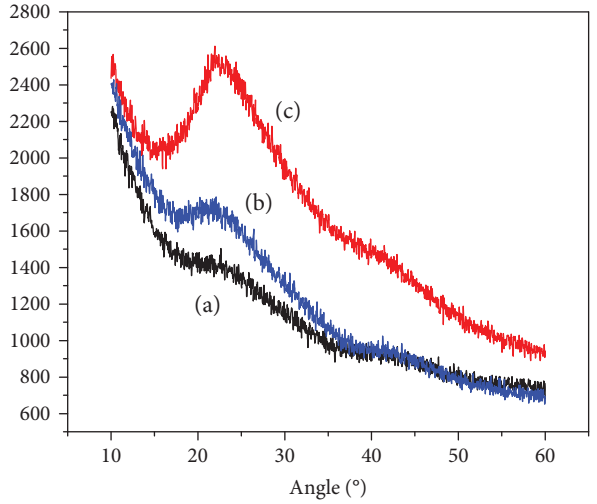

Figure 6: X-rays of HEC/PAAm xerogel (a) and HEC/PAAm xerogel with ASA incorporated by synthesis (b) and by swelling (c).

[26]; these phenomena are associated with the functional groups of the polymer-solvent system, the entropy change, and the solvent-polymer interaction parameter [26–28]. The LCST is attributed to the change in the dipole moment of the molecule by increasing the temperature of the polymer. The UCST temperature is attributed to the decrease in the entropy of the system that occurs when the solution is cooled. It should be remembered that for a polymer to dissolve in a solvent, the functional groups of both must be similar and the entropy must increase [29]. The HEC/PAAm gel has an LCST of 41°C, which indicates that below this temperature the release of the drug will be presented; this temperature and a particle size between 124 and 167 microns were determined by turbidimetry. These values are between normal for cellulose derivatives such as hydroxypropyl cellulose/PAAM as reported by Castro et al..

Figures 7 and 8 show the release of ASA from HEC/PAAm hydrogels at three temperatures in buffer solution and ethanol-water, respectively. In both graphs, it is observed that around 120 minutes the release is done more quickly and then more slowly until a maximum concentration is obtained around 480 minutes. The release of ASA is constant from the first hour, releasing 0.3 mg/hr·m. The simulation was done in Matlab.

The results obtained from the release in buffer (Figure 7) are also consistent with the relationship between the released concentration and the temperature as reported in bibliographic sources since the lowest concentration was at 37°C with 0.1657 mg/mL and the highest at 39°C with 0.3144 mg/mL. In regard to ethanol-water release data (Figure 8) for the same type of gel, it can be seen that as the temperature increases, the concentrations of drug released tend to decrease. On the other hand, it is observed that the HEC/PAAm gel at 35°C in ethanol-water released more amount of ASA (0.3941 mg/mL).

With the results obtained from the drug releases made in the two types of films and using the different solvents, the kinetic study was performed using the mathematical model represented in Equation 2.3, proposed by Higuchi in 1963 and Korsmeyer and Peppas in 1983, where M_t/M_∞ represents the fraction of drug released, k is a constant of proportionality, and n is the mode of transport of the drug [30]. To know if the mechanism of drug release is of Fickian or anomalous type, the mode of transport n should be calculated. Where n has a value of 0.5, the release of the drug follows the Fickian diffusion mechanism; if n is different from 0.5, the diffusion mechanism is considered non-Fickian or anomalous, and when n is equal to 1, it is considered to follow the Schott diffusion mechanism [31, 32].

Table 1 shows the values of n obtained for the release of ASA from the hydrogels in the xerogel state both incorporated by swelling and in the synthesis and in both solvents used, at three temperatures. Unfortunately, the results of the kinetics of ASA are very irregular, and the values of n are less than 0.5, so they do not correspond to any of the intervals described by Katime (2004), which indicates the existence of several simultaneous processes to the phenomenon of dissemination of ASA. These results are consistent with those reported by Aragón et al. [33].

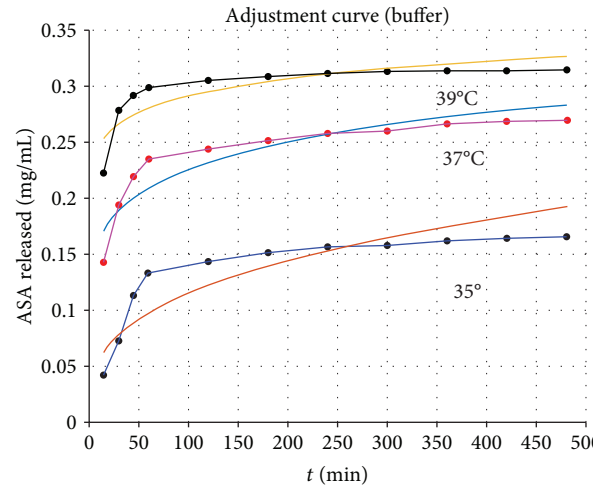

Figure 7: Adjustment curve for ASA released with buffer solution experimental data using Matlab.

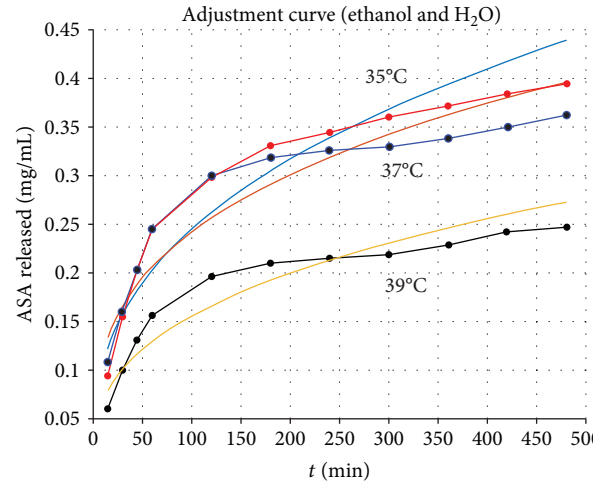

Figure 8: Adjustment curve for ASA released with ethanol-water solution experimental data using Matlab.

The adjustment of the experimental data was made using the Higuchi model, using the Matlab software version 2016, (Supplementary Materials (available here), which the program used). For the two solutions of ethanol-water and buffer for the temperatures of 35, 37, and 39°C, it is observed that as one for each temperature, in the case of buffer solution the curves were better adjusted to the data, while in regard to ethanol water solution no adjustment to the data is observed.

On the other hand, we have ANOVA for the data as shown in Table 2, in the two solutions with the temperatures of 35, 37, and 39°C. The error calculated for the simulated data and with the Matlab software has a greater error in the first-order model, three decimal places in a range 0.0042-0.0084, and for the Higuchi model error of eleven decimal places in a range of $9.169E-11$ to $6.52E-11$.

The R^2 confidence level for the first-order model of 0.442-0.790 or below 80% for both solvents indicates that it is

Table 1: Values of n calculated for the kinetics of ASA release from xerogels.

Hydrogel	Method of incorporation	Solvent of release	35 C		37°C		39°C	
			n	k	n	k	n	k
HEC/PAAm	Swelling	Buffer	0.1485	0.4353	0.3249	0.1558	0.0733	0.6594
HEC/PAAm	Swelling	E_A	0.3701	0.113	0.3131	0.1582	0.3576	0.1218

Table 2: ANOVA data from the "first-order" equation and Higuchi model simulation.

Solvent	Temperature (°C)	First order			Higuchi model data		
		Error	R^2	F^0	Error	R^2	F^0
Buffer	35	0.0044	0.432	$8.4101E-06$	$6.6615E^{-11}$	0.902	$8.41005E-06$
Buffer	37	0.0059	0.581	$1.2142E-06$	$7.5046E^{-11}$	0.941	$1.21422E-06$
Buffer	39	0.0042	0.442	$1.6866E-05$	$9.1696E^{-11}$	0.882	$1.68663E-05$
Ethanol-water	35	0.0084	0.790	$3.887E-07$	$6.8622E^{-11}$	0.949	$6.7894E-07$
Ethanol-water	37	0.0080	0.734	$9.1803E-07$	$7.5030E^{-11}$	0.939	$1.40442E-06$
Ethanol-water	39	0.0057	0.442	$4.7177E-07$	$6.5236E^{-11}$	0.947	$8.01275E-07$

not the "first order," while for the Higuchi model the value of R^2 is in the range of 0.882-0.947 or, in other words, above 90% for both solutions, which indicates that the release of ASA is done by this model. Another important value to measure is that F^0 is not statistically significant for the "first order" for both solvents and at all temperatures; contrary to this, the Higuchi model suggests that it is statistically significant.

The controlled release of ASA is 0.35 mg/hour, which is enough for the application of a dermatological compress to control or eliminate acne. At the beginning of the dermatological infection, the temperature rises and becomes red, with a temperature up to 39°C, where a greater amount of ASA will be released; later, the skin will lower the temperature due to the action of the drug, which will mean that less amount of drug is needed, to ensure that the amount of this drug is slow to avoid a possible allergy to the drug.

The active release of the drug is possible on the skin due to the biomacromolecules present in the skin, due to temperature, pH, stimulation, etc. This release of the drug is active due to the diffusion of ASA contained in the drug matrix towards the epidermis of the skin (Figure 9). It is expected to prove with primary bioessays to conclude the work in a next investigation.

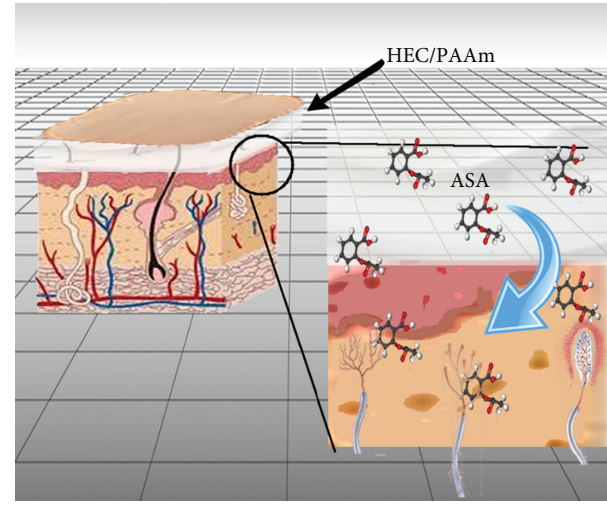

Figure 9: Schematic representation of ASA of the hydrogel entering the dermis.

4. Conclusions

The incorporation of ASA in the HEC/PAAm gels was possible by means of swelling, without modifying the drug in the incorporation. On the other hand, in the incorporation of ASA in the synthesis of the HEC/PAAm gel, the drug is in smaller quantity; in SEM microscopy, it is observed that ASA tends to form arborecencias and not form defined crystals, together with the appearance of the gel which changed the color yellow.

The spectrum of FTIR has the characteristic bands of the drug ASA, 2921 and 2863 cm^{-1}, whose assignments correspond to the CH_3 and CH_2 groups that are part of both the polymer and the ASA molecule. The DSC showed that the drug is present in the gel at 115°C; in the DMA, it is shown that the HEC/PAAm gel has chain movement. The drug release is carried out according to the "Higuchi" model, in ethanol-water and buffer solutions, and it is simulated; the ANOVA of the data informs us that it has a confidence level of 90%. In the application of this drug in a dermatological pad for the control or elimination of acne, at the beginning this has redness and a temperature rise, taking that at 39, 37, and 35°C the release at a higher temperature is constant with time.

Data Availability

The simulation data used to support the findings of this study are included within the supplementary information file.

Conflicts of Interest

The authors declared no potential conflicts of interest with respect to the research, authorship, and/or publication of this article.

Funding

This research was supported financially by Tecnologico Nacional de Mexico/Instituto Tecnologico de Ciudad Madero.

Supplementary Materials

Simulation in Matlab to obtain the adjustment curve, error, and coefficients of the experimental data from the ASA released in solution ethanol water and buffer. *(Supplementary Materials)*

References

[1] J. K. L. Tan and K. Bhate, "A global perspective on the epidemiology of acne," *British Journal of Dermatology*, vol. 172, pp. 3–12, 2015.

[2] D. H. Suh and H. H. Kwon, "What's new in the physiopathology of acne?," *British Journal of Dermatology*, vol. 172, pp. 13–19, 2015.

[3] I. A. Katime, O. K. Trabanca, and D. K. Trabanca, "Materiales inteligentes: hidrogeles macromoleculares; algunas aplicaciones biomédicas," *Anales de la Real Sociedad Española de Química*, no. 4, pp. 35–50, 2005.

[4] N. Sun, T. Wang, and X. Yan, "Synthesis and investigation of a self-assembled hydrogel based on hydroxyethyl cellulose and its in vitro ibuprofen drug release characteristics," *RSC Advances*, vol. 7, no. 16, pp. 9500–9511, 2017.

[5] M. Kalagasidis Krušić, M. Ilić, and J. Filipović, "Swelling behaviour and paracetamol release from poly(N-isopropylacrylamide-itaconic acid) hydrogels," *Polymer Bulletin*, vol. 63, no. 2, pp. 197–211, 2009.

[6] S. MojtabaTaghizadeh and R. S. Javan, "Preparation and investigation of chitosan nanoparticles including salicylic acid as a model for an oral drug delivery system," *e-Polymers*, vol. 10, no. 1, 2013.

[7] G. J. Alonso, J. L. A. Rivera, A. M. M. Mendoza, and M. L. H. Mendez, "Effect of temperature and pH on swelling behavior of hydroxyethyl cellullose-acrylamide hydrogel," *e-Polymers*, vol. 7, no. 1, 2013.

[8] C. Gerlach, Buford, M. Davies, and Dacula, "Patent Issued for Salicylic Acid Gel Health & Medicine Week," US Patent 2014/0323445 A1.

[9] C. A. Castillo-Miranda, A. Beatriz Morales-Cepeda, C. F. Castro-Guerrero et al., "Deposition of ibuprofen crystals on hydroxypropyl cellulose/polyacrylamide gel: experimental and mathematic modeling releasing," *International Journal of Polymer Science*, vol. 2016, Article ID 2634104, 8 pages, 2016.

[10] C. F. Castro-Gurrero, *Síntesis y caracterización de nanogeles y microgeles a partir de derivados de celulosa y poli(acrilatos), Tesis de Doctorado en Ciencias en Ingeniería Química*, Instituto Tecnológico de Cd. Madero, 2009.

[11] J. A. Hinkley and S. H. Gehrke, "Tensile properties of a cellulose ether hydrogel," NASA Langley Technical Reports Server, NASA/TM-2003-212417, 2003.

[12] E. R. Kenawy, D. C. Sherrington, and A. Akelah, "Controlled release of agrochemical molecules chemically bound to polymers," *European Polymer Journal*, vol. 28, no. 8, pp. 841–862, 1992.

[13] M. V. Risbud, A. A. Hardikar, S. V. Bhat, and R. R. Bhonde, "pH-sensitive freeze-dried chitosan-polyvinyl pyrrolidone hydrogels as controlled release system for antibiotic delivery," *Journal of Controlled Release*, vol. 68, no. 1, pp. 23–30, 2000.

[14] K. Makino, J. Hiyoshi, and H. Ohshima, "Effects of thermosensitivity of poly (N-isopropylacrylamide) hydrogel upon the duration of a lag phase at the beginning of drug release from the hydrogel," *Colloids and Surfaces B: Biointerfaces*, vol. 20, no. 4, pp. 341–346, 2001.

[15] Y. Luo, K. R. Kirker, and G. D. Prestwich, "Cross-linked hyaluronic acid hydrogel films: new biomaterials for drug delivery," *Journal of Controlled Release*, vol. 69, no. 1, pp. 169–184, 2000.

[16] T. Higuchi, *Journal of Pharmaceutical Sciences*, vol. 52, no. 12, pp. 1145–1149, 1963.

[17] R. Korsmeyer and N. Peppas, "Macromolecular and modeling aspects of swelling-controlled systems," in *Controlled Release Delivery Systems*, T. J. Roseman and S. Z. Mansdorf, Eds., pp. 77–90, Elsevier, New York, N.Y., USA, 1983.

[18] A. I. Katime, T. O. Katime, and D. Katime Trabanca, *Los materiales inteligentes de este milenio: Los hidrogeles macromoleculares: Síntesis, propiedades y aplicaciones*, Servicio editorial de la Universidad del País Vasco, 2004.

[19] T. Nita, "Synthesis of antimicrobial polymer composition and in vitro drugs release study," *e-Polymers*, vol. 8, no. 1, 2013.

[20] L. Yang and T. Wang, "Preparation of cellulosic drug-loaded hydrogel beads through electrostatic and host-guest interactions," *Journal of Applied Polymer Science*, vol. 135, no. 31, 2018.

[21] A. C. Rodríguez-Llimos, D. Chiappetta, M. E. Széliga, A. Fernández, and C. Bregni, "Micropartículas de alginato conteniendo paracetamol," *Ars Pharmaceutica*, vol. 44, no. 4, pp. 333–342, 2003.

[22] P. Petrov, E. Petrova, B. Tchorbanov, and C. B. Tsvetanov, "Synthesis of biodegradable hydroxyethylcellulose cryogels by UV irradiation," *Polymer*, vol. 48, no. 17, pp. 4943–4949, 2007.

[23] P. Petrov, E. Petrova, R. Stamenova, C. B. Tsvetanov, and G. Riess, "Cryogels of cellulose derivatives prepared via UV irradiation of moderately frozen systems," *Polymer*, vol. 47, pp. 6481–6484, 2006.

[24] C. Muthuselvi, M. Dhavachitra, and S. Pandiarajan, "Growth and characterization of aspirin crystal in the phosphoric acid medium," *Journal of Chemical and Pharmaceutical Research*, vol. 8, no. 5, pp. 804–814, 2016.

[25] C. Aubrey-Medendorp, S. Parkin, and T. Li, "The confusion of indexing aspirin crystals," *Journal of Pharmaceutical Sciences*, vol. 97, no. 4, pp. 1361–1367, 2008.

[26] P. J. Flory, *Principles of Polymer Chemistry, Ed*, Cornell University Press, Ithaca, N. Y, USA, 1953.

[27] D. Patterson, "Free volume and polymer solubility. a qualitative view," *Macromolecules*, vol. 2, no. 6, pp. 672–677, 1969.

[28] P. J. Flory and W. J. Leonard Jr, "Thermodynamic properties of solutions of helical polypeptides," *Journal of the American Chemical Society*, vol. 87, no. 10, pp. 2102–2108, 1965.

[29] J. I. Kroschwitz, *Concise Encyclopedia of Polymer Science and Engineering*, John Wiley & Sons, 1990.

[30] V. Sáez, E. Hernández, and A. L. Sanz, "Mecanismos de liberación de fármacos desde materiales polímeros," *Revista Iberoamericana de Polímeros*, vol. 5, no. 1, p. 55, 2004.

[31] I. Katime, J. E. Puig, and E. Mendizábal, *Hidrogeles Poliméricos para Uso Médico*, Revista Universidad de Guadalajara, 1999, Número 14.

[32] I. Katime, N. Valderruten, and J. R. Quintana, "Controlled release of aminophylline from poly (N-isopropylacrylamide--co-itaconic acid) hydrogels," *Polymer International*, vol. 50, no. 8, pp. 869–879, 2001.

[33] F. J. Aragón, S. R. González, G. N. Brizuela, and V. L. Oliver, "Estudio cinético de liberación in vitro en un biomaterial compuesto por HAP-200/POVIAC/$CaCO_3$," *Revista Iberoamericana de Polímeros*, vol. 10, no. 2, pp. 119–130, 2009.

Hindawi
International Journal of Polymer Science
Volume 2018, Article ID 2768120, 7 pages
https://doi.org/10.1155/2018/2768120

Research Article

Anticancer Effects of Cyclocarya paliurus Polysaccharide (CPP) on Thyroid Carcinoma In Vitro and In Vivo

Zhiwei He,[1] Fangfang Lv,[2] Yueli Gan,[1] Jing Gu,[1] and Ting Que[1]

[1]*Shanghai Post and Telecommunication Hospital, Shanghai 200040, China*
[2]*Fudan University Shanghai Cancer Center, Shanghai 200032, China*

Correspondence should be addressed to Ting Que; tque@outlook.com

Zhiwei He and Fangfang Lv contributed equally to this work.

Received 14 September 2018; Revised 19 October 2018; Accepted 23 October 2018; Published 27 December 2018

Guest Editor: Jianxun Ding

In this study, we explored the role and mechanisms of Cyclocarya paliurus polysaccharide on cell apoptosis in thyroid cancer (TC) cells. The apoptosis of thyroid cancer cells *in vitro* and tumor tissues *in vivo* induced by Cyclocarya paliurus polysaccharide was determined by MTT assay and flow cytometric assay. The downstream molecules including phosphop-protein kinase B (p-Akt), Akt, B-cell lymphoma 2 (Bcl-2), and Bcl-2-associated X protein (Bax) in tumor tissue were evaluated by western blotting. MTT and flow cytometry assay *in vitro* revealed Cyclocarya paliurus polysaccharide-induced apoptosis of thyroid cancer cell line in a manner of time-dependent and dose-dependent. *In vivo* assay showed 50 mg/kg and 100 mg/kg Cyclocarya paliurus polysaccharide significantly suppressed the proliferation of thyroid cancer in mice. Western blotting showed downregulation of p-Akt, Akt, and Bcl-2 and upregulation of Bax. These results suggest that Cyclocarya paliurus polysaccharide may enhance thyroid cancer cell apoptosis by suppressing the activation of p-Akt, Akt, and Bcl-2 and activating Bax, which provide a novel use of CPP as a thyroid cancer treatment.

1. Introduction

Plant polysaccharides are natural polymeric macromolecules generally composed of more than ten monosaccharide units joined by glycosidic bonds, playing an important role in life-support activities. Biological activities of polysaccharides have been broadly investigated since the 1940s. Plant polysaccharides have biological effects such as immunoregulation, anticancer, antiaging, serum glucose-depressing, and lipid-depressing [1–5]. And recently a growing number of studies have demonstrated the significant advantages of polysaccharides in the prevention and treatment of critical or chronic diseases in human such as cancers, cardiovascular diseases, and diabetes [6–8].

Moreover, there are some limitations of present therapy against thyroid cancer. Patients with different types of thyroid cancer exhibited poor or modest response to traditional chemotherapy [9]. Till date, present goals are to identify novel agents to improve response and progression-free survival. Researches show that most of the plant polysaccharides perform anticancer effect through strengthening immune function against cancer cells by regulating the levels of cytokines secreted by the host cells [10]. On the other hand, cytotoxic polysaccharides possess tumor cytotoxicity, which showed direct interactions with cancer cells [11]. However, the effects of Cyclocarya paliurus polysaccharide on thyroid carcinoma are still largely unknown.

In the past decade, progress has been made to understand the molecular mechanisms of thyroid cancer. The best represented advances in genetic and epigenetic events occurring in thyroid cancer was Akt, which was reported to be involved in several major pathways [12]. Hyperactivation of Akt promotes cell transformation and tumorigenesis in multiple tumors. In addition, Bcl-2 family of proteins is a major intracellular modulator of apoptotic signaling, which exist in normal and neoplastic thyroid tissue [13]. It was reported

that overexpression of Bcl-2 in thyroid carcinoma cells increased oncogenic addiction of cells. Another molecule influencing the apoptotic balance in cancer tissues is Bax. It has been assumed that the ratio of Bcl-2/Bax determines cell death [14].

In the present study, we investigate the mechanism by which polysaccharides isolated by Cyclocarya paliurus and determine its possible anticancer properties. Furthermore, we established a mouse model to reveal the underlying mechanism of anticancer effects *in vitro* and *in vivo*.

2. Materials and Methods

2.1. Reagents. Plant materials and preparation of C. paliurus polysaccharides were obtained previously [15]. The leaves of C. paliurus were collected from a planting base in Enshi, Hubei Province, China. Sugar content was measured by the phenol-sulfuric acid colorimetric method with D-glucose as a standard at 490 nm. Phospho-Akt1 (S246) polyclonal antibody was purchased from R&D. AKT antibody was purchased from Rockland. Bcl-2 monoclonal antibody, Bax polyclonal antibody, GAPDH, and HRP Mouse mAb were purchased from MultiSciences.

2.2. Cell Lines. Thyroid carcinoma cell lines (FRO, ARO, 8505C, SW579, K1, FTC133, and BCPAP) were purchased from FuHeng Cell Center, Shanghai, China. The cells were cultured in RPMI-1640 medium (Invitrogen, Carlsbad, CA, USA) with 10% fetal bovine serum (FBS), 100 units/mL penicillin (Sigma-Aldrich, St. Louis, USA), and 0.1 mg/mL streptomycin (Sigma-Aldrich, St. Louis, USA). All cells were maintained in a humidified incubator containing 5% humidified CO_2 at 37°C.

2.3. Animals. All animal procedures were approved by the Animal Care and Use Committee of the institution in compliance with the Guide for the Care and Use of Laboratory Animals. Forty male BALB/c nude mice (18–20 g, 5–6 week age) were obtained from a commercial vendor (Beijing Huafukang Bioscience Co. Inc., Beijing, China, permit number: SCXK-JING 2014-0004). All the mice were housed under pathogen-free conditions in accordance with laboratory animal care and allowed free access to sterilized food and water. After FRO cells were harvested, tumor inoculation was performed in the right foreleg (5×10^6 cells/mice). Mice in NC and TC groups were orally administered with distilled water. Tumor volume was quantified with caliper, using the formula as follows: tumor volume = 0.5 × length × width2. At the time of sacrificing, tumor tissues were quickly dissected and weighed.

2.4. MTT Assay. The inhibition effect of CPP on seven human thyroid carcinoma cell lines (FRO, ARO, 8505C, SW579, K1, FTC133, and BCPAP cells) was measured by MTT assay in vitro. Briefly, the thyroid carcinoma cells (2×10^4 cells/well) were incubated in 96-well plates with 0.2 mL cell culture medium at 37°C. Cells were allowed to adhere for 24 h, then were incubated in the culture containing CPP with different concentration (0, 30, and 100 μg/mL) for extra 48 h. After the exposure to CPP, 20 μL of MTT assay reagent were added to each well, and the cells continued to be cultured for 1 h. After the medium was removed, 50 μL of DMSO were added to each well and were incubated for 10 min. The absorbance value of the plate was read at 570 nm by the microplate reader. The inhibition rate was calculated as follows: growth inhibitory rate (%) = (1-absorbance of the experimental group/absorbance of the blank control group) × 100%.

2.5. Flow Cytometry. Flow cytometry was performed to identify cell apoptosis by using Annexin V-FITC/PI kit (Qiangen, China), followed by the manufacturer's instructions. After incubation with Cyclocarya paliurus polysaccharide, cells were collected and washed with phosphate-buffered saline (PBS) and stained with Annexin V-FITC/PI. Binding buffer (150 μL) and Annexin-V-FITC (5 μL) were added into each tube and incubated at room temperature for 15 min. Subsequently, binding buffer (100 μL) and PI (5 μL) were also added and incubated for 5 min. At least 10000 cells in each sample were acquired by flow cytometry FC500 (Beckman Coulter, USA) and analyzed with CXP analysis software 2.2 (Beckman Coulter, Inc.).

2.6. Western Blotting. Tumor tissues isolated from mice and collected by surgical manipulation were quickly frozen in liquid nitrogen and sliced to a thickness of 8 μm using a microtome (Leica CM1900, Berlin, Germany). Total protein was extracted from cells and tumor tissues using ice-cold RIPA lysis buffer (Beyotime, Shanghai, China). The concentration was calculated by a bicinchoninic acid (BCA) assay kit (Beyotime, Shanghai, China). 30 μg of proteins were separated using 10% sodium dodecyl sulfate polyacrylamide gel electrophoresis (SDS-PAGE, Bio-Rad, CA, USA) and transferred to a polyvinylidene difluoride (PVDF) membrane. After blocked with 5% nonfat milk for 1 h, samples were incubated with primary antibodies against p-Akt (1 : 1000) polyclonal antibody, Akt (1 : 1000), Bcl-2 (1 : 1000), Bax (1 : 1000), and GAPDH (1 : 1000) at 4°C overnight. After washed with Tris-buffered saline/Tween 20 (TBST), the membrane was incubated with HRP-conjugated secondary antibody (1 : 5000) for 1 h at room temperature. Washed three times with TBST, the protein was detected with an enhanced chemiluminescence (ESL) western blot detection system (Millipore, Bedford, MA, USA). GAPDH was considered to be reflective of the relative protein expression.

2.7. Statistical Analysis. All values were expressed as mean ± standard deviation (SD). All experimental data were analyzed using SPSS 21.0 software (IBM Corp., USA). Comparisons between groups were conducted using a paired *t*-test. Comparisons between two groups were performed using an independent sample *t*-test. Comparisons among multiple groups were assessed by one-way analysis of variance (ANOVA). Enumeration data were expressed as percentage and analyzed by chi-square test. A value of $p < 0.05$ was indicative of statistical significance.

3. Results

3.1. Extraction and Content Determination of CPP. In this study, we isolated polysaccharide from C. paliurus by water extraction and ethanol precipitation. To confirm purity of

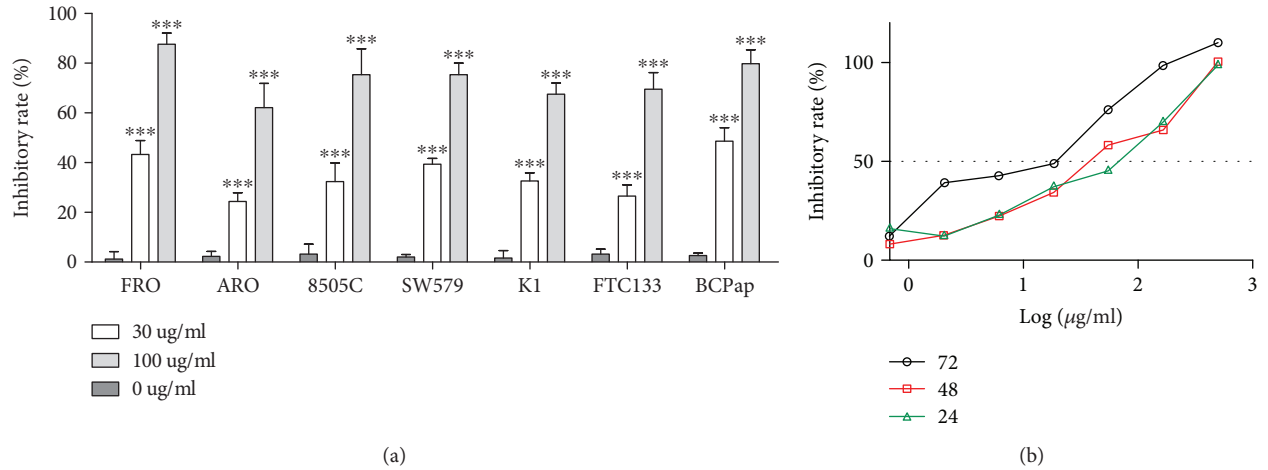

Figure 1: Inhibitory rate of thyroid carcinoma cell lines induced by CPP. (a) Inhibitory rates of a panel of thyroid carcinoma cell lines (FRO, ARO, 8505C, SW579, K1, FTC133, and BCPAP) that treated with CPP (0 μg/mL, 30 μg/mL, and 100 μg/mL) are presented. (b) Inhibitory rates of FRO cells treated with CPP for 24 h, 48 h, and 72 h. The results were expressed as a percentage of the control, which was set at 100%. Data were presented as mean ± SD. $^{*}p < 0.05$ compared with control. $^{**}p < 0.01$ compared with control. $^{***}p < 0.001$ compared with control. All experiments were performed triplicate.

polysaccharide, we further analyzed the sugar contents by the phenol-sulfuric acid colorimetric method. The purity of polysaccharide was determined to be 89.5%.

3.2. Growth Inhibitory Effect of CPP on Thyroid Carcinoma Cell Lines. The growth inhibitory rate of CPP with different levels on seven human thyroid carcinoma cell lines was evaluated to characterize the antithyroid cancer effect of CPP and screen for the cell line with the most effective inhibition induced by CPP. Cell viability of cell lines was analyzed by MTT assay. The cell growth was significantly inhibited in all of the seven thyroid carcinoma cell lines after incubated with 30 and 100 μg/mL of CPP ($p < 0.001$, Figure 1(a)). And the effect of CPP in 100 μg/mL on growth inhibition of thyroid carcinoma cells was more significant than that in 30 μg/mL.

The inhibitory rate on anaplastic thyroid carcinoma-derived FRO cells was approximately 50% at the CPP concentration of 30 μg/mL, only slightly lower than that on differentiated thyroid carcinoma-derived BCPAP cells (%). However, the inhibitory rate on FRO was up to 90% at the concentration of 100 μg/mL, which is higher than all other thyroid carcinoma cell lines tested including BCPAP cells. Therefore, anaplastic thyroid carcinoma-derived FRO cells were selected and used for further investigation.

We further investigated the effect of 100 μg/mL CPP on FRO for 24 h, 48 h, and 72 h. As shown in Figure 1(b), FRO cells treated for 72 h presented higher inhibitory effect, when compared to those of 48 h and 24 h, with no significance. These results indicating that the inhibitory effect of CPP possessed dose-dependent and time-dependent.

3.3. Apoptosis Assay of Tumor Tissues Induced by CPP. Mice treated with PBS were served as control. As shown in Figure 2(a), 50 mg/kg and 100 mg/kg for 30 days significantly decreased the tumor weight, when compared with PBS group. During the period of dosing with CPP, tumor volume in mice increased (Figure 2(b)). Annexin V-FITC double staining was performed to detect tumor cell apoptosis in tumor tissues of mice (Figures 2(c)–2(f)). Treatment of 50 mg/kg and 100 mg/kg CPP resulted in a significant apoptosis of tumor cells in mice by 17.7 ± 2.3% and 21.3 ± 2.6% ($p < 0.001$).

3.4. Expressions of p-Akt, Akt, Bcl-2, and Bax Proteins in Tumor Tissues Regulated by CPP. Protein (Figure 3) expressions of p-Akt, Akt, Bcl-2, and Bax after the mice were sacrificed were evaluated in all three treatment groups. 50 mg/kg and 100 mg/kg treatment of CPP significantly raised p-Akt/Akt protein expressions by 77.6% and 48.1% (Figure 3(b), $p < 0.01$). The Bcl-2 protein expressions decreased by 78.5% and 69.2% (Figure 3(c), $p < 0.01$). The Bax protein expression had elevated to 1.67-fold and 2.23-fold (Figure 3(d), $p < 0.001$). CPP had a strong promoting effect on apoptosis, indicating functional involvement of p-Akt, Akt, Bcl-2, and Bax in apoptosis induced by CPP.

4. Discussion

The infiltration of inflammatory cells usually could be found in thyroid cancer, including lymphocytes, macrophages, and mast cells. Although the role of these cells in cancer and function mechanism is not entirely clear, most of the experiments show that these cells promote the development of tumor. Therefore, inflammatory molecules can be a potential thyroid cancer treatment target, while immunotherapy gradually become the focus in the treatment of thyroid cancer in recent years. As reported, qing qian liu polysaccharide has been proven to have the function of immune regulation and can inhibit the release of IL-6 and TNF-β by macrophages stimulated by LPS [16]. Cyclocarya paliurus polysaccharide is a kind of natural plant polysaccharide extracted from Cyclocarya paliurus. Because of its special physical and chemical effects and small side effects, it has become a

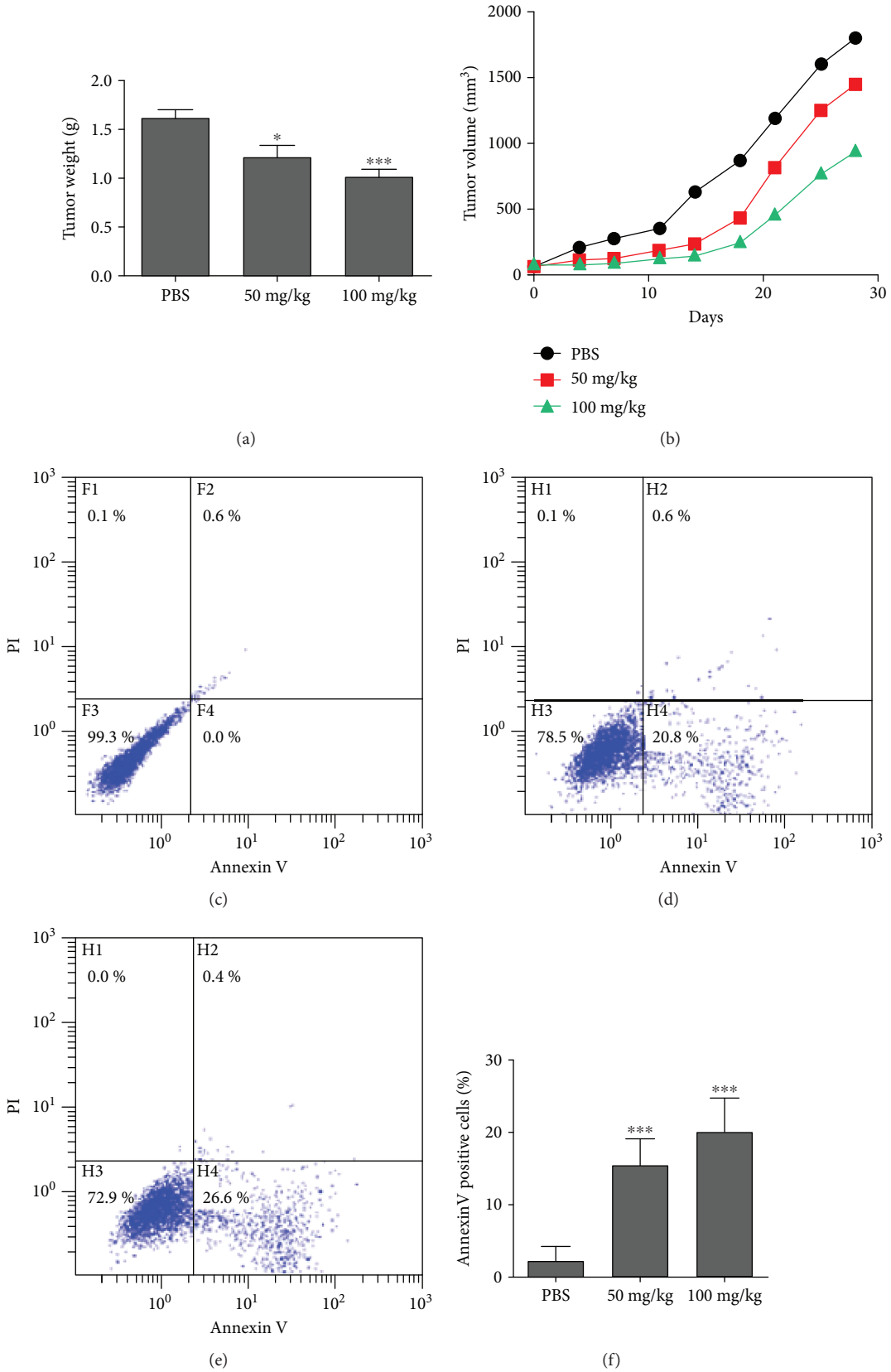

Figure 2: Effect on tumor weight and apoptosis induced by CPP. (a) and (b) presented the tumor weight of mice with specific treatment. In (c), (d), (e), and (f), apoptotic cells were quantified by flow cytometry after stained with Annexin V and PI. Data were presented as mean ± SD. $^{*}p < 0.05$ compared with control. $^{**}p < 0.01$ compared with control. $^{***}p < 0.001$ compared with control. All experiments were performed triplicate.

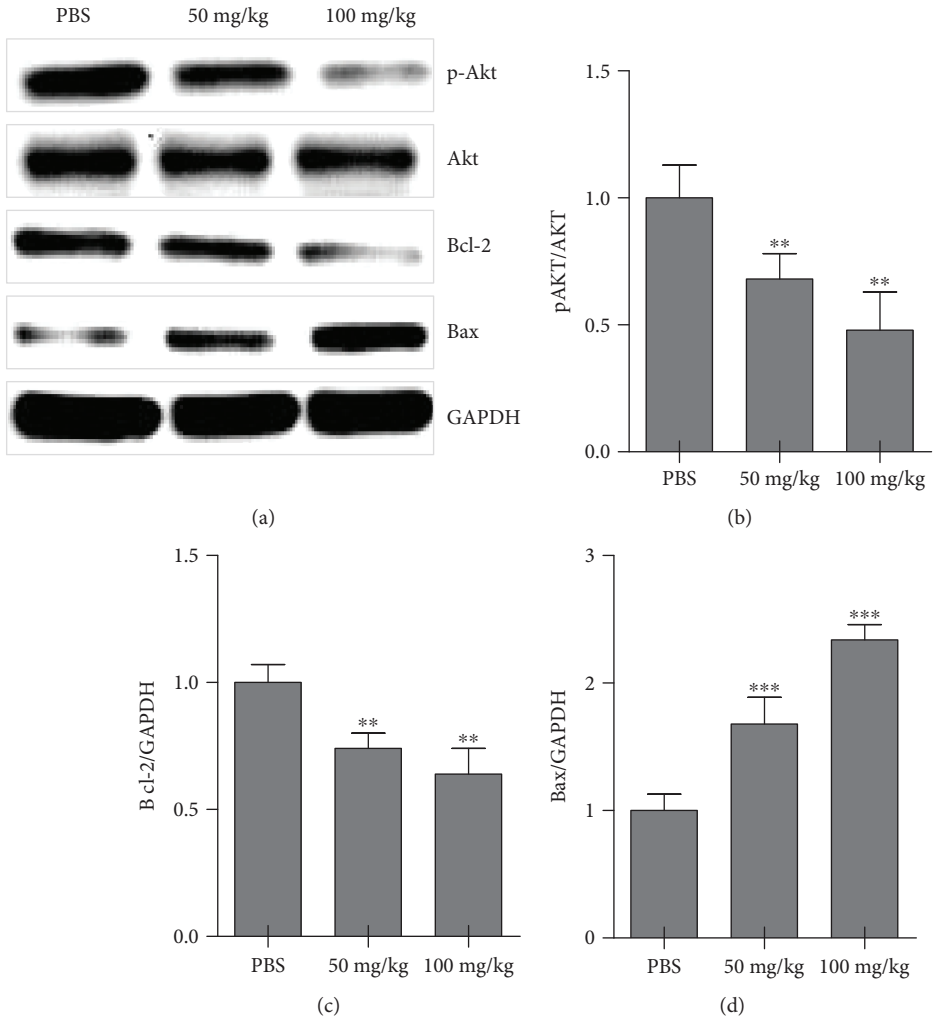

Figure 3: Effect on p-Akt, Akt, Bcl-2, and Bax protein levels induced by CPP. (a) The expression of p-Akt, Akt, Bcl-2, and Bax in tumor tissues are detected by immunoblotting. GAPDH is served as loading control. (b), (c), and (d) presented the relative expression of p-AKT, Bcl-2, and Bax proteins. Data were presented as mean ± SD from three independent experiments. $^{*}p < 0.05$, $^{**}p < 0.01$, and $^{***}p < 0.001$ compared with control. All experiments were performed triplicate.

potential active compound. Currently, studies on the anticancer capacities of polysaccharides focused on the apoptotic effect. The cytotoxicity of the components from Inonotus obliquus was identified in human prostatic carcinoma cell PC3 and breast carcinoma MCF-7 cell [17, 18]. *In vivo* and *in vitro* studies have confirmed polysaccharides from P. However, the signal pathways involved in the apoptosis of cancer cells are complex, and the signal mechanisms of apoptosis are often different in different tumor cell types.

In this study, we isolated polysaccharide from C. paliurus by water extraction and ethanol precipitation. To confirm the contents of polysaccharide, we further measured the sugar contents by the phenol-sulfuric acid colorimetric method. The total content of polysaccharide was determined to be 89.5%. Previous study showed that CPP exerts antiproliferation effect on various tumor cell lines [17–19]. We observed CPP inhibited cell proliferation and induced apoptosis in a pair of thyroid carcinoma cell lines including FRO, ARO, 8505C, SW579, K1, FTC133, and BCPAP. Also, a similar trend was observed in a mouse model. Tumor weight of mice was significantly reduced after treated with CPP.

In our previous study, we explored the potential mechanism of apoptosis of human colon cancer cell HT29 induced by CPP. MTT colorimetric assay was used to detect that Cyclocarya paliurus polysaccharides could significantly inhibit the proliferation of human colon cancer cell HT29. Our previous results suggested that apoptosis induction may be the main mechanism of antitumor effect of CPP. The results of flow cytometry showed that the polysaccharide could induce apoptosis of human colon cancer cell line HT29, and the typical morphological characteristics of apoptotic cells could be observed. As a major strategy for cancer therapeutics, Annexin V/PI staining was conducted to determine whether the cytotoxic effect was related to the apoptotic process. We found that after dosing with CPP, the percentages of early and late apoptotic tumor cells were markedly increased. All these data indicated that CPP induced apoptosis in thyroid tumor.

To understand the possible molecular mechanisms of thyroid cancer cytotoxicity, we explored the related mechanisms. The PI3K/AKT pathway is the most studied frequently mutated network in human cancer [20]. Overactivation of this protein is associated with tumor growth, invasion, and drug resistance. Our results confirmed that CPP markedly downregulated p-Akt and Akt protein levels. Considering p-Akt is the active form of Akt, our data suggested that CPP inhibited active form of Akt directly and indirectly.

In general, cellular life and death are regulated by the Bcl-2 family proteins and the balance between Bcl-2 and Bax. Abnormal expression of Bcl-2 and Bax contribute to tumor survival and growth. Furthermore, Bcl-2 and Bax regulate cell apoptosis process in an independent way [21]. Mitochondrial membrane associated Bcl-2 modulates the expression of some apoptotic factors that usually sequestered in the mitochondrial intermembrane space. Bax plays an essential role in rescuing the sensitivity of apoptosis [22]. If Bcl-2 failed to exert the antiapoptosis role, Bax will form a channel in the mitochondrial outer membrane that facilitate apoptosis [23]. Here, we revealed that CPP markedly reduced Bcl-2 protein levels and elevated Bax protein levels.

To summarize, CPP has a remarkable inhibition in thyroid tumor growth both *in vitro* and *in vivo*, making it of significance in studies. CPP exerts an anticancer effect on thyroid cancer cells through p-Akt, Akt, Bcl-2, and Bax pathways. Our data suggest a potential strategy as a promising therapy for thyroid cancer.

Data Availability

The data used to support the findings of this study are included within the article.

Ethical Approval

Approval for the present study was obtained by the Ethics Committee of the Shanghai Post and Telecommunication Hospital (Shanghai, China).

Consent

All patients admitted to the study provided informed consent for their participation of the present study and the publication of this data.

Conflicts of Interest

The authors declare that they have no competing interests.

Authors' Contributions

TQ was responsible for the study conception and design and revised the manuscript; ZH and FL performed the experiments and drafted the manuscript; YG and JG analyzed the data. All authors read and approved the final manuscript.

Acknowledgments

This work was funded by the Health and Family Planning Commission Foundation of Shanghai (No. 201540289).

References

[1] M. Sundberg-Kövamees, J. Grunewald, and J. Wahlström, "Immune cell activation and cytokine release after stimulation of whole blood with pneumococcal C-polysaccharide and capsular polysaccharides," *International Journal of Infectious Diseases*, vol. 52, pp. 1–8, 2016.

[2] J. Chen, J. Ding, W. Xu et al., "Receptor and microenvironment dual-recognizable nanogel for targeted chemotherapy of highly metastatic malignancy," *Nano Letters*, vol. 17, no. 7, pp. 4526–4533, 2017.

[3] Y. Zhang, T. Lv, M. Li et al., "Anti-aging effect of polysaccharide from *Bletilla striata* on nematode *Caenorhabditis elegans*," *Pharmacognosy Magazine*, vol. 11, no. 43, pp. 449–454, 2015.

[4] Y. G. Li, D. F. Ji, S. Zhong, Z. Q. Lv, and T. B. Lin, "Cooperative anti-diabetic effects of deoxynojirimycin-polysaccharide by inhibiting glucose absorption and modulating glucose metabolism in streptozotocin-induced diabetic mice," *PLoS One*, vol. 8, no. 6, article e65892, 2013.

[5] D. Qin, X. Yang, S. Gao, J. Yao, and D. J. McClements, "Influence of hydrocolloids (dietary fibers) on lipid digestion of protein-stabilized emulsions: comparison of neutral, anionic, and cationic polysaccharides," *Journal of Food Science*, vol. 81, no. 7, pp. C1636–C1645, 2016.

[6] Y. Jiang, Y. Chang, Y. Liu et al., "Overview of *Ganoderma sinense* polysaccharide–an adjunctive drug used during concurrent chemo/radiation therapy for cancer treatment in China," *Biomedicine & Pharmacotherapy*, vol. 96, pp. 865–870, 2017.

[7] J. Zhang, S. Fan, Y. Mao et al., "Cardiovascular protective effect of polysaccharide from *Ophiopogon japonicus* in diabetic rats," *International Journal of Biological Macromolecules*, vol. 82, pp. 505–513, 2016.

[8] D. Li, J. Han, J. Ding, L. Chen, and X. Chen, "Acid-sensitive dextran prodrug: a higher molecular weight makes a better efficacy," *Carbohydrate Polymers*, vol. 161, pp. 33–41, 2017.

[9] V. Bernet and R. Smallridge, "New therapeutic options for advanced forms of thyroid cancer," *Expert Opinion on Emerging Drugs*, vol. 19, no. 2, pp. 225–241, 2014.

[10] N. Wang, J. Yang, J. Lu et al., "A polysaccharide from *Salvia miltiorrhiza* Bunge improves immune function in gastric cancer rats," *Carbohydrate Polymers*, vol. 111, pp. 47–55, 2014.

[11] C. Caro and D. Pozo, "Polysaccharide colloids as smart vehicles in cancer therapy," *Current Pharmaceutical Design*, vol. 21, no. 33, pp. 4822–4836, 2015.

[12] M. Xing, B. R. Haugen, and M. Schlumberger, "Progress in molecular-based management of differentiated thyroid cancer," *The Lancet*, vol. 381, no. 9871, pp. 1058–1069, 2013.

[13] C. S. Mitsiades, P. Hayden, V. Kotoula et al., "Bcl-2 overexpression in thyroid carcinoma cells increases sensitivity to Bcl-2 homology 3 domain inhibition," *The Journal of Clinical Endocrinology & Metabolism*, vol. 92, no. 12, pp. 4845–4852, 2007.

[14] Z.-g. Zhang, J. Zou, Y. Huang, and L. Wu, "Kinetin inhibits proliferation of hepatic stellate cells by interrupting cell cycle and induces apoptosis by down-regulating ratio of Bcl-2/

Bax," *Journal of Huazhong University of Science and Technology [Medical Sciences]*, vol. 35, no. 5, pp. 672–678, 2015.

[15] J. Y. Yin, S. P. Nie, C. Zhou, Y. Wan, and M. Y. Xie, "Chemical characteristics and antioxidant activities of polysaccharide purified from the seeds of Plantago asiatica L," *Journal of the Science of Food and Agriculture*, vol. 90, no. 2, pp. 210–217, 2010.

[16] Z. Wang, J. Xie, Y. Yang et al., "Sulfated *Cyclocarya paliurus* polysaccharides markedly attenuates inflammation and oxidative damage in lipopolysaccharide-treated macrophage cells and mice," *Scientific Reports*, vol. 7, no. 1, 2017.

[17] H. Zhang, Y. Jing, and G. Wu, "Inhibitory effects of crude polysaccharides from Semen vaccariae on benign prostatic hyperplasia in mice," *Journal of Ethnopharmacology*, vol. 145, no. 2, pp. 667–669, 2013.

[18] Z. Luo, H. Zeng, Y. Ye et al., "Safflower polysaccharide inhibits the proliferation and metastasis of MCF-7 breast cancer cell," *Molecular Medicine Reports*, vol. 11, no. 6, pp. 4611–4616, 2015.

[19] T. Shinbo, S. Fushida, T. Tsukada et al., "Protein-bound polysaccharide K suppresses tumor fibrosis in gastric cancer by inhibiting the TGF-β signaling pathway," *Oncology Reports*, vol. 33, no. 2, pp. 553–558, 2015.

[20] B. Han, P. Jiang, Z. Li et al., "Coptisine-induced apoptosis in human colon cancer cells (HCT-116) is mediated by PI3K/Akt and mitochondrial-associated apoptotic pathway," *Phytomedicine*, vol. 48, pp. 152–160, 2018.

[21] S. Gaumer, I. Guénal, S. Brun, L. Théodore, and B. Mignotte, "Bcl-2 and Bax mammalian regulators of apoptosis are functional in *Drosophila*," *Cell Death & Differentiation*, vol. 7, no. 9, pp. 804–814, 2000.

[22] S. Zhu, T. Li, J. Tan et al., "*Bax* is essential for death receptor-mediated apoptosis in human colon cancer cells," *Cancer Biotherapy & Radiopharmaceuticals*, vol. 27, no. 9, pp. 577–581, 2012.

[23] T. Moldoveanu, A. V. Follis, R. W. Kriwacki, and D. R. Green, "Many players in BCL-2 family affairs," *Trends in Biochemical Sciences*, vol. 39, no. 3, pp. 101–111, 2014.

Hindawi
International Journal of Polymer Science
Volume 2018, Article ID 5136185, 13 pages
https://doi.org/10.1155/2018/5136185

Research Article

Structural Characterization, Antioxidant Activity, and Biomedical Application of *Astragalus* Polysaccharide Degradation Products

Jian-Min Wang, Xin-Yuan Sun, and Jian-Ming Ouyang

Institute of Biomineralization and Lithiasis Research, Jinan University, Guangzhou 510632, China

Correspondence should be addressed to Xin-Yuan Sun; sunxinyuan1985@163.com and Jian-Ming Ouyang; toyjm@jnu.edu.cn

Received 20 April 2018; Revised 7 August 2018; Accepted 29 August 2018; Published 30 September 2018

Academic Editor: Mingqiang Li

To study the antioxidant capacity of *Astragalus* polysaccharides (APS) with different molecular weights, we used hydrogen peroxide to degrade original *Astragalus* polysaccharide (APS0) with an initial molecular weight of 11.03 kDa and obtained three degraded polysaccharides with molecular weights of 8.38 (APS1), 4.72 (APS2), and 2.60 kDa (APS3). The structures of these polysaccharides were characterized by ^{1}H NMR, ^{13}C NMR, FT-IR, and GC/MS. The degradation process did not cause significant changes in the main chain structure of APS. The monosaccharide component of APS before and after degradation was slightly changed. The antioxidant ability *in vitro* (removing hydroxyl and ABTS radicals and reducing ability) and in cells (superoxide dismutase and malondialdehyde generation) of these polysaccharides is closely related to their molecular weight. If the molecular weight of APS is very high or low, it is not conducive to their activity. Only APS2 with moderate molecular weight showed the greatest antioxidant activity and ability to repair human kidney epithelial (HK-2) cells. Therefore, APS2 can be used as a potential antistone polysaccharide drug.

1. Introduction

Radix Astragali is one of the most popular medicinal herbs in China, and it has been used for more than 2000 years. One of its main active ingredients is *Astragalus* polysaccharides (APS), which show antioxidation, antitumor, and antiaging properties and cardiovascular, liver, and kidney protective effects [1, 2].

The polysaccharide property is closely related to its molecular weight, acid group content, monosaccharide composition, glycosidic linkage type, and main chain structure [3–6]. Given the different varieties, qualities, and processing methods, a certain difference exists in its monosaccharide composition and structure [7]. Wang et al. [6] separated APS with a molecular weight of 3.6×10^4 Da from *A. membranaceus* roots by hot water extraction method. The main chain of APS is made up of α–D–$(1 \rightarrow 4)$–Glc and $(1 \rightarrow 6)$–α–D–Glcp, and the branching point is located at O-6. Fu et al. [8] obtained APS with a molecular weight of approximately 3.01×10^5 Da from Mongolian *Astragalus* using low concentration of ethanol for precipitation and gel chromatography for purification. Spectral analysis results of ^{1}H NMR and ^{13}C NMR showed that the APS backbone has a 1,3-linked β-D-Gal residue and the branched portion has β-Glc, 1,6-linked α-Gal; 1,5-linked β-Xyl; 1,4-linked β-Gal; β-D-Gal, 1,2-linked α-Rha; and 1,2,4-linked α-Rha residues.

The molecular weight affects the antioxidant ability of the polysaccharide. In addition, optimal antioxidant ability will vary depending on the type of polysaccharide. Liu et al. [9] reported that *Ganoderma lucidum* polysaccharide (GLP_L1) with low molecular weight (5.2 kDa) has a higher ability to scavenge free radicals, superoxide radicals, and hydrogen peroxide than the component (GLP_L2) with high molecular weight (15.4 kDa). At a concentration of 10 mg/mL, the scavenging rates of GLP_L1 to hydroxyl radical and superoxide anion are close to 75% and 90%, respectively, whereas the scavenging ability of GLP_L2 is only 50% and 60%, respectively. Ma et al. [10] isolated four kinds of polysaccharides, namely, GLP1 (>10 kDa), GLP2 (8–10 kDa), GLP3 (2.5–8 kDa), and GLP4 (<2.5 kDa), from *G. lucidum* by ultrasonic method. At the concentration of 0.5 mg/mL, the reducing ability was in the following order: GLP2 > GLP1 > GLP3 > GLP4, showing that the GLP2 polysaccharide with moderate molecular weight had the best reducing ability. Sheng and

Sun [11] obtained four polysaccharides, namely, CPA-1, CPA-2, CPA-3, and CPA-4, from *Athyrium multidentatum* (Doll.) Ching by H_2O_2 degradation method, and their molecular weights were 14.53, 12.37, 11.55, and 6.40 kDa, respectively. The DPPH scavenging rates of the four polysaccharides with a concentration of 30 μg/mL were 63.35%, 50.23%, 42.45%, and 30.01%, respectively, showing that the polysaccharide with high molecular weight had the greatest scavenging activity.

Free radical-induced oxidative stress is thought to be one of the major causes of kidney disease, including kidney stones [12]. Polysaccharides can remove free radicals in vitro and act as antioxidants to protect living organisms from oxidative damage [13]. Khan [14] certified that free radicals can cause renal epithelial cell damage and allow urine crystals to attach to the damaged epithelial cell layer through simulation of the kidney environment in vitro. This research also proved that renal cell injury induced by free radicals can produce an environment conducive to crystal growth, accelerating the formation of stones. Antioxidant activity means that some antioxidants can protect cells against the damage of reactive oxygen species [15], such as superoxide, singlet oxygen, and hydroxyl radicals. Thus, research and exploring potent natural compounds with antioxidant activities and low cytotoxicity from plants have become very important in the field of biomedicine.

Based on this fact, the effects of the molecular weight of APS on its antioxidant capacity and cell repair ability were studied. The results of this study will provide enlightenment for screening for the optimal active polysaccharides.

2. Experimental Method

2.1. Reagents and Instruments. Astragalus polysaccharides (95% purity) produced by Shaanxi Ciyuan Biology Co. Ltd.; 30% hydrogen peroxide; anhydrous ethanol; trichloroacetic acid (CCl_3COOH); o-phenanthroline; $K_4[Fe(CN)_6]$; ferrous sulfate ($FeSO_4 \bullet 7H_2O$); potassium bromide (KBr); D_2O (99.9%, Sigma); ascorbic acid (Vc); and ferric chloride ($FeCl_3$) were all purchased from Guangzhou Chemical Reagent Factory.

Human kidney proximal tubular epithelial (HK-2) cells were purchased from Shanghai Cell Bank, Chinese Academy of Sciences (Shanghai, China). Dulbecco's modified Eagle's medium (DMEM) and fetal bovine serum were purchased from HyClone Biochemical Products Co. Ltd. (UT, USA). Cell culture plates were purchased from Wuxi NEST Biotechnology Co. Ltd. (Wuxi, China). Malondialdehyde (MDA) kit and superoxide dismutase (SOD) kit were purchased from Jiancheng Institute of Biotechnology (China). Hematoxylin-eosin (HE) kit was purchased from Shanghai Beyotime Biotech Co. Ltd. (Shanghai, China).

The apparatus used in this paper were the following: KQ2200DB Ultrasonic Cleaning Instrument (Kunshan Ultrasonic Instruments Co. Ltd.), Ubbelohde capillary viscometer (0.45 mm, Qihang Glass Instrument Factory, Shanghai, China), conductivity meter (DDS-11A, LEICI, Shanghai, China), ultraviolet-visible spectrophotometer (Cary 500, Varian, Palo Alto, CA, USA), Fourier-transform infrared spectrometer (Equinox 55, Bruker, Karlsruhe, Germany), enzyme mark instrument (Safire2, Tecan, Männedorf, Switzerland), nuclear magnetic resonance (Varian Bruker-600 MHz, Bruker, Germany), 7890A-5975C gas chromatography-mass spectrometer (Agilent, USA), and fluorescence microscope (22DI-E-D282, Leica, Solms, Germany).

2.2. Experimental Methods. We followed the methods of Bhadja et al. [16].

2.2.1. Degradation of Polysaccharides. About 1.2 g original Astragalus polysaccharide (APS0) was weighed and dissolved in 20 mL distilled water. H_2O_2 solution was added to the reaction system—90°C water bath degradation for 2 h. The degradation reaction was cooled at room temperature, at which point the solution pH was adjusted to 7.0 by adding 2 mol/L NaOH solution. The degraded solution was then concentrated to one-third of its original volume at 60°C. The product was precipitated by adding three volumes of anhydrous ethanol. After filtration, the degraded polysaccharide was obtained by drying. The above experimental procedure was repeated by changing the H_2O_2 concentration at 4%, 6%, and 14%; degraded Astragalus polysaccharides with different molecular weights were obtained.

2.2.2. Measurement of Molecular Weights of Polysaccharides. According to the literature [17], the molecular weight was determined by Ubbelohde viscosity method at 25 ± 0.2°C. After determining the drop time T of each polysaccharide in the viscometer, the relative viscosity η_r and the specific viscosity η_{sp} were calculated, where $\eta_r = T_i/T_0$ and $\eta_{sp} = \eta_r - 1$, where T_i and T_0 are the drop time of polysaccharide solution and deionized water. According to the one-point method, the intrinsic viscosity $[\eta] = [2(\eta_{sp} - \ln \eta_r)]^{1/2}/c$, where c is the concentration of the sample to be tested. The molecular weights of each polysaccharide before and after degradation were calculated based on $[\eta]$ values. The relationship between the intrinsic viscosity $[\eta]$ of the polymer solution and the molecular weight M of the polymer can be expressed by the empirical equation of Mark-Houwink: $[\eta] = \kappa M^{\alpha}$, where κ and α are the two parameters of the empirical equation and are constants related to polymer morphology, solvent, and temperature.

2.2.3. Analysis of Carboxylic Group Content. The carboxyl group (–COOH) content of APS was measured by conductometric titration. The conductivity titration curve was plotted using the conductivity value as the Y-axis and the used NaOH volume as the X-axis. The conductivity titration curve can be divided into three parts, a conductivity reduction stage (A), an equilibrium stage (B), and a conductivity increase stage (C). Three tangent lines are constructed from the three-stage curve, and the intersection is a stoichiometric point. The intersection of lines A and B gives the volume of NaOH (V_1) that excessive HCl and $-SO_3H$ consumed; the intersection of lines B and C gives the volume of NaOH (V_2) that excessive HCl and $-SO_3H$ and the –COOH of the APS consumed together; so, $V_2 - V_1$ (platform portion) is the NaOH volume that the –COOH of the APS consumed

alone. The –COOH content can be obtained according to the following formula [18]:

$$-\mathrm{COOH}(\%) = \frac{C_{\mathrm{NaOH}} \times (V_2 - V_1) \times 45/1000}{C_{\mathrm{sample}} \times 40/1000} \times 100, \quad (1)$$

wherein C_{NaOH} (mol/L) represents the molar concentration of NaOH, C_{sample} (g/L) represents the mass concentration of the polysaccharide, 45 g/mol is the molar mass of –COOH, and 40 mL is the solution volume of polysaccharide. The final value is the average of three parallel experiments.

2.2.4. Fourier-Transform Infrared Spectroscopy (FT-IR) Analysis. A dried polysaccharide sample (2.0 mg) was mixed with KBr (200 mg). After grinding and pressing into KBr pellet, scanning was performed between the ranges of 4000 cm^{-1} to 400 cm^{-1} with a resolution of 4 cm^{-1}.

2.2.5. ^{1}H NMR and ^{13}C NMR Detection of APS. According to the literature [19], 20 mg of fully dried APS1 polysaccharides was weighed and added to a NMR tube containing 0.5 mL of deuterated water (D_2O), which is completely dissolved and placed in the magnetic field of the nuclear magnetic resonance spectrometer for detection.

2.2.6. Monosaccharide Component Detection of APS by GC-MS. According to the literature [20], 10 mg of APS1 polysaccharide was added to a 121°C sealed container containing 2.5 $\mathrm{mol{\cdot}L^{-1}}$ trifluoroacetic acid (TFA) (2 mL) for 90 minutes. The solution was concentrated to dryness under reduced pressure, and then the TFA was removed with MeOH to a neutral solution and concentrated to dryness under reduced pressure. The residue was dissolved in 2 mol/L NH_4OH (1 mL) and 1 $\mathrm{mol{\cdot}L^{-1}}$ fresh $NaBD_4$ (1 mL). The reaction was carried out at room temperature for 2.5 h and stirring was done at room temperature. Then two drops of acetic acid were added to decompose excess $NaBD_4$ until no bubbles were produced. The solution was concentrated to dryness under reduced pressure. The filtrate was added with MeOH to remove boric acid and dried in vacuo. 1 mL of acetic anhydride was added and acetylated at 100°C for 2.5 h. The acetylated product was extracted with dichloromethane. The organic layer was washed with distilled water, dried, and analyzed by GC-MS. The HP-5MS capillary column (15 m × 250 μm × 0.25 μm) was programmed, and the temperature was raised from 135°C to 180°C at 0.5°C/min, then to 190°C at 10°C/min, and up to 310°C at 40°C/min. Helium acts as carrier gas, with a column flow rate of 0.6 mL/min. The acetylated product was identified by debris ions in GC-MS and relative retention times in GC. The structure is identified by peaks and assessed by peak area. Standard monosaccharides (rhamnose, arabinose, fucose, xylose, mannose, glucose, and galactose) are used as reference.

2.2.7. Hydroxyl Radical (•OH) Scavenging Activity of APS with Different Molecular Weights. The •OH scavenging ability of polysaccharide in vitro was detected by H_2O_2/Fe system method [21]. The four different molecular weight polysaccharide solutions (60 μg/mL, 1 mL) were incubated with phenanthroline (2.5 mmol/L, 1 mL), ferrous sulfate (2.5 mmol/L, 1 mL), and hydrogen peroxide (20 mmol/L, 1 mL) in phosphate buffer (20 mmol/L, 1 mL, pH 7.4) for 90 min at 37°C. The absorbance measured at 536 nm was designated A_1. The absorbance when hydrogen peroxide (H_2O_2) was replaced with distilled water and polysaccharide solution was A_2 and A_3, respectively. Ascorbic acid (Vc) was used as the positive control group. The ability to scavenge hydroxyl radicals was calculated using the following equation:

$$\text{Scavenging effect}(\%) = \frac{(A_3 - A_1)}{(A_2 - A_1)} \times 100\%. \quad (2)$$

2.2.8. ABTS Radical Scavenging Activity of APS with Different Molecular Weights. ABTS was oxidized to produce a stable blue-green cationic radical $ABTS^+$. The antioxidant reacts with $ABTS^+$ to cause the reaction to fade and initiate a change in the absorbance of a particular wavelength segment to determine the size of the antioxidant to remove ABTS free radicals [22].

The ABTS radical scavenging activity of polysaccharides was performed according to [23] with slight modification. 7 mmol/L ABTS solution was mixed with 2.45 mmol/L potassium persulfate aqueous solution, and then the mixture was incubated in the dark at room temperature for 12–16 h. Then 3 mL $ABTS^+$ solution was added to 1 mL polysaccharide solutions of various concentrations in a test tube. After reacting for 6 min at room temperature, the absorbance was measured at 734 nm.

$$\text{Scavenging effect}(\%) = \left[1 - \frac{(A_1 - A_2)}{A_0}\right] \times 100\%. \quad (3)$$

where A_0 is the control group without polysaccharide, A_1 is the experiment group, and A_2 is the blank group without reagents (the absorbance of polysaccharide solution A_2 was 0).

2.2.9. Reducing Power of APS with Different Molecular Weights. Using the Prussian blue method [24], the polysaccharide sample may reduce the positive Fe^{3+} ions into Fe^{2+} ions in potassium ferricyanide ($K_4[Fe(CN)_6]$) to form Prussian blue and develop at 700 nm. That is, the greater the absorbance at 700 nm is, the stronger is the reduction of polysaccharide [25].

2 mL APS with different molecular weights (60 μg/mL) was mixed with 2 mL phosphate buffer solution (PBS) (pH = 6.6) and 2 mL 1% $K_4[Fe(CN)_6]$. The mixture was incubated at 50°C for 20 min. 2 mL 10% trichloroacetic acid was added to the mixture which was then centrifuged for 10 min at 3000 r/min. The supernatant (2 mL) was mixed with 0.5 mL $FeCl_3$ (0.1%, *w*/*v*) solution and 2 mL distilled water. The mixture was shaken well and left to stand for 10 min. Then the absorbance was measured at 700 nm. Phosphate buffer was used as negative control, and Vc was used as positive control for comparison.

Table 1: Physicochemical properties and FT-IR characteristic absorption peaks of original and degraded APS.

	H_2O_2 concentration $C_{(H2O2)}$ (%)	Mean molecular weight (Mr/Da)	–COOH content (%)	Relative intensity of –COOH absorption peak*	Functional group characteristic absorption peak			
					–OH	–COOH	$-CH_2$	Sugar ring
APS0	0	11.03	16.8	1.4	3394.8	1617.1	2927.4	1115.5, 1087.4, 1030.5, 763.5
APS1	4	8.39	16.7	1.2	3393.7	1618.1	2931.3	1106.1, 1082.8, 1022.8, 764.8
APS2	6	4.72	17.2	1.6	3392.7	1616.7	2932.9	1110.8, 1081.9,1023.6, 762.5,
APS3	14	2.60	16.2	1	3396.3	1622.1	2930.8	1113.7, 1082.1, 1027.7, 761.9

*$(100\text{-}T_{APS0}) : (100\text{-}T_{APS1}) : (100\text{-}T_{APS2}) : (100\text{-}T_{APS3})$, where T represents the light transmittance.

2.2.10. Cell Culture. HK-2 cells were cultured in DMEM medium containing 10% fetal bovine serum, 100 U/mL penicillin, and100 μg/mL streptomycin antibiotic with a pH of 7.4 and cultured in a 5% CO_2-humidified environment of 37°C. Cells were passaged by trypsin digestion. Upon reaching 80%–90% confluent, cells were gently blown after trypsinization to form a cell suspension for the following cell experiments.

2.2.11. Superoxide Dismutase (SOD) Activity Detection. SOD activity was assessed using a commercially available kit based on the autooxidation of hydroxylamine. The cell suspension was inoculated in 24-well plates with a cell concentration of 5×10^4 cell/mL and 500 μL per well and was incubated for 24 h in an incubator at 37°C. The experimental model was divided into three groups: (1) control group: only serum-free medium was added, (2) injury group: serum-free medium containing 2.6 mmol/L oxalate was added for 3.5 h, and (3) repair group: 60 μg/mL of APS solutions with different molecular weights was added to the injured cells and repaired for 10 h. At the indicated time points, the treated cells were homogenized in 100 mmol/L Tris-HCl buffer and centrifuged at 10,000 rpm for 20 min and then the SOD activity was determined using assay kits. The absorbance of the supernatant was then measured directly by a microplate reader at 550 nm with a reference wavelength of 600 nm.

2.2.12. Malondialdehyde (MDA) Detection. For lipid peroxidation assay, we used a commercial kit to quantify the generation of MDA according to the manufacturer's protocol. Cell culture and polysaccharide treatment were performed using a method similar to that of SOD measurement. After the repair effect was completed, the cells were harvested by trypsinization and cellular extracts were prepared by sonication in ice-cold buffer (50 mM Tris-HCl, pH 7.5, 5 mM EDTA, and 1 mM DTT). After sonication, lysed cells were centrifuged at 10000 rpm for 20 min to remove debris. The supernatant was subjected to the measurement of MDA levels by detecting the absorbance at 532 nm.

2.2.13. Hematoxylin and Eosin (HE) Staining. Cell suspension with a cell concentration of 5×10^4 cells/mL was inoculated per well in 12-well plates, 1 mL of DMEM containing 10% fetal bovine serum was added per well, and the cells were incubated for 24 h. Cell culture and polysaccharide treatment were performed using a method similar to that of SOD measurement. After the repair was completed, the supernatant was removed by aspiration and washed 2 times with PBS. Then the cells were fixed with 4% polyoxymethylene at room temperature for 15 min. After fixation, the cells were stained with hematoxylin stain for 15 minutes. The cells were then washed with distilled water for 2 min to remove excess stains. Thereafter, the cells were stained with an eosin staining solution for 5 min. The cells were washed with pure water for 2 min to remove excess eosin. After treatment, the cells were observed under a microscope, the nuclei were stained purple, and the cytoplasm was stained pink.

2.2.14. Statistical Analysis. Experimental data were expressed as mean ± SD. The experimental results were analyzed statistically using SPSS 13.0 software. The differences of means between the experimental groups and the control group were analyzed by Tukey's test. $p < 0.05$ indicates significant difference; $p < 0.01$ indicates extremely significant difference.

3. Results

3.1. Degradation of APS. Original *Astragalus* polysaccharide (APS0) with a molecular weight of 11,033 Da was degraded by H_2O_2 with concentrations of 4%, 6%, and 14%. Three kinds of degraded APS, namely, APS1, APS2, and APS3, with the molecular weights of 8376, 4716, and 2600 Da, respectively, were obtained.

3.2. Change in the Contents of the –COOH in APS before and after Degradation. The content of the –COOH in APS was measured by conductivity titration. The results are shown in Table 1. The carboxyl content of three degraded APS was between 16.2% and 17.2%, which only slightly changed (16.8%) before degradation.

The carboxyl group content of APS2 (17.2%) increased slightly. The reason is that hydroxyl radicals produced by the H_2O_2 degradation system break the sugar chain, exposing the carboxyl groups. Thus, high levels of carboxyl were detected in polysaccharides with low molecular weight after degradation [26]. Chang et al. [27] degraded the original polysaccharide with a molecular weight of 1.29×10^2 kDa by ethanol precipitation and obtained two degraded polysaccharides with molecular weights of 60.0 and 52 kDa. The content of uronic acid was increased from 70.8% before degradation to 79.5% and 86.2%.

The carboxyl group content (16.9%) of APS3 decreased slightly, probably because free radicals generated by high concentration of H_2O_2 (14%) led to oxidative decarboxylation of

polysaccharides, allowing the carboxyl groups in the polysaccharide chain to be converted into other groups, such as –OH [28].

3.3. Structural Characterization of APS by FT-IR Spectra. Figure 1 shows the FT-IR spectra of four APS. The FT-IR spectra of polysaccharides before and after degradation were similar, and no new peaks appeared, which indicated that the degradation of H_2O_2 did not cause significant effect on the overall structure of polysaccharides.

The absorption peaks of all four APS are shown in Table 1. The strong absorption band at 3392.7 cm^{-1} corresponds to the absorption peak of the stretching vibration of –OH in the polysaccharide. The absorption band at 2932.9 cm^{-1} corresponds to the stretching vibration of C–H [29]. The two distinct absorbance peaks, at about 1616.7 and 1417.9 cm^{-1}, suggested the presence of uronic acids. The absorption peaks at 1113.7 and 1027.7 cm^{-1} indicate that the polysaccharide contains α-glucose residues [30].

As the polysaccharide of each sample has the same mass (2.0 mg), the intensity of the absorption peak can reflect the content of the characteristic functional groups (such as the –COOH) [31]. Compared with the original polysaccharide before degradation, the absorption peaks of the –OH and –COOH at 3408 and 1620 cm^{-1} were enhanced and the peaks of APS2 were the strongest, which was probably due to the exposure of the –OH and –COOH of polysaccharides after degradation, thus increasing their content [32, 33]. The intensity change of the absorption peak of the –COOH is consistent with the change rule of the measured content of the –COOH (Table 1).

3.4. Structural Analysis of APS by ^1H NMR and ^{13}C NMR. The polysaccharides were characterized by ^1H and ^{13}C NMR spectroscopy and typical spectra are shown in Figure 2.

3.4.1. ^1H NMR. Table 2 lists the attribution of each line in the ^1H NMR spectra of APS1 and APS2. The ^1H NMR spectrum of APS1 was similar to that of APS2 (Table 2). For APS2, the signal peaks at δ5.31 and δ4.87 ppm correspond to the chemical shifts of H-1 of (1→4)–α–D–Glcp and (1→6)–α–D–Glcp, respectively. The highly overlapping peak at δ3.42–3.88 ppm belongs to the H-2, H-3, H-4, H-5, and H-6 signals of (1→4)–α–D–Glcp and (1→6)–α–D–Glcp of polysaccharides [34]. The proton signals at δ5.12 and 5.08 ppm belong to the H-1 signal of (1→6)–α–D–Gal and (1→)–α–D–Rha, respectively, of polysaccharide.

3.4.2. ^{13}C NMR Spectrum. Table 3 lists the attribution of the lines in the ^{13}C NMR spectra of APS1 and APS2. The ^{13}C NMR spectrum of APS1 was similar to that of APS2. For APS2, the signal at δ103.7 ppm belongs to the C-1 signal peak of β–D–Glcp of polysaccharide. The signals at δ99.6, δ71.5, δ73.2, δ76.7, δ71.2, and δ60.4 ppm are attributed to C-1, C-2, C-3, C-4, C-5, and C-6 signals of (1→4)–α–D–Glcp, respectively. The signals at δ71.9, δ73.1, δ69.3, δ70.4, and δ65.6 ppm are attributed to C-2, C-3, C-4, C-5, and C6 signals of (1→6)–α–D–Glcp, respectively [34, 35]. The signals at δ100.2, δ72.7, δ72.3, δ81.2, and δ73.3 ppm are attributed to C-1, C-2, C-3, C-4, and C-5 signal peaks of (1→4)–GalA, respectively [36]. The signals at δ92.1, δ72.2, δ70.1, δ83.7, and δ69.0 ppm correspond to the C-1, C-2, C-3, C-4, and C-5 signal peaks of (1→)–α–D–Rha, respectively. The signals at δ70.5, δ72.4, and δ63.7 ppm are attributed to the C-4, C-5, and C-6 signal peaks of (1→6)–α–D–Gal, respectively.

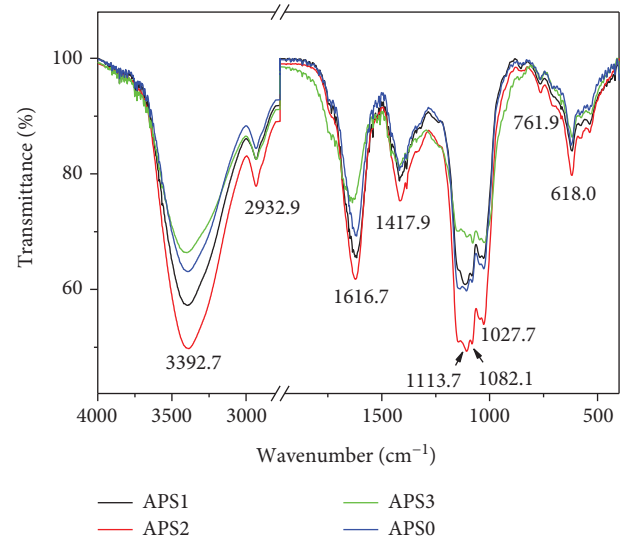

FIGURE 1: Infrared spectrum of APS with different molecular weights.

3.5. Monosaccharide Composition of APS. The GC spectra of APS1, APS2, APS3, and 7 standard monosaccharides after derivatization were obtained by GC-MS, as shown in Figure 3. The retention time of each monosaccharide peak in APS is consistent with the retention time of standard monosaccharides of glucose, arabinose, rhamnose, and galactose (Figure 3(a)). According to the peak area, the molar ratio of monosaccharides in APS1 can be calculated as 11.4 : 7.8 : 0.7 : 1 (Figure 3(b)). The molar ratio of monosaccharides in APS2 is 13.9 : 8.2 : 1.2 : 1 (Figure 3(c)). The molar ratio of monosaccharides in APS3 is 13.3 : 8.4 : 1.1 : 1 (Figure 3(d)).

3.6. Differences in Scavenging Capacity of •OH Radicals of Polysaccharides with Different Molecular Weights. Among the reactive oxygen free radicals in the body, hydroxyl radicals (•OH) are known as the strongest oxidants, which can induce damage of surrounding biological macromolecules, such as certain proteins, nucleic acids, and unsaturated fatty acids. Such injuries can cause aging, cancer, and other diseases [37].

The •OH scavenging capacity of the four kinds of APS is shown in Figure 4. The •OH scavenging rate increased with the increase in APS concentration from 0.15 mg/mL to 3 mg/mL. The IC_{50} of APS0, APS1, APS2, APS3, and the positive control group (Vc) were 3.1, 2.7, 2.4, 4.2, and 0.06 mg/mL, respectively, which indicated that all APS had the ability to remove •OH radicals and APS2 with moderate molecular weight had the strongest scavenging

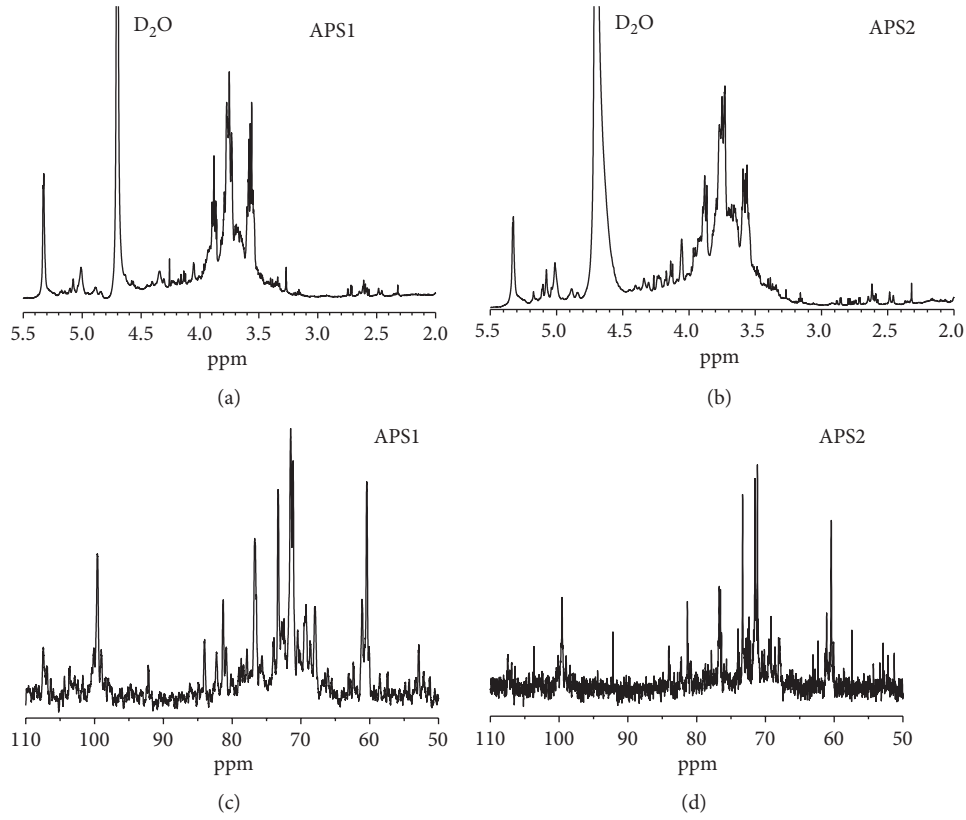

Figure 2: Nuclear magnetic resonance spectra of APS1 and APS2. (a) ^{1}H NMR spectrum of APS1; (b) ^{1}H NMR spectrum of APS2; (c) ^{13}C NMR spectrum of APS1; (d) ^{13}C NMR spectrum of APS2.

Table 2: Structure characterization of APS1 and APS2 by ^{1}H NMR spectra.

	Composition*	Chemical shifts (δppm)					
		H-1	H-2	H-3	H-4	H-5	H-6
APS1	(1 → 6)-α-D-Glcp	4.89	3.48	3.63	3.40	3.85	3.64
	(1 → 4)-α-D-Glcp	5.33	3.55	3.87	3.56	3.73	3.70
	β-D-Glcp	5.18					
	(1 → 6)-α-D-Gal	5.10					
	(1→)-α-D-Rha	5.08					
	(1 → 4)-GalA	4.96					
APS2	(1 → 6)-α-D-Glcp	4.87	3.46	3.63	3.42	3.87	3.63
	(1 → 4)-α-D-Glcp	5.31	3.53	3.88	3.54	3.76	3.71
	β-D-Glcp	5.19					
	(1 → 6)-α-D-Gal	5.12					
	(1→)-α-D-Rha	5.08					
	(1 → 4)-GalA	4.97					

*Gal: galactose; Glcp: glucose; Rha: rhamnose; GalA: glucuronic acid.

Table 3: Structure characterization of APS1 and APS2 by ^{13}C NMR spectra.

	Composition*	Chemical shifts (δppm)					
		C-1	C-2	C-3	C-4	C-5	C-6
APS1	β-D-Glcp	103.6					
	(1 → 4)-α-D-Glcp	99.6	71.5	73.3	76.7	71.1	60.4
	(1 → 4)-GalA	100.1	72.6	72.4	81.3	73.3	
	(1 → 6)-α-D-Glcp		71.8	73.0	69.3	70.4	65.7
	(1→)-α-D-Rha	92.2	72.3	70.1	83.7	69.0	
	(1 → 6)-α-D-Gal				70.5	72.4	63.6
APS2	β-D-Glcp	103.7					
	(1 → 4)-α-D-Glcp	99.6	71.5	73.2	76.7	71.2	60.4
	(1 → 4)-GalA	100.2	72.7	72.3	81.2	73.3	
	(1 → 6)-α-D-Glcp		71.9	73.1	69.3	70.4	65.6
	(1→)-α-D-Rha	92.1	72.2	70.1	83.7	69.0	
	(1 → 6)-α-D-Gal				70.5	72.4	63.7

*Gal: galactose; Glcp: glucose; Rha: rhamnose; GalA: glucuronic acid.

capacity. At a concentration of 2.5 mg/mL, the scavenging rate of APS2 (63.4%) was twice as high as that of APS3 (31.7%) with the lowest molecular weight and it was also obviously higher than that of APS0 (45.3%) with the highest molecular weight. However, the scavenging rates of the four polysaccharides were all less than that of Vc (97.8%).

3.7. Differences of ABTS Radical Scavenging Capacity of APS with Different Molecular Weights. Four kinds of APS with different molecular weights all had an obvious scavenging effect on ABTS free radicals (Figure 5) and showed a dose-dependent relationship in the concentration range of 0.15–3 mg/mL. At the concentration of 2.5 mg/mL, the scavenging

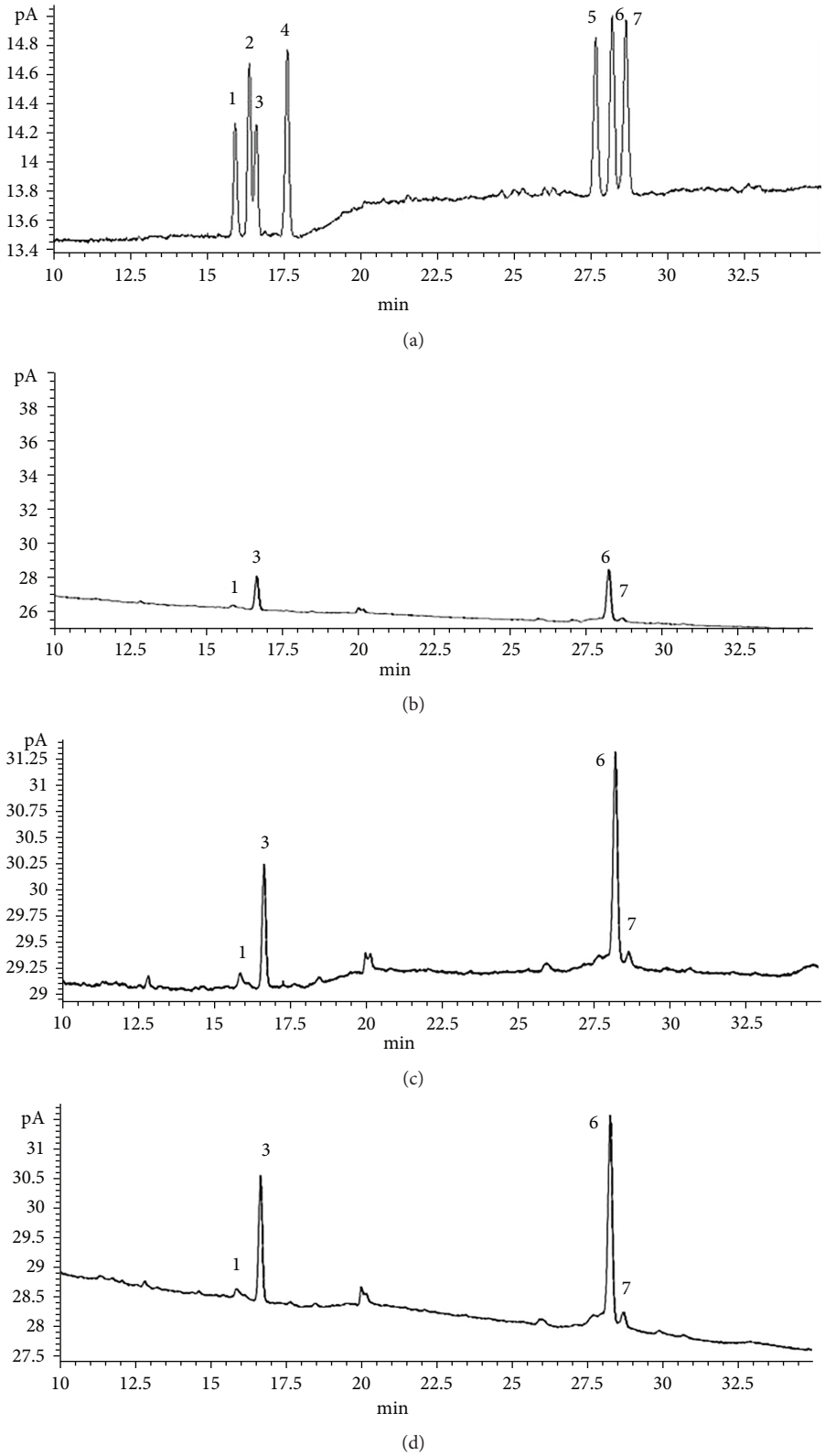

Figure 3: Gas chromatography-mass spectrometry (GC-MS) results of APS. (a) Gas chromatogram of standard monosaccharides. (b) Monosaccharide component of APS1. (c) Monosaccharide component of APS2. (d) Monosaccharide component of APS3. 1: rhamnose; 2: fucose; 3: arabinose; 4: xylose; 5: mannose; 6: glucose; 7: galactose.

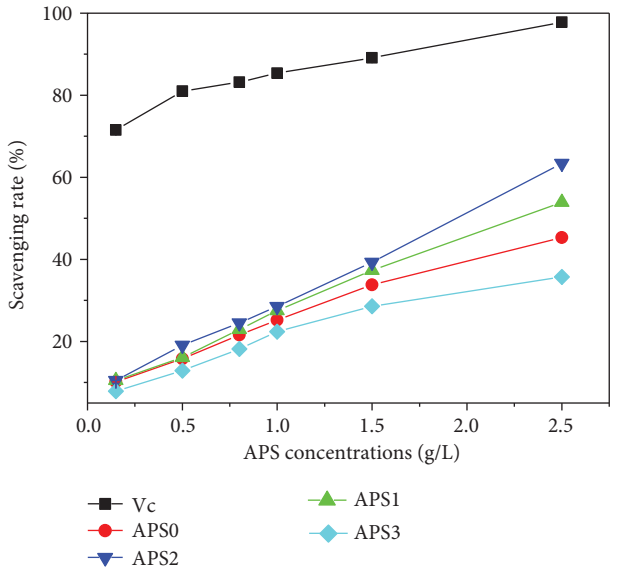

Figure 4: Hydroxyl radical scavenging capacity of APS with different molecular weights.

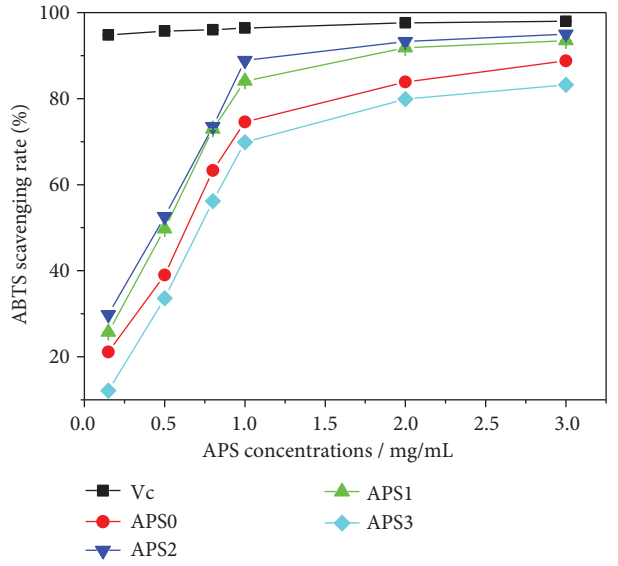

Figure 5: ABTS radical scavenging capacity of APS with different molecular weights.

rates of APS0, APS1, APS2, and APS3 were 88.8%, 93.5%, 95%, and 83.2%, respectively, which indicated that APS2 with moderate molecular weight had the highest antioxidant activity and was slightly lower than Vc (98%).

3.8. Differences of Reducing Ability of APS with Different Molecular Weights. The reducing ability of materials in vivo provides hydrogen atoms to destroy the free radical reaction chain, so as to achieve antioxidation. Therefore, the reducing ability is an important indicator of the potential antioxidant capacity of antioxidants.

As shown in Figure 6, the reducing ability of each polysaccharide showed a concentration-dependent manner.

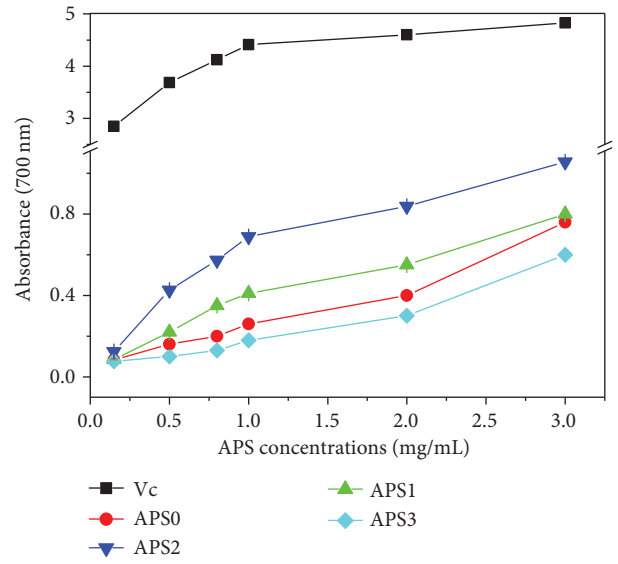

Figure 6: Reducing power of APS with different molecular weights.

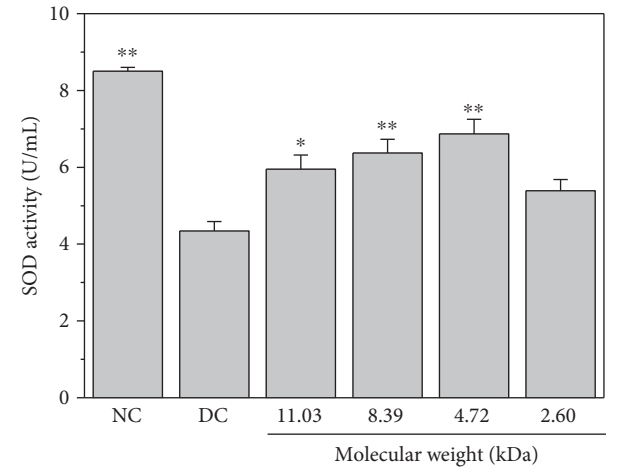

Figure 7: Changes of SOD activity after the damaged HK-2 cells were repaired by APS with different molecular weights for 10 h. NC: normal control; DC: damaged control. Compared with the DC group, $*$ indicates $p < 0.05$. $**$ indicates $p < 0.01$.

When the concentration was 2.5 mg/mL, the ability of the four polysaccharides to reduce Fe^{3+} was in the following order: APS2 (1.06) > APS1 (0.8) > APS0 (0.76) > APS3 (0.6). APS2 had the highest reducing ability.

3.9. Changes of SOD Activity in Damaged Cells and APS-Repaired Cells. The reduction of SOD activity in organism implies decreased ability to resist free radical-induced damage in organism [38]. Figure 7 shows the changes of SOD activity in damaged HK-2 cells after polysaccharide repair for 10 h. It can be seen that the activity of intracellular SOD increases first and then decreases with the decrease of APS molecular weight. The SOD activity in the control group was 8.5 ± 0.1 U/mL, and it decreased to 4.34 ± 0.25 U/mL after 2.6 mmol/L oxalate damage. After

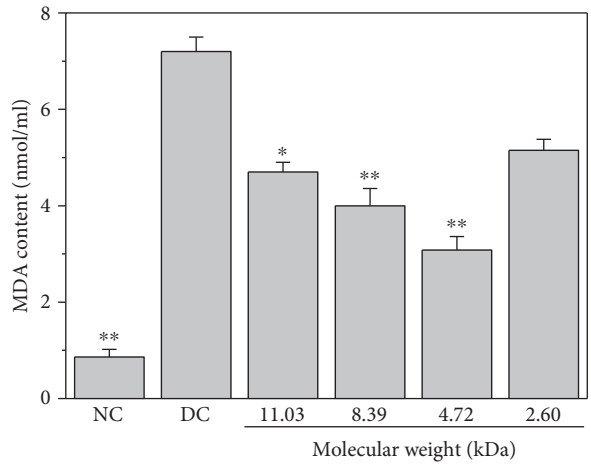

Figure 8: Changes of MDA content after the damaged HK-2 cells were repaired by APS with different molecular weights for 10 h. NC: normal control; DC: damaged control. Compared with the DC group, $*$ indicates $p < 0.05$. $**$ indicates $p < 0.01$.

damaged cells were repaired by APS0, APS1, APS2, and APS3 for 10 h, the SOD activity increased to 5.95 ± 0.38, 6.3 ± 0.36, 6.87 ± 0.37, and 5.39 ± 0.29 U/mL, respectively. APS2 with moderate molecular weight has the strongest ability to enhance SOD activity.

3.10. Changes of MDA Content in Damaged Cells and APS-Repaired Cells. The change of MDA content usually reveals the level of lipid peroxidation *in vivo* and indirectly reflects the degree of cell injury [39]. After the cells were injured by 2.6 mmol/L oxalate, the release of MDA increased from 0.86 ± 0.16 nmol/mL (control group) to 7.2 ± 0.3 nmol/mL (Figure 8), indicating that HK-2 cells suffered oxidative damage. When the damaged cells were repaired by APS0, APS1, APS2, and APS3 for 10 h, the generation content of MDA decreased from 7.2 ± 0.3 nmol/mL to 4.7 ± 0.3, 4.0 ± 0.3, 3.08 ± 0.28, and 5.15 ± 0.23 nmol/mL, respectively. That is, APS inhibit the release of MDA to the outside of the cells. Especially, APS2 with moderate molecular weight has the strongest ability to inhibit MDA release.

3.11. Cell Morphology Repair of APS with Different Molecular Weights in HK-2 Cells. The morphological changes of renal proximal tubule epithelial cells (HK-2) after repair by APS with different molecular weights were observed by hematoxylin and eosin staining (Figure 9). Normal HK-2 grows tightly and is plump. After oxidative damage by 2.6 mmol/L oxalic acid, the inherent form of HK-2 cells was lost. The cell volume was reduced, and nuclei staining was enhanced. Many dense apoptotic bodies were formed. After repair in injured HK-2 cells by APS with different molecular weights, the cell number increased and the cell morphology recovered similar to normal cells in varying degrees. Especially for the APS2-repaired cells, the morphology is the closest to normal cells. By contrast, APS3 with a lower molecular weight and APS0 with a higher molecular weight were less effective than APS2.

4. Discussion

4.1. Chemical Structure of APS. The structure of polysaccharides is the basis for their biological activity. Many factors affect the biological activity of polysaccharides, including molecular weight, acid group content, monosaccharide composition, ligand type, and main chain structure [3–6]. In the present study, the monosaccharide composition and type of sugar residues of APS were analyzed by ^{1}H NMR, ^{13}C NMR, GC-MS, and FT-IR spectroscopy.

From the results of comprehensive analysis (Figures 1–3), α- and β-glycosidic bonds exist in the four kinds of APS. The main structure is that the main chain is composed of $(1 \rightarrow 4)$ connected Glcp and the branch point is located at the C-6 position of $(1 \rightarrow 6)$ connected Glcp, both containing 1,4-linked glucuronic acid fragments (Figure 10). The main structure is basically consistent with the structure illustrated by Li and Zhang [29]. Fu et al. [8] also found that APS mainly consist of glucose, rhamnose, xylose, and galactose, which is inconsistent with our results in that the monosaccharides of APS consisted of rhamnose, arabinose, fucose, sugar, mannose, glucose, and galactose. Even with the same species of polysaccharides, differences will exist in their monosaccharide components due to their origin, processing method, separation process, and purification conditions [27].

The main chain structures of the four polysaccharides were similar from FT-IR results (Figure 1), but the absorption peak intensities of characteristic functional group of the polysaccharides before and after degradation were different (Table 1). This finding is mainly because the hydroxyl radicals produced by H_2O_2 degradation can attack the polysaccharide glycosidic bonds and cleave them, resulting in the change of side chain structure but not the main chain structure in polysaccharides. For example, Tian et al. [40] analyzed the chitosan structure before and after H_2O_2 degradation by infrared spectroscopy and nuclear magnetic resonance. The depolymerization only leads to changes of side groups, and no distinct change takes place in the structures of the main chain.

4.2. Effects of Molecular Weight on the Activity of APS Polysaccharides

4.2.1. Reasons for the Low Activity in Low-Molecular Weight APS. For different types of plant polysaccharides, the range of molecular weights that exhibit the best bioactivity is different. When the molecular weight of APS is very low, an active polymeric structure might not form, resulting in the loss of polysaccharide activity [41]. In low-molecular weight polysaccharide, the unique bond linking method of polysaccharide and their three-dimensional structure (conformation) based on intramolecular hydrogen bond of polysaccharide will be destructed. The carbonyl group in low-molecular weight polysaccharide changed to be in an open chain, whereas in high-molecular weight polysaccharide, it was attached to a ring molecule. The destruction of the ring structure will break the hydrogen bond structure of the polysaccharide molecule, leading to reduced bioactivity.

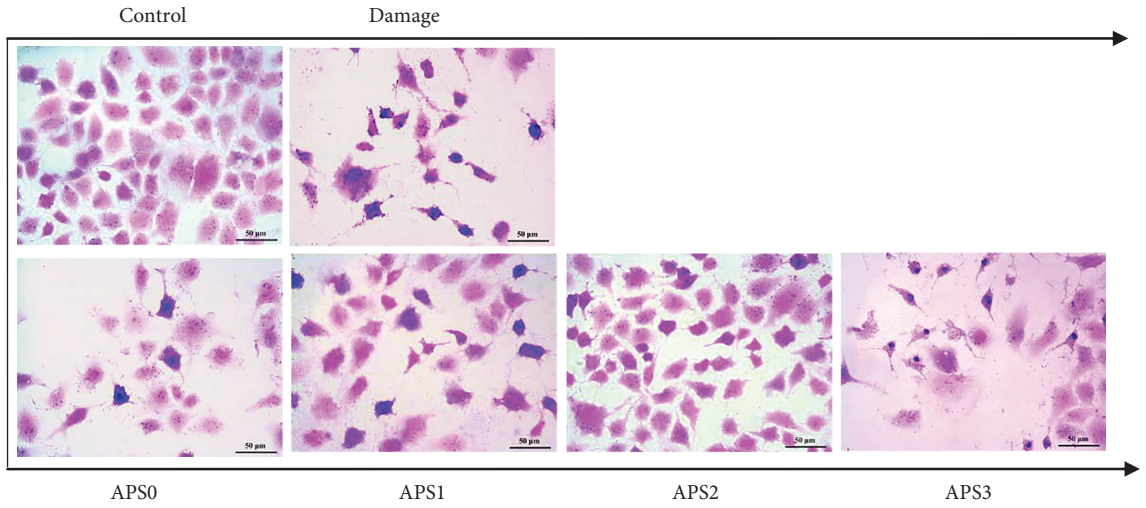

Figure 9: Morphological changes after the damaged HK-2 cells were repaired by APS with different molecular weights. Oxalic acid concentration: 2.6 mmol/L, injury time: 3.5 h; polysaccharide concentration: 60 μg/mL, repair time: 10 h.

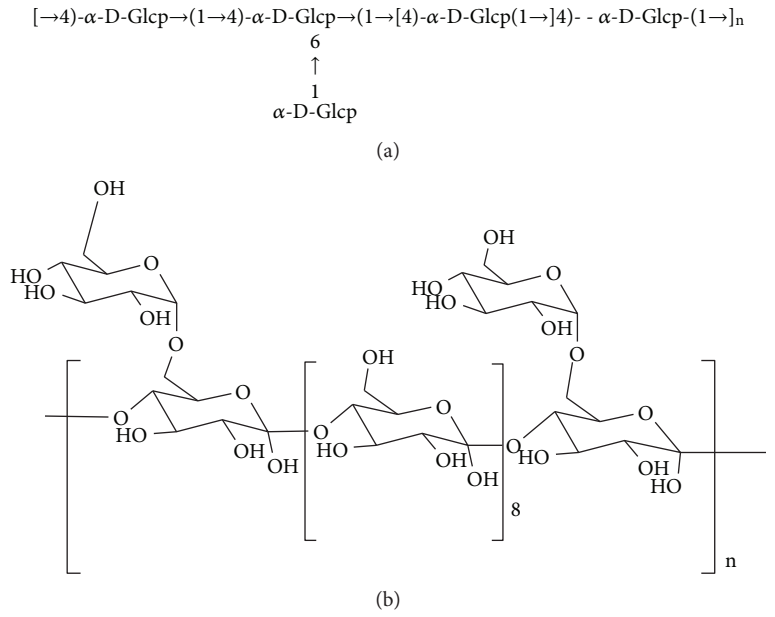

Figure 10: Molecular structure of APS. (a) Chain structure; (b) skeleton structure.

Polysaccharide has two mechanisms of clearing the hydroxyl radical: the first is to remove the already-generated hydroxyl radicals and the second is to inhibit the generation of hydroxyl radicals [42]. The former mechanism is related to that hydroxyl radical can quickly capture the hydrogen atom of the C-H chain of polysaccharide and form H_2O, whereas, the carbon atom of polysaccharide generates a single electron and turns into carbon free radical which then will be oxidized to be a peroxy radical that decomposes harmless products to organism [43]. The latter mechanism is related to the transition of metal ions that catalyze the generation of hydroxyl radicals, so the chelating ability may affect the hydroxyl radicals [44].

Hydroxyl radical can quickly capture the hydrogen atom of the C-H chain of polysaccharide and form H_2O [43]. In addition, the acid group of polysaccharide (such as –COOH) can decrease the production of hydroxyl radicals through the inactivating Fenton reaction. The carboxyl group content has considerable effect on scavenging •OH radicals [45]. APS contained many hydroxyl groups and carboxyl groups in each monomer unit. Polysaccharides with low molecular weights would have more reductive hydroxyl group or carboxyl group terminals (on per unit mass basis) to accept and eliminate the free radicals [46]. The chain structure of APS3 with the lowest molecular weight suffered significant destruction, and its molecular structure was the most loose. Therefore, the ability of APS3 to clear free radicals was the lowest. Chen et al. [47] reported that when the hydroxyl groups from polysaccharide are replaced with sulfuric acid groups, the antioxidant activity of polysaccharides decreases,

which also indicates that the reduction in the number of hydroxyl groups will reduce the antioxidant activity of polysaccharides. Lai et al. [48] extracted two molecular weights of mung bean polysaccharides by ethanol precipitation. At a concentration of 0.8 mg/mL, the DPPH free radical scavenging rate (70.2%) of mung bean polysaccharide with low molecular weight (45 kDa) was weaker than that of mung bean polysaccharide (91.6%) with high molecular weight (83 kDa).

4.2.2. Reasons for the Low Activity in High-Molecular Weight APS. APS0 has high molecular weight, molecular volume, and viscosity and relatively low solubility, which affect its biological activity. The biological activity of polysaccharides is closely related to the single-helix structure of the main chain and hydrophilic group (hydroxyl group) located on the surface of the spirochetes [49]. Another reason is because the polysaccharide with high molecular weight has a more compact structure and stronger intramolecular hydrogen bonds, resulting in less exposure of effective active groups. Qi et al. [50] found that the polysaccharide chain has a reduction and a nonreducing end. The greater the molecular weight of polysaccharides is, the lesser the reduction and nonreducing end contents are and the weaker the antioxidant activity is.

Polysaccharide degradation can effectively improve its antioxidant capacity. After degradation of APS0 to the polysaccharide with a suitable molecular weight, the branching degree of the polysaccharide becomes small, providing sufficient spatial extent to form a regular helical structure, which favors the exposure of more hydroxyl groups to the surface of the helical structure and is good for exerting bioactivity.

For example, *Lycium barbarum* polysaccharides with low molecular weight (10.2 kDa) have anticancer activity, whereas those with high molecular weight (6.50×10^3 kDa) have no anticancer activity [51]. Similarly, *Ligusticum chuanxiong* polysaccharide with low molecular weight has a strong reducing ability [52]. At a concentration of 5 mg/mL, the IC_{50} values of reduction capacity of three kinds of *Rhizoma chuanxiong* polysaccharides with molecular weights of 2.83×10^4, 1.23×10^4, and 6.31×10^4 Da are 1.05, 1.1, and 0.84 mg/mL, respectively. However, the immunoregulatory effect of *Opuntia* polysaccharides with high molecular weight (133 kDa) on macrophages is better than that of *Opuntia* polysaccharides with low molecular weight (168 kDa) [53].

4.2.3. APS with Moderate Molecular Weight Has the Strongest Activity. As shown in Figures 4–6, the antioxidant capacity of APS was in the following order: APS2 > APS1 > APS0 > APS3, and APS2 had the strongest antioxidant capacity. APS with a very high (APS0) or low (APS3) molecular weight had weakened antioxidant capacity. The ability of each polysaccharide to repair damaged HK-2 cells also showed the same activity sequence.

A number of studies have also confirmed that polysaccharides with moderate molecular weight have more conducive activity [54, 55]. For example, Im et al. [54] studied the immunomodulatory and antitumor functions of aloe polysaccharides with different molecular weights. The results showed that the inhibitory rate of aloe polysaccharide G2E1DS2 (Mw = 5–400 kDa) with moderate molecular weight on the growth of S180 cells in mice was 91.53%. The inhibition rates of G2E1DS3 (>400 kDa) with the highest molecular weight and G2E1DS1 (<5 kDa) with the lowest molecular weight were only 14.87% and 15.89%, respectively. Fan et al. [55] isolated three polysaccharides (DDP1, DDP2, and DDP3) with molecular weights of 51.5, 26.1, and 6.95 kDa, respectively, from *Dendrobium denneanum* by hot water extraction. At the concentration of 2 mg/mL, the scavenging ability of the three polysaccharides to •OH, DPPH, and ABTS radicals was in the following order: DDP2 > DDP1 > DDP3. Moreover, the antioxidant capacity of DDP2 with moderate molecular weight (26.1 kDa) was the strongest.

Chen et al. [5] obtained three kinds of APS, namely, APS1-1, APS2-2, and APS3-3, by DEAE resin column chromatography, with molecular weights of 112, 98.3, and 20.4 kDa, respectively, and with the uronic acids content of 0.0%, 5.9%, 11.6%, respectively. Their corresponding total antioxidant capacities were 1152.8, 1566.3, and 1580.4 μmol/L, respectively, at the concentration of 2 mg/mL. These findings showed that polysaccharides with a high uronic acid content and a low molecular weight have great antioxidant ability. There are two variables (molecular weight and uronic acid content) in this study, and it is difficult to determine which factor is the most important in affecting antioxidant activity. In our study, we obtained four different molecular weight APS by H_2O_2 degradation method and the differences of their carboxyl content were small (ranging from 16.2% to 17.2%). Therefore, the influence of the carboxyl group content on the antioxidant ability can be avoided. At the same time, the molecular weight of APS used in our study ranged from 2.60 to 1.03 kDa, which is much less than what Chen et al. [5] reported. We also found that only APS with moderate molecular weight showed the greatest antioxidant capacity.

5. Conclusions

Three degraded APS with molecular weights of 8.38, 4.72, and 2.60 kDa were obtained by degradation of primitive APS (APS0, Mw 11.03 kDa) with different concentrations of H_2O_2. The results of ^{1}H NMR, ^{13}C NMR, FT-IR, and GC-MS showed no significant difference in the main chain structure of the four polysaccharides. All four polysaccharides had (1 → 4)–D–glucose as the main chain and (1 → 6)–D–glucose linkage as the branch chain. The monosaccharide component of APS before and after degradation was slightly changed. APS with four molecular weights had the ability to scavenge hydroxyl and ABTS radicals and good reducing ability. The antioxidant capacity of APS was in the following order: APS2 > APS1 > APS0 > APS3, that is, the antioxidant effect of APS2 with moderate molecular weight was the best. Moreover, the polysaccharides showed good ability to enhance SOD activity, inhibit MDA release, and recover cell morphology. APS, especially APS2, can be used as potential antioxidative drugs for renal protection.

Data Availability

The data used to support the findings of this study are included within the article.

Conflicts of Interest

The authors declare no competing financial interest.

Acknowledgments

This research work was granted by the National Natural Science Foundation of China (nos. 21701050 and 81670644) and the China Postdoctoral Science Foundation (no. 2017M612837).

References

[1] R. Z. Zhong, M. Yu, H. W. Liu, H. X. Sun, Y. Cao, and D. W. Zhou, "Effects of dietary Astragalus polysaccharide and Astragalus membranaceus root supplementation on growth performance, rumen fermentation, immune responses, and antioxidant status of lambs," *Animal Feed Science and Technology*, vol. 174, no. 1-2, pp. 60–67, 2012.

[2] Y. Fan, Y. Hu, D. Wang et al., "Effects of Astragalus polysaccharide liposome on lymphocyte proliferation in vitro and adjuvanticity in vivo," *Carbohydrate Polymers*, vol. 88, no. 1, pp. 68–74, 2012.

[3] Y. Yu, M. Shen, Q. Song, and J. Xie, "Biological activities and pharmaceutical applications of polysaccharide from natural resources: a review," *Carbohydrate Polymers*, vol. 183, pp. 91–101, 2018.

[4] J. H. Xie, M. L. Jin, G. A. Morris et al., "Advances on bioactive polysaccharides from medicinal plants," *Critical Reviews in Food Science and Nutrition*, vol. 56, Supplement 1, pp. S60–S84, 2015.

[5] R.-Z. Chen, L. Tan, C.-G. Jin et al., "Extraction, isolation, characterization and antioxidant activity of polysaccharides from Astragalus membranaceus," *Industrial Crops and Products*, vol. 77, pp. 434–443, 2015.

[6] K.-p. Wang, J. Wang, Q. Li et al., "Structural differences and conformational characterization of five bioactive polysaccharides from Lentinus edodes," *Food Research International*, vol. 62, pp. 223–232, 2014.

[7] M. Jin, K. Zhao, Q. Huang, C. Xu, and P. Shang, "Isolation, structure and bioactivities of the polysaccharides from Angelica sinensis (Oliv.) Diels: a review," *Carbohydrate Polymers*, vol. 89, no. 3, pp. 713–722, 2012.

[8] J. Fu, L. Huang, H. Zhang, S. Yang, and S. Chen, "Structural features of a polysaccharide from Astragalus membranaceus (Fisch.) Bge. var. mongholicus (Bge.) Hsiao," *Journal of Asian Natural Products Research*, vol. 15, no. 6, pp. 687–692, 2013.

[9] W. Liu, H. Wang, X. Pang, W. Yao, and X. Gao, "Characterization and antioxidant activity of two low-molecular-weight polysaccharides purified from the fruiting bodies of Ganoderma lucidum," *International Journal of Biological Macromolecules*, vol. 46, no. 4, pp. 451–457, 2010.

[10] C.-w. Ma, M. Feng, X. Zhai et al., "Optimization for the extraction of polysaccharides from Ganoderma lucidum and their antioxidant and antiproliferative activities," *Journal of the Taiwan Institute of Chemical Engineers*, vol. 44, no. 6, pp. 886–894, 2013.

[11] J. Sheng and Y. Sun, "Antioxidant properties of different molecular weight polysaccharides from Athyrium multidentatum (Doll.) Ching," *Carbohydrate Polymers*, vol. 108, pp. 41–45, 2014.

[12] P. Wang, X. Jiang, Y. Jiang et al., "In vitro antioxidative activities of three marine oligosaccharides," *Natural Product Research*, vol. 21, no. 7, pp. 646–654, 2007.

[13] K. W. Kim and R. L. Thomas, "Antioxidative activity of chitosans with varying molecular weights," *Food Chemistry*, vol. 101, no. 1, pp. 308–313, 2007.

[14] S. R. Khan, "Hyperoxaluria-induced oxidative stress and antioxidants for renal protection," *Urological Research*, vol. 33, no. 5, pp. 349–357, 2005.

[15] R. Wang, P. Chen, F. Jia, J. Tang, F. Ma, and B. Xu, "Characterization and antioxidant activities of polysaccharides from Panax japonicus C.A. Meyer," *Carbohydrate Polymers*, vol. 88, no. 4, pp. 1402–1406, 2012.

[16] P. Bhadja, C.-Y. Tan, J.-M. Ouyang, and K. Yu, "Repair effect of seaweed polysaccharides with different contents of sulfate group and molecular weights on damaged HK-2 cells," *Polymer*, vol. 8, no. 5, p. 188, 2016.

[17] J.-Y. Yin, S.-P. Nie, Q.-B. Guo, Q. Wang, S. W. Cui, and M.-Y. Xie, "Effect of calcium on solution and conformational characteristics of polysaccharide from seeds of Plantago asiatica L," *Carbohydrate Polymers*, vol. 124, pp. 331–336, 2015.

[18] L. Luo, M. Wu, L. Xu et al., "Comparison of physicochemical characteristics and anticoagulant activities of polysaccharides from three sea cucumbers," *Marine Drugs*, vol. 11, no. 12, pp. 399–417, 2013.

[19] R. Li, W.-c. Chen, W.-p. Wang, W.-y. Tian, and X.-g. Zhang, "Antioxidant activity of Astragalus polysaccharides and antitumour activity of the polysaccharides and siRNA," *Carbohydrate Polymers*, vol. 82, no. 2, pp. 240–244, 2010.

[20] S. Bhatia, P. Rathee, K. Sharma, B. B. Chaugule, N. Kar, and T. Bera, "Immuno-modulation effect of sulphated polysaccharide (porphyran) from Porphyra vietnamensis," *International Journal of Biological Macromolecules*, vol. 57, pp. 50–56, 2013.

[21] J. Jiang, F. Kong, N. Li, D. Zhang, C. Yan, and H. Lv, "Purification, structural characterization and in vitro antioxidant activity of a novel polysaccharide from Boshuzhi," *Carbohydrate Polymers*, vol. 147, pp. 365–371, 2016.

[22] Y. Cai, Q. Luo, M. Sun, and H. Corke, "Antioxidant activity and phenolic compounds of 112 traditional Chinese medicinal plants associated with anticancer," *Life Sciences*, vol. 74, no. 17, pp. 2157–2184, 2004.

[23] R.-B. Xu, X. Yang, J. Wang et al., "Chemical composition and antioxidant activities of three polysaccharide fractions from pine cones," *International Journal of Molecular Sciences*, vol. 13, no. 12, pp. 14262–14277, 2012.

[24] K. I. Berker, B. Demirata, and R. Apak, "Determination of total antioxidant capacity of lipophilic and hydrophilic antioxidants in the same solution by using ferric-ferricyanide assay," *Food Analytical Methods*, vol. 5, no. 5, pp. 1150–1158, 2012.

[25] M. Hassasroudsari, P. Chang, R. Pegg, and R. Tyler, "Antioxidant capacity of bioactives extracted from canola meal by subcritical water, ethanolic and hot water extraction," *Food Chemistry*, vol. 114, no. 2, pp. 717–726, 2009.

[26] Z. Zhao, J. Li, X. Wu et al., "Structures and immunological activities of two pectic polysaccharides from the fruits of Zizyphus jujuba Mill. cv. jinsixiaozao Hort," *Food Research International*, vol. 39, no. 8, pp. 917–923, 2006.

[27] S. C. Chang, B. Y. Hsu, and B. H. Chen, "Structural characterization of polysaccharides from Zizyphus jujuba and evaluation of antioxidant activity," *International Journal of Biological Macromolecules*, vol. 47, no. 4, pp. 445–453, 2010.

[28] J. Tang, J. Nie, D. Li et al., "Characterization and antioxidant activities of degraded polysaccharides from Poria cocos sclerotium," *Carbohydrate Polymers*, vol. 105, pp. 121–126, 2014.

[29] S.-g. Li and Y.-q. Zhang, "Characterization and renal protective effect of a polysaccharide from Astragalus membranaceus," *Carbohydrate Polymers*, vol. 78, no. 2, pp. 343–348, 2009.

[30] J.-Y. Yin, B. C.-L. Chan, H. Yu et al., "Separation, structure characterization, conformation and immunomodulating effect of a hyperbranched heteroglycan from Radix Astragali," *Carbohydrate Polymers*, vol. 87, no. 1, pp. 667–675, 2012.

[31] L. Sun, L. Wang, J. Li, and H. Liu, "Characterization and antioxidant activities of degraded polysaccharides from two marine Chrysophyta," *Food Chemistry*, vol. 160, pp. 1–7, 2014.

[32] M. A. Chaouch, J. Hafsa, C. Rihouey, D. Le Cerf, and H. Majdoub, "Depolymerization of polysaccharides from Opuntia ficus indica: antioxidant and antiglycated activities," *International Journal of Biological Macromolecules*, vol. 79, pp. 779–786, 2015.

[33] C. Q. Qin, Y. M. Du, and L. Xiao, "Effect of hydrogen peroxide treatment on the molecular weight and structure of chitosan," *Polymer Degradation and Stability*, vol. 76, no. 2, pp. 211–218, 2002.

[34] Y. Li, Y.-L. Wang, L. Li et al., "Structural characterization of polysaccharides from the roots of Urtica fissa," *Journal of Asian Natural Products Research*, vol. 11, no. 11, pp. 951–957, 2009.

[35] Z.-Y. Zhu, R.-Q. Liu, C.-L. Si et al., "Structural analysis and antitumor activity comparison of polysaccharides from Astragalus," *Carbohydrate Polymers*, vol. 85, no. 4, pp. 895–902, 2011.

[36] W. Fan, S. Zhang, P. Hao, P. Zheng, J. Liu, and X. Zhao, "Structure characterization of three polysaccharides and a comparative study of their immunomodulatory activities on chicken macrophage," *Carbohydrate Polymers*, vol. 153, pp. 631–640, 2016.

[37] F. Hecht, C. F. Pessoa, L. B. Gentile, D. Rosenthal, D. P. Carvalho, and R. S. Fortunato, "The role of oxidative stress on breast cancer development and therapy," *Tumor Biology*, vol. 37, no. 4, pp. 4281–4291, 2016.

[38] C. M. Muth, Y. Glenz, M. Klaus, P. Radermacher, G. Speit, and X. Leverve, "Influence of an orally effective SOD on hyperbaric oxygen-related cell damage," *Free Radical Research*, vol. 38, no. 9, pp. 927–932, 2009.

[39] H. Chen, H. Yoshioka, G.-S. Kim et al., "Oxidative stress in ischemic brain damage: mechanisms of cell death and potential molecular targets for neuroprotection," *Antioxidants & Redox Signaling*, vol. 14, no. 8, pp. 1505–1517, 2011.

[40] F. Tian, Y. Liu, K. Hu, and B. Zhao, "The depolymerization mechanism of chitosan by hydrogen peroxide," *Journal of Materials Science*, vol. 38, no. 23, pp. 4709–4712, 2003.

[41] S. Alban and G. Franz, "Characterization of the anticoagulant actions of a semisynthetic curdlan sulfate," *Thrombosis Research*, vol. 99, no. 4, pp. 377–388, 2000.

[42] B. Li, S. Liu, R. Xing et al., "Degradation of sulfated polysaccharides from Enteromorpha prolifera and their antioxidant activities," *Carbohydrate Polymers*, vol. 92, no. 2, pp. 1991–1996, 2013.

[43] X. T. Li, Y. K. Zhang, H. X. Kuang et al., "Mitochondrial protection and anti-aging activity of Astragalus polysaccharides and their potential mechanism," *International Journal of Molecular Sciences*, vol. 13, no. 2, pp. 1747–1761, 2012.

[44] J. Wang, Q. Zhang, Z. Zhang, and Z. Li, "Antioxidant activity of sulfated polysaccharide fractions extracted from Laminaria japonica," *International Journal of Biological Macromolecules*, vol. 42, no. 2, pp. 127–132, 2008.

[45] J. Fan, Z. Wu, T. Zhao et al., "Characterization, antioxidant and hepatoprotective activities of polysaccharides from Ilex latifolia Thunb," *Carbohydrate Polymers*, vol. 101, pp. 990–997, 2014.

[46] J. Wang, S. Hu, S. Nie, Q. Yu, and M. Xie, "Reviews on mechanisms ofin vitroantioxidant activity of polysaccharides," *Oxidative Medicine and Cellular Longevity*, vol. 2016, Article ID 5692852, 13 pages, 2016.

[47] Y. Chen, H. Zhang, Y. Wang, S. Nie, C. Li, and M. Xie, "Sulfated modification of the polysaccharides from Ganoderma atrum and their antioxidant and immunomodulating activities," *Food Chemistry*, vol. 186, pp. 231–238, 2015.

[48] F. Lai, Q. Wen, L. Li, H. Wu, and X. Li, "Antioxidant activities of water-soluble polysaccharide extracted from mung bean (Vigna radiata L.) hull with ultrasonic assisted treatment," *Carbohydrate Polymers*, vol. 81, no. 2, pp. 323–329, 2010.

[49] A. Inoue, N. Kodama, and H. Nanba, "Effect of maitake (Grifola frondosa) D-fraction on the control of the T lymph node Th-1/Th-2 proportion," *Biological & Pharmaceutical Bulletin*, vol. 25, no. 4, pp. 536–540, 2002.

[50] H. Qi, T. Zhao, Q. Zhang, Z. Li, Z. Zhao, and R. Xing, "Antioxidant activity of different molecular weight sulfated polysaccharides from Ulva pertusa Kjellm (Chlorophyta)," *Journal of Applied Phycology*, vol. 17, no. 6, pp. 527–534, 2005.

[51] M. Zhang, X. Tang, F. Wang, Q. Zhang, and Z. Zhang, "Characterization of Lycium barbarum polysaccharide and its effect on human hepatoma cells," *International Journal of Biological Macromolecules*, vol. 61, pp. 270–275, 2013.

[52] J.-F. Yuan, Z.-Q. Zhang, Z.-C. Fan, and J.-X. Yang, "Antioxidant effects and cytotoxicity of three purified polysaccharides from Ligusticum chuanxiong Hort," *Carbohydrate Polymers*, vol. 74, no. 4, pp. 822–827, 2008.

[53] I. A. Schepetkin, G. Xie, L. N. Kirpotina, R. A. Klein, M. A. Jutila, and M. T. Quinn, "Macrophage immunomodulatory activity of polysaccharides isolated from Opuntia polyacantha," *International Immunopharmacology*, vol. 8, no. 10, pp. 1455–1466, 2008.

[54] S. A. Im, S. T. Oh, S. Song et al., "Identification of optimal molecular size of modified Aloe polysaccharides with maximum immunomodulatory activity," *International Immunopharmacology*, vol. 5, no. 2, pp. 271–279, 2005.

[55] Y. Fan, X. He, S. Zhou, A. Luo, T. He, and Z. Chun, "Composition analysis and antioxidant activity of polysaccharide from Dendrobium denneanum," *International Journal of Biological Macromolecules*, vol. 45, no. 2, pp. 169–173, 2009.

Hindawi
International Journal of Polymer Science
Volume 2018, Article ID 9269154, 7 pages
https://doi.org/10.1155/2018/9269154

Research Article

Mechanism of MCP-1 in Acute Lung Injury and Advanced Therapy by Drug-Loaded Dextrin Nanoparticle

Zheng Cao,[1] Jing-Lan Liu,[2] Shen Wu,[1] and Qiao Wang[1]

[1]*Emergency Department, Shanghai Ninth People's Hospital, School of Medicine, Shanghai Jiao Tong University, Shanghai, China*
[2]*The International Peace Maternity & Child Health Hospital of the China Welfare Institute, Shanghai, China*

Correspondence should be addressed to Qiao Wang; wangqiao1298@126.com

Received 11 July 2018; Revised 7 August 2018; Accepted 15 August 2018; Published 27 September 2018

Academic Editor: Jianxun Ding

Objective. To observe the expression of monocyte chemotactic protein 1 (MCP-1) in acute lung injury (ALI) rat model, to characterize its effect on the development and progression of ALI, and to identify the potential new drug delivery approach during in vivo experiment. *Method*. The effects of different doses of lipopolysaccharide (LPS) on human pulmonary artery endothelial cells (HPAEC) were tested. For the animal experiments, thirty Sprague-Dawley (SD) rats were divided into physiological saline control group (NC group), the LPS model group (L group), the antagonist RS102895 combined with LPS group (R + L group), and the antagonist RS102895-loaded polyaldehyde dextran nanoparticles combined with LPS group (DNPR + L group). The blood gas analysis and dry/wet weight ratio were detected 24 hours after interventions. The levels of inflammatory factors, tumor necrosis factor-α (TNF-α) and interleukin-1β (IL-1β), were tested by ELISA. The expression of monocyte chemoattractant protein-1 (MCP-1) in lung tissues was examined through Western blot, and the change of MCP-1 mRNA expression level was detected by performing RT-PCR. *Result*. LPS was responsible for inducing ALI in rats, and the degree of cell damage was dose-dependent. Blood gas analysis of L group showed that PaO2 and PaO2/FiO2 levels were significantly lower than those of the NC group ($P < 0.05$), while the dry/wet weight ratio of lung tissues in L group increased ($P < 0.05$). Inflammatory factors including TNF-α and IL-1β and the expression of MCP-1 in both protein and mRNA levels were higher in L group than in the NC group ($P < 0.05$). The inhibition of the interaction between MCP-1 and chemokines receptor 2 (CCR2) by antagonist RS102895 can significantly alleviate the ALI in rats, which is accompanied by a significant decrease of inflammatory factors and MCP-1 expression ($P < 0.05$). Compared with R + L group, treatment with DNPR and LPS combination significantly improved the condition of rats and decreased the level of TNF-α, IL-1β, and MCP-1 expression ($P < 0.05$). *Conclusion*. In ALI, RS102895 can inhibit the MCP-1/CCR2 interaction, therefore, retarding the progress of ALI. Because of the high transfection efficiency of inhibitor RS102895packgaed by polyaldehyde dextran nanoparticles, this phenomenon particularly reached a significant level. The results imply new insights for the treatment of ALI.

1. Introduction

Acute lung injury (ALI) and its severe stage, acute respiratory distress syndrome (ARDS), are defined as acute pneumonia and tissue damaged disease. The clinical symptoms include acute hypoxemic respiratory failure, reduced pulmonary compliance, excessive pulmonary inflammation, pulmonary edema, and diffuse alveolar damage due to an imbalance of pulmonary gas exchange and blood flow [1, 2]. ALI is mainly caused by acute inflammations induced by infection, trauma, or gastric acid sucking [3–5]. Up until now, researchers have made great progress in the pathogenesis of ALI and ARDS by proposing various treatments; however, the morbidity and mortality of these diseases remain high [6–8].

The pathogenesis of ALI is very complicated as alveolar macrophages play a key role in the development of ALI. Alveolar macrophage is the most common nonparenchymal cells in lung tissue. Once activated by bacterial or viral infection, macrophages generate and release a large number of inflammatory cytokines and chemokines, at the same time, transport a large number of leukocytes to the lesion [9, 10]. Meanwhile, cell signaling is activated through multilevel

signal transduction with a cascade of inflammatory transcription factors activation, inflammatory cytokines genes overexpression, excessive immune response, and inflammatory response [11]. Chemokines are crucial in leukocyte recruitment, activation, and related functions as well as in the progression of inflammation. Previous work showed dextran sulfate-graft-methotrexate conjugate therapeutic value and targeted the SR-expressed activated macrophages in the treatment of collagen-induced arthritis [12]. On account of the small size, nanoparticles possess greater physical activity, enabling contact between the molecules and target cells, and improving therapeutic efficacy [13, 14]. Self-assembled nanoparticles with chemokine receptor antagonist RS102895 and polyaldehyde dextran were prepared to improve lung injury for this study.

In this study, in vitro HPAEC model is used to study the effect of LPS on cell damage. Then a rat model of LPS-induced ALI was built and evaluated by blood gas analysis. Furthermore, we compared the inhibition efficiency between direct administration and polyaldehyde dextran-coated nanoparticles with antagonist RS102895, expecting to find a better approach to achieve high-efficiency inhibitor delivery with less extra injury. Finally, in this study, we discuss the underlying mechanism of MCP-1 in ALI rat model and provide new therapeutic ideas for the clinical treatment of ALI.

2. Materials and Methods

Cell lines. The culture medium of HPAEC and endothelial cells were purchased from ScienCell (Carlsbad, CA, USA).

(1) Animals. Thirty adult male Sprague-Dawley rats weighing 200–220 g were purchased from Shanghai SLAC Laboratory Animal Co., Ltd (Shanghai, China).

(2) Reagents. DPBS and trypsin were purchased from Gibco (Carlsbad, CA, USA); LPS was purchased from Sigma (St. Louis, MO, USA); CCK-8 ELISA kit was purchased from Beyotime Biotechnology (Shanghai, China); Annexin V-APC/7-AAD kit was purchased from BioLegend (San Diego, CA, USA); TNF-α and IL-1β ELISA kit were purchased from R&D system (Minneapolis MN, USA); MCP-1 antibody was purchased from BioLegend (San Diego, CA, USA); the design and synthesis of MCP-1 mRNA primer were by Invitrogen (Carlsbad, CA, USA); RNA and RNAase H-reverse transcriptase were purchased from Invitrogen (Carlsbad, CA, USA); and RS102895 was purchased from Santa Cruz Biotechnology, Inc. (Santa Cruz, CA, USA). Dextran was purchased from Nobilus, Kutno Company. Sodium periodate was purchased from Sigma-Aldrich Company. Ethylene glycol was purchased from Chempur, Piekary Slaskie Company.

2.1. Cell Treatment. Logarithmic phase HPAEC cells in good conditions were digested and adjusted to a density of 1×10^5 cells per mL with culture media supplemented with 10% fetal bovine serum and 1% penicillin and streptomycin and then were plated 1 mL per well into a 12-well plate. The cells were grown until confluence reached 70%–80% before the LPS treatment. The supernatant of culture media was removed, and the cells were washed once using Dulbecco's phosphate-buffered saline (DPBS). Then cells were divided into control group and experimental groups: experimental groups were treated with different concentrations of LPS solutions (100 ng/mL, 500 ng/mL, and 1 μg/mL), while the control group was treated with culture media. Each treatment was done in triplicate. All groups of cells were cultured in a humidified atmosphere with 5% CO_2 at 37°C.

2.2. Cell Viability. After LPS interventions for 24 h, the supernatant was removed, and the cells were washed twice using DPBS. 1.1 mL CCK-8 working solutions (0.1 mL CCK : 1 mL culture medium) were then added to each well. Culture supernatants were collected 4 hours after incubation and added into a 96-well plate (100 μL per well). Absorbance for collected culture supernatants was measured at 450 nm.

2.3. Apoptosis Assay. The cells were harvested 24 h after LPS treatments, washed twice with binding buffer, and suspended in 500 μL annexin V binding buffer. Following that, the cells were stained with 2 μL Annexin V-APC and 5 μL 7-AAD at room temperature for 10 min protected from light. The stained cells were then subjected to flow cytometry for analysis.

2.4. ALI Model of SD Rats. Thirty SD rats were randomly divided into four groups: (1) normal saline control group (NC group) which rats received intraperitoneal injection of 2 mL/kg saline; (2) LPS group which rats received 10 mg/kg LPS by intraperitoneal injection; (3) antagonist RS102895 combined with LPS (R + L group) which rats received intraperitoneal injection of 2 mL/kg RS102895 and 10 mg/kg LPS injection 24 hours after the antagonist treatment; and (4) the antagonist RS102895-loaded polyaldehyde dextran nanoparticles combined with LPS (DNPR + L group) which rats received intraperitoneal injection with 2 mg/kg RS102895 formulated nanoparticle and LPS (10 mg/kg) injection 24 hours after nanoparticle injection. Rats were sacrificed 24 hours after each intervention, and samples were collected for further use.

2.5. Preparation of RS102895-Loaded NPs. Sodium periodate (2 g) was added to 200 mL of dextran (50 mg/mL dissolved in distilled water). After 1 hour, ethanediol was added to the mixture. Secure the mixture with the dialysis membrane bag and precipitate the distilled water for 3 days and dried for 24 hours after participation. The characteristics of polyaldehyde dextran (PAD) were tested by hydroxylamine hydrochloride method. Dried polyaldehyde dextran (1 g) was dissolved in distilled water (10 mL, 30°C) and mixed with 0.01 g/mL RS102895 solution. After stirred for 30 min, pH was adjusted to 7.4 with sodium hydroxide or hydrochloric acid. The mixture was set for dialysis for 30 min.

2.6. Measurement of Characteristics of RS102895 Formulations. The drug encapsulation efficiency (EE) and loading efficiency (LE) were calculated to characterize the efficiency

of NPs production. LE was defined as the ratio of the mass of RS102895 in NPs to the total mass of NPs, and EE was the percentage of the mass of RS102895 to the mass of the total used RS102895 for NPs preparation. The mass and purity of RS102895 in NPs were evaluated by HPLC (Malvern Instruments, UK). All measurements were performed in triplicate.

2.7. Arterial Blood Gas Analysis. 24 hours after LPS treatments, 0.5 mL blood was drawn from rat celiac artery by 1 mL syringe and used for blood gas analysis.

2.8. Lung Wet/Dry Weight Ratio. After scarifying the rats, the inferior lobe of the right lungs was excised, cleaned, and weighed to obtain wet weight (W). The lungs were then dried in 80°C oven until the weight stayed constant, and the lungs were weighed again to obtain dry weight (D). The W/D ratio was then calculated.

2.9. TNF-α and IL-1β Measurement. The left lung tissues of rats were taken, and bronchoalveolar lavage (BAL) samples were obtained by lavaging the lungs for 1 min for 3 cycles. The lavage fluid was pooled and kept at −20°C for further use. Enzyme-linked immunosorbent assay (ELISA) was performed according to the instructions of TNF-α and IL-1β ELISA kits. The absorbance was measured at 450 nm, and the concentration of proteins was calculated based on their standard curves.

2.10. Western Bolt. The lung tissues of rats in each group were collected, excised, and washed three times with precooled PBS. The tissues were lysed and homogenized. The lysate of tissue was centrifuged, and the top clear supernatant was electrophoresed by SDS-PAGE. The protein strip was then transferred to the PVDF membrane and blocked with 5% skim milk. After blocking, the membrane was washed 5 times for 5 min each using 1X TBST buffer. MCP-1 antibody (1 : 1000 dilution) and β-actin antibody (1 : 1000 dilution) were added to the membrane and incubated at 4°C overnight. After washing 5 times with TBST, a secondary antibody was added at a concentration of 1 : 5000 and incubated for 1 hour at 37°C. ECL developer was applied, and the membrane that was subjected to Quantity One Software was used for data analysis.

2.11. RT-PCR. The mRNA expression of MCP-1 was measured by RT-PCR, and β-actin was included as internal reference. Lung tissues were lysed in Trizol reagent, and then the mixtures were homogenized to ensure complete breakdown of the tissues. The tissue lysates were set still at room temperature for 5 min. Following that, chloroform was added, and the whole mixture was vortexed for 1 min. The mixture was incubated for 3 min at room temperature and then centrifuged at 12000g for 1 min at 4°C. The top clear layer was carefully transferred into a new RNAse free Eppendorf tube, and an equal amount of isopropanol was added to precipitate RNA. The samples were centrifuged for 15 min to participate the RNA pellets. Each pellet was washed once with 75% ethanol, air dried, and then dissolved in RNAse-free water. The concentration and purity of RNA were determined by using Nanodrop. PCR was performed to amplify the cDNA of the target gene. RT-PCR was used to determine the expression of MCP-1 mRNA in each group.

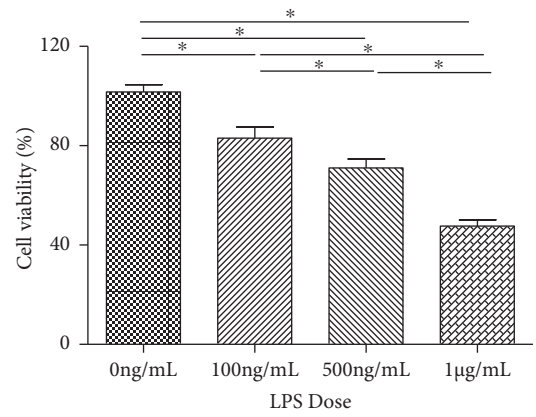

Figure 1: Effects of LPS doses on human pulmonary artery endothelial cell viability.

2.12. Statistical Analysis. SPSS 18 software was used for statistical analysis. Data were presented in mean ± standard deviation format. Between-group comparisons were carried out by one-way analysis of variance (One-way ANOVA). Multiple-group comparisons were conducted by F test. A significant level of each test was set to be $P < 0.05$.

3. Results

3.1. Characterization of NPs. In this study, the LE of nanoparticle was 23.1 ± 7.1%. The EE of RS102895 nanoparticle was 40.4 ± 4.7%. The average size of RS102895 nanoparticle was found to be around 145 ± 32.9 nm.

3.2. Cell Viability. Compared with the control group (0 ng/mL LPS), the HPAEC cell viability significantly decreased in response to the increased dose of LPS interventions. The dosage of LPS interventions was 100 ng/mL, 500 ng/ml, and 1 μg/mL, correspondingly, the cell viabilities were 83 ± 4.58, 71.00 ± 3.61, and 47.67 ± 2.51. The differences among each group were significant ($P < 0.05$) (Figure 1).

3.3. Cell Apoptosis. To further confirm the effect of LPS on cell viability, Annexin V-APC/7-AAD flow cytometry was used to detect cell apoptosis. The percentages of apoptosis were 37.10 ± 1.73 and 46.27 ± 1.55 after 100 ng/ml and 500 ng/ml LPS interventions (Figure 2). The difference between the two groups was statistically significant ($P < 0.05$). With a further increase of LPS dose, the apoptosis percentage increased to 54.60 ± 2.80, which is statistically higher than those of 100 ng/mL and 500 ng/mL ($P < 0.05$).

3.4. Blood Gas Analysis. According to the blood gas analysis data, PaO_2 and PaO_2/FiO_2 of LPS group were lower than those of NC group; the difference between the groups was statistically significant ($P < 0.05$). The PaO_2/FiO_2 of LPS group was less than 300 mmHg, which met the clinical diagnostic standard of ALI. PaO_2 and PaO_2/FiO_2 of group R + L

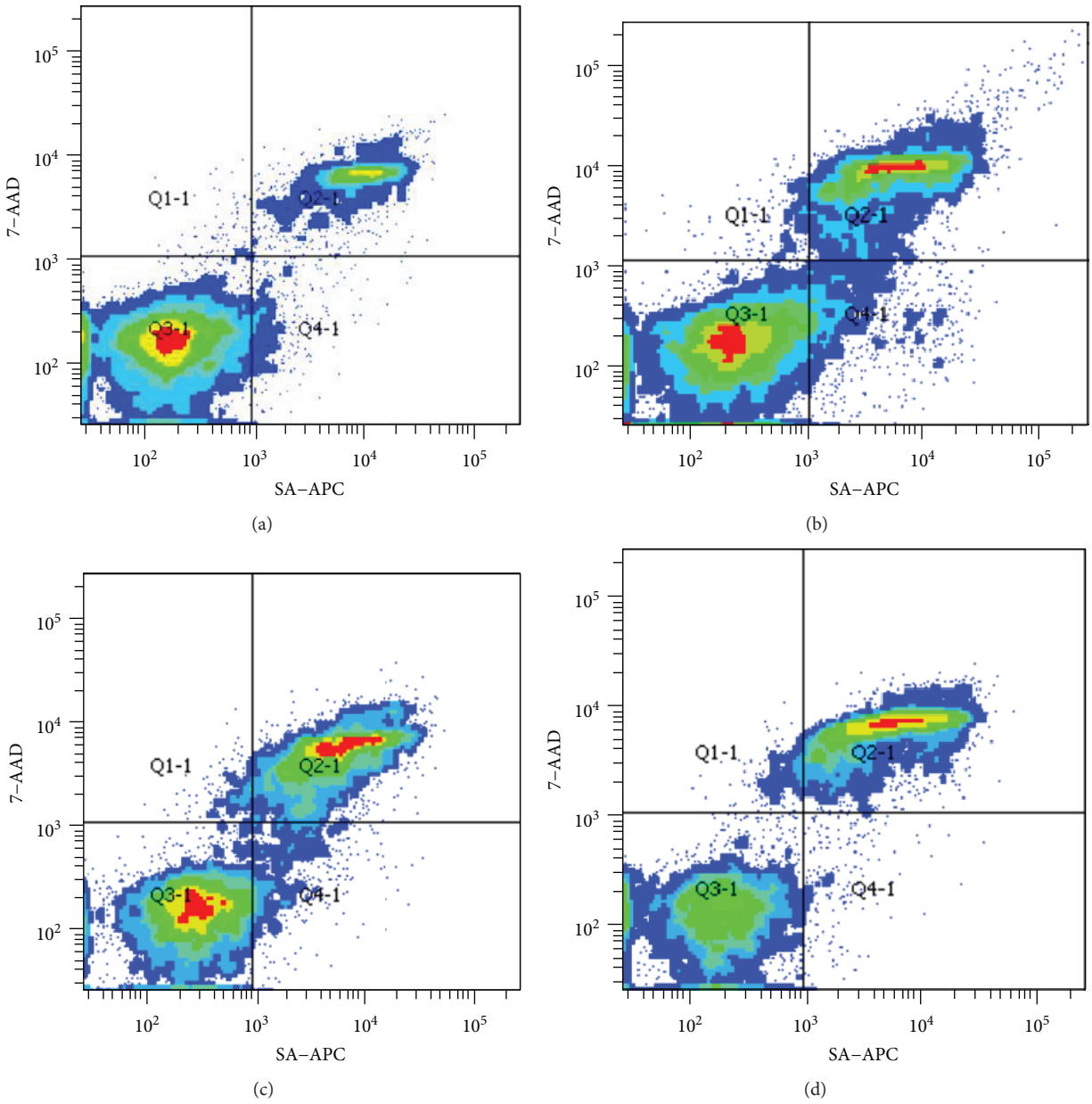

Figure 2: Effects of LPS doses on human pulmonary artery endothelial cell apoptosis. (a) Negative control (LPS 0 ng/mL); the rate of apoptosis of cells without LPS stimulating. (b) The rate of apoptosis of cells with LPS stimulating in 100 ng/mL. (c) The rate of apoptosis of cells with LPS stimulating in 500 ng/mL. (d) The rate of apoptosis of cells with LPS stimulating in 1 μg/mL.

were significantly higher than group L but significantly lower than those of NC group ($P < 0.05$) (Table 1). Compared to group R + L, PaO_2 and PaO_2/FiO_2 of group DNPR + L were significantly lower ($P < 0.05$) (Table 1).

3.5. Lung Wet/Dry Weight Ratio. 24 hours after LPS induced in ALI models, rats in group L were in poor physiological conditions with low activity and poor mental state, while the activities of rats in the NC group were normal. The lung wet/dry weight ratio of LPS group was significantly higher than that of the NC group ($P < 0.05$). The lung wet/dry weight ratio of group R + L was significantly lower than group L but significantly higher than the NC group ($P < 0.05$). The lung wet/dry weight ratio of group DNPR + L was significantly decreased compared to group R + L ($P < 0.05$) (Table 1).

3.6. TNF-α and IL-1β Measurement. The level of TNF-α and IL-1β in BALF were measured by using commercial ELISA kits. The concentrations of TNF-α and IL-1β in BALF significantly increased in the LPS group compared with the NC group ($P < 0.05$). The concentration of TNF-α increased from 61.51 ± 6.22 to 440.34 ± 29.06, while the concentration of IL-1β increased from 45.38 ± 4.55 to 341.19 ± 27.51. Antagonist RS102895 pretreatment remarkably decreased the levels of TNF-α and IL-1β compared to LPS alone group ($P < 0.05$) (Table 2). Concentration levels of TNF-α and

Table 1: Effects of LPS and LPS/CCR2 antagonist interventions on PaO_2, PaO_2/FiO_2, and wet/dry weight ratio in LPS-induce ALI rat models ($\bar{x} \pm s$, $n = 10$).

Group	PaO_2 (mmHg)	PaO_2/FiO_2 (mmHg)	Wet/dry weight ratio
NC group	104.30 ± 7.36	458.70 ± 12.05	4.05 ± 0.15
L group	$61.50 \pm 7.18^{*\#}$	$261.30 \pm 7.07^{*\#}$	$6.02 \pm 0.44^{*\#}$
R + L group	$83.30 \pm 3.83^{*}$	$331.30 \pm 9.87^{*}$	$5.02 \pm 0.33^{*}$
DNPR + L group	$95.78 \pm 4.51^{\#}$	$379.85 \pm 8.19^{\#}$	$4.47 \pm 0.43^{\#}$
F value	114.07	1027.386	90.662
P value	0.000	0.000	0.000

*Compared with NC group ($P < 0.05$); #: compared with R + L group ($P < 0.05$).

Table 2: Effects of LPS and LPS/CCR2 antagonist interventions on TNF-α and IL-1β in LPS-induce ALI rat models by ELISA ($\bar{x} \pm s$, $n = 10$).

Group	TNF-α (pg/mL)	IL-1β (pg/mL)
NC Group	61.51 ± 6.22	45.38 ± 4.55
L Group	$440.34 \pm 29.06^{*\#}$	$341.19 \pm 27.51^{*\#}$
R + L Group	$150.24 \pm 25.55^{*}$	$101.08 \pm 10.61^{*}$
DNPR + L Group	$120 \pm 21.43^{\#}$	$86 \pm 9.47^{\#}$
F value	766.85	833.09
P value	0.000	0.000

*Compared with NC group ($P < 0.05$); #: compared with R + L group ($P < 0.05$).

IL-1β in group DNPR + L were significantly lower than those in group R + L ($P < 0.05$).

3.7. The Expression Level of MCP-1 in Lung Tissue. The expression level of MCP-1 significantly increased in the LPS group compared to the control group ($P < 0.05$). The increase was markedly inhibited by the preinjection of RS102895 ($P < 0.05$). However, the inhibition was not effective enough to counteract the MCP-1 increase induced by LPS posttreatment, as the MCP-1 level was still significantly higher than the control group ($P < 0.05$). The expression of the MCP-1 protein in group DNPR + L was significantly lower than those in group R + L, but the expression of the MCP-1 protein in group DNPR + L was still significantly higher than that in NC ($P < 0.05$, $P < 0.05$, Figure 3).

3.8. MCP-1 mRNA Expression. The expression of MCP-1 mRNA in lung tissue was examined by real-time fluorescence quantitative PCR. Compared with the NC group, MCP-1 mRNA expression in LPS group increased by 9.13 ± 1.15 times, and the difference was statistically significant ($P < 0.05$). Compared with the LPS group, the expression of MCP-1 mRNA in R + L group decreased by 2.55 ± 0.43 times, and the difference was statistically significant ($P < 0.05$). In addition, the expression of MCP-1 mRNA in R + L group was higher than that in the control group, and the difference was statistically significant ($P < 0.05$).

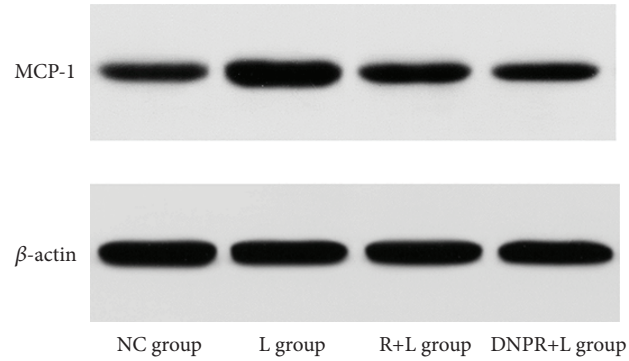

Figure 3: Effects of LPS and LPS/CCR2 antagonist interventions on the expression level of MCP-1 by Western blot. The result of Western blot shows that under LPS stimulating the expression is upregulated, and direct administration of RS102895 can reduce the expression of MCP-1 to some extent but not to the condition without LPS stimulating. Nanoparticles can significantly reduce the MCP-1 expression.

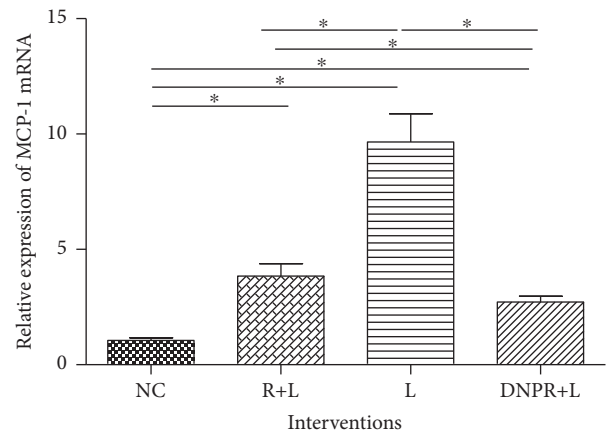

Figure 4: Effects of LPS and LPS/CCR2 antagonist interventions on MCP-1 mRNA expression by quantitative real-time PCR.

Compared to NC, the expression of MCP-1 mRNA in group DNPR + L significantly increased ($P < 0.05$, Figure 4).

4. Discussion

ALI is a disease characterized by acute pneumonia and tissue injury [15]. The incidence of the disease is high and the overall mortality rate amounts to 40% [16]. Bacterial infection is the most common cause of ALI, which may cause lung or systemic inflammation. LPS is the main component of gram-negative bacteria. It is reported that LPS can activate cytokines through a series of cell signal transduction, which promote the release of a large number of inflammatory factors, subsequently induce cell apoptosis, and lead to the occurrence of ALI [17–20]. In this study, in vitro experiments investigated the effects of different doses of LPS (100 ng/mL, 500 ng/mL, and 1 μg/mL) on human pulmonary artery endothelial cells. The experimental results showed that LPS can induce an inflammatory reaction. As the LPS dosage

increased, the cell survival rate decreased gradually along with the apoptosis rate significantly increased ($P < 0.05$).

MCP-1, which belongs to the chemokine family, is a secretory protein that plays an important role in the development of inflammation [21]. Moderate or controlled inflammation is a positive and protective response to multiple injuries, while over or uncontrolled inflammation is harmful and pernicious. Studies have shown that the expression of MCP-1 and MCP-1 mRNA increase significantly when the body suffers chronic and acute inflammations [22, 23]. In addition, the overexpression of MCP-1 can aggravate the occurrence of tissue damage [24]. By binding to its major receptor—CCR2, MCP-1 recruits mononuclear cells, macrophages, and induces cytokine expression [25–27]. MCP-1/CCR2 pathway is reported to be involved in the pathogenesis of cardiovascular diseases, diabetes, transplantation, and cancer [28–30]. Kalnins et al. suggested that interruption of MCP-1/CCR2 interaction is a promising immunosuppressive therapy for heart transplantation in rats [31]. Gibon et al. also proposed that inhibition of the interaction between MCP-1 and CCR2 weakened their cell chemotaxis abilities [32]. Here, our in vivo study also provided evidence that the blockage of this ligand-receptor axis by CCR antagonists not only effectively reduces the levels of inflammatory cytokines but also reduces chemokines, which, overall, attenuates acute lung injury symptoms in LPS-induced ALI rat model. However, during our study, we found out that direct administration of the antagonist RS102895 is not effective enough for treatment. Therefore, we alternated the way for delivering the inhibitor. We polymerize dextran into polyaldehyde dextran and taken this polymer as a vector vehicle to transfer the inhibitor into intracellular space, and with the help of the nanoparticles, the inhibit efficiency raised from 60% to 80%.

However, our results also indicated that the protective effects of MCP-1/CCR2 blockage cannot counteract the effects of LPS challenge evidenced by significant differences between R + L group and NC group. The MCP-1/CCR2 pathway is only one of many pathways in systematic disease such as acute lung injury. LPS is recognized by toll-like receptors on the membrane of antigen-presenting cells, which triggers LPS/TLR/MyD88/IRAK/TRAF/NF-κB signaling pathway [33, 34]. The activation of NF-κB results in more inflammatory cytokines and chemokines such as TNF-α, IL-1β, and MCP-1. If the MCP-1 expression level keeps increasing, more leukocytes would be attracted accompanied by an increase of TNF-α and IL-1β. This loop is endless and overwhelming. Interventions which are able to inhibit LPS/TLR/MyD88/NF-κB signaling pathway must be more effective to prevent the negative consequences.

In conclusion, the MCP-1/CCR2 signaling contributes to the pathogenesis of acute lung injury. In order to test whether MCP-1/CCR2 pathway could be a potential therapeutic target for ALI treatment and molecules interfering with MCP-1/CCR2 interaction could be studied and regarded as a promising ALI therapy, future clinical trials should be taken into consideration. And our method to deliver the inhibitor through self-synthesized nanoparticles may provide a more efficient way for drug delivery. Furthermore, aside from inhibition of MCP-1/CCR2 interaction, inhibition of TLR/MyD88/NF-κB signaling pathway might be a more promising treatment for acute lung injury.

Data Availability

The data used to support the findings of this study are available from the corresponding author upon request.

Ethical Approval

Approval for the present study was obtained by the Ethics Committee of Shanghai Ninth People's Hospital (Shanghai, China).

Consent

All subjects participating in the image acquisition signed the consent form.

Conflicts of Interest

We declare that we have no financial and personal relationships with other people or organizations.

Authors' Contributions

Zheng Cao designed the study and performed the experiments. Qiao Wang analyzed the data. All authors read and approved the manuscript. Qiao Wang was responsible for study conception and design and revised the manuscript; Zheng Cao and Jing-Lan Liu performed the experiments and drafted the manuscript; and Zheng Cao and Shen Wu analyzed the data. All authors read and approved the final manuscript.

Acknowledgments

The article is supported by grant 51673190 from the National Natural Science Foundation of China, and the data and materials used to support the findings of this study are included in the published article.

References

[1] G. D. Rubenfeld, E. Caldwell, E. Peabody et al., "Incidence and outcomes of acute lung injury," *The New England Journal of Medicine*, vol. 353, no. 16, pp. 1685–1693, 2005.

[2] N. B. Yu, "Therapeutic experience of the application of anisodamine on acute lung injury," *Journal of Acute Disease*, vol. 5, no. 5, pp. 382–385, 2016.

[3] G. M. Mutlu and G. R. Budinger, "Incidence and outcomes of acute lung injury," *The New England Journal of Medicine*, vol. 354, no. 4, pp. 416-417, 2006.

[4] P. Toy, O. Gajic, P. Bacchetti et al., "Transfusion-related acute lung injury: incidence and risk factors," *Blood*, vol. 119, no. 7, pp. 1757–1767, 2012.

[5] F. Dias-Freitas, C. Metelo-Coimbra, and R. Roncon-Albuquerque Jr., "Molecular mechanisms underlying hyperoxia acute lung injury," *Respiratory Medicine*, vol. 119, pp. 23–28, 2016.

[6] V. von Dossow-Hanfstingl, "Advances in therapy for acute lung injury," *Anesthesiology Clinics*, vol. 30, no. 4, pp. 629–639, 2012.

[7] S. Guo, Y. Fu, S. Xiong, and J. Lv, "Corilagin protects the acute lung injury by ameliorating the apoptosis pathway," *Biomedicine & Pharmacotherapy*, vol. 95, pp. 1743–1748, 2017.

[8] S. Rajasekaran, D. Pattarayan, P. Rajaguru, P. S. Sudhakar Gandhi, and R. K. Thimmulappa, "MicroRNA regulation of acute lung injury and acute respiratory distress syndrome," *Journal of Cellular Physiology*, vol. 231, no. 10, pp. 2097–2106, 2016.

[9] S. Herold, K. Mayer, and J. Lohmeyer, "Acute lung injury: how macrophages orchestrate resolution of inflammation and tissue repair," *Frontiers in Immunology*, vol. 2, p. 65, 2011.

[10] C. H. Han, P. X. Zhang, and W. W. Liu, "Macrophage polarization is related to the pathogenesis of decompression induced lung injury," *Medical Gas Research*, vol. 7, no. 3, pp. 220–223, 2017.

[11] P. Störmann, T. Lustenberger, B. Relja, I. Marzi, and S. Wutzler, "Role of biomarkers in acute traumatic lung injury," *Injury*, vol. 48, no. 11, pp. 2400–2406, 2017.

[12] M. Yang, J. Ding, X. Feng et al., "Scavenger receptor-mediated targeted treatment of collagen-induced arthritis by dextran sulfate-methotrexate prodrug," *Theranostics*, vol. 7, no. 1, pp. 97–105, 2017.

[13] Y. Zhang, F. Wang, M. Li et al., "Self-stabilized hyaluronate nanogel for intracellular codelivery of doxorubicin and cisplatin to osteosarcoma," *Advanced Science*, vol. 5, no. 5, article 1700821, 2018.

[14] N. Lomis, S. Westfall, L. Farahdel, M. Malhotra, D. Shum-Tim, and S. Prakash, "Human serum albumin nanoparticles for use in cancer drug delivery: process optimization and in vitro characterization," *Nanomaterials*, vol. 6, no. 6, p. 116, 2016.

[15] A. G. Proudfoot, D. F. McAuley, M. J. D. Griffiths, and M. Hind, "Human models of acute lung injury," *Disease Models & Mechanisms*, vol. 4, no. 2, pp. 145–153, 2011.

[16] Y. Cao, Y. Lyu, J. Tang, and Y. Li, "MicroRNAs: novel regulatory molecules in acute lung injury/acute respiratory distress syndrome," *Biomedical Reports*, vol. 4, no. 5, pp. 523–527, 2016.

[17] J. Lei, Y. Wei, P. Song et al., "Cordycepin inhibits LPS-induced acute lung injury by inhibiting inflammation and oxidative stress," *European Journal of Pharmacology*, vol. 818, pp. 110–114, 2018.

[18] N. A. Maniatis, A. Kotanidou, J. D. Catravas, and S. E. Orfanos, "Endothelial pathomechanisms in acute lung injury," *Vascular Pharmacology*, vol. 49, no. 4–6, pp. 119–133, 2008.

[19] Y. L. Wang, X. Y. Guo, W. He, R. J. Chen, and R. Zhuang, "Effects of alliin on LPS-induced acute lung injury by activating PPARγ," *Microbial Pathogenesis*, vol. 110, pp. 375–379, 2017.

[20] G. Deng, H. He, Z. Chen et al., "Lianqinjiedu decoction attenuates LPS-induced inflammation and acute lung injury in rats via TLR4/NF-κB pathway," *Biomedicine & Pharmacotherapy*, vol. 96, pp. 148–152, 2017.

[21] A. Yadav, V. Saini, and S. Arora, "MCP-1: chemoattractant with a role beyond immunity: a review," *Clinica Chimica Acta*, vol. 411, no. 21-22, pp. 1570–1579, 2010.

[22] J. Panee, "Monocyte chemoattractant protein 1 (MCP-1) in obesity and diabetes," *Cytokine*, vol. 60, no. 1, pp. 1–12, 2012.

[23] J. N. Hilda and S. D. Das, "TLR stimulation of human neutrophils lead to increased release of MCP-1, MIP-1α, IL-1β, IL-8 and TNF during tuberculosis," *Human Immunology*, vol. 77, no. 1, pp. 63–67, 2016.

[24] E. A. Boström, E. Kindstedt, R. Sulniute et al., "Increased eotaxin and MCP-1 levels in serum from individuals with periodontitis and in human gingival fibroblasts exposed to pro-inflammatory cytokines," *PLoS One*, vol. 10, no. 8, article e0134608, 2015.

[25] Y. Hu, N. D. Kodithuwakku, L. Zhou et al., "*Levo*-corydalmine alleviates neuropathic cancer pain induced by tumor compression via the CCL2/CCR2 pathway," *Molecules*, vol. 22, no. 6, 2017.

[26] H. Zhang, Y. Li, M. de Carvalho-Barbosa et al., "Dorsal root ganglion infiltration by macrophages contributes to paclitaxel chemotherapy-induced peripheral neuropathy," *The Journal of Pain*, vol. 17, no. 7, pp. 775–786, 2016.

[27] S. Al-Mazidi, M. Alotaibi, T. Nedjadi, A. Chaudhary, M. Alzoghaibi, and L. Djouhri, "Blocking of cytokines signalling attenuates evoked and spontaneous neuropathic pain behaviours in the paclitaxel rat model of chemotherapy-induced neuropathy," *European Journal of Pain*, vol. 22, no. 4, pp. 810–821, 2018.

[28] J. Kalliomäki, B. Jonzon, K. Huizar, M. O'Malley, A. Andersson, and D. M. Simpson, "Evaluation of a novel chemokine receptor 2 (CCR2)-antagonist in painful diabetic polyneuropathy," *Scandinavian Journal of Pain*, vol. 4, no. 2, pp. 77–83, 2013.

[29] Y. He, X. Xu, T. Zhu, M. Tang, J. Mei, and Y. Si, "Resident arterial cells and circulating bone marrow-derived cells both contribute to intimal hyperplasia in a rat allograft carotid transplantation model," *Cellular Physiology and Biochemistry*, vol. 42, no. 4, pp. 1303–1312, 2017.

[30] Y. Wang, H. Ni, H. Li et al., "Nuclear factor kappa B regulated monocyte chemoattractant protein-1/chemokine CC motif receptor-2 expressing in spinal cord contributes to the maintenance of cancer-induced bone pain in rats," *Molecular Pain*, vol. 14, 2018.

[31] A. Kalnins, M. N. Thomas, M. Andrassy et al., "Spiegelmer inhibition of MCP-1/CCR2 – potential as an adjunct immunosuppressive therapy in transplantation," *Scandinavian Journal of Immunology*, vol. 82, no. 2, pp. 102–109, 2015.

[32] E. Gibon, T. Ma, P. G. Ren et al., "Selective inhibition of the MCP-1-CCR2 ligand-receptor axis decreases systemic trafficking of macrophages in the presence of UHMWPE particles," *Journal of Orthopaedic Research*, vol. 30, no. 4, pp. 547–553, 2012.

[33] Y. Luo, W. Che, and M. Zhao, "Ulinastatin post-treatment attenuates lipopolysaccharide-induced acute lung injury in rats and human alveolar epithelial cells," *International Journal of Molecular Medicine*, vol. 39, no. 2, pp. 297–306, 2017.

[34] X. Ding, S. Jin, Y. Tong et al., "TLR4 signaling induces TLR3 up-regulation in alveolar macrophages during acute lung injury," *Scientific Reports*, vol. 7, no. 1, article 34278, 2017.

Hindawi
International Journal of Polymer Science
Volume 2018, Article ID 3592843, 12 pages
https://doi.org/10.1155/2018/3592843

Research Article

Comparison of Rheological, Drug Release, and Mucoadhesive Characteristics upon Storage between Hydrogels with Unmodified or Beta-Glycerophosphate-Crosslinked Chitosan

Emilia Szymańska, Anna Czajkowska-Kośnik, and Katarzyna Winnicka

Department of Pharmaceutical Technology, Faculty of Pharmacy, Medical University of Białystok, Mickiewicza 2c, Białystok 15-222, Poland

Correspondence should be addressed to Emilia Szymańska; esz@umb.edu.pl

Received 19 April 2018; Revised 25 July 2018; Accepted 15 August 2018; Published 19 September 2018

Academic Editor: Mingqiang Li

The physicochemical characteristics of beta-glycerophosphate-crosslinked chitosan hydrogels were investigated upon long-term storage at ambient, accelerated, and refrigerated conditions and compared to unmodified chitosan formulations. Additionally, the impact of chitosan modification on the ex vivo mucoadhesive performance in contact with porcine vaginal mucosa and on the drug release profile from hydrogels was evaluated. Viscosity and mechanical properties of formulations with unmodified chitosan decreased significantly upon storage regardless of tested conditions as a result of hydrolytic depolymerization. Introduction of ion crosslinker exerted stabilizing effect on physicochemical performance of chitosan hydrogels but only upon storage at refrigerated conditions. Beta-glycerophosphate-modified chitosan formulations preserved organoleptic, rheological behavior, and hydrogel structure up to 3-month storage at $4 \pm 2^{\circ}$C. Viscosity variations upon storage influenced markedly mucoadhesive properties and drug release rate from hydrogels.

1. Introduction

Application of multifunctional polymers as effective excipients in drug delivery systems is a current and attractive concept in pharmaceutical technology [1]. Among various polymer materials, chitosan (CS)—an abundantly accessible polysaccharide, owing to its biodegradability and biocompatibility is extensively investigated for a number of pharmaceutical and medical applications, comprising prolonged drug release delivery systems [2], wound dressings [3], cartilage and bone tissue engineering scaffolds [4, 5], nanocarriers for gene delivery [6], or vaccine adjuvants [7].

CS is commercially possessed by deacetylation of chitin derived mainly from the exoskeleton of crustaceans, though alternative production methods by fungal fermentation have been also explored to provide CS with more defined characteristics [8]. Due to polycationic behavior, CS structure can be certainly modified and utilized into diverse semisolid or solid vehicles. Hence, CS may be regarded to be a promising tool not only in pharmaceutical [9] but also in cosmetic [10] or food industry [11].

CS displays mucoadhesive potential enabling interaction with mucin via electrostatic or hydrogen bonding. Mucoadhesiveness, providing an intimate contact between CS-based dosage form and mucosal tissue, appears to be beneficial, especially in terms of CS application in technology of drug carriers for local: nasal [12], ocular [2], buccal [13], or vaginal delivery [14]. Additionally, with regard to capability of swelling and creating hydrogel matrix, CS may be useful in the development of modified release delivery systems [15, 16]. In recent years, particular attention has been directed to the use of CS as an antimicrobial adjunctive [17, 18]. This capability of increasing the pharmacological action of an antimicrobial agent provides the opportunity for combination therapy in which CS acts as the effective excipient and simultaneously as an active part of the treatment.

Regarding abovementioned advantages of CS, experimental research was conducted to investigate CS usability as pharmaceutical excipient in technology of vaginal hydrogels for the treatment of mycotic vaginosis. Designed semisolid platforms displayed favorable ability to interact with porcine vaginal mucosa confirmed in ex vivo studies followed with enhanced anti-*Candida* activity compared to commercially available preparation with clotrimazole [19, 20]. Nonetheless, because of fast and uncontrollable disintegration in an acidic environment and poor rheological behavior with regard to vaginal administration, further improvement of CS structure was needed. Previously presented data showed that CS crosslinked with beta-glycerophosphate disodium (bGP) demonstrated a promising potential for the development of mucoadhesive hydrogels with feasible rheological and mechanical properties [20].

Even though CS is regarded as a multifunctional compound in the technology of drug carriers, only a limited number of pharmaceutical products with CS (apart from hemostatic dressings, products for wound healing, or nutraceuticals) are commercially available. One of the main drawbacks, limiting the application of CS in pharmaceutical technology, is its susceptibility to environmental conditions (especially with regard to humidity and temperature) as well as processing factors, which in consequence might impact the physicochemical and pharmaceutical performance of polymer's dosage form upon storage [21]. According to the literature, modification of CS structure via grafting, chemical, or ionic crosslinking may overcome the problems of reduced long-term stability of polymer-based drug delivery systems [22–24]. Since, to our best knowledge, only limited number of studies have been devoted to the issue of long-term stability data of CS-based dosage forms, therefore, the goal of the current paper was to examine the influence of crosslinking with bGP on the physicochemical performance of CS hydrogels with a model antifungal agent upon storage. Designed semisolid platforms with bGP/CS were characterized by organoleptic, rheological, mucoadhesive properties and compared to unmodified CS-based hydrogels. The impact of CS modification on the drug release profile from hydrogels upon storage was also examined.

2. Materials and Methods

2.1. Materials. High-quality medium molecular weight CS (200–400 kDa; viscosity 370–390 mPa·s at 25°C, 1% (*w*/*w*) in 1% (*v*/*v*) acetic acid) with deacetylation degree 80% was obtained from Heppe Medical CS GmbH (Haale, Germany). Clotrimazole was a gift from Ziaja Ltd. (Gdańsk, Poland). bGP disodium salt hydrate and Cremophor EL were obtained from Sigma–Aldrich (Steinheim, Germany). Acetic acid 80%, glycerolum 85%, disodium hydrogen phosphate, potassium dihydrogen phosphate, sodium acetate, and sodium hydroxide were purchased from Chempur (Piekary Śląskie, Poland). Methanol (HPLC grade) was purchased from Merck (Darmstadt, Germany). Vaginal mucoadhesive gel Replens™ was acquired from APC Instytut Sp. z o.o. (Warsaw, Poland). Water for HPLC was distilled and passed through a reverse osmosis system Milli Q Reagent Water System (Billerica, MA, USA).

2.2. Experimental Procedure

2.2.1. Hydrogels with Unmodified or bGP-Crosslinked CS. Hydrogels with clotrimazole were prepared using mechanical stirrer according to the previously described technique [20]. Briefly, CS base with concentration of 3% or 4% (*w*/*w*) was obtained by dissolving proper amount of polymer in a gently heated acetic acid solution (the weight ratio CS : glacial acetic acid was 0.6 : 1.0) [25] and stirred until homogenous mixtures appeared. To prepare bGP-modified CS hydrogels, the appropriate amount (necessary to simulate vaginal pH 4.5) of cold 45% (*w*/*w*) aqueous solution of bGP (the weight ratio CS to bGP 1 : 0.63) was added dropwise to the cold CS base with continuous agitation. Subsequently, suitable amount of unmodified CS or bGP/CS base was carefully added to a mixture of humectant, preservative, and clotrimazole solubilized in Cremophor EL to obtain uniform dispersion of drug in the hydrogel matrix. Hydrogels' composition is displayed in Table 1.

2.2.2. Long-Term Evaluation of Hydrogels. Hydrogel formulations were subjected to long-term stability studies under defined conditions of humidity and temperature according to ICH guideline [26]. Briefly, hydrogels closed in sealed polyethylene containers and additionally in cardboard packages to prevent from light exposure were kept in humidity chambers (CTC 256 Memmert GmbH, Schwabach, Germany) maintained at 25± 2°C/60 ± 5% relative humidity (RH) and 40± 2°C/70 ± 5% RH as well as in the refrigerator at 4 ± 2°C. At specific time intervals (displayed in Table 2), macroscopic performance, pH and viscosity values, drug particle's diameter, and drug content uniformity followed with mechanical and mucoadhesive performance were evaluated. Formulations were maintained for at least 1 h at ambient temperature prior analysis.

(1) Macroscopic and Microscopic Analysis. Organoleptic analysis in terms of consistency, odor, and color was performed in accordance to the European Pharmacopoeia (Eur. Ph.) by placing hydrogel in a thin layer on a glass slide [27].

Particles size analysis was accomplished using an optical microscope Motic BA 400 (Moticon, Wetzlar, Germany) with magnifications 100x and 400x. Concisely, 0.5 mg of each formulation (corresponding to 10 μg of clotrimazole) was located on a glass slide and the longest dimension from edge to edge of drug particles was defined for particles present in at least three areas of observation [28].

(2) Viscosity Measurement. The apparent viscosity was measured according to Eur. Ph. [27] using a digital rotational Brookfield RVDV-III ULTRA Viscometer (Brookfield Engineering Laboratories, Germany) at ambient temperature. Each hydrogel sample (0.5 g) was placed in the thermostated sampler holder of the viscometer, allowed to equilibrate for 10 min at 25± 1°C, and then C-52 spindle was lowered into

Table 1: Composition of hydrogels with unmodified CS (F1, F2) or bGP-crosslinked CS (F3, F4).

Ingredient (g)	Category	Hydrogel with			
		Unmodified CS		bGP-modified CS	
		F1	F2	F3	F4
CS	Gelling agent	3.0	4.0	3.0	4.0
bGP 45% (*w*/*w*)	Ion crosslinker	—	—	4.2	5.6
Clotrimazole	API	2.0	2.0	2.0	2.0
Glycerolum	Humectant	5.0	5.0	5.0	5.0
Cremophor EL	Solubilizer	6.0	6.0	6.0	6.0
D-Glucono-1,5-lactone and sodium benzoate	Preservative	1.0	1.0	1.0	1.0
Acetic acid	Vehicle	Up to 100.0	Up to 100.0	Up to 100.0	Up to 100.0

Table 2: Time intervals applied for stability studies [26].

Stability studies	Storage conditions	The minimum period of storage	Time intervals (months)
Long term	25 ± 2°C/60 ± 5% RH	12 months	1, 3, 6, 12
	4 ± 2°C	6 months	1, 3, 6
Accelerated	40± 2°C/75 ± 5% RH	6 months	1, 3, 6

the sample. The shear rate was 6/s. Each experiment was performed at least three times.

(3) pH Determination. The pH of hydrogels was estimated by a glass electrode of the pH meter Orion-3 Star (Thermo Scientific, Waltham, MA, USA) in triplicate.

(4) Drug Content Uniformity. Drug content uniformity was evaluated after the extraction of hydrogel samples with absolute ethanol, centrifugation at 4000 rpm for 20 min, and filtration through 0.45 μm nylon filters. Samples were next suitably diluted with mobile phase and determined for clotrimazole content by HPLC method according to [19]. Separations were performed at ambient temperature on 5 μm Zorbax Eclipse XDB–C18 (4.6 mm × 150 mm) column (Agilent, Waldbronn, Germany). The mobile phase consisted of methanol-phosphate buffer pH 7.4 (4 : 1, *v*/*v*), the flow rate was 1.0 mL/min, and the retention time was 5.3 min. The detector was set to 210 nm. The standard calibration curve was linear over the range of 1 to 100 μg/mL ($R^2 = 0.995$).

(5) Mechanical Properties. Mechanical properties were evaluated using Texture Analyser TA.XT Plus (Stable Micro System, UK) equipped with a backward extrusion measuring system A/BE (25 mm diameter). Each preparation (30.0 ± 0.2 g) was located in a measuring vessel, and then a disc was compressed with a speed of 2 mm/s into the sample to a defined depth of 5 mm. The experimental parameters were established during preliminary study. All measurements were carried out at 25 ± 2°C. From the force-time curves, the values of consistency were calculated and the hardness parameter was recorded using Texture Exponent 32 software. Each experiment was carried out at least three times.

(6) Ex Vivo Mucoadhesive Properties. Ex vivo mucoadhesive behavior of hydrogels in contact with porcine vaginal mucosa was evaluated according to a method defined previously [15] with using Texture Analyser TA.XT. Plus (Stable Micro Systems, Godalming, UK) equipped with the measuring system A/GMP. Briefly, freshly excised porcine vaginal mucosa was adhered by double-sided tape to the platform below the texture analyzer probe whilst hydrogel sample (1.5 mL) was set on the upper probe and secured with the attached support collar. The experiments were conducted at 37 ± 1°C. Prior to analysis, the support collar was removed and the probe was lowered onto the surface of the porcine vaginal mucosa with a speed of 0.5 mm/s. After keeping a contact time for 180 s with contact force 0.5 N, the surfaces were separated at a constant rate of 0.1 mm/s. The maximum detachment force (F_{max}) as a function of displacement was recorded directly from Texture Exponent 32 software, and the work of adhesion (W_{ad}) was calculated from the area under the force vs. distance curve. Each experiment was performed six times.

(7) In Vitro Drug Release Studies. Due to unfavorable organoleptic and rheological changes observed for hydrogels upon their storage at ambient and accelerated conditions, in vitro dissolution studies were performed only for formulations with preserved rheological and mechanical behavior upon 6-month storage at 4 ± 2°C. Drug release was measured through natural cellulose membrane (Cuprophan with MWCO 10000 Da, Medicell, London, UK) using an Enhancer cell (Agilent Technologies, Cary, USA) [29] and USP dissolution Apparatus II (Agilent 708-DS, Agilent Technologies, Cary, USA). Each formulation (1.0 g) was placed in the drug reservoir on the top of the membrane making certain that no entrapped air was present at the interface of the dosage form and the membrane (diffusion area 3.80 cm^2). The dissolution medium was 100 mL acetic buffer (pH 4.5) with addition of 1% surfactant to retain sink conditions. The temperature of medium was maintained at 37 ± 1°C, and a stirring rate was 75 rpm. Samples (2 mL) were withdrawn at the predetermined time points, filtered through 0.45 μm CA paper filters, diluted with mobile phase, and

quantified using HPLC method. Withdrawn samples were replaced with equal volume of fresh medium. All release experiments were carried out in triplicate.

2.3. Statistical Analysis. Quantitative variables were expressed as the mean ± standard deviation (SD) or the median by using MS Excel software. A statistical analysis of mucoadhesive measurements was accomplished using a nonparametric Kruskal–Wallis test, with the Statistica 12.0 software. Measurements were considered significant at $p < 0.05$.

3. Results and Discussion

3.1. Characterization of Hydrogels upon Storage. Stability evaluation provides the critical characteristics of the drug dosage form in terms of its physicochemical or biopharmaceutical properties, and thus it is crucial for the full assessment of product quality during preformulation analysis. Basically, for drug products, a comparative stability data in both long term (at 25°C/60% RH for 12 months) and accelerated conditions (40°C/75% RH) is required to define an acceptable product shelf-life [26]. Given these premises, the effect of ion crosslinking on CS hydrogel physicochemical characteristics upon storage at 25°C/60% RH and 40°C/75% RH was studied. Regarding the fact that CS is recommended to store at low temperatures (2–8°C) [27], additional examination of formulations upon storage at 4 ± 2°C was also provided.

Directly after preparation, all hydrogels possessed smooth, uniform consistency and off-white color resulting from the presence of suspended clotrimazole (Figure S1). Significant organoleptic differences were noticed upon first months of storage at ambient conditions. Hydrogels with unmodified CS (F1, F2) became yellowish within one month at 25°C/60% RH, and the color alterations were deepened over time. After 3-month storage, loss of gel structure and homogeneity of formulations F1 and F2 was observed. It should be noted that hydrogels with bGP-modified CS (F3 and F4) remained stable in terms of organoleptic properties within 3-month storage. Nonetheless, upon 6-month storage at 25°C/60% RH, a substantial liquidation with visible drug particle sedimentation and simultaneous color changes occurred in all examined hydrogels (Figure S2).

The most profound and particularly fast alterations in hydrogel performance appeared upon their storage at 40°C/75% RH. When hydrogels with unmodified chitosan (F1 and F2) were subjected to accelerated stability studies, loss of homogeneity follow with color changes and drug particle sedimentation occurred just upon 1-month storage period. Regarding formulations with bGP/CS (F3 and F4), a significant enhancement in the structure stiffness was observed over time and after 3 months at 40°C/75% RH, hydrogels transformed into brown solid state formulations (Figure S3). The observed time-delayed sol/gel transition was probably attributed to thermosensitivity of CS in the presence of ion crosslinker, which affected the time and the temperature of CS gelling [30].

Notably, all hydrogel formulations remained organoleptically stable up to 3 months at refrigerated conditions. Upon their 6-month storage at 4 ± 2°C, no alterations in bGP/CS hydrogels' appearance were observed whereas substantial changes in consistency with simultaneous drug particle sedimentation in hydrogels with unmodified CS (F1 and F2) occurred (Figure S4).

The microscopic analysis of all investigated formulations revealed no considerable change in average particle size of suspended clotrimazole upon storage at refrigerated conditions although the presence of few aggregates of drug particles was observed in hydrogels F1 and F2 (Figure 1).

Due to the presence of undesirable changes in hydrogels' organoleptic properties followed with loss of their homogeneity upon 3-month and 6-month storage at accelerated or ambient conditions (Figures S2 and S3), respectively, formulations F1–F4 were excluded from further long-term analysis. Evaluation of drug content uniformity was performed for these hydrogel formulations, which preserved their viscosity and organoleptic properties upon storage. As it is presented in Table 3, clotrimazole was found to be chemically stable in hydrogels F1 and F2 upon 3-month storage at ambient and refrigerated conditions and upon 1-month at 40°C/75% RH. Regarding bGP/CS hydrogels, the drug content was found to be uniform and was within acceptable USP limit 90%–110% after storage in all investigated storage conditions [31].

A slight increase in pH values of hydrogels F1 and F2 was observed after 3-month storage at 40°C/75% RH and 6-month at 25°C/60% RH in contrast to formulations F3 and F4, which displayed decreasing pH trend upon storage regardless of temperature conditions (Table 3). Nonetheless, at the end of the stability studies, all hydrogels displayed the pH values below 4.5, which was maintained within the physiological range 3.5–4.9 [32].

3.2. Viscosity and Mechanical Measurements. To assess the influence of ion crosslinking on the rheological behavior of CS hydrogels upon storage, the viscosity measurements were performed. The intrinsic viscosity of CS defines the ability to form viscous solution and is proportional to the polymer average molecular weight [33]. Figure 2 displays the viscosity variations upon storage at different conditions.

Freshly prepared hydrogels F3 and F4 displayed lower viscosities compared to unmodified CS formulations (F1 and F2) most likely as a consequence of greater ionic strength resulted from the introduction of bGP. All formulations exhibited non-Newtonian pseudoplastic behavior, and the presence of bGP improved thixotropic properties of CS hydrogels [20].

It can be seen that viscosity of hydrogels with unmodified CS (F1 and F2) decreased significantly over time regardless of tested conditions. Formulation F2, with higher concentration of CS, displayed more profound viscosity variations and loss of more than 40%, 50%, and 90% of the initial value after 3-month storage at 4 ± 2°C, 25°C/60%RH, and 40°C/75% RH was observed, respectively. Similarly, Chattopadhyay and Inamdar observed the impact of CS concentration on the viscosity of polymer solution over storage [34]. Interestingly, the presence of ion crosslinker exerted stabilizing effect on CS hydrogels' viscosity but only upon their storage at

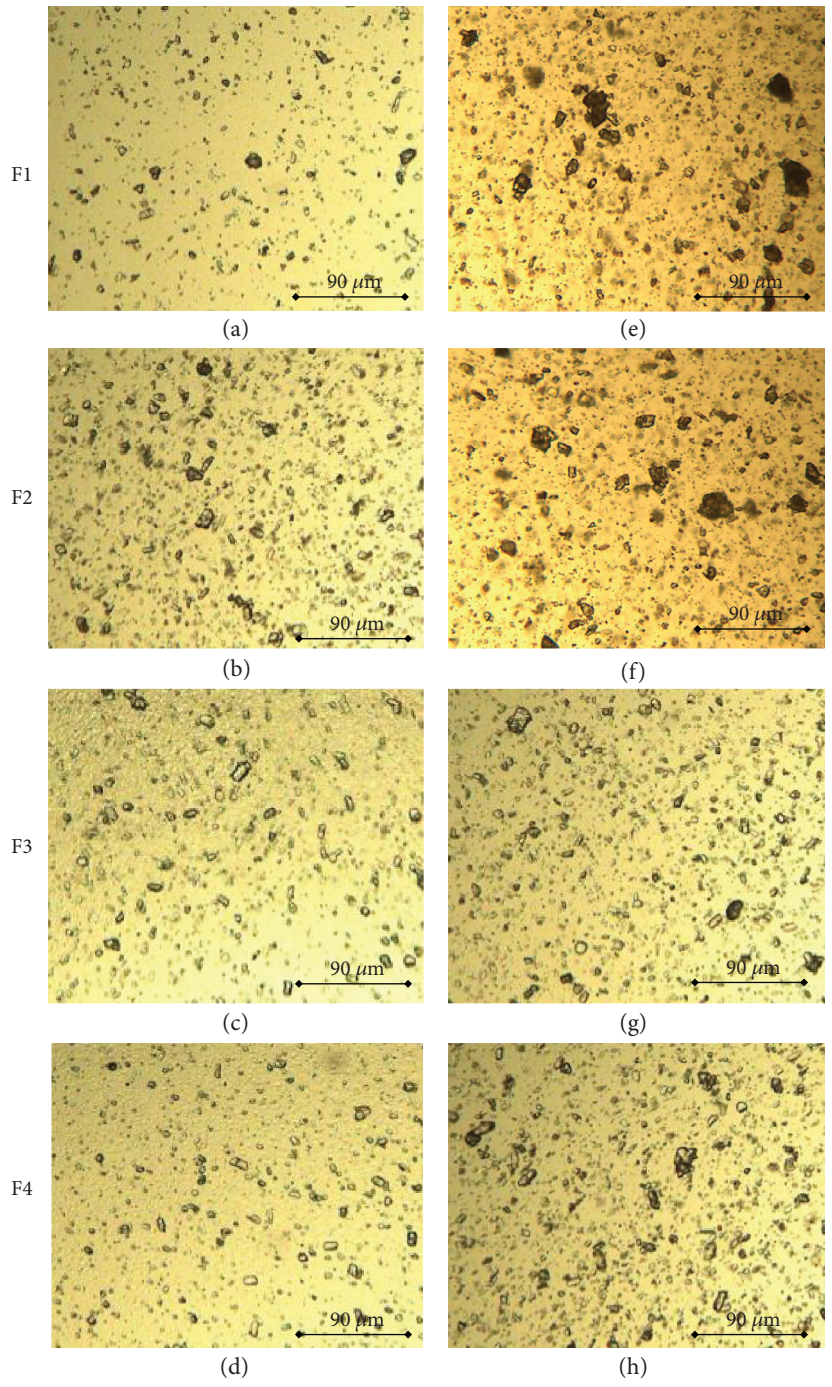

Figure 1: The optical images of hydrogels with unmodified CS (F1, F2) or with bGP-crosslinked CS (F3, F4) after preparation (a–d) and upon 3-month (F1, F2) (e–f) or 6-month storage (g–h) at refrigerated conditions (F3, F4).

refrigerated conditions. After 3 months at $4 \pm 2^{\circ}$C, hydrogels F3 and F4 displayed comparable viscosity values to those obtained for freshly prepared formulations (Figure 2(c)). Nonetheless, after a period of 6 months, a drop of more than 15% and 25% in viscosity parameter of formulations F3 and F4 was noticed, respectively. In contrast, profound viscosity variations of bGP/CS hydrogels were noticed upon their storage at ambient and accelerated conditions. An increase in viscosity values and solidification of formulations F3 and F4 was obtained within a period of 3 months at 40°C/75% RH (Figure 2(b)). Conversely, a slight decrease in viscosity parameter upon their 3-month storage at 25°C/60% RH was noticed and after 6 months, a significant drop in viscosity of bGP/CS hydrogels (approximately 40% of the initial value) was recorded.

The substantial viscosity alterations observed particularly in hydrogels with unmodified CS may be attributed to partial degradation of CS in organic acid solution [33, 35, 36]. In

Table 3: Changes in organoleptic properties, clotrimazole content, and drug particle size in hydrogels with unmodified CS (F1, F2) or with bGP-crosslinked CS (F3, F4) upon storage compared to values obtained to freshly prepared formulations.

Storage time (months)	Parameter	Hydrogel with Unmodified CS		Hydrogel with bGP-crosslinked CS	
		F1	F2	F3	F4
	pH	4.06 ± 0.02	4.08 ± 0.01	4.54 ± 0.04	4.56 ± 0.03
0	Particle size range (μm)	6.0–49.5	6.0–47.0	4.0–40.0	4.0–41.5
	Drug content (%)*	95.6 ± 4.9	98.2 ± 3.5	97.3 ± 4.1	97.4 ± 3.3
25°C/60% RH					
	pH*	4.16 ± 0.05	4.23 ± 0.05	4.51 ± 0.04	4.53 ± 0.02
1	Particle size range (μm)	7.5–52.5	7.5–57.0	6.0–29.5	5.0–48.5
	Drug content (%)*	94.8 ± 3.3	96.1 ± 4.2	96.5 ± 3.5	97.1 ± 3.9
	pH*	4.40 ± 0.02	4.38 ± 0.03	4.35 ± 0.02	4.27 ± 0.03
3	Particle size range (μm)	7.0–58.0	6.0–54.5	4.0–41.0	4.0–34.5
	Drug content (%)*	94.6 ± 5.9	92.4 ± 5.1	98.1 ± 4.1	95.2 ± 4.5
	pH*	4.31 ± 0.02	4.39 ± 0.01	4.26 ± 0.02	4.23 ± 0.02
6	Particle size range (μm)	*n.d.*	*n.d.*	*Sedimentation*	*Sedimentation*
	Drug content (%)*	*n.d.*	*n.d.*	*n.d.*	*n.d.*
40°C/75% RH					
	pH*	4.20 ± 0.03	4.24 ± 0.05	4.56 ± 0.04	4.51 ± 0.02
1	Particle size diameter (μm)	*Sedimentation*	*Sedimentation*	10.0–53.0	5.0–61.0
	Drug content (%)*	*n.d.*	*n.d.*	96.5 ± 3.5	97.1 ± 3.9
	pH*	4.40 ± 0.02	4.48 ± 0.02	4.36 ± 0.01	4.29 ± 0.03
3	Particle size range (μm)	*n.d.*	*n.d.*	5.0–44.5	4.5–37.0
	Drug content (%)*	*n.d.*	*n.d.*	93.1 ± 7.1	94.2 ± 6.8
4 ± 2°C					
	pH*	4.10 ± 0.05	4.03 ± 0.05	4.56 ± 0.04	4.53 ± 0.02
1	Particle size range (μm)	12.0–58.5	7.5–65.0	8.0–59.0	10.5–45.0
	Drug content (%)*	94.3 ± 3.8	96.1 ± 4.2	96.5 ± 3.5	97.1 ± 3.9
	pH*	4.10 ± 0.02	4.12 ± 0.02	4.31 ± 0.02	4.37 ± 0.03
3	Particle size range (μm)	*Sedimentation*	6.0–59.5	11.0–40.0	5.0–45.5
	Drug content (%)*	*n.d.*	95.1 ± 8.4	98.1 ± 4.7	95.2 ± 4.5
	pH*	4.23 ± 0.03	4.29 ± 0.03	4.28 ± 0.03	4.37 ± 0.01
6	Particle size range (μm)	*n.d.*	*n.d.*	6.5–46.0	5.0–40.0
	Drug content (%)*	*n.d.*	*n.d.*	94.1 ± 4.9	96.0 ± 3.7

*$n = 3$, mean ± SD; n.d.: not determined.

overall, storage temperature and CS concentration were found to accelerate the rate of hydrolysis of unmodified CS [33, 34]. Our findings from stability analysis at refrigerated conditions are in the agreement with studies accomplished by Nguyen et al., which revealed that the ratio of CS decomposition in acetic acid environment could be reduced upon storage at 4 ± 2°C [35]. In contrast, Ruel-Gariépy et al. observed poor stability of bGP/CS thermogelling solutions below room temperature as gelation of the systems occurred upon 3-month storage at refrigerated conditions [37]. Similarly, Supper et al. indicated that the CS/bGP thermogelling solutions intended for parenteral administration possessed reduced physicochemical stability both under ambient and refrigerated conditions [38]. Nonetheless, in the present studies, much higher CS concentration was used for hydrogel preparation (3-4%) as compared to the abovementioned studies, and it could be regarded as one of the factor improving hydrogel stability. In addition, the ability of bGP to balance the effect of the presence of acetic acid solution might have slowed down the rate of CS degradation and in consequence maintained the viscosity parameters over storage.

To assess deeper insight into the internal structure of prepared hydrogels upon their storage, the mechanical properties: hardness and consistency—parameters reflecting the degree of difficulty in loss of initial formulations' structure,

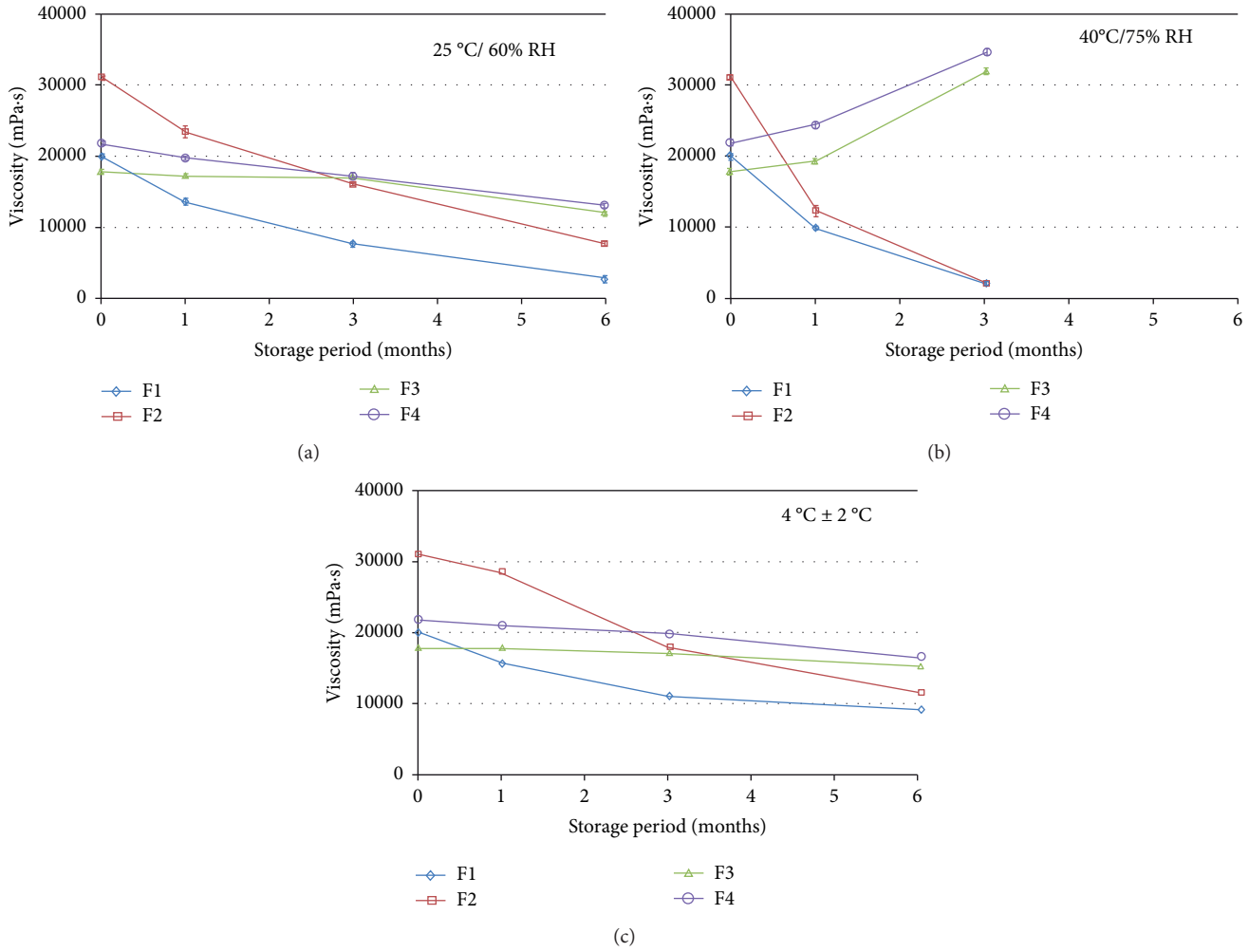

Figure 2: Variations in viscosity values of hydrogels with unmodified CS (F1, F2) or with bGP-crosslinked CS (F3, F4) upon storage at ambient (a), accelerated (b), and refrigerated conditions (c); $n = 3$, mean ± SD.

were examined (Figures 3(a)–3(f)). A correlation between investigated mechanical performance and hydrogel viscosity was displayed (Figure 2).

Noticeable drop in hardness and consistency values upon storage in all tested conditions was observed for hydrogels with unmodified CS (F1 and F2). Hydrogels with bGP/CS preserved their mechanical properties upon storage at 4 ± 2°C up to 6 months. However, differences in structural behavior were recorded when formulations F3 and F4 were subjected to stability studies under accelerated and ambient conditions. Loss of bGP/CS hydrogels' hardness (more than 30% of the initial values) was noticed upon 6-month storage at 25°C/60% RH whereas substantially thicker and firmer structure of formulations F3 and F4 after 3 months at 40°C/75% RH was observed.

3.3. Mucoadhesion Studies. Mucoadhesive tests were conducted for all hydrogel formulations stored for up to six months and displayed in Figure 4. Because of profound loss of homogeneity followed with a major drop in viscosity values (which hinder the ability to maintain in a support collar of mucoadhesive probe), formulations F1 and F2 were excluded from mucoadhesive measurements at accelerated conditions as well as upon 3- and 6-month storage at ambient and refrigerated conditions, correspondingly.

Results obtained from ex vivo mucoadhesive measurements upon storage clearly displayed that the ability to adhere to porcine vaginal mucosa differed significantly between unmodified and ion-crosslinked CS formulations. bGP/CS hydrogels stored at 4 ± 2°C exhibited comparable mucoadhesive behavior compared to freshly prepared formulations within 3-month storage. However, after 6 months, a decrease in ability to adhere to porcine vaginal mucosa of bGP/CS hydrogels was noticed. Similarly, upon storage at ambient conditions, formulations with bGP/CS (F3 and F4) tended to lose their mucoadhesive properties after a period of 3 months. In contrast, a significant drop in F_{max} and W_{ad} values ($p < 0.05$) of formulations with unmodified CS (F1 and F2) was recorded just after 1-month storage at 4 ± 2°C and 25°C/60% RH (Figure 4). The observed variations in mucoadhesive performance were most likely influenced by changes in viscosity and mechanical properties of CS hydrogels during storage. Sufficiently high viscosity and preserved hydrogel structure appear to be crucial for

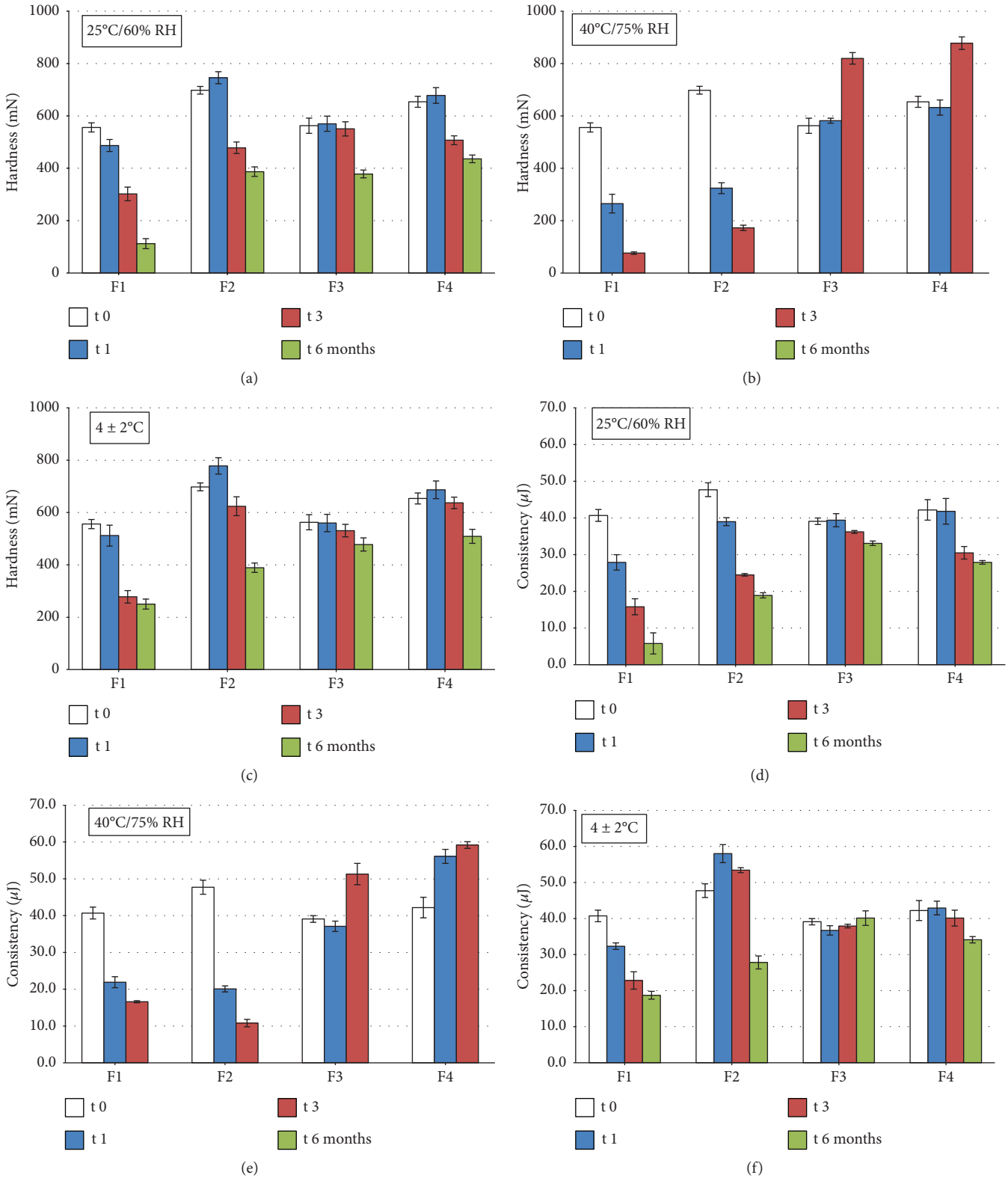

Figure 3: Hardness (a–c) and consistency (d–f) of hydrogels with unmodified CS (F1, F2) or with bGP-crosslinked CS (F3, F4) directly after preparation and upon 6-month storage at ambient (a, d), accelerated (b, e), and refrigerated conditions (c, f) ($n = 3$, mean ± SD).

the formation of the linkage between polymer and mucosal tissue. However, a considerable reduction in hydrogels' mucoadhesiveness could be also attributed to a decrease in their cohesive properties (defined as attractive forces existing between the hydrogel layers) resulting from loss of viscosity.

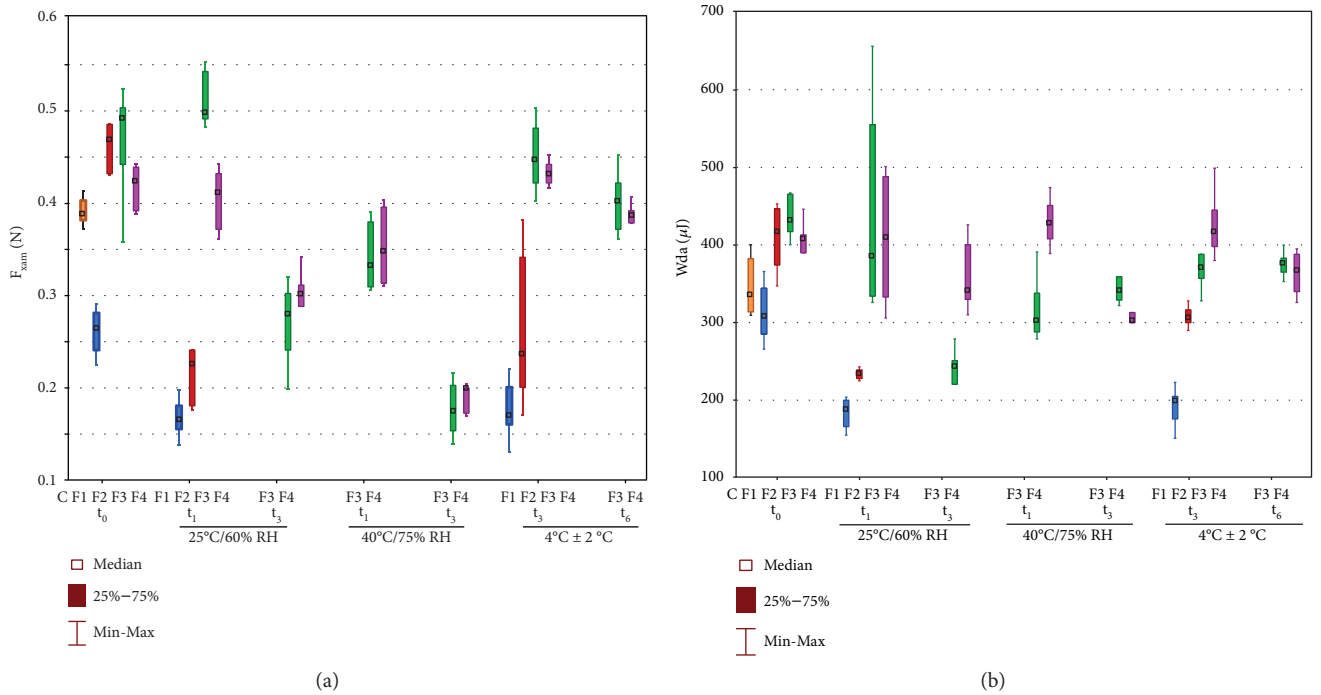

FIGURE 4: Box-plot graphs presenting mucoadhesive properties: (a) maximum force of detachment (F_{max}) and (b) work of adhesion (W_{ad}) of hydrogels with unmodified CS (F1, F2) or with bGP-crosslinked CS (F3, F4) directly after preparation (t_0) and upon 1-month (t_1), 3-month (t_3), or 6-month (t_6) storage at ambient, accelerated, and refrigerated conditions ($n = 6$, median); C: control, mucoadhesive vaginal gel Replens™.

Unexpectedly, upon storage at accelerated conditions, formulations F3 and F4 were found to lose their ability to interact with mucosal tissue, regardless of simultaneous increase in their viscosity (Figure 2(b)) and mechanical properties (Figures 3(b)–3(e)). This could be attributed to the time-delayed gelation process that occurred in bGP/CS hydrogels, responsible for reduced CS chain mobility. That drop in polymer flexibility may have diminished mucoadhesive capacity of hydrogels.

3.4. In Vitro Drug Release Studies. To determine the influence of bGP crosslinking on drug release profile from CS hydrogels upon storage, dissolution tests with using the enhancer cell (equipped with Cuprophan membrane) were performed for CS formulations stored at refrigerated conditions. Because of substantial rheological changes observed for CS hydrogels upon storage at ambient and accelerated conditions, formulations F1–F4 were not analyzed in terms of drug dissolution profile. As compared to drug release rate achieved for freshly prepared formulations (Figure 5(a)), no considerable changes in drug release behavior of all hydrogels were observed after 1 month at $4 \pm 2^{\circ}C$ (Figure 5(b)). However, upon 3-month storage, formulations F1 and F2 exhibited substantially faster clotrimazole release rate, most probably as a consequence of loss in hydrogels' viscosity. In contrast, hydrogels F3 and F4 stored for 3 months at $4 \pm 2^{\circ}C$ displayed only little alterations in drug release profile (Figure 5(c)). Substantial changes ($p < 0.05$) in drug dissolution rate from bGP/CS hydrogels occurred upon 6-month storage, and considerable differences ($p < 0.05$) in drug release curve were recorded especially with regard to formulation F3 (with lower CS concentration) (Figure 5(d)). The obtained results point on the impact of rheological characteristic of pharmaceutical semisolid dosage forms on their drug release properties.

4. Conclusions

The poor long-term stability of CS is a considerable drawback in the development of CS pharmaceutical preparations. In order to overcome stability challenges faced by unmodified CS formulations, physical modification (by addition of ion crosslinker) of CS hydrogels with model antifungal agent was investigated. The effect of bGP on organoleptic, physicochemical, and pharmaceutical performance of CS hydrogels was examined upon storage at ambient, accelerated, and refrigerated conditions according to ICH guideline.

A clear dependence of environmental storage conditions on CS hydrogel characteristics was displayed, and the most profound and particularly fast organoleptic and viscosity changes appeared at accelerated conditions. Notably, the introduction of bGP was shown to stabilize CS hydrogels, especially upon storage at refrigerated conditions. Formulations with bGP-crosslinked CS preserved rheological, mucoadhesive behavior, and hydrogel structure up to 3-month storage at $4 \pm 2^{\circ}C$. In addition, no significant alterations in physical appearance and drug content in

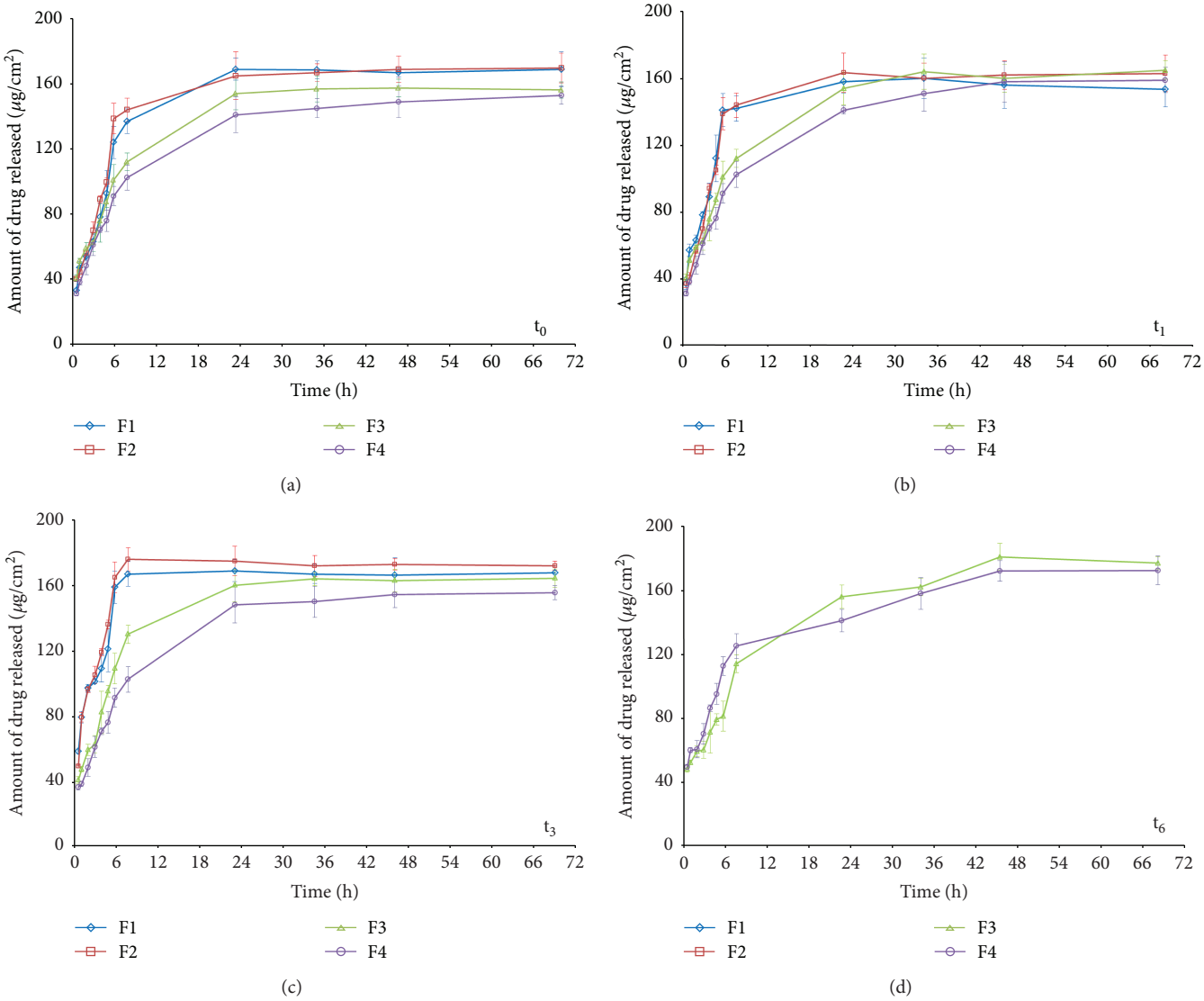

FIGURE 5: Amount of clotrimazole per unit area (μg/cm^2) released from hydrogel with unmodified CS (F1, F2) or with bGP-crosslinked CS (F3, F4): (a) directly after preparation (t_0) and (b) upon 1-month (t_1), (c) 3-month (t_3), or (d) 6-month (t_6) storage at refrigerated conditions ($n = 3$, mean ± SD).

formulations with bGP/CS (F3 and F4) for up to 6-month storage at 4°C and 25°C/60% RH were observed. In contrast, hydrogels with unmodified CS were found to have poor physicochemical stability both under ambient and refrigerated conditions, especially with regard to their viscosity and mechanical properties.

Data Availability

Access to additional data from microscopic analysis would be available upon request to the corresponding author. All other information underlying the findings of the paper is available within the manuscript.

Conflicts of Interest

The authors declare no conflict of interest.

Acknowledgments

This research work was supported by Medical University of Białystok grant (number N/ST/ZB/17/006/2215).

Supplementary Materials

The following is available as a separate file. Figure S1: optical images of hydrogels with unmodified CS (F1, F2) or with bGP-crosslinked CS (F3, F4) after preparation. Figure S2: macroscopic appearance of hydrogels with unmodified CS (F1, F2) or with bGP-crosslinked CS (F3, F4) after 6-month storage at ambient conditions. Figure S3: macroscopic appearance of hydrogels with unmodified CS (F1, F2) or with bGP-crosslinked CS (F3, F4) after 3-month storage at accelerated conditions. Figure S4: macroscopic appearance of hydrogels with unmodified CS (F1, F2) or with bGP-

crosslinked CS (F3, F4) after 6-month storage at refrigerated conditions. *(Supplementary Materials)*

References

[1] A. Srivastava, T. Yadav, S. Sharma, A. Nayak, A. Akanksha Kumari, and N. Mishra, "Polymers in drug delivery," *Journal of Biosciences and Medicines*, vol. 4, no. 1, pp. 69–84, 2016.

[2] J. R. Franca, G. Foureaux, L. L. Fuscaldi et al., "Bimatoprost-loaded ocular inserts as sustained release drug delivery systems for glaucoma treatment: *in vitro* and *in vivo* evaluation," *PLoS One*, vol. 9, no. 4, pp. e95461–e95472, 2014.

[3] F. Saporito, G. Sandri, S. Rossi et al., "Freeze dried chitosan acetate dressings with glycosaminoglycans and traxenamic acid," *Carbohydrate Polymers*, vol. 184, pp. 408–417, 2018.

[4] J. Venkatesan, I. Bhatnagar, and S. K. Kim, "Chitosan-alginate biocomposite containing fucoidan for bone tissue engineering," *Marine Drugs*, vol. 12, no. 1, pp. 300–316, 2014.

[5] B. Choi, S. Kim, B. Lin, B. M. Wu, and M. Lee, "Cartilaginous extracellular matrix-modified chitosan hydrogels for cartilage tissue engineering," *ACS Applied Materials & Interfaces*, vol. 6, no. 22, pp. 20110–20121, 2014.

[6] Y. H. Lee, H. I. Park, and J. S. Choi, "Novel glycol chitosan-based polymeric gene carrier synthesized by a Michael addition reaction with low molecular weight polyethylenimine," *Carbohydrate Polymers*, vol. 137, pp. 669–677, 2016.

[7] A. Smith, M. Perelman, and M. Hinchcliffe, "Chitosan: a promising safe and immune-enhancing adjuvant for intranasal vaccines," *Human Vaccines & Immunotherapeutics*, vol. 10, no. 3, pp. 797–807, 2014.

[8] P. N. Vaingankar and A. R. Juvekar, "Fermentative production of mycelial chitosan from Zygomycetes: media optimization and physico-chemical characterization," *Advances in Bioscience and Biotechnology*, vol. 05, no. 12, pp. 940–956, 2014.

[9] T. A. Ahmed and B. M. Aljaeid, "Preparation, characterization, and potential application of chitosan, chitosan derivatives, and chitosan metal nanoparticles in pharmaceutical drug delivery," *Drug Design, Development and Therapy*, vol. 10, pp. 483–507, 2016.

[10] I. Aranaz, N. Acosta, C. Civera et al., "Cosmetics and cosmeceutical applications of chitin, chitosan and their derivatives," *Polymer*, vol. 10, no. 2, p. 213, 2018.

[11] T. T. Nguyen, A. R. Barber, K. Corbin, and W. Zhang, "Lobster processing by-products as valuable bioresource of marine functional ingredients, nutraceuticals, and pharmaceuticals," *Bioresources and Bioprocessing*, vol. 4, no. 1, pp. 27–46, 2017.

[12] S. Baltzley, A. Mohammad, A. H. Malkawi, and A. M. Al-Ghananeem, "Intranasal drug delivery of olanzapine-loaded chitosan nanoparticles," *AAPS PharmSciTech*, vol. 15, no. 6, pp. 1598–1602, 2014.

[13] G. Tejada, M. G. Barrera, G. N. Piccirilli et al., "Development and evaluation of buccal films based on chitosan for the potential treatment of oral candidiasis," *AAPS PharmSciTech*, vol. 18, no. 4, pp. 936–946, 2017.

[14] A. Almomen, S. Cho, C. H. Yang et al., "Thermosensitive progesterone hydrogel: a safe and effective new formulation for vaginal application," *Pharmaceutical Research*, vol. 32, no. 7, pp. 2266–2279, 2015.

[15] E. Szymańska, K. Winnicka, A. Amelian, and U. Cwalina, "Vaginal chitosan tablets with clotrimazole—design and evaluation of mucoadhesive properties using porcine vaginal mucosa, mucin and gelatine," *Chemical and Pharmaceutical Bulletin*, vol. 62, no. 2, pp. 160–167, 2014.

[16] F. Notario-Pérez, A. Martín-Illana, R. Cazorla-Luna et al., "Influence of chitosan swelling behaviour on controlled release of tenofovir from mucoadhesive vaginal systems for prevention of sexual transmission of HIV," *Marine Drugs*, vol. 15, no. 2, pp. 50–66, 2017.

[17] I. Younes, S. Sellimi, M. Rinaudo, K. Jellouli, and M. Nasri, "Influence of acetylation degree and molecular weight of homogeneous chitosans on antibacterial and antifungal activities," *International Journal of Food Microbiology*, vol. 185, pp. 57–63, 2014.

[18] M. Egusa, R. Iwamoto, H. Izawa et al., "Characterization of chitosan nanofiber sheets for antifungal application," *International Journal of Molecular Sciences*, vol. 16, no. 11, pp. 26202–26210, 2015.

[19] E. Szymańska, K. Winnicka, P. Wieczorek, P. Sacha, and E. Tryniszewska, "Influence of unmodified and β-glycerophosphate cross-linked chitosan on anti-Candida activity of clotrimazole in semi-solid delivery systems," *International Journal of Molecular Sciences*, vol. 15, no. 10, pp. 17765–17777, 2014.

[20] E. Szymańska, K. Sosnowska, W. Miltyk, M. Rusak, A. Basa, and K. Winnicka, "The effect of β-glycerophosphate crosslinking on chitosan cytotoxicity and properties of hydrogels for vaginal application," *Polymer*, vol. 7, no. 11, pp. 2223–2244, 2015.

[21] E. Szymańska and K. Winnicka, "Stability of chitosan—a challenge for pharmaceutical and biomedical applications," *Marine Drugs*, vol. 13, no. 4, pp. 1819–1846, 2015.

[22] M. Fernandes, I. C. Gonçalves, S. Nardecchia, I. F. Amaral, M. A. Barbosa, and M. C. L. Martins, "Modulation of stability and mucoadhesive properties of chitosan microspheres for therapeutic gastric application," *International Journal of Pharmaceutics*, vol. 454, no. 1, pp. 116–124, 2013.

[23] C. Liu, E. Thormann, P. M. Claesson, and E. Tyrode, "Surface grafted chitosan gels. Part II. Gel formation and characterization," *Langmuir*, vol. 30, no. 29, pp. 8878–8888, 2014.

[24] A. N. Allam, V. F. Naggar, and S. S. El Gamal, "Formulation and physicochemical characterization of chitosan/acyclovir co-crystals," *Pharmaceutical Development and Technology*, vol. 18, no. 4, pp. 856–865, 2013.

[25] M. Rinaudo, G. Pavlov, and J. Desbrières, "Influence of acetic acid concentration on the solubilization of chitosan," *Polymer*, vol. 40, no. 25, pp. 7029–7032, 1999.

[26] "International conference on harmonisation of technical requirements for registration of pharmaceuticals for human use, ICH harmonised tripartite guideline, evaluation for stability data Q1E," April 2018, http://www.ich.org/fileadmin/Public.../Guidelines/.../Q1E_Guideline.pdf.

[27] *The European Pharmacopoeia 7.0*, Council of Europe, Strasbourg, France, 2011.

[28] EMA, *ICH Topic Q4B Annex 12 Analytical Sieving General Chapter*March 2018, http://www.ema.europa.eu/docs/en_GB/document_library/Scientific_guideline/2010/01/WC500044305.pdf.

[29] "In vitro release testing and in vivo bioequivalence documentation," in *Guidance for Industry: SUPAC-SS Non-Sterile Semisolid Dosage Forms. Scale-up and Postapproval Changes:*

Chemistry, Manufacturing and Controls, pp. 19–24, FDA-SUPAC-SS, Rockville, MD, USA, 1999.

[30] A. Chenite, M. Buschmann, D. Wang, C. Chaput, and N. Kandani, "Rheological characterisation of thermogelling chitosan/glycerol-phosphate solutions," *Carbohydrate Polymers*, vol. 46, no. 1, pp. 39–47, 2001.

[31] *The United States Pharmacopeia USP 34-NF 29*, The United States Pharmacopeial Convention, Rockville, MD, USA, 2011.

[32] W. Y. Chien, "Drug delivery: vaginal route," in *Encyclopedia of Pharmaceutical Technology, vol. 2*, J. Swarbrick, Ed., pp. 1339–1361, Informa Healthcare, New York, NY, USA, 3rd edition, 2007.

[33] S. E. Harding, "Some observations on the effects of bioprocessing on biopolymer stability," *Journal of Drug Targeting*, vol. 18, no. 10, pp. 732–740, 2010.

[34] D. P. Chattopadhyay and M. S. Inamdar, "Aqueous behaviour of chitosan," *International Journal of Polymer Science*, vol. 2010, Article ID 939536, 7 pages, 2010.

[35] T. T. B. Nguyen, S. Hein, C. H. Ng, and W. F. Stevens, "Molecular stability of chitosan in acid solutions stored at various conditions," *Journal of Applied Polymer Science*, vol. 107, no. 4, pp. 2588–2593, 2008.

[36] B. Martini, S. Dimida, E. de Benedetto, M. Madaghiele, and C. Demitri, "Study on the degradation of chitosan slurries," *Results in Physics*, vol. 6, pp. 728-729, 2016.

[37] E. Ruel-Gariépy, A. Chenite, C. Chaput, S. Guirguis, and J.-C. Leroux, "Characterization of thermosensitive chitosan gels for the sustained delivery of drugs," *International Journal of Pharmaceutics*, vol. 203, no. 1-2, pp. 89–98, 2000.

[38] S. Supper, N. Anton, N. Seidel, M. Riemenschnitter, C. Schoch, and T. Vandamme, "Rheological study of chitosan/polyol-phosphate systems: influence of the polyol part on the thermo-induced gelation mechanism," *Langmuir*, vol. 29, no. 32, pp. 10229–10237, 2013.

Hindawi
International Journal of Polymer Science
Volume 2018, Article ID 3286491, 9 pages
https://doi.org/10.1155/2018/3286491

Research Article

Achyranthes bidentata Polysaccharide along with Anti-IL-5 Antibody Inhibits Allergic Lung Inflammation and Airway Hyperresponsiveness Mice Induced by House Dust Mites

Jian Sun,[1] Shiwei Sheng,[2] and Gang Zhao[1]

[1]*Department of Emergency, Shanghai Jiao Tong University Affiliated Sixth People's Hospital, Shanghai 200233, China*
[2]*Department of Nuclear Medicine, Shanghai Jiao Tong University Affiliated Sixth People's Hospital, Shanghai 200233, China*

Correspondence should be addressed to Gang Zhao; zhaogang64369181@sohu.com

Received 16 April 2018; Accepted 6 June 2018; Published 28 August 2018

Academic Editor: Jianxun Ding

Bronchial asthma is a chronic inflammatory disease which has become prevalent worldwide. There are millions of new patients and thousands of people die from asthma. Asthma is characterized with infiltration by eosinophils in pulmonary parenchyma, high serum IgE, and cytokines like IL-4, IL-5, and IL-13 secreted by allergen-specific T helper cell-2 (Th2) cells. Products of eosinophils are considered as negative regulators that work on remodeling lung tissue, including airway thickening, fibrosis, and angiogenesis. *Achyranthes bidentata* polysaccharide (ABPS) is a kind of polysaccharide extracted from the dry root of *Achyranthes* plant *Achyranthes bidentata*. ABPS is reported to have multiple biological functions and acts on the human immune system. ABPS can induce production of TNF-α in macrophage, enhance the killing ability of NK cells, and promote the proliferation of B cells. Besides this, ABPS is reported that can induce apoptosis of eosinophils by upregulating the expression of proteins involved in apoptosis. In this study, we constructed chronic allergic asthma mice model induced by house dust mites (HDM) with airway hyperresponsiveness (AHR) and found that anti-IL-5 mAb and ABPS treatment can both decrease inflammatory cells infiltration especially eosinophils and decrease the level of serum IgE and HDM-specific IgG1. The level of IFN-γ is increased and AHR is improved, and a more significant phenomenon was observed in anti-IL-5 mAb and ABPS combined treatment.

1. Introduction

Bronchial asthma is a chronic inflammatory disease of the airway [1] which has become increasingly prevalent worldwide. It is estimated that over 300 million individuals suffered from asthma worldwide and 250 thousand people dies from asthma every year [2–4]. The number is also predicted to reach about 400 million over in the next decades [5].

Asthma is characterized by eosinophils infiltration into the pulmonary parenchyma and airways [6]. The products of eosinophils are considered as negative moleculars to lung tissue remodel, including airway thickening, fibrosis, and angiogenesis, and asthma exacerbate [7, 8]. It is proved that asthma is a complex and heterogenic disease which can be subdivided into several phenotypes due to clinical, physiological, and inflammatory markers [9, 10]. Eosinophilic asthma is one of these phenotypes characterized by increased serum or sputum eosinophils, which means the number of eosinophils correlates with disease severity [11]. Usually, patients with severe asthma and refractory eosinophilic phenotype will suffer frequent asthma exacerbations.

Inhaled glucocorticoids (GCs) were typically the gold-standard treatment to asthma patients because of their suppression of multiply inflammatory mechanisms in parallel and being able to reduce AHR and degree of disease activity [12]. However, the side effects of GCs have been

well documented, GCs require lifetime therapy for most of the asthma patients whose symptoms usually return if GCs are withdrawn [5]. Meanwhile, another common concern for GCs therapy is the various clinical response in the patients with asthma [13].

Current biological treatment strategies focused on specific targeting of Th2-associated cytokines [14]. Recent research revealed that periostin could be a novel biomarker for bronchial asthma in downstream of IL-13 signaling [15]. Also, it is well accepted that Th2-derived interleukin-5 (IL-5) plays a key role in developing and maturing of eosinophils, enhancing their adhesion to endothelial cells lining the postcapillary venules, activating, secreting, and prolonging survival through apoptosis inhibition in the tissues [16]. It has been well-known that IL-5 is upregulated within the airways of both atopic and nonatopic asthmatic patients and that the expression of IL-5 negative related with pulmonary function [17, 18]. Therefore, IL-5 was considered a promising target to treat eosinophil-mediated inflammation in asthma patients and other eosinophil-related conditions [11]. And, *Achyranthes bidentata* polysaccharide, used as traditional Chinese medicine, possessed the effect of improving the proliferation activity and cytokine production of lymphocytes, antitumor functions, and immunomodulatory functions [19–21]. Previous study showed dietary supplementation with the ABPS greatly increased the peripheral lymphocyte proliferation in a concentration-dependent manner in piglets. The main effect of ABPS was focused on strengthen muscles and bones remodeling. Pharmacological findings suggested ABPS is reported as an effective inhibitor of Th1/Th2 dysregulation; therefore, we considered ABPS a promising strategy to treat eosinophil-mediated inflammation in asthma.

Murine models are often used to study the delineation mechanisms and critical mediators of asthma with conflicting results which suggested that the dominant mechanism and mediators required for asthma induction differ on the use of model and the method of allergen sensitization [6]. Though animal models induced by ovalbumin (OVA) have been used in most studies, there are difficulties in evaluating recurrence and maintaining chronic inflammation [1]. And the study previously confirmed that when more closely resembles ambient allergen exposure in human subjects used in a murine model, the IgE will act as a more critical role in the pathogenesis of allergic asthma and mucosa pathology [6]. House dust mites (HDM) allergens are considered as the most important risk factor for the development of allergic diseases [22], and the chronic murine HDMs model has been considered as an improved preclinical in vivo model to assess the efficacy and mechanism of action of potential novel therapeutics for asthmatic disease which was recently shown to be effective in response to anti-interleukin-13 (anti-IL-13) treatment [23].

Here, in an HDM-induced chronic asthma murine model of lung inflammation, we assessed the effect of anti-IL-5 mAb and ABPS treatment, respectively, or combined in asthma. We analyzed the change of inflammatory cells especially eosinophils and cytokines in BALF as well as the change of IgE and HDM-specific IgG1 levels in serum.

2. Materials and Methods

2.1. Materials. Extraction of ABPS: take 50 g dry roots of plant *Achyranthes bidentata*, grind it into powder, and extract it with 10 volumes of 75% ethanol; then recover ethanol and sediment is obtained by lyophilization. The residue was extracted with 10 volumes of water, then concentrated, and finally added with 95% ethanol to precipitate. The precipitate obtained is dissolved in water and trichloroacetic acid is added to remove the protein and the supernatant is taken after centrifugation. The supernatant was added with 95% ethanol to obtain a precipitate. The precipitate was washed successively with absolute ethanol, acetone, and ether and freeze-dried to obtain a crude product of *Achyranthis* polysaccharide. The extracted Acetyltalatisamine Achyranthan was reddish-brown powder. After acid hydrolysis, the ratio of hydrolysate to fructose and glucose was determined by high performance liquid chromatography (HPLC).

2.2. Animals. Female C57BL/6 mice of SPF clean grade (6–8 weeks old) were purchased from Shanghai SLAC Laboratory Animal Co., LTD. All animals were held in regular 12 h dark/light cycles at 25°C and were bred and maintained in the high-efficiency particulate air filter-exhausted ventilated cages. The mice received food and water ad libitum. All the animal procedures were conducted in concordance with the Institutional Ethical Committees for Use of Experimental Animals.

2.3. Allergen Sensitization of Murine Models. Fifty C57BL/6 mice were randomly divided into five groups, as control group, asthma group, anti-IL-5 mAb treated group, ABPS treated group, and anti-IL-5 mAb-ABPS combined group. Mice were sensitized to house dust mite (HDM) extracts (Greer, Lenoir, NC, USA) by subcutaneous injections of 50 μg HDM adsorbed to 2 mg of alum [$Al(OH)_3$] gel (Sigma Chemical Co., St. Louis, MO, USA) on days 0 and 7 and challenged intranasally with 25 μg of HDM in 50 μL of PBS for 4 consecutive days a week for 3 weeks. Controls received only alum and were challenged with saline (0.9% NaCl) instead of HDM. Necropsy was performed 24 h after the final allergen challenge.

2.4. Medicine Treatment. To assess the different effect of medicine in chronic allergic murine asthma model, different therapeutic agents were dosing to corresponding groups: anti-IL-5 mAb group were treated with 100 μg of rat anti-mouse IL-5 mAb (Abcam Shanghai Trade Co., LTD, Shanghai, China) 2 h before the first intranasal HDM application and thrice weekly before necropsy; ABPS group were treated with follow operations: after the second sensitization of HDM, intraperitoneal injection of 70 mg/kg per day, and in sensitized phase, ABPS were administered intraperitoneally 1 h prior until the mice were sacrificed.; anti-IL-5 mAb-APBS combined group were treated with both of this two organics.

2.5. Assess of Airway Hyperresponsiveness to Methacholine. Airway hyperresponsiveness (AHR) of mice to methacholine was measured before necropsy. Mice were placed in

individual chambers and exposed to nebulized methacholine (6.25 mg/mL, Sigma, St Louis, MO) for 2 min. And after exposure, enhanced pause (Penh) was measured during methacholine exposure and change in mean Penh was used as an indicator of airway responsiveness.

2.6. Bronchoalveolar Lavage Fluid Collection and Cell Counting. Before dissection, the bronchoalveolar lavage fluid (BALF) was performed by twice instillation of 0.8 mL ice-cold PBS then centrifuged (1500 rpm, 5 min, 4°C). The supernatant was immediately aliquoted and stored at −70°C for subsequent measurement of cytokine content. The precipitation was resuspended in 0.5 mL of PBS, and the total number of cell was counted by Neubauer chamber. 100 cells in cytospin were prepared and stained by Rosenfeld's stain to evaluate differential cell counts.

2.7. Lung Histology. After the collection of BALF, the left lung lobe was immersed in 10% phosphate-buffered formalin for 24 h, followed by 70% ethanol, and embedded in paraffin. Tissues sections of 5 μm were then stained with H&E (haematoxylin and eosin) to assess histopathological changes. The slides were manually examined under a light microscope ×100.

2.8. Cytokine and Immunoglobulin Assays. The concentration of IFN-γ (R&D system, Minneapolis, MN, USA) in the BALF and serum was measured by ELISA kits. The minimum detectable concentration was 2 pg/mL.

Serum IgE levels were detected by Mouse IgE ELISA kits (Becton, Dickinson and Company, New Jersey, USA) and manipulated as follows: 100 μL of rat anti-mouse IgE monoclonal antibody were added to each well, plated, and incubated at 4°C overnight. After being washed and blocked with PBS containing 1% skim milk mouse sera were incubated overnight at 4°C, and antibody binding was assessed by the addition of 100 μL of biotinylated anti-mouse IgE detection mAb and streptavidin-horseradish peroxidase conjugate (SAv-HRP) incubated at 37°C for 1 h. After the addition of the enzyme substrate, plates were read at 450 nm in an ELISA reader (Bio-Rad, Richmond, CA, USA). The purified mouse IgE antibody was used for the total IgE standard. The minimum detectable concentration was 2 ng/mL.

HDM specific IgG1 was measured by ELISA kit. HDM was coated overnight at 4°C with 100 μL of 5 μg/mL HDM in carbonate buffer (0.05 mol/L, pH 9.6) and by detecting HDM specific IgG1 binding with biotinylated rat anti-mouse IgG1 detection mAb and SAv-HRP. The other procedures are the same with detection serum IgE.

2.9. Flow Cytometry Assays. Centrifuge the BALF fluid and resuspend cells into cell suspension. Loading Percoll in different density (1.085, 1.080, 1.075, and 1.070) to a centrifuge tube. Pipetting the cell suspension under Percoll carefully and centrifuging (1500 rp, 25 min at room temperature). Eosinophils were loaded between 1.075 and 1.070 density ladder. Wash eosinophils with PBS twice and resuspend with binding buffer, dying with Annexin-V in the dark for 15 min; PI was added before flowing.

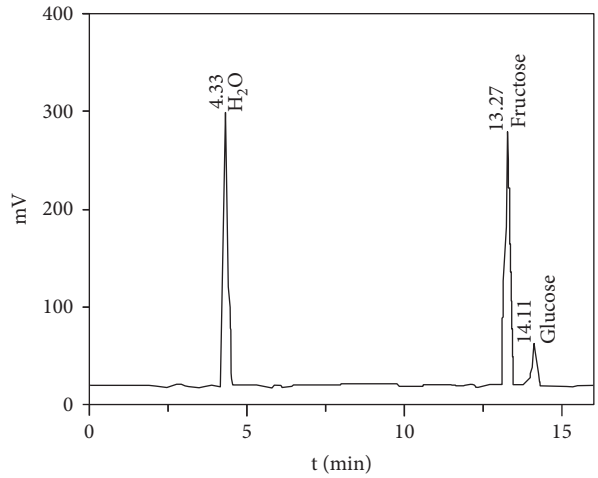

Figure 1: HPLC analysis of the ratio of fructose to glucose in hydrolyzed *Achyranthes* polysaccharides extracted Acetyltalatisamine Achyranthan was hydrolyzed, and the ratio of fructose to glucose was measured. From the data, we know that at about the 13th minute fructose was separated and glucose was separated at the 14th minute. The ratio of the two was about 4 to 1 (fructose to glucose).

2.10. Statistics. The differences among the groups were analyzed using InStat 2.01 software (GraphPad, San Diego, CA, USA). Data are given as means + SEM for normally distributed. For comparison, multiple groups ANOVA or Kruskal–Wallis with parametric (Bonferroni) or nonparametric (Dunn's) posttest, respectively, was performed. For all tests, P values less than 0.05 were considered significant.

3. Results

3.1. Extraction and Component Analysis of Acetyltalatisamine Achyranthan. After repeated extraction and precipitation, reddish-brown powder is obtained. After acid hydrolysis, a series of preparations are performed to detect the ratio of fructose to glucose by HPLC. Fructose was separated at about 13th minute (13.27th minute) and glucose was separated at one minute later (14.11th minute). The ratio of fructose and glucose was about 4 to 1 (Figure 1).

3.2. Effect of Therapeutic Agent on Airways Hyperresponsiveness. In order to investigate the effect of therapeutic agent on AHR in our murine chronic allergic inflammation model, plethysmography was conducted to detect changes in respiratory dynamics following exposure to methacholine with a concentration of 6.25 mg/mL. The results showed an increased sensitivity to methacholine challenge after HDM exposure. And Penh is significantly higher than the control group ($P < 0.01$) (Figure 2). And the AHR to methacholine was significantly decreased with the treatment of anti-IL-5 mAb ($P < 0.05$) and ABPS ($P < 0.05$), or the combined treatment group ($P < 0.01$) (Figure 1).

3.3. Effect of Anti-IL-5 mAb and ABPS Combined Treatment on Pulmonary Inflammation. The total inflammatory cells,

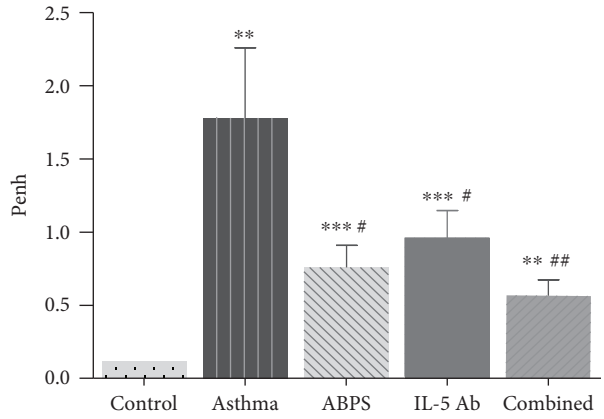

Figure 2: Effect of anti-IL-5 mAb and ABPS treatment on hyperresponsiveness induced by methacholine. Airway response of control, asthma group, or therapy group to methacholine (24 h after exposure to HDM). Data was presented as mean Penh + SEM and was from one experiment, with $n = 10$ mice per group. $^{**}P < 0.01$, $^{***}P < 0.001$, compared to the control group. $^{\#}P < 0.05$, $^{\#\#}P < 0.01$, compared to the asthma group. The significance of the data was evaluated by one-way ANOVA with Bonferroni's multiple comparison test compared to control.

eosinophils, neutrophils, mononuclear/macrophages, and lymphocytes in BALF fluid was significantly elevated in HDM-challenge mice versus saline control mice as shown in Table 1 (versus control, $P < 0.001$, $P < 0.001$, $P < 0.01$, $P < 0.001$, $P < 0.01$, separatively). Anti-IL-5 mAb or ABPS treatment can significantly decrease the number of total cells, eosinophils, neutrophils, and lymphocytes (versus asthma group, $P < 0.01$, $P < 0.001$, $P < 0.01$, $P < 0.01$, separatively under anti-IL-5 mAb group. $P < 0.05$, $P < 0.01$, $P < 0.05$, $P < 0.05$, separatively under ABPS group.), especially in the combined group (versus asthma group, $P < 0.05$, $P < 0.001$, $P > 0.05^{*}$, $P < 0.01$, separatively).

Inhibition of lung inflammation infiltration by anti-IL-5 mAb and ABPS treatment, respectively, or combined was also confirmed by histology examination. The results showed the inflammatory cells infiltration into peribronchial and perivascular areas in asthma group as compared to the control using H&E staining. Treatment of anti-IL-5 mAb and ABPS can both reduce the magnitude of inflammatory cells infiltration into the peribronchiolar and perivascular connective tissues as compared to asthma group (Figure 3), and this phenomenon is more significant in combined treatment group (Figure 3).

3.4. Effect of Anti-IL-5 mAb and ABPS Combined Treatment on Immune Function. Classically, the mutual inhibition balance of Th1/Th2 was broken in patients with asthma. And the Th1 cells were often inhibited in asthma patients. The effect of anti-IL-5 mAb and ABPS treatment on immune function was detected, and the results showed that HDM sensitization and challenge induced significant decrease of IFN-γ both in the BALF fluid and in serum (versus Asthma, $P < 0.05$, $P < 0.05$ in BALF and $P < 0.01$, $P < 0.05$ in serum) as shown in Figure 3. After combining treatment, the concentration of IFN-γ both in the BALF fluid and in serum significantly increased (versus asthma group, $P < 0.01$, $P < 0.001$), which is better than only anti-IL-5 mAb or ABPS treatment (Figure 4).

3.5. Effect of Anti-IL-5 mAb and ABPS Combined Treatment on Serum IgE and HDM-Specific IgG1. Usually, Th2 cell immune responses are associated with the production of IgG1 and IgE antibody. The results of the assays showed that exposure to HDM resulted in the increase generation of HDM-specific IgG1 and IgE in serum ($P < 0.001$). And the treatment of anti-IL-5 mAb or ABPS can decrease the levels of both serum IgE and HDM-specific IgG1 ($P < 0.01$, $P < 0.05$ in anti-IL-5 mAb group, $P < 0.05$, $P < 0.05$ in ABPS group), similar before, anti-IL-5 mAb and ABPS combined group has significantly reduced on the levels of both serum IgE and HDM-specific IgG1 ($P < 0.001$, $P < 0.01$) (Figure 5).

3.6. Effect of Anti-IL-5 mAb and ABPS Combined Treatment on Apoptosis. To identify the function of inducing apoptosis of anti-IL-5 mAb and ABPS combined treatment, the proportion of eosinophils derived from BALF was analyzed. As the results, the proportion of eosinophils from asthma group was higher than control group ($P < 0.01$). After treatment, the proportion of eosinophils from treatment group was markedly elevated ($P < 0.01$), especially in anti-IL-5 mAb and ABPS combined treatment group (Figure 6).

4. Discussion

Animal models were an invaluable tool in translational research, especially mouse models with a large selection of specific reagents and techniques which have made major contributions to the understanding of asthma pathophysiology and the main characters of the disease [24]. The increasing focus on asthma research is severe asthma because of unmet medical need. And the current findings emphasise the necessity of developing reproducible asthma exacerbation models to provide the opportunities for pharmacological intervention studies.

OVA is the classical allergen for asthma models because of its low costs, useless and well-known immunological characteristics [22], and being able to produce an airway inflammation model exhibiting plentiful human asthma-like cellular and pathophysiological features. However, there is an increasing concern about the prolonged exposure to OVA by inducing tolerance in the animals [25]. Additionally, in human subjects, a big proportion of asthma is due to aeroallergens, and OVA-induced asthma is far from being a common event. Therefore, asthma animal models sensitized by common allergens might be more relevant tools to the study of human asthma [26]. To date, several kinds of allergen extracts or purified proteins which are more clinically relevant have become useful in animal models such as fungi, HDMs (i.e., *Dermatophagoides farina* (*Der f*) and *Dermatophagoides pteronyssinus* (*Der p*)), cockroach, ragweed, and pollen spores [27–31]. HDMs are one of the most common allergens in asthma patients. 50–85% asthma patients are typically allergic to HDMs with increased levels of HDM-specific IgE [32]. The exposure to HDM can overcome the

Table 1: The total and sorting cell count of each group in BALF ($^{*}10^{4}$/mL, $\bar{x} \pm s$).

Group	n	Total cells	Eosinophils	Neutrophils	Mononuclear/macrophages	Lymphocytes
Control	10	4.261 ± 0.689	0.2052 ± 0.0319	1.7502 ± 0.1862	0.3782 ± 0.0322	2.8912 ± 0.2381
Asthma	10	$19.35 \pm 3.802^{***}$	$8.9862 \pm 1.0763^{***}$	$4.2198 \pm 0.7621^{**}$	$4.2781 \pm 0.5621^{***}$	$7.2671 \pm 1.9761^{**}$
ABPS	10	$9.78 \pm 3.66^{*}$	$3.543 \pm 0.856^{**}$	$2.933 \pm 0.659^{*}$	$2.045 \pm 0.4533^{**}$	$6.0941 \pm 1.543^{*}$
IL-5 Ab	10	$11.44 \pm 3.04^{**}$	$2.76 \pm 0.55^{***}$	$3.37 \pm 0.544^{**}$	$3.04 \pm 0.665^{***}$	$5.4941 \pm 1.333^{**}$
Combined group	10	$7.98 \pm 1.5600^{*}$	$1.6782 \pm 0.0963^{***}$	2.0672 ± 0.3219	$1.0621 \pm 0.2875^{*}$	$4.5912 \pm 0.6782^{**}$

Data was presented as mean + SEM and was from one experiment.* $P < 0.05$; ** $P < 0.01$; *** $P < 0.001$. The significance of the data was evaluated by one-way ANOVA with Bonferroni's multiple comparison test compared to control.

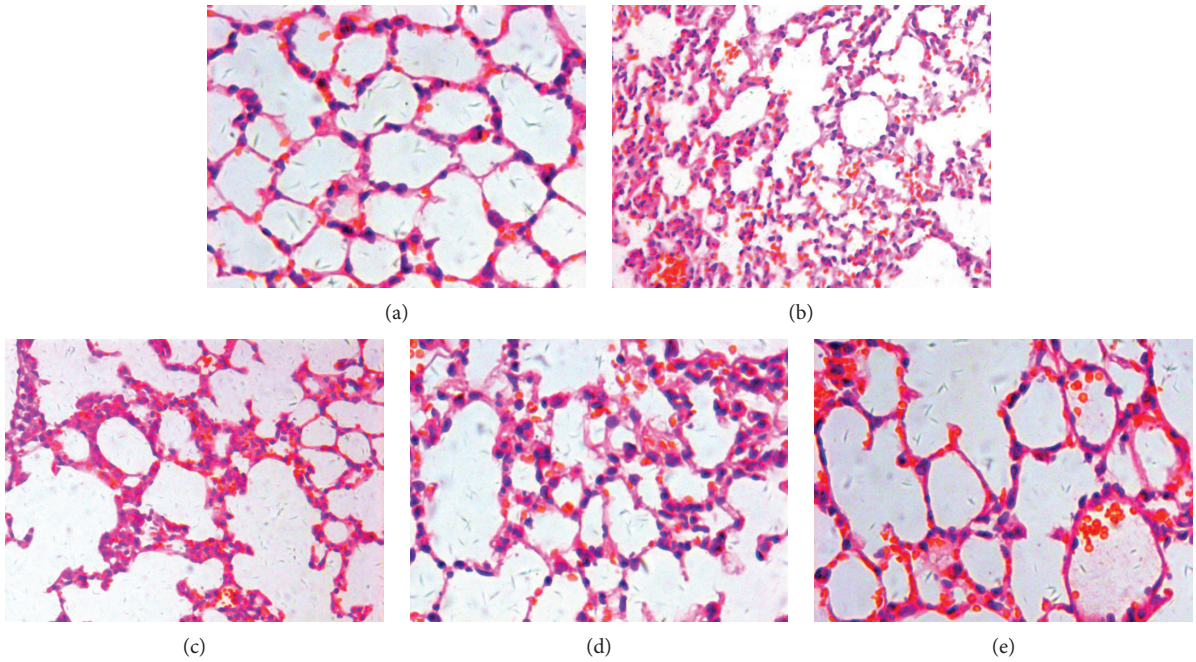

Figure 3: Effect of anti-IL-5 mAb and ABPS, respectively, or combined treatment on airway inflammation (H&E, magnification ×100). Exposure to HDM increases airway inflammatory cell infiltration and treatment decreased it, which is more remarkable in the anti-IL-5 mAb and ABPS combined treatment group. (a, b, c, d, e) represents control, asthma group, ABPS group, anti-IL-5 and anti-IL-5 mAb, and ABPS combined group, respectively.

limitation of prolonged exposure to OVA models of tolerogenic response and allow us to investigate changes related to chronic, persistent allergen exposure. Remodeling of the airways with increased mucous cell density and AHR can be constructed by prolonged exposure to HDM and remains elevated for a while after discontinuation of HDM exposure [33]. Meanwhile, it is well known that chronic exposure to inhaled allergens can induce an inflammatory response in the lung leading to clinical symptoms of asthma [10]. Therefore, in this article we choose the HDM extracts to induce the chronic allergic asthma model in order to mimic the clinical process of human subjects better.

According to our data, we successfully constructed the chronic allergic lung inflammation model induced by HDM with a significant increase of inflammatory cells especially eosinophils, AHR, serum total IgE, and HDM-specific IgG1 and the decrease of IFN-γ, which verifies that chronic exposure to HDM is able to cause cellular infiltration of the airways by immune and inflammatory cells [10] and lays foundation for the research of anti-IL-5 mAb treatment of eosinophilic asthma.

Although, GCs are the gold-standard treatment for asthma. It still remains some disadvantage for those patients with GC-refractory eosinophilic asthma and requires unmet medical need. Given that airway inflammation is the key to asthma pathogenesis, new therapies targeting key cells and mediators that drive the inflammatory responses in the asthmatic lung is becoming hotspot [11]. Allergic inflammation is well marked by prominent infiltration of eosinophils and Th2 lymphocytes. It has been reported that IL-5 plays an important role for the regulation of eosinophil maturation, recruitment, survival, and their release into the blood, and eosinophils are a prominent feature in the pulmonary inflammation which is associated with allergic asthma. Thus, IL-5 has been proposed to be a potential molecular target in the treatment of asthma [34]. Similarly, there are reports which proved that ABPS also effectively works on the inhibition of dysregulation of Th1/Th2 in asthma. ABPS was

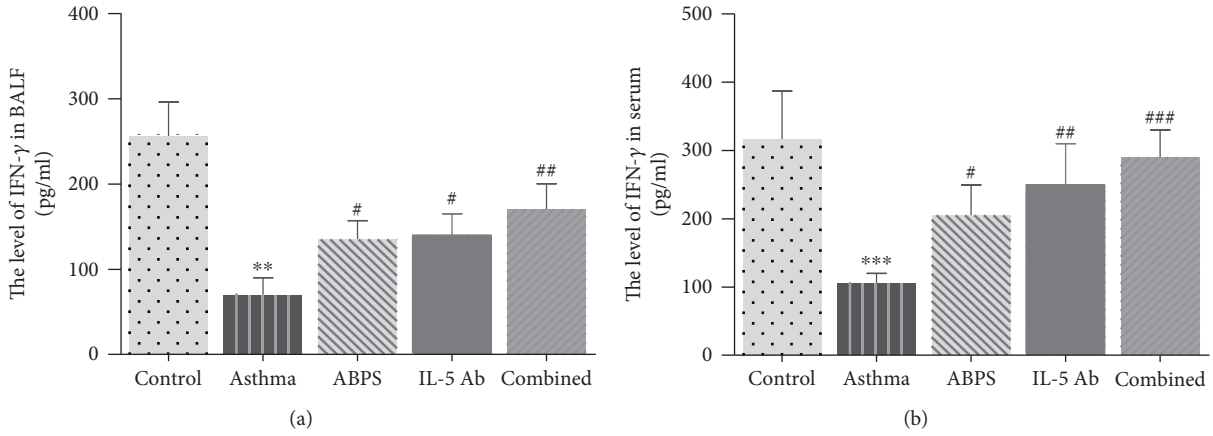

Figure 4: The levels of IFN-γ in BALF (a) and serum (b) of control, asthma group, anti-IL-5 mAb, and ABPS, respectively, or combined treatment group were detected by ELISA. Data was presented as mean Penh + SEM and was from one experiment, with $n = 10$ mice per group. $^{**}P < 0.01$, $^{***}P < 0.001$, compared to the control group. $^{\#}P < 0.05$, $^{\#\#}P < 0.01$, $^{\#\#\#}P < 0.001$, compared to the asthma group. And the levels of IFN-γ detected from combined treatment group was significantly higher than individual treatment group. The significance of the data was evaluated by one-way ANOVA with Bonferroni's multiple comparison test compared to control.

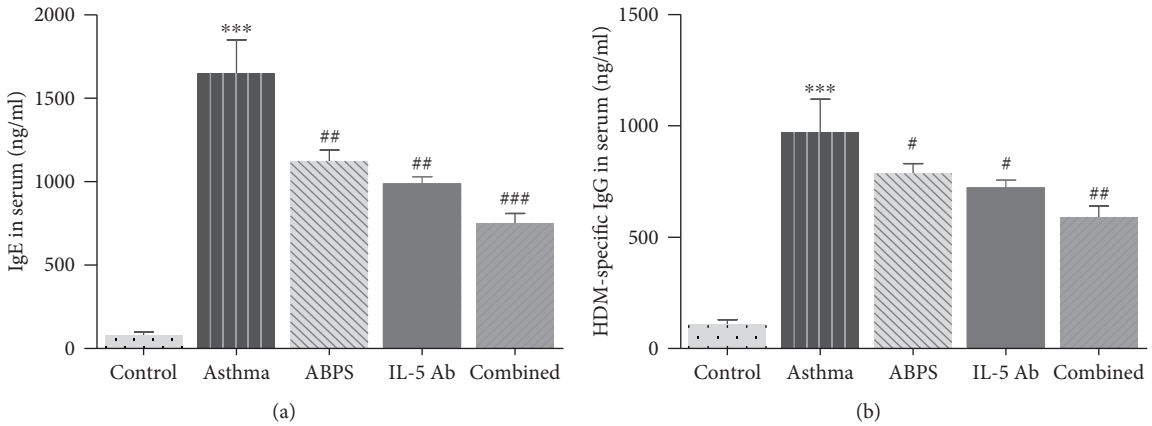

Figure 5: Effect of anti-IL-5 mAb and ABPS, respectively, or combined treatment on the levels of IgE and HDM-specific IgG1. Levels of HDM-specific IgG1 (a) and IgE (b) in serum were measured by ELISA data presented as mean ± SEM and are from one experiment, with $n = 10$ mice per group. $^{***}P < 0.001$, compared to the control group. $^{\#}P < 0.05$, $^{\#\#}P < 0.01$, $^{\#\#\#}P < 0.001$, compared to the asthma group. The significance of the data was evaluated by one-way ANOVA with Bonferroni's multiple comparison test compared to control.

shown to markedly enhance DC maturation and differentiation *in vitro* through providing extra IL-12 and MHC II and upregulating antigen presentation, leading to activating $CD4^+$ T cells [35]. Therefore, we tested the effect of ABPS on asthma and combined with IL-5 antibody in the treatment of asthma. Although this primary studies showed that anti-IL-5 mAb and ABPS treatment can improve disease status in asthma animal models, respectively, it has been proven inadequate in clinical patients with moderate, controlled asthma. Given the knowledge that asthma has several phenotypes, anti-IL-5 mAb and ABPS combined treatment is supposed to be effective in the patients with eosinophilic asthma [36]. In order to identify the hypothesis, we use HDMs to construct a chronic murine asthma model with large number of eosinophils infiltrated and assess the effect of anti-IL-5 mAb and ABPS, respectively, or combined treatment on eosinophilic asthma.

In order to determine the effect of anti-IL-5 mAb and ABPS combined treatment on eosinophilic asthma, we administrate anti-IL-5 mAb and ABPS combined treatment at the time of initial intranasal exposure to HDM three weeks until necropsy which shows dramatical inhibition to the infiltration of the lung tissue and airway by eosinophils. The results showed that anti-IL-5 mAb and ABPS combined treatment was found to reduce HDM-induced chronic asthma responses significantly. Anti-IL-5 mAb and ABPS combined treatment can improve the AHR and reduce inflammatory cell infiltration, especially eosinophils.

Asthma is caused by IgE-mediated hypersensitivity reactions, and the increase of serum IgE is the main character of asthma. Meanwhile, IFN-γ is the typical mediators secreted by Th1 cells which plays an important role in the development of asthma. It has been reported that IL-5 can help IL-4 to promote the production of IgE. When IL-5 and IL-4

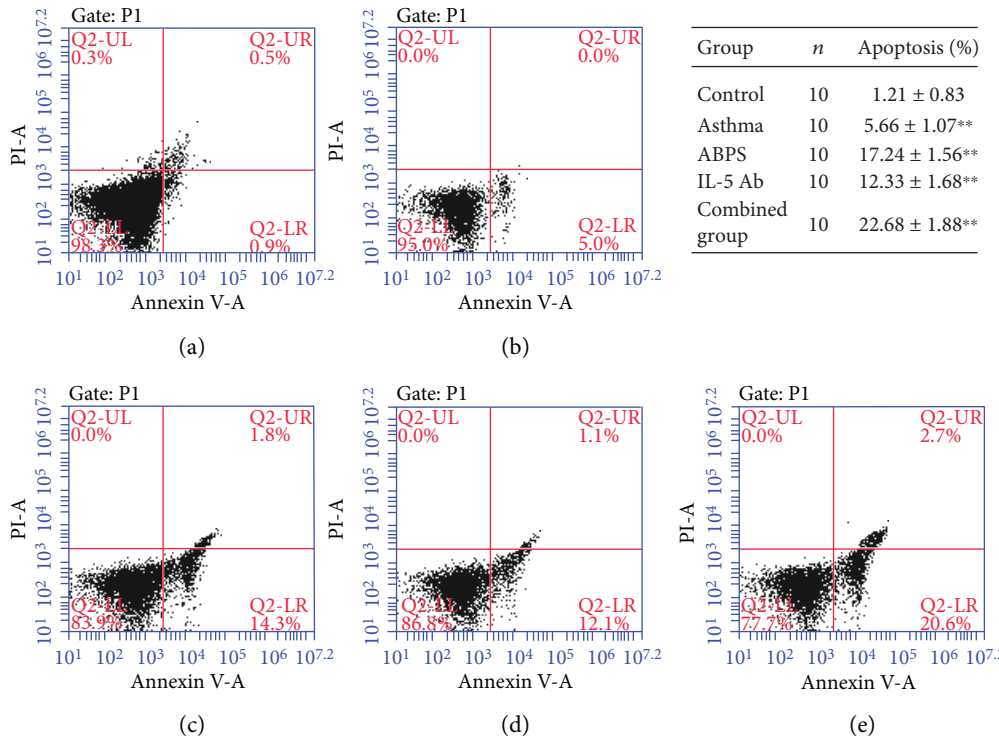

Group	n	Apoptosis (%)
Control	10	1.21 ± 0.83
Asthma	10	5.66 ± 1.07**
ABPS	10	17.24 ± 1.56**
IL-5 Ab	10	12.33 ± 1.68**
Combined group	10	22.68 ± 1.88**

Figure 6: Effect of combined treatment on apoptosis proportion of EOS in BALF by AnnexinV-PI. Proportions of different apoptosis stage presented as above. (a, b, c, d, e) represents control, asthma group, ABPS group, anti-IL-5 and anti-IL-5 mAb, and ABPS combined group, separatively. ** $P < 0.01$, compared to the control group. The significance of the data was evaluated by one-way ANOVA with Bonferroni's multiple comparison test compared to control.

stimulated B lymphocytes at the same time, the production of IgE will increase more than a dozen times compared to IL-4 stimulating alone which means IL-5 also plays an important role in IgE-mediated type I allergic reaction. Additionally, downregulation of IgE can not only decrease the degranulation of mast cells and macrophages but also inhibit the FcεRI-mediated Th2 cells inflammation [37]. Adjust the differentiation direction of Th cell subtypes and the imbalance of Th1/Th2 cells through upregulating IFN-γ or downregulating the level of Th2 cytokine has been recommended as the new approach to treat asthma patients [38]. Theoretically, anti-IL-5 mAb can combine to IL-5 to inhibit IL-5 and downregulate the production of IgE thus to weaken Th2 inflammatory responses and relatively upregulated IFN-γ can enhance the function of Th1 cells. Therefore, in this study we also detected the effect of combining anti-IL-5 mAb and ABPS on IgE and IFN-γ to explore asthma pathogenesis more deeply and find the potential value of anti-IL-5 mAb and ABPS combined treatment in asthma. Th2 immune responses are often associated with the production of IgG1, and ABPS is a sufficient inhibitor to Th1/Th2 dysregulation [10]. We also analyzed the level of HDM-specific IgG1. Taken together, the results showed that anti-IL-5 mAb and APBS can significantly decrease the level of serum IgE and HDM-specific IgG1 and increase the level of IFN-γ, which provides a potential target to treat asthma patients.

In summary, we have shown that anti-IL-5 mAb and ABPS combined treatment results in significantly decreasing of eosinophil infiltration into the lung and improvement of airway function in HDM-induced mouse models of eosinophilic asthma. A combination of anti-IL-5 mAb and ABPS presented excellent therapeutic effects on asthma. These effects correlated with a significant improvement of AHR, a significant reduction of pulmonary inflammatory cells infiltration, an increase of IFN-γ, and a reduction of serum IgE and HDM-specific IgG1, indicating that anti-IL-5 mAb and ABPS therapy promoted Th1 cytokine secretion and suppressed Th2 cytokine secretion thus attenuated the accumulation of eosinophilic. Our study verified that anti-IL-5 mAb and ABPS combined treatment is a promising therapy for the improvement of eosinophilic asthma.

Data Availability

The data used to support the findings of this study are included within the article.

Conflicts of Interest

The authors declare no conflict of interest.

References

[1] J. H. Ahn, C. H. Kim, Y. H. Kim et al., "Inflammatory and remodeling events in asthma with chronic exposure to house dust mites: a murine model," *Journal of Korean Medical Science*, vol. 22, no. 6, pp. 1026–1033, 2007.

[2] R. Buhl, "Omalizumab (Xolair) improves quality of life in adult patients with allergic asthma: a review," *Respiratory Medicine*, vol. 97, no. 2, pp. 123–129, 2003.

[3] E. D. Bateman, S. S. Hurd, P. J. Barnes et al., "Global strategy for asthma management and prevention: GINA executive summary," *The European Respiratory Journal*, vol. 31, no. 1, pp. 143–178, 2008.

[4] L. J. Akinbami, J. E. Moorman, and X. Liu, "Asthma prevalence, health care use, and mortality: United States, 2005–2009," *National Health Statistics Reports*, no. 32, pp. 1–14, 2011.

[5] R. Divekar and D. Lal, "Recent advances in biologic therapy of asthma and the role in therapy of chronic rhinosinusitis," *F1000Research*, vol. 7, p. 412, 2018.

[6] M. Ollé-Monge, M. J. Cruz, S. Gomez-Ollés, I. Ojanguren, J. Vanoirbeek, and X. Muñoz, "Effect of anti-IgE in occupational asthma caused by exposure to low molecular weight agents," *Allergy*, vol. 72, no. 11, pp. 1720–1727, 2017.

[7] S. W. Yancey, O. N. Keene, F. C. Albers et al., "Biomarkers for severe eosinophilic asthma," *The Journal of Allergy and Clinical Immunology*, vol. 140, no. 6, pp. 1509–1518, 2017.

[8] A. H. Nissim Ben Efraim and F. Levi-Schaffer, "Tissue remodeling and angiogenesis in asthma: the role of the eosinophil," *Therapeutic Advances in Respiratory Disease*, vol. 2, no. 3, pp. 163–171, 2008.

[9] G. P. Anderson, "Endotyping asthma: new insights into key pathogenic mechanisms in a complex, heterogeneous disease," *The Lancet*, vol. 372, no. 9643, pp. 1107–1119, 2008.

[10] K. E. Burrows, C. Dumont, C. L. Thompson, M. C. Catley, K. L. Dixon, and D. Marshall, "OX40 blockade inhibits house dust mite driven allergic lung inflammation in mice and in vitro allergic responses in humans," *European Journal of Immunology*, vol. 45, no. 4, pp. 1116–1128, 2015.

[11] G. M. Walsh, "Therapeutic potential of targeting interleukin 5 in asthma," *BioDrugs*, vol. 27, no. 6, pp. 559–563, 2013.

[12] P. J. Barnes, I. M. Adcock, and K. Ito, "Histone acetylation and deacetylation: importance in inflammatory lung diseases," *The European Respiratory Journal*, vol. 25, no. 3, pp. 552–563, 2005.

[13] W. E. Berger, "New approaches to managing asthma: a US perspective," *Therapeutics and Clinical Risk Management*, vol. 4, no. 2, pp. 363–379, 2008.

[14] K. Izuhara, H. Matsumoto, S. Ohta, J. Ono, K. Arima, and M. Ogawa, "Recent developments regarding periostin in bronchial asthma," *Allergology international*, vol. 64, Supplement, pp. S3–10, 2015.

[15] J. Sahota and D. S. Robinson, "Update on new biologics for intractable eosinophilic asthma: impact of reslizumab," *Drug Design, Development and Therapy*, vol. 12, pp. 1173–1181, 2018.

[16] P. M. O'Byrne, "The demise of anti IL-5 for asthma, or not," *American Journal of Respiratory and Critical Care Medicine*, vol. 176, no. 11, pp. 1059-1060, 2007.

[17] Q. Hamid, M. Azzawi, S. Ying et al., "Expression of mRNA for interleukin-5 in mucosal bronchial biopsies from asthma," *The Journal of Clinical Investigation*, vol. 87, no. 5, pp. 1541–1546, 1991.

[18] J. G. Karras, K. McGraw, R. A. McKay et al., "Inhibition of antigen-induced eosinophilia and late phase airway hyperresponsiveness by an IL-5 antisense oligonucleotide in mouse models of asthma," *The Journal of Immunology*, vol. 164, no. 10, pp. 5409–5415, 2000.

[19] Q. Chen, Z. Liu, and J. H. He, "*Achyranthes bidentata* polysaccharide enhances immune response in weaned piglets," *Immunopharmacology and Immunotoxicology*, vol. 31, no. 2, pp. 253–260, 2009.

[20] X. Zhu, Y. Pan, L. Zheng, L. Cui, and Y. Cao, "Polysaccharides from the Chinese medicinal herb *Achyranthes bidentata* enhance anti-malarial immunity during *Plasmodium yoelii* 17XL infection in mice," *Malaria Journal*, vol. 11, no. 1, p. 49, 2012.

[21] L. Q. Jin, Z. J. Zheng, Y. Peng, W. X. Li, X. M. Chen, and J. X. Lu, "Opposite effects on tumor growth depending on dose of *Achyranthes bidentata* polysaccharides in C57BL/6 mice," *International Immunopharmacology*, vol. 7, no. 5, pp. 568–577, 2007.

[22] T. Baqueiro, M. Russo, V. M. G. Silva et al., "Respiratory allergy to *Blomia tropicalis*: immune response in four syngeneic mouse strains and assessment of a low allergen-dose, short-term experimental model," *Respiratory Research*, vol. 11, no. 1, p. 51, 2010.

[23] K. L. Tomlinson, G. C. G. Davies, D. J. Sutton, and R. T. Palframan, "Neutralisation of interleukin-13 in mice prevents airway pathology caused by chronic exposure to house dust mite," *PLoS One*, vol. 5, no. 10, article e13136, 2010.

[24] A. T. Nials and S. Uddin, "Mouse models of allergic asthma: acute and chronic allergen challenge," *Disease Models & Mechanisms*, vol. 1, no. 4-5, pp. 213–220, 2008.

[25] R. K. Kumar, C. Herbert, and P. S. Foster, "The "classical" ovalbumin challenge model of asthma in mice," *Current Drug Targets*, vol. 9, no. 6, pp. 485–494, 2008.

[26] H. Smith, "Animal models of asthma," *Pulmonary Pharmacology*, vol. 2, no. 2, pp. 59–74, 1989.

[27] E. G. Barrett, K. Rudolph, L. E. Bowen, B. A. Muggenburg, and D. E. Bice, "Effect of inhaled ultrafine carbon particles on the allergic airway response in ragweed-sensitized dogs," *Inhalation Toxicology*, vol. 15, no. 2, pp. 151–165, 2003.

[28] S. P. Chapoval, K. Iijima, E. V. Marietta et al., "Allergic inflammatory response to short ragweed allergenic extract in HLA-DQ transgenic mice lacking CD4 gene," *Journal of Immunology*, vol. 168, no. 2, pp. 890–899, 2002.

[29] B. Fuchs and A. Braun, "Improved mouse models of allergy and allergic asthma–chances beyond ovalbumin," *Current Drug Targets*, vol. 9, no. 6, pp. 495–502, 2008.

[30] J. Chesné, F. Braza, G. Chadeuf et al., "Prime role of IL-17A in neutrophilia and airway smooth muscle contraction in a house dust mite–induced allergic asthma model," *Journal of Allergy and Clinical Immunology*, vol. 135, no. 6, pp. 1643–1645.e5, 2015.

[31] R. L. Warner, N. W. Lukacs, S. D. Shapiro et al., "Role of metalloelastase in a model of allergic lung responses induced by cockroach allergen," *The American Journal of Pathology*, vol. 165, no. 6, pp. 1921–1930, 2004.

[32] S. Sagar, H. Akbarshahi, and L. Uller, "Translational value of animal models of asthma: challenges and promises," *European Journal of Pharmacology*, vol. 759, pp. 272–277, 2015.

[33] J. R. Johnson, R. E. Wiley, R. Fattouh et al., "Continuous exposure to house dust mite elicits chronic airway inflammation and structural remodeling," *American Journal of Respiratory and Critical Care Medicine*, vol. 169, no. 3, pp. 378–385, 2004.

[34] J. Corren, "Inhibition of interleukin-5 for the treatment of eosinophilic diseases," *Discovery Medicine*, vol. 13, no. 71, pp. 305–312, 2012.

[35] X. He, X. Wang, J. Fang et al., "The genus *Achyranthes*: a review on traditional uses, phytochemistry, and pharmacological activities," *Journal of Ethnopharmacology*, vol. 203, pp. 260–278, 2017.

[36] I. D. Pavord, S. Korn, P. Howarth et al., "Mepolizumab for severe eosinophilic asthma (DREAM): a multicentre, double-blind, placebo-controlled trial," *The Lancet*, vol. 380, no. 9842, pp. 651–659, 2012.

[37] Z. Peng, "Vaccines targeting IgE in the treatment of asthma and allergy," *Human Vaccines*, vol. 5, no. 5, pp. 302–309, 2009.

[38] D. A. Randolph, R. Stephens, C. J. L. Carruthers, and D. D. Chaplin, "Cooperation between Th1 and Th2 cells in a murine model of eosinophilic airway inflammation," *Journal of Clinical Investigation*, vol. 104, no. 8, pp. 1021–1029, 1999.

Hindawi
International Journal of Polymer Science
Volume 2018, Article ID 1782734, 8 pages
https://doi.org/10.1155/2018/1782734

Research Article

Identification of a Novel Anticancer Oligopeptide from *Perilla frutescens* (L.) Britt. and Its Enhanced Anticancer Effect by Targeted Nanoparticles *In Vitro*

Dong-Liang He,[1,2] Ri-Ya Jin,[1] Hui-Zhen Li,[1] Qing-Ye Liu,[1] and Zhi-Jun Zhang[1]

[1]*School of Chemical Engineering and Technology, North University of China, Taiyuan, China*
[2]*Department of Environmental Engineering, Taiyuan Institute of Technology, Taiyuan, China*

Correspondence should be addressed to Zhi-Jun Zhang; zjzhang@nuc.edu.cn

Received 14 April 2018; Revised 15 June 2018; Accepted 26 June 2018; Published 9 August 2018

Academic Editor: Jianxun Ding

Objective. *Perilla frutescens* (L.) Brittis is a dietary herbal medicine and has anticancer effect. However, little is known about its anticancer peptides. This study is aimed at identifying cytotoxic oligopeptides which are loaded by a drug delivery system, to explore its anticancer application. *Methods*. The oligopeptides were isolated from enzymatic hydrolysates of *Perilla* seed crude protein by using ultrafiltration, gel filtration chromatography, and reversed-phase high-performance liquid chromatography (RP-HPLC). The structure of the oligopeptide was determined using a peptide sequencer, and its anticancer effect was examined by the MTT assay. PSO (*Perilla* seed oligopeptide), the most potent anticancer oligopeptide, was loaded by chitosan nanoparticles (NPs) modified by hyaluronic acid (HA). Then, the particle size, zeta potential, encapsulation efficiency (EE), drug loading efficiency (LE), the cumulative release rates of NPs, and its cytotoxic effect on cancer cells were investigated. *Results*. Three fractions were isolated by the chromatography assay. The third fraction has a broad-spectrum and the strongest anticancer effect. This fraction was further purified and identified as SGPVGLW with a molecular weight of 715 Da and named as PSO. Then, PSO was loaded by HA-conjugated chitosan to prepare HA/PSO/C NPs, which had a uniform size of 216.7 nm, a zeta potential of 35.4 mV, an EE of 38.7%, and an LE of 24.3%. HA/PSO/C NPs had a slow release rate *in vitro*, with cumulative release reaching to 81.1%. Compared with free PSO, HA/PSO/C NPs showed notably enhanced cytotoxicity and had the strongest potency to human glioma cell line U251. *Conclusion*. This study demonstrated that PSO, a novel oligopeptide from *Perilla* seeds, has a broad-spectrum anticancer effect and could be encapsulated by NPs, which enhanced tumor targeting cytotoxicity with obvious controlled release. Our study indicates that *Perilla* seeds are valuable for anticancer peptide development.

1. Introduction

Perilla frutescens (L.) Britt. has a long cultivation history of more than two thousand years [1] and has been identified as a medicine-food homology plant by the Ministry of Health, China [2]. The seed of *Perilla frutescens* has been regarded as one of the major officinal parts and has special anticancer effects [3], has neuroprotective ability [4], boosts memory [5, 6], improves eyesight [7], lowers blood lipid and blood pressure [8], and inhibits platelet aggregation. Proteins comprise 20%~23% of the total mass of *Perilla frutescens* seeds and can be up to 28%~45% after being defatted. However, the *Perilla frutescens* seed is only a kind of vegetable healthcare oil, and the by-product after oil extraction has not acquired wide attention. Extensive research on protein resource of *Perilla frutescens* seeds is necessary for the purpose of efficient use.

Safe and effective anticancer drugs have always been the important directions in the drug research and development field. Oligopeptides, as short-chain polypeptides, have been considered promising candidates due to potent activity, higher safety, and absorbability. They can induce apoptosis of cancer cells, destroy membranaceous cell and organelle structures, change the pH level inside the cell and tumor microenvironment, and enhance immune responses to tumor by the body. And oligopeptides present low toxicity

or nontoxicity to normal cells. Thus, an oligopeptide has emerged as one of the hot topics in the anticancer drug field. Several oligopeptides have been carried out on clinical stage against tumor, such as tyroserleutide [9] and tyroservatide [10, 11]. Plitidepsin (Aplidin®), a cyclic depsipeptide, has been evaluated in a phase III clinical trial for multiple myeloma [12]. Tasidotin (ILX651), a depsipeptide from sea slug, has reached a phase II clinical trial for advanced or metastatic non-small-cell lung cancer [13]. These oligopeptides are nature products isolated from the body of animals and plants, and so far, they can yield better anticancer effect after synthesis and ingeniously structural modification. Therefore, screening anticancer oligopeptides from *Perilla frutescens* might be meaningful for the development of *Perilla* protein.

Oligopeptide utilization is limited by their nature, such as instability, short half-life, and easy degradation in plasma; however, these deficiencies could be overcome by using macromolecular peptide delivery systems and tumor-targeting agents [14]. Chitosan is a natural cationic polymer and can be used as a drug delivery system due to its good biodegradability and biocompatibility [15]. Hyaluronic acid (HA) binds to its receptor (CD44) to participate in the regulation of tumor growth and metastasis. Based on this feature, initiative targeting effect on tumor can be acquired by using the binding activity between HA and CD44 [16, 17]. It has been reported that HA-conjugated chitosan nanoparticles (NPs) can be effectively utilized as an active tumor-targeting drug carrier.

In this study, oligopeptides were isolated and purified from *Perilla* meal protein, and their anticancer effects were screened. Then, the most potent antitumor oligopeptide was encapsulated by NPs using HA-conjugated chitosan, and its targeting cytotoxicity to several tumor cells was evaluated.

2. Materials and Methods

2.1. Preparation of Defatted Flour and Crude Protein. After drying at 37°C for 2 h, *Perilla* seeds were milled and passed through a 60-mesh-size sieve. The sieved flour was defatted by using 3 times volume of petroleum ether with stirring for 30 min in an extractor. After repeating for 3 times and drying at 50°C for 1 h, the defatted flour was obtained.

The flour was suspended in water with a biomass-to-volume ratio of 1 : 10, with pH adjusted to 10 by adding sodium hydroxide. After incubation for 60 min at 55°C, the alkali-aided solubilized proteins were collected in supernatant by centrifugation. Isoelectric protein precipitation was applied by the addition of hydrochloric acid (HCl), followed by centrifugation at 10,000 rpm at 4°C for 20 min.

2.2. Protein Hydrolysis, Ultrafiltration, and Isolation. Perilla crude protein was dissolved into water (30 mg/ml); then, alcalase (more than 1.9×10^4 U/g) was added (Novozymes, Denmark). After incubation for 6 hours at 60°C and pH 9.5, the enzyme in the hydrolysate was inactivated at 100°C, followed by cooling to 37°C and then centrifuging to collect the supernatant. Hydrolysate fractions with molecular weight smaller than 3 kDa were obtained through centrifugation with an ultrafiltration tube with 3 kDa cut-off (Millipore, Temecula, CA, USA). Oligopeptide fractions below 3 kDa were further purified by Sephadex G-25 (1.6 cm × 100 cm) preequilibrated with distilled water. Oligopeptides were eluted with distilled water at 0.5 ml/min and collected one tube per 4 min. Aliquots were monitored by measuring the absorbance at 214 nm and pooled within the same peak area. The cytotoxic activity of lyophilized fractions was evaluated by the MTT assay.

2.3. Oligopeptide Purification by Reversed-Phase High-Performance Liquid Chromatography (RP-HPLC). Oligopeptide was dissolved in water (0.5 mg/ml) and then was purified by RP-HPLC with the C18 column (4.6 × 250 mm, 5 μm, Agilent, USA). The conditions were as follows: a linear gradient of acetonitrile containing 0.1% TFA increasing from 5% to 40% over 60 min and a flow rate of 1.0 ml/min. The fractions were collected, lyophilized, and named PSO (*Perilla* seed oligopeptide).

2.4. Molecular Mass and Sequence Analysis. The amino acid sequence was determined by the Edman degradation method using a protein sequencer (PPSQ-23A, Shimadzu, Japan). And the molecular mass was analyzed by Agilent 6210 time-of-flight LC/MS (Agilent Technologies, Santa Clara, CA).

2.5. Preparation of PSO-Loaded NPs. Purified PSO was dissolved in water (1.0 mg/ml); then, the same volume of 2.5 mg/ml chitosan aqueous solution in 0.1 mol/l acetic acid (pH 4.0) was added. After stirring for 10 min, tripolyphosphate was added (0.15 mg/ml). After continuous stirring for 30 min, precipitation was collected by centrifugation at 14,000 rpm for 30 min, and then PSO-loaded chitosan was obtained by lyophilization.

1-Ethyl-3-(3-dimethylaminopropyl)carbodiimide (EDC) was added to 3 mg/ml HA aqueous solution. After EDC was dissolved completely, N-hydroxysuccinimide was added; then, the pH was adjusted to 7.5. After incubation at 37°C for 3 hours, lyophilized powder of PSO-loaded chitosan was suspended in HA solution with a biomass ratio of 4 : 1. After stirring for 24 hours, the mixture was centrifuged at 14,000 rpm at 4°C for 60 min; then, PSO-loaded HA-conjugated chitosan (HA/PSO/C) NPs were obtained by lyophilization.

2.6. Characterization of HA/PSO/C NPs. HA/PSO/C NPs were suspended in water (30 mg/ml) and then were ultrasonicated for 5 min. A particle analyzer (Zetasizer Nano ZS90, Malvern Instruments Ltd., United Kingdom) was used to assay the mean particle size and zeta potential of HA/PSO/C NPs. All measurements were performed in triplicate.

2.7. Encapsulation Efficiency (EE) and Drug Loading Efficiency (LE) of HA/PSO/C NPs. 1 mg of HA/PSO/C NPs was degraded by 10% HCl and then diluted with ethanol to 10 ml. PSO concentration was assayed by high-performance liquid chromatography (HPLC). EE was defined as the percentage of the mass of the loaded PSO to the total mass of the consumed PSO in HA/PSO/C NPs preparation, and

LE was defined as the percentage of loaded-PSO mass to NPs mass.

2.8. In Vitro Drug Release Profiles. 1.5 mg of HA/PSO/C NPs was suspended in phosphate-buffered saline (PBS, pH 7.4) (0.5 mg/ml) and then was transferred into a dialysis membrane bag (2000 of molecular weight cut-off, Sangon, Shanghai, China) which was soaked in 30 ml PBS. The whole dialysis system was shaken at 37°C in an incubator. At different time intervals, 1 ml of released solution was collected for HPLC analysis, and the equivalent volume of fresh PBS was compensated. The cumulative release of PSO was measured in triplicate.

2.9. Cell Culture and Reagents. Cell lines of human glioma (U251), human lung carcinoma (A549), human colorectal carcinoma (HCT116), human gastric carcinoma (MGC-803), and human hepatocellular carcinoma (HepG2) were purchased from the Chinese Academy of Sciences (Shanghai, China) and were maintained in DMEM containing 10% fetal bovine serum at 37°C in a humidified incubator supplemented with 5% CO_2.

2.10. Measurement of Inhibition on Cell Proliferation through the MTT Method. The cancer cells in the logarithmic phase were trypsinized to single-cell suspension, and a 96-well plate was seeded with 0.2×10^5 cells per well. After overnight incubation, medium containing the indicated sample was added in a total volume of 100 μl. After the designated time point, 10 μl of the MTT reagent was added into corresponding wells of the plate, and the optical density (OD) at a wavelength of 450 nm was detected with a microplate reader. Proliferation rates were defined as the percentage of the corresponding sample OD to the vehicle control OD, which was set at 100%. Dose-response curves and the concentration inhibiting proliferation by 50% (IC50) were generated with GraphPad Prism 4.0 (GraphPad Software, La Jolla, CA).

2.11. Statistical Processing. Data were presented as mean ± standard deviation (SD) and processed with Statistical Product and Service Solutions 19.0 (SPSS 19.0). Statistical analysis was performed via one-way analysis of variance. $P < 0.05$ suggested that the difference had statistical significance.

3. Results and Discussions

Anticancer peptides, which can directly kill cancer cells with little damage to normal human cells, are new kinds of anticancer drugs and have become a hot spot in new anticancer drug research [18]. Hundreds of anticancer peptides have been found so far [19]. And appropriate structural modifications lead to more potent efficacy of anticancer peptides. In the present study, a novel anticancer oligopeptide was isolated from *Perilla frutescens* seeds. And the anticancer effect was enhanced by form modification through HA-conjugated chitosan.

Oligopeptides smaller than 3 kDa were separated by ultrafiltration from alcalase hydrolysate of *Perilla* crude protein. After isolation by Sephadex G-25, oligopeptide fractions were separated into three major fraction peaks (Figure 1(a)), named as $PSO_{(G25)}1$, $PSO_{(G25)}2$, and $PSO_{(G25)}3$. After pooling and lyophilization, the cytotoxicity of these eluted products was examined by the MTT assay (Figure 1(b)). Compared with $PSO_{(G25)}1$ and $PSO_{(G25)}2$, $PSO_{(G25)}3$ showed the strongest anticancer effect by evaluating the trend presenting the lowest proliferative activity on several cancer cells (U251, A549, HCT116, and HepG2) at both dosages of 1 mg/ml and 5 mg/ml, and the inhibitive effect was in a dose-dependent manner in that 5 mg/ml showed significant inhibition than 1 mg/ml ($P < 0.05$). Although $PSO_{(G25)}3$ did not show the strongest anticancer effect on MGC-803, 5 mg/ml $PSO_{(G25)}3$ still led to a significant decrease in proliferation compared to the vehicle group ($P < 0.001$). This result indicated that $PSO_{(G25)}3$, as a novel anticancer oligopeptide, possessed a broad spectrum of anticancer activities. $PSO_{(G25)}3$ showed a mild cytotoxicity to HepG2 (hepatocellular carcinoma cell line) and MGC-803 (gastric carcinoma cell line) and a moderate cytotoxicity to HCT116 (colorectal carcinoma cell line) and A549 (lung carcinoma cell line). Remarkably, $PSO_{(G25)}3$ possessed the strongest antiproliferative activity to U251 (glioma cell line), which might be correlated to its neurological function. It has been recorded that *Perilla frutescens* seeds were used as the main ingredient to treat neurological diseases, such as anxiety, in the prescription from Chinese ancient works "Yan Shi Ji Sheng Fang." In addition, $PSO_{(G25)}1$ showed relative higher inhibitive effect against MGC-803, compared to $PSO_{(G25)}2$ and $PSO_{(G25)}3$, which indicated the gastric carcinoma preference of $PSO_{(G25)}1$. Taken together, we focused our further study on $PSO_{(G25)}3$ for structural analysis, modification, and its anticancer efficacy.

Then, lyophilized $PSO_{(G25)}3$ was purified by RP-HPLC and determined the sequence of Ser-Gly-Pro-Val-Gly-Leu-Trp, which was named as PSO. PSO molecular mass was practically measured as 715.33 Da (Figure 2), which was anastomosed essentially with theoretical calculated molecular mass (715 Da).

Anticancer peptides are increasingly getting attention; however, deficiencies still exist, such as low natural production, short half-life [20], and less potent bioactivity in plasma [21], as well as easy degradation [19]. Enhancing the stability and tumor-targeting effects of anticancer peptides will definitely improve their antitumor effects. Chitosan nanoparticle carriers have distinct advantages of water solubility, electropositivity, low toxicity, biodegradability, biocompatibility, mass production, and controlled release [22]. In this study, we aimed to use chitosan as a drug delivery system to encapsulate PSO and hope to extend its release, stability, and half-life. HA is an important constituent of the extracellular matrix and is characterized as a natural and linear mucopolysaccharide with electronegativity, biodegradation, and biocompatibility. Research indicates that HA-specific receptors include CD44, RHAMM, LYVE-1, and HARE [23, 24]. CD44 are highly expressed on the surface of various cancer cells, such as glioma [25], ovarian cancer [26], and lung adenocarcinoma [27]. This characteristic can be applied to the formulation development of pharmaceutical agents for greatly increasing the drug concentration in the target cells [28].

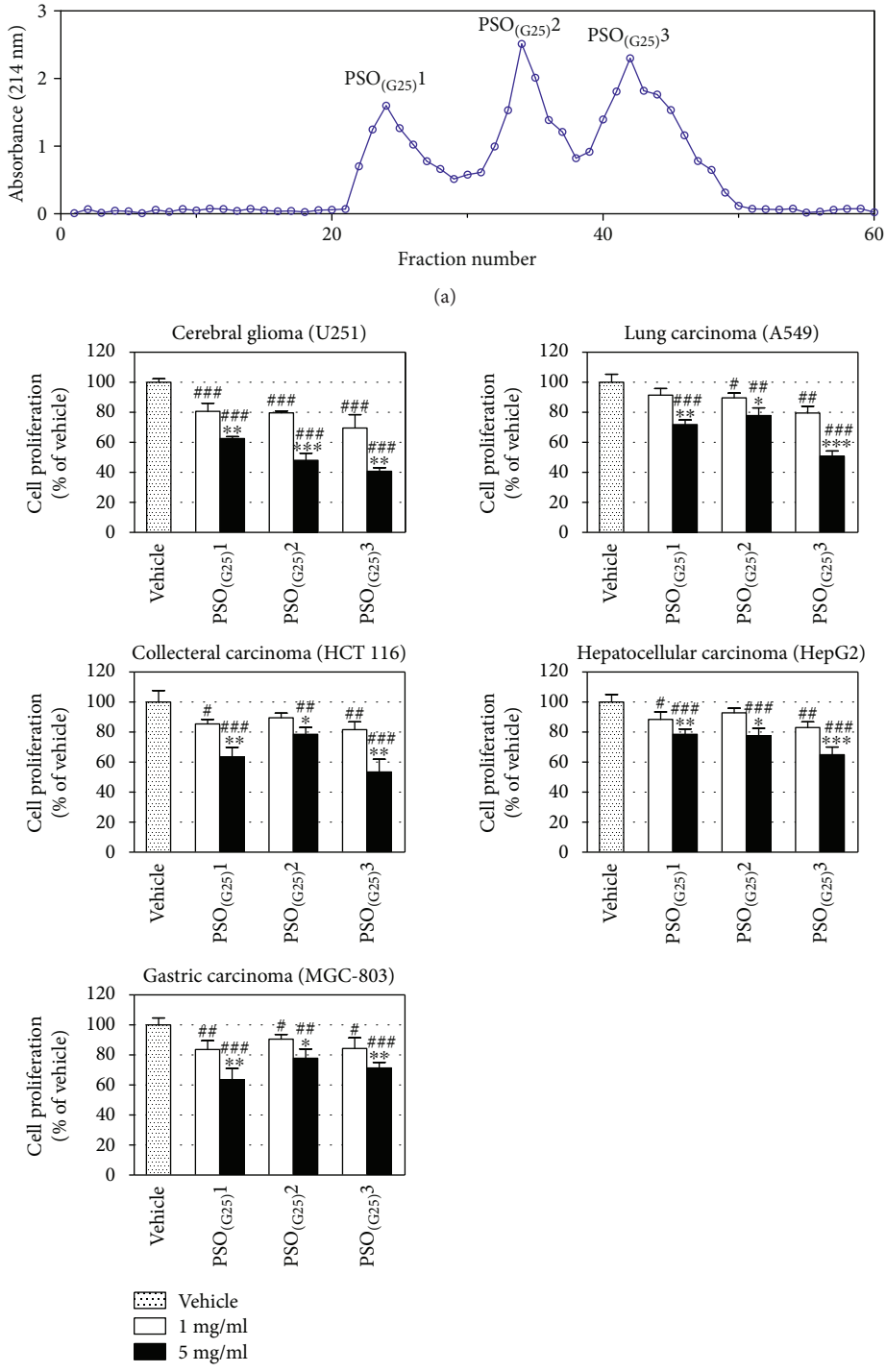

Figure 1: Purification of oligopeptides and their cytotoxicity screening. (a) Gel filtration chromatography on a Sephadex G-25 column, and there were three peaks, $PSO_{(G25)}1$, $PSO_{(G25)}2$, and $PSO_{(G25)}3$. (b) Anticancer effect of three fractions on U251, A549, HCT116, HepG2, and MGC-803 with 1 mg/ml or 5 mg/ml for 24 h, measured by the MTT assay. Percentages of cell proliferation were normalized by optical density values of the vehicle group (as 100%). Data are shown as means ± SD ($n = 5$). $*$ denotes $P < 0.05$, $**$ denotes $P < 0.01$, and $***$ denotes $P < 0.001$; comparisons were performed between groups of 1 mg/ml and 5 mg/ml of every fraction. # denotes $P < 0.05$, ## denotes $P < 0.01$, and ### denotes $P < 0.001$; comparisons were performed against the vehicle group.

In this study, electronegative HA covalently bound to electropositive chitosan via EDC to formulate assembly into NPs with drug loading activity. As shown in Figure 3, HA/PSO/C NPs presented even distribution in particle size with a mean value of 216.7 ± 4.5 nm (Table 1). The sharp main peak suggested that HA/PSO/C NPs had a fairly

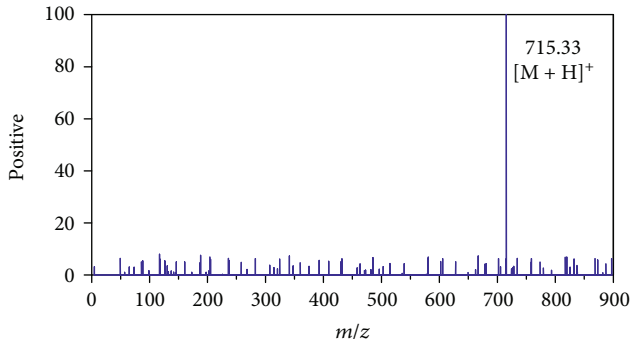

Figure 2: LC/MS analysis of PSO. Consistent with theoretical calculated molecular mass, molecular weight of purified PSO was about 715.33 Da analyzed by Agilent 6210 time-of-flight LC/MS.

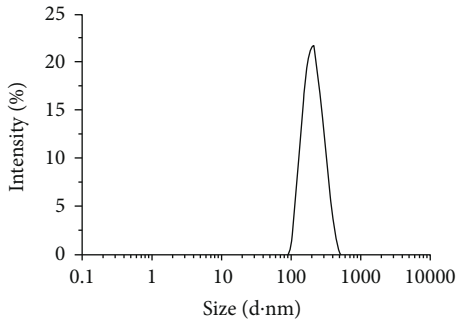

Figure 3: Particle size distribution profiles of HA/PSO/C NPs. Particle size distribution curves of HA/PSO/C NPs measured by a particle analyzer.

Table 1: Characterization of HA/PSO/C NPs (mean ± SD, $n = 3$).

	Particle size (nm)	Zeta potential (mV)	EE (%)	LE (%)
HA/PSO/C	216.7 ± 4.5	35.4 ± 3.2	38.7 ± 4.5	24.3 ± 1.2

narrow size distribution, indicating acceptable size uniformity. The mean zeta potential was 35.4 ± 3.2 mV (Table 1), indicating a satisfactory stability. Moreover, Table 1 also showed EE and LE of HA/PSO/C NPs at 38.7 ± 4.5% and 24.3 ± 1.2%, respectively, indicating successful loading.

The drug release behavior of PSO from HA/PSO/C NPs was also investigated in the release medium of PBS (pH 7.4) at 37°C, according to the ascending velocity of cumulative release curve. As shown in Figure 4, an initial burst release of PSO was noted to 60.7 ± 1.3% within 8 hours. The loaded drug was gradually released from 8 hours to 36 hours, whereas the release velocity became slower. After 36 hours, it hit a release plateau. At the end of the 48-hour release, 81.1 ± 2.3% of PSO was released. The release study indicated that HA/PSO/C NPs had the acceptable abilities of sustained release which could be the contribution from chitosan. Thus, it is speculated that the drug delivery NPs could enhance and prolong the anticancer efficacy of PSO with sustained release

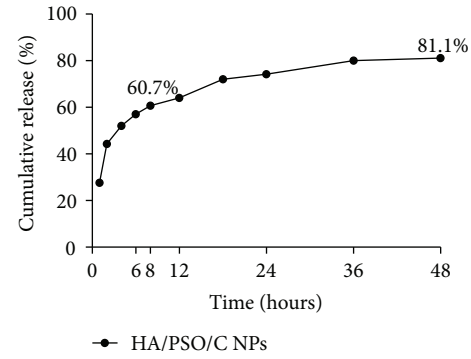

Figure 4: Cumulative release curve. PSO cumulatively released from HA/PSO/C NPs was quantified using HPLC until 48 h. Data are shown as means ± SD ($n = 3$).

into the intracellular tumor microenvironment and reduce systemic cytotoxicity because of the slow release behavior in blood circulation. Taken together, these results of characterization and controlled release suggested that HA/PSO/C NPs were successfully prepared.

Because HA/PSO/C NPs were speculated to be enriched around the tumor and were offered the selection by the contribution from HA due to their binding to specific receptors on the surface of the tumor cell [23, 24], the anticancer effects between HA/PSO/C NPs and PSO were compared to prove it. As shown in Figure 5, 1 mg/ml HA/PSO/C NPs showed inhibitive effect against proliferation of all 5 kinds of cancer cells. Compared with 1 mg/ml PSO, HA/PSO/C NPs showed notably stronger cytotoxic effect on 5 cancer cells ($P < 0.01$) and exhibited the strongest inhibition on U251 (human glioma cell line), then followed by the inhibition on A549 (human lung carcinoma cell line). Furthermore, as shown in Figure 6, HA/PSO/C NPs and PSO could inhibit U251 proliferation with both dose-dependent manner and time-dependent manner. IC50s of HA/PSO/C NPs at 24 hours and 48 hours were 0.39 mg/ml and 0.22 mg/ml, respectively, whereas IC50s of PSO at 24 hours and 48 hours were 2.00 mg/ml and 0.49 mg/ml, respectively. Both IC50s of HA/PSO/C NPs were more potent than IC50s of PSO, which indicated the enhanced potency of PSO by HA-conjugated chitosan NPs. These results suggested that HA/PSO/C NPs worked well for anticancer on various cancer cells. Chitosan and HA worked together to achieve the activity increase. Chitosan, serving as a type of scaffold and macromolecule carrier, has obviously sustained-release property [29]. Drugs can freely diffuse from the chitosan scaffold or even can be released due to the degradation of chitosan [30]. However, the adhesion ability to cells by chitosan is less effective than that by HA. HA affects the adherence and migration ability of tumor cells [31] through binding with specific receptors, such as CD44 [32]. CD44 variants are achieved after splicing and modification and then overexpressed on the surface of tumor cells in abnormal conditions. Overexpressed CD44 variants promote tumorigenicity, migration, and invasion, as well as the binding capability to HA [33]. Therefore, HA, serving as the targeted agent, increases the drug concentration around

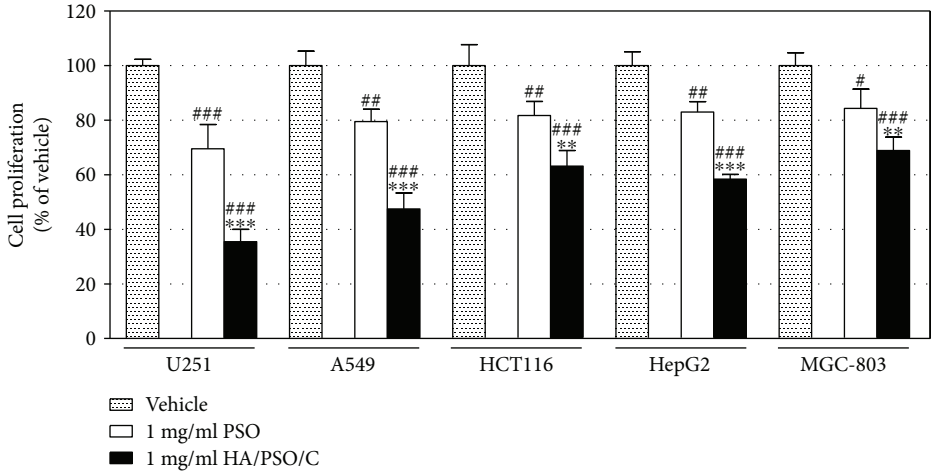

Figure 5: Cytotoxicity of HA/PSO/C NPs on various cancer cells. Anticancer effect of HA/PSO/C NPs or free PSO on U251, A549, HCT116, HepG2, and MGC-803 with 1 mg/ml for 24 h, measured by the MTT assay. Percentages of cell proliferation were normalized by optical density values of the vehicle group (as 100%). Data are shown as means ± SD ($n = 5$). ∗∗ denotes $P < 0.01$, and ∗∗∗ denotes $P < 0.001$; comparisons were performed between groups of HA/PSO/C NPs and PSO. # denotes $P < 0.05$ ## denotes $P < 0.01$, and ### denotes $P < 0.001$; comparisons were performed against the vehicle group.

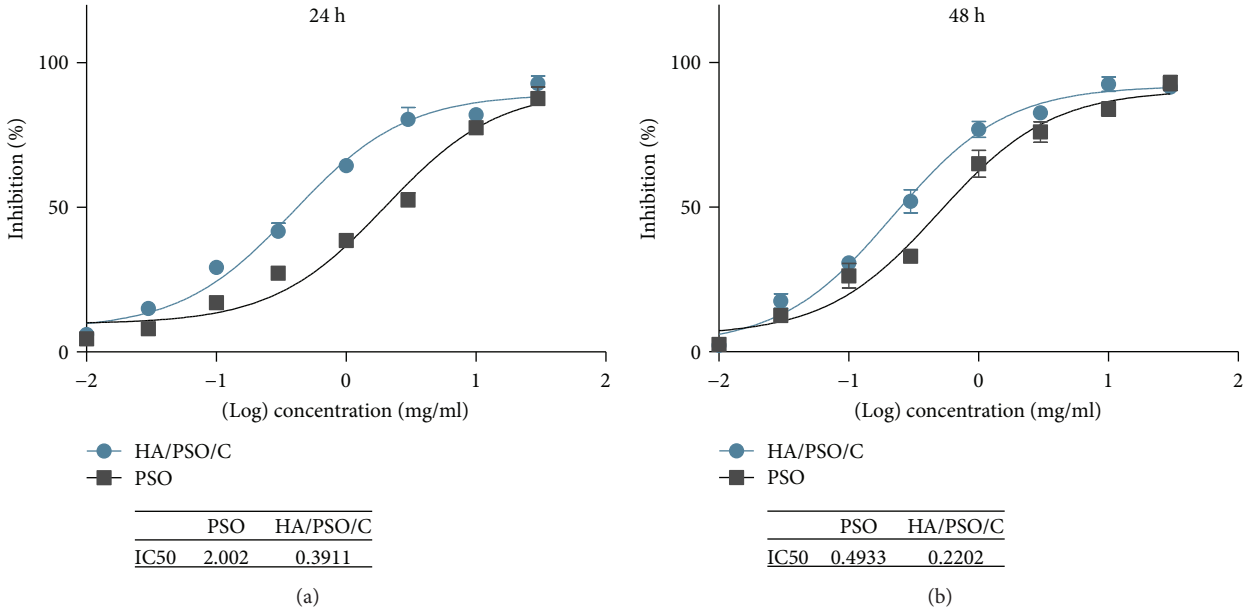

	PSO	HA/PSO/C
IC50	2.002	0.3911

(a)

	PSO	HA/PSO/C
IC50	0.4933	0.2202

(b)

Figure 6: Enhanced cytotoxicity of PSO by nanodevices on the U251 cell. IC50 values measured for free PSO or HA/PSO/C NPs on the U251 cell at 24 h (a) and 48 h (b). Cell proliferation inhibition was measured by the MTT assay. Data are shown as means ± SD ($n = 5$).

cancer cells, whereas it decreases the drug concentration in normal tissues. Taken together, the combined application of chitosan and HA can modify PSO more effectively.

4. Conclusion

In this study, we isolated a novel anticancer oligopeptide, PSO, from *Perilla frutescens* seeds. PSO was successfully encapsulated by HA-conjugated chitosan and showed a broad-spectrum anticancer cytotoxicity with active targeting. Efficient utilization of meal protein from *Perilla frutescens* seeds, which is the by-product after oil extraction, can provide improvement of comprehensive utilization of *Perilla*. Moreover, PSO might be worth taking on further research as an anticancer candidate.

Abbreviations

EE: Encapsulation efficiency
HA: Hyaluronic acid
HA/PSO/C: PSO-loaded hyaluronic acid-conjugated chitosan
HCl: Hydrochloric acid
HPLC: High-performance liquid chromatography

LE: Drug loading efficiency
NPs: Nanoparticles
OD: Optical density
PBS: Phosphate-buffered saline
PSO: *Perilla* seed oligopeptide
RP-HPLC: Reversed-phase high-performance liquid chromatography.

Data Availability

The data used to support the findings of this study are available from the corresponding author upon request.

Conflicts of Interest

No conflict of interest was declared by all authors.

Acknowledgments

This study was supported by a grant from the National Natural Science Foundation of China (no. 51603195) and a grant from the Science and Technology Research Program in Social Development of Shanxi Province (no. 201603D321031).

References

[1] M. Nitta, J. K. Lee, and O. Ohnishi, "Asian perilla crops and their weedy forms: their cultivation, utilization and genetic relationships," *Economic Botany*, vol. 57, no. 2, pp. 245–253, 2003.

[2] T. Zhang, C. Song, L. Song et al., "RNA sequencing and coexpression analysis reveal key genes involved in α-linolenic acid biosynthesis in *Perilla frutescens* seed," *International Journal of Molecular Sciences*, vol. 18, no. 11, 2017.

[3] M. Asif, "Health effects of omega-3, 6, 9 fatty acids: *Perilla frutescens* is a good example of plant oils," *Oriental Pharmacy and Experimental Medicine*, vol. 11, no. 1, pp. 51–59, 2011.

[4] G. Zhao, C. Yao-Yue, G. W. Qin, and L. H. Guo, "Luteolin from purple Perilla mitigates ROS insult particularly in primary neurons," *Neurobiology of Aging*, vol. 33, no. 1, pp. 176–186, 2012.

[5] A. Y. Lee, B. R. Hwang, M. H. Lee, S. Lee, and E. J. Cho, "*Perilla frutescens* var. *japonica* and rosmarinic acid improve amyloid-$\beta_{25\text{-}35}$ induced impairment of cognition and memory function," *Nutrition Research and Practice*, vol. 10, no. 3, pp. 274–281, 2016.

[6] J. Lee, S. Park, J. Y. Lee, Y. K. Yeo, J. S. Kim, and J. Lim, "Improved spatial learning and memory by perilla diet is correlated with immunoreactivities to neurofilament and α-synuclein in hilus of dentate gyrus," *Proteome Science*, vol. 10, no. 1, p. 72, 2012.

[7] L. Zhang, Y. J. Peng, Y. M. Niu, H. Fan, Y. J. Gao, and M. H. Chen, "Determination the contents of lutein and β-carotene in *Perilla frutescens*," *China Food Additives*, vol. 5, pp. 121–125, 2016.

[8] T. Shimokawa, A. Moriuchi, T. Hori et al., "Effect of dietary alpha-linolenate/linoleate balance on mean survival time, incidence of stroke and blood pressure of spontaneously hypertensive rats," *Life Sciences*, vol. 43, no. 25, pp. 2067–2075, 1988.

[9] Z. Y. Xiao, J. B. Jia, L. Chen, W. Zou, and X. P. Chen, "Phase I clinical trial of continuous infusion of tyroserleutide in patients with advanced hepatocellular carcinoma," *Medical Oncology*, vol. 29, no. 3, pp. 1850–1858, 2012.

[10] J. B. Jia, W. Q. Wang, and G. Lin, "Advances of tyroserleutide and tyroservaltide as novel anti-cancer agents," *Chinese Journal of New Drugs and Clinical*, vol. 28, no. 6, pp. 401–404, 2009.

[11] X. Jin, M. Li, L. Yin, J. Zhou, Z. Zhang, and H. Lv, "Tyroservatide-TPGS-paclitaxel liposomes: tyroservatide as a targeting ligand for improving breast cancer treatment," *Nanomedicine*, vol. 13, no. 3, pp. 1105–1115, 2017.

[12] S. Alonso-Álvarez, E. Pardal, D. Sánchez-Nieto et al., "Plitidepsin: design, development, and potential place in therapy," *Drug Design, Development and Therapy*, vol. 11, pp. 253–264, 2017.

[13] D. Rawat, M. Joshi, P. Joshi, and H. Atheaya, "Marine peptides and related compounds in clinical trial," *Anti-Cancer Agents in Medicinal Chemistry*, vol. 6, no. 1, pp. 33–40, 2006.

[14] G. L. Bidwell, "Peptides for cancer therapy: a drug-development opportunity and a drug-delivery challenge," *Therapeutic Delivery*, vol. 3, no. 5, pp. 609–621, 2012.

[15] V. K. Mourya and N. N. Inamdar, "Trimethyl chitosan and its applications in drug delivery," *Journal of Materials Science. Materials in Medicine*, vol. 20, no. 5, pp. 1057–1079, 2009.

[16] V. Orian-Rousseau, "CD44, a therapeutic target for metastasising tumours," *European Journal of Cancer*, vol. 46, no. 7, pp. 1271–1277, 2010.

[17] A. K. Yadav, P. Mishra, and G. P. Agrawal, "An insight on hyaluronic acid in drug targeting and drug delivery," *Journal of Drug Targeting*, vol. 16, no. 2, pp. 91–107, 2008.

[18] Y. F. Xiao, M. M. Jie, B. S. Li et al., "Peptide-based treatment: a promising cancer therapy," *Journal of Immunology Research*, vol. 2015, Article ID 761820, 13 pages, 2015.

[19] D. Wu, Y. Gao, Y. Qi, L. Chen, Y. Ma, and Y. Li, "Peptide-based cancer therapy: opportunity and challenge," *Cancer Letters*, vol. 351, no. 1, pp. 13–22, 2014.

[20] S. Marqus, E. Pirogova, and T. J. Piva, "Evaluation of the use of therapeutic peptides for cancer treatment," *Journal of Biomedical Science*, vol. 24, no. 1, p. 21, 2017.

[21] H. Qin, Y. Ding, A. Mujeeb, Y. Zhao, and G. Nie, "Tumor microenvironment targeting and responsive peptide-based nanoformulations for improved tumor therapy," *Molecular Pharmacology*, vol. 92, no. 3, pp. 219–231, 2017.

[22] R. C. Cheung, T. B. Ng, J. H. Wong, and W. Y. Chan, "Chitosan: an update on potential biomedical and pharmaceutical applications," *Marine Drugs*, vol. 13, no. 8, pp. 5156–5186, 2015.

[23] K. Park, M. Y. Lee, K. S. Kim, and S. K. Hahn, "Target specific tumor treatment by VEGF siRNA complexed with reducible polyethyleneimine-hyaluronic acid conjugate," *Biomaterials*, vol. 31, no. 19, pp. 5258–5265, 2010.

[24] C. Surace, S. Arpicco, A. Dufaÿ-Wojcicki et al., "Lipoplexes targeting the CD44 hyaluronic acid receptor for efficient transfection of breast cancer cells," *Molecular Pharmaceutics*, vol. 6, no. 4, pp. 1062–1073, 2009.

[25] R. H. Eibl, T. Pietsch, J. Moll et al., "Expression of variant CD44 epitopes in human astrocytic brain tumors," *Journal of Neuro-Oncology*, vol. 26, no. 3, pp. 165–170, 1995.

[26] J. D. Sacks and M. V. Barbolina, "Expression and function of CD44 in epithelial ovarian carcinoma," *Biomolecules*, vol. 5, no. 4, pp. 3051–3066, 2015.

[27] V. N. Nguyen, T. Mirejovský, L. Melinová, and V. Mandys, "CD44 and its v6 spliced variant in lung carcinomas: relation to NCAM, CEA, EMA and UP1 and prognostic significance," *Neoplasma*, vol. 47, no. 6, pp. 400–408, 2000.

[28] A. Avigdor, P. Goichberg, S. Shivtiel et al., "CD44 and hyaluronic acid cooperate with SDF-1 in the trafficking of human CD34+ stem/progenitor cells to bone marrow," *Blood*, vol. 103, no. 8, pp. 2981–2989, 2004.

[29] F. Khademi, R. A. Taheri, A. Yousefi Avarvand, H. Vaez, A. A. Momtazi-Borojeni, and S. Soleimanpour, "Are chitosan natural polymers suitable as adjuvant/delivery system for anti-tuberculosis vaccines?," *Microbial Pathogenesis*, vol. 121, pp. 218–223, 2018.

[30] P. Lim Soo, J. Cho, J. Grant, E. Ho, M. Piquette-Miller, and C. Allen, "Drug release mechanism of paclitaxel from a chitosan-lipid implant system: effect of swelling, degradation and morphology," *European Journal of Pharmaceutics and Biopharmaceutics*, vol. 69, no. 1, pp. 149–157, 2008.

[31] J. A. Gomes, R. Amankwah, A. Powell-Richards, and H. S. Dua, "Sodium hyaluronate (hyaluronic acid) promotes migration of human corneal epithelial cells in vitro," *The British Journal of Ophthalmology*, vol. 88, no. 6, pp. 821–825, 2004.

[32] S. Koochekpour, G. J. Pilkington, and A. Merzak, "Hyaluronic acid/CD44H interaction induces cell detachment and stimulates migration and invasion of human glioma cells in vitro," *International Journal of Cancer*, vol. 63, no. 3, pp. 450–454, 1995.

[33] G. Mattheolabakis, L. Milane, A. Singh, and M. M. Amiji, "Hyaluronic acid targeting of CD44 for cancer therapy: from receptor biology to nanomedicine," *Journal of Drug Targeting*, vol. 23, no. 7-8, pp. 605–618, 2015.

Hindawi
International Journal of Polymer Science
Volume 2018, Article ID 1708172, 13 pages
https://doi.org/10.1155/2018/1708172

Review Article

Competitive Biological Activities of Chitosan and Its Derivatives: Antimicrobial, Antioxidant, Anticancer, and Anti-Inflammatory Activities

Suyeon Kim

Engineering Department, Pontificia Universidad Católica del Perú (PUCP), Av. Universitaria 1801, Lima 32, Peru

Correspondence should be addressed to Suyeon Kim; skim@pucp.pe

Received 20 April 2018; Accepted 19 June 2018; Published 19 July 2018

Academic Editor: Yu Tao

Chitosan is obtained from alkaline deacetylation of chitin, and acetamide groups are transformed into primary amino groups during the deacetylation. The diverse biological activities of chitosan and its derivatives are extensively studied that allows to widening the application fields in various sectors especially in biomedical science. The biological properties of chitosan are strongly depending on the solubility in water and other solvents. Deacetylation degree (DDA) and molecular weight (MW) are the most decisive parameters on the bioactivities since the primary amino groups are the key functional groups of chitosan where permits to interact with other molecules. Higher DDA and lower MW of chitosan and chitosan derivatives demonstrated higher antimicrobial, antioxidant, and anticancer capacities. Therefore, the chitosan oligosaccharides (COS) with a low polymerization degree are receiving a great attention in medical and pharmaceutical applications as they have higher water solubility and lower viscosity than chitosan. In this review articles, the antimicrobial, antioxidant, anticancer, anti-inflammatory activities of chitosan and its derivatives are highlighted. The influences of physicochemical parameters of chitosan like DDA and MW on bioactivities are also described.

1. Introduction

Natural polymers are considered environmentally friendly alternatives widely used in medical, agricultural, food, and environmental industries and so on due to their especially renewable, sustainable, and nontoxic properties [1]. Especially in biomedical filed, the natural polymers play very important role. Polysaccharide polymers are the most efficient applicants for the preparation of biomedical products. There are mainly two types of polysaccharides: (i) homopolysaccharides, one type of monomer unit; (ii) heteropolysaccharides, two or more types of monomer unit [2]. They possess a wide range of molecular weights and a significant number of functional groups that give a rise to chemical modification availability [3]. Among the many different sorts of polysaccharides, cellulose (bacterial cellulose and nanocellulose) [4–9], starch [10–14], seaweed (alginate, carrageenan, fucoidan, and ulvan) [15–18], chitin, and chitosan are mainly studied. Due to their attractive abilities to improve the pharmacokinetics and pharmacodynamics of small drug, protein, and enzyme molecules, macromolecular polysaccharides have been receiving significant attention [2, 3]. Polysaccharide polymers demonstrated very efficient attachments of bioactive therapeutic agents, which leads to an increase in the duration of activity [2]. The bioactive agents can bind covalently to polysaccharide backbone structures.

Chitosan is a biopolysaccharide obtained by a de-N-deacetylation process of chitin which is the primary structural polymer in arthropod exoskeletons [19–22]. Chitosan contains three types of reactive groups which are the primary amine group and the primary and secondary hydroxyl groups at C-2, C-3, and C-6 positions, respectively [15]. Among the three reactive groups, the primary amine at the C-2″ position of the glucosamine residues is the most considerable functional groups for biological activities of chitosan [23]. Chitosan has received a significant attention for several

decades due to their unique biological activities. This review aims to supply the recent information about the competitive biological activities of chitosan and its derivatives for medical and pharmaceutical applications. Among many biological activities of chitosan and its derivatives discovered so far, antimicrobial, antioxidant, anticancer, and anti-inflammatory activities were described with recently published outcomes.

2. Chitosan

After cellulose, chitin is the most abundant natural mucopolysaccharide and commonly found as constituent of the exoskeleton in animals, particularly in crustaceans, mollusks, and insects [19–22]. Chitosan is derived from alkaline deacetylation of chitin composing of 2-amino-2-dedoxyd-glucose and 2-acetamino-dedoxy-d-glucose units linked with b-(1 → 4) bonds (Figure 1) [19, 20]. In the process of deacetylation of chitin, the acetamide groups are transformed to the primary amino groups, which are the principal functional groups of chitosan. Chitosan possesses 5–8% nitrogen in the molecules in form of the primary aliphatic amine groups, which makes chitosan proper for typical reactions of amines [19, 23]. The degree of deacetylation of chitosan is referred to the molar fraction of N-acetylated units (DA) or percentage of acetylation (DA%). The high viscosity and low solubility of chitosan limit its biological applications since the attractive biological properties of chitosan are strongly depending on the solubility in water and other commonly used solvents [24]. The degree of deacetylation (DDA) makes an important role to decide its bioactivities as they are directly related to the cationic behavior of chitosan, and the protonation of the amino groups occurs in aqueous acidic solutions [21, 22, 25–28].

The functional amino groups in chitosan are easily modified by chemical reaction and that results in the changes of the mechanical and physical properties. High molecular weight of chitosan allows less availability for its bioactivities, and thus, depolymerization by hydrolysis of polymer chains is frequently performed to acquire low molecular or oligomers of chitosan. In acid hydrolysis, temperature and acidic concentrations were critical factors affecting on the results [29]. The enzymatic degradation of chitosan is getting an attention since it possesses many advantages like milder condition, high specificity, no modification of sugar rings, and mass production comparing to chemical hydrolysis [30]. Common nonspecific enzymes like lysosome, chitinase, pectinase, and cellulose are employed [21]. Proteolytic enzymes, such as pepsin, papain, pronase [31, 32], hepatopancreas [33], and chitosanase [30], were also studied to obtain the low molecular weight of chitosan. Chitosan oligosaccharide (COS) is an oligomer of chitosan, which usually has a degree of polymerization (DP) < 50–55 and an average molecular weight (MW) < 10,000 kDa [34]. COS has good water solubility and low viscosity and thus has more favorable applicant than chitosan in biomedical applications. Aranaz and his colleagues well reported the relations between the biological characteristics and MW and the deacetylation degree of chitosan [21]. When the DDA increases, the solubility of

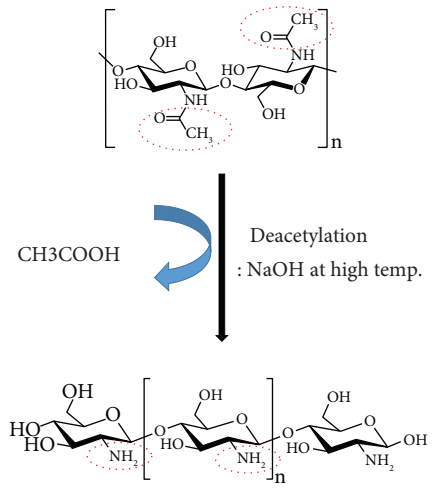

Figure 1: Schematic presentation of chitin deacetylation with alkaline.

chitosan also increases and the more possible interactions are permitted between the available sites of chitosan and other molecules. Thus, the mucoadhesive capacity of chitosan polymers increases with an increase of DDA by providing higher numbers of reactive amino groups available for interaction with other molecules [35, 36]. The cationic characteristic of chitosan is pH dependence (pKa 6.3) and makes it ready to interact with negatively charged molecules such as proteins, therapeutic DNA or RNA, fatty acids, bile acids, phospholipids, and anionic polyelectrolytes [35, 37, 38]. Besides the MW and DDA of chitosan, other physicochemical properties like polydispersity (MW/MN) and crystallinity or the pattern of acetylation might be also considered since they affect on mechanical and biological activities of chitosan [24].

Chitosan and its derivatives are extensively studied in medical and pharmaceutical fields due to their competitive biological properties like biocompatibility, biodegradability, nontoxicity, and analgesic, antitumor, hemostatic, hypocholesterolemic, antimicrobial, and antioxidant properties and so on [35, 39]. These properties are very advantageous in biomedical applications of tissue engineering, wound healing, excipients for drug delivery, and gene delivery [37, 38, 40–42]. The preparations of chitosan-based biomedical materials are varied such as finely divided powders, films, membranes, gels, coatings, nanoparticles, suspensions, and hydrogels, and they can influence their biomedical activity [24]. Depending on the operation purpose, types of drug, and healing target, the preparation manner can be varied.

3. Antimicrobial Activity

The antimicrobial activity has been considered the most essential and influential bioactivity of chitosan and employed not only to the preparation of biomedical materials but also to the functionalization of other polymeric materials including fibers and food conservation [43–51]. The most concerned problem found in hospital and healthcare institutions is infections by microorganism, and thus the

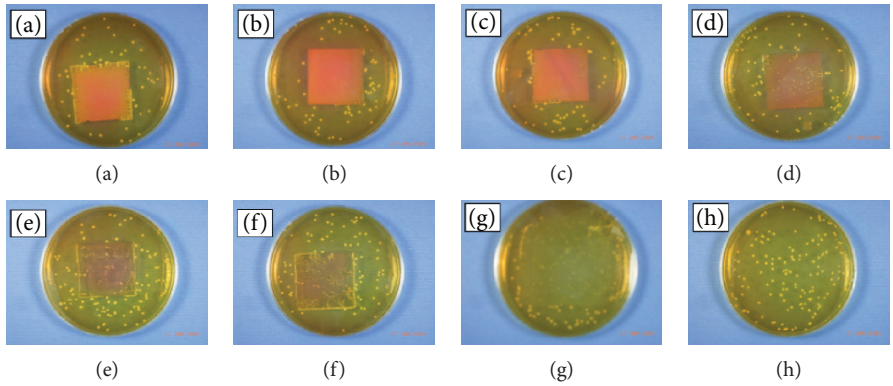

Figure 2: Effect of the DDA of chitosan on the growth inhibition of *S. aureus*. Higher DDA was more effective on inhibiting the growth of *S. aureus*: (a) DD 92.2%; (b) DD 90.1%; (c) DD 88.0%; (d) DD 83.9%; (e) DD 79.7%; (f) DD 75.5%; (g) PVC; (h) control (adapted from [59]).

antimicrobial activity should be primarily considered in biomedical materials. The exposure of subcutaneous tissue caused by wounds like cut, surgery, burn, and so on provides a moist, warm, and nutritious environment that is very suitable for growing the microorganisms [52]. The wound infections are seriously considered since they can cause an increase of trauma and a burden on financial resources to the patients. The mechanism of antimicrobial activity of chitosan is not yet fully understood although numerous researches have been carried out so far. The antimicrobial effect of chitosan is much higher comparing to chitin due to the numbers of the amine groups that is responsible for cationic property of chitosan. Positively charged chitosan at acidic condition might interact with negatively charged residues of carbohydrates, lipids, and proteins located on the cell surface of bacteria, which subsequently inhibit the growth of bacteria [21, 22]. Thus, the electronic property of chitosan plays a very important role in the inhibition mechanism of microorganisms. The high density of positive charge on the structure of chitosan or its derivatives generates strong electrostatic interaction that is affiliated with DDA. With this theory, chitosan is more promising for the inhibition of Gram-negative than Gram-positive bacterium since the negatively charged cell surfaces interact more with positively charged chitosan [22, 43, 47, 53]. However, many researches demonstrated that the chitosan was a more efficient inhibitor against Gram-positive compared to Gram-negative microorganism in their experimental results [44, 45, 54–58].

Takahashi and his colleagues tested the influence of DDA of chitosan on the antimicrobial activity against *Staphylococcus aureus* using two different testing methods, that is, incubation using a mannitol salt agar medium and a conductimetric assay [59]. In both testing methods, the DDA of chitosan played a dominant role in the inhibition of *Staphylococcus aureus* growing (the higher DDA showed the higher rate of inhibition) (Figure 2).

Jung et al. and Younes et al. also achieved similar results about the antimicrobial activity depending on chitosan DDA [60, 61]. When the DDA was nearly 100% (99%), chitosan inhibited almost all types of bacteria tested at the minimum inhibitory concentration (MIC).

There is another theory proposed about the inhibition mechanism of chitosan, that is, an inhibition of RNA and protein synthesis by permeation into the cell nucleus and eventually rupture and leakage of intracellular component. In this theory, the MW is the most decisive factor on the activity [20–22]. The low MW of chitosan was found that easily penetrates into the cell wall of bacteria, combining with DNA and inhibiting the synthesis of mRNA and DNA transcription. With the increase of MW, the permeation into the cell nucleus capacity is decreased. In the case of high MW chitosan, it binds to the negatively charged components on the bacterial cell wall forming an impermeable layer around the cell and consequently changes the cell permeability and blocks transport into the cell [38, 62].

Apart from the MW and DDA, the solubility, pH, and temperature environment are also affecting on the antimicrobial activity of chitosan. At a lower pH, the positive ionic charge increases and chitosan is more absorbed by bacterial cells [20–22]. Benhabile et al. experimented the antimicrobial potential of chitin, chitosan, and its N-acetyl chito- and chito-oligomers against four Gram-positive bacteria (*Staphylococcus aureus* ATCC 25923 and ATCC 43300, *Bacillus subtilis*, and *Bacillus cereus*) and seven Gram-negative bacteria (*Escherichia coli*, *Pseudomonas aeruginosa*, *Salmonella typhimurium*, *Vibrio cholerae*, *Shigella dysenteriae*, *Prevotella melaninogenica*, and *Bacteroides fragilis*) [63]. In this publication, both N-acetyl chito- and chito-oligomers were more effective on the inhibition activity against all tested microorganism than chitosan and chitin, and the decisive effect of DDA and MW on antimicrobial activity was well proved. When DDA is the same (~80%), the effect of MW on the inhibition capacity against *Escherichia coli* was studied by Liu et al. [64]. The authors tested the MW from 55 to 155 kDa, and the lower MW has the higher activity of inhibition against *Escherichia coli*.

Jeon and his colleagues presented the antimicrobial potential of chitosan microparticles against *Escherichia coli*, *Salmonella enterica*, *Klebsiella pneumonia*, and *Streptococcus uberis* [65]. The chitosan microparticles showed a broad-spectrum antimicrobial activity, and when high concentration of chitosan microparticles was applied, the activity

increased. Despite the many studies realized so far, still there is a limitation to conclude about the clear relation between antimicrobial capacity of chitosan and its MW and DDA. It might be due to many other factors affecting the inhibition rate such as sorts of bacterial strains and conditions of biological testing [66]. To expect the synergetic effect of the antimicrobial activity, the incorporation with other promising compounds [43, 44, 67–69] and the modification of structure of chitosan molecules are attempted [26, 70–72]. The phytochemicals like phenolic compounds are broadly attempted to improve antimicrobial activity of chitosan by grafting into the structure [44, 73]. Kim et al. reported the antibacterial effect of chitosan-phytochemical (caffeic acid, ferulic acid, and sinapic acid) conjugates on acne-related bacteria *P. acnes*, *S. epidermidis*, *S. aureus*, and *P. aeruginosa*, and the results exhibited higher (synergetic) antimicrobial effects than that of unconjugated chitosan [73]. Eom et al. prepared the conjugates of chitosan and ferulic acid in the presence of β-lactam antibiotics, and their synergetic antibacterial effect against methicillin-resistant *Staphylococcus aureus* was achieved [74].

4. Antioxidant Activity

Free radical reaction is considered the major cause of several specific human disease and has become an intense interested theme to scientists. Due to its atomic or molecular structure, free radicals are unstable and very reactive. Thus, they tend to pair up with other molecules and atoms to be more stable state [75]. Phaniendra and his colleagues defined free radical as an atom or molecule containing one or more unpaired electrons in a valence shell or outer orbit and is capable of independent existence [76].

In human body, reactive oxygen species (ROS) are produced during the normal metabolism and they oxidize biomolecules, such as lipids, proteins, carbohydrates, and DNA, ultimately leading to oxidative stress [20]. The term of ROS is used not only for oxygen-derived free radicals like superoxide, hydroxyl radical, and nitric oxide but also for nonradical oxygen derivatives of high reactivity like singlet oxygen, hydrogen peroxide, peroxynitrite, and hypochlorite [75, 77]. In biological system, mitochondria are the main responsible for ROS generation during physiological and pathological states and their own ROS scavenging mechanisms required for cell survival [78]. Besides the normal cellular metabolism, there are many exogenous sources to generate ROS such as ozone exposure, hyperoxia, ionizing radiation, and heavy metal ions [79]. In cell metabolism, various enzymes such as catalase, superoxide dismutase, and glutathione peroxidase are involved as a part of the cellular defense system against ROS-mediated cellular injury [80]. When excessive ROS are generated in cellular metabolism, the defense mechanism is not able to protect cellular system and thus the oxidative stress is caused. The oxidative stress in the human body can cause various pathogenic processes including aging, cancer, wrinkle formation, rheumatoid arthritis, inflammation, hypertension, dyslipidemia, atherosclerosis, myocardial infraction, angina pectoris, heart failure, and neurodegenerative diseases such as Alzheimer, Parkinson, and amyotrophic lateral sclerosis [80–84]. In this aspect, an increasing interest in antioxidant agents is very natural.

Therefore, the antioxidant activity of chitosan has been getting high attention from many scientists. Chitosan has shown a notable scavenging activity against different radical species presenting a great potential for an extensive applications. The scavenging activity of chitosan derivatives against free radicals comes through donating hydrogen atom, and several theories were proposed by Xie et al. [85]:

(i) The hydroxyl groups in the polysaccharide unit can react with hydroxyl radicals by the typical H-abstraction reaction.

(ii) OH can react with the residual-free amino groups NH_2 to form stable macromolecules radicals.

(iii) The NH_2 groups can form ammonium groups NH_3^+ by absorbing H^+ from the solution, and then they react with OH through addition reactions.

The DDA and MW of chitosan are also the major factors deciding the scavenging capacity of chitosan [21]. Different with chitosan, chitin is an insoluble polymer in water and thus the major limitation exists for being a useful antioxidant agent.

The NH_2 groups in chitosan are responsible for free radical scavenging, and they can be protonated in acidic solution. There are many publications about the effect of MW and DDA on the scavenging capacity of chitosan. Mahdy Samar and his colleagues experimented an antioxidant activity with various chitosan samples with different DDA and MW and obtained results as high rate of DDA and low MW of chitosan has higher antioxidant activity [27]. Hajji et al. studied three types of chitosan obtained by deacetylation of chitin extracted from Tunisian marine sources shrimp *(Penaeus kerathurus)* waste (DDA: 88%), crab *(Carcinus mediterraneus)* shells (DDA: 83%), and cuttlefish *(Sepia officinalis)* bones (DDA: 95%) [86]. In the test of antioxidant activity, chitosan from cuttlefish with 95% DDA showed the highest value of scavenging effect on DPPH-free radical. Kim and Thomas evaluated the antioxidant activity of chitosan with different MW like 30, 90, and 120 kDa and proved that higher antioxidant activity acquired with lower MW of chitosan (30 kDa) [87]. Sun and his colleagues studied about chitosan oligomers with different MW and tested the scavenging capacity against superoxide anion and hydroxyl radical [88]. In both superoxide anion and hydroxyl radical, the chitosan oligomers presented relative stronger scavenging activity with lower MW. The antioxidant activity of enzymatically degradated chitosan against hydrogen peroxide, 2, 2-diphenyl-1-picrylhydrazyl radical, and chelating ferrous ion was reported by Chang et al. [89]. The results showed that lower MW of chitosan (~2.2 kDa) has the highest impact on the scavenging capacity. Li et al. prepared the low MW of chitosan by oxidative degradation using hydrogen peroxide and tested scavenging capacity against hydroxyl radical [90]. The results indicated that the MW of chitosan (lower

MW has better activity) and concentration were attributed to free radical scavenging effect.

Although the antioxidant activity of chitosan has been proven through many researches, the level of activity is not very satisfactory due to the lack of a H-atom donor to serve as a good chain-breaking antioxidant [91]. The scavenging capacity of free radicals is related to bond dissociation energy of O–H or N–H and the stability of the formed radicals. Due to strong intramolecular and intermolecular hydrogen bonds in chitosan molecules, the OH and NH_2 groups are difficult to dissociate and react with hydroxyl radicals [85]. The various modifications of chitosan molecules to improve the activity were accomplished by grafting functional groups into molecular structure. Among the many tries, the grafting of polyphenols onto chitosan was the most actively studied. Most of polyphenols are found from natural sources and considered safe and environmentally benign materials. After recognizing their strong antioxidant activity, polyphenols have been extensively studied in the area of nutrient, food manufacturing, pharmaceuticals, and medicals [92–98]. The grafting reaction of chitosan and polyphenols was mostly assisted by enzymes [72, 99–101]. In the enzyme-catalyzed reaction, phenolic compounds are oxidized to *o*-quinones which are highly reactive electrophilic compounds further covalently graft to nucleophilic amine groups in chitosan through Schiff-base and/or Michael-type addition reaction [45, 72]. After modification of chitosan by grafting polyphenols, the antioxidant activity was remarkably increased due to the synergetic effects obtained from both chitosan and polyphenols. Figure 3 shows the grafting mechanism of chitosan and catechin by laccase-mediated oxidation reaction (Figure 3(a)) and an increase of antioxidant activity on the chitosan film after grafting catechol (Figure 3(b)).

5. Anticancer Activity

The general cancer treatments performed clinically using chemotherapy, radiotherapy, and surgery have considerably extended the life expectancy of patients. Many current anticancer drugs have nonideal pharmacological properties such as low aqueous solubility, irritating nature, lack of stability, rapid metabolism, and nonselective drug distribution, and they can cause several adverse consequences, including suboptimal therapeutic activity, dose-limiting side effects, and poor-patient quality of life [102, 103]. Thus, many scientists are inspired to search for more effective and harmless medication for cancer-suffering patients. Chitosan and its derivatives are considered the potential anticancer polysaccharide naturally obtained. Many efforts on searching an efficient anticancer agent from natural products lead an increasing interest in polysaccharides. Zong et al. published a review article about the anticancer activity of polysaccharides from fungi, plants, algae, animals, and bacteria [104]. They resumed the inhibition mechanism of tumor growth by polysaccharides as the following:

(i) Prevention of tumorigenesis by oral consumption of active preparations

(ii) Direct anticancer activity, such as the induction of tumor cell apoptosis

(iii) Immunopotentiation activity in combination with chemotherapy

(iv) Inhibition of tumor metastasis

An intrinsic antitumor activity of chitosan and its derivatives with low MW was verified through *in vitro* and *in vivo* experiments [105]. Along with antimicrobial and antioxidant activities, the DDA and MW of chitosan and its derivatives are also the major factors deciding antitumor activity. The effects of the DDA and MW of chitosan oligomers on antitumor activity *in vitro* were investigated by Park et al. [106]. The lower MW and higher DDA (higher solubility) are promising factors for the development of antitumor agents derived from chitosan in *in vitro* tests with Human PC3 (prostate cancer cell), A549 (carcinomic human alveolar basal epithelial cell), and HepG2 (hepatocellular carcinoma cell). Azuma and his colleagues well reviewed about the antitumor activity of COS *in vivo* and *in vitro* cell models showing an effectiveness on tumor growing, reduction of the number of metastatic colonies, suppressing cancer cell growing, and enhancement of acquired immunity [107]. COS has comparatively short chain length and readily soluble in water. Jeon and Kim examined the antitumor activity of COS with different molecular weight against S180 (sarcoma 180 solid) and U14 (uterine cervix carcinoma number 14) tumor cell-bearing mice [108]. The results proved that the antitumor activity was clearly dependent on MW and the range of MW 1.5 to 5.5 kDa effectively inhibited the growth of both tumor cells S180 and U14 in the mice. At the same time, the mice survived more days without weight loss. In several studies, nanoparticles prepared with chitosan showed direct inhibition activity to the proliferation of human tumor cell by inducing apoptosis and growth suppression without signs of neurological toxicity or weight loss proving the safeness of chitosan nanoparticles in the mouse model [109–111]. Xu et al. described that the antitumor activity of chitosan nanoparticles might be related to anti-angiogenic activity that is correlated with vascular endothelial growth factor receptor (VEGFR2) production and subsequent blockage of vascular endothelial growth factor-(VEGF-) induced endothelial cell activation [109]. The stearic acid-g-chitosan oligosaccharide (CSO-SA) micelles were studied for antitumor drug or gene delivery carriers [112, 113]. Hydrophobic drug, podophyllotoxin, was successfully loaded in the CSO-SA micelles demonstrating a sustained release and *in vitro* anticancer effects for suppressing against human breast carcinoma (MCF-7) cells, human lung cancer cells (A549), and human hepatoma cell line (Bel-7402) [112]. Polyethylenimine-conjugated stearic acid-g-chitosan showed good DNA-binding capacity (formation of gene delivery complex) with effectively suppressing the tumor (above 60% tumor inhibition) without systematic toxicity [113]. There are also many other studies about the chitosan and chemically/physically

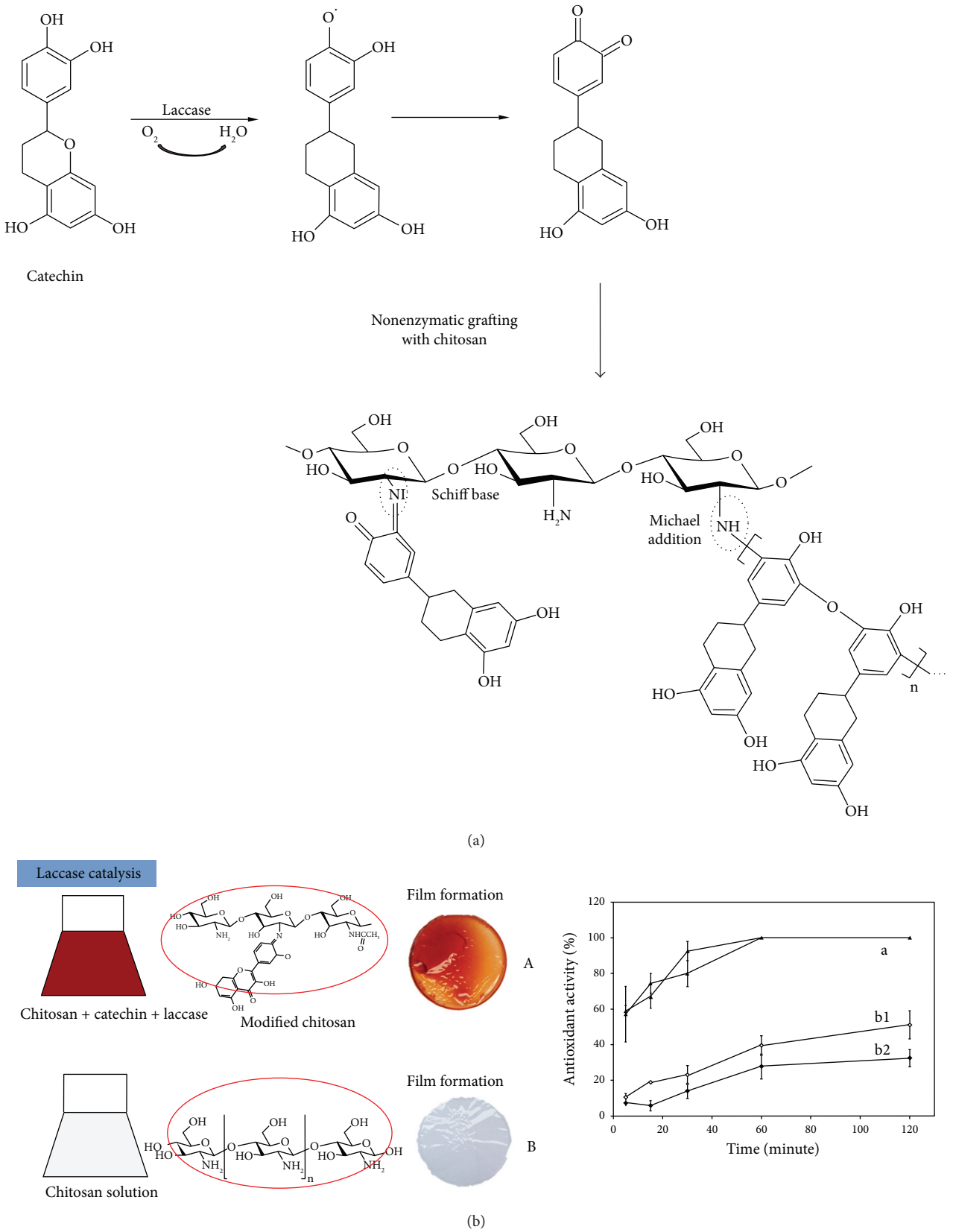

Figure 3: (a) Schematic presentation of enzymatic oxidation of catechin by laccase and nonenzymatic grafting with chitosan and (b) enzymatically modified chitosan film with catechin flavonoids (A) and unmodified chitosan film (B). After modification with catechin, the antioxidant activity of films reached to 100% in 60 minutes while chitosan film (b) showed less than 40% of radical reduction. b1: 95% of DDA; b2: 64% of DDA (adapted and modified from [26]).

Table 1: Anticancer and antitumor activity of chitosan involved preparations tested in various cancer cells.

Cancer types	Used CS form	Tested cells	Remarkable results	Ref.
Breast cancer	SCS[1], SBCS[2]	MCF-7, MDA-MB-231	Inhibition cell proliferation and inducing apoptosis	[114]
	CS[3]	MDA-MB-231, MCF-7, T47D	Inhibition cell proliferation, inducing apoptosis nontoxic to fibroblast L929 normal cells	[102]
	Docetaxel-CN[4]	MCF-7	Inhibition cell proliferation, nontoxic to normal cells	[115]
	FA-CS-UA-NPs[5]	MCF-7	Inhibition cell viability, inhibition tumor growth (reduction of size)	[116]
	MCN[6]	MCF-7	Inhibition cell proliferation	[117]
Prostate cancer	CA[7] scaffolds	LNCaP, C4-2, C4-2B, TRAMP-C2	Good interaction with immune cells, including tumor-infiltrating B cells	[118]
	CS-EGCG NP[8]	22Rv1	Inhibition tumor growth (reduction of size)	[119]
	GC-based CNPs[9]	PC-3	long-term tumor growth inhibition	[120]
	CHGC[10]	LNCaP, PC-3	Inhibition tumor growth (reduction of size)	[121]
	FA-CS PLGA NP[11]	DU145	Inhibition cell proliferation	[122]
	CS-AGR2 siRNA NP[12]	PC-3	Inhibition cell viability	[123]
Colon cancer	CSHA[13] membranes	HT29, DLD-1, HCT116, SW480,	In situ inhibitory effect on cancer cell	[124]
Liver cancer	Bio-CS NP[14]	SMMC7721	In situ inhibition cell proliferation, in vitro and in vivo efficient cell targeting	[125]
	CS, CSHA[13] membranes	Huh7, HepG2, Hep3B, SKHep-1	Inhibition cell proliferation	[124]
Esophageal cancer	CS NP	CAF cell from cancer patient	Inhibition cell proliferation, antimetastatic ability	[126]
Oral cancer	CLCS NP[15]	SCC-9	Reduction cell viability	[118]
	CS	HSC-3, HSC-4, Ca9-22, and HaCaT	Reduction cell viability	[127]

SCS[1]: sulfated chitosan; SBCS[2]: sulfated benzaldehyde chitosan; CS[3]: chitosan; docetaxel-CN[4]: docetaxel-loaded chitosan nanoparticle; FA-CS-UA-NPs[5]: folate-chitosan nanoparticles loaded with ursolic acid; MCN[6]: magnetic chitosan nanoparticles; CA[7]: chitosan-alginate; CS-EGCG NP[8]: chitosan nanoparticles encapsulating epigallocatechin-3-gallate; GC-based CNP[9]: glycol chitosan-based chitosan nanoparticles; CHGC[10]: glycol chitosan; FA-CS PLGA NP[11]: folic acid conjugated-chitosan functionalized poly (D,L-lactide-co-glycolide) nanoparticles; CS-AGR2 siRNA NP[12]: chitosan-based AGR2 siRNA nanoparticle; CSHA[13]: hyaluronan- (HA-) grafted chitosan; bio-CS NP[14]: biotinylated chitosan nanoparticles; CLCS NP[15]: curcumin-loaded chitosan-coated nanoparticles.

modified chitosan or chitosan derivatives for various types of cancer treatment *in vivo* and *in vitro*. Most of the studies commonly demonstrated that chitosan involved anticarcinogenic tools that are very efficient on the inhibition of cell proliferation, inducing apoptosis, cell viability, reduction of tumor size, cell targeting, less side effect, and low toxicity. In Table 1, the summarized several literatures about the anticancer effects of chitosan involved anticarcinogenic tools on breast, prostate, esophageal, liver, oral cancer cells, and so on.

6. Anti-Inflammatory Activity

Inflammation is the first protective response to infection or injury of human body driven in a tissue compartment by a specific set of immune and inflammatory cells with the aim of restoring its structural and functional integrity after exposure to an adverse stimulus [128]. Numerous researches have carried out about the anti-inflammatory and proinflammatory properties of chitosan and its derivatives. Davydova and his colleagues tested the anti-inflammatory activity of chitosan with high (MW: 115 kDa) and low molecular weight (MW: 5.2 kDa), and both chitosan samples presented an intensified induction of anti-inflammatory IL-10 cytokine in animal blood and suppression of colitis progress [129]. The authors concluded that the main contribution to anti-inflammatory activity of chitosan was driven by structural elements comprising its molecule, but not depending on MW. Friedman et al. reported the inhibition capacity of chitosan-alginate nanoparticles against inflammatory cytokines and chemokines induced by *P. acnes*, and the results showed that chitosan-alginate nanoparticles efficiently inhibited *P. acnes*-induced cytokine production in human monocytes and keratinocyte in a dose-dependent manner [130]. Besides inhibition capacity, they also showed high specificity of controlled drug delivery potential for topical therapeutics. Oliveira et al. examined the inhibition of proinflammatory cytokines and anti-inflammatory activities of chitosan film [131]. From the achieved results, a reduction of TNF-α (proinflammatory cytokines) in 3~10 days of cells cultured on chitosan film and significant increase of anti-inflammatory cytokines IL-10 and TGF-β1 are presented. Anti-inflammatory activities of COS were demonstrated by many scientists notwithstanding that the exact mechanism is not yet fully understood. Chung et al. studied two types of COS with high (70 kDa) and low molecular weight (MW:

<1 kDa), and their anti-inflammatory capacity was compared [132]. In low molecular weight COS, the significant inhibition effect against IL-4, IL-13, and TNF-α cytokines was found showing the potential in alleviating the allergic inflammation *in vivo*. Li et al. proposed the mechanism of the lipopolysaccharide-induced NF-κB-dependent inflammatory gene expression by COS, which was associated with reduced NF-κB nucleus translocation [133]. NF-κB is an important transcription factor in mediating the proinflammatory responses. Similar study was carried out by Ma et al. [134], and the positive effect of pretreatment with COS on the suppression of LPS-induced NF-κB and AP-1 activation in macrophages was explained. The results explained that COS is a potential inhibitor against NF-κB- and AP-1-mediated inflammation responses in macrophage by showing the suppression of the LPS-induced c-fos (proto-oncogene) expression in macrophages in a concentration-dependent manner. Yang and his colleagues reported COSs with different MW: COS-A (10 kDa < MW < 20 kDa) and COS-C (1 kDa < MW < 3 kDa) [135]. In both COS samples, the remarkable inhibition activity was observed against the LPS-induced nitric oxide production of RAW 264.7 cells by 50.2% and 44.1%, respectively, without cytotoxicity. Comparing to COS-A, COS-C (lower MW) has a higher level of inhibition activity at lower concentration applied. Li et al. reported the proinflammatory and inflammatory activities of COS (obtained by enzymatic hydrolysis using chitosanase) on cytokines [136]. The authors examined the level of proinflammatory cytokines like IL-1β, IL-6, and TNF-α and anti-inflammatory cytokine IL-2 in mouse osteoarthritis (OA) model. The reduction of serum expression of proinflammatory cytokines and enhancement of anti-inflammatory activity were achieved. Apart from that, the relief of knee joint swelling symptom of mouse model was observed by measuring the changes of the diameter of the knee joint.

7. Future Prospects

Chitosan and its derivatives are extensively studied for medical and pharmaceutical applications. Their unique and attractive bioactivities have been proved through in situ and in vitro experiments. They are easy to obtain in nature with low-cost processes via alkaline deacetylation of chitin. Besides that, the possible acquirement of raw materials by reusing of by-products from food processing industries is also very competitive. Taking into account their many advantages, the interest on the industrial applications of chitosan and its derivatives might be constantly increased. The commercialization of products prepared with chitosan and its derivatives is not yet very common and easy to find. In the future, the effort might be made for easier accessibility of costumers to commercial products in the market. To get more confidence on the chitosan-based commercial products from customers, more fundamental studies on the natural polysaccharides with useful bioactivities might be accomplished including the mechanism of bioactivities of chitosan molecules. This review might help to clarify what have been the most considered among many advantages of chitosan and its derivatives for medical applications in the literatures and will motivate many scientists to work on both fundamental studies and more variety industrial applications.

8. Conclusion

Chitosan and its derivatives possess very attractive biological activities. The potential availability of chitosan and its derivatives in biomedical applications was mainly focused in this review article like antimicrobial, antioxidant, anticancer, and anti-inflammatory activities. Countless researches have been carried out and have commonly reported excellent activities without toxicity. The MW and DDA of chitosan were the most decisive factors affecting on the biological activities mentioned in this review. Thus, in many cases, the hydrolysis of chitosan to reduce the MW to improve their functionality in diverse manners and its effects on biological activities were studied in parallel. The excellent results have been shown through the many scientists, but still there are many challenges required to be explored to explain their mechanism of bioactivities. This review will contribute to the authors working not only on the preparation of chitosan-based biomedical products but also on the evaluation of their specific biological activities.

Conflicts of Interest

The authors declare that they have no conflicts of interest.

Acknowledgments

This research was carried out by the Materials Modification Research Group at the Pontificia Universidad Católica del Perú (PUCP). The author would like to acknowledge Grant 151-2017-FONDECYT from CONCYTEC (Peru).

References

[1] C. Wang, X. Gao, Z. Chen, Y. Chen, and H. Chen, "Preparation, characterization and application of polysaccharide-based metallic nanoparticles: a review," *Polymers*, vol. 9, no. 12, pp. 1–13, 2017.

[2] R. L. Reis, N. M. Neves, J. F. Mano, M. E. Gomes, A. P. Marques, and H. S. Azevedo, "Natural-based polymers for biomedical applications, 2008," in *Chapter 1, Polysaccharides as Carriers of Bioactive Agents for Medical Applications*, R. Pawar, W. Jadhav, S. Bhusare, B. R. Farber, D. Itzkowitz, and A. Domb, Eds., pp. 3–53, Woodhead Publishing, 2008.

[3] A. Basu, K. R. Kunduru, E. Abtew, and A. J. Domb, "Polysaccharide-based conjugates for biomedical applications," *Bioconjugate Chemistry*, vol. 26, no. 8, pp. 1396–1412, 2015.

[4] G. F. Picheth, C. L. Pirich, M. R. Sierakowski et al., "Bacterial cellulose in biomedical applications: a review," *International Journal of Biological Macromolecules*, vol. 104, pp. 97–106, 2017.

[5] M. Jorfi and E. J. Foster, "Recent advances in nanocellulose for biomedical applications," *Journal of Applied Polymer Science*, vol. 132, no. 14, pp. 1–19, 2015.

[6] M. H. Kwak, J. E. Kim, J. Go et al., "Bacterial cellulose membrane produced by *Acetobacter* sp. A10 for burn wound dressing applications," *Carbohydrate Polymers*, vol. 122, pp. 387–398, 2015.

[7] F. C. A. Silveira, F. C. M. Pinto, S. da Silva Caldas Neto, M. de Carvalho Leal, J. Cesário, and J. L. de Andrade Aguiar, "Treatment of tympanic membrane perforation using bacterial cellulose: a randomized controlled trial," *Brazilian Journal of Otorhinolaryngology*, vol. 82, no. 2, pp. 203–208, 2016.

[8] G. F. Picheth, M. R. Sierakowski, M. A. Woehl et al., "Lysozyme-triggered epidermal growth factor release from bacterial cellulose membranes controlled by smart nanostructured films," *Journal of Pharmaceutical Sciences*, vol. 103, no. 12, pp. 3958–3965, 2014.

[9] N. Lin and A. Dufresne, "Nanocellulose in biomedicine: current status and future prospect," *European Polymer Journal*, vol. 59, pp. 302–325, 2014.

[10] N. H. Zakaria, N. Muhammad, and M. Abdullah, "Potential of starch nanocomposites for biomedical applications," *IOP Conference Series: Materials Science and Engineering*, vol. 209, article 012087, 2017.

[11] F. G. Torres, O. P. Troncoso, C. G. Grande, and D. A. Díaz, "Biocompatibilty of starch-based films from starch of Andean crops for biomedical applications," *Materials Science and Engineering*, vol. 31, no. 8, pp. 1737–1740, 2011.

[12] K. Sakeer, T. Scorza, H. Romero, P. Ispas-Szabo, and M. A. Mateescu, "Starch materials as biocompatible supports and procedure for fast separation of macrophages," *Carbohydrate Polymers*, vol. 163, pp. 108–117, 2017.

[13] B. Komur, F. Bayrak, N. Ekren et al., "Starch/PCL composite nanofibers by co-axial electrospinning technique for biomedical applications," *BioMedical Engineering OnLine*, vol. 16, no. 1, pp. 40–13, 2017.

[14] S. Eaysmine, P. Haque, T. Ferdous, M. A. Gafur, and M. M. Rahman, "Potato starch-reinforced poly (vinyl alcohol) and poly (lactic acid) composites for biomedical applications," *Journal of Thermoplastic Composite Materials*, vol. 29, no. 11, pp. 1536–1553, 2016.

[15] J. Venkatesan, B. Lowe, S. Anil et al., "Seaweed polysaccharides and their potential biomedical applications," *Starch*, vol. 67, no. 5-6, pp. 381–390, 2015.

[16] J. Venkatesan, I. Bhatnagar, P. Manivasagan, K. H. Kang, and S. K. Kim, "Alginate composites for bone tissue engineering: a review," *International Journal of Biological Macromolecules*, vol. 72, pp. 269–281, 2015.

[17] H. Liu, J. Cheng, F. Chen et al., "Biomimetic and cell-mediated mineralization of hydroxyapatite by carrageenan functionalized graphene oxide," *ACS Applied Materials & Interfaces*, vol. 6, no. 5, pp. 3132–3140, 2014.

[18] A. Alves, R. A. Sousa, and R. L. Reis, "*In vitro* cytotoxicity assessment of ulvan, a polysaccharide extracted from green algae," *Phytotherapy Research*, vol. 27, no. 8, pp. 1143–1148, 2013.

[19] S. Islam, M. A. Rahman Bhuiyan, and M. N. Islam, "Chitin and chitosan: structure, properties and applications in biomedical engineering," *Journal of Polymers and the Environment*, vol. 25, no. 3, pp. 854–866, 2017.

[20] B. K. Park and M.-M. Kim, "Applications of chitin and its derivatives in biological medicine," *International Journal of Molecular Sciences*, vol. 11, no. 12, pp. 5152–5164, 2010.

[21] I. Aranaz, M. Mengíbar, R. Harris et al., "Functional characterization of chitin and chitosan," *Current Chemical Biology*, vol. 3, no. 2, pp. 203–230, 2009.

[22] I. Younes and M. Rinaudo, "Chitin and chitosan preparation from marine sources. Structure, properties and applications," *Marine Drugs*, vol. 13, no. 3, pp. 1133–1174, 2015.

[23] I. Aranaz, R. Harris, and A. Heras, "Chitosan amphiphilic derivatives. Chemistry and applications," *Current Organic Chemistry*, vol. 14, no. 3, pp. 308–330, 2010.

[24] J. Kumirska, M. X. Weinhold, J. Thöming, and P. Stepnowski, "Biomedical activity of chitin/chitosan based materials—influence of physicochemical properties apart from molecular weight and degree of N-acetylation," *Polymer*, vol. 3, no. 4, pp. 1875–1901, 2011.

[25] A. Grenha, S. al-Qadi, B. Seijo, and C. Remuñán-López, "The potential of chitosan for pulmonary drug delivery," *Journal of Drug Delivery Science and Technology*, vol. 20, no. 1, pp. 33–43, 2010.

[26] S. Kim, K. I. Requejo, J. Nakamatsu, K. N. Gonzales, F. G. Torres, and A. Cavaco-Paulo, "Modulating antioxidant activity and the controlled release capability of laccase mediated catechin grafting of chitosan," *Process Biochemistry*, vol. 59, pp. 65–76, 2017.

[27] M. Mahdy Samar, M. H. el-Kalyoubi, M. M. Khalaf, and M. M. Abd el-Razik, "Physicochemical, functional, antioxidant and antibacterial properties of chitosan extracted from shrimp wastes by microwave technique," *Annals of Agricultural Science*, vol. 58, no. 1, pp. 33–41, 2013.

[28] N. Qinna, Q. Karwi, N. al-Jbour et al., "Influence of molecular weight and degree of deacetylation of low molecular weight chitosan on the bioactivity of oral insulin preparations," *Mar Drugs*, vol. 13, no. 4, pp. 1710–1725, 2015.

[29] C. T. Tsao, C. H. Chang, Y. Y. Lin, M. F. Wu, J. L. Han, and K. H. Hsieh, "Kinetic study of acid depolymerization of chitosan and effects of low molecular weight chitosan on erythrocyte rouleaux formation," *Carbohydrate Research*, vol. 346, no. 1, pp. 94–102, 2011.

[30] D. R. Yao, M. Q. Zhou, S. J. Wu, and S. K. Pan, "Depolymerization of chitosan by enzymes from the digestive tract of sea cucumber Stichopus japonicus," *African Journal of Biotechnology*, vol. 11, no. 2, pp. 423–428, 2012.

[31] A. B. Kumar and R. N. Tharanathan, "A comparative study on depolymerization of chitosan by proteolytic enzymes," *Carbohydrate Polymers*, vol. 58, no. 3, pp. 275–283, 2004.

[32] V. Y. Novikov and V. A. Mukhin, "Chitosan depolymerization by enzymes from the hepatopancreas of the crab *Paralithodes camtschaticus*," *Applied Biochemistry and Microbiology*, vol. 39, no. 5, pp. 464–468, 2003.

[33] C. Muanprasat and V. Chatsudthipong, "Chitosan oligosaccharide: biological activities and potential therapeutic applications," *Pharmacology & Therapeutics*, vol. 170, pp. 80–97, 2017.

[34] S. Rodrigues, M. Dionísio, C. R. López, and A. Grenha, "Biocompatibility of chitosan carriers with application in drug delivery," *Journal of Functional Biomaterials*, vol. 3, no. 3, pp. 615–641, 2012.

[35] T. M. Ways, W. M. Lau, and V. Khutoryanskiy, "Chitosan and its derivatives for application in mucoadhesive drug delivery systems," *Polymer*, vol. 10, no. 3, pp. 1–37, 2018.

[36] D. Enescu and C. E. Olteanu, "Functionalized chitosan and its use in pharmaceutical, biomedical, and biotechnological research," *Chemical Engineering Communications*, vol. 195, no. 10, pp. 1269–1291, 2008.

[37] R. Cheung, T. Ng, J. Wong, and W. Chan, "Chitosan: an update on potential biomedical and pharmaceutical applications," *Marine Drugs*, vol. 13, no. 8, pp. 5156–5186, 2015.

[38] M. Zhang, X. H. Li, Y. D. Gong, N. M. Zhao, and X. F. Zhang, "Properties and biocompatibility of chitosan films modified by blending with PEG," *Biomaterials*, vol. 23, no. 13, pp. 2641–2648, 2002.

[39] Y. Yuan, B. M. Chesnutt, W. O. Haggard, and J. D. Bumgardner, "Deacetylation of chitosan: material characterization and *in vitro* evaluation via albumin adsorption and pre-osteoblastic cell cultures," *Materials*, vol. 4, no. 8, pp. 1399–1416, 2011.

[40] S. Ahmed and S. Ikram, "Chitosan based scaffolds and their applications in wound healing," *Achievements in the Life Sciences*, vol. 10, no. 1, pp. 27–37, 2016.

[41] Y. Zhang, T. Sun, and C. Jiang, "Biomacromolecules as carriers in drug delivery and tissue engineering," *Acta Pharmaceutica Sinica B*, vol. 8, no. 1, pp. 34–50, 2018.

[42] L. M. Bakar, M. Z. Abdullah, A. A. Doolaanea, and S. J. A. Ichwan, "PLGA-chitosan nanoparticle-mediated gene delivery for oral cancer treatment: a brief review," *Journal of Physics: Conference Series*, vol. 884, article 012117, 2017.

[43] S. Kim, J. Nakamatsu, D. Maurtua, and F. Oliveira, "Formation, antimicrobial activity, and controlled release from cotton fibers with deposited functional polymers," *Journal of Applied Polymer Science*, vol. 133, no. 8, pp. 4305401–4305411, 2016.

[44] S. Kim, M. M. Fernandes, T. Matamá, A. Loureiro, A. C. Gomes, and A. Cavaco-Paulo, "Chitosan–lignosulfonates sono-chemically prepared nanoparticles: characterisation and potential applications," *Colloids and Surfaces B: Biointerfaces*, vol. 103, pp. 1–8, 2013.

[45] C. Silva, T. Matamá, S. Y. Kim et al., "Antimicrobial and antioxidant linen via laccase-assisted grafting," *Reactive and Functional Polymers*, vol. 71, no. 7, pp. 713–720, 2011.

[46] L. F. Zemljič, J. Volmajer, T. Ristić, M. Bracic, O. Sauperl, and T. Kreže, "Antimicrobial and antioxidant functionalization of viscose fabric using chitosan–curcumin formulations," *Textile Research Journal*, vol. 84, no. 8, pp. 819–830, 2014.

[47] Z. Zhang, L. Chen, J. Ji, Y. Huang, and D. Chen, "Antibacterial properties of cotton fabrics treated with chitosan," *Textile Research Journal*, vol. 73, no. 12, pp. 1103–1106, 2003.

[48] M. G. Tardajos, G. Cama, M. Dash et al., "Chitosan functionalized poly-ε-caprolactone electrospun fibers and 3D printed scaffolds as antibacterial materials for tissue engineering applications," *Carbohydrate Polymers*, vol. 191, pp. 127–135, 2018.

[49] U. V. Brodnjak, A. Jesih, and D. Gregor-Svetec, "Chitosan based regenerated cellulose fibers functionalized with plasma and ultrasound," *Coatings*, vol. 8, no. 4, p. 133, 2018.

[50] M. Petriccione, F. Mastrobuoni, M. Pasquariello et al., "Effect of chitosan coating on the postharvest quality and antioxidant enzyme system response of strawberry fruit during cold storage," *Food*, vol. 4, no. 4, pp. 501–523, 2015.

[51] Y. Xing, Q. Xu, S. Yang et al., "Preservation mechanism of chitosan-based coating with cinnamon oil for fruits storage based on sensor data," *Sensors*, vol. 16, no. 7, pp. 1–23, 2016.

[52] L. J. Bessa, P. Fazii, M. di Giulio, and L. Cellini, "Bacterial isolates from infected wounds and their antibiotic susceptibility pattern: some remarks about wound infection," *International Wound Journal*, vol. 12, no. 1, pp. 47–52, 2015.

[53] E. Malinowska-Pańczyk, H. Staroszczyk, K. Gottfried, I. Kolodziejska, and A. Wojtasz-Pajak, "Antimicrobial properties of chitosan solutions, chitosan films and gelatin-chitosan films," *Polimery*, vol. 61, pp. 735–741, 2015.

[54] R. C. Goy, S. T. B. Morais, and O. B. G. Assis, "Evaluation of the antimicrobial activity of chitosan and its quaternized derivative on *E. coli* and *S. aureus* growth," *Revista Brasileira de Farmacognosia*, vol. 26, no. 1, pp. 122–127, 2016.

[55] H. K. No, N. Y. Park, S. H. Lee, and S. P. Meyers, "Antibacterial activity of chitosans and chitosan oligomers with different molecular weights," *International Journal of Food Microbiology*, vol. 74, no. 1-2, pp. 65–72, 2002.

[56] K. Divya, S. Vijayan, T. K. George, and M. S. Jisha, "Antimicrobial properties of chitosan nanoparticles: mode of action and factors affecting activity," *Fibers and Polymers*, vol. 18, no. 2, pp. 221–230, 2017.

[57] M. Kaya, T. Baran, M. Asan-Ozusaglam et al., "Extraction and characterization of chitin and chitosan with antimicrobial and antioxidant activities from cosmopolitan Orthoptera species (Insecta)," *Biotechnology and Bioprocess Engineering*, vol. 20, no. 1, pp. 168–179, 2015.

[58] Z. Zhong, R. Xing, S. Liu, L. Wang, S. Cai, and P. Li, "Synthesis of acyl thiourea derivatives of chitosan and their antimicrobial activities in vitro," *Carbohydrate Research*, vol. 343, no. 3, pp. 566–570, 2008.

[59] T. Takahashi, M. Imai, I. Suzuki, and J. Sawai, "Growth inhibitory effect on bacteria of chitosan membranes regulated with deacetylation degree," *Biochemical Engineering Journal*, vol. 40, no. 3, pp. 485–491, 2008.

[60] E. J. Jung, D. K. Youn, S. H. Lee, H. K. No, J. G. Ha, and W. Prinyawiwatkul, "Antibacterial activity of chitosans with different degrees of deacetylation and viscosities," *International Journal of Food Science and Technology*, vol. 45, no. 4, pp. 676–682, 2010.

[61] I. Younes, S. Sellimi, M. Rinaudo, K. Jellouli, and M. Nasri, "Influence of acetylation degree and molecular weight of homogeneous chitosans on antibacterial and antifungal activities," *International Journal of Food Microbiology*, vol. 185, pp. 57–63, 2014.

[62] L. Y. Zheng and J. F. Zhu, "Study on antimicrobial activity of chitosan with different molecular weights," *Carbohydrate Polymers*, vol. 54, no. 4, pp. 527–530, 2003.

[63] M. S. Benhabiles, R. Salah, H. Lounici, N. Drouiche, M. F. A. Goosen, and N. Mameri, "Antibacterial activity of chitin, chitosan and its oligomers prepared from shrimp shell waste," *Food Hydrocolloids*, vol. 29, no. 1, pp. 48–56, 2012.

[64] N. Liu, X. G. Chen, H. J. Park et al., "Effect of MW and concentration of chitosan on antibacterial activity of *Escherichia coli*," *Carbohydrate Polymers*, vol. 64, no. 1, pp. 60–65, 2006.

[65] S. J. Jeon, M. Oh, W. S. Yeo, K. N. Galvão, and K. C. Jeong, "Underlying mechanism of antimicrobial activity of chitosan microparticles and implications for the treatment of infectious diseases," *PLoS One*, vol. 9, no. 3, pp. e92723–e92710, 2014.

[66] M. Kong, X. G. Chen, K. Xing, and H. J. Park, "Antimicrobial properties of chitosan and mode of action: a state of the art review," *International Journal of Food Microbiology*, vol. 144, no. 1, pp. 51–63, 2010.

[67] S. Kumar-Krishnan, E. Prokhorov, M. Hernández-Iturriaga et al., "Chitosan/silver nanocomposites: synergistic antibacterial action of silver nanoparticles and silver ions," *European Polymer Journal*, vol. 67, pp. 242–251, 2015.

[68] S. Ghosh, T. K. Ranebennur, and H. N. Vasan, "Study of antibacterial efficacy of hybrid chitosan-silver nanoparticles for prevention of specific biofilm and water purification," *International Journal of Carbohydrate Chemistry*, vol. 2011, Article ID 693759, 11 pages, 2011.

[69] D. dos Santos Lima, B. Gullon, A. Cardelle-Cobas et al., "Chitosan-based silver nanoparticles: a study of the antibacterial, antileishmanial and cytotoxic effects," *Journal of Bioactive and Compatible Polymers*, vol. 32, no. 4, pp. 397–410, 2017.

[70] A. Amato, L. M. Migneco, A. Martinelli, L. Pietrelli, A. Piozzi, and I. Francolini, "Antimicrobial activity of catechol functionalized-chitosan versus *Staphylococcus epidermidis*," *Carbohydrate Polymers*, vol. 179, pp. 273–281, 2018.

[71] T. M. Tamer, M. A. Hassan, A. M. Omer et al., "Antibacterial and antioxidative activity of O-amine functionalized chitosan," *Carbohydrate Polymers*, vol. 169, pp. 441–450, 2017.

[72] F. Sousa, G. M. Guebitz, and V. Kokol, "Antimicrobial and antioxidant properties of chitosan enzymatically functionalized with flavonoids," *Process Biochemistry*, vol. 44, no. 7, pp. 749–756, 2009.

[73] J.-H. Kim, D. Yu, S. H. Eom et al., "Synergistic antibacterial effects of chitosan-caffeic acid conjugate against antibiotic-resistant acne-related bacteria," *Marine Drugs*, vol. 15, no. 6, p. 167, 2017.

[74] S.-H. Eom, S. K. Kang, D. S. Lee et al., "Synergistic antibacterial effect and antibacterial action mode of chitosan-ferulic acid conjugate against methicillin-resistant Staphylococcus aureus," *Journal of Microbiology and Biotechnology*, vol. 26, no. 4, pp. 784–789, 2016.

[75] S. Bhattacharya, "Reactive oxygen species and cellular defense system," in *Free Radicals in Human Health and Disease*, V. Rani and U. C. S. Yadav, Eds., pp. 17–29, Springer, New Delhi, India, 2015.

[76] A. Phaniendra, D. B. Jestadi, and L. Periyasamy, "Free radicals: properties, sources, targets, and their implication in various diseases," *Indian Journal of Clinical Biochemistry*, vol. 30, no. 1, pp. 11–26, 2015.

[77] V. I. Lushchak, "Free radicals, reactive oxygen species, oxidative stress and its classification," *Chemico-Biological Interactions*, vol. 224, pp. 164–175, 2014.

[78] P. Patlevič, J. Vašková, P. Švorc Jr, L. Vaško, and P. Švorc, "Reactive oxygen species and antioxidant defense in human gastrointestinal diseases," *Integrative Medicine Research*, vol. 5, no. 4, pp. 250–258, 2016.

[79] E. Birben, U. M. Sahiner, C. Sackesen, S. Erzurum, and O. Kalayci, "Oxidative stress and antioxidant defense," *World Allergy Organization Journal*, vol. 5, no. 1, pp. 9–19, 2012.

[80] A. Bhattacharyya, R. Chattopadhyay, S. Mitra, and S. E. Crowe, "Oxidative stress: an essential factor in the pathogenesis of gastrointestinal mucosal diseases," *Physiological Reviews*, vol. 94, no. 2, pp. 329–354, 2014.

[81] P. Pittayapruek, J. Meephansan, O. Prapapan, M. Komine, and M. Ohtsuki, "Role of matrix metalloproteinases in photoaging and photocarcinogenesis," *International Journal of Molecular Sciences*, vol. 17, no. 6, p. 868, 2016.

[82] S.-J. Yoo, E. Go, Y. E. Kim, S. Lee, and J. Kwon, "Roles of reactive oxygen species in rheumatoid arthritis pathogenesis," *Journal of Rheumatic Diseases*, vol. 23, no. 6, pp. 340–347, 2016.

[83] M. Abbas and M. Monireh, "The role of reactive oxygen species in immunopathogenesis of rheumatoid arthritis," *Iranian Journal of Allergy, Asthma, and Immunology*, vol. 7, pp. 195–202, 2008.

[84] T. Rahman, I. Hosen, M. M. T. Islam, and H. U. Shekhar, "Oxidative stress and human health," *Advances in Bioscience and Biotechnology*, vol. 3, no. 7, pp. 997–1019, 2012.

[85] W. Xie, P. Xu, and Q. Liu, "Antioxidant activity of water-soluble chitosan derivatives," *Bioorganic & Medicinal Chemistry Letters*, vol. 11, no. 13, pp. 1699–1701, 2001.

[86] S. Hajji, I. Younes, M. Rinaudo, K. Jellouli, and M. Nasri, "Characterization and in vitro evaluation of cytotoxicity, antimicrobial and antioxidant activities of chitosans extracted from three different marine sources," *Applied Biochemistry and Biotechnology*, vol. 177, no. 1, pp. 18–35, 2015.

[87] K. W. Kim and R. L. Thomas, "Antioxidative activity of chitosans with varying molecular weights," *Food Chemistry*, vol. 101, no. 1, pp. 308–313, 2007.

[88] T. Sun, D. Zhou, J. Xie, and F. Mao, "Preparation of chitosan oligomers and their antioxidant activity," *European Food Research and Technology*, vol. 225, no. 3-4, pp. 451–456, 2007.

[89] S.-H. Chang, C.-H. Wu, and G.-J. Tsai, "Effects of chitosan molecular weight on its antioxidant and antimutagenic properties," *Carbohydrate Polymers*, vol. 181, pp. 1026–1032, 2018.

[90] H. Li, Q. Xu, Y. Chen, and A. Wan, "Effect of concentration and molecular weight of chitosan and its derivative on the free radical scavenging ability," *Journal of Biomedical Materials Research Part A*, vol. 102, no. 3, pp. 911–916, 2014.

[91] M. Božič, S. Gorgieva, and V. Kokol, "Laccase-mediated functionalization of chitosan by caffeic and gallic acids for modulating antioxidant and antimicrobial properties," *Carbohydrate Polymers*, vol. 87, no. 4, pp. 2388–2398, 2012.

[92] S. Khurana, K. Venkataraman, A. Hollingsworth, M. Piche, and T. Tai, "Polyphenols: benefits to the cardiovascular system in health and in aging," *Nutrients*, vol. 5, no. 10, pp. 3779–3827, 2013.

[93] S. Kumar and A. K. Pandey, "Chemistry and biological activities of flavonoids: an overview," *The Scientific World Journal*, vol. 2013, Article ID 162750, 16 pages, 2013.

[94] D. Vauzour, A. Rodriguez-Mateos, G. Corona, M. J. Oruna-Concha, and J. P. E. Spencer, "Polyphenols and human health: prevention of disease and mechanisms of action," *Nutrients*, vol. 2, no. 11, pp. 1106–1131, 2010.

[95] H. R. Fuller, E. L. Humphrey, and G. E. Morris, "Naturally occurring plant polyphenols as potential therapies for inherited neuromuscular diseases," *Future Medicinal Chemistry*, vol. 5, no. 17, pp. 2091–2101, 2013.

[96] Q. Zhou, L. L. Bennett, and S. Zhou, "Multifaceted ability of naturally occurring polyphenols against metastatic cancer," *Clinical and Experimental Pharmacology and Physiology*, vol. 43, no. 4, pp. 394–409, 2016.

[97] M. Agrawal, "Natural polyphenols based new therapeutic avenues for advanced biomedical applications," *Drug Metabolism Reviews*, vol. 47, no. 4, pp. 420–430, 2015.

[98] N. Braidy, R. Grant, S. Adams, and G. J. Guillemin, "Neuroprotective effects of naturally occurring polyphenols on quinolinic acid-induced excitotoxicity in human neurons," *The FEBS Journal*, vol. 277, no. 2, pp. 368–382, 2010.

[99] A. O. Aytekin, S. Morimura, and K. Kida, "Synthesis of chitosan–caffeic acid derivatives and evaluation of their antioxidant activities," *Journal of Bioscience and Bioengineering*, vol. 111, no. 2, pp. 212–216, 2011.

[100] M. Božič, J. Štrancar, and V. Kokol, "Laccase-initiated reaction between phenolic acids and chitosan," *Reactive and Functional Polymers*, vol. 73, no. 10, pp. 1377–1383, 2013.

[101] A. Aljawish, I. Chevalot, B. Piffaut et al., "Functionalization of chitosan by laccase-catalyzed oxidation of ferulic acid and ethyl ferulate under heterogeneous reaction conditions," *Carbohydrate Polymers*, vol. 87, no. 1, pp. 537–544, 2012.

[102] F. Salehi, H. Behboudi, G. Kavoosi, and S. K. Ardestani, "Chitosan promotes ROS-mediated apoptosis and S phase cell cycle arrest in triple-negative breast cancer cells: evidence for intercalative interaction with genomic DNA," *RSC Advances*, vol. 7, no. 68, pp. 43141–43150, 2017.

[103] T. Iwamoto, "Clinical application of drug delivery systems in cancer chemotherapy: review of the efficacy and side effects of approved drugs," *Biological & Pharmaceutical Bulletin*, vol. 36, no. 5, pp. 715–718, 2013.

[104] A. Zong, H. Cao, and F. Wang, "Anticancer polysaccharides from natural resources: a review of recent research," *Carbohydrate Polymers*, vol. 90, no. 4, pp. 1395–1410, 2012.

[105] B. Sarmento and J. Neves, Eds.T. Cunha, B. Teixeira, B. Santos, M. Almeida, G. Dias, and J. Neves, "Chitosan-based systems for biopharmaceuticals: delivery, targeting and polymer therapeutics," in *Chapter 5. Biological and Pharmacological Activity of Chitosan and Derivatives*, B. Sarmento and J. Neves, Eds., Wiley, 2012.

[106] J. K. Park, M. J. Chung, H. N. Choi, and Y. I. Park, "Effects of the molecular weight and the degree of deacetylation of chitosan oligosaccharides on antitumor activity," *International Journal of Molecular Sciences*, vol. 12, no. 1, pp. 266–277, 2011.

[107] K. Azuma, T. Osaki, S. Minami, and Y. Okamoto, "Anticancer and anti-inflammatory properties of chitin and chitosan oligosaccharides," *Journal of Functional Biomaterials*, vol. 6, no. 1, pp. 33–49, 2015.

[108] Y. Jeon and S.-K. Kim, "Antitumor activity of chitosan oligosaccharides produced in ultrafiltration membrane reactor system," *Journal of Microbiology and Biotechnology*, vol. 12, pp. 503–507, 2002.

[109] Y. Xu, Z. Wen, and Z. Xu, "Chitosan nanoparticles inhibit the growth of human hepatocellular carcinoma xenografts through an antiangiogenic mechanism," *Anticancer Research*, vol. 30, pp. 5103–5110, 2010.

[110] L. Qi and Z. Xu, "In vivo antitumor activity of chitosan nanoparticles," *Bioorganic & Medicinal Chemistry Letters*, vol. 16, no. 16, pp. 4243–4245, 2006.

[111] L. Qi, Z. Xu, X. Jiang, Y. Li, and M. Wang, "Cytotoxic activities of chitosan nanoparticles and copper-loaded nanoparticles," *Bioorganic & Medicinal Chemistry Letters*, vol. 15, no. 5, pp. 1397–1399, 2005.

[112] X. Huang, X. Huang, X. H. Jiang et al., "*In vitro* antitumour activity of stearic acid-*g*-chitosan oligosaccharide polymeric micelles loading podophyllotoxin," *Journal of Microencapsulation*, vol. 29, no. 1, pp. 1–8, 2012.

[113] F. Q. Hu, W. W. Chen, M. D. Zhao, H. Yuan, and Y. Z. Du, "Effective antitumor gene therapy delivered by polyethylenimine-conjugated stearic acid-g-chitosan oligosaccharide micelles," *Gene Therapy*, vol. 20, no. 6, pp. 597–606, 2013.

[114] Z. H. Mirzaie, S. Irani, R. Mirfakhraie et al., "Docetaxel–chitosan nanoparticles for breast cancer treatment: cell viability and gene expression study," *Chemical Biology & Drug Design*, vol. 88, no. 6, pp. 850–858, 2016.

[115] H. Jin, J. Pi, F. Yang et al., "Folate-chitosan nanoparticles loaded with ursolic acid confer anti-breast cancer activities *in vitro* and *in vivo*," *Scientific Reports*, vol. 6, no. 1, article 30782, 2016.

[116] J. Varshosaz, F. Hassanzadeh, H. S. Aliabadi, F. R. Khoraskani, M. Mirian, and B. Behdadfar, "Targeted delivery of doxorubicin to breast cancer cells by magnetic LHRH chitosan bioconjugated nanoparticles," *International Journal of Biological Macromolecules*, vol. 93, pp. 1192–1205, 2016.

[117] S. J. Florczyk, G. Liu, F. M. Kievit, A. M. Lewis, J. D. Wu, and M. Zhang, "3D porous chitosan-alginate scaffolds: a new matrix for studying prostate cancer cell-lymphocyte interactions in vitro," *Advanced Healthcare Materials*, vol. 1, no. 5, pp. 590–599, 2012.

[118] L. Mazzarino, G. Loch-Neckel, L. D. S. Bubniak et al., "Curcumin-loaded chitosan-coated nanoparticles as a new approach for the local treatment of oral cavity Cancer," *Journal of Nanoscience and Nanotechnology*, vol. 15, no. 1, pp. 781–791, 2015.

[119] N. Khan, D. J. Bharali, V. M. Adhami et al., "Oral administration of naturally occurring chitosan-based nanoformulated green tea polyphenol EGCG effectively inhibits prostate cancer cell growth in a xenograft model," *Carcinogenesis*, vol. 35, no. 2, pp. 415–423, 2014.

[120] H. Y. Yoon, S. Son, S. J. Lee et al., "Glycol chitosan nanoparticles as specialized cancer therapeutic vehicles: sequential delivery of doxorubicin and Bcl-2 siRNA," *Scientific Reports*, vol. 4, no. 1, pp. 1–12, 2015.

[121] J. Xu, J. Yu, X. Xu et al., "Development, characterization, and evaluation of PSMA-targeted glycol chitosan micelles for prostate cancer therapy," *Journal of Nanomaterials*, vol. 2014, Article ID 462356, 13 pages, 2014.

[122] N. L. Dhas, P. P. Ige, and R. R. Kudarha, "Design, optimization and in-vitro study of folic acid conjugated-chitosan functionalized PLGA nanoparticle for delivery of bicalutamide in prostate cancer," *Powder Technology*, vol. 283, pp. 234–245, 2015.

[123] A. Mohandas, K. S. Snima, R. Jayakumar, and V.-K. Lakshmanan, "Chitosan based AGR2 siRNA nanoparticle delivery system for prostate cancer cells," *Journal of Chitin and Chitosan Science*, vol. 1, no. 2, pp. 161–165, 2013.

[124] P.-H. Chang, K. Sekine, H.-M. Chao, S.-H. Hsu, and E. Chern, "Chitosan promotes cancer progression and stem cell properties in association with Wnt signaling in colon and hepatocellular carcinoma cells," *Scientific Reports*, vol. 8, no. 45751, pp. 1–14, 2017.

[125] M. Cheng, W. Zhu, Q. Li, D. Dai, and Y. Hou, "Anti-cancer efficacy of biotinylated chitosan nanoparticles in liver cancer," *Oncotarget*, vol. 8, no. 35, pp. 59068–59085, 2017.

[126] P. D. Potdar and A. U. Shetti, "Evaluation of anti-metastatic effect of chitosan nanoparticles on esophageal cancer-associated fibroblasts," *Journal of Cancer Metastasis and Treatment*, vol. 2, no. 7, pp. 259–267, 2016.

[127] Y. S. Wimardani, D. F. Suniarti, H.-J. Freisleben, S. I. Wanandi, and M.-A. Ikeda, "Cytotoxic effects of chitosan

against oral cancer cell lines is molecular-weight-dependent and cell-type-specific," *International Journal of Oral Research*, vol. 3, article e1, 2012.

[128] J. Gallo, M. Raska, E. Kriegova, and S. B. Goodman, "Inflammation and its resolution and the musculoskeletal system," *Journal of Orthopaedic Translation*, vol. 10, pp. 52–67, 2017.

[129] V. N. Davydova, A. A. Kalitnik, P. A. Markov, A. V. Volod'ko, S. V. Popov, and I. M. Ermak, "Cytokine-inducing and anti-inflammatory activity of chitosan and its low-molecular derivative," *Applied Biochemistry and Microbiology*, vol. 52, no. 5, pp. 476–482, 2016.

[130] A. J. Friedman, J. Phan, D. O. Schairer et al., "Antimicrobial and anti-inflammatory activity of chitosan-alginate nanoparticles: a targeted therapy for cutaneous pathogens," *The Journal of Investigative Dermatology*, vol. 133, no. 5, pp. 1231–1239, 2013.

[131] M. I. Oliveira, S. G. Santos, M. J. Oliveira, A. L. Torres, and M. A. Barbosa, "Chitosan drives anti-inflammatory macrophage polarisation and pro-inflammatory dendritic cell stimulation," *European Cells and Materials*, vol. 24, pp. 136–153, 2012.

[132] M. J. Chung, J. K. Park, and Y. I. Park, "Anti-inflammatory effects of low-molecular weight chitosan oligosaccharides in IgE-antigen complex-stimulated RBL-2H3 cells and asthma model mice," *International Immunopharmacology*, vol. 12, no. 2, pp. 453–459, 2012.

[133] Y. Li, H. Liu, Q. S. Xu, Y. G. du, and J. Xu, "Chitosan oligosaccharides block LPS-induced O-GlcNAcylation of NF-κB and endothelial inflammatory response," *Carbohydrate Polymers*, vol. 99, pp. 568–578, 2014.

[134] P. Ma, H. T. Liu, P. Wei et al., "Chitosan oligosaccharides inhibit LPS-induced over-expression of IL-6 and TNF-α in RAW264.7 macrophage cells through blockade of mitogen activated protein kinase (MAPK) and PI3K/Akt signaling pathways," *Carbohydrate Polymers*, vol. 84, no. 4, pp. 1391–1398, 2011.

[135] E. J. Yang, J. G. Kim, J. Y. Kim, S. Kim, N. Lee, and C. G. Hyun, "Anti-inflammatory effect of chitosan oligosaccharides in RAW 264.7 cells," *Central European Journal of Biology*, vol. 5, no. 1, pp. 95–102, 2010.

[136] Y. Li, L. Chen, Y. Liu, Y. Zhang, Y. Liang, and Y. Mei, "Anti-inflammatory effects in a mouse osteoarthritis model of a mixture of glucosamine and chitooligosaccharides produced by bi-enzyme single-step hydrolysis," *Scientific Reports*, vol. 8, no. 1, article 5624, 2018.